ISBN 978-82-326-3798-0 (printed version)
ISBN 978-82-326-3799-7 (electronic version)
ISSN 1503-8181

Doctoral theses at NTNU, 2019:100

Solveig Vassenden

Rock Breaking Under Rolling TBM Disc Cutters in Hard Rock Conditions

Visualization and documentation of craks

NTNU
Norwegian University of
Science and Technology
Faculty of Engineering
Department of Geoscienceand Petroleum

NTNU
Norwegian University of
Science and Technology

Doctoral theses at NTNU, 2019:100

NTNU

NTNU
Norwegian University of
Science and Technology

Solveig Vassenden

Rock Breaking Under Rolling TBM Disc Cutters in Hard Rock Conditions

Visualization and documentation of craks

Thesis for the degree of Philosophiae Doctor

Trondheim, March 2019

Norwegian University of Science and Technology
Faculty of Engineering
Department of Geoscienceand Petroleum

NTNU
Norwegian University of
Science and Technology

NTNU
Norwegian University of Science and Technology

Thesis for the degree of Philosophiae Doctor

Faculty of Engineering
Department of Geoscienceand Petroleum

ISBN 978-82-326-3798-0 (printed version)
ISBN 978-82-326-3799-7 (electronic version)
ISSN 1503-8181

Doctoral theses at NTNU, 2019:100

Printed by Skipnes Kommunikasjon as

Abstract

Since the world's first TBM started boring in 1800s the development of the boring technology has been a continuous process. The diameter of the TBM, the penetration rate and the efficiency in hard rock have increased in correlation with improved steel quality, larger disc cutters, adjusted cutter spacing, higher thrust force and higher torque. Different prediction models are established to estimate consumption of time, costs and cutter wear. Downtime caused by cutter changes, due to abrasion and wear, brings down the overall advance rate and affects the total economy of a project. Experiences from previous TBM projects show that the TBM is boring about 40% of the total boring time, and that cutter change takes about 15 % of the time. A small increase in cutter life can therefore give a considerable saving potential, looking at material costs and time spent. The TBM manufacturing companies are continuously working to improve penetration rate and to lower the costs in the boring process.

FAST-Tunn is a joint research project dealing within TBM technology, involving a cluster of industrial partners, governmental bodies and academia/research. The aim of the FAST-Tunn project has been to improve the efficiency of new cutters in terms of 25 % increased durability, by investigating rock breaking mechanisms, steel quality and abrasivity. This Ph.D.-study is one out of two scholarships within the FAST-Tunn project.

A large amount of resources have already been, and is expected to be, invested in different research projects aiming for improved cutter quality and more efficient TBMs, but do we really knows what is actually happening at this interface of materials? The number, length, orientation, type of cracks and the distance between them are all important responses to be detected and documented in order to increase the understanding of rock breaking under disc cutters of a TBM. Such knowledge can be used to optimize the TBM cutter head design, the cutter design and the operation of new TBMs, in order to decrease the cutter wear, and thereby increase the cutter life and the overall efficiency of the TBM. The knowledge can also be used to increase the utilization potential of a TBM at ongoing projects.

This Ph.D.-Study seeks to improve the understanding of rock breaking by establishing a cost and time efficient method to visualize and document the rock breaking under the cutters of a full size TBM and under the cutter of a linear cutter test, and to use this method to document the effect of the cutter head speed, measured in revolutions per minute.

The combination of sampling by core drilling at the face of two ongoing tunnel projects, geological mapping, sound velocity measurements, dye penetrant and the quantification of crack and core sample properties, have proven to be a both economical and time efficient way to detect and document the rock braking under a disc cutter of a full size TBM.

Given constant operating conditions, there is a considerable variation of fracture patterns, and the rock breaking under the cutters of a TBM is much more complex than presented in literature. The concept model of rock breaking under the cutters of a TBM can be considered as a generalized and idealized presentation of the rock breaking, but is does not represent the great variety of fracture patterns and rock surfaces in front of a full size TBM.

The study of cracks in core samples from two sites with different geologies and different RPMs, indicates that more cracks are initiated, and the cracks are longer and penetrates deeper into

the rock when the RPM is reduced. There is also a better distribution of dip angles, dip directions and point of origin in reference to the cutter groove. This implies a higher chipping potential, as the probability of intersection of cracks increases. This seems to be the main trend for two different geologies.

From the available data, the findings from the LCT indicates that there are some differences in the effects of the disc cutter on a TBM and a LCT, with respect to the distribution of dip angles and the relative distribution of vertical depths from the 0-line, relative to the maximum vertical depth from the 0-line in the core samples from the LCT and a full size TBM.

Acknowledgements

Ever since my first lesson about TBMs at the Norwegian University of Science and technology, given by Professor emeritus **Einar Broch** in 2004, I was deeply fascinated by this machines. A huge machine, utilizing enormous thrust forces to break intact rock masses, leaving a perfect circular hole. For me, this was the perfect proof of humankind's arrogance towards nature and millions of years with rock formation. From this point on, I had a dream of visiting a full size TBM. Through FAST-Tunn, this Ph.D.-study gave me the opportunity not only to fulfill my dream, but also to study this fascinating rock breaking process under the disc cutters and to fully experience the daily life on a TBM in operation, and get to know the opportunities and limitations of a TBM. The breakthrough at the Nedre Røssåga headrace tunnel will forever be one of the greatest experiences of my life.

Eivind, thank you for your supervising through all these years. For your contagious engagement, your positivism and your calmness when I have been in despair or even in panic. You have been patient and encouraging; you have supported my wishes and given me the opportunity to make this Ph.D. my own. And last, but not least, you have believed in me even when I have not. I am going to miss early morning discussions over a cup of coffee in your office.

To **Charlie**, thank you for valuable input towards the end of this work.

Beside the great experiences with TBMs, I want to thank the **FAST-Tunn** project and its participants for unlimited access to project data, and for facilitating this study throughout the project. Among all the participant, I give a special thanks to **Tobias Anderson** for unconditional facilitation, and valuable discussions and inputs along the way, and to **Sindre Log** for taking me to India and introducing me to my first TBM.

At the point where I had many core samples, and no visible cracks, I was really close to quitting the study. I am therefore so grateful that **Robert Sturk** not only followed my presentation at Fjellsprengningskonferansen, but also that he gave thoughts to my problem and took the trouble of contacting Eivind and tell him about **Mats Olson**. Mats Olson invited me to his home in Stockhom, and gave me the advice to use the dye penetrant. Without Robert and Mats, this study could have ended before it really started.

I also wat to thank **Marit Haugen** in SINTEF for her contribution to naming the rock types in the samples from the Nedre Røssåga headrace tunnel. I also want to thank **Filip Dahl, Kjartan Følke, Trond Erik Larsen, Niklas Haugen, Joakim Eggen** and **Simon Hagen** at the rock engineering laboratory at NTNU/SINTEF for all their help advices and patience with me and all my core samples.

To my friends **Kay, Rune, Max, Arnt Erik and Eivind;** thank you for helping me out in the tunnel, for inviting me into your daily life in the tunnel, and for answering all my questions and for shearing all this invaluable details about the TBM and the boring process that helped me improve my study.

Core drilling at the face of a TBM tunnel involves heavy lifting, crawling through narrow passages, being hungry, dirty, soaking vet and tired. **Robert** and **Rolf Martin**, you were the best field assistants I could possibly ask for. Thank you.

Being a Ph.D.-candidate could sometimes feel quite lonely, being the only one working with these tiny details. My fellow Ph.D.-students, **Javier, Helene** and **Karl Gunnar** have contributed in professional discussions, but mostly in a non-professional way by being supportive and understanding, and for creating sense of community within the loneliness. Thank you.

Through his master thesis, **Eirik Hannestad** contributed with valuable findings concerning sound velocity measurements, and I learned a lot from supervising his work.

My employer, **Multiconsult**, consented three years leave of absence to this Ph.D.- study, and I am so thankful that I had the change to finish this study without any concerns regarding my future, and I hope that my years of work can benefit Multiconsult in Trondheim in some way.

It is for sure, I would never have finished this work without the support and love from **Mamma, Pappa** and **Kristin**, and **Maya** and **Snotas** waggly tails and never-ending wish for a run.

Thank you to **Moje** and **Moste** for making me dinner, to my brother **Håvard** and my sister-in-law **Guro** for their care, and to my nephew **Ole** for being the most adorable preoccupation from science.

At last, thanks to **Mattis.** The love of my life and my personal ski waxer.

Table of contents

Table of figures

Table of tables

List of acronyms and abbreviations

AMR Project	Alimineti Madhava Reddy Project
BWI	Bit Wear Index
CLI	Cutter Life Index
DRI	Drilling Rate Index
FAST-Tunn	Future Advanced Steel Technology for Tunneling
HP TBM	High Performance TBM
ISRM	International Society for Rock Mechanics
KICT	LCT facilities at Korea Institute of Civil Engineering and Building Technology
LCT	Linear Cutter Test
LNS	Leonard Nilsen & Sønner AS
MR imaging	Magnetic resonance imaging
NTH	The Norwegian Institute of Technology in Trondheim (until: 1996)
NTNU	The Norwegian University of Technology and Science (from: 1996)
Robbins	The Robbins Company
RPM	Revolutions Per Minute
RQD	Rock Quality Designation
SBU	Small Boring Unit
SJ-value	Sievers's J-value
TBM	Tunnel Boring Machine

A	Area of between 0-line and maximal vertical distance from 0-line to surface line
a	Area between surface line and 0-line
d	Vertical depth from 0-line to surface line at the cutter groove
D	Maximal vertical distance from 0-line to surface line
k_{area}	Ratio that describes the area left to be chipped
k_{depth}	Ratio that describes the cutter position in relation to the intact rock mass on the sides
$k_{\text{surface length}}$	Ratio that describes the roughness of the surface line
$k_{\text{surface variation}}$	Ratio that describes the chipping potential in terms of unevenness of the surface
l	Length of 0-line
L	Length of surface line
λ	Horizontal distance between the minimum and the maximum vertical distance from 0-line to surface line

1 Introduction

1.1 Background

Since the world's first tunnel boring machine, from now on referred to as TBM, started boring in 1800s the development of the boring technology has been a continuous process. The diameter of the TBM, the penetration rate and the efficiency in hard rock have increased in correlation with improved steel quality, larger disc cutters, adjusted cutter spacing, higher thrust force and higher torque. Different prediction models have been established to estimate consumption of time, costs and cutter wear. The empirical model for TBM performance from the Norwegian University of Science and Technology (NTNU) has been active for several decades, and is continuously improved through implementation of data from completed projects and further research.

Downtime caused by cutter changes, due to abrasion and wear, brings down the overall advance rate and affects the total economy of a project. Experiences from previous TBM projects show that the TBM is boring about 40% of the total boring time, and that cutter change takes about 15 % of the time. A small increase in cutter life can therefore give a considerable saving potential, looking at material costs and time spent. The TBM manufacturing companies are continuously working to improve penetration rate and to lower the costs in the boring process.

In 2011, a cluster of industrial partners, governmental bodies and academia/research initiated the research project *Future Advanced Steel Technology for Tunneling* (FAST-Tunn). The aim of the FAST-Tunn project has been to improve the efficiency of new cutters in terms of 25 % increased durability, by investigating rock breaking mechanisms, steel quality and abrasivity. This Ph.D.-study is one out of two scholarships within the FAST-Tunn project.

A large amount of resources have already been, and is expected to be, invested in different research projects aiming for improved cutter quality and more efficient TBMs, but so far, there are no available documentation of what is actually happening at this interface of materials. The number, length, orientation, type of cracks and the distance between them are all important responses to be detected and documented in order to increase the understanding of rock breaking under disc cutters of a TBM.

In the NTNU prediction model, the rotation speed of the cutter head (RPM) is included in the formulas for estimations of cutter life and the TBM performance. As for the overall understanding of rock breaking under disc cutters, documentation of rock breaking using different RPMs can be valuable knowlegde. Such knowledge can be used to optimize the TBM cutter head design and the cutter design and the operation of new TBMs, in order to decrease the cutter wear, and thereby increase the cutter life and the overall efficiency of the TBM. The knowledge can also be used to increase the utilization potential of a TBM at ongoing projects.

Linear cutter tests (LCT) are used for both estimation of cutter wear and TBM performance, but also for calibration of numerical models and testing of new cutters. During a LCT, one full size disc cutter is used to cut several horizontal, parallel and straight grooves. Any possible effects of concentric cutting, gravity and interaction between two or more neighbor cutters are therefore not included in the results.

1.2 Objectives of thesis

To substantiate the FAST-Tunn project main objective; "*to improve the efficiency of new cutters in terms of 25 % increased durability*", this Ph.D. study seeks to **increase the understanding of the rock breaking under a disc cutter of a full size TBM**.

In this context, it is claimed that an improved understanding of rock breaking will provide a valuable knowledge to the process of increasing the cutter life or the penetration rate. Thereby it contributes to the achievement of the main objective of the FAST-Tunn project.

The increased understanding of rock breaking will be addressed through three main objectives;

1. Establish an economical and time efficient method to detect and document the rock breaking under the disc cutters of a full size TBM in hard rock in order to verify, disprove or differentiates the interpretation of rock breaking under disc cutters
2. Document the effect of different RPMs concerning rock breaking under the disc cutters of a full size TBM in hard rock
3. Detect and document the rock breaking under the disc cutter in a linear cutter, and compare this with the results from a full size TBM in order to document any similarities or differences in the effect of a disc cutter in a LCT and on a full size TBM.

1.3 Research questions

The three objectives of this thesis are addressed through the following research questions which are grouped in the same three categories as the main objectives:

1. Document rock breaking:

1.1 How can a high number of useful samples be collected from the face of a TBM tunnel, in a cost and time efficient way, without influencing the excavation of the tunnel unnecessary?
1.2 How can the effect of disc cutters be detected and documented in a cost and time efficient way?
1.3 How deep into the rock mass is the rock mass affected by the cutters?
1.4 Can the concept model of rock breaking under the cutters of a TBM be verified, or would the findings lead to a revision or differentiation of the drawing?
1.5 Is there any correlation between cracks found in chips compared to those in the core samples?

2. Document effect of different RPMs:

2.1 Is it possible to identify similar responses of disc cutters in two different geologies?
2.2 Is it possible to identify different responses of disc cutters using different RPMs within the same geology?
2.3 Does the RPM affect the shape of the surface line of the core samples?

3. Document rock breaking under disc cutters in LCT:

   3.1 Is it possible to identify similar effects of disc cutters on a TBM and in a LCT?

Through laboratory tests on samples from a reference rock type and samples from two different TBM projects these questions have been elaborated. A detailed description of the projects and the relevant rock type is given in chapter 2.7 *Description of selected sites and testing facilities*.

1.4 Limitations of the work presented in this thesis

The limitations of this Ph.D.-study are listed below:

- This Ph.D.-study focuses on hard rock TBM Tunneling. The tunneling of soft ground is not within the scope of the study.
- Neither drill & blast tunneling, cut and cover tunneling nor roadheader tunneling will be evaluated.
- The effect of foam or other additives will not be evaluated in this study.
- The data used in this thesis are based on samples from two different TBM projects, one double shield TBM and one open gripper TBM from the Robbins Company. Both machines using 19" and 20" cutters. Other types of TBMs, other cutter sizes or TBM cutters with tungsten carbide inserts or similar methods are not included.
- The rock samples in this study have been collected from ongoing projects, and the sampling is adjusted to the excavation of the tunnel. This has placed a limitation on number of sample series and number of samples in each series. A certain variability in grain size, mineral content and fracturing must be expected.
- Evaluation of rock breaking mechanisms and failure modes is not included in the study.
- RPM is chosen as the operational parameter to study, and the effects of thrust, torque and different operators of the TBM are not included.
- All rock mass parameters are provided by the TBM supplier and SINTEF, and represents the properties in a given section in the tunnels, and not exactly at the same chainages as the samples.
- Except the samples from the LCT-testing, the author has collected all samples and done the geological mapping included in this thesis. The samples from the LCT-testing have been collected by Yongbeom Seo.
- All operation parameters for the TBMs are provided by the contractors and the TBM supplier. Some of the parameters are measured while boring, but due to technical problems some of the parameters are manually logged by the TBM operator.

1.5 Sites and testing facilities

In order to study rock breaking under rolling disc cutters of a full size TBM in hard rock, samples from ongoing TBM projects had to be included. This study is based on samples from two ongoing TBM projects, and samples from a reference location. In addition, samples from

a rock specimen tested at the LCT facilities at Korea Institute of Civil Engineering and Building Technology (KICT) in Gumi, South-Korea are included.

The following sites have been selected for sampling and testing:

- The Alimineti Madhava Reddy Project in Andhra Pradesh, India
- The Nedre Røssåga headrace tunnel for a new power plant in Hemnes, Norway
- The Iddefjord granite, used for LCT- testing in Korea
- The Tronhjemite quarry at Støren, Norway
- LCT Facilities at the Korea Institute of Civil Engineering and Building Technology (KICT) in Gumi, South-Korea

A detailed description of the sites and the projects is given in chapter 2.7 *Description of selected sites and testing facilities*.

1.6 Publications

The FAST-Tunn Project in general has been presented on a number of occasions, both in Norway and internationally, whilst selected preliminary results have been presented by the Ph.D.-candidate in three papers, two oral presentations and one poster. Below is an overview of the papers prepared by the author:

- Fjellsprengningskonferansen 2013 : Paper and oral presentation
  FAST-Tunn; a research project to increase the TBM cutter efficiency with 25 %, (Vassenden & Grøv, 2013)
- Fjellsprengningskonferansen 2016 : Paper and oral presentation
  Rock breaking under disc cutters of a TBM – A part of the research project FAST-Tunn (Vassenden, 2016)
- World Tunnel Congress 2017: Paper and poster presentation
  Rock Breaking Under the Disc Cutters of a TBM – a Part of the Research Project FAST-Tunn (Vassenden & Grøv, 2017)

1.7 Outline of the thesis

The thesis is comprised of eight chapters, whilst all raw data is provided in totally 10 appendixes.

Chapter 1 presents the objectives, research questions, a short introduction of the selected sites and testing facilities and the limitations of the study.

Chapter 2 presents the technical background for the objectives and goals of this thesis, and contains theoretical considerations supporting the objectives and the research questions, including the research project that this Ph.D.-study is a part of, and describes this thesis' contribution to the research project. It also presents detailed information of the selected sites and testing facilities for fieldwork and laboratory testing. Some of the site properties are decisive for the research methodology used in this Ph.D.-study, and therefore this chapter has been included prior to the chapter describing the research methodology.

Chapter 3 presents the Ph.D.-project plan, and gives a brief discussion of reasons for changes from the original project plan.

Chapter 4 presents the research methodology, and includes the arguments and rationales for selecting the research methodologies and a discussion of the various benefits and shortcomings linked to the chosen methods.

Chapter 5 and 6 presents the results obtained from the field and laboratory testing.

Chapter 7 discusses the findings and the methods presented in chapter 5, and presents a short summary of the findings in each category. This chapter also presents a few issues that were identified as outstanding, though not elaborated in this thesis, but which has an impact on rock breaking assessments.

Chapter 8 contains the main findings of this thesis, and presents the answers to the research questions presented in chapter 3.

The appendixes presents background information and data about samples that form the basis of this thesis, and some results that are not included in the thesis.

2 Technical background

2.1 Tunnel Boring Machine history

The history of TBMs, goes back to the beginning of the 1800s. During some decades, the technique developed rapidly from boring of holes with small diameters to excavation of larger parts of the tunnel face. In 1856, Charkes Wilson patented the first machine that excavated the entire face using disc cutters on a rotating cutter head. This machine is considered as the first modern TBM (Maidl, et al., 2008). Different TBM and cutter designs were then developed and tested continuously the next 100 years in order to achieve machines that were more efficient. In 1952, James S. Robbins designed the first open gripper TBM. This machine had disc cutters as the only excavating tool, and it was the first machine that was usable for excavation of harder rock types (Tunnels & Tunneling, 2009). Since then, the TBMs have become bigger, stronger and more efficient, and now excavating tunnels worldwide.

The first full face excavated tunnel in Norway was a 73 meters long raise tunnel with a diameter of 1 meter, at Tokke hydroelectric power project in 1967. Five years later, in 1972, the first tunnel was excavated by a TBM. This was a 4,3 km long sewage tunnel in Trondheim, with a diameter of 2,3 meters. The TBM was a second hand machine, and the Norwegian contractor made use of a German contractor to operate the TBM (Hansen, 2017). From 1972 to 1992 more than 49 tunnels, and a total of 250 km, were excavated by the use of TBMs. Most of these tunnels were bored due to the development of hydroelectric power projects, but there were also excavation of sewage tunnels, including the 40 km long VEAS tunnel through Oslo, Bærum and Asker. The majority of these tunnels had relatively small cross sections, and diameters of less than 4,5 meters. Two of the tunnels were road tunnels, with diameters exceeding 6 meters (Hansen, 1998).

The first TBM tunnels in Norway were bored mainly in soft rocks like limestone, schists and phyllites. Through the end of 1970s and beginnings of the 1980s projects in hard rocks like granites and gneisses were completed. In this period, The Norwegian Institute of Technology, NTH, (now: Norwegian University of Science and Technology, NTNU) carried out wide-ranging field studies and investigations on cuter wear and TBM performance in hard rock. The experienced from previous projects and the investigations revealed the need for improved TBMs for hard rock boring. As a result, The Robbins Company, in cooperation with Statkraft, introduced the first High Performance TBM (HP TBM) in 1988. These TBMs were provided with 19-inch cutters with a new and impoved bearing, rated 312 kN/ cutter, in comparison with the previous 17-inch cutters rated 250 kN/ cutter. These improvements resulted in a 50-60 % increased cutter penetration, given in millimeters per revolution of the cutter head (Hansen, 2017).

A majority of the Norwegian bedrock consists of competent hard rock. Compared to less competent and softer types of rock the need for rock support is relatively less, and they are well suited for drill and blast excavation. During the 1980s, the Norwegian contractors became very competent in the conventional drill-and-blast technology, and excavated tunnels at a low cost and with a high efficiency. Despite the improved performances by the HP TBMs they were outdistanced by the drill and blast excavation, and after the completion of Meråker hydroelectric power project in 1992, there were no TBMs in operation in Norway for more than 20 years.

From 1992 and up to this date the TBM technology have developed rapidly, resulting in bigger and stronger machines, and 20 inch cutters, making them more suitable for hard rock types. At the same time, the increase of excavation of tunnels close to existing infrastructure and settlements have caused challenges related to vibrations, noise and limited construction sites. Internationally, the TBM is dominating, though not in hard rock but in soil, and TBM constitutes approximately 60-80 % of all tunneling worldwide (FAST-Tunn, 2011). In Norway, excavation by TBM have been considered at an early stage for some projects, but the method have been rejected due to cost and lack of TBM experience among Norwegian contractors, project owners and consultants.

In October 2012 the Norwegian National Rail Administration announced that the Follobanen project from Oslo to Ski, is going to be excavated by TBM-technology, starting by the end of 2016 (The Norwegian National Rail Administration, 2012). This was a remarkable decision that caught the interest of the tunneling industry not only in Norway. In 2014, the same governmental body indicated that the tenders for the Ulriken tunnel next to Bergen would be opened for TBM excavation as well as conventional drill & blast (The Norwegian National Rail Administration, 2012) and in May 2014 they signed a contract for TBM excavation (The Norwegian National Rail Administration, 2014). Finally, on the 25th of January 2013 Leonhard Nilsen & Sønner AS and The Robbins Company signed a Letter of Intent to lease a TBM for use in a new head race tunnel at Statkraft's hydroelectric power plan at Nedre Røssåga (Leonhard Nilsen & Sønner AS, 2013). These three projects might be the beginning of a new TMB history in Norway.

LNS completed the excavation of the headrace tunnel at Røssåga was in December 2015, and Skanska Strabag completed the excavation of Ulriken tunnel in August 2017. From December 2016, Acciona Ghella excavates at the Follobanen project using four TBMs. The excavations are expected completed by November 2018.

2.2 Previous and current research on TBM technology and performance

Since the world's first TBM started boring in 1800s the development of the boring technology has been a continuous process. The diameter of the TBM, the penetration rate and the efficiency in hard rock have increased in correlation with improved steel quality, larger disc cutters, adjusted cutter spacing, higher thrust force and higher torque (Maidl, et al., 2008). Different prediction models are established to estimate consumption of time, costs and cutter wear. Some of the well-known models are the NTNU-model (Bruland, 2000), (Macias, 2016), the model from the Colorado School of Mines (CSM-model), (Rostami & Ozdemir, 1993) , (Rostami, 1997) and the Q_{TBM}-model (Barton, 2000). In addition, several numerical models are established to see the effect on the cutters, the cutter head and the rock interface (Innaurato & Oreste, 2011), (Entacher, et al., 2012), (Alvarez, et al., 2000) and (Cho, et al., 2009). Even a probabilistic model has been developed for that purpose (Laughton, 1998).

Knowledge from different research projects and data from completed projects have continuously served the prediction models and the numerical models with more precise and adequate parameters, and the models have been, and will be further revised.

Downtime caused by cutter changes, due to abrasion and wear, brings down the overall advance rate and affects the total economy of the project. The process of cutter wear, cutter

design, material technology and operating parameters as Revolutions Per Minute (RPM) and thrust have therefore been important areas of research (Maidl, et al., 2008), (Tunneling Journal, oct/nov 2011), (Sänger, 2006), (Entacher, et al., 2012).

Another important factor influencing several parts of the boring process is the rock mass-steel interface and the subsequent rock breaking. This is a generic topic, and competence in rock breaking, and general rock mechanics and the process of rock breaking under the impact of an intender have been studied from different angles of attack. This rock breaking have an influence on both the mining and tunneling industries, as well as for all situations with a steel – geological material interface. Numerical modeling (Hajiabdolmajid, et al., 2002) and experiences from completed projects and field studies (Bruland, 2000), (Eide, 2014), (Macias, 2016) have contributed to improved understanding of rock breaking under different conditions. In addition, there has been a continuous process of optimizing laboratory tests and development of new laboratory test for prediction of costs and performance has (Kou, et al., 1997), (Bruland, 2000) (Rinne, 2008), (Yilmaz, 2009), (Dahl, et al., 2011), (Macias, et al., 2016).

Since the beginning of the 2000s three wide-ranging research projects on TBM related subjects have been completed. One of them was Technology Innovation in Underground Construction (Tunnconstruct). This was a research project were 41 partners from 11 countries of the European Union participated. The partners included clients, industry, small and medium-sized enterprises, manufacturers, research institutions, and universities. The project lasted for four years, and finished in 2009 (International Tunnelling and Underground Space Association, 2011).

In addition, the TBM manufacturing companies are continuously working to improve penetration rate and to lower the costs in the boring process. Two of the large TBM-manufacturers, The Robbins Company and Herrenknecht AG both have their own research and development divisions, and they have also been involved in two different research projects, Future Advance Steel Technology for Tunneling (FAST-Tunn) and ABROCK respectively.

ABROCK is a project with several research units (ETH Zürich, LFU Innsbruck, TU München, MU Leoben, EPF Lausanne, CSM Golden) and industrial partners (construction companies, clients, consulting engineers and TBM experts) were the objective was *"analysis and prediction of penetration and cutter wear for TBM-tunnels in rock"* (ABROCK Reseach Project, 2013).

2.3 FAST-Tunn

FAST-Tunn is a joint research project dealing with TBMs, involving a cluster of industrial partners, governmental bodies and academia/research. The industrial partners are BASF, Babendererde Engineering, BMS Steel, Leonard Nilsen & Sønner AS, Scana Steel and The Robbins Company. The governmental bodies are The Norwegian National Rail Administration (Bane Nord from 1.1.2017) and The Norwegian Research Council. The academia and research partners are NTNU and SINTEF.

The aim of the FAST-Tunn project is quoted from the FAST-Tunn project description: *"An important aim of the FAST-Tunn project is to improve the efficiency of new cutters in terms of 25 % increased durability, introducing the need of possible new steel alloys and cutter*

layout/geometry. Before testing in mid-scale or full scale, numerical modeling and laboratory testing are important tools to understand the governing physical mechanisms in the interaction geological material and rolling disc cutters at the tunnel face, the mechanical properties of the geologic material and the cutter steel as well as the failure mechanism at the point of interface" (FAST-Tunn, 2011).

The FAST-Tunn project meets the need to compensate the development of the TBM-technology with new cutter steel to allow an excavation method that enables the machine capacities to be fully utilized at the rock-steel interface. The main objectives of the projects is to 1) to develop more efficient system for excavation of hard rock with cutter rings for TBMs and 2) to improve the capabilities of the NTNU model for performance prediction of tunneling operations in Norway (Grøv, 2014).

Through the different partners, the project and its co-workers there is access to knowledge, software, field data and testing facilities at different levels. Both steel alloys and rock was planned to be tested in the tribo-corrosion-, drillability- and rock engineering laboratory at NTNU/SINTEF. Suggested cutter steel alloys, cutter design and operating parameters were further tested in small and midscale tests, and later on in full scale at ongoing TBM projects. Field data and the results from the testing were then applied for improving the numerical models, and the NTNU-prediction model. The project took into account cross-disciplinary competence to both solve and document the prevailing interfaces and interactions through the available resources.

This Ph.D.-study is one out of two scholarships within the FAST-Tunn project. Francisco Javier Macias defended his thesis "*Performance Predictions and Cutter Life Assessments*" (Macias, 2016) in December 2016.

In addition, Yongbeom Seo is writing his Ph.D.-thesis on "*Numerical modeling of rock breaking in hard rock in TBM tunneling*" in cooperation with the FAST-Tunn project, but with private financing.

The author's contribution to the FAST- Tunn project is illustrated in Figure 2.1.

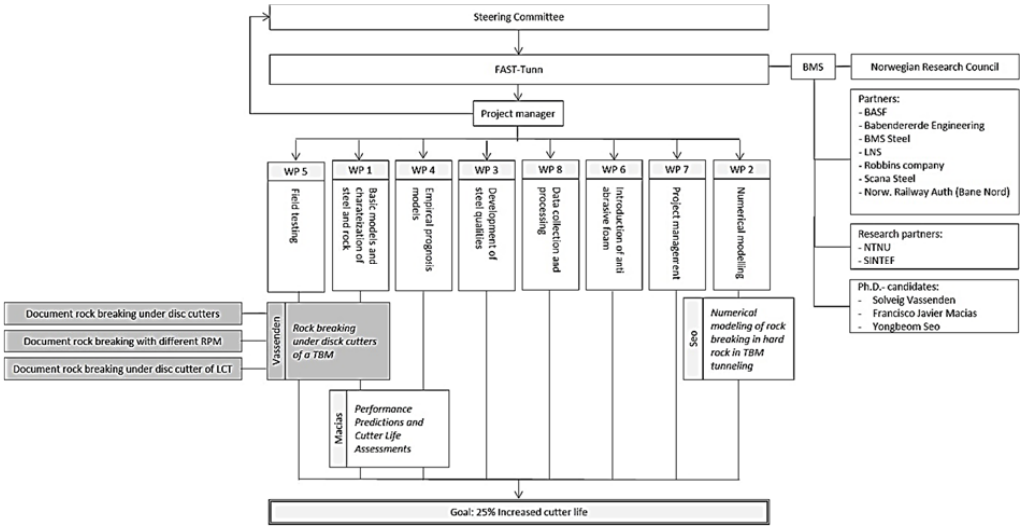

Figure 2.1: Overview of the FAST-Tunn project. The authors' contribution in colored area.

2.4 Documentation of rock breaking

Excavating tunnels with TBMs is a complex process. The TBM performance depends on four types of parameters; project specific parameters, rock mass properties, TBM parameters and performance parameters (Maidl, et al., 2008). Examples of project specific parameters are location, purpose of project, contractor, project owners and the choice of muck removal systems. For a given project, rock type or rock types, geological formations, quarts content, the uniaxial compressive strength (UCS) of the rocks, rock quality designation (RQD), characteristics of discontinuities and the presence of water are important rock mass parameters. Both the project specific parameters and the expected rock mass parameters influences the choice of TBM and thereby TBM related parameters as type of TBM, the diameter, the necessary power, torque and thrust force. In addition, the RPM, cutter materials, the cutter design and the cutter spacing are examples of TBM specific parameters. Examples of performance parameters are the need of rock support, the cutter wear and maintenance.

To be able to estimate the cutter wear, the penetration rate and the advance rate at a given project, several prediction models have been established over the years. In 1976, Graham introduced a simplified prediction model based on the normal force per cutter, the RPM and the UCS of the rock (Graham, 1976). Later on, multiple parameter predicting models, such as the Q_{TBM} model, the CSM model and the NTNU model where established.

The NTNU model is a continuation of the model presented in the NTH project report "Hard Rock Tunnel Boring" in 1976 (NTH, 1976). The NTNU model includes machine parameters, rock mass properties and rock drillability (Blindheim, 1979), (Bruland, 2000), (Macias, 2016). The model is based on an empirical understanding of the rock breaking mechanisms in combination with mapped degree of fracturing and the laboratory testing that is done at the NTNU/SINTEF drillability laboratory (Dahl, et al., 2011). The laboratory testing is based on the

NTH test (Selmer-Olsen & Lien, 1960), originally developed in the late 1950s for evaluating the drillability of rocks by percussive drilling, but the tests have been applied for tunnel boring since 1972 (Blindheim & Bruland, 1998).

The Drilling Rate Index™ (DRI™) was introduced in 1970 (Selmer-Olsen & Blindheim, 1970), and represents the rocks ability to be crushed by repeated impacts, corrected for the surface hardness of the rock. The index is dependent on the Brittleness Value (S_{20}) (Hjelmer & Matern, 1943) and the Sievers' J-Value (SJ) (Sievers, 1950). To estimate the wear rate of the drilling tool, the DRI™ is corrected for time dependent abrasion on tungsten carbide, using the Abrasion Value (AV) (Selmer-Olsen & Lien, 1960). The Bit Wear Index™ (BWI™) represents the expected wear rate. From 1980-1983, the Cutter Life Index™ (CLI™) was developed (NTH, 1983). The CLI™ is assessed from the SJ-value and the Abrasion Value Cutter Steel (AVS). The AVS is regarded as a measure of time dependent abrasion on cutter ring steel, and the test method is based on the AV testing.

The three indexes obtained, DRI™, BWI™ and CLI™, have been trademarked. The drillability laboratory, and the indexes developed at the SINTEF/ NTNU joint drillability laboratory, constitute a global reference for characterisation of rock mass abrasion. Given NTNUs and SINTEFs participation in the FAST-Tunn project, the NTNU prediction model was a logical basis for this thesis.

In the NTNU model the total cost of a TBM project consist of costs related to rig, the TBM, back up and muck removal system, wage and cutters. Rig, TBM, back up and muck removal costs can be considered as fixed costs per meter tunnel. The wage and the cutter related cost depends on the cutter life and the advance rate, and are elements of uncertainty concerning the total cost.

Experiences from several previous TBM projects in hard rock show that cutter change takes about 15 % of the available time. Figure 2.2 shows the time consumption during boring at three different TBM projects from 1998-2012 (Johannessen, et al., 1998), (Maidl, et al., 2008), (The Robbins Company, 2012). This figure shows that for these three projects the time for cutter inspection and change is around 14 %. In comparison, the TBM bores 30-40 % of the total available time. This proves that the processes of cutter change and cutter maintenance are very time consuming. A small increase in cutter life can therefore give a considerable saving potential, looking at material costs and time spent. At the Follobanen project, a 10 % increase in cutter life would generate a 20-25 million NOK saving, due to material costs. Including time saving due to less cutter changing, another 125 million NOK can be saved (FAST-Tunn, 2011). In addition, an increased cutter life will directly reduce the environmental footprint, and reduce the risk of accidents and injuries for the workers changing the cutters at the tunnel face.

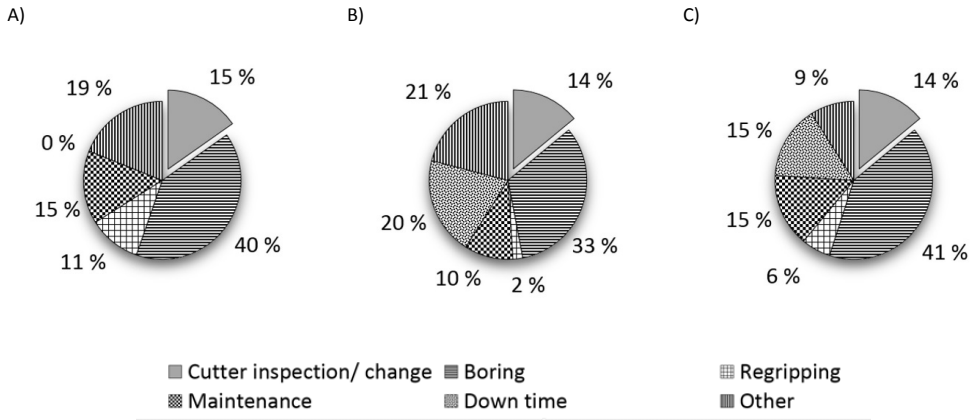

Figure 2.2: Time consumption during boring of A) the Meråker hydroelectric power plant tunnel in Norway (Johannessen, et al., 1998) B) the Manapouri underwater tunnel in New Zealand (1998) (Maidl, et al., 2008) and C) An average month at the Alimineti Madhava Reddy (AMR) Project in India (2012) (The Robbins Company, 2012).

The cutter life depends on rock and steel properties, cutter design, the operation of the TBM and geological conditions (Rostami & Ozdemir, 1993), (Bruland, 2000), (Barton, 2000). Both the cutter related parameters and the TBM operation can be changed and optimized during a project, but the geological conditions cannot be modified. Penetration tests are performed a number of times throughout the excavation to achieve the highest possible penetration per minute. This empirical approach is very efficient at site, but in in a wider perspective it is a short-term gain, as it does not challenge the established way of thinking and thereby contribute to further innovation of the TBM technology. To do that, it is essential to know what is happening in the rock mass when it is exposed to the load from the rolling cutters of a TBM. Four variations of concept models for rock breaking under disc cutters can be seen in Figure 2.3 and Figure 2.4. All these concept models involve radial cracking from under the disc cutter.

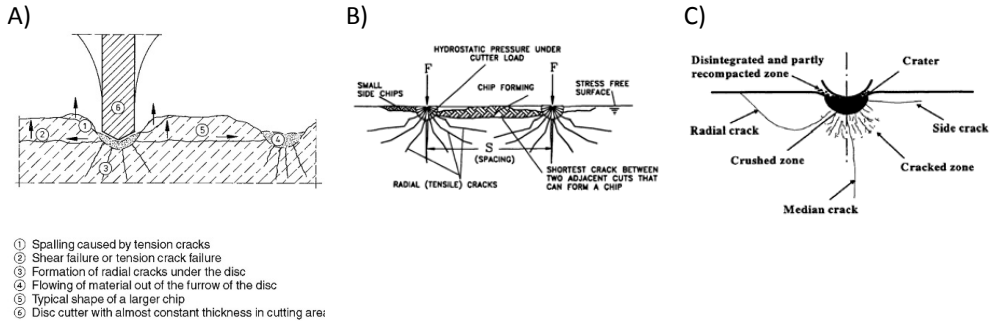

Figure 2.3: Variations of concept models of rock breaking by A) (Büchi, 1984). B) (Rostami & Ozdemir, 1993). C) (Kou, et al., 1997).

Figure 2.4 presents a well-known and commonly accepted interpretation of rock breaking under the rolling cutters of a TBM (Bruland, 2000). There is an extensive theoretical knowledge of development of cracks in brittle and ductile materials and rock breaking (Dieter & Bacon, 1988), (Rinne, 2008), (Wittaker, et al., 1992). Results from several laboratory tests have been published (Ozdemir & Nilsen, 1999), (Innaurato & Oreste, 2011), (Yin, et al., 2014), (Entacher, et al., 2014), (Macias, et al., 2016). Experiences from previous projects all over the world, with a great variety of geology have also been published (Boniface, 2000), (Jung, et al., 2011), (Balchi, 2008), (Bilgin, et al., 2005), (Gong, et al., 2012), (Macias, et al., 2017). A direct response in the rock mass being exposed to the dynamic loads caused by the cutters on a TBM would be initiation of new cracks in the rock mass in front of the TBM. However, there are no available research work that verifies, disproves or differentiates the interpretation presented in Figure 2.4. A large amount of resources have already been, and is expected to be, invested in different research projects aiming for improved cutter quality and more efficient TBMs, but do we really know what is actually happening at this interface of materials? The main focus of this study is thus to focus on an improved understanding of the interface of a rolling disc cutter at a hard rock tunnel face.

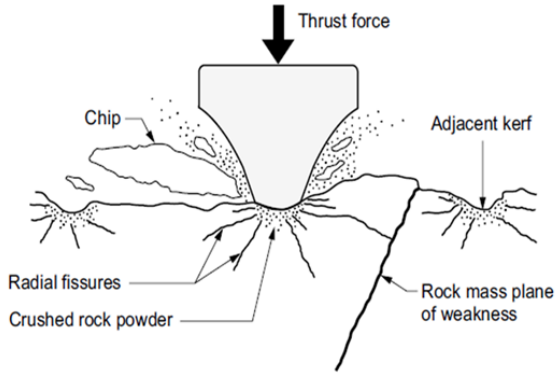

Figure 2.4: A concept model of the interpretation of rock breaking under the cutters of a TBM modified from (NTH, 1983).

The number, length, orientation, type of such new cracks and the distance between them are all important responses to detect and document in order to increase the understanding of rock breaking under disc cutters of a TBM. This knowledge can be used to optimize the TBM cutter head design, the cutter design and the operation of new TBMs, in order to decrease the cutter wear, and thereby increase the cutter life and the overall efficiency of the TBM. The knowledge can also be used to increase the utilization potential of a TBM at ongoing projects.

This is related to the first objective of this Ph.D.-study.

When a method to detect and document the rock breaking under the disc cutters of a full size TBM is established, the effect of any changes in cutter head design, cutter design or TBM operation parameters, such as thrust, torque, RPM and the TBM operator, on rock breaking can be documented.

In this Ph.D.-study, TBM operational parameters, and RPM in particular, was selected as the preferable parameter to study. In the following sections, the background for this choice will be given.

2.5 RPM as study parameter

According to NTNU model, the cutter life can be measured as cubic meters per cutter, hours per cutter or meters per cutter. This means that an increase in cutter life can be achieved by reducing the wear of the cutter or by increasing the efficiency of the cutter through an increased net penetration.

The choice of TBM design for a specific project is based on location, purpose of project preliminary investigations concerning rock type or rock types, geological formations, quarts content, the UCS of the rocks, RQD and the presence of water. The design includes the type of TBM, the diameter, the necessary power, torque and thrust force that needs to be installed, the cutter spacing and a cutter design that is assumed to be suitable. At site, only adjustments concerning cutter design, cutter materials and the operation of the TBM within its limits can be done to increase the cutter life or increase the net penetration. In addition, the process is affected by parameters that vary through the project, like variable geological conditions and the TBM operator. This complexity implies numerous possible combinations of factors, and a number of combinations may give the same result. To fully understand the rock breaking under disc cutters of a TBM each parameter must be studied separately, keeping the other parameters constant.

Cutter materials and cutter design are not within the author's qualifications and thereby not a part of the scope of this Ph.D.-study, leaving operational parameters as RPM, thrust and torque as potential parameters. Ideally, all three parameters should be studied, but within the time limitation of this Ph.D.-study only one parameter could be fully studied.

In the NTNU-model the cutter life depends on the surface hardness of the rock and the rocks ability to induce wear on the cutter ring steel (Dahl, et al., 2011), the diameter of the TBM, the number of cutters and their diameter, the quartz content and the RPM. The net penetration rate is a function of the basic penetration rate, calculated as mm/rev, and the RPM, whereas thrust and torque are not included in the formulas in the NTNU prognosis model. Within the scope and limitations of the FAST-Tunn Project, RPM was the preferable parameter to study.

The choice of the TBM operational parameter was also discussed with Tobias Andersson, the TBM Construction Manager at Nedre Røssåga headrace tunnel and LNS´ contact within FAST-Tunn. From previous TBM projects, he had experienced that the operators often tries to increase the RPM as much as possible to gain a high net penetration rate. The net penetration is measured in meters per hour and is assessed by the penetration in millimeters per revolution and the RPM. Increased RPM can therefore compensate for a lower net penetration. A high RPM might give considerable vibrations on the TBM, and thereby increased need of maintenance. In addition, the rolled meters per cutter per hour increases with an increase of the RPM, increasing the frequency of the cutter change. From a contractor's point of view, Andersson was interested in looking into the effect of changed RPM on rock breaking in order to lower the RPM.

From the two different arguments presented above, RPM was chosen as the preferable TBM operational parameter to study in this Ph.D.-study.

$$I_0 = i_0 * RPM * \left(\frac{60}{1000}\right) (m/h) \quad [2.1]$$

$I_0 = Basic\ penetration\ rate\ (m/h)$
$i_0 = net\ penetration\ rate\ (mm/rev)$

Beside the two FAST-Tunn related arguments presented above, documenting the effect of different RPMs was interesting from a rock mechanical point of view. The uniaxial- and triaxial compression strength of a rock specimen depends on geological properties as grain size, the mineral components, grain cementation between the mineral grains, pre-existing cracks, porosity and degree of anisotropy. In addition to the geological properties, the compressive strength of a rock specimen depend on testing parameters as the specimen's volume, the preparation of the specimen, the machine stiffness and the loading rate (Vutkuri, et al., 1978). With an a high loading rate, the time to failure becomes shorter, and because of that the interaction between pre-existing cracks gets weaker and less new cracks are generated. This results in smaller rock deformation, less weakening and a higher measured compressive strength than with lower strain rates (Okubo, et al., 1990), (Martin & Chandler, 1994), (Brady & Brown, 2006), (Hashiba, et al., 2006), (Yang, 2015).

If rock breaking under a disc cutter of a TBM is analog to the rock failure during uniaxial and triaxial compressive strength testing, the RPM might be analog to the loading rate. This can impliy that a lowering of the RPM might result in better interaction between existing cracks; both the pre-existing and the new TBM initiated cracks, as well as more TBM initiated cracks. A documentation of rock breaking with different RPMs can give valuable knowledge of the effect of different RPMs concerning rock breaking.

This is related to the second objective of this Ph.D.-study.

2.6 Linear Cutter Test

The linear cutter test (LCT) is considered a full-scale test, and provides a direct measure of rock cuttability of a preferred rock specimen. This test is not a part of the NTNU-prediction model, but data from this test can be used to; predict cutter life and penetration rate as a part of the preliminary investigations (Gong & Zhao, 2008), study the optimum cutter spacing, (Cho, et al., 2009), study rock breaking mechanisms under disc cutters (Entacher, et al., 2014), verify numerical models (Cho, et al., 2013) and make comparisons with data from ongoing projects (Balchi, 2008). Figure 2.5 shows a schematic drawing of the Linear Cutter Test device at the Colorado School of Mines (Gertsch, et al., 2007).

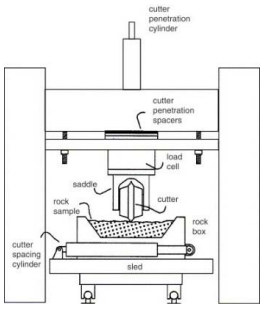

Figure 2.5: Schematic drawing of the linear cutting machine at the Colorado School of Mines (Gertsch, et al., 2007).

During a LCT, one full size disc cutter are used to cut several horizontal, parallel and straight grooves. Any possible effects of concentric cutting, gravity and interaction between two or more neighbor cutters will not be included in the results. By fulfilling the main objective of this Ph.D.-study, the rock breaking under the disc cutters of a LCT in hard rock can be detected and documented, and compared to the results from a full size TBM.

This is related to the third objective of this Ph.D.-study.

2.7 Description of selected sites and testing facilities

Through their participation in the FAST-Tunn project, the contractor Leonard Nilsen & Sønner AS (LNS) and TBM-manufacturer The Robbins Company (Robbins) made their ongoing tunnel projects available for field sampling. The field sampling for this Ph.D-study was performed at the Alimineti Madhava Reddy (AMR) Project in India and at the Nedre Røssåga headrace tunnel in Norway.

In addition, the Tronhjemite from the Tronhjemite quarry at Støren in Norway was used as reference rock type for sound velocity measurements, and the Iddefjord granite from the Iddefjord granite quarry at Skriverøya in southern Norway was used as the rock specimen that were tested at the LCT at KICT South Korea.

2.7.1 The Alimineti Madhava Reddy Project, India

The Alimineti Madhava Reddy Project (AMR Project) is a water transfer tunnel located 100 km south of Hyderabad, in the state of Andhra Pradesh in India, see Figure 2.6. The Government of Andhra Pradesh is project owner, and Jaiprakash Associates Ltd. is the contractor. The tunnel length is 43,5 km, and it is excavated by two Robbins double shield machines, and concrete lining is mounted continuously, along with the excavation. The excavation started in 2008, and is not finished by November 2017. The machine properties, presented in Table 2.1, are provided by Robbins.

Table 2.1: Machine properties at the AMR Project.

TBM	Robbins Double shield
TBM diameter	10,02 m
Number of cutters	67
Cutter diameter	20 ” cutters on 19” bearings
Cutter spacing	74,6 mm
Initial tip of cutters	¾ “
Stroke length	1,6 m
Maximum thrust	25 000 kN
Maximum thrust per cutter	373 kN/c

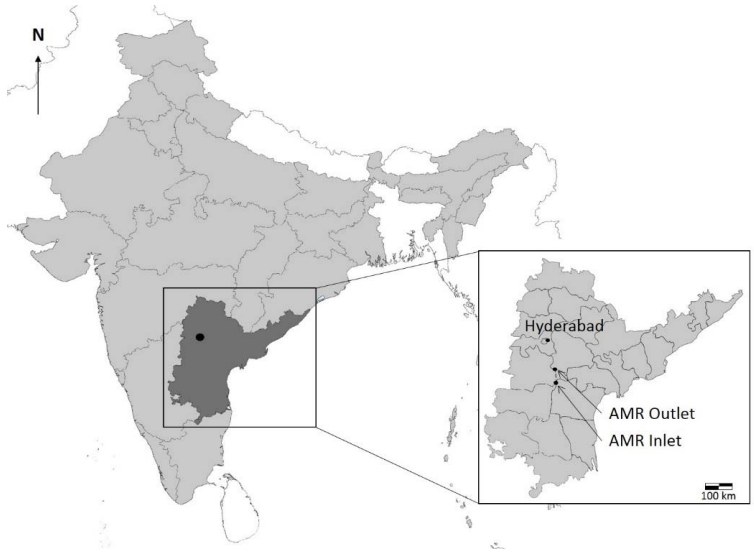

Figure 2.6: Map showing the location of the AMR Project.

The geology changes along the tunnel line, and includes quartzite, shales and granite. The average overburden is around 300 meters, varying from 140 to 480 meters, see longitudinal section in Figure 2.7. The samples used in this study are from chainages 11572,8 and 11578,8, seen from the outlet, and were collected in February 2013. From now on, these chainages will be referred to as 11573 and 11579. Table 2.2 shows mechanical properties for the rock mass between chainage 11558-11616 (SINTEF, 2013). According to the petrographic analysis the rock type is massive, non-foliated with magmatic texture and medium to coarse grain size. It is spotted, greyish-greenish with black spots. From the mineral content, it can be considered a monzo granite. The results of the XRD-analyses are presented in Table 2.3.

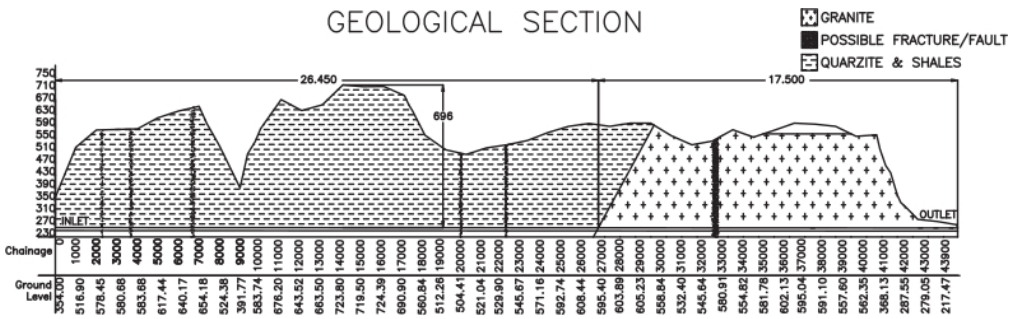

Figure 2.7: Geological section for the AMR (Scialpi, et al., 2012).

Table 2.2: Rock mass properties chainage 11558-11616.

DRI^{TM}	43 – 45 (Medium)
CLI^{tm}	5,4 – 5,5 (Very low)
Sievers's J-value	3,3 – 3,7 (Very high)
AVS	39 – 41 (Very high)
Brittleness value, S_{20}	47,5 – 50,9 (Medium)
Flakiness index	1,28
Point load strength, I_{s50}	11 – 14,9 MPa (Very high)
Estimated UCS from I_{s50}	275 – 372 MPa (Extremely high)
Density	2,62 – 2,63 g/cm^3
Quartz content	34 – 36 %
Rock type	monzo granite

Table 2.3: Mineral content chainage 11558-11616.

Mineral	Volume %
Quartz	34 – 36
Plagioclase	25 – 27
Alkali feldspar	33 – 34
Mica	4
Chlorite	2 – 3

2.7.2 The Nedre Røssåga headrace tunnel, Norway

The Nedre Røssåga headrace tunnel is a headrace tunnel for the new Nedre Røssåga power plant in the municipality of Hemnes in Norway, see Figure 2.8. The excavation started in November 2013, and breakthrough was in December 2015. Statkraft Energi AS is the project owner, and LNS was the tunnel contractor. The tunnel length is 7,4 km, and it was excavated by a Robbins open gripper machine. There was no concrete lining or shotcrete mounted in the tunnel. The machine properties, presented in Table 2.4, are provided by Robbins and LNS.

Table 2.4: Machine properties at Nedre Røssåga headrace tunnel.

TBM	Robbins Open gripper
TBM diameter	7,23 m
Number of cutters	46
Cutter diameter	19 ” cutters
Cutter spacing	78,6 mm
Initial tip of cutters	¾ “
Stroke length	1,83 m
Maximum thrust	14 324 kN
Maximum thrust per cutter	312 kN/c

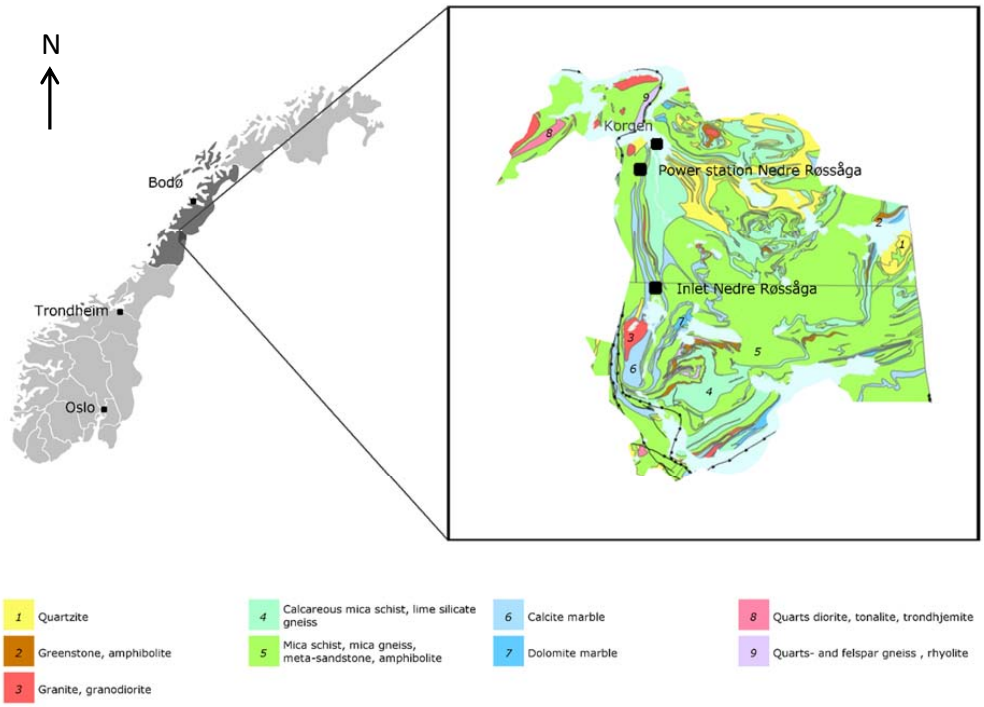

Figure 2.8: Map showing the location for the Nedre Røssåga headrace tunnel (NGU, 2017).

The tunnel is located in metamorphic and magmatic rocks in the uppermost allochthon of the Caledonian orogeny. The rock types are metamorphic like mica schists and mica gneisses, partly with calcareous percentage, pervaded by layers of quartzite, marble and metasandstone, and plutonic rocks as granite or granodiorite. The rock types in the area dates back 359-443 million years, and are defined as a Silurian and Devonian metamorphic and plutonic rocks (Bjerkgård, et al., 1995).

From the preliminary investigations, the geology was expected to vary from quartzite, granite and gneisses to mica schist, marble and limestone. The average overburden is around 150 meters, varying from 50 to 200 meters. The predicted geological longitudinal section is

presented in Figure 2.9. The samples used in this study are from chainages 1184,2, 3112,6, 5437,5, 5458,0 and 5478,0 and were collected in the period from July 2014 to July 2015. From now on, these chainages will be referred to as 1184, 3112, 5437, 5458 and 5478.

Table 2.5 shows mechanical properties for the rock mass at the chainages of interest. All the samples are tested at the NTNU/SINTEF Geology Engineering Laboratory, on behalf of Robbins, LNS and FAST-Tunn. The results are presented in different laboratory reports from SINTEF, prepared for the various parties involved in the Nedre Røssåga headrace tunnel project. The laboratory reports are therefore confidential, and specific references will not be given in this thesis.

Senior research scientist, Marit Haugen, at SINTEF Building and Infrastructure Department of Architecture, Materials and Structures, has made a petrographic analyze of the rock samples used in this Ph.D.-study. The analysis is not presented in any written report, and it is only valid for the specified chainages. The petrographic analysis is provided in the following sections (Haugen, 2015).

At chainage 1184, a massive, slightly foliated and fine grained rock with metamorphic texture is found. It is spotted, white and grey with black spots. From the mineral content, it can be considered as a granodioritic gneiss with thin layers of mica schist. At chainage 3112 the rock type is massive, slightly foliated and fine grained with metamorphic texture. It is spotted, white and grey with black layers. From the mineral content, it can be considered as a calcareous rock with biotite and a considerable quartz content. At chainage 5437-5478 the rock type is massive, foliated and fine grained rock with metamorphic texture. It is dark to light grey, with black layers. From the mineral content, it can be considered as a gneiss with garnet and some lime.

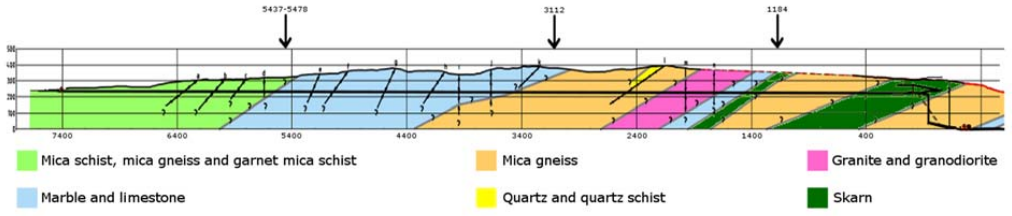

Figure 2.9: Predicted geological section for the Nedre Røssåga headrace tunnel from the tender documents, and locations for field sampling (Norconsult, 2013).

Table 2.5: Rock mass properties at chainages 1010-1149, 2970-3149 and 5400-5478.

	1010-1149	2970 – 3149	5400-5478
DRI^{TM}	45 - 51 (Medium)	38 - 40 (Low)	45 (Medium)
CLI^{TM}	4,7 - 13-3 (Extremely low - medium)	4,5 - 7,3 (Extremely low - low)	5 (Extremely low)
Sievers's J-value	2- 2,3 (Extremely low - very low)	1,9 - 3,8 (Extremely low – very low)	1,7 (Extremely low)
AVS	12 - 33 (Low- high)	21 - 34 (Medium - high)	24 (Medium)
Brittleness value, S_{20}	51 - 53 (Medium to high)	45 - 57 (Medium to high)	48 - 54 (Medium to high)
Flakiness index	1,3 - 1,32	1,33 - 1,44	1,4
Point load strength, I_{s50}	Not tested	Not tested	Not tested
UCS	62 - 92 MPa (High)	65 - 139 MPa (High)	92-124 MPa (High to very high)
Density	2,67 - 2,71 g/m^3	2,66 - 2,88 g/m^3	2,78 g/m^3
Quartz content	Not tested	Not tested	Not tested
Rock type	Granodioritic gneiss with layers of mica schist	Calcareous rock with biotite and a high quartz content	Gneiss with garnet and some lime

The mineral contents at the different chainages were not tested, as the information was not considered relevant for the results of this Ph.D.-study.

2.7.3 The Trondhjemite quarry at Støren, Norway

The Trondhjemite quarry is operated by Trøndergranitt AS and is owned by Norblock AS. It is located in the municipality of Midtre Gauldal, 50 km south of Trondheim, in Norway, se Figure 2.10. The quarry mainly produces rock blocks for dry stone walls, facing bricks and monument materials.

The bedrock of the Støren area is a part of the Trondheim Nappe Complex, largely consisting of metamorphosed sedimentary rocks and local mafic to ultramafic volcanic rocks. The trondhjemite in this area dates back 432 million years and is defined as a silurian plutonic rock (Nilsen, et al., 1987).

According to the petrogragraphic analysis the rock is massive, non-foliated rock with magmatic texture and fine to medium grain size texture. It is spotted, white to light grey with black spots. From the mineral content, it can be considered a quarts diorite, and it is usually named trondhjemite. At the Trondhjemite quarry, the trondhjemite is massive, with a very limited number of cracks and joints, giving good conditions for core sampling.

The trondhjemite has traditionally been used as a reference sample at the SINTEF Rock Engineering Laboratory at NTNU, Trondheim. Although the trondhjemite appear seemingly homogeneous with no visible foliation, several rock mechanical tests have indicated that both the texture and rock mechanical properties of the rock vary to some extent in the quarry. Rock mass properties and mineral content of the trondhjemite can be seen in Table 2.6 and Table 2.7.

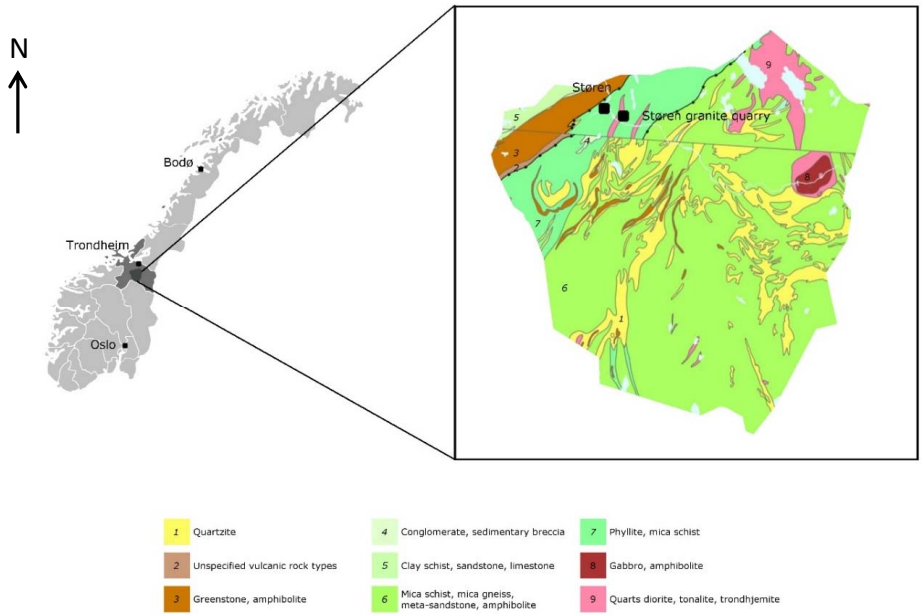

Figure 2.10: Map showing the location for the Tronhjemite quarry at Støren, Norway (NGU, 2017).

Table 2.6: Rock mass properties for the tronhjemite (Dahl, 2015).

DRI^{TM}	51 (Medium)
CLI^{TM}	6,3 (Low)
Sievers's J-value	3,6 (Very low)
AVS	27,5 (High)
Brittleness value, S_{20}	56,1 (High)
Flakiness index	1,33
Point load strength, I_{s50}	27,2 MPa
UCS	196 MPa (Very high)
Density	2,69 g/cm^3
Quartz content	26 %
Rock type	Quarts diorite (trondhjemitE)

Table 2.7: Mineral content for the trondhjemite from XRD analysis (Dahl, 2015).

Mineral	Volume %
Quartz	31
Plagioclase	53
Mica	9
Pyroxene	2
Epidote	4

2.7.4 The Iddefjord granite quarry at Skriverøya, Norway

The Iddefjord granite quarry is operated by JOGRA Steinindustri and owned by AP Sten Sweden AB. It is located at Skriverøya, 10 km south of Halden in Norway, se Figure 2.11. The quarry mainly produces rock blocks for dry paving stone, floor tiles and facing bricks and monument materials.

The Iddefjord granite forms the northern part of the Swedish Bohus batholith and ranges in composition from diorite to granite. The granite consists of 13 individual plutons, and the mechanism of intrusion is related to block subsidence rather than forceful intrusion. The Iddefjord granite dates back 925 million years, and is defined as a late riphean plutonic rock (Pedersen & Maaløe, 1990).

According to the petrographic analysis the rock is massive, non-foliated rock with magmatic texture and fine grain size texture. It is spotted, white to light grey with some grey and black spots. From the mineral content, it can be considered a granite, and it is usually named Iddefjord granite. Rock mass properties and mineral content of the Iddefjord granite can be seen in Table 2.8 and Table 2.9.

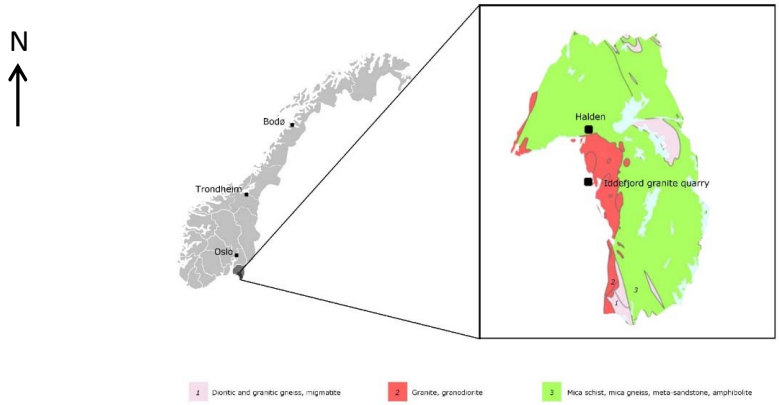

Figure 2.11: Map showing the location for the Iddefjord granite quarry at Skriverøya, Norway (NGU, 2017).

Table 2.8: Rock mass properties for the Iddefjord granite (Dahl, 2015).

DRI^{TM}	58 (High)
CLI^{TM}	6,8 (Low)
Sievers's J-value	5,0 (Low)
AVS	31,5 (High)
Brittleness value, S_{20}	61,9 (Very high)
Flakiness index	Not tested
Point load strength, I_{s50}	Not tested
UCS	188 MPa (Very high)
Density	2,6 g/cm^3
Quartz content	25 %
Rock type	Granite

Table 2.9: Mineral content for the Iddefjord granite from XRD analysis (Dahl, 2015).

Mineral	Volume %
Quartz	25
Plagioclase	32
Feldspar	35
Mica	8

2.7.5 LCT facilities at the Korea Institute of Civil Engineering and Building Technology (KICT), South-Korea

The linear cutting machine is owned and managed by Korea Institute of Civil Engineering and Building Technology in Seoul in South Korea.

The machine consists of a hydraulic unit, a controller, a specimen mold, a load cell, and a frame with actuators that move in the X, Y, and Z directions, see Figure 2.12. Three-directional components of loads acting on a cutter can be measured simultaneously by a three-directional load cell. The three-directional load cell can measure the cutter forces of maximum 500 kN in the x and y directions and a maximum of 1 000 kN in the z direction.

The experimental set up parameters such as rock specimen, the disc cutter, number of cutting lines, cutter spacing and penetration depth can be changed changes according to the purpose of the test and the client's needs. The testing can be done with sequential or random cutting operation.

Prior to testing, all rock specimens were casted in steel molds by mortar to secure their confinement.

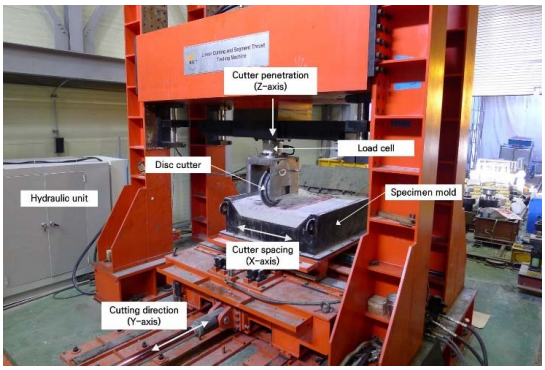

Figure 2.12: The linear cutting machine at KICT (KICT, 2015).

3 Point of departure for research works

The basis of this Ph.D.-study is the project description approved by NTNU in March 2013. This plan was based on literature studies and ambitions within the participants of the FAST-Tunn project and the ideas of the Ph.D.-candidate and the supervisors.

Below is an abstract of the original Ph.D. project description with the title *Mechanical properties of geological material influencing abrasion of cutter steel for TBM-boring.*

3.1 Project description

3.1.1 Objectives

The main goal of the study is to detect, map and analyze the fractures in the rock due to the impact of disc cutters on a TBM, and to investigate the effect of impact time (RPM, *author's remark*).

In order to achieve that goal there are several underlying objectives or sub tasks to be solved:

- Collect core samples from the tunnel faces after boring with different RPM at ongoing TBM projects in hard rock
- Map and analyze the cracks in the collected core samples, and compare with existing theories on cracking
- Modify the point load test apparatus by installing disc cutter shaped indenters and a fixed-time control to imitate the boring conditions
- Run tests with the modified point load tester with varying duration, different shaped indenters and /or different steel alloys
- Map and analyze the cracks in samples after laboratory testing to see the effect of time, and to compare with cracking in cores from ongoing TBM projects
- Map and analyze the cracks from different shapes of indenters and steel alloys
- Compare the results from the modified point load test with results from the standardized test
- Establish a 2D numerical model for rock breaking and stress distribution under a disc cutter and correlate it with results from laboratory testing and samples from the field
-

3.1.2 Field investigations

In order to prove, reject or differentiate the hypothesis of rock fracturing during boring with a TBM investigations and observations in the field are necessary. The field investigations will take place at the AMR-project in India, and preferable other sites where The Robbins Company is the TBM supplier. One such project is the Røssåga project being undertaken by the Norwegian contractor Leonhard Nilsen & Sønner AS. If this TBM-tunneling starts, and runs according to plan, samples from the project will be included in the study.

The aim of the field investigations is to collect core samples from the tunnel face and larger chips from the same chainage during boring. In order to document the effect of impact time, the cores will be sampled after boring with different circular speed, measured in rotations per minute. To detect the extent of sideway fracture propagation and the interaction between the fractures the collaring of the cores should be both directly in the groove from the disk cutter and in between two grooves. The loading conditions at the center cutters differ a lot

from the load conditions at the gauge cutters. The cores should therefore be located in between the center and the gauge cutters. Due to limited access to the face, the cores must be drilled through the inspection hole, and adjustments will take place.

3.1.3 Laboratory testing

Rock strength is one of the material parameters influencing the advance rate of a TBM. The most used test to decide the rock strength is the uniaxial or triaxial compression test where the rock sample is exposed to an increasing axial loading, with or without confining pressure until rock failure. This testing gives good results, but the duration of this test is much longer than the impact time from a disc cutter.
The point load test was developed in the early 1970s as an alternative to the compression test (Broch & Franklin, 1972). In a point load test, the rock failure is caused by induced tensile stresses in the sample. The different load values from the point load test have been correlated with the results from the uniaxial/triaxial tests, and a ratio between the values has been established, see [3.1]. The conditions during a point load test, with respect to the short duration of the test and the loading conditions are more comparable with the conditions during boring with disc cutters than during a uniaxial/triaxial test. The apparatus is easy to use, and it is a low cost method.

$$\sigma_c = k * \sigma_{point\ load} \qquad [3.1]$$

σ_c= *Compression strength of rock*
k= *rock type constant*
$\sigma_{point\ load}$= *Point load strength*

By installing disc cutter shaped indenters and a fixed-time control, the conditions will be even more comparable to a TBM disc cutter. From classic fracture mechanics of materials we know that the impact time is of significant importance when it comes to fracture development and fracture growth (Rinne, 2008), (Dieter & Bacon, 1988) and (Maidl, et al., 2008). At the time the project description was prepared, the important basis for this Ph. D. study was to modify the point load test to make it more suitable for testing rock in the purpose of TBM boring with respect to fracture propagation and impact time. The testing apparatus can be used to perform tests with different shape of indenters and different steel alloys.

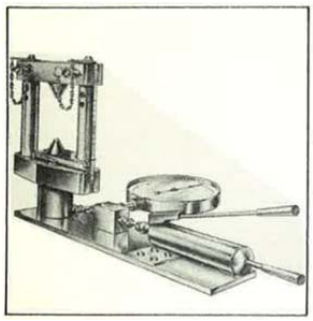

Figure 3.1: Apparatus for point load testing (Broch & Franklin, 1972).

When the point load apparatus is modified, tests will be performed according to real impact time during TBM boring. To detect and document the effect of time, the test samples need to

be a homogenous rock or concrete, and preferably a material that has been tested by NTNU/SINTEF before, so that the standard rock characteristics as uniaxial compression strength, shear strength and fracture angle are known. Tests with different shaped indenters and steel alloys can be performed to detect possible effects of improvements to the cutters.

3.1.4 Analysis of laboratory and field samples

To analyze the effect of time during the modified point load test, the samples need to be analyzed with respect to degree of fracturing, types of fracturing and the extent of fracture propagation, both laterally and towards the depth of the cores. This requires studies of thin sections by use of a microscope. The thin sections need to be prepared both parallel and perpendicular to the direction of the load. The same analyses will be carried out for the core samples from the tunnel face and the larger chips collected during boring.

3.1.5 Numerical modeling

Numerical modeling is a useful tool for prediction of stresses, strains and rock failure under disc cutters. If a numerical model is calibrated against field data and laboratory tests, one can change different parameters one by one, and see the effect without having to carry out expensive, time consuming, and in worst case inconclusive filed experiments. A numerical model will never be an exact representation of in-situ conditions, but it can give valuable information of the effect of changing one or more parameters. The planned numerical modeling will utilize coding developed within the FAST-Tunn project in addition to the software Phase^2 from RockScience. The model in Phase ^{2} will be a 2D model, in the plane parallel to the cutter direction, where the main objective is to study the response mechanisms in the rock. Knowledge about the response mechanisms can support the theories concerning rock breaking and failure mechanisms. The model will be correlated against the results from the laboratory testing.

3.1.6 Expected results

The expected results of the study is to:

- Prove, reject or differentiate the hypothesis of rock breaking under a disc cutter
- Improve the understanding of tool-rock interaction
- Establish a modified point load test that is more suitable for TBM purposes
- Determine the effect of time during the modified point load test
- Detect the possible rock breaking effect of improved disc cutters
- Detect any correlation with existing drillability parameters
- Establish a 2D numerical model that is correlated with field observations and laboratory tests
- Contribute to fulfill the aim of the FAST-Tunn project; to “improve the efficiency of new cutters in terms of 25 % increased durability, introducing the need of possible new steel alloys and cutter layout/geometry” (FAST-Tunn, 2013).

3.2 Remarks

Due to unforeseen challenges, unexpected findings and contributions from the participants of the FAST-Tunn project, the plan was be revised during the course of the study. The main revisions and the reasons for those are described below. The performed research

methodology is presented in chapter 4 *Research methodology.* The adjustments have been incorporated with due discussions and approval of the supervisor.

3.2.1 Major changes

One of the objectives within the FAST-Tunn project was to develop an improved cutter ring by using a new alloy and/or change the cutter geometry to increase the cutter life by 25 %. The original plan was, as described, to perform laboratory tests with these new cutters. The development of the new cutters took much longer time than expected, and they were not available for testing in due time to be included in this Ph.D.-study.

During the project period, the FAST-Tunn project decided to perform a LCT for calibration of a numerical model that was developed at SINTEF for the simulations of the interaction between the cutter and the rock mass. This decision gave the opportunity to include samples from the LCT in this study, and to gain valuable information about rock breaking under the disc cutter. The consequence on this Ph.D.-study was as follows:

Due to the delay of delivery of the new cutters and the decision to conduct scaled testing at KICT in Korea, the original planned point load testing was abandoned and studies of samples from the LCT were done instead.

On initiative by its participants, The FAST-Tunn project decided to establish a numerical model to study the wear of the cutters and any effects of a changed geometry of the cutters, and the wish was that the numerical modeling became a part of the two Ph.D.-studies within the project. This request was the main reason why numerical modeling was included in the original project plan.

When Ph.D.-candidate Yongbeom Seo and his thesis "*Numerical modeling of rock breaking in hard rock in TBM tunneling*" was included in the FAST-Tunn project, he met the request from the FAST-Tunn project members on numerical modelling. A simplified 2D model would nevertheless neither have contributed with any new information or value to the project nor to this thesis.

At the same time, the process of detection, visualization and documentation of cracks had become more extensive than originally planned. The consequence of these circumstances to the thesis was as follows:

Due to the extensive rock breaking study and the limited potential of a valuable contribution from the numerical modelling, the numerical modelling was excluded from the project plan.

4 Research methodology

4.1 Choice of sites

4.1.1 The AMR Project and the Nedre Røssåga headrace tunnel

Because the properties of rock masses and rock types can change considerably over a short distance, studies of these circumstances are challenging. In order to achieve reliable results, a high number of samples is needed. In addition, as described in chapter2 *Technical background*, the tunnel excavation by TBMs is an extremely complex process, with a high number of potential variable parameters. To minimize the uncertainties and keeping as many machine related parameters as possible constant, only two TBM projects were chosen for field sampling for this Ph.D.-study, the AMR Project in India and the Nedre Røssåga headrace tunnel in Norway were chosen. Both tunnels were excavated in hard rock, with Robbins TBMs.

Given the required continuous access to the tunnel through LNS´ and Robbins´ participation in the FAST-Tunn project, and the favorable location, the Nedre Røssåga headrace tunnel was a preferable site for field sampling. In addition, the TBM was an open gripper machine and no lining or shotcrete were applied and thus the rock mass was easily accessible through the whole excavation period. Nedre Røssåga headrace tunnel was therefore chosen as the main site.

In anticipation of a late startup at the Nedre Røssåga headrace tunnel compared to the study time schedule, another site had to be chosen. The main focus was to test the sampling procedure and the analysis of the samples, and to collect field samples from another geology than the one expected at Nedre Røssåga headrace tunnel. The FAST-Tunn project had chosen the AMR Project in India as a suitable candidate site to test new steel alloy and to run tests using anti-abrasion agent. The TBM was a Robbins double shield machine, giving limited access to the rock mass, but rock samples from this site was already tested at the NTNU/SINTEF Geology Engineering Laboratory, and the geology was to a certain extent mapped by two master students from the Department of Civil and Environmental Engineering doing their thesis on the testing of the anti-abrasion agent. The installation of the anti-abrasion agent system ensured some down time on the TBM, which gave good access to sampling. The AMR Project was therefore chosen as the second site for field sampling.

In order to study the rock breaking under the rolling disc cutters of a TBM as an independent limited process, it is essential to identify all parameters and elements that directly or indirectly influence the rock breaking. In order to do that, and to gain a better understanding of the whole process of TBM excavation, the author attended several shifts at the two chosen sites and spent a lot of time discussing and learning from the TBM operators and the other members of the TBM crew. From this the author learned, among other things, that the TBM operators operated the TBM differently, using different operating “philosophies”. By “philosophy” the author means ways for operating the TBM. These differences applies for both sites, but also for the different operators at the same site.

Below, some quotations from the TBM operators are presented (TBM operators AMR project, February 2013), (TBM operators Nedre Røssåga headrace tunnel, April 2014 - December 2015):

- "I keep the thrust at a maximum level, and then I increase the RPM until the vibrations gets to strong."
- "I adjust both the RPM and the thrust to achieve the highest possible penetration per revolution."
- "I keep the thrust at a constant level close to its maximum, and then I adjust the RPM to achieve the highest possible penetration per minute."
- "I increase the RPM until it is around 5-5.5, and then I adjust the thrust to keep the torque at a reasonable level."
- "I never bore the last centimeter of the stroke, because boring the last centimeter will increase the pressure in the stuffing box in the hydraulic cylinder. This increased pressure will, after several repetitions lead to wear of the cylinders. The increased pressure in the cylinders is not transferred to the cutters."

These big differences in how the operators operate the TBM might affect the rock braking, and a change of the operator might be a potentially variable parameter. However, with a proper planning and relevant instructions and procedures it can be kept constant.

Disadvantages of only two sites:

- Limited number of rock types / different geologies limits the area of application
- It is more difficult to reveal site specific results
- More vulnerable to unexpected down time

Advantages of only two sites:

- More samples from each site and thereby reducing the uncertainties associated with rock mass
- The type of TBM, cutter size and design, machine properties and the operators are unchanged
- An increased probability that the sampling strokes are bored the same way and that the sampling is done similar each time
- By limiting the number of sites it is easier to map the geology and get familiar with the rock mass through the tunnel
- Better communication and cooperation with the personnel at the TBM when the number of hours spent together increases
- Sampling can be adjusted to fit similar geologies to order to compare the results
- Sampling can easier be adjusted to the daily routine at the site

Keeping the limitations and the two first objectives of this Ph.D.-study study in mind; "*To establish an economical and time efficient method to detect and document the rock breaking under the disc cutters of a full size TBM, and to document the effect of different RPMs concerning rock breaking under the disc cutters of a full size TBM in hard rock",* the advantages of having access to two sites only was found to be greater than the disadvantages.

4.1.2 The Trondhjemite quarry

Because of its homogenous rock mass, with previous thorough documented characteristic properties and the favorable location, the Trondhjemite quarry at Støren was an obvious choice of site for sampling of reference core samples. At the quarry at Støren, a Small Boring Unit (SBU) from Robbins was installed for testing, and samples were tested for this purpose.

4.1.3 The LCT facilities at KICT

The choices of testing facilities, the use of Iddefjord granite and the set up during the testing were made by the FAST-Tunn participants. The author did not provide any premises for these decisions, and have not been present during testing.

The purpose of the testing was to study crack propagation in the rock, rock chip analysis and roughness measurements on the rock surface after the linear cutting test, for calibration of numerical modeling of the cutting process. Depending on cutting sequences during the tests, differences of cutter acting force and rock chips were also checked.

KICT has provided the results of the tests in an experimental report for NTNU /FAST-Tunn. The results are not relevant to the work in this Ph.D.-study and will not be presented here. For further details, see (KICT, 2015).

4.2 Sampling

In the following, the abbreviations presented in Table 4.1 are used to name samples and data series.

Table 4.1: Abbreviations used to name samples and data series.

Site	Abbreviation
The AMR Project	AMR
The Nedre Røssåga headrace tunnel	R
The Linear Cutter Test facilities	LCT
The Trondhjemite granite quarry	S

4.2.1 Sampling methods and procedures

Choice of sampling method

Keeping in mind that the selected sites involved both an open gripper TBM and a double shield TBM, the sampling procedure had to be feasible at both sites. Both tunnels were under excavation during the field sampling, and the work had to be adjusted to the daily routine at site to avoid additional downtime caused by the sampling. This implies that the sampling procedure needed to be uncomplicated and require easy accessible equipment.

Sampling from the face of a TBM tunnel can be done in two different ways, either in front of the cutter head, or through the inspection hole in the cutter head. At the AMR Project, concrete lining is installed continuously, and this limits the potential space in front of the cutter head as soon as a lining ring is installed. Even if the cutter head is fully retracted at the end of a stroke, there is a maximum 1,6 meters available space. At Nedre Røssåga headrace tunnel, the stroke length was 1,8 meters, adding an extra 20 centimeters to the available space, making sampling in front of the cutter head more suitable. Staying in front of the cutter head can be associated with a potential risk of loose rocks falling from the tunnel surface or the face itself. Independent of available space, work in front of the cutter face could only be carried out if the rock mass is stable enough. This can change along the tunnel, so the sampling procedure had to be adaptable to the rock mass quality. In addition, personnel, the necessary equipment and the rock samples has to be transported through the inspection hole. The inspection hole in the cutter head has a diameter of approximately 60 centimeters and it

is approximately 50 centimeters deep. A picture showing the dimension of the inspection hole is presented in Figure 4.1. Both transportation of equipment and samples, and sampling through the inspection hole is therefore challenging, given the limited degree of freedom inside and through the inspection hole.

Figure 4.1: Inspection hole at the ARM Project.

Ideally, several cutter grooves should be included in one sample to study the rock breaking under the disc cutters and the interaction between the cutters. In addition, the sampling depth should be adjustable to different sites. In the early stage of this study, the impact depth of the cutters were unknown, and the sampling procedure had to allow sampling depths up to 50 centimeters.

From the limitations given by the available space, and the required depth of sampling, two sampling procedures were taken into account; cutting by wire saw or an angle grinder and core drilling.

Both a wire saw and an angle grinder can be used to cut cubes or rectangular prisms that include several cutter grooves in one sample. Both tools imply preparatory work, by setting up the equipment, and this is quite time consuming. In addition, the operator needs comprehensive training to use the equipment.

The diameter of the inspection hole limits the size of the angle grinder wheel to a diameter of 50 centimeters, giving a sampling depth of maximum 25 centimeters. A wire saw would fulfil the required sampling depth.

The size of the cube or rectangular prisms could not exceed the size of the inspection hole, and with a sampling depth of 50 centimeters, the dimension of the cube or prisms had to be adjusted to the inspection hole. Given the distance between the cutters, a maximum of seven cutter grooves could be included in one sample, reducing the possible thickness of the sample to less than 10 centimeters. A sample including three or four cutter grooves could be 40-50 centimeters, see Figure 4.2. Because of the spherical wheel of angle grinders, the actual sampling size would be considerably smaller if the sampling is done through the inspection hole. In practice, sampling by using an angle grinder through the inspection hole is not possible unless the sampling size and depth is reduced considerably. One possible way to circumvent

the limitations of the inspection hole is to excavate small caverns in the surface of the tunnel, place the samples there, and then collect the samples when the TBM has bored pass this cavern. This is a time consuming process, and as it will influence the excavation process, it is a quite expensive method as well.

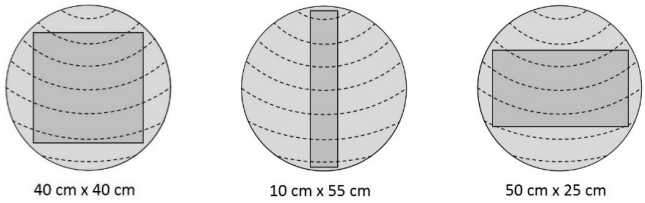

Figure 4.2: Potential dimensions of cubes and prisms that can be transported through the inspection hole in the cutter head. Dotted lines represents the cutter grooves.

The weight of the samples was another factor that needed to be taken into account. A sample of 40x40x50 cm^3 could potentially weigh around 200 kg. Even a sample of 10x55x50 cm^3 could potentially weigh around 70 kg. Handling and transportation of these samples would be challenging and time consuming.

Another challenging factor concerning sawing of samples is how to loosen the sample from the face of the tunnel without damaging the samples. A big contact area, like 40x40 cm^2 would require a large force to break loose the sample in the bottom of the sample. The potential of damaging the sample was considered to be quite high.

The last factor concerning cutting of cubes or prisms that was considered, was the consequence the sampling had for the next stroke of boring. Leaving a big hole in the face would increase the risk of broken cutters due to hits or other impact factors. Because of the large diameter cutters, the hole after a sample with a width of 10 centimeters and a height of 55 centimeters would have a much lower damaging potential than a hole after a sample with a width of 55 centimeters and a height of 10 centimeters.

The advantages and disadvantages of core drilling was also closely elaborated before the actual sampling commenced.

As for the cutting equipment, the core drilling equipment also imply some preparatory work, by setting up the equipment. As opposed to the cutting tool, this only involve one expansion bolt, and it is not very time consuming. The equipment could then be relocated for further sampling in a circular sphere around the bolt by loosening and tightening the bolt. In addition, the operator does not need comprehensive training to use the equipment. Setting up the equipment in front of the cutter head would not cause any problem, but a main concern was whether the equipment would fit in the inspection hole or not, and whether it was possible to set it up through the inspection hole. From the size of the equipment it was theoretically possible, but only an actual setup could provide the answer.

Core drills come in various lengths, so the required sampling depth of 50 centimeters was achievable. Core drills that can be used with handheld equipment are produced with various

diameters, ranging from 2 centimeters and up to 40 centimeters, and five or six cutter grooves could then be included in one sample.

The weight of a 50 centimeters long core with a diameter of 40 centimeters could potentially weigh 170 kg, and as for the cubes and prisms handling and transportation of these samples would be challenging and time consuming. A bisection of the diameter of the core would reduce the number of cutter grooves to three, and the weight to around 40 kg.

As for the cutting sampling procedure, loosening the cores from the face without damaging the samples was considered. A core with a diameter of 40 centimeters would have a considerable less contact area than a cube of 40x40 cm^2, and would require a smaller impact or force to be loosened. The potential risk of damaging the samples are lower when less force is needed to break them loose.

If the diameter of the cores are in the upper range of the available dimensions, broken cutters might be a problem, as discussed earlier.

A cube or a prism can be cut in slices and give valuable information about the propagation of cracks between the cutter grooves and along the grooves. A cylinder cannot provide the same amount of information unless it has a considerably large diameter, and smaller diameters require more samples to achieve the same information.

A summary of the advantages and disadvantages for the methods are presented in Table 4.2.

Table 4.2: Advantages and disadvantages for the methods considered.

	Cutting cubes or prisms	Core drilling
Time consume	÷	+
Cost	÷	+
Availability of equipment	÷	+
A high number of cutter grooves in one sample	+	÷
Weight of big samples	÷	÷
Sampling depth	÷ / +	+
Need for comprehensive training before use	÷	+
Risk of damaging the sample when loosening	÷	+
Risk of damaged cutters if the samples are big	÷	÷
Information value for each sample	+	÷

Despite the obvious advantage of getting more information from each sample by cutting cubes or prisms, core drilling was chosen as the favorable method of sampling. It is clearly the most time and cost efficient way to sample, given the time and space available, and the equipment is easy accessible and it does not require a comprehensive training before using. The drawback of less information per sample is compensated by the efficiency of the sampling, and the possibility to get many samples in a short time. This makes it a less vulnerable method than the cutting, where the success factor depends on the quality of one sample. Besides, the method is flexible and it can easily be adjusted to fit the conditions at site.

The first field sampling was going to take place at the AMR Project in India, and the core drills had to be brought along from Norway. At this point, core drilling through the inspection hole with a large diameter drill core was only a theoretically possibility. To make sure that there

would be enough space, a core diameter of 104 millimeters was chosen. With a cutter spacing of 74,6 mm, this core could cover two cutter grooves or more than half of the cutter spacing if the core was centered over one cutter groove.

Sampling at the AMR Project

As expected, the core drilling at the AMR Project had to be done through the inspection hole. Experiences from the sampling show that it is possible to drill the cores through the inspection hole, but that it is challenging to set up the equipment and to adjust it to get the preferred location of the cores. One unexpected challenge was to avoid getting water in the engine of the drilling equipment. The machine had only a limited sector of orientation without getting water in the engine. Because of this, the cutter head and the drilling equipment had to be reallocated more often than expected to be able to obtain the samples. Due to the available space, a core diameter of 150 millimeters was evaluated to be the upper limit of drill core diameters. Looking at the time consume the set up and the adjusting of the core location took considerably more time than the drilling itself. With some training, it was possible to drill three cores in one hour, once all the equipment is located in the cutter head.

With some minor variances, the cores were either centered over a cutter groove or centered in between two cutter grooves. The inspection hole covers cutter groove number 32 – 41, counted from the center, but it was only possible to get samples from cutter groove number 34 – 38. Two pictures from the core drilling at the AMR Project can be seen in Figure 4.3.

During the visit to the AMR Project, the contractor experienced some technical problems with the TBM and the conveyer belt, causing the machine to start and stop several times during a stroke. In total, only 10-12 full strokes of 1,6 meters were bored. Because of that, all the samples from the AMR Project were drilled at two different faces, but only 6 meters apart. The same TBM operator bored both the two actual strokes. The operator choose the operational mode of the TBM based on his "philosophy"; "*To keep the thrust at a constant level close to its maximum, and then I adjust the RPM to achieve the highest possible penetration per minute"*. At this point of the study, the main objective was to detect and document the rock breaking under the disc cutters of a full size TBM, and samples from strokes bored with different RPMs were not being considered. The author had no influence on the operational parameters. Some average values for the last 50 centimeters of the sample strokes can be seen in Table 4.3. This data is provided by the operator.

Table 4.3: Manually logged average performance of the TBM during boring of sampling strokes.

Chainage [m]	11572,8	11578,8
Date of sampling	25.02.2013	26.02.2013
RPM	5,9	5,5
Thrust force [kN]	16000	16000
Torque [kNm]	No data	No data
Pressure[bar]	No data	No data
Cutter load [tonn/disc]	No data	No data
Penetration [mm/min]	25	27
Penetration [mm/rev]	No data	No data
Penetration [m/h]	1,50	1,60

After the core drilling, the orientation of the cores, the cutter groove, the distance from the center and sector were registered for all the core samples before they were loosened from

the face using a small crow bar. To avoid damaging or interfering the potential cutter induced cracks directly under the cutter, the crow bar was placed perpendicular to the cutter groove. The cutter wear for cutter number 32 – 41 were also registered. The cores from the AMR Project are named AMR_[chainage]_[core number]_[cutter groove number], for example AMR_11573_1_34.

A) B)

Figure 4.3: Core drilling at the AMR Project. A) Challenging conditions, with limited space in and around the inspection hole. B) Location of some cores from the AMR Project.

Sampling at the Nedre Røssåga headrace tunnel

Due to stable and good quality rock mass at Nedre Røssåga headrace tunnel, all the sampling could take place in front of the cutter head. The sampling was done at five different faces, after fully completed strokes. The chainages were chosen in comparison with LNS, to ensure access to the face. The sampling strokes at chainages 1184 and 3112 were bored by one operator, and the sampling strokes at chainages 5437, 5458 and 5478 were bored by another operator. The first operator did not bore the last centimeter of the stroke, as discussed in chapter 4.1 *Choice of sites*, whereas the other operator bored the last centimeter. For all the sampling strokes the two operators were instructed to keep the RPM constant at the predefined value for at least the last 50 centimeters of the strokes and to keep the thrust as constant as possible. They were also instructed to manually log the operational parameters during the last 50 centimeters of the strokes. Some average values for the last 50 centimeters of the sampling strokes can be seen in Table 4.4. This data is provided by the operators.

Table 4.4: Manually logged average performance of the TBM during boring of sampling strokes.

Chainage [m]	1184,2	3112,6	5437,5	5458,0	5478,0
Date of sampling	14.07.2014	10.02.2015	21.07.2015	22.07.2015	23.07.2015
RPM	7,5	5	3	6,5	5
Thrust force [kN]	14000	14000	16000	15500	16000
Torque [kNm]	1800	No data	2100	2200	2200
Pressure[bar]	220	220	240	240	250
Cutter load [tonn/disc]	26	26	28	28	29
Penetration [mm/min]	40	No data	26	60	43
Penetration [mm/rev]	5,5	No data	8	9	8,6
Penetration [m/h]	2,48	1,70	1,60	3,50	2,50

Prior to the sampling stroke at chainage 1184, the author did not influence the operational parameters. At this chainage, the operator chose a RPM of 7,5. At chainage 3112 the author could chose the RPM. In order to compare the samples with the samples from the AMR Project, the favorable RPM had been between 5,5 and 6. Due to heavy vibrations in the TBM using this RPM, the RPM had to be lowered to 5. At chainage 5437, 5458 and 5478 the author could chose the RPM. In order to compare the samples with the previous samples, RPMs of 5 and 7,5 were preferable in addition to a RPM of 3. Due to heavy vibrations in the TBM using a RPM of 7,5, the RPM had to be lowered to 6,5.

Compared to the sampling at the AMR Project, sampling in front of the cutter head was less time consuming and it was considerably easier to adjust the equipment to get the preferred locations of the core samples. With some training and optimization of the location of the equipment, eight cores could be bored using only one expansion bolt. Drilling in front of the cutter head also made it possible to use two machines at the same time. With some training and planning, it was possible to bore 4-5 cores per machine in one hour, once the equipment is in front of the cutter head.

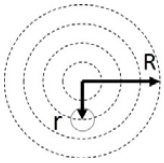

$$\frac{r}{R} = k \qquad [4.1]$$

r = distance from the center of the TBM to a given cutter groove (m)
R = radius of the TBM (m)

The TBMs at the AMR Project and the Nedre Røssåga headrace tunnel have different diameters, and different cutter spacing. To get the most comparable samples, it was preferable to get samples with the same relative positioning. The ratio between the distance from the center of the TBM to cutter grooves number 34 – 38 and the radius of the TBM at the AMR Project was calculated by formula [4.1]. The ratio was used to find the corresponding cutter grooves for the TBM at the Nedre Røssåga headrace tunnel. Cutter grooves number 22 – 25 were found to be the corresponding cutter grooves, see Table 4.5. Two pictures from the core drilling at the Nedre Røssåga headrace tunnel can be seen in Figure 4.4.

Table 4.5: Calculated radius ratios at the AMR Project and at the Nedre Røssåga project.

AMR Project		Nedre Røssåga headrace tunnel	
Cutter groove no.	r/R-ratio	Cutter groove no.	r/R-ratio
32	0,524	20	0,501
33	0,539	21	0,524
34 *	0,553	22 *	0,546
35 *	0,567	23 *	0,569
36 *	0,582	24 *	0,592
37 *	0,596	25 *	0,615
38 *	0,611	26	0,638
39	0,625	27	0,660
40	0,639	28	0,683
41	0,654	29	0,706

After drilling, the orientation of the cores, the cutter groove, the distance from the center and sector were registered for all the core samples before they were loosened from the face using a small crow bar. To avoid damaging or interfering the potential cutter induced cracks directly under the cutter, the crow bar was placed perpendicular to the cutter groove. The cutter wear for cutter numbers 20 – 29 were also registered.

The cores from the Nedre Røssåga headrace tunnel are named R_[chainage]_[sample set]-[core number]_[cutter groove number], for example R_1184_1-2_25.

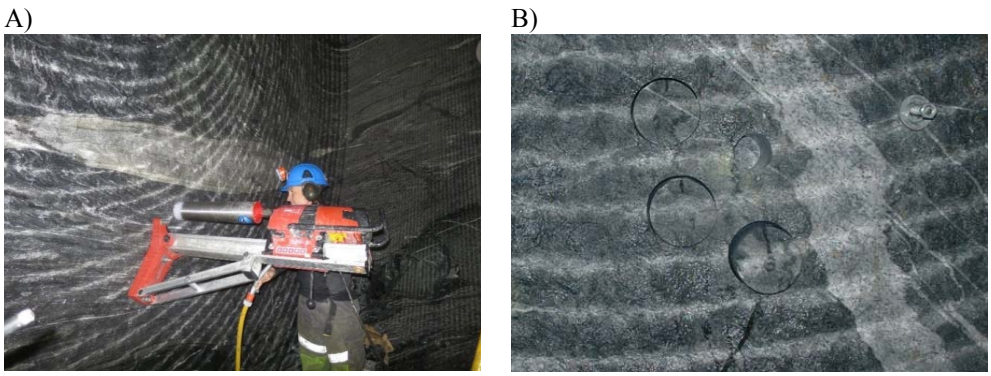

Figure 4.4: A) Core drilling into the face of the Nedre Røssåga headrace tunnel. B) Picture showing a typical sampling pattern.

Sampling of chips

An indirect way to study the efficiency of the rock breaking under disc cutters is by recording chips sizes, chip shapes and crack patterns in the chips (Bruland, 2000). In his thesis, Bruland shows that the chip size is a function of cutter load, and that both length, width and thickness increases with increased cutter load. He also shows that chip shape reflect the efficiency of the chipping, pointing out that the width of the largest chips often is larger than the cutter spacing at high cutter loads and that the length and thickness of the largest chips may be larger than the average size occurring at a higher cutter load. Bruland found that "*the general trend is that the shape of the chips moves from flat and elongated at low thrust leves towards more elongated, and even more cubic shape at higher thrust levels".*

By combining the thickness and the shape of the chip, it is possible to estimate the depth of the cutter groove. The ratio between the chip thickness and the depth of the cutter groove, kurf depth factor, decreases with increasing thrust, and the ratio may be used as an indicator of the cutting efficiency. Figure 4.5 and equation [4.2] describe the kurf depth factor

In addition to the indication of cutting efficiency, Bruland points out that this ratio may be an indicator of the rock breaking mechanisms that form the chip. *"A visual interpretation of the chip cross sections in Figure 4.5 indicates that the chip taken at the highest thrust level to a large extent is formed by tensile cracks originating from the cutter edge. The contribution from shear failure must be quite low. The chip cross section from the lowest thrust level may suggest a somewhat different distribution between tensile and shear failure, but with the tensile failure still dominating the chip formation".*

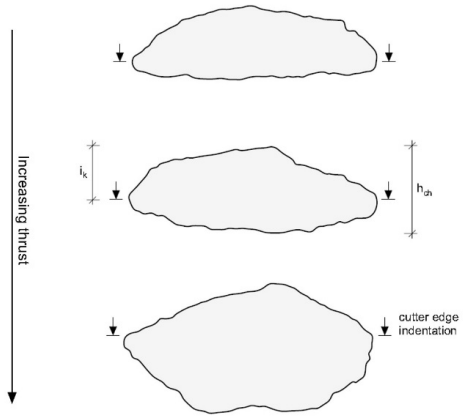

$$\frac{i_k}{h_{ch}} = f_{cgd} \qquad [4.2]$$

i_k = *kerf depth at chip forming [mm]*
h_{ch} = *maximum chip thicknes [mm]*
f_{kd} = *kerf depth factor*

Figure 4.5: Calculation of cutter kerf depth factor (Bruland, 2000).

Because the size and the shape of a chip most likely is a combination of new cracks propagating between neighboring cutters towards existing cracks and the lengthening of existing cracks from previous passes of the cutter, cross sections of chips may give valuable information about cutting efficiency and how the crack formation is developing.

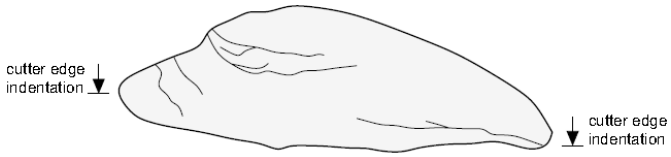

Figure 4.6: Typical cross section of a chip according to Brulands analysis (Bruland, 2000).

Figure 4.6 shows a, according to Brulands analysis, typical cross section of a chip (Bruland, 2000). Bruland writes that "*there are at least three different cracks that have propagated from the cutter. It is likely that at least two of these cracks have been made during the previous pass of the cutter than the pass that made the chip. It is however not all of the large chips that contains cracks which may be identified as cracks from previous passes of the cutter, i.e. some large chips may be formed by only one pass of the cutter".*

Figure 4.7 shows typical cross section of chips dependent on rock type and thrust (Bruland, 2000).

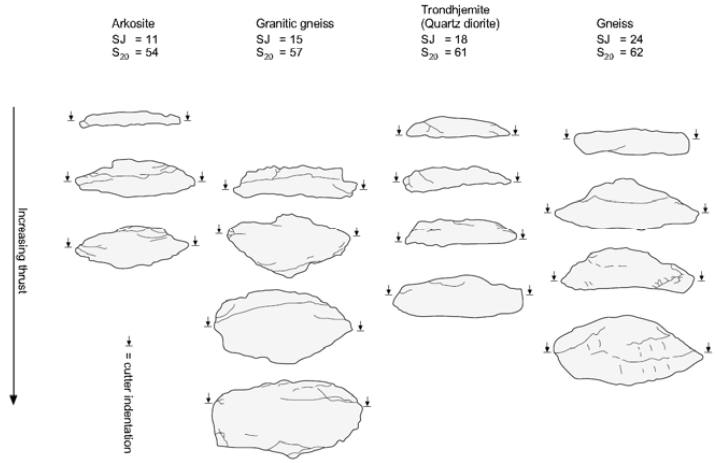

Figure 4.7: Typical cross section of chips dependent on rock type and thrust (Bruland, 2000).

As a supplement to the core samples, it was decided to collect chips at the sampling strokes to compare the findings in the core samples with cracks in the chips. At the AMR Project, the chips were collected from the conveyor belt at the end of the sampling stroke. At the Nedre Røssåga headrace tunnel, it was not possible to collect chips directly from the conveyor belt, so the chips were collected at the tip outside the tunnel, at the end of the sampling stroke.

A representative selection of chips were collected from both sites. In order to compare the finding in the core samples with cracks in the chips, it was important that the chips were likely to have been chiped from the area between two cutter grooves. The final selection of chips to be included in this study were done in cooperation with Bruland.

The chips are named [Site]_[chainage]_[chip number]_[part of chip]-[which side of chip], for example R_1184_3_A-B.

Sampling at Trondhjemite granite quarry

Because the purpose of the sampling at the Trondhjemite quarry was to get reference samples for laboratory testing, core drilling with the same equipment that was used at the AMR Project and at the Nedre Røssåga headrace tunnel was chosen without any other considerations.

The sampling took place on a vertical, wire sawed wall with no visible cracks or intrusions interfering the sampling area. Location can be seen in Figure 4.8.

The chips are named S_[core number]-[core sample within the core] for example S_2-1.

Figure 4.8: Core drilling at a vertical wall at the Trondhjemite quarry.

Sampling at the LCT facilities at KIT

The author has not been present during testing or sampling at the LCT facilities. Al information about the setup, equipment and sampling is provided by Yongbeom Seo, who were present during testing and sampling (Seo, 2016).

The linear cutting machine was controlled and managed by KICT. Ph.D.-candidate Yongbeom Seo participated in every work for obtaining rock chips, coring and measuring the roughness on the rock surface, as well as assisting KICT during the tests.

Five specimens of Iddefjord granite were shipped from Norway and used for the testing. The dimensions of the specimens were 1300×1150×400 millimeters and the specimens were casted in steel molds by mortar to secure their confinement.

By combining the following parameters, 17 different testing conditions were chosen by the participants of the FAST-Tunn Project:

- Two disc cutters with diameters of 19” and 6,5”
- Disc cutter spacing of 40, 80, 100 mm
- Penetration depths of 2, 3, 4, 6, 8 mm
- Sequential and random cutting operation

Sequential cutting operation means that the lines are cut with a predefined spacing from one side of the specimen towards the other side, until the desired number of lines are cut. With random cutting operation, the desired number of lines are cut in random order, causing the cutter to be relocated sideways in both directions and with irregular intervals until the desired number of lines are cut. The predefined cutter spacing is constant. The two cutting operations are illustrated in Figure 4.9. A rock specimen after testing, prior to core drilling can be seen in Figure 4.10.

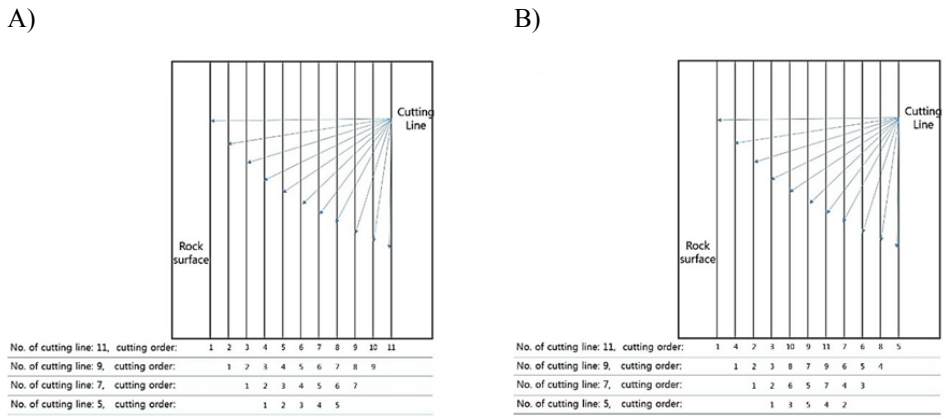

Figure 4.9: Cutting orders with A) sequential cutting, and B) random cutting (KICT, 2015).

Figure 4.10: Core drilling after testing. Note that the core drilling were performed from the bottom of the specimen (photo: Yongbeom Seo).

To compare the results with the core samples from the AMR Project and the Nedre Røssåga headrace tunnel, the author requested that the cores samples were centered over a cutter groove and in between two cutter grooves. The author had no influence on which cutting test the samples were from or which cutter lines that was chosen. The sampling was done by core drilling, drilling from the bottom of the specimen and upwards, causing some challenges to a

precise location of the core samples. Due to limitations of the equipment, the diameter of the core samples were 55 mm.

In total, eight core samples from two different tests were collected from the rock block used at the linear cutter test performed at KICT. Table 4.6 shows number of core samples from each test. A summary of relevant information for the two tests is presented in Table 4.6. Note that the penetration depth was kept constant, and that the average force represents the average normal force in the cutter during the test.

The chips are named LCT_[cutter spacing]_[sampling serie]-[core sample]- for example LCT_80_2-2.

Table 4.6: Number of samples from two tests at the linear cutter test.

Number of samples		Cutter diameter	Cutter spacing	Penetration depth	Cutting operation	Number of cutting lines	Average load on cutter
Over cutter groove	Between cutter grooves						
2	2	19”	80 mm	4 mm	Sequential	7	27,7 t
2	2	19”	100 mm	4 mm	Sequential	7	22,0 t

4.2.2 Collection of geological and TBM related data

Collection of data from the TBM

During drilling all operational parameters and the TBM performance were logged continuously at both the AMR Project and the Nedre Røssåga headrace tunnel. Cutter head thrust force and stroke position during boring of the sample stroke at chainage 1157 at the AMR Project can be seen in Figure 4.11. A complete presentation of relevant operational parameters and TBM performance for all sampling strokes can be found in Appendix A *Operational parameters and TBM performance*. The data is provided by Robbins and LNS.

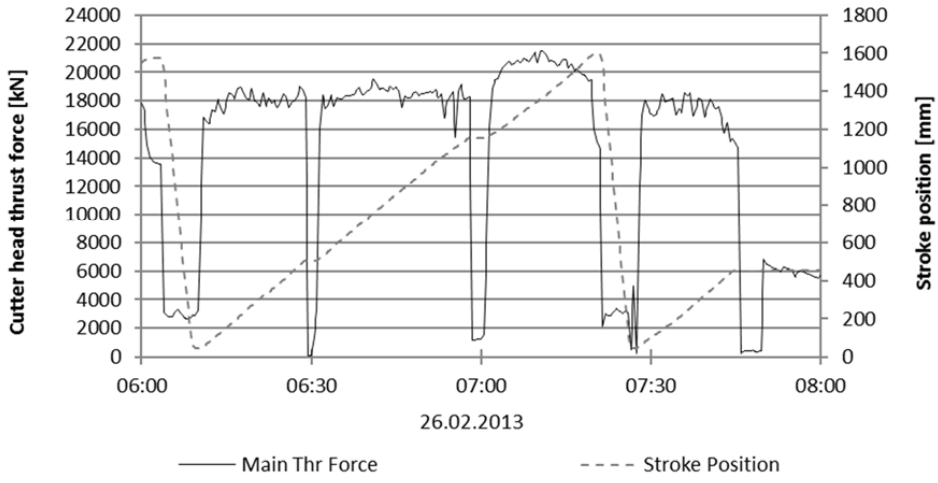

Figure 4.11: Cutter head thrust force and stroke position during the sample stroke at chainage 11579 at the AMR Project.

Geological mapping

An extensive geological mapping was carried out at both tunnel sites. The purpose of this mapping was to identify local structures, number of joint sets and the orientation of these joint sets in order to recognize them and separate them from the cracks and fissures induced by the TBM cutters. The mapping cannot, without additional information, be used for prediction modelling, rock support evaluation or any other TBM operational purposes. An example of geological mapping of the tunnel roof and walls from chainage 1182 to 18842 and the tunnel face at chainage 1184 at the Nedre Røssåga headrace tunnel, can be seen in Figure 4.12. The section to the left represents a fold out of the tunnel from the lower part of the wall on the left side of the tunnel to the lower part of the wall on the right side of the tunnel, seen from above. The circle to the right represents the face at chainage 1184. A complete geological mapping from the two sites can be seen in Appendix B *Geological mapping*.

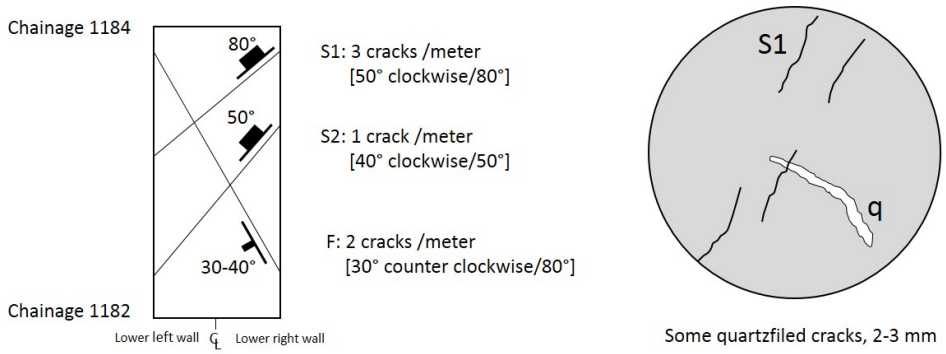

Figure 4.12: Part of geological mapping at chainage 1184 at the Nedre Røssåga headrace tunnel.

At the AMR Project, concrete lining was installed continuously, and the only accessible rock surface was at the face of the tunnel. Because of limited access to the face, some observations from outside the tunnel was also implemented. At the Nedre Røssåga headrace tunnel, no lining or shotcrete was installed, and the entire tunnel was accessible during the construction time. This accessibility gave good premise for geological mapping, and made it possible to ensure representative sampling strokes.

At both sites, a detailed mapping of the face was carried out during the core drilling.

4.3 Visual inspection of samples

4.3.1 Visual inspection of the core samples

The first step to identify cracks induced by the TBM cutters was by a visual inspection of the core samples from the Nedre Røssåga headrace tunnel and the AMR-project. Before inspection, dirt and fines were removed with flowing water, but no mechanical cleaning was done. All the core samples were then visually inspected in three different conditions; dry, moistened with water and moistened with methylated alcohol. The use of methylated alcohol is commonly used among concrete engineers to check for micro cracks and fissures during

curing of concrete. The alcohol evaporates faster from the smooth, less absorptive surface of the concrete than from the rough surface of micro cracks, making the cracks easy visible for a short amount of time (Aalberg, April 2013).

In the core samples from the AMR Project, these inspections revealed one fresh crack that was likely to have been induced by the TBM cutters, otherwise only preexisting open cracks with or without filling were observed. Not even directly under the cutter groove. The cores were then cut in the longitudinal direction, perpendicular or parallel to the cutter groove to look for cracks inside the core, but with negative results. Four pictures of one of the cores from the AMR are presented in Figure 4.13.

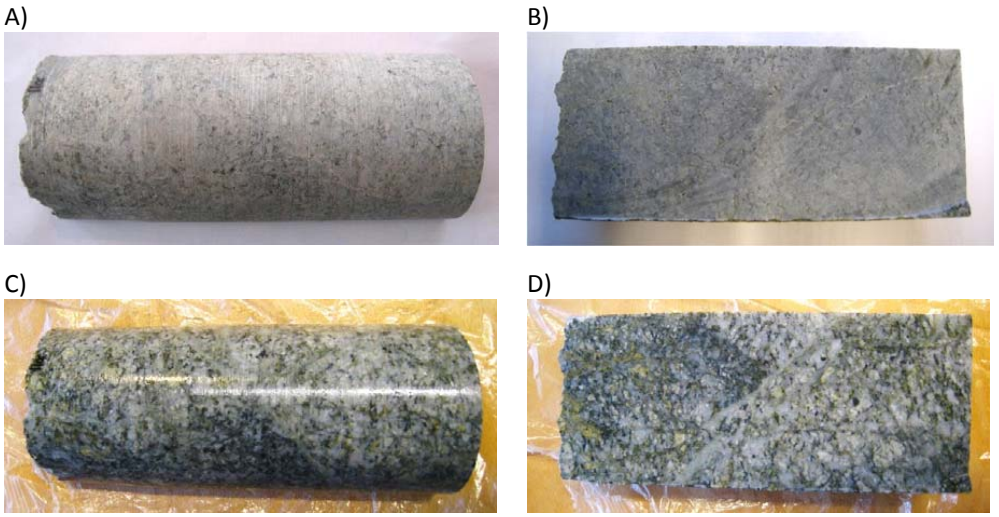

Figure 4.13: Visual inspection of one core from the AMR Project. A) Dry surface of core. B) Dry plane through the core. C) Core surface moistened with methylated alcohol. D) Plane through the core moistened with methylated alcohol.

In the cores from the Nedre Røssåga headrace tunnel and from the linear cutter test, a limited number of cracks were identified. There were no difference in the visibility of cracks whether the cores were dry or moistened with water. A few more cracks were visible when the cores were moistened with methylated alcohol, but still the number of visible cracks were unexpectedly low.

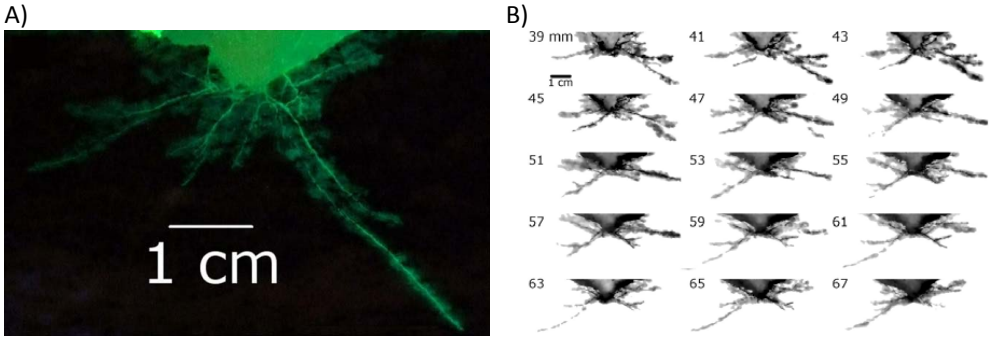

Figure 4.14: Cross sections of cracks under disc cutter in an augengneiss after a linear cutter test at the Montanuniversität in Leoben (Entacher, et al., 2014). A) Crack pattern visualized by a liquid two-component epoxy resin with a fluorescent additive. B) Cross sections of cracks every 2 mm.

The original plan was to use the visually identified cracks to define areas of interest for creating thin sections, as proven very effective by Entacher, Schuller and Galler. They used thin sections to study cracks and crack patterns under disc cutters after a linear cutter test, see Figure 4.14. The lack of cracks in the cores from the AMR Project necessitated a revision of the plan. Thin sections could still be created, but the location and orientation of the section would be a pure conjecture, and would only represent a very limited area. A worst case scenario was to create a high number of thin sections that was useless for this purpose. Random creation of thin sections would not only be incompatible with the objective of establishing an economical and time efficient method; it would also make the cores unusable for other purposes. After a thorough evaluation, creation of thin sections were temporary rejected as an investigation method. Note that this decision was made before the sampling started at the Nedre Røssåga headrace tunnel.

4.3.2 Visual inspection of chips

As described in chapter 4.2 *Sampling*, chips were collected from both the Nedre Røssåga headrace tunnel and the AMR-project. From the collected chips, a representative selection of the chips with a width and shape that made it probable that they were broken loose between two cutter grooves, were made. The only exception is chip R_1440_1. This chip has the properties of a chip broken loose between three cutter grooves. The final selection of chips was done in cooperation with Amund Bruland.

Depending on the size, the chosen chips were cut in two, three or four slices, perpendicular to what is the assumed cutter grooves. All the selected chips, and two examples can be seen in Figure 4.15.

The cut chips were then visually inspected to detect cracks likely to have been induced by the cutters. There were no visible cracks in the chips from the AMR Project, and some in the chips from the Nedre Røssåga headrace tunnel.

A)

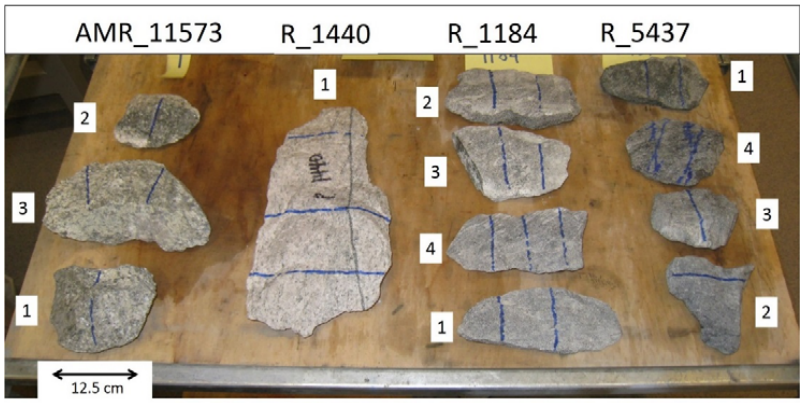

B)

C)

Figure 4.15: A) The chosen chips before cutting. B) Chip from the Nedre Røssåga headrace tunnel, chainage 1184. C) Chip from the AMR Project, chainage 11576.

4.4 Sound velocity measurements

4.4.1 Background for the choice of sound velocity measurements

The lack of visible cracks in the cores from the AMR Project necessitated a revision of the original plan. The possibility of X-ray photographing, magnetic resonance imaging (MR), investigations by an optic tele viewer in small borehole in the cores and sound velocity measurements along the core samples were evaluated as alternative methods for crack detecting.

The suitability of the four methods were discussed with the relevant research communities at NTNU and SINTEF. This simplified feasibility study indicated that both MR, optic tele viewer and sound velocity measurements could be possible methods to identify cracks in the cores. X-ray photographing were not suitable for this purpose without slicing the cores, causing the same dilemma as with the thin sections; random slicing and cores unusable for other purposes.

MR was found to be a possible, but very expensive method. It was also a high uncertainty regarding the likelihood of good results. On the other hand, the use of an optic tele viewer was found to be a both time and cost efficient method with the possibilities of good results.

The drawback of this method was that, with no visible cracks, the positioning of the small boreholes had to be more or less random.

As for the optic tele viewer, the use of sound velocity measurements was found to be a cost and time efficient method, with a high probability of good results. In addition, it is a non-destructive method, making the cores usable for other purposes after the investigation.

A summary of the advantages and disadvantages for the methods are presented in Table 4.7.

Table 4.7: Advantages and disadvantages for the methods considered.

	Cost	Time consumption	Destructive /non destructive	Potential
X-ray photographing	÷	÷	Destructive	+
Magnetic resonance imaging (MR)	÷	÷	Non destructive	÷/+
Optic tele viewer	+	+	Destructive	+
Sound velocity measurements	+	÷	Non destructive	+

With the first objective of the Ph.D.-study in mind, the MR imaging was rejected because of the high costs and high uncertainty regarding the possibility of good results. The X-ray photographing was rejected because of the uncertainty of slicing the cores with no visible cracks as guidelines. Applying either an optic tele viewer or sound velocity measurements were evaluated as equal methods as regard cost, time consumption and the potential of getting good results. Because of the benefits of a non-destructive method, the sound velocity measurements were chosen as the alternative method of crack detecting.

Ultrasonic testing is a widely used non-destructive testing methods for rock material characterization. The method is based on the generation, transmission and reception of compressional sound waves. The pulse length and the pulse frequencies of the sound waves can be adjusted to the purpose of the measuring. Sound velocity measurements can be used to define the mechanical properties of intact rock, or to define geological structures of the rock mass (Onur, et al., 2012). If an ultrasonic pulse that propagates through a geological sample meets a discontinuity, the direct pulse signal is obstructed, and this causes a time delay compared with the travel time of pulses in homogeneous core samples. If several measurements are performed along the core, this delay can make it possible to locate the position of the discontinuity.

4.4.2 Equipment and set-up

The interpretation of rock breaking under the cutters presented in Figure 2.4 shows a radial cracking under the disc cutter of the TBM. With this fracture pattern in mind, two hypothesis were defined;

1) The sound velocity will increase with increasing distance from the face, as the effect of the cutters on the TBM at a certain distance from face will be insignificant
2) The sound velocity will be higher measured parallel to the cutter groove than measured perpendicular to it, given that the cracking is radial to the cutters

A principle presentation of the hypothesis concerning sound velocity measurements can be seen in Figure 4.16.

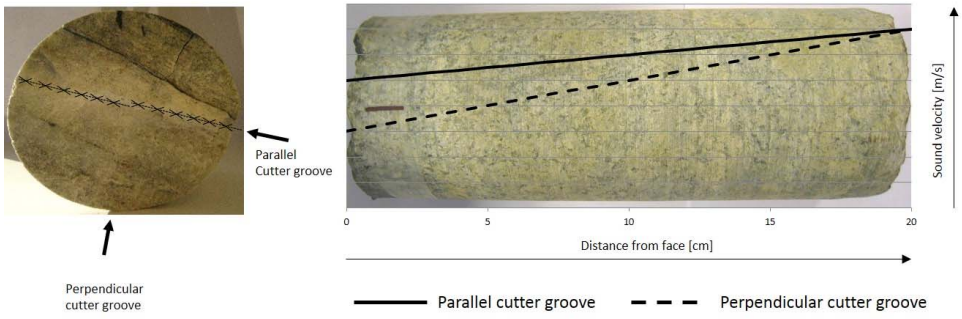

Figure 4.16: A principle presentation of the hypothesis concerning sound velocity measurements.

The International Society for Rock Mechanics´ (ISRM) standard procedure for laboratory measuring of sound velocity implies measurements in the longitudinal direction of the core (ISRM, 1978). The scope of this thesis, to study the depth and comprehensiveness of initiated cracks from the cutters required images to be made along the axes of the core samples. Therefore, in order to investigate potential TBM related cracking, sound velocity measurements had to be carried out radial to the cores. Radial measuring of sound velocity in order to detect anisotropy has been proven to give good results (Eitzenberger, 2002) and (Chryssanthakis & Tunbridge, 2004) and (Eitzenberger, 2012).

As a direct consequence of the radial measuring, the contact area between the core and the transducers is confined to be a straight line with a very restricted area. Both Eitzenberger, Chryssanthakis and Tunbridge used curved wave-guides with the same radii as the cores to increase the contact area between the core and the transducers.

For this Ph.D.-study, the purpose of the sound velocity measurement was to get an indication of cracks in the core by detecting potential changes in sound velocity through the core. The quantity of the sound velocity was less important. For the preliminary measurements, it was therefore decided to try measuring without a wave-guide.

In order to ensure diametrically opposite positioning of the transducers, reduce the sources of error and ensure repeatability, a frame where both the core and the transducers could be relocated step less, was constructed. Once the sample is located in the frame, it can be relocated with the preferred step length, whereas the two transducers can be slided sideways during relocation of the sample. Two pictures of the framework can be seen in Figure 4.17.

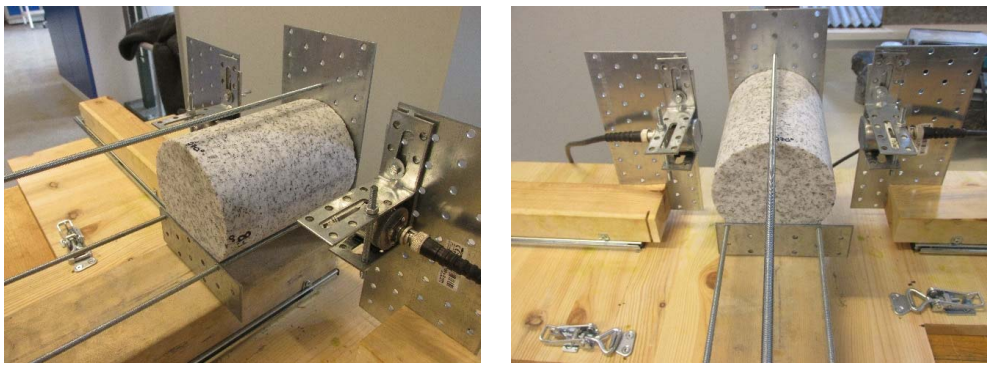

Figure 4.17: Constructed frame for sound velocity measurements.

The sound velocity measurements were performed at the NTNU and SINTEFs laboratory facilities in Trondheim, Norway. The test apparatus used was a Pundit Lab from Proceq. This apparatus has been designed especially for field testing, being light, portable and simple to use, but it is also used in standard laboratory testing at the NTNU / SINTEF laboratories. The apparatus generates ultrasonic pulses and accurately measures the time of their transmission through the sample.

The apparatus consists of a pulse generator, piezoelectric transducers, coupling agents, signal amplifier and an analyses system. The signal generator produces an electrical pulse of a certain wave form, which the piezoelectric emitter converts into an ultrasonic pulse. The ultrasonic pulse then propagate through the rock sample and arrive at a receiving transducer that converts the ultrasonic wave pulses into an electrical pulse. The received signal is then amplified, and the travel time of the pulse is recorded. The apparatus only detects the time taken for the first pulse arrival to propagate through the sample, and no later arrivals is detected. When using transducers with a diameter of 30 mm, the recorded pulse velocity represents the sound velocity in the 30 millimeters thick area between the two transducer, but the conditions under the center of the transducer has the highest impact in the recorded pulse. In order to determine the velocity of the pulse, the distance that the pulse travels in the material must be measured in order to calculate the velocity. A block diagram of the equipment is shown in Figure 4.18.

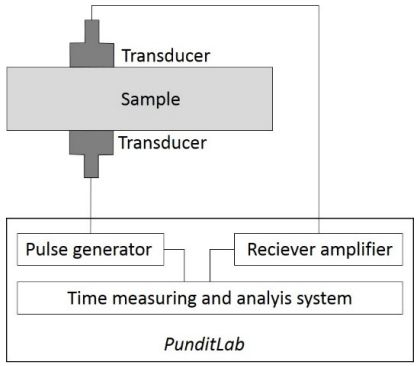

Figure 4.18: A block diagram of the equipment.

Different combinations of continuous and discontinuous measurements, different transducer sizes and a wide range of frequencies were tested to find the optimal setup for the measurements. In addition, several measurements were carried out with the same setup to ensure repeatability. After each measurement, the signal strength of the recorded waveform was controlled as it gives a clear indication of the quality of the received signal. According to the producer of the Pundit Lab, the best results are obtained when the received signal strength is around 75 % (Proceq, 2014). A low signal strength may be caused by an uneven core sample or inadequate acoustic coupling between the transducers and sample surface. Two examples from measurements with respectively low and high signal strength are presented in Figure 4.19. To obtain good acoustic contact between the transducers and the core sample, an aqueous transmission gel for electro-medical procedures, Dane-gel, was used as couplant. This gel was easily removed with rinsing water after the measurements.

Repeatability and the quality of the signal strength were good guidelines to conclude with the optimal setup for the purpose of these measurements. The signal strength was also controlled during the measurements as a quality assurance of the measured values. The chosen setup parameters are listed in Table 4.8.

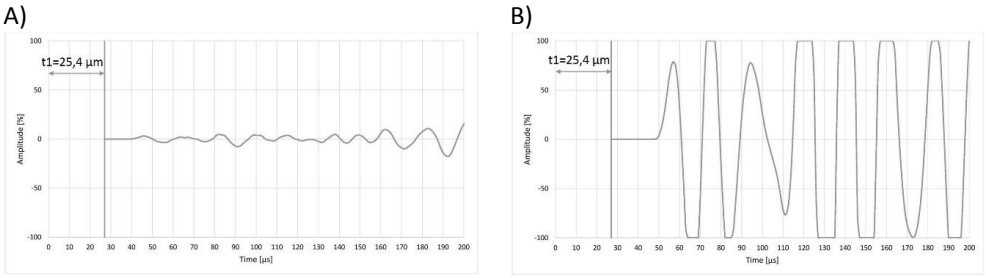

Figure 4.19: Two examples of signal strengths with different set ups. A) Low signal strength. B) High signal strength.

Table 4.8: Setup information for sound velocity measurements

Apparatus	Pundit Lab from Proceq
Diameter of transducers	30 mm
Probe frequency	150 kHz
Pulse amplitude	125 V
Rx probe gain	1
Time frame	0,2 ms
Measurement type	Direct
Number of events	100
Number of readings	1

With the purpose of the sound velocity measurements in mind, one measuring every 5 millimeters along the core was considered as a sufficient sampling pattern. With a transducer diameter of 30 mm, this results in a constant 2 centimeters overlap. The first measurement

was done with the transducers placed at the top of the core sample, and the last measurement was done with the transducers placed at the bottom of the core sample, see Figure 4.20. A small stress is applied to hold the transducers in place. All the measurements along one core sample is from now on referred to as a series of measurements.

Prior to every series of measurements, the Pundit Lab was calibrated with a calibration rod with declared values for frequency [kHz] and travel time [µs]. The diameter of the core sample was also measured in order to calculate the sound velocity.

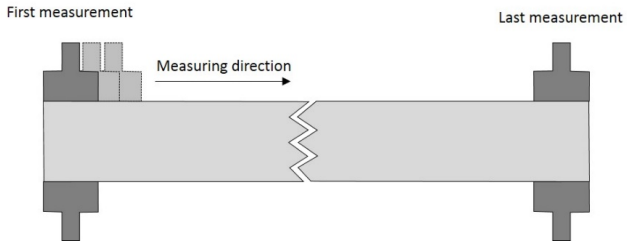

Figure 4.20: A principle sketch showing the positioning of the transducers.

4.4.3 Reference measurements

As a reference measurement and a quality assurance on setup and repeatability, preliminary measurements were carried out on a 14 centimeters long, intact core of trondhjemite from the Trondhjemite quarry at Støren, Norway. As described in chapter 2.7.3 *The Trondhjemite quarry at Støren, Norway*, the trondhjemite is a mainly homogenous rock with thorough documented characteristic properties, including sound velocity, which make it very suitable for reference measurements.

The sound velocity was measured in two directions, perpendicular to each other. In the following, these two directions are referred to as the 0-180° and the 90-270° direction. A picture showing the two directions can be seen in Figure 4.21A. The measurements show that the sound velocity varied slightly along the core, independent of measuring direction, and that there were some differences between the two directions. To check the validity of the measurements, the measuring procedure were repeated four times on the same core sample. The measured velocities from one of the series are shown in Figure 4.21B and Figure 4.21C. Note that the scale along the x.axis is different in the two figures, and that the points in the graph represents the location of the center point of the 30 millimeters diameter transducers. As the figures show, the deviation along the core and in the two measuring directions is small compared to the high measured sound velocity in the core sample. All measurements were congruent, with a maximum deviation of 40 m/s. The average deviation within the four series was 22 m/s.

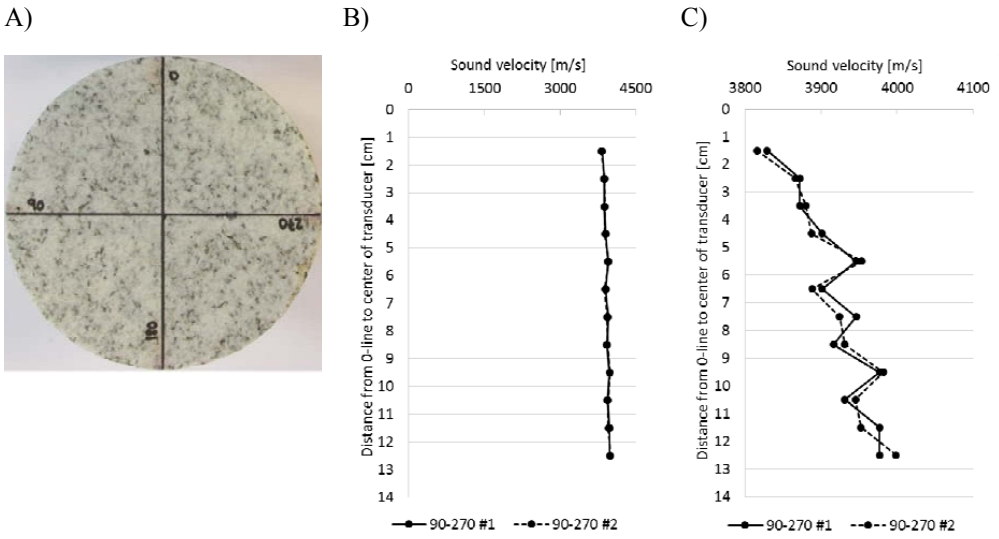

Figure 4.21: A) Intact core sample S_9-2 of Trondhjemite. B) One series of measured sound velocities series in intact core sample S_9-2. C) The same series of measured sound velocities series in intact core sample S_9-2 with another scale along the x-axis.

In addition, sound velocity measurements have been carried out on the other 15 core samples from the Trondhjemite quarry at Støren. These measurements were carried out to document if and how much the sound velocity changes along an intact core sample from a homogenous rock mass. These measurements show that the minimum deviation on measured sound velocities within the cores is 72 m/s in the 0-180 diretion and 71 m/s in the 90-270 direction. The maximum difference is 234 m/s in both directions. The average difference between the measured sound velocities in the two directions is 48 m/s.

In their report on sound velocity measurements in a borehole at Forsmark site investigation, Chryssanthakis and Tunbrige concludes that variations in temperature, thickness of transmission gel and seating of the transducers can cause differences in velocity of about ± 15 m/s (Chryssanthakis & Tunbridge, 2004). Eitzenbergs measurements on cores of steel and aluminium show a standard deviation of ± 10 m/s (Eitzenberger & Nordlund, 2002). A maximum deviation of 40 m/s, and an average deviation of 22 m/s thereby verified that the apparatus and the chosen settings gave reliable results.

At this point, the setup and quality of the measurements were validated, and the sound velocity profile of the intact trondhjemite core sample was well-documented. The next step was to investigate if one, or more known cracks could be detected by sound velocity measurements, and if possible which geometries of the crack, or cracks that could be detected.

An ideal condition for these investigations would have been one, planar crack with constantly decreasing width, from totally open to totally closed, towards the bottom of the core. An exaggerated sketch of this geometry can be seen in Figure 4.22A. This idealized crack would have given valuable information about if and how the width of the crack affects the measured

sound velocity, and thereby if the method was suitable for detecting cracks in the core samples from the AMR Project and the Nedre Røssåga headrace tunnel.

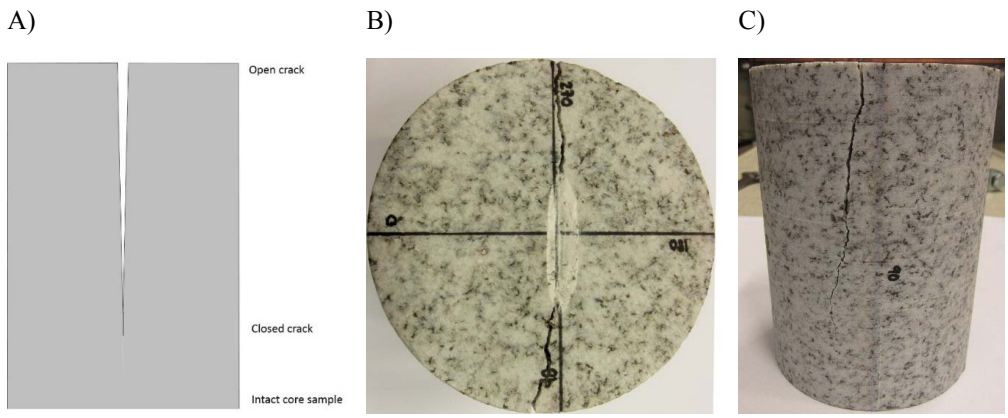

Figure 4.22: A) Ideal geometry of crack in a core sample. B) Initiated crack along the 90-270 axis at the top of core sample S_9-2. C) Initiated crack along the 90-270 axis in core sample S_9-2.

In order to initiate a crack close to the preferred geometry, the core sample was partly cloved with an applied load. A part of a used cutter ring from a TBM was used as an indenter and a point load was applied in the 90-270° direction of the core, see Figure 4.23. By using a low confinement stress and a low loading rate, a semi-planar crack with decreasing width along the core length was initiated. It was of great interest to keep the base of the core intact so that measured values in this section could be compared with the preliminary results. The geometry of this crack can be seen in Figure 4.22B and B.

Figure 4.23: Apparatus used to partially clove the core sample.

The details of the apparatus, confinement pressure and loading are not relevant to the results of the sound velocity measurements, and will not be presented in this thesis. A detailed description of the process is presented in Eirik Hannestads master thesis "*Use of indentation tests to study the rock breaking mechanisms"* (Hannestad, 2015).

Once the crack was initiated, the sound velocity measurements were repeated, using the exact same points of measuring. Measurements in the 0-180° direction were then perpendicular to the crack, and the measurements in the 90-270° direction were parallel to the crack.

A complete review and discussion of the findings and the method will be given in chapter 6.1 *Reference measurements of sound velocity* and in chapter 7.7 *On the sound* velocity measurements, but in order to allow the reader to follow the author's argumentation for further work, some findings and conclusions are presented below.

The measured sound velocities after initiation of crack compared to the measured sound velocity in the 0-180 direction in the intact core can be seen in Figure 4.24.

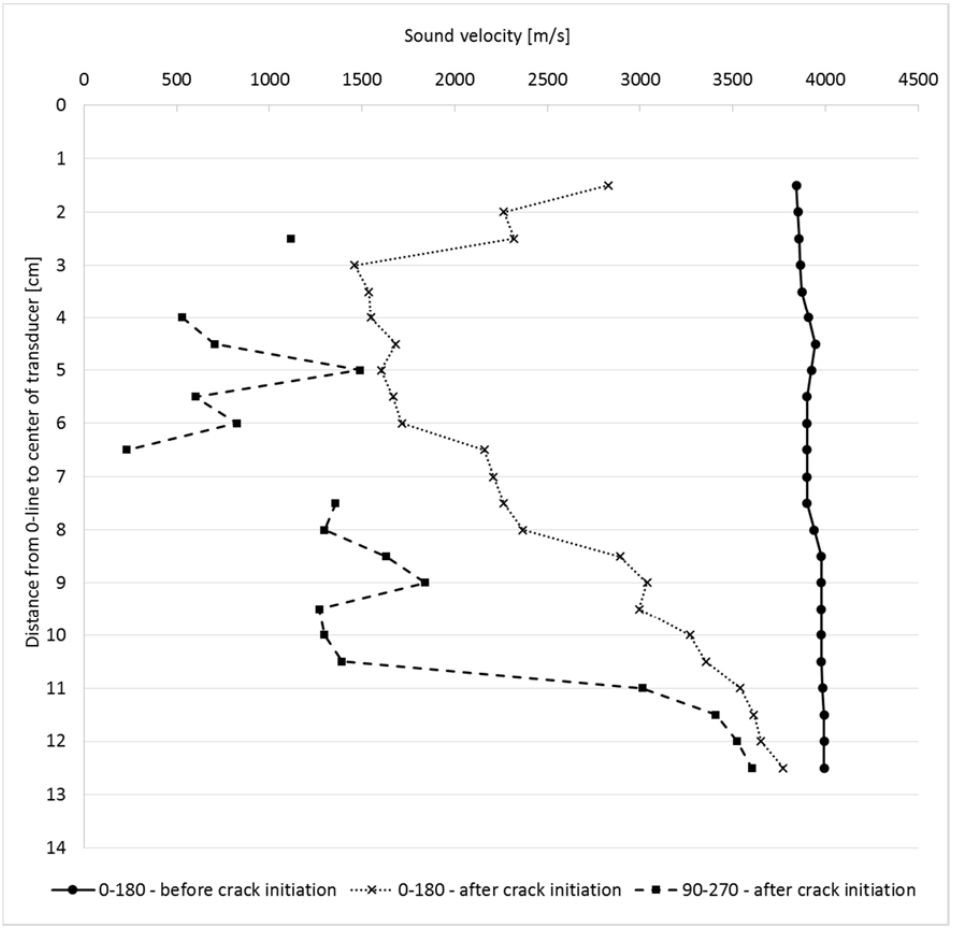

Figure 4.24: Measured sound velocities in core sample S_9-2 after initiation of crack, compared to measured sound velocities in the intact core sample.

To a great extent, the measured values in the 0-180° direction verifies the first hypothesis that the sound velocity increases with increasing distance from the face. The high sound velocity measured in the upper part of the core is most likely due to some crushed rock in the crack caused by the cutter ring during loading and cracking. The deviation between the measurements before and after crack initiation in the bottom of the core might be due to some micro cracking, not visible by visual inspection of the core.

The measured sound velocities along the 90-270° direction varies a lot, and at some measuring points it was not possible to achieve any measurements. One possible explanation could be that the straight line between the transducers in these points fully or partially runs along the open crack. The transducers cannot measure sound velocity through air and therefore no measurements in these points can be done. Because of the lacking measurements it´s not possible to verify the second hypothesis based on these measurements, but since the rest of the measurements correlates so good it cannot be set aside either.

These reference measurements show that it is possible to get reliable and repeatable results with the chosen equipment and set up. They also show that it is possible to detect cracks by sound velocity measurements, and that there is a good correlation between measured sound velocity and the length and width of a crack. The accuracy of the method would probably be better with a smaller diameter of the transducers, but as a method to check for potential cracking in the core samples, it was found to be suitable.

To verify the suitability of the method, the author initiated a further study through a master thesis at the NTNU. In 2015 Eirik Hannestad submitted his master's thesis "*Use of indentation tests to study rock breaking mechanisms induced by a TBM disc cutter*" to the Department of Geology and Mineral at NTNU, Norway. The thesis includes an evaluation of the suitability of sound velocity measurements to identify cracks as described above. Hannestad concluded that there are some uncertainties related to this method, but that it gives a qualified indication of whether there are cracks in the core or not, and how long these cracks are, given that the measurements are carried out perpendicular to the cracks (Hannestad, 2015).

Since the cores from the AMR Project were cut in the longitudinal direction, it was not possible to do sound velocity measurements on them. Sound velocity measurements were carried out on 20 of the core samples from the Nedre Røssåga headrace tunnel. These measurements were carried out every 1 centimeters, both parallel and perpendicular to the cutter groove. These measurements gave good indication of more cracking than what had been detected by visual inspection. Even though sound velocity measurements was found to be a suitable method to get an indication on whether there were cracks in the core sample, and to some extent the length of the cracks, it could not be used to identify the number of cracks, or their orientation and location in the core. To fulfill the first objective of the Ph.D.-study the cracks had to be visualized in some way.

After giving a speech about the preliminary results and the lack of visible cracks at the Fjellsprengningskonferansen in 2013, the author's supervisor was contacted by one of the listeners who recommended contacting Mats Olsson for a further discussion on visualization of cracks.

4.5 Visualization of cracks

4.5.1 Background and product description

Mats Olsson has 35 years of experience of rock blasting and is the founder and director of EDZ-consulting, a company working with quality in blasting and research work on smooth blasting. Olsson has used dye penetrant to identify and document cracks induced from blasting. Among other places he has used this technique at the TASS tunnel, in Äspö HRL in Sweden (Olsson, et al., 2009) and after wire sawing in tunnel at Citybanan, in Stockholm in Sweden (Christiansson, et al., 2013). Figure 4.25 shows two examples of cracks visualized by dye penetrant.

On Olssons recommendation, dye penetrant was tested on the cores from the AMR Project and the Nedre Røssåga headrace tunnel (Olsson, 2014).

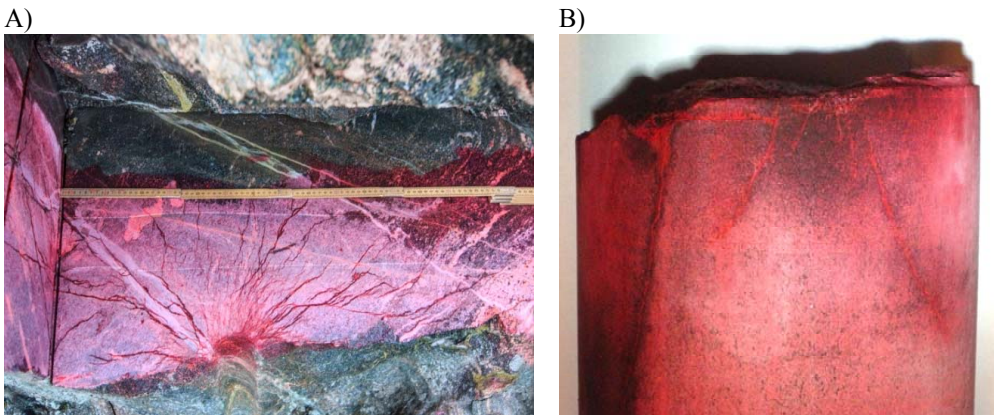

Figure 4.25: A) Visualization of cracks induced from blasting (foto: Mats Olsson). B) Visualization of TBM related cracks in a core sample from the Nedre Røssåga headrace tunnel.

Penetrant testing is a non-destructive material testing method, and can be used to visualize cracks, pores, laminations and other defects that are open to the surface of different materials. The penetrant can be used on non-porous or absorbent materials such as steel, aluminum, copper, plastic, glass, ceramics and rock (Bycotest AB, January 2007). The penetrant penetrates into any defects in the material, and the defects are visualized by application of a developer that sucks the penetrant from the defects to the surface. The defects appear clearly as red lines against the white background that the developer forms. Defects down to about 10-20 micrometers can be detected, and it is widely used within the nuclear, shipyards, airline, engineering, automotive and oil industries (Bycotest AB, January 2007), (Olsson, 2014).

The following products from Bycotest AB, Sweden, were used for the crack visualization;

- BYCOTEST RP20 Dye Penetrant from Bycotest AB, Sweden.
- BYCOTEST C10 Cleaner – Remover
- BYCOTEST D30A Developer

All three products were applied by spray can.

4.5.2 Procedure for application of penetrant

The recommended procedure for the application of penetrant is described in the product data sheet from Bycotest AB. With minor adjustments, this procedure was followed for application of penetrant on the core samples from the AMR Project, the Nedre Røssåga headrace tunnel and the linear cutter test on the Iddefjord granite, and on the chips from the two tunnel sites. In the following, both the core samples and the chips will be referred to as the samples.

The procedure can be summarized in five steps;

1. Preparation and cleaning of the core samples and chips
2. Application of penetrant
3. Penetration time
4. Removal of surplus
5. Application of developer

In the following, a detailed description of the different steps will be given. Note that the application of the cleaner, the penetrant and the developer were performed in a fume cupboard to avoid inhaling aerosols.

To ensure that the core samples and the chips were free of contamination that may prevent the penetrant from entering the discontinuities a proper cleaning of the samples is necessary. As described in the section about visual inspection of the core samples, dirt and fines had already been removed by flowing water. Since the core samples were not contaminated by mud, grease, rust or any other incrustation, rinsing water was sufficient, and no mechanical cleaning was performed. To ensure that there were not any impurities in the discontinuities, the BYCOTEST C10 Cleaner was applied on the cores.

Any remaining water or solvents may impair the function of the penetrant. After cleaning, the core samples were therefore left to dry for at least 48 hours.

After drying, the penetrant was applied to the samples by spraying. Suitable penetration time depends on the properties of the penetrant, the temperature of its application, the material of the test substance and the type of discontinuities to be indicated. Penetration time may vary from five to 60 minutes. For the samples used for this Ph.D.-study, the cracks and discontinuities needed a minimum of 15 minutes to absorb the penetrant. The penetration must not, under any circumstances be allowed to dry during penetration time, and the use of a fume cupboard increased the risk of the samples drying out. To keep the samples wet throughout the penetration time, more penetrant was applied every five minute. The samples were also wrapped in a thin plastic foil. A picture from the application of the penetrant can be seen in Figure 4.26a.

After 15 minutes, the surplus penetrant was dried off with a clean cloth. Then the core samples were carefully rinsed by letting a small amount of slowly running lukewarm water. To avoid water from rinsing the penetrant out of the cracks, the water was applied at the bottom of the core and then slowly ran along the core sample. The chips were rinsed with a wet cloth.

After rinsing the samples they were dried off with a cloth and placed in the fume cupboard to dry as quickly as possible.

Once the samples were dry, a thin layer of BYCOTEST developer was applied. When sprayed on, the developer makes a white film on the sample surface, and after some minutes the cracks visualizes as red lines on the white surface. The cracks are only visible as lines a limited time before the area around the cracks is colored red as well. Generally, the visualization of the cracks take between five and 30 minutes. For the samples used for this Ph.D.-study, the visualization took five to seven minutes, depending on the rock type. In general, it is preferable to perform the first visual inspection of the sample immediately after applying the developer or as soon as it has dried, as this facilitates the interpretation of the cracks. In this study, the samples were visually inspected from the developer was applied until the development time was completed. A picture from the application of the developer can be seen in Figure 4.26B.

After the visual inspection of the samples, the developer was carefully rinsed of using a small amount of running water and then the samples were left to dry. For some samples, removing the developer helped distinguish cracks with a short distance in between, or one short crack crossing a longer and more pronounced crack. The cleaning also made the samples more suitable for further investigations, as gloves no longer were needed to handle the samples.

A) B)

Figure 4.26: A) Application of penetrant. B) Core sample after application of developer, but before the cracks were fully developed.

The penetrant was a success and revealed a considerable amount of cracks. Using the information obtained from the geological mapping it was possible to sort out cracks that were TBM initiated and cracks that existed naturally at the sites.

In addition to the quality of visualizing cracks, the use of dye penetrant is a non-destructive method, and the cores can be used for other purposes afterwards. It is time efficient, generating results in a short amount of time, and does not require laboratory facilities. The product is inexpensive, and using dye penetrant from spray can minimize the consumption.

Therefore, this method fulfill the premises in the first objective of the Ph.D.-study.

Final remark; the use of the dye penetrant is not suitable to document cracks on top of the core samples because the rough surface on top of the core samples result in a considerable uncertainty.

4.6 Documentation of rock breaking and TBM initiated cracks

4.6.1 Photographs

All core samples and chips were photographed before and after use of the dye penetrant. The photos were taken every 90 degrees around the core sample and on top of the core. Figure 4.27 shows photographs of a core sample from chainage 1184 at the Nedre Røssåga headrace tunnel. The photograph in Figure 4.27B was taken ten minutes after the cracks first visualized in the surface, and therefore no individual cracks can be seen in this picture. The areas with one or more cracks can be seen as dark red areas in the top of the core sample. In Figure 4.27C, two single cracks are marked with black arrows.

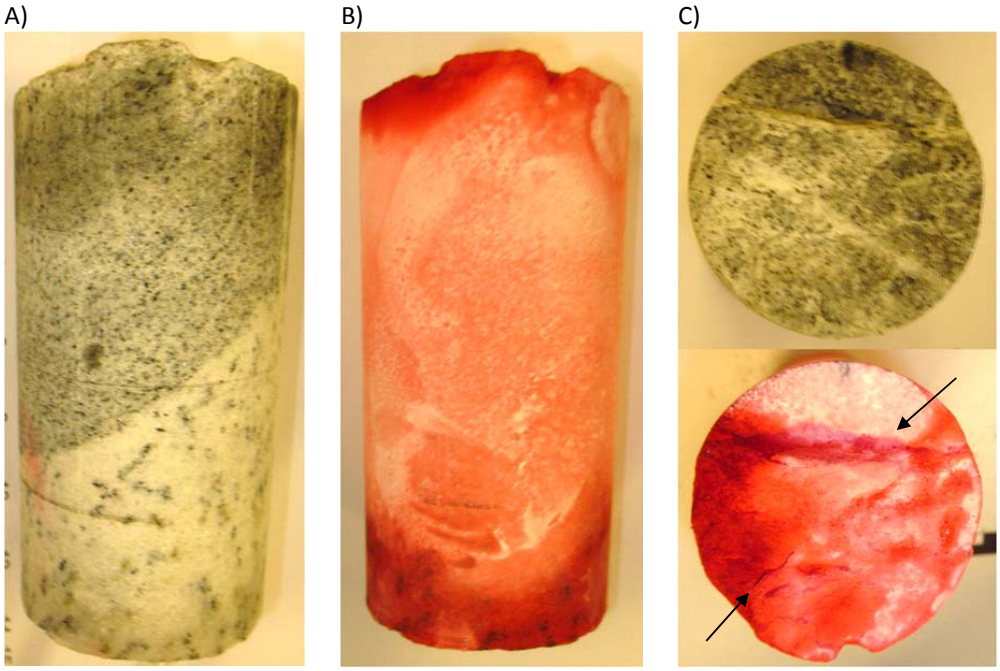

Figure 4.27: Photographs of a core sample from chainage 1184 at the Nedre Røssåga headrace tunnel A) Picture taken from the side before use of dye penetrant. B) Picture taken from the side after use of dye penetrant. C). Picture taken from the top before and after use of dye penetrant.

4.6.2 Digital foldouts

The mapping and documentation of cracks in the samples were done in scale 1:1 by drawing the cracks on a cylinder of thin, transparent plastic foil wrapped tight around the core sample, or placed on top of the chips.

All cracks were mapped in scale 1:1 in a three-step process.

1. Before use of penetrant
2. After application of penetrant and developer
3. After removing the developer

Using the information from the geological mapping it was possible to detect the cracks that were not TBM related. This crack detection was easiest done before application of the penetrant and the developer. After application of the developer, the samples were visually inspected throughout the complete development time of the cracks, and newly visualized cracks were mapped and documented. After cleaning of developer, a complemental mapping was performed, including any newly visualized cracks or corrections to the previous mapping.

In addition to the cracks, the surface along the edge of the core sample, the cutter groove and the foliation, if any, were mapped. For the chips, the outlines of the chips were drawn. An example of a plastic foil cylinder after mapping and the outline and four cracks in two chips from the Nedre Røssåga headrace tunnel are presented in Figure 4.28.

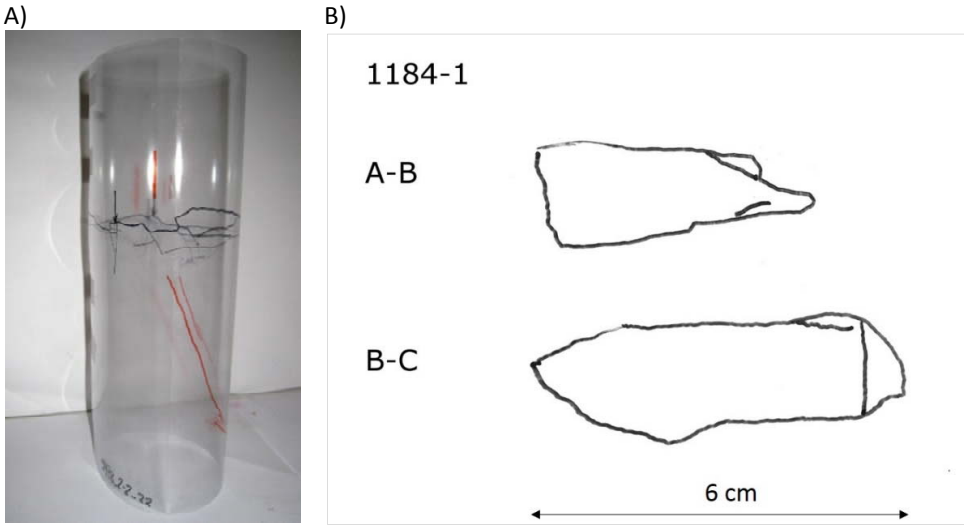

Figure 4.28: A) A plastic foil cylinder after mapping. B) Two cross sections of one chip from the Nedre Røssåga headrace tunnel.

When the mapping was completed, the plastic foil cylinder was opened, flattened and scanned in order to create a two dimensional digital foldout, representing the surface of each core sample. Three definitions in relation to this digitalization were defined by the author for the works in this study;

- The 0-line is defined by the highest point of the core sample when it is in a vertical position
- The surface line is the
- The basis point for the digital foldout is where the core sample is tangent to an imaginary horizontal line, leaving the foldout to present the core sample in a counter clockwise direction

Note that the 0-line and the basis point of the digital foldout define the reference system for all mapped cracks and the core surfaces, and that by these definitions, the reference system is valid for all samples, independent of the position on the tunnel face. The two definitions are schematically illustrated in Figure 4.29, and one example of a digitalized foldout of one core from the Nedre Røssåga Project can be seen in Figure 4.30. The arrow in Figure 4.30 represents the center of the cutter groove.

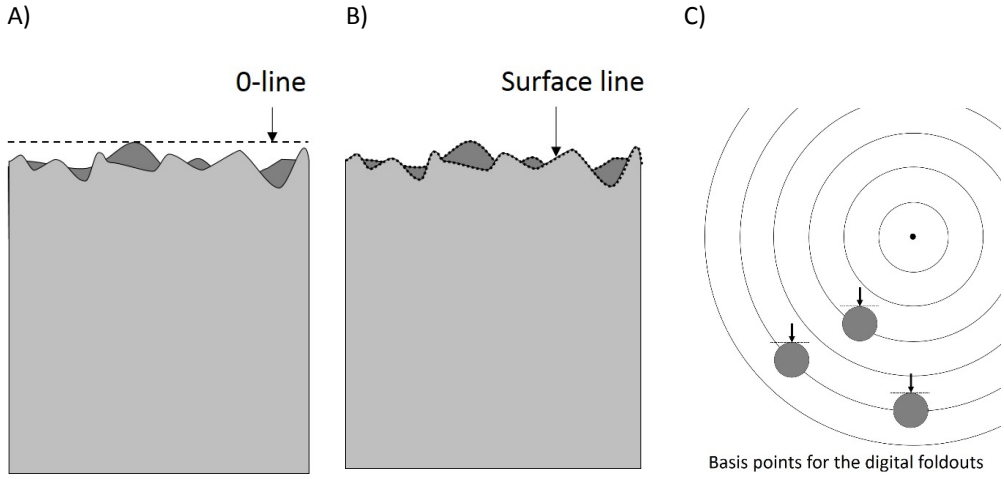

Figure 4.29: Author's definition of A) the 0-line. B) The surface line. C) The basis point for the digital foldout, shown with arrows.

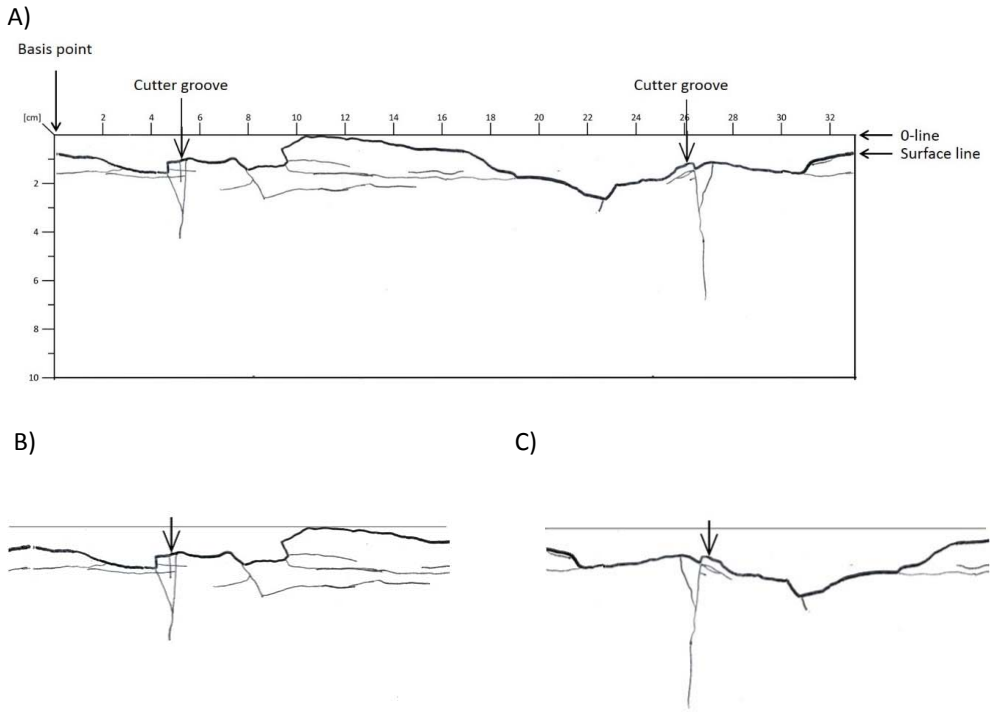

Figure 4.30: Digitalized foldout of a core sample R_5478_2-2_22 at the Nedre Røssåga headrace tunnel. The arrows represent the center of the cutter grooves. A) Complete foldout. B) Foldout of anterior half of core sample, seen counter clockwise the rotational direction of the cutter head. C) Foldout of posterior half of core sample, seen counter clockwise the rotational direction of the cutter head.

4.6.3 Quantification of cracks and core samples

In this study, the definition of the point of origin for a crack is where the crack intersects the surface line of the core. If the crack does not intersect the surface, the point of origin is defined as the vertical projection of the cracks upper end on the surface line. The left end of cracks with dip of less than 3° are defined as the initiation point. These three definitions are illustrated in Figure 4.31.

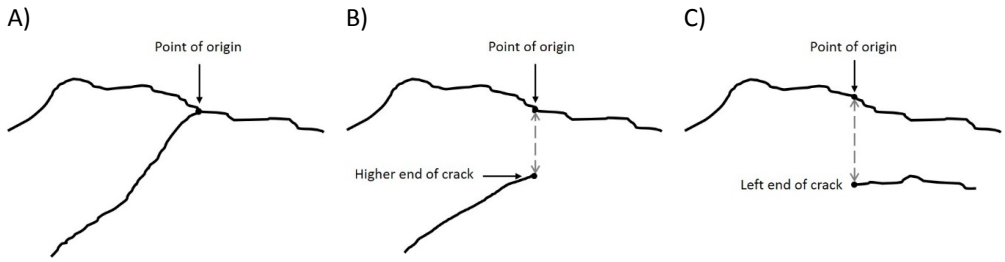

Figure 4.31: Author's definition of point of origin. A) When the crack intersects the surface line. B) The crack does not intersect the surface line. C) When the dip of the crack is less than 3°.

In order to establish a standard procedure for documentation of rock breaking under disc cutters in core samples from different areas of the tunnel face and different core diameters, nine measurable crack properties were defined by author, and thereafter quantified in millimeters, degrees or right/left;

1) The horizontal distance from the basis point to the point of origin of the crack, measured counter clockwise on the core sample, and from left to right on the foldout [mm]
2) The horizontal length of the crack [mm]
3) The vertical length of a crack [mm]
4) The total length of the crack [mm]
5) The dip of the crack, measured in degrees from the horizontal line [°]
6) The dip direction of a crack, towards right or left on the fouldout [right/left]
7) The vertical distance from the 0-line to the lower end of a crack [mm]
8) The vertical distance from the point of origin to the end of a crack [mm]
9) The vertical distance from the surface line to the point of origin of the crack when this is below the surface line [mm]

The nine properties are schematically presented in Figure 4.32.

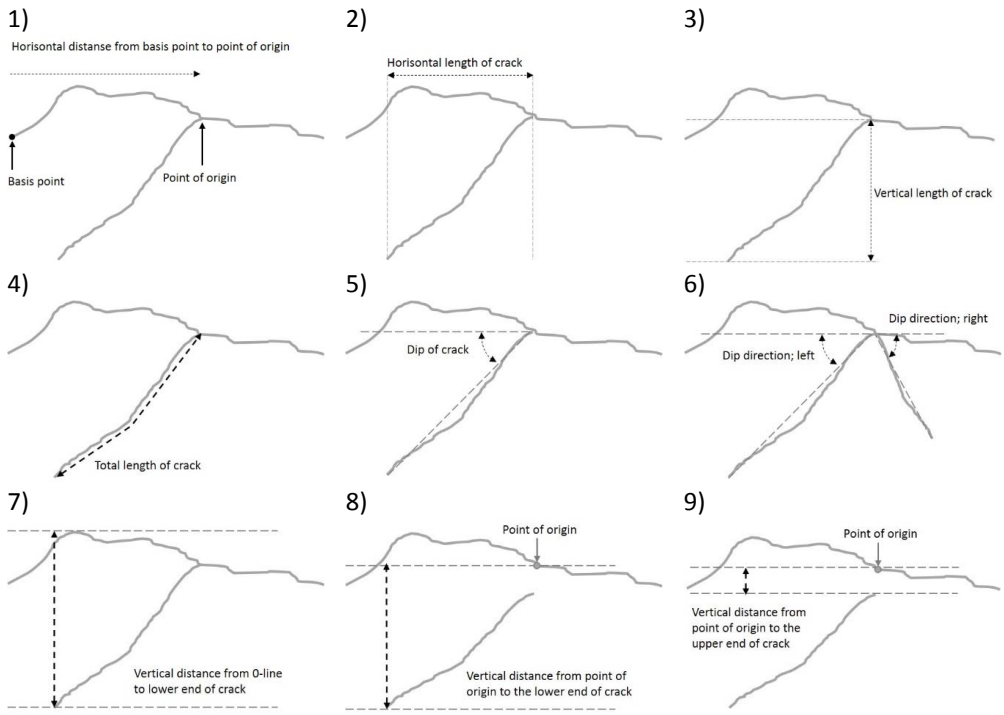

Figure 4.32: The author's definition of nine measureable properties for cracks detected at the surface of the core. The numbering corresponds to the list presented above.

In addition, two measurable core sample properties were defined and quantified;

10) The horizontal distance from the horizontal 0-point to the two cutter grooves, measured counter clockwise [mm]
11) The horizontal 0-point to the intersection points of the foliation, if any, measured counter clockwise [mm]

These properties are schematically presented in Figure 4.33.

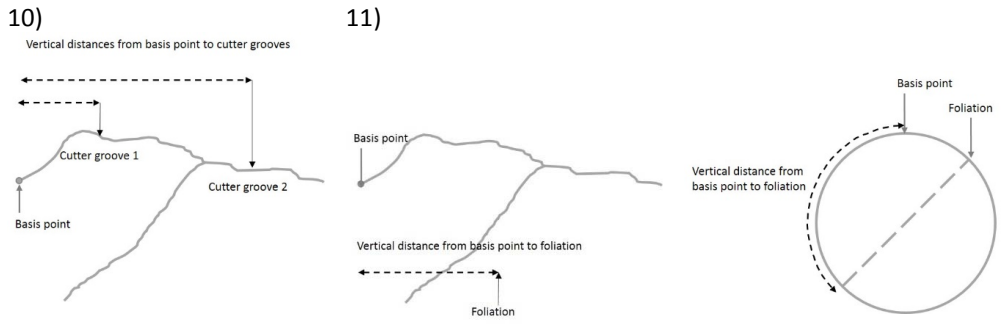

Figure 4.33: The author's definition of two measureable properties for the core samples. The numbering corresponds to the list presented above.

For comparison of the core samples, another six core sample properties, presented in Figure 4.34, were measured for each half of the core samples;

12) The circumference of the core sample[mm]
13) The length of the surface line along the circumference of the core sample [mm]
14) The horizontal distance between the highest and lowest point on the surface line [mm]
15) The vertical distance between the highest and lowest point on the surface line [mm]
16) The vertical distances from the 0-line to the cutter grooves [mm]
17) The area between the 0-line and the surface line [mm^2]

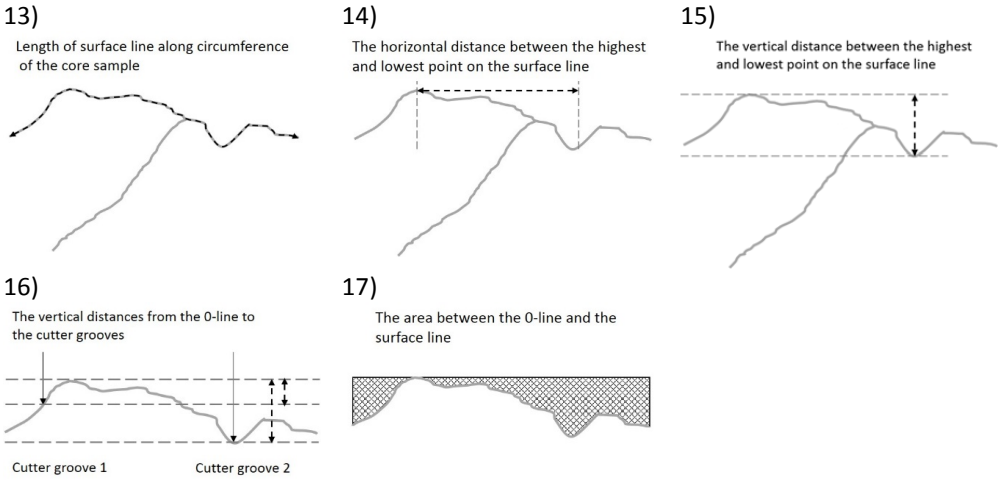

Figure 4.34: The author's definition of six core sample properties used to compare the core samples. The numbering corresponds to the list presented above.

These 17 quantified properties made it possible to document and compare the core samples and the rock breaking in each core sample.

From the obtained data, a digital presentation of the distribution of initiation points along the circumference of the core, the foliation and the cutter groove was created. The digital presentation of core R_1184_1-1_21 is presented in Figure 4.35.

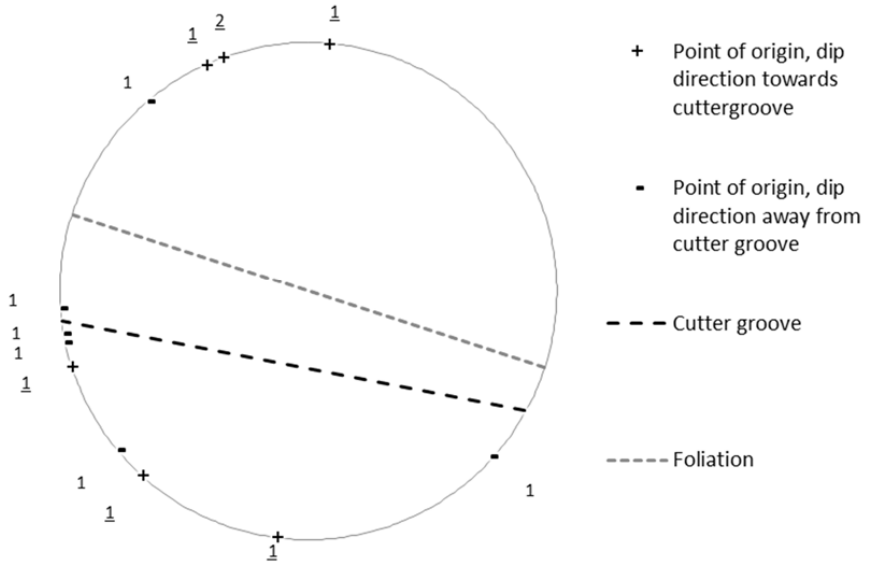

Figure 4.35: Digitalization of crack distribution along the circumference of core R_1184_1-1_21.

4.7 Practical use of obtained data

The foldouts and the data set of quantified properties of the cracks and the core samples provides an extensive documentation of rock breaking under the disc cutters of a TBM, and thereby fulfill the first objective of this Ph.D.-study.

To provide the answer to if, or how, the RPM effects the rock breaking, and whether it is possible to define some trends within or across geology and RPM, and thereby fulfill the second objective of this study, an extensive analysis of the measured crack and core sample properties was then carried out. To provide an adequate explanation of the results of the analysis is not within the scope of this Ph.D.-study.

Within the possibilities of the 17 defined measureable properties described in the previous chapter, the further analysis were done with three different areas focus areas;

A) The data set in its entirety
B) Data from all samples within a specific RPM
C) Data from all samples within a specific geology

The author has defined the geologies at chainage 1184 and 3112 at the Nedre Røssåga headrace tunnel as comparable enough to group as one geology. This result in three different groups of geology, including the geology at the AMR Project, see Table 4.9. The background of this choice will be discussed in detail in chapter 7 *Discussion*.

Table 4.9: Definitions of geologies used in the analysis.

Chainage	RPM	Geology 1	Geology 2	Geology 3
R_1184	R_RPM = 7,5	x		
R_3112	R_RPM = 5	x		
R_5437	R_RPM = 3		x	
R_5478	R_RPM = 5		x	
R_5458	R_RPM = 6,5		x	
AMR_11573	AMR_RPM = 5,5			x
AMR_11579	AMR_RPM = 5,9			x

4.7.1 Crack data analysis

Within the areas of interest, the following crack properties and combinations of properties were analyzed and itemized as follow:

Item no. 1) Number of cracks

Item no. 2) Distribution of the dip angles and the dip directions
Item no. 3) Distribution of the horizontal lengths of the cracks
Item no. 4) Distribution of the vertical lengths of the cracks
Item no. 5) Distribution of the total lengths of the cracks

Item no. 6) Distribution of vertical distance from surface line to crack end
Item no. 7) Distribution vertical distance from 0-line to crack end

Item no. 8) Distribution of horizontal distance from the point of origin to the cutter groove
Item no. 9) Distribution of number of cracks on the two sides of the cutter groove
Item no. 10) Distribution of cracks perpendicular and parallel to the cutter groove

Item no. 11) Dip of cracks versus average horizontal length of cracks
Item no. 12) Dip of cracks versus average vertical length of cracks
Item no. 13) Dip of cracks versus average total length of cracks

Item no. 14) Dip of cracks versus average vertical distance from surface to crack end
Item no. 15) Dip of cracks versus average vertical distance from 0-line to crack end
Item no. 16) Dip of cracks versus horizontal distance from the point of origin to the cutter groove

Item no. 17) Horizontal distance from point of origin to cutter groove versus dip angles and dip direction of crack
Item no. 18) Horizontal distance from point of origin to cutter groove versus total length of crack
Item no. 19) Horizontal distance from point of origin to cutter groove versus vertical distance from surface line to end of crack
Item no. 20) Horizontal distance from point of origin to cutter groove versus vertical distance from 0-line to end of crack

Dip of cracks versus average horizontal distance from point of origin to cutter groove makes no sense, and is not analyzed.

In addition, the following properties of the surface of the core samples were analyzed and itemized as follow:

Item no. 21) Ratio between the measured area between 0-line and surface line, and the theoretically calculated area of a rectangle with length of half the circumference of the core sample and a height of the vertical distance between the highest and lowest point of the core sample.
Item no. 22) Ratio between half the circumference of the core sample and the length of the surface line
Item no. 23) Ratio between vertical distance from the 0-line to lowest point on the surface line and the vertical distance from the 0-line to the cutter groove
Item no. 24) Ratio between the horizontal distance between the highest and lowest point on the surface line and half the circumference of the core sample

In the following, assumptions, remarks and explanations relevant for some of the chosen properties presented above will be given.

4.7.2 Remarks and explanations

The number in the heading of the following chapters correlates with the item numbers in the lists above.

Item no. 3, 4 and 5 – Horizontal, vertical and total length of cracks

As presented in chapter 4.6.3 *Quantification of cracks and core samples*, both horizontal, vertical and total length of the cracks have been measures. As presented in Figure 4.32, the total length of the crack is measures along the crack, including every curve. A theoretically calculated length of the crack from the vertical and horizontal length would not include any deviation from a straight line. Even though the difference between the theoretically calculated length of the crack and the actually measured total length of the crack is small, the author has chosen to include and present all three parameters.

Item no. 8 - Distribution of horizontal distance from the point of origin to the cutter groove

As opposed to the linear path for a cutter in a linear cutter test, the cutters on a TBM runs along circular paths with different radiuses. To document if this has any effect on the rock breaking, the distribution of both sides of the cutter groove was analyzed. Definition of the circle line, the center side and the outside of the cutter groove are illustrated in Figure 4.36.

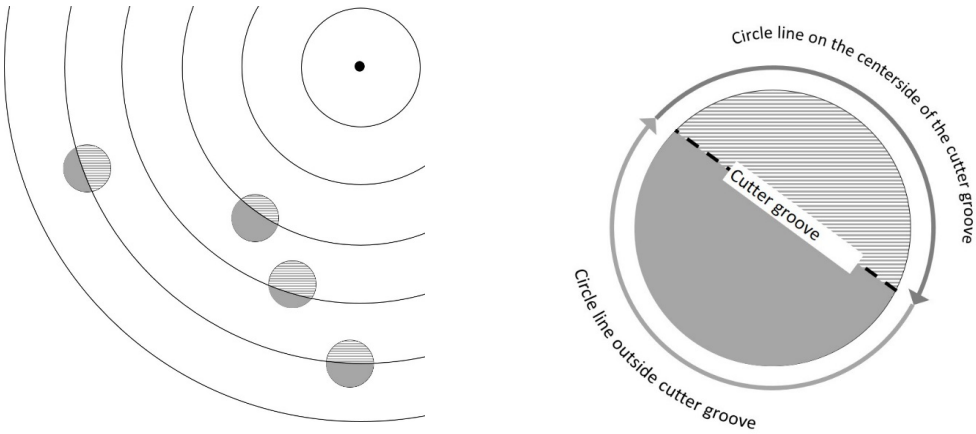

Figure 4.36: Definition of the circle line, the center side and the outside of the cutter groove.

Item no. 9 and 10 - Distribution cracks in relation to the cutter groove

The criteria of segmentation described above only differentiates between the center side and the out side of the cutter groove, and presuppose that the cutter groove is passing through the center point of the core. This is not the case for all cores, see Figure 4.37. This potential difference in area on the two sides of the cutter groove must be considered. To do that, the initiationpoints at the surface are projected vertically from the circel line to the cutter groove, and horisontally to an imaginary line passing through the center of the core, perpendicular to the cutter groove. The average distance between the cracks on both sides of the cuttergroove can then be calculated for both sides of cutter groove. The real area on both sides is also considered. By area, the author mean the calculated area of a circle with the same diamteter as the core sample.

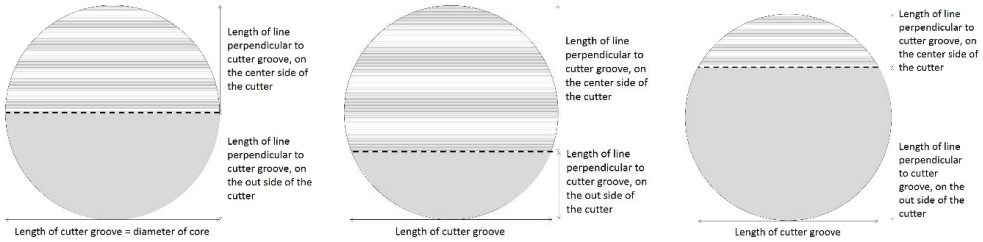

Figure 4.37: Illustration of area on both sides of the cutter groove depends on how the core sample is centered over the cutter groove.

To fully document the rock breaking it was preferable to study the distribution of cracks along and perpendicular to the cutter groove in each core. To do this, all the cracks and their orientation were projected to an imaginary line, parallel or perpendicular to the cutter groove. A projection to an imaginary line perpendicular to the cutter groove is illustrated in Figure 4.38. The projection of cracks groove in each core sample from sampling chainage R_1184 are

presented in Figure 4.39. The dotted line marks the cutter spacing. Negative values represents the outside of the cutter groove. All cracks are included in this plot.

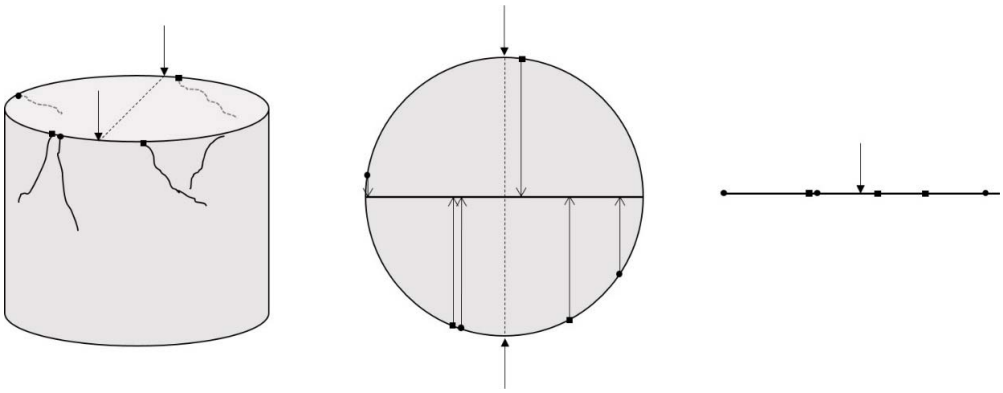

Figure 4.38: Procedure for projecting the point of origin of any crack and its orientation to an imaginary line, perpendicular to the cutter groove.

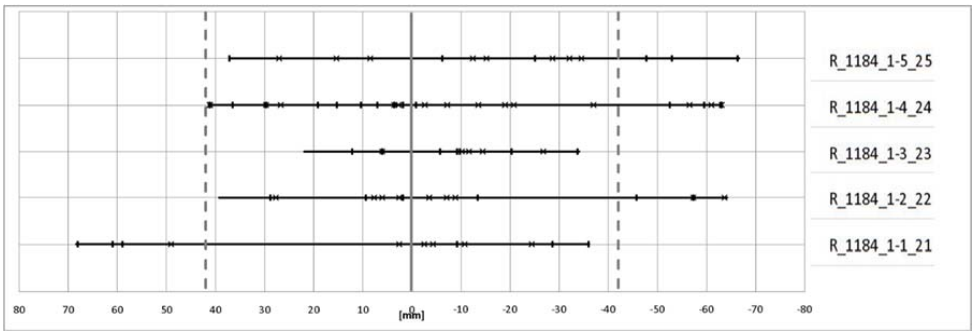

Figure 4.39: Cracks projected to an imaginary line perpendicular to the cutter groove in each core sample from sampling chainage R_1184. The dotted line marks the cutter spacing. Negative values represents the outside of the cutter groove. All cracks are included.

Item no. 21, 22, 23 and 24 - Ratios describing the surface of the core samples

The surface between two cutter grooves at the face of a tunnel varies with the chipping, and a cross section perpendicular to the cutter grooves will depend on whether there have been recent chipping or not . If the chipping process is generalized, three surface shapes and potentials of chipping can be defined, see Figure 4.40;

A) Right after chipping, low chipping potential
B) I between two chippings, medium chipping potential
C) Right before chipping, high chipping potential.

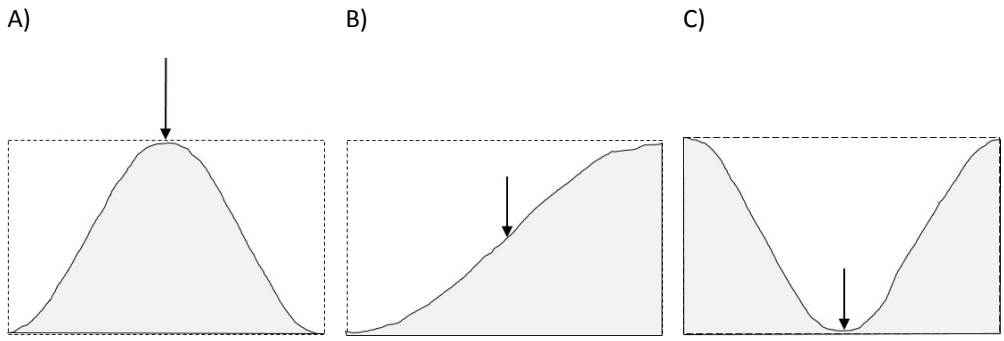

Figure 4.40: Three generalized stages of the chipping process. A) Right after chipping, low chipping potential. B) In between two chippings, medium chipping potential. C) Right before chipping, high chipping potential.

The length and amount of cracks in a core sample from a surface with a high chipping potential could potentially differ significantly from a core sample from a surface with a low chipping potential.

To ensure a representative selection of core samples with respect to chipping potential, four different ratios were calculated for each half of each core sample;

- k_{area} describe the amount of rock mass that is left to be chipped, see Figure 4.41 and equation [4.1]
- $k_{surface\ length}$ describe the roughness of the surface, see Figure 4.42 and equation [4.2]
- k_{depth} describe the vertical variation of the surface, see Figure 4.43A and equation [4.3]
- $k_{surface\ variation}$ describe the horizontal variation of the surface, see Figure 4.43B and equation [4.4]

Table 4.10 shows the expected relations between the ratios with different chipping potential.

Table 4.10: Expected relations between the ratios with different chipping potential.

Low chipping potential		Medium chipping potential		High chipping potential
k_{area}	>=	k_{area}	=<	k_{area}
$k_{surface\ length}$	>=	$k_{surface\ length}$	=<	$k_{surface\ length}$
k_{depth}	<	k_{depth}	<	k_{depth}
$k_{surface\ variation}$	>=	$k_{surface\ variation}$	=<	$k_{surface\ variation}$

A variation in combinations of these factors for each core sample indicate a representative selection of core samples with respect to chipping potential.

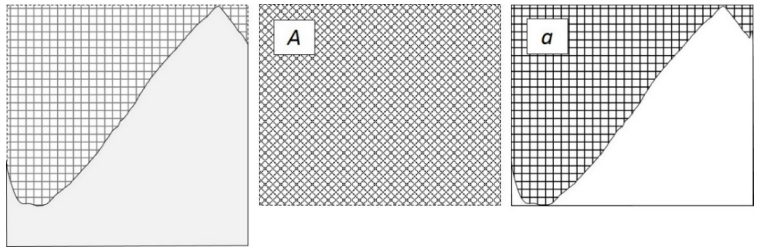

$$k_{area} = \frac{A - \mathrm{a}}{A} \qquad [4.3]$$

Figure 4.41: Ratio between the measured area between 0-line and surface line, and the theoretically calculated area of a rectangle with length of half the circumference of the core sample and a height of the vertical distance between the highest and lowest point of the core sample.

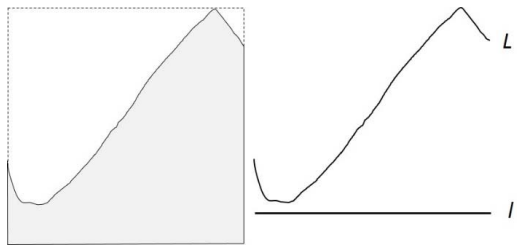

$$k_{surface\ length} = \frac{L - l}{l} \qquad [4.4]$$

Figure 4.42: Ratio between half the circumference of the core sample and the length of the surface line.

A)

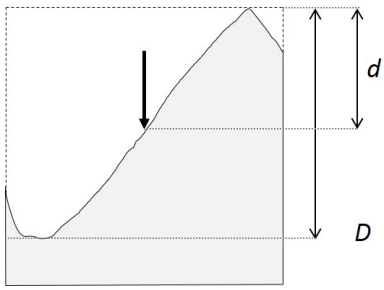

$$k_{depth} = \frac{d}{D} \qquad [4.5]$$

B)

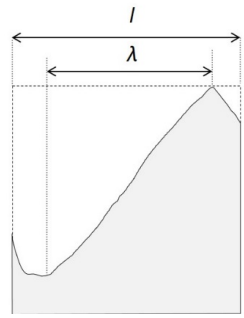

$$k_{surface\ variation} = \frac{\lambda}{l} \qquad [4.6]$$

Figure 4.43: A) Ratio between the vertical distance between the highest and lowest point on the core sample and the vertical distance from the 0-line to the cutter groove. B) Ratio between the horizontal distance between the highest and lowest point on the core sample and half the circumference of the core sample.

5 Results and analysis of rock breaking

In total, 108 core samples and 12 chips are included in this Ph.D.-study. Table 5.1 gives an overview of number of samples from each site, and the investigations that are carried out on these samples.

Table 5.1: Number samples and performed investigations.

Samples	Number of samples	Sound velocity measurements	Dye penetrant	Digital foldout	Quantification of cracks	Data analysis	Core surface analysis
Cores from the AMR-project	6		x		x		
Cores from the Nedre Røssåga headrace tunnel	64	x	x	x	x	x	x
Cores from the Trondhjemite quarry	3	x					
Cores from the Linear Cutter Test	8		x	x	x	x*	
Chips from the AMR-project	3		x	x			
Chips from the Nedre Røssåga headrace tunnel	9		x				

*) To a less extent than the core samples from the Nedre Røssåga headrace tunnel, due to less available data

Geological mapping and TBM performance parameters are presented in the following appendices:

- Appendix A: Operational parameters and TBM performance
- Appendix B: Geological mapping

All the core samples and chips used in this Ph.D.-study are presented in the following appendices:

- Appendix C: Core samples from the AMR Project
- Appendix D: Core samples from the Nedre Røssåga headrace tunnel
- Appendix E: Core samples from the LCT
- Appendix F: Core samples from the Trondhjemite granite quarry
- Appendix G: Chips from the AMR Project and the Nedre Røssåga headrace tunnel

In addition, the following appendices present the complete set of findings:

- Appendix H: Sound velocity measurements and digital foldouts
- Appendix I: Surfaces
- Appendix J: Data analysis of cracks from the Nedre Røssåga headrace tunnel

5.1 Rock breaking at the AMR Project

Only one out of six core samples from the AMR Project was a perfect cylinder. The five other core samples were either split into several larger pieces or even consisted of crushed parts with gravel sized pieces at the top of the core. Figure 5.1 shows core sample AMR_11579_1-3_34 where the 3-4 first centimeters from the face consisted of gravely pieces. The plane passing through the core sample on the right side is an open preexisting crack with some filling of feldspar or brittle and porous quarts.

Figure 5.1: Core sample AMR_11579_1-3_34.

As described in the previous chapter about visual inspection of the cores, these inspections did not reveal any fresh cracks that was likely to have been induced by the TBM cutters, only preexisting cracks with or without filling. In order to look for cracks inside the core samples they were cut in the longitudinal direction, perpendicular or parallel to the cutter grooves. This splitting made it impossible to perform sound velocity measurements on the cores, but regardless of the splitting, they were unsuitable for sound velocity measurements because of the heavy fracturing along preexisting cracks.

By the use of dye penetrant both outside the cores and on the cut surface, the author was able to detect four fresh cracks that were likely to have been induced by the cutters of the TBM. In addition, four reopened preexisting cracks both with and without filling was detected.

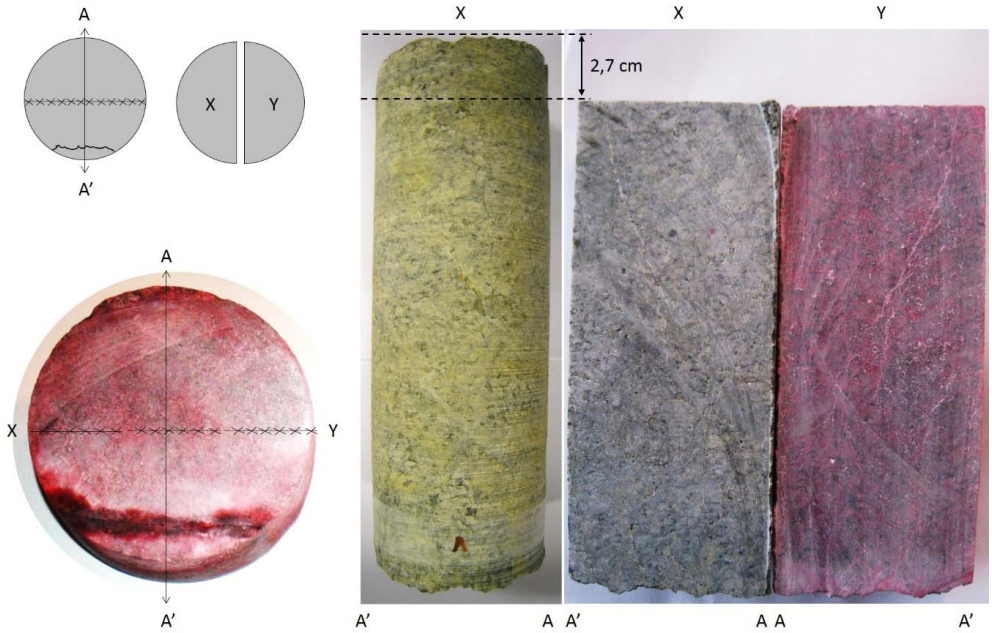

Figure 5.2: Core sample AMR_11573_1-1_38.

Figure 5.2 shows core sample AMR_11573_1-1_38 before and after use of dye penetrant. As the figure shows, the upper 2,7 centimeters of AMR_11573_1-1_38 was sliced before the core sample was split perpendicular to the cutter groove. The crack visible on the slice is a preexisting open crack. No fresh crack were detected in this core sample. This indicates that at this location, crack initiation does not reach beyond a distance of 2,7 centimeters from the tunnel face.

Figure 5.3 shows core sample AMR_11579_1-1_36. With two exceptions, the dark red lines of dye penetrant visualize preexisting cracks, both with and without filling of feldspar or porous quartz. These fillings absorb the dye penetrant better than the rest of the cores, making them appearing as cracks when the developer is applied. This proves the importance of a good visual examination of the core sample before the dye penetrant is applied.

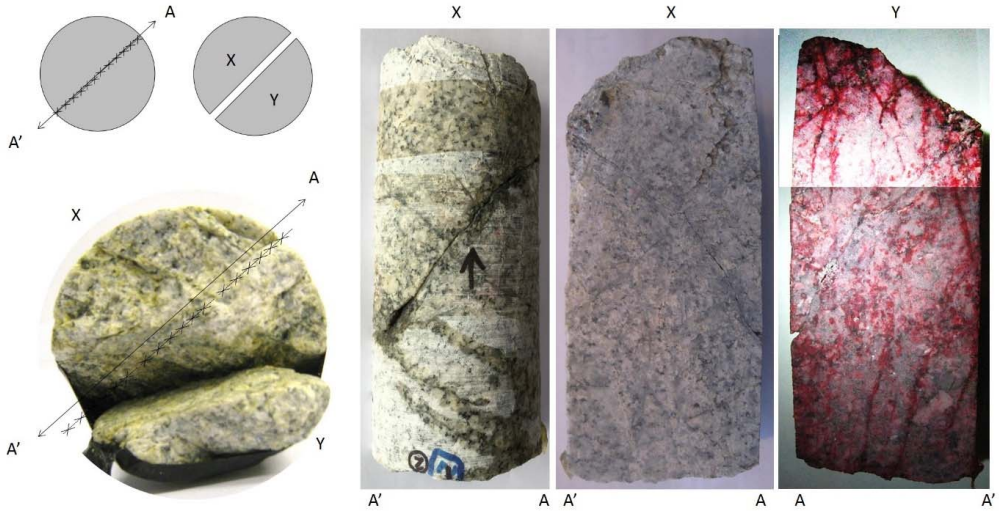

Figure 5.3: Core sample AMR_11579_1-1_36.

The author could, by the methods chosen for this Ph.D.-study, only detect eight cracks that are likely to have been induced by the cutters on the TBM. As a consequence of this, the cracks were not quantified for further analysis. The eight cracks that are likely to have been induced by the cutters are highlighted in Figure 5.4. A complete presentation of the core samples and the cross sections is presented in Appendix C.

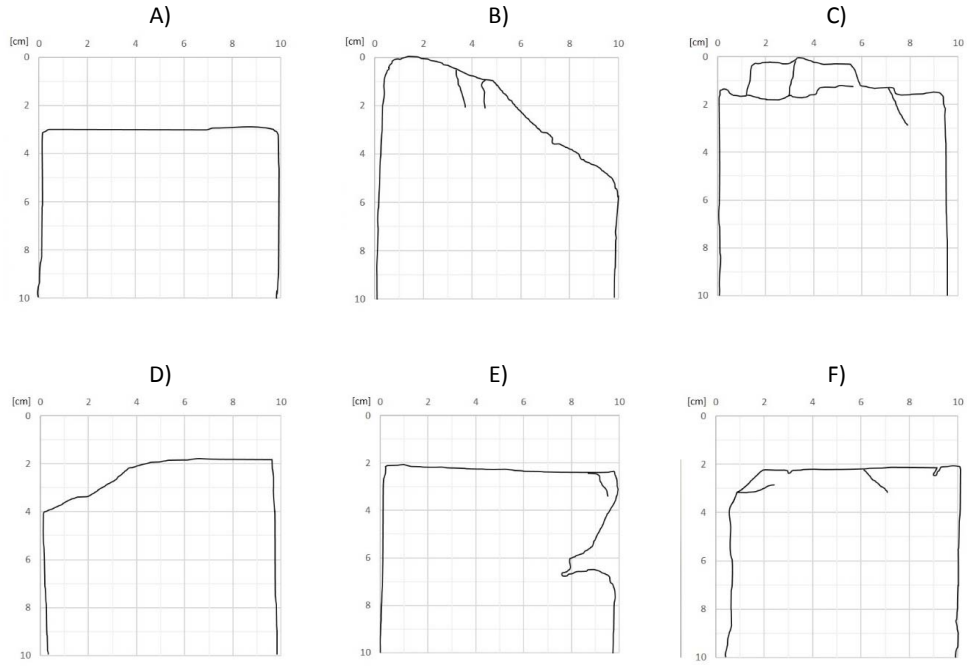

Figure 5.4: Cross sections and detected cracks in the core samples from the AMR Project. A) AMR_11573_1-1_38. B) AMR_11579_1-1_36. C) AMR_11573_1-2_37-38. D) AMR_11573_1-3_34. E) AMR_11573_1-4_34-35. F) AMR_11573_1-5_35.

5.2 Rock breaking at the Nedre Røssåga headrace tunnel

The findings presented in this chapter are based on 64 cores, from five different test series, as presented in Table 5.2: Number of cores in the test series at the Nedre Røssåga headrace tunnel.

Table 5.2: Number of cores in the test series at the Nedre Røssåga headrace tunnel.

Chainage	RPM	Number of cores
1184	7,5	5
3112	5	17
5437	3	16
5458	6,5	16
5478	5	10

5.2.1 Digitalized foldouts

The digitalized foldouts have been used to create cross-section imitations that show detected cracks in relation to the cutter groove in each core sample. Note that the cross-sections only are imitations, as they represent each half of the core sample. The area to the left of the

cutter grooves is on the center side of the cutter groove, whereas the area to the right is on the outside of the cutter groove.

A complete set of cross-sections can be seen in appendix I. In addition, the complete foldout for each core sample can be seen in appendix D *Core samples from the Nedre Røssåga headrace tunnel*.

Below is a selection of three digitalized foldouts that show the great variety of crack patterns. The arrows indicate the center of the cutter grooves.

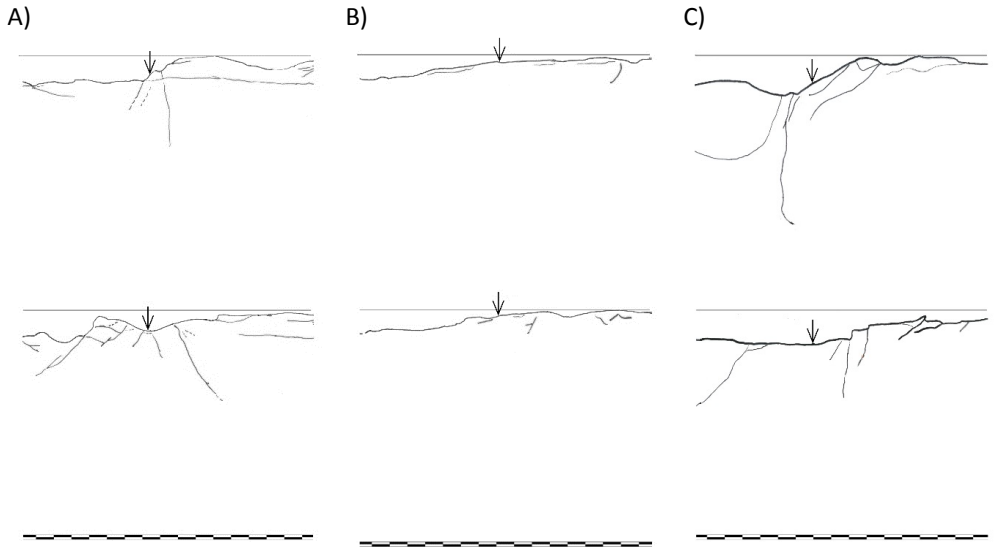

Figure 5.5: Cross-sections for a section of core samples from the Nedre Røssåga headrace tunnel. A) Core sample R_1184_1-4_24. B) Core sample R_3112_1-2_22. C) Core sampe5437_3-1_22.

5.2.2 Item no. 21, 22, 23 and 24 - Surfaces

The distribution of calculated surface ratios for the core samples from the five sampling chainages at the Nedre Røssåga headrace tunnel are presented in Figure 5.6 and Figure 5.7. For definition of the different ratios, see Figure 4.41, Figure 4.42 and Figure 4.43.

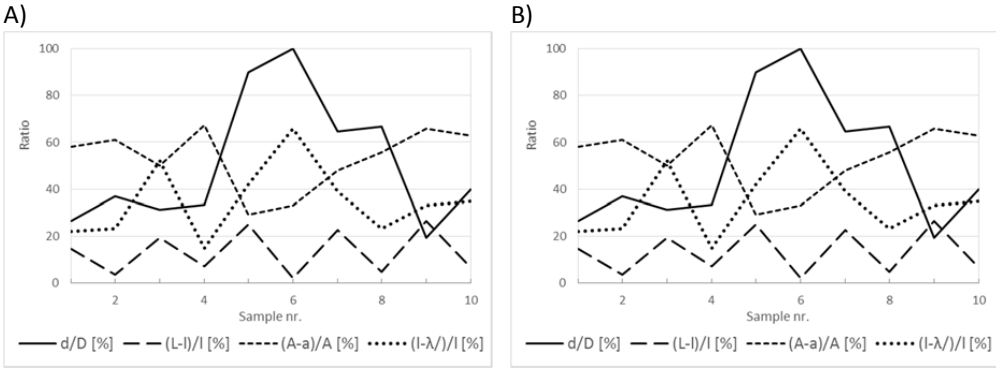

Figure 5.6: The distribution of ratios describing the surfaces of the core samples from Geology 1 at the Nedre Røssåga headrace tunnel. A) Sampling chainage R_1184. B) Sampling chainage 3112.

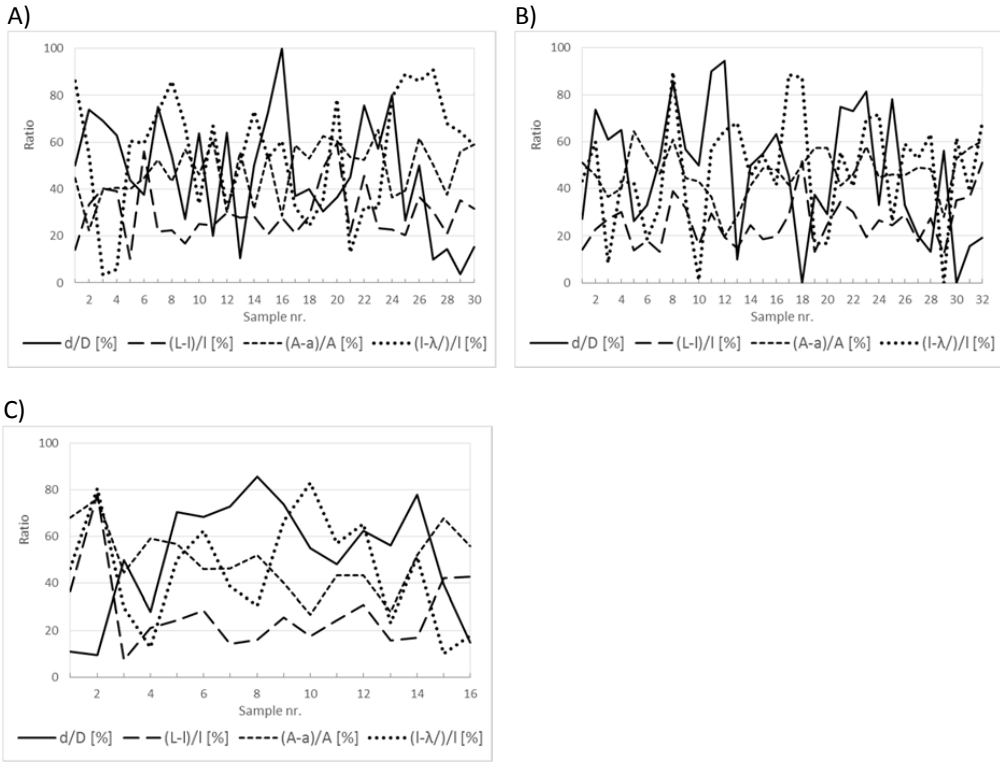

Figure 5.7: The distribution of ratios describing the surfaces of the core samples from Geology 2 at the Nedre Røssåga headrace tunnel. A) Sampling chainage R_5437 B) Sampling chainage R_5458. C) Sampling chainage R_5478.

In addition, the distribution of the vertical distance from the 0-line to surface line at the crack initiation points can give an indication of the variations of surfaces. Figure 5.8 shows this distribution for the core samples from the Nedre Røssåga headrace tunnel. This figure shows that the core samples from the lowest RPM within each geology have the highest share of cracks with a high vertical distance between the surface line and the 0-line in the point of origin, but that there are still small differences between the different sampling chainages, except R_5458.

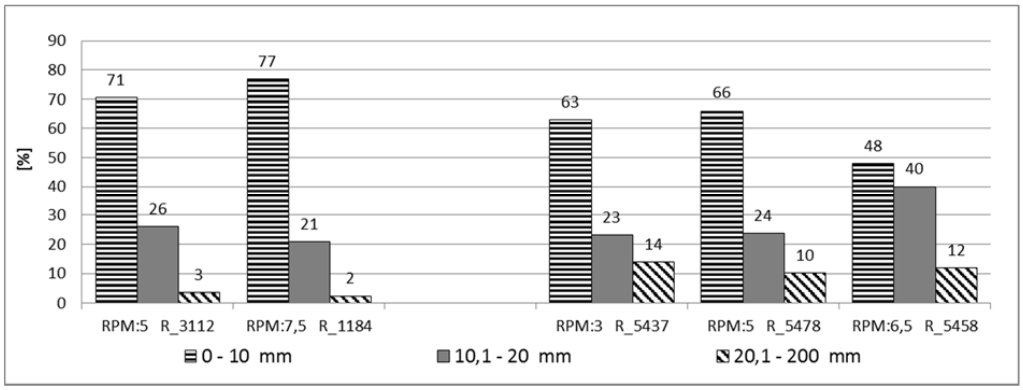

Figure 5.8: The distribution of vertical distances from 0-line to surface line at the crack initiation points in the core samples from the Nedre Røssåga headrace tunnel.

5.2.3 Detected cracks

In the following, all data will be presented in accordance with the list of crack data analysis in chapter 4.7.1 Crack data analysis. For definition of the different items, see chapter 4.6.3 *Quantification of cracks and core samples*.

Unless particularly commented in the following, all cracks and core samples are included in the analysis. More details can be seen in appendix J *Data analysis of cracks from the Nedre Røssåga headrace tunnel*.

Item no. 1 - Number of cracks

From the 64 core samples included in this study, 1243 individual cracks have been identified and documented. The distribution of cracks in each core sample is presented in Figure 5.9.

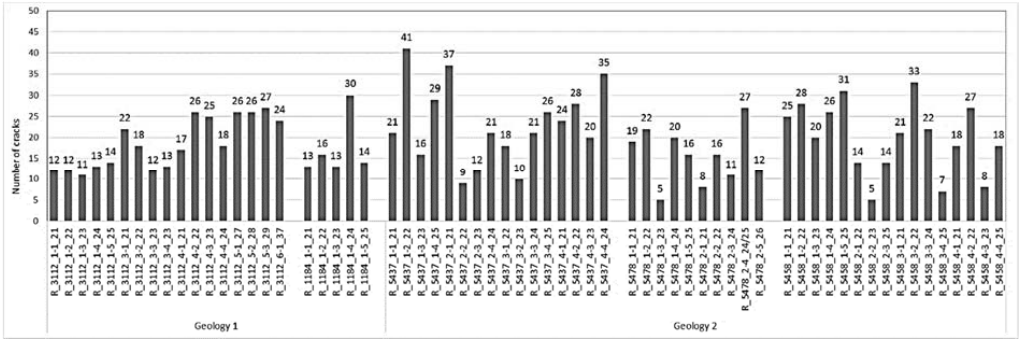

Figure 5.9: Number of detected cracks in each core sample from the Nedre Røssåga headrace tunnel.

Figure 5.10 shows the number of cracks and the calculated average number of cracks within the two geologies and the different RPMs. The plots show that the average number of cracks in a core sample varies from five to 41, and the average is 19,4 cracks per core sample. These plots also show that there is a difference between the different geologies, and between the different sampling chainages.

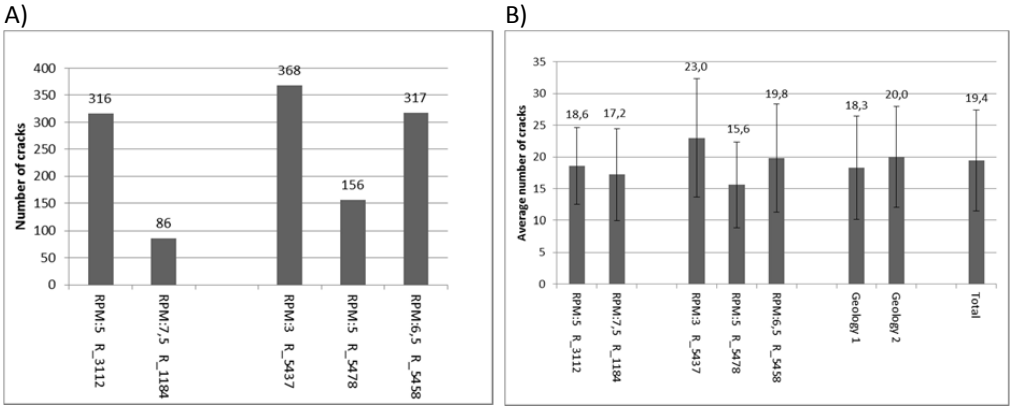

Figure 5.10: A) Number of detected cracks from each sampling stroke at the Nedre Røssåga headrace tunnel. B) Average number of detected cracks from each sampling stroke at the Nedre Røssåga headrace tunnel.

Item no. 2 - Distribution of the dip angles and the dip directions

Figure 5.11 shows the distribution of measured dip for the cracks from the Nedre Røssåga headrace tunnel. Independent of RPM and geology, most cracks have a dip below 30 degrees from the horizontal line. This amounts to around 40 % of the cracks. Except for the core samples from sampling chainage R_5478, there are more cracks with dip between 61 and 90 ° than between 31 and 60 °. This amounts to approximately 32 % and 27 % of the cracks.

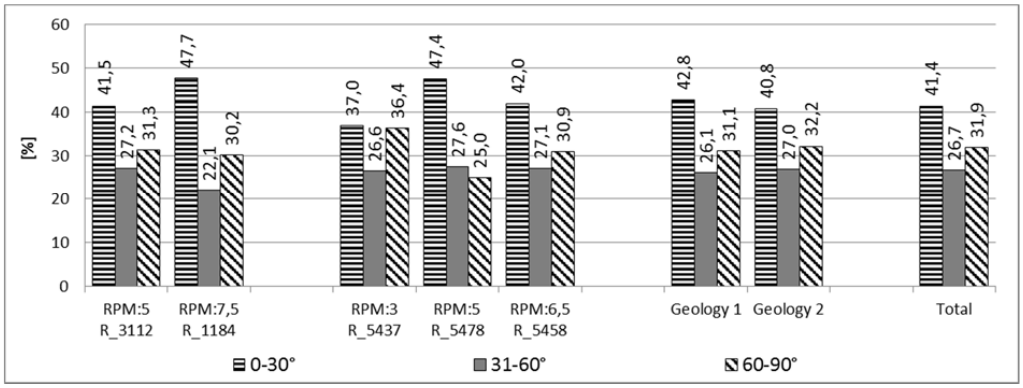

Figure 5.11: Distribution of dip angles for the cracks in the core samples from the Nedre Røssåga headrace tunnel.

An accumulated frequency distribution of the dip angles shows that except the number of cracks with dip angles of 0 °, the distribution of dip angles is even for all RPMs and both geologies.

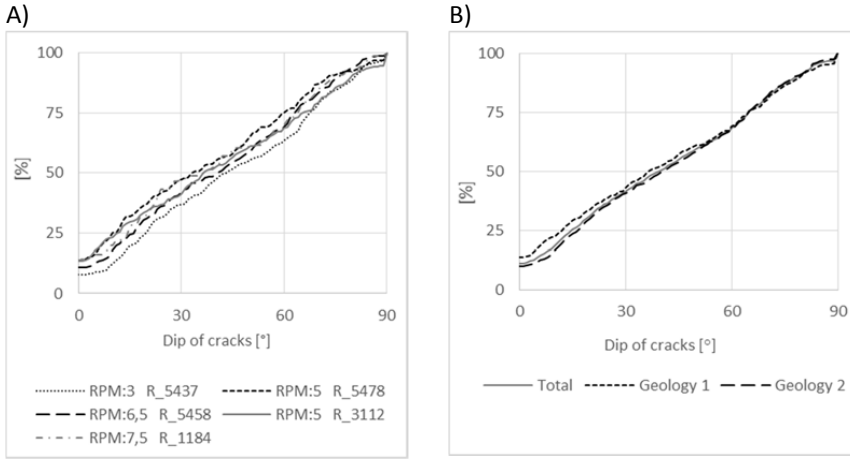

Figure 5.12: An accumulative frequency distribution of dip angles for the cracks in the core samples from the Nedre Røssåga headrace tunnel. A) All the sampling chainages individually. B) The two geologies individually and the total distribution for the core samples.

When cracks with dip less than 3 ° are excluded, more than half of the cracks have an orientation away from the cutter groove, independent of RPM and geology. This can be seen in Figure 5.13.

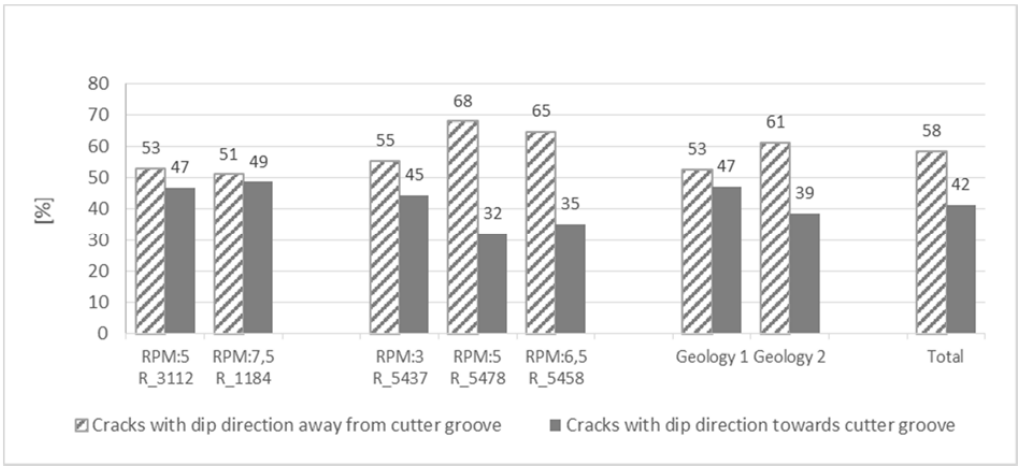

Figure 5.13: Distribution of dip direction for the cracks in the core samples from the Nedre Røssåga headrace tunnel.

Item no. 3 - Distribution of the horizontal lengths of the cracks

More than 70 % of all cracks, independent of geology and RPM, have a horizontal length of less than 15 mm, and only about 10 % have horizontal lengths that exceeds 30 mm. The exact distribution can be seen in Figure 5.14. The maximum horizontal lengths measured in the core samples from the five sampling chainages are, in the same order as in the plot below; 160, 139, 128, 96 and 149 mm.

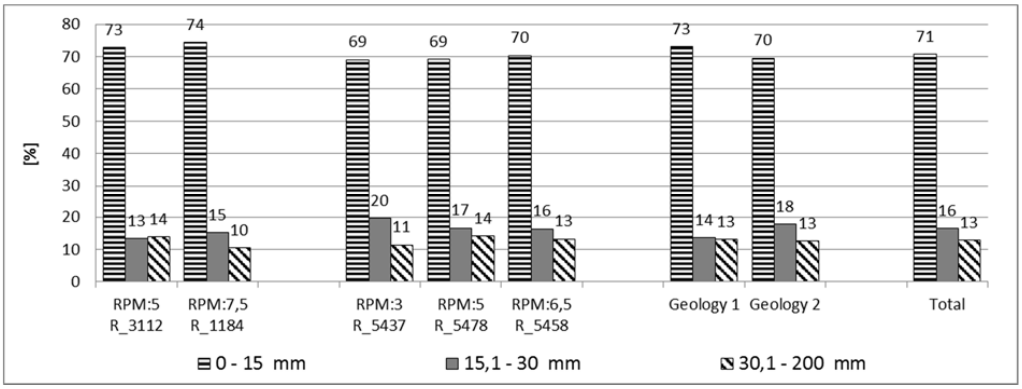

Figure 5.14: Distribution of horizontal length of cracks in the core samples from the Nedre Røssåga headrace tunnel.

Item no. 4 - Distribution of the vertical lengths of the cracks

More than 65 % of all cracks, independent of RPM and geology, have a vertical length of less than 15 mm, and only about 10 %have vertical lengths that exceeds 30 mm. The exact

distribution can be seen in Figure 5.15. The maximal vertical lengths measured in the core samples from the five sampling chainages are, in the same order as in the plot below; 142, 120, 120, 84 and 94 mm.

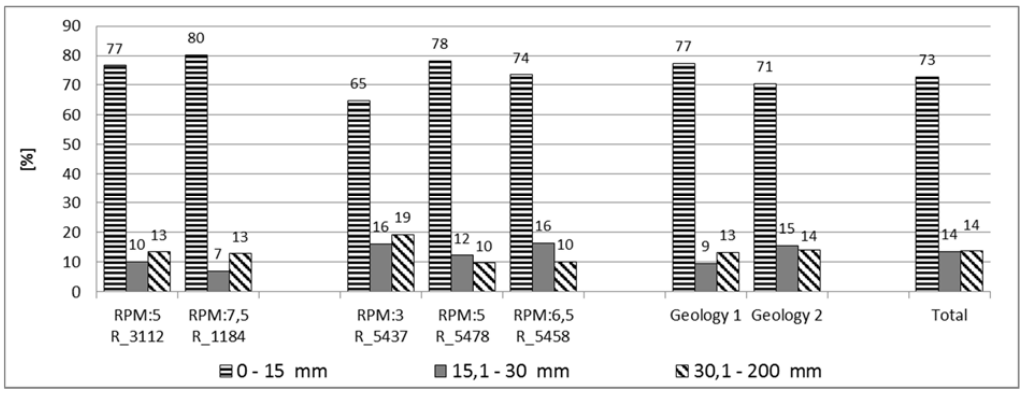

Figure 5.15: Distribution of vertical length of cracks in the core samples from the Nedre Røssåga headrace tunnel.

Item no. 5 - Distribution of the total lengths of the cracks

More than 59 % of all cracks, independent of RPM and geology, have a total length of less than 20 mm, and only about 15 % have total lengths that exceeds 40 mm. The exact distribution can be seen in Figure 5.16.

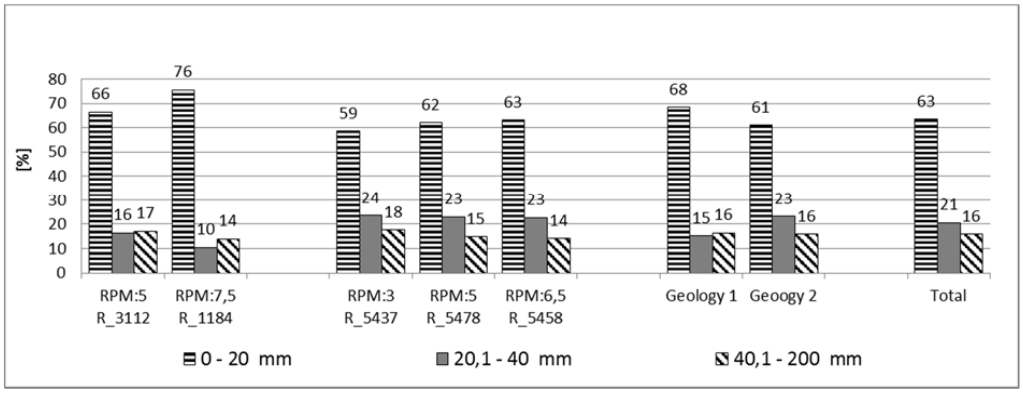

Figure 5.16: Distribution of total length of cracks in the core samples from the Nedre Røssåga headrace tunnel.

Figure 5.17 shows the accumulative frequency distribution of the total length for all documented cracks in the core samples from the Nedre Røssåga headrace tunnel. This plot shows that 80 % of all cracks have a total length of less than 35 mm. Only 10 % of the cracks have total lengths that exceeds 55 mm.

The maximal total lengths measured in the core samples from the five sampling chainages are, in the same order as in the plot above; 160, 139, 151, 101 and 155 mm.

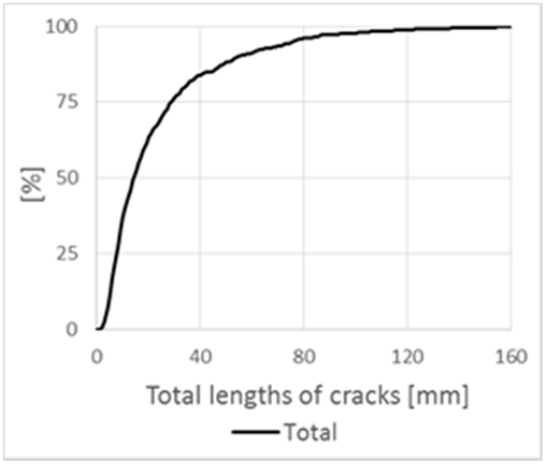

Figure 5.17: Accumulative frequency distribution of total length of cracks in the core samples from the Nedre Røssåga headrace tunnel.

Item no. 6 – Distribution of vertical distance from surface line to crack end

In the following *vertical distance from surface line to crack end* is referred to as *vertical depth from surface line.*

More than 67 % of all cracks, independent of RPM and geology reaches a vertical depth from surface line of less than 20 mm, and only about 10 % reaches a vertical depth that exceeds 40 mm. The exact distribution can be seen in Figure 5.18.

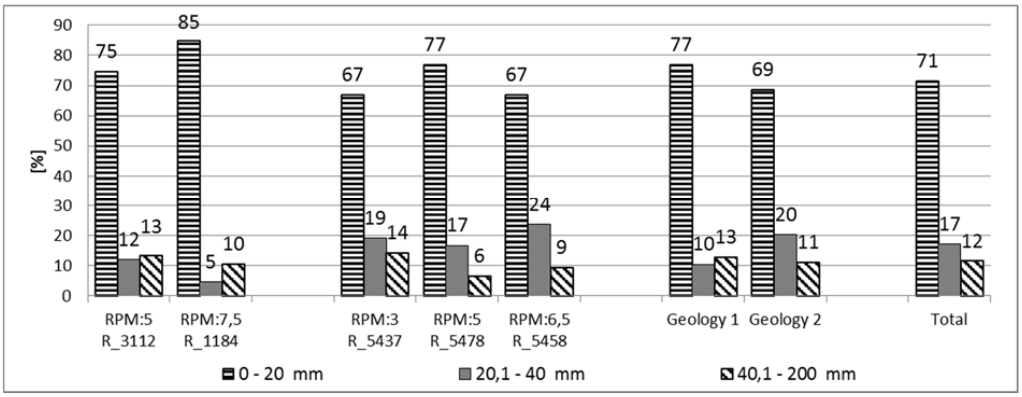

Figure 5.18: Distribution of depth from the surface line for cracks in the core samples from the Nedre Røssåga headrace tunnel.

Figure 5.19 shows the accumulative frequency distribution of the vertical depths from the surface line for all documented cracks in the core samples from the Nedre Røssåga headrace tunnel. This plot shows that 80 % of all cracks have a vertical depth from the surface line of less than 28 mm. Only 10 % of the cracks have vertical depths from the surface line that exceeds 43 mm.

The maximal vertical distances from the surface line measured in the core samples from the five sampling chainages are, in the same order as in the plot above; 154, 120, 120, 130, and 96 mm.

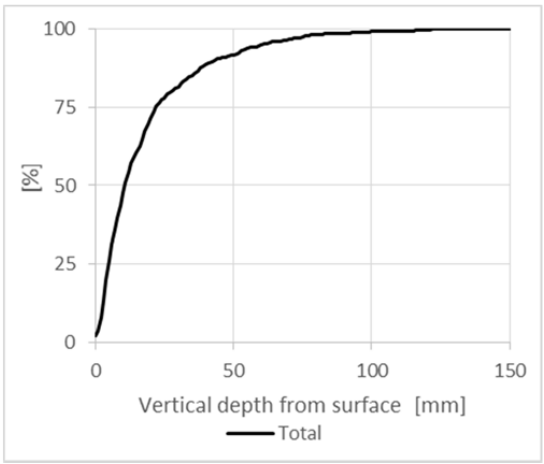

Figure 5.19: Accumulative frequency distribution of vertical depth from the surface line for cracks in the core samples from the Nedre Røssåga headrace tunnel.

Item no. 7 – Distribution of vertical distance from 0-line to crack end

In the following *vertical distance from 0-line to crack end* is referred to as *vertical depth from surface line.*

The distribution of vertical depth from the 0-line can be seen in Figure 5.20. This plot shows that there is more variation between the geologies in relation to vertical depth from the 0-line than it is in relation to vertical depth from the surface. In geology 2, there is a more even distribution between the intervals of 20 millimeters than in geology 1. In geology 2, only 40 % of the cracks have a vertical distance from the 0-line of less than 20 mm. In geology 1, this share is 60 %. The difference in share of cracks with vertical distance from the 0-line exceeding 40 millimeters is less, with 21 % in geology 2 and 18 % in geology 1.

The differences between the different RPMs within the two geologies are smaller than between the two geologies. The exception is in the core samples from sampling chainage R_5458. In these core samples, there are more cracks with vertical depth between 20 and 40 millimeters than cracks with vertical depth between 0 and 20 mm.

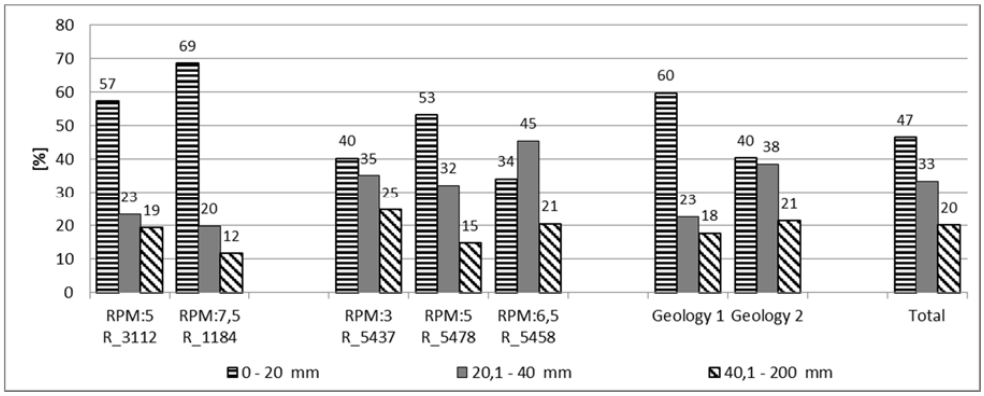

Figure 5.20: Distribution of vertical depth from the 0-line line for cracks in the core samples from the Nedre Røssåga headrace tunnel.

Figure 5.21 shows the accumulative frequency distribution of the vertical depths from the 0-line for all documented cracks in the core samples from the Nedre Røssåga headrace tunnel. This plot shows that 80 % of all cracks have a vertical depth from the 0-line line of less than 41 mm. Only 10 % of the cracks have vertical depths from the 0-line that exceeds 59 mm.

The maximal vertical distances from the 0-line measured in the core samples from the five sampling chainages are, in the same order as in the plot above; 158, 127, 123, 133 and 115 mm.

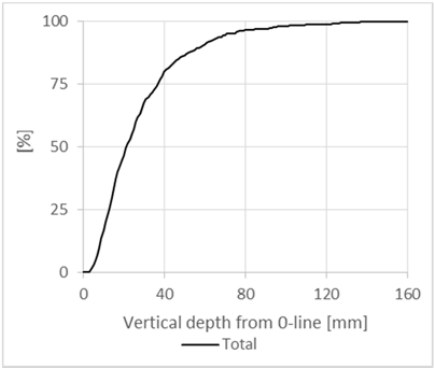

Figure 5.21: Accumulative frequency distribution of vertical depth from the 0-line for cracks in the core samples from the Nedre Røssåga headrace tunnel.

Item no. 8 - Distribution of horizontal distance from the point of origin to the cutter groove

Core sample R_5437_2-2_22 are not included in this evaluation due to incomplete core sample. Core sample R_5478_2-4_24/25 are not icluded due to sampling in between two cutter grooves.

As describes in chapter 4.6.3 *Quantification of cracks and core samples*, the point of origin for all cracks with a dip of less than 3 ° is defined as the left end of the crack on the digitalized

foldouts. Within the possibilities of the methods used in this Ph.D.-study it is not possible to define a precise point of origin for these cracks. The cracks with dip less than 3 ° are therefore not included in this evauation. This will be further discussed in chapter 7 *Discussion.*

Figure 5.22 shows the distribution of distribution of horizontal distance from the point of origin to the cutter groove for the cracks in the core samples from the Nedre Røssåga headrace tunnel. Note that the cutter spacing at Nedre Røssåga headrace tunnel was 78.6 mm. The reason why some points of origins have a point of origin that exceeds the half cutter spacing of 39,3 millimeters is because the core samples are not located excaxtly over the cutter groove. Also note that core sample R_1184-1-3_23 has a diamter of 55 mm. This affects the distribution to some extent, but because the majority of the cracks have a point of origin in relation ot the cutter groove of less than 40 mm, the core sample is included in this analyzis.

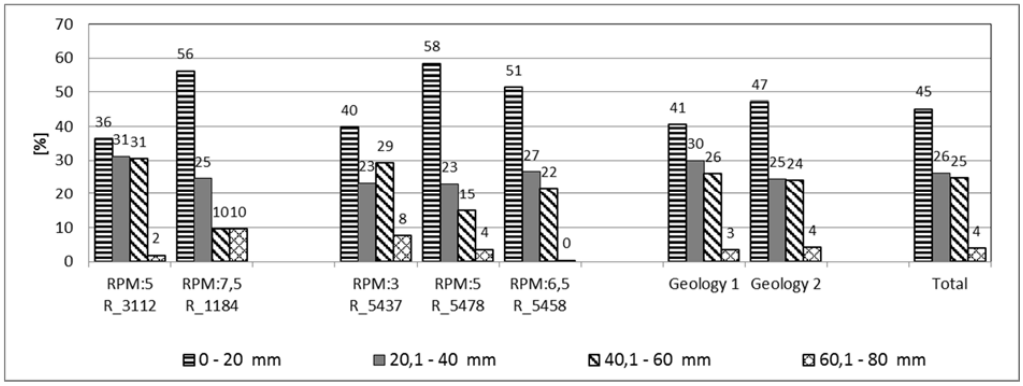

Figure 5.22: Distribution of distribution of horizontal distance from the point of origin to the cutter groove for cracks in the core samples from the Nedre Røssåga headrace tunnel. Cracks with dip < 3° are not included.

Figure 5.23 shows a accumulative frequency distribution of p distribution of horizontal distance from the point of origin to the cutter groove for cracks in the core samples from the Nedre Røssåga headrace tunnel. This plot shows that 50 % of the cracks have a point of origin in relation to the cutter groove of less than 24 mm. 70 % of all cracks have a point of origin less than half the cutter spacing of 39 mm.

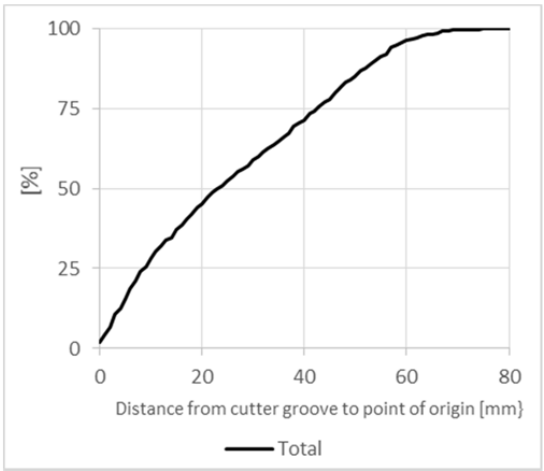

Figure 5.23: Accumulative frequency distribution of distribution of horizontal distance from the point of origin to the cutter groove for cracks in the core samples from the Nedre Røssåga headrace tunnel. Cracks with dip < 3° are not included.

Item no. 9 - Distribution of number of cracks on the two sides of the cutter groove

Core sample R_5437_2-2_22 and R_5478_2-4_24/25 are not included in these evaluations. Cracks with dip < 3° are included. This choise will be discussed in chapter 7.3 *On the rock breaking at the Nedre Røssåga* headrace tunnel.

Figure 5.24 shows the average number of crakcs with point of origin on the outside and on the center side of the cutter groove. This plot shows that, indpendent of geology and RPM, there have been documented more cracks on the outside of the cutter groove than on the center side in the core samples.

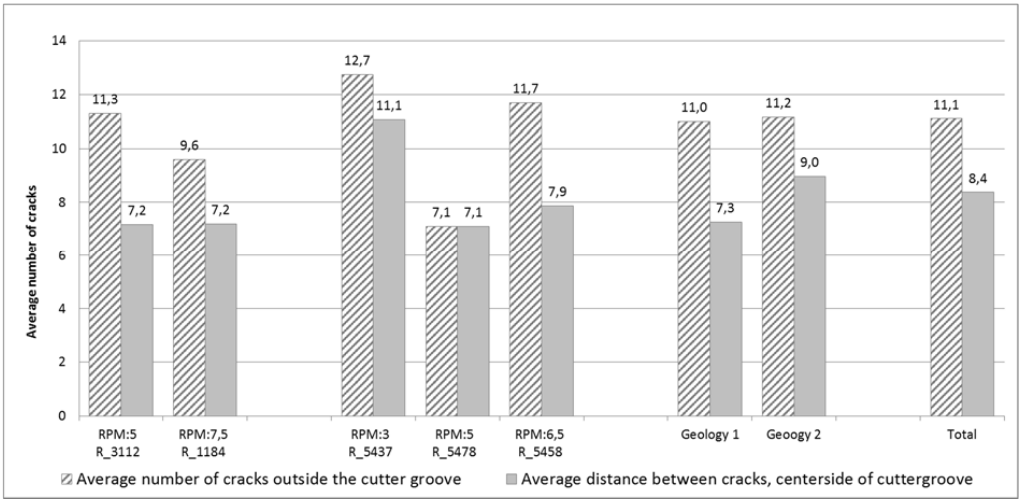

Figure 5.24: Average number of cracks with point of origin on the center side and outside the cutter groove in the core samples from the Nedre Røssåga headrace tunnel. Cracks with dip < 3° are not included.

Item no. 10 - Distribution of cracks perpendicular and parallel to the cutter groove

Core samples R_5437_2-2_22 and R_5478_2-4_24/25 are not included in thses evaluations. Cracks with dip < 3° are included. This choise will be discussed in chapter 7.3 On the rock breaking at the Nedre Røssåga headrace tunnel

As described in chapter 4.7.2 Remarks and explanations, the previous plot ony differentiates between the center side and the out side of the cutter groove, and presuppose that the cutter groove is passing through the center point of the core. This data, hovewer, suggests that this is not the case for all core samples. This potential difference in area on the two sides of the cutter groove must be considered. To do that, the initiationpoints at the surface are projected from the circel line to the cutter groove, and to an imaginary line passing through the center of the core, perpendicular to the cutter groove. The average distance between the cracks on both sides of the cutter groove can then be calculated for both sides of cutter groove. The real area on both sides is also considered.

Figure 5.25 shows the calculated average distance per crack along a fictive line perpendicular to the cutter grooves in the core samples. This is calculated by using the summarized number of cracks and the summarized length of the fictive line perpendicular the cutter grooves in each group. This plot shows that there is less difference between the two sides of the cutter than it was when only the number of cracks was considered. For both geologies, there is a higher average distance between the cracks outside the cutter groove than on the center side of the cutter groove, but this is not valid for the individual sampling chainages in geology 2. In the core samples from sampling chainage R_5437 there average distance is equal on both sides. For sampling chainage R_5458 the average distance between the cracks is highest on the center side of the cutter groove and lowest on the outside of the cutter groove, while it is opposite for sampling chainage R_5478.

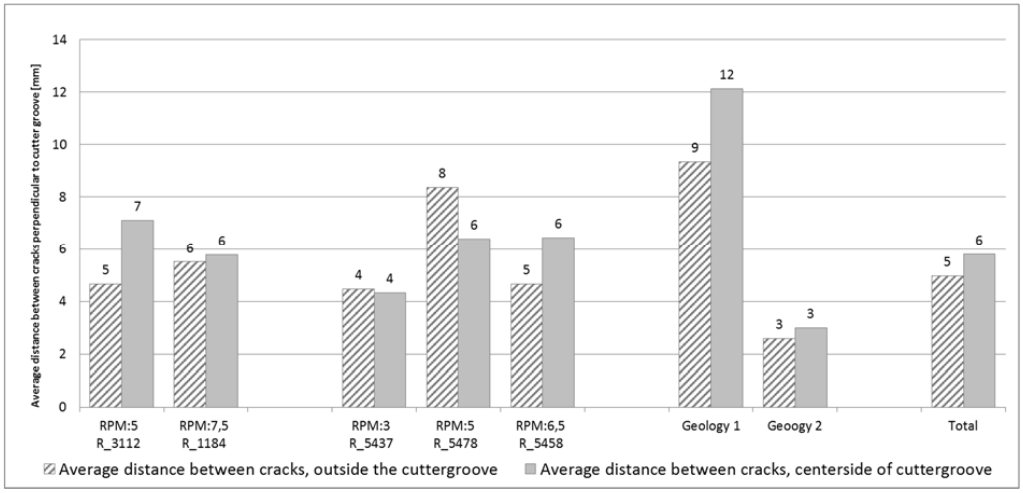

Figure 5.25: Average distance between cracks perpendicular cutter groove on the center side and outside the cutter groove, and totally in the core samples from the Nedre Røssåga headrace tunnel.

Figure 5.26 shows the calculated average distance per crack along the cutter groove in the core samples. This is calculated by using the summarized number of cracks and the summarized length of the cutter grooves in each group. With this approach, the average

distance between the cracks is highest on the center side of the cutter groove, independent of geology and RPM, except for the core samples from R_5478. For these core samples, the average distance between the cracks is equal on both sides of the cutter groove.

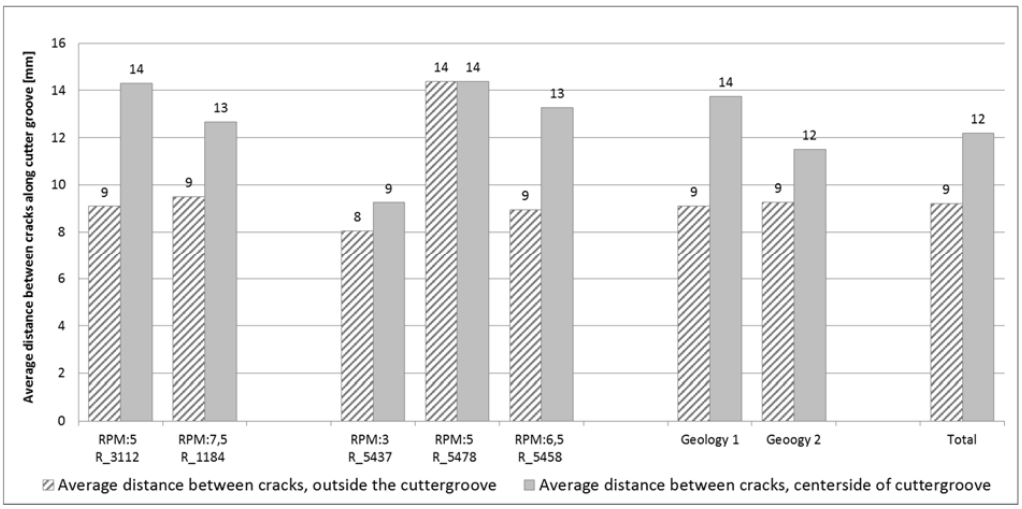

Figure 5.26: Average distance between cracks along cutter groove on the center side and outside the cutter groove, and totally in the core samples from the Nedre Røssåga headrace tunnel.

Figure 5.27 shows the calculated average are per crack in the core samples. These values are calculated by using the summarized number of cracks and the summarized area between the cutter groove and the circumference of the core on each side of the cutter groove in each group. By way of comparison, the area of a circle with a diameter of 10,4 centimeters is 8586 mm^2. As for the plot above, this plot shows that the average area per crack is highest on the center side of the cutter groove, independent of geology and RPM.

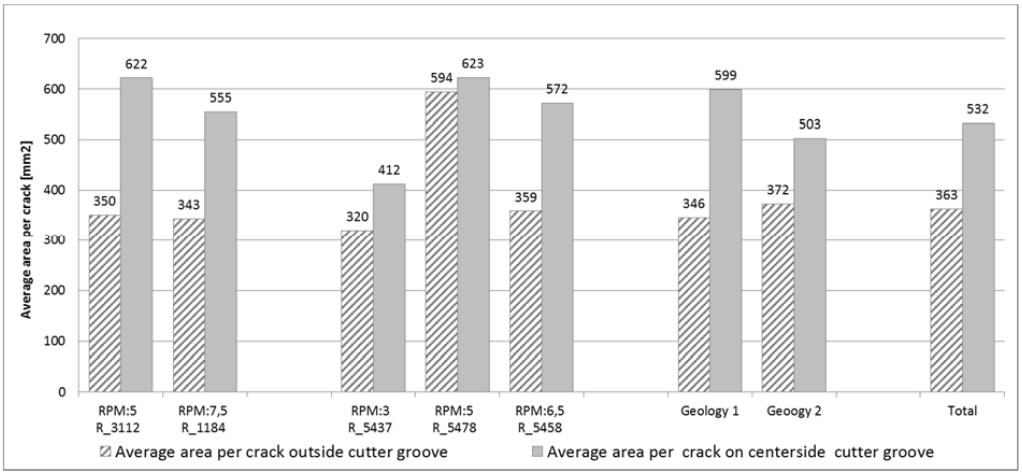

Figure 5.27: Average area per crack on the center side and outside the cutter groove, and totally in the core samples from the Nedre Røssåga headrace tunnel.

Item no. 11 - Dip of cracks versus average horizontal length of cracks

Figure 5.28 shows the calculated average horizontal length of cracks with dips within intervals of 10 ° in the core samples from the Nedre Røssåga headrace tunnel. These plots show that there are some differences between the RPMs and the two geologies. In geology 1, the calculated average horizontal length of the cracks are higher in the core samples from R_3112 compared to R_1184 as long as the dip of the cracks are less than 60 °. From 60 ° to 90 °, the cracks from R_1184 have a higher calculated average horizontal length. In geology 2, there are more variations, but the core samples from R_5437 have the highest calculated average horizontal length except for the cracks with dip from 0° to 10 °.

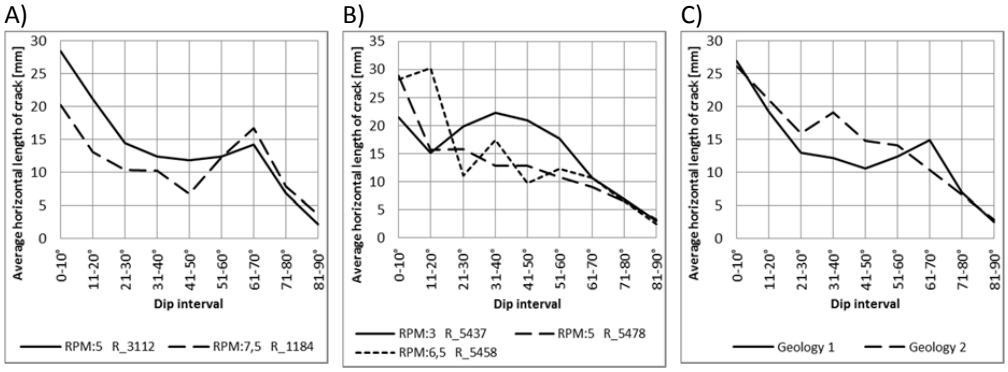

Figure 5.28: Calculated average horizontal lengths of cracks with dips within intervals of 10 ° in the core samples from the Nedre Røssåga headrace tunnel. A) Sampling chainage R_3112 and R_1184. B) Sampling chainages R_5437, R_5478 and R_5458. C) Geology 1 and geology 2.

Item no. 12 - Dip of cracks versus average vertical length of cracks

Figure 5.29 shows the calculated average vertical length of cracks with dips within intervals of 10 ° in the core samples from the Nedre Røssåga headrace tunnel. These plots show that there are some differences between the RPMs and the two geologies. As for the horizontal length of cracks, the calculated average vertical length of the cracks are higher in the core samples from R_3112 compared to R_1184 as long as the dip of the cracks are less than 60 °. From 60 ° to 90 °, the cracks from R_1184 have a higher calculated average horizontal length.

In geology 2, there are more variations, but the core samples from R_5437 have the highest calculated average horizontal length except for the cracks with dip from 0° to 30 °.

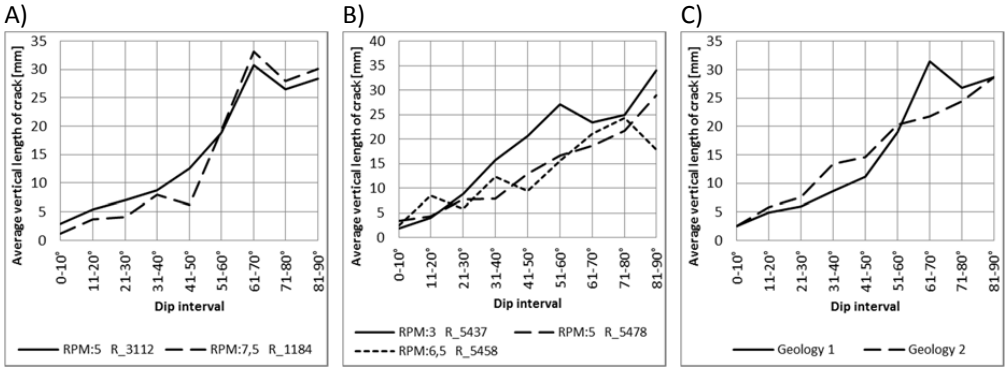

Figure 5.29: Calculated average vertical lengths of cracks with dips within intervals of 10 ° in the core samples from the Nedre Røssåga headrace tunnel. A) Sampling chainage R_3112 and R_1184. B) Sampling chainages R_5437, R_5478 and R_5458. C) Geology 1 and geology 2.

Item no. 13 - Dip of cracks versus average total length of cracks

Figure 5.30 shows the calculated average total length of cracks with dips within intervals of 10 ° in the core samples from the Nedre Røssåga headrace tunnel. These plots show that there are some differences between the RPMs and the two geologies. As for the horizontal and vertical length of cracks, the calculated average vertical length of the cracks are higher in the core samples from R_3112 compared to R_1184 as long as the dip of the cracks are less than 60 °. From 60 ° to 90 °, the cracks from R_1184 have a higher calculated average total length.

In geology 2, there are more variations, but the core samples from R_5437 have the highest calculated average total length except for the cracks with dip from 0° to 30 °.

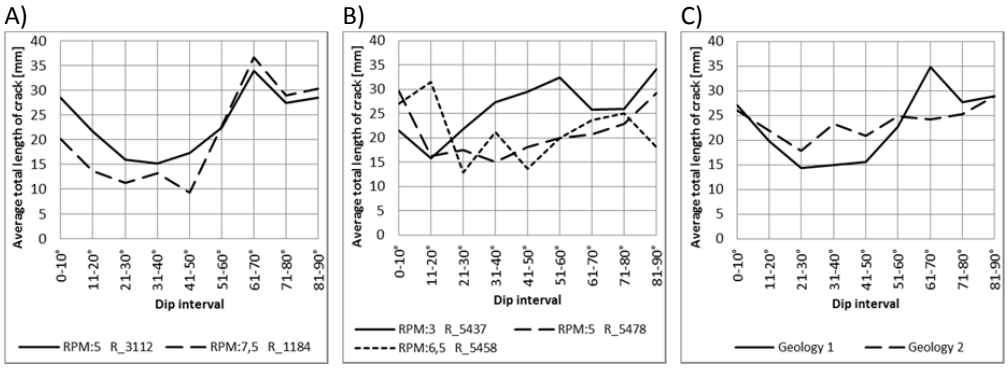

Figure 5.30: Calculated average total lengths of cracks with dips within intervals of 10 ° in the core samples from the Nedre Røssåga headrace tunnel. A) Sampling chainage R_3112 and R_1184. B) Sampling chainages R_5437, R_5478 and R_5458. C) Geology 1 and geology 2.

Item no. 14 - Dip of cracks versus average vertical distance from surface to crack end

In the following *vertical distance from surface line to crack end* is referred to as *vertical depth from surface line.*

Figure 5.31 shows the calculated average vertical depth from the surface line for cracks with dips within intervals of 10 ° in the core samples from the Nedre Røssåga headrace tunnel. These plots show that there are some differences between the RPMs and the two geologies. In geology 1, the average vertical depth from the surface line is higher in the core samples from R_3112 than in the core samples from R_1184, independent of dip of cracks.

In geology 2, there are more variations, but the core samples from R_5437 have the highest calculated average total length except for the cracks with dip from 0° to 30 ° and the cracks with dip between 71 to 80 °.

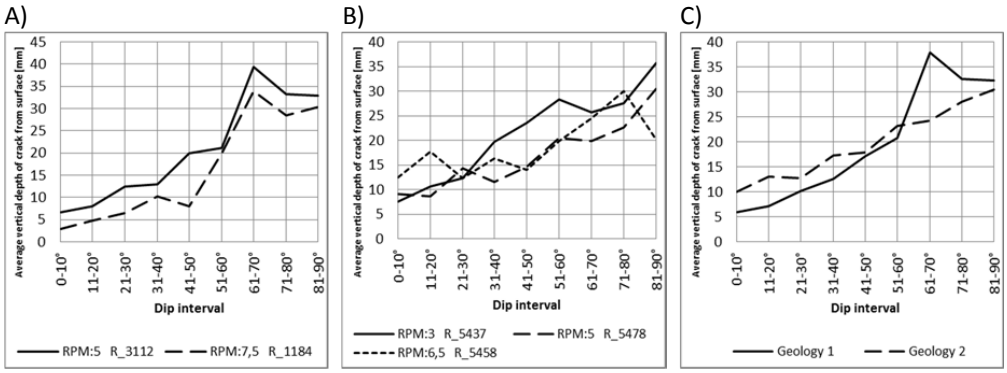

Figure 5.31: Calculated average vertical depths from the surface line for the cracks with dips within intervals of 10 ° in the core samples from the Nedre Røssåga headrace tunnel. A) Sampling chainage R_3112 and R_1184. B) Sampling chainages R_5437, R_5478 and R_5458. C) Geology 1 and geology 2.

Figure 5.32 shows the calculated vertical depth from the surface line for all cracks in the core samples from the Nedre Røssåga headrace tunnel. This plot shows that the average calculated vertical depth from the surface line is 18 millimeters in both geologies, but that there are some differences between the different RPMs. In geology 1, the calculated average vertical depth from the surface is higher in the core samples from R_3112 than in the core samples from R_1184. In geology 2, the highest average vertical depth from the surface line is in the core samples from R_5437 and that it is lowest in the core samples from R_5478.

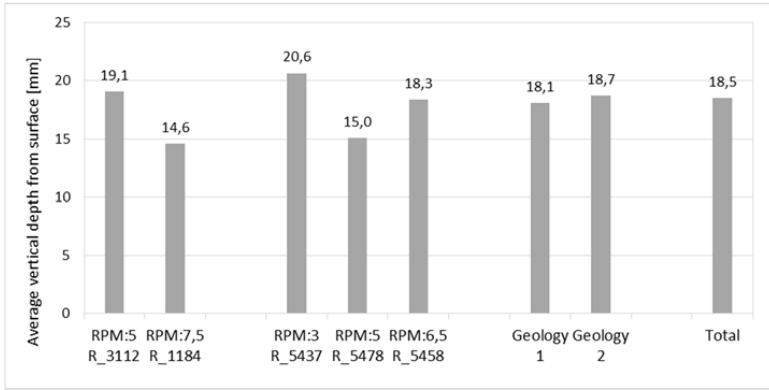

Figure 5.32: Calculated average vertical depths from the surface line for all cracks in the core samples from the Nedre Røssåga headrace tunnel.

Item no. 15 - Dip of cracks versus average vertical distance from 0-line to crack end

In the following *vertical distance from surface line to crack end* is referred to as *vertical depth from the 0-line.*

Figure 5.33 shows the calculated average vertical depth from the 0-line line for cracks with dips within intervals of 10 ° in the core samples from the Nedre Røssåga headrace tunnel. These plots show that there are some differences between the RPMs and the two geologies. In geology 1, the average vertical depth from the surface line is higher in the core samples from R_3112 than in the core samples from R_1184, independent of dip of cracks.

In geology 2, there are more variations, but the core samples from R_5437 have the highest calculated average total length except for the cracks with dip from 0° to 30 ° and the cracks with dip between 71 to 80 °.

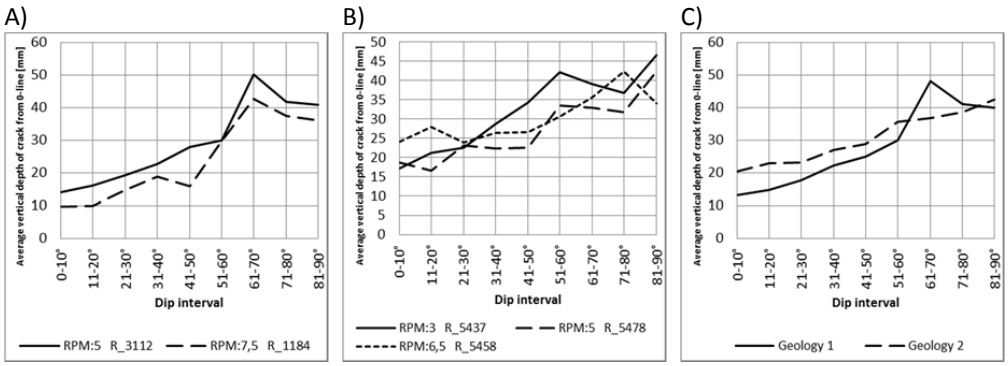

Figure 5.33: Calculated average vertical depths from the 0-line line for the cracks with dips within intervals of 10 ° in the core samples from the Nedre Røssåga headrace tunnel. A) Sampling chainage R_3112 and R_1184. B) Sampling chainages R_5437, R_5478 and R_5458. C) Geology 1 and geology 2.

Figure 5.34 shows the calculated vertical depth from the 0-line line for all cracks in the core samples from the Nedre Røssåga headrace tunnel. This plot shows that there are some differences between the different RPMs and the two geologies. In geology 1, the calculated average vertical depth from the surface is higher in the core samples from R_3112 than in the core samples from R_1184. In geology 2, the highest average vertical depth from the surface line is in the core samples from R_5437 and that it is lowest in the core samples from R_5478.

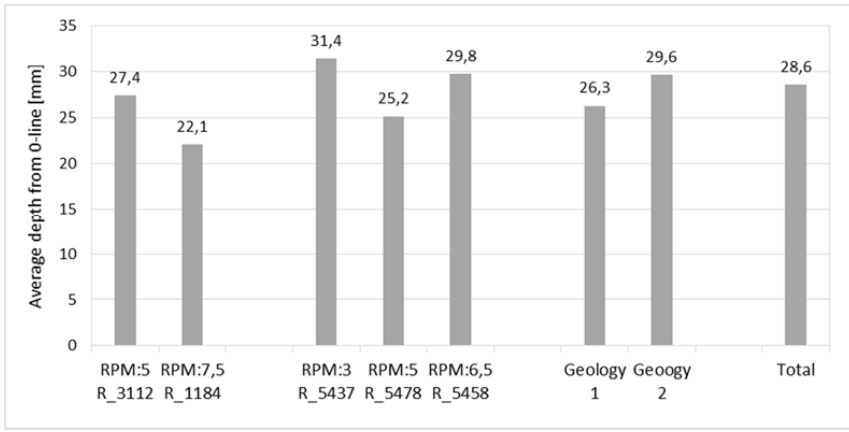

Figure 5.34: Calculated average vertical depths from the 0-ine line for all cracks in the core samples from the Nedre Røssåga headrace tunnel.

Item no. 16 - Dip of cracks versus horizontal distance from the point of origin to the cutter groove

Cracks with dip < 3° and core sample R_5437_2-2_22 and R_5478_2-4_24/25 are not included in this evaluation.

Figure 5.35 and Figure 5.36 show the distribution of dip inclinations related to horizontal distance from the point of origin to the cutter groove in the core samples from the Nedre Røssåga headrace tunnel.

For geology 1, the distribution of dip inclinations are more evenly distributed, independent of point of origin in the core samples from R_3112 compared to the core samples from R_1184. For geology 2, the distribution of dip inclinations are more evenly distributed, independent of point of origin in the core samples from R_5437 compared to the core samples from R_1184. Within geology 2, the most even distribution is in the core samples from R_5437.

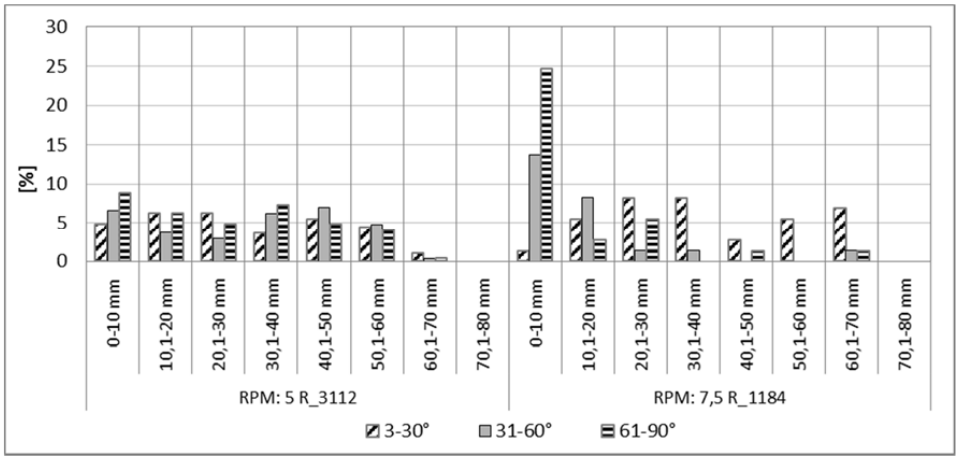

Figure 5.35: Distribution of dip inclinations in relation to horizontal distance from the point of origin to the cutter groove for the core samples from geology 1 at the Nedre Røssåga headrace tunnel.

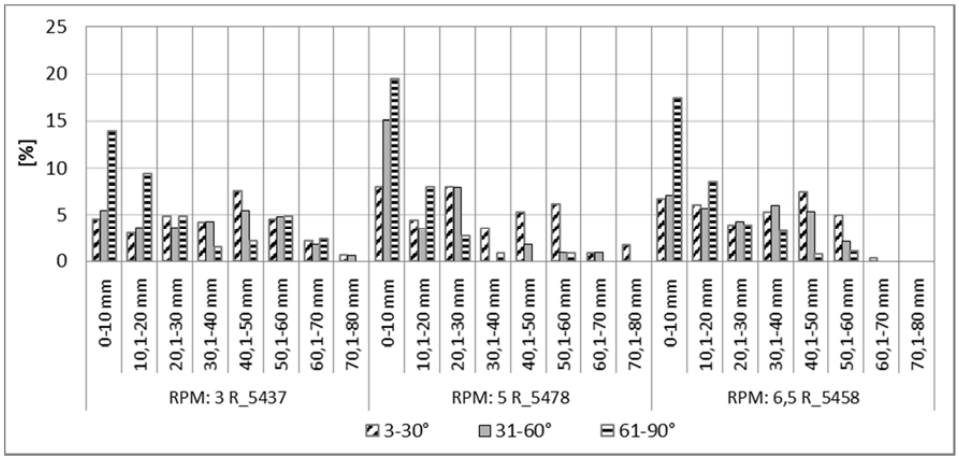

Figure 5.36: Distribution of dip inclinations in relation to horizontal distance from the point of origin to the cutter groove for the core samples from geology 2 at the Nedre Røssåga headrace tunnel.

Item no. 17 - Horizontal distance from point of origin to cutter groove versus dip angles and dip direction of crack

Cracks with dip < 3° and core sample R_5437_2-2_22 and R_5478_2-4_24/25 are not included in these evaluations.

Figure 5.37 shows the distribution of dip directions related to the point of origin in relation to the cutter groove for the core samples from the Nedre Røssåga headrace tunnel. This plot shows that there is a more even distribution of dip directions in the core samples from R_3112 and R_5437 than in the other core samples. The core samples from R_5478 have the most uneaven distribution.

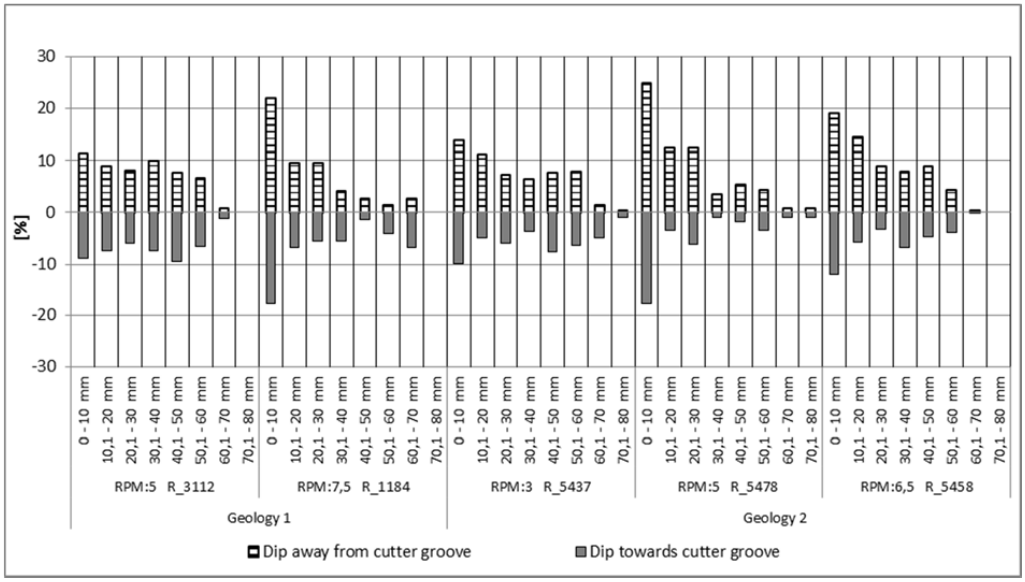

Figure 5.37: Distribution of dip directions in relation to horizontal distance from the point of origin to the cutter groove for the core samples from the Nedre Røssåga headrace tunnel.

The plot above differentiates between dip directions towards and away from the cutter groove and the absolute point of origin in relation to the cutter in to consideration. Figure 5.39 and Figure 5.40 show dip values, dip directions and the exact point of origin in relation to the cutter groove for all cracks in geology 1 and 2 at the Nedre Røssåga headrace tunnel. Negative distances to the point of origin represent the cracks on the outside of the cutter groove, and the positive distances represent cracks on the center side of the cutter groove. Negative dip values represents cracks with dip towards the cutter groove, and the positive values represents cracks with dip away from the cutter groove, see definitions in Figure 5.38.

Figure 5.39 presents the data from the core samples from R_3112 and R_1184. The figure shows that there is a more even distribution between dips, dip directions and point of origin in relation to the cutter groove for the core samples from R_3112 than for the core samples from R_1184. At both sampling chainages, there is a slight predominance of cracks with dip away from the utter grove, and cracks with point of origin on the outside of the cutter groove.

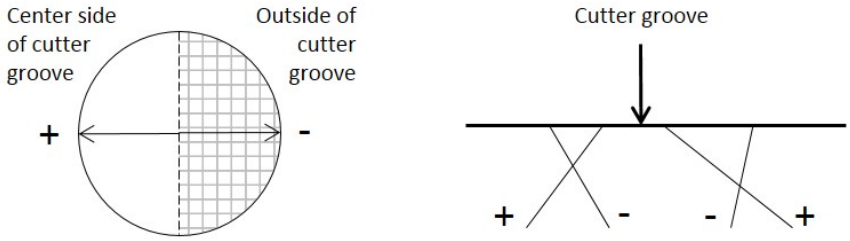

Figure 5.38: Definitions of positive and negative values of dip and distances from the point of origin to the cutter groove.

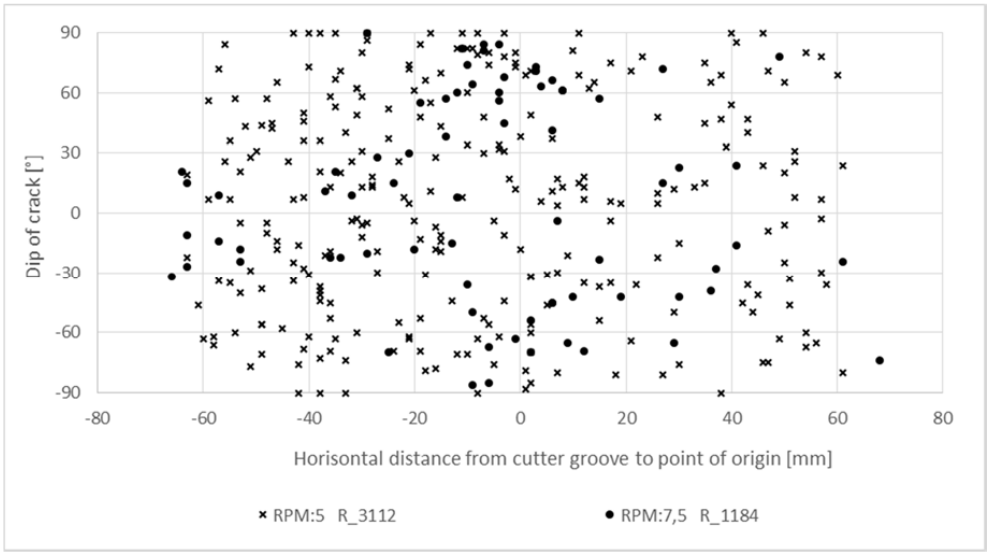

Figure 5.39: Dip inclinations, dip direction and exact point of origin in relation to the cutter groove for all cracks with dip >3° in the core samples from geology 1 at the Nedre Røssåga headrace tunnel.

Figure 5.40 presents the data from the core samples from R_5437, R_5478 and R_5458. The figure shows that there is a more even distribution between dip inclinations, dip directions and point of origin in relation to the cutter groove for the core samples from R_5437 than for the core samples from R_5478 and R_5458. At the same time, there is a more even distribution in the core samples from R_5478 than from R_5458. At all sampling chainages, there is a slight predominance of cracks with dip away from the cutter grove, and cracks with point of origin on the outside of the cutter groove.

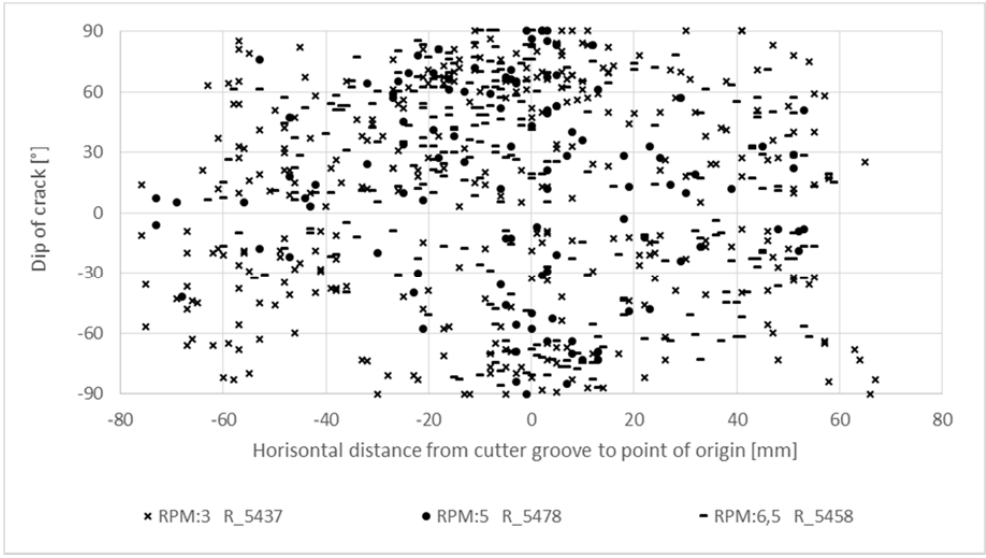

Figure 5.40: Dip inclinations, dip direction and exact point of origin in relation to the cutter groove for all cracks with dip >3° in the core samples from geology 2 at the Nedre Røssåga headrace tunnel.

Item no. 18 - Horizontal distance from point of origin to cutter groove versus total length of crack

Cracks with dip < 3° and core sample R_5437_2-2_22 and R_5478_2-4_24/25 are not included in this evaluations.

Figure 5.41 presents the data from the core samples from R_3112 and R_1184. This plot shows that there is a more even distribution between the total lengths and point of origin in relation to the cutter groove for the core samples from R_3112 than for the core samples from R_1184. At both sampling chainages, there is a slight predominance of cracks point of origin on the outside of the cutter groove.

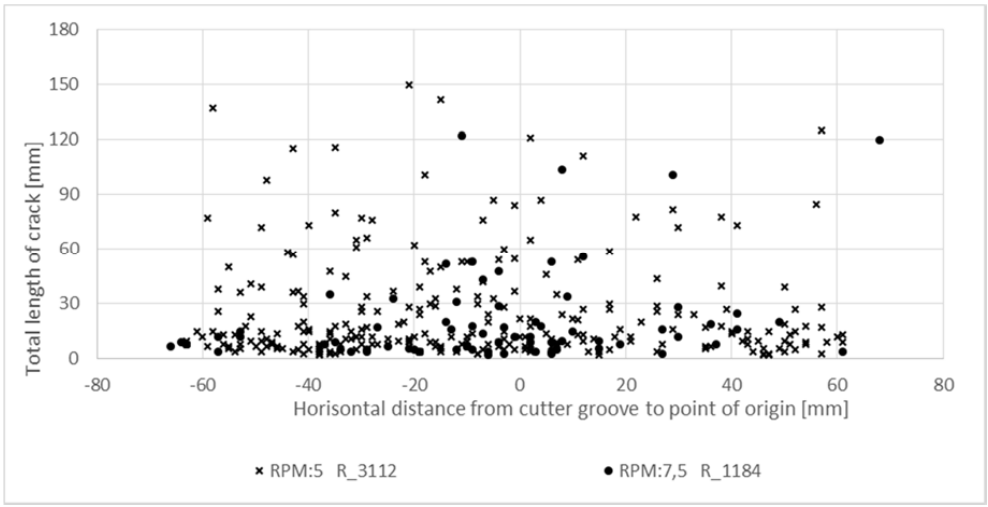

Figure 5.41: Total length of cracks and exact horizontal distance from the point of origin to the cutter groove for all cracks with dip >3° in the core samples from geology 1 at the Nedre Røssåga headrace tunnel.

Figure 5.42 presents the data from the core samples from R_5437, R_5478 and R_5458. This plot shows that there is a more even distribution between the total lengths and point of origin in relation to the cutter groove for the core samples from R_5437 than for the core samples from R_5478 and R_5458. At the same time, there is a more even distribution in the core samples from R_5478 than from R_5458. At all sampling chainages, there is a slight predominance of cracks point of origin on the outside of the cutter groove.

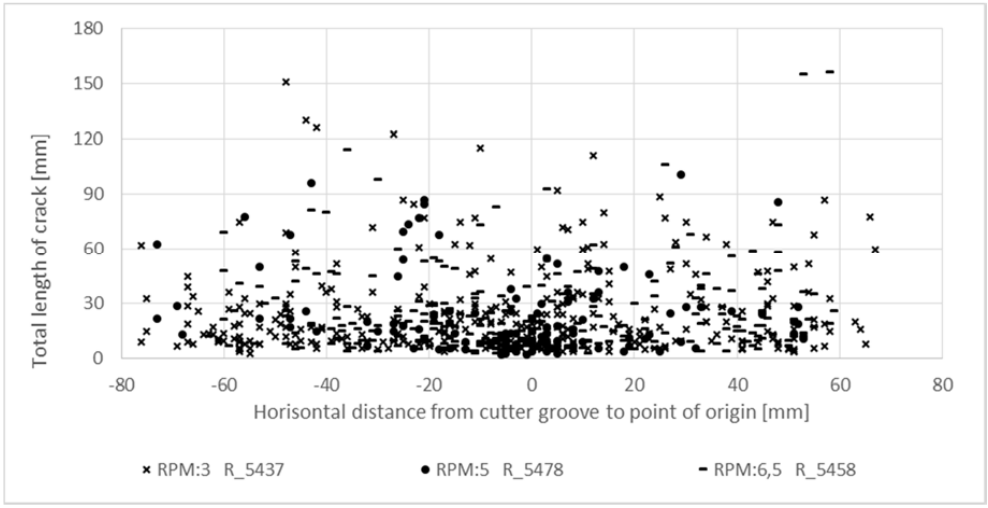

Figure 5.42: Total length of cracks and exact horizontal distance from the point of origin to the cutter groove for all cracks with dip >3° in the core samples from geology 2 at the Nedre Røssåga headrace tunnel.

Item no. 19 - Horizontal distance from point of origin to cutter groove versus vertical distance from surface line to end of crack

In the following *vertical distance from surface line to crack end* is referred to as *vertical depth from surface line.*

Cracks with dip < 3° and core sample R_5437_2-2_22 and R_5478_2-4_24/25 are not included in these evaluations.

Figure 5.43 presents the data from the core samples from R_3112 and R_1184. This plot shows that there is a more even distribution between the vertical depths from the surface line and point of origin in relation to the cutter groove for the core samples from R_3112 than for the core samples from R_1184. At both sampling chainages, there is a slight predominance of cracks point of origin on the outside of the cutter groove.

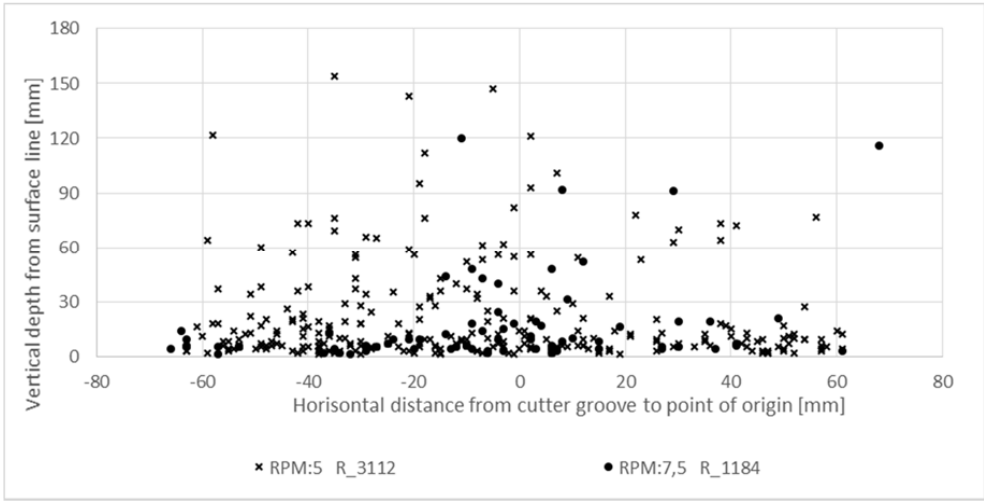

Figure 5.43: Depth from the surface line of cracks and exact point of origin in relation to the cutter groove for all cracks with dip >3°in the core samples from geology 1 at the Nedre Røssåga headrace tunnel.

Figure 5.44 presents the data from the core samples from R_5437, R_5478 and R_5458. This plot shows that there is a more even distribution between the vertical depth from the surface line and point of origin in relation to the cutter groove for the core samples from R_5437 than for the core samples from R_5478 and R_5458. At the same time, there is a more even distribution in the core samples from R_5458 than from R_5478. At both sampling chainages, there is a slight predominance of cracks point of origin on the outside of the cutter groove.

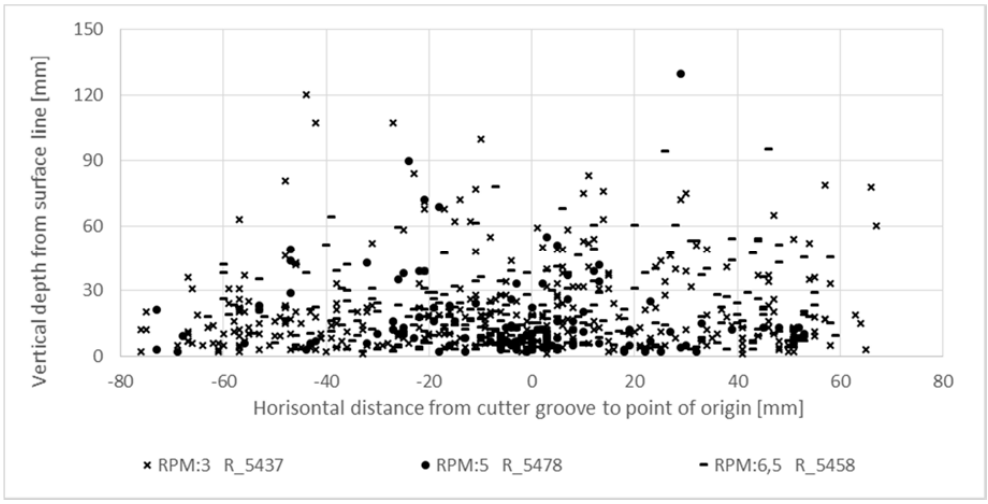

Figure 5.44: Depth from the surface line of cracks and exact point of origin in relation to the cutter groove for all cracks with dip >3°in the core samples from geology 2 at the Nedre Røssåga headrace tunnel.

Item no. 20 - Horizontal distance from point of origin to cutter groove versus vertical distance from 0-line to end of crack

In the following *vertical distance from surface line to crack end* is referred to as *vertical depth from 0-line.*

Cracks with dip < 3° and core sample R_5437_2-2_22 and R_5478_2-4_24/25 are not included in these evaluations.

Figure 5.45 presents the data from the core samples from R_3112 and R_1184. This plot shows that there is a more even distribution between the vertical depths from the 0-line and point of origin in relation to the cutter groove for the core samples from R_3112 than for the core samples from R_1184. At both sampling chainages, there is a slight predominance of cracks point of origin on the outside of the cutter groove.

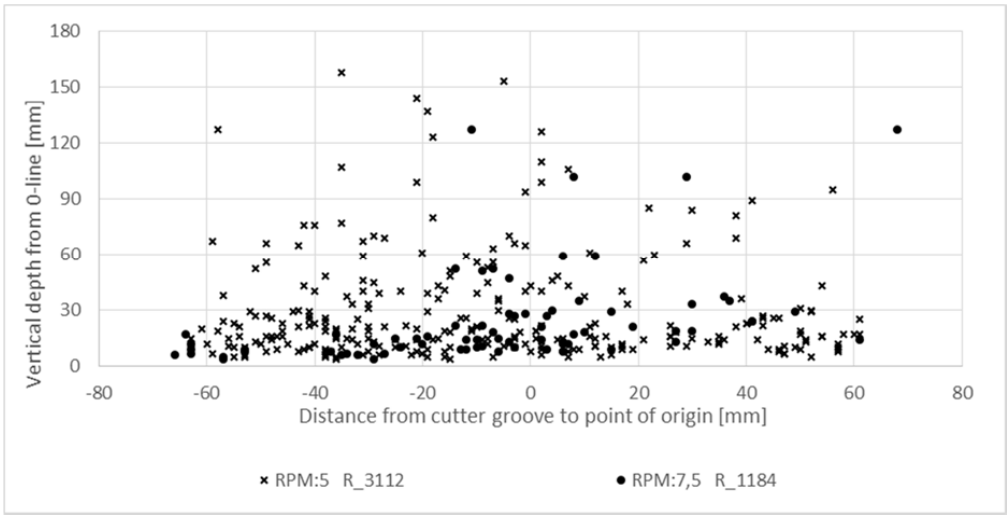

Figure 5.45: Depth from the 0-line of cracks and exact point of origin in relation to the cutter groove for all cracks with dip >3° in the core samples from geology 1 at the Nedre Røssåga headrace tunnel.

Figure 5.46 presents a linear trend line for the data from the core samples from R_5437, R_5478 and R_5458. This plot shows that there is a more even distribution between the vertical depth from the 0-line line and point of origin in relation to the cutter groove for the core samples from R_5437 than for the core samples from R_5478 and R_5458. At the same time, there is a more even distribution in the core samples from R_5478 than from R_5458. At both sampling chainages, there is a slight predominance of cracks point of origin on the outside of the cutter groove.

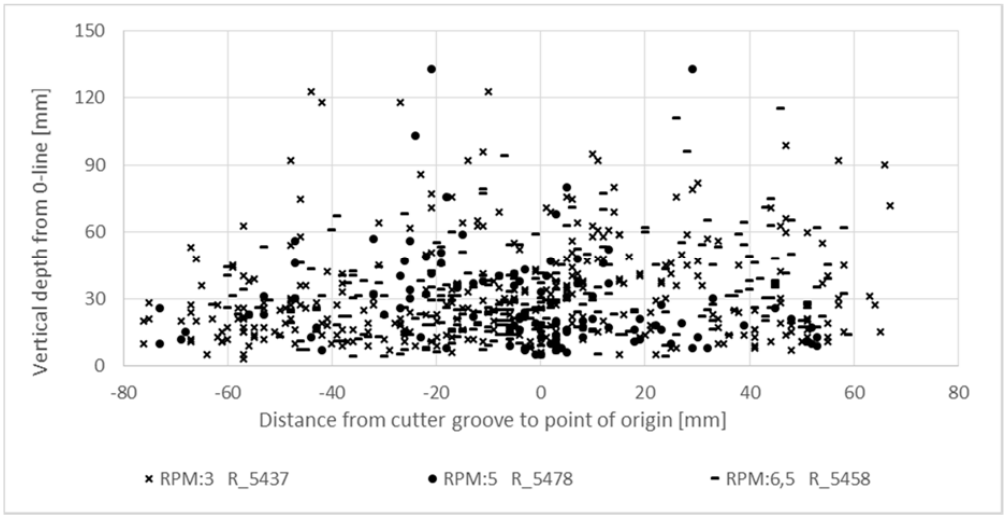

Figure 5.46: Depth from the 0-line of cracks and exact point of origin in relation to the cutter groove for all cracks with dip >3° in the core samples from geology 2 at the Nedre Røssåga headrace tunnel.

5.3 Rock breaking at the LCT

Due to the low number of core samples, the small diameter and the positioning of the core samples, there are uncertainties concerning a direct comparison of the findings from the Nedre Røssåga headrace tunnel with the findings from the linear cutter test. Nevertheless, a comparison of the accumulative frequency distributions of dip inclinations, total length and vertical depth from the 0-line and the distribution of dip direction in relation to the cutter groove can give some indications concerning any similarities or differences in rock breaking under the disc cutter of a LCT and the disc cutters of a full size TBM. In addition, and a visual evaluation of the fracturing patterns can give some indications concerning similarities and differences in fracturing patterns.

Figure 5.47 shows a selection of three digitalized foldouts that presents three different types of crack patterns in the core samples from the LCT. The digitalized foldouts show that there is a variety of crack patterns and surfaces in the core samples from the LCT. Note that Figure 5.47C represents a core sample that was located between two cutter grooves, and therefore has no cutter groove passing over the core sample.

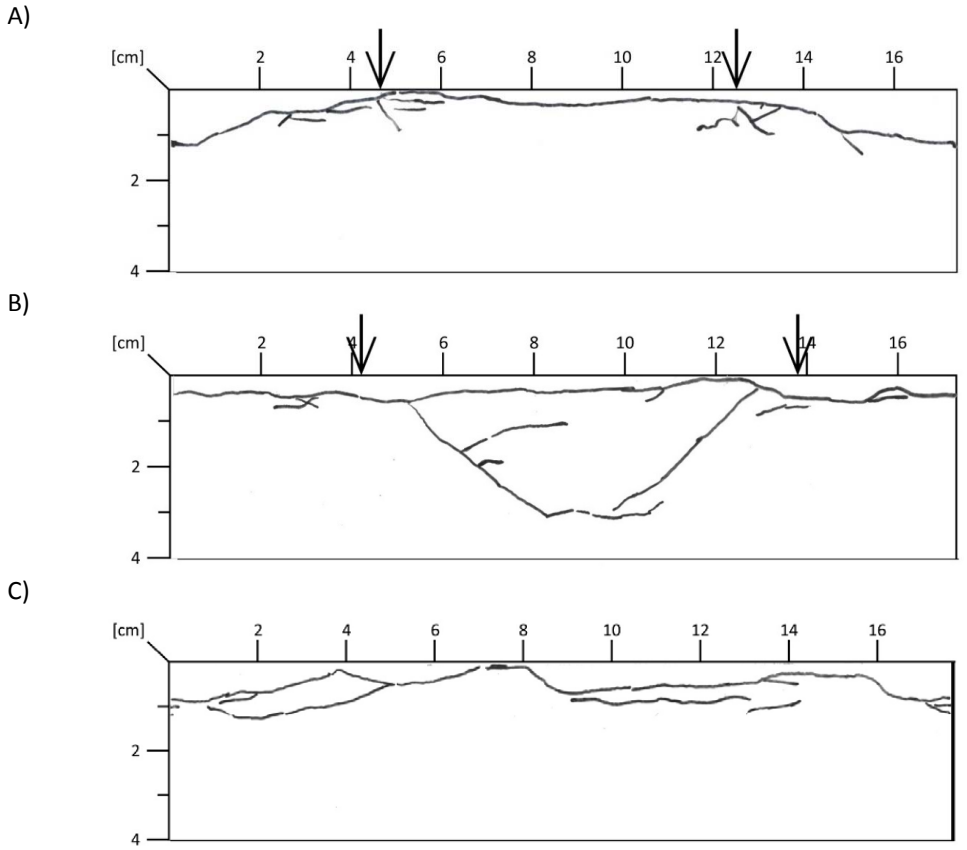

Figure 5.47: Digitalized foldout with crack patterns. The arrows represent the center of the cutter groove. A) Core sample LCT_80_1-1. B) Core sample LCT_80_1-2. C) Core sample LCT_100_2-1. Note that this core sample is from the area between two cutter grooves, and therefore does not have any cutter groove markings.

Figure 5.48 shows the accumulative frequency distribution of dip angle and the distribution of dip directions in reference to the cutter groove. These plots show that the distribution of dip directions in relation to the cutter groove is almost identical in the core samples from the LCT and the full size TBM at the Nedre Røssåga headrace tunnel, and that there is a difference in the accumulative distribution of dip angles.

A) B)

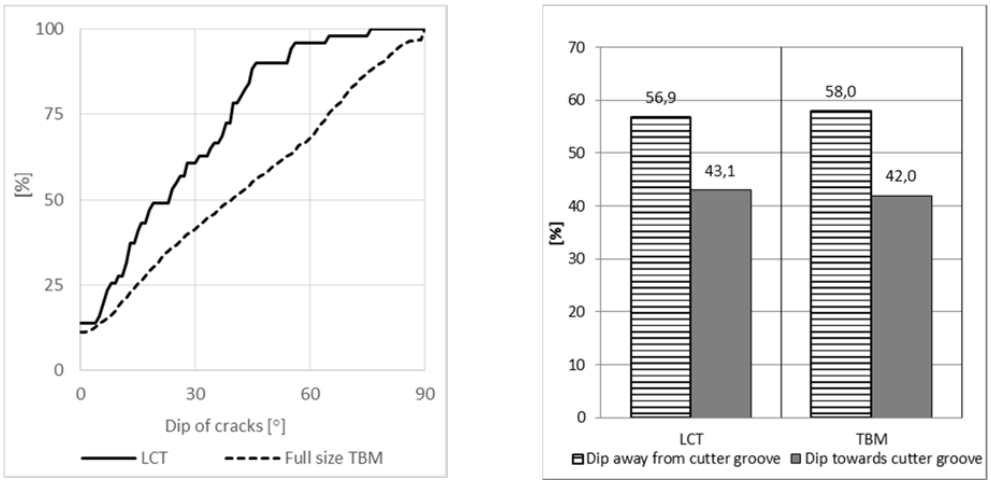

Figure 5.48: A) Accumulative frequency distribution of dip inclinations. B) Distribution of dip directions in reference to the cutter groove.

A) B)

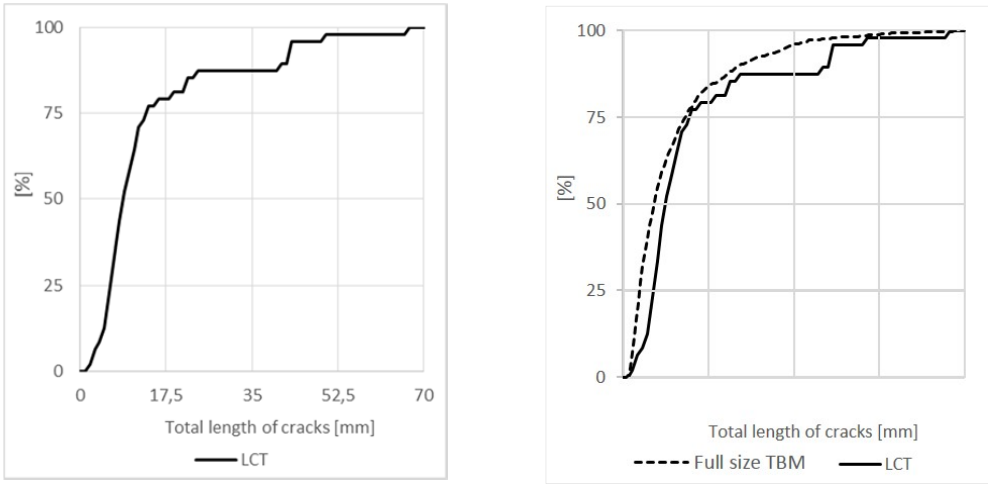

Figure 5.49: A) Accumulative frequency distribution of total length. B) Accumulative frequency distribution of total length of cracks, adjusted to the maximum total length within both series.

Figure 5.49 shows the accumulative frequency distribution of total lengths in the core samples from the LCT and the accumulative frequency distribution of total lengths of cracks, adjusted to the maximum total lengths in the core samples from the LCT and the full size TBM. The first plot shows that the maximum total length of the cracks in the core samples from the LCT is 70 mm, and that 50 % of the cracks have a total length of less than 9 mm.

The second plot shows that, despite a low number of documented cracks in the core samples from the LCT, there are similarities between the distributions of total lengths, relative to the maximum length within both groups.

Figure 5.50 shows the accumulative frequency distribution of vertical depths from the 0-line in the core samples from the LCT and the accumulative frequency distribution of vertical depths from the 0-line, adjusted to the maximum vertical depth from the 0-line in the core samples from the LCT and the full size TBM. The first plot shows that the maximum vertical depth from the 0-line for the cracks in the core samples from the LCT is 32 mm, and that 50 % of the cracks have a total length of less than 8 mm.

The second plot shows that there is a more even distribution of measured vertical depths from the 0-line in the core samples form the LCT than in the core samples from the Nedre Røssåga headrace tunnel.

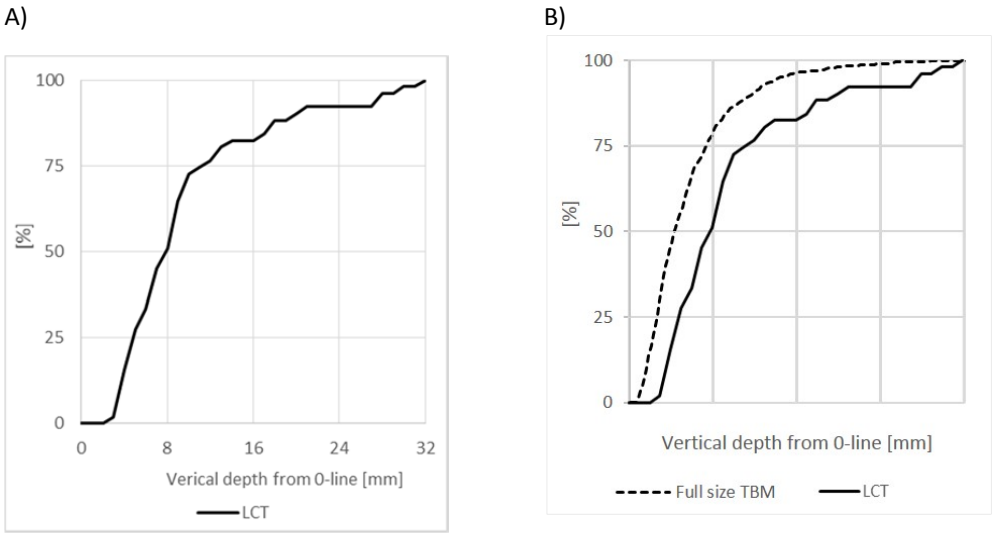

Figure 5.50: A) Accumulative frequency distribution of vertical depths from the 0-line. B) Accumulative frequency distribution of vertical depths from the 0-line, adjusted to the maximum vertical depth from the 0-line within both series.

5.4 Chips

In order to supplement and support the findings from the core samples, cracks in chips from the AMR Project and the Nedre Røssåga headrace tunnel was identified and documented. In total, 102 cracks were identified and documented in the selected chips. Note that some of the

cracks were documented in two cuts of the same chip, and that the 102 detected cracks therefor are not 102 individual cracks.

The detected cracks in the cut chips from the different chainages are presented in the following chapters. Note that the figures do not present the correct scale and that the aspect ratio between the different samples is not correct. For more details, see *Appendix G: Chips from the AMR Project and the Nedre Røssåga headrace tunnel*.

Table 5.3: Number of samples, cuts and cracks from the sampling chainages at the AMR Project and the Nedre Røssåga headrace tunnel.

Chainage	Number of samples	Number of cuts	Documented cracks
AMR_11573	3	4	13
R_1184	4	9	37
R_1440	1	3	25
R_5437	4	6	27

5.4.1 The AMR Project

Chainage 11573

The detected cracks in the cut chips from chainage 11573 at the AMR Project can be seen in Figure 5.51. In total, 13 cracks were documented on the four cuts. Compared to the number of cracks identified in the core samples from the AMR Project, the number of detected cracks in the chips are relatively high.

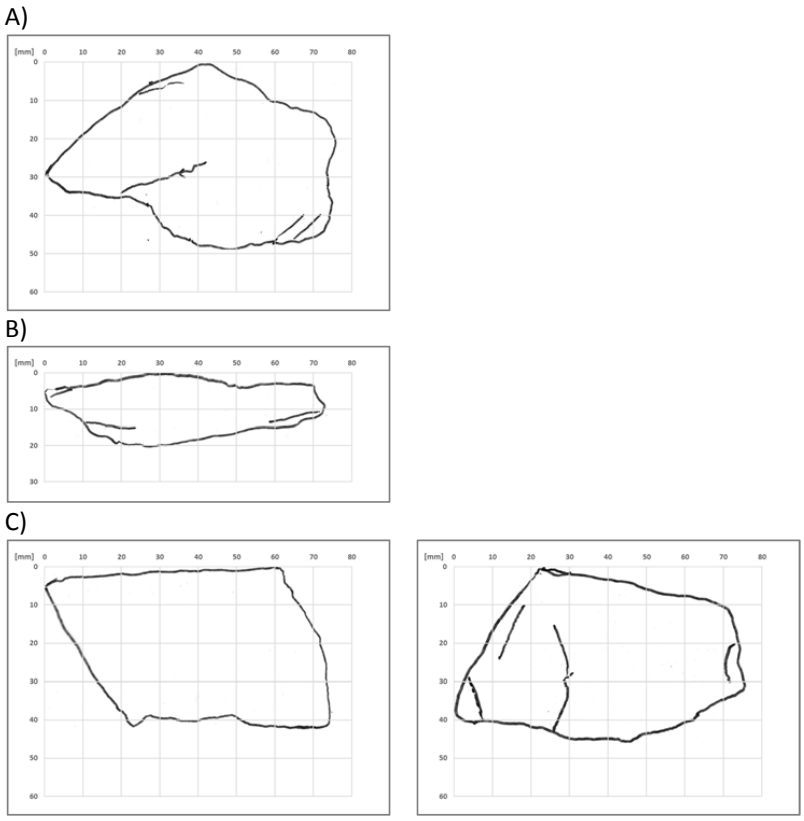

Figure 5.51: Detected cracks in cut chips from chainage 11573 at the AMR Project
A) AMR_11573_1-A-B. B) AMR_11573_2-A-B. C) AMR_11573_3-A-B and AMR_11573_3-B-C.

5.4.2 The Nedre Røssåga headrace tunnel

As the following figures show, there were detected and documented several cracks in the chips from the Nedre Røssåga headrace tunnel. AS the figures show, the average number of cracks is higher in the chips from Geology 2 than in the chips from Geology 1. Independent of geology, the average number of cracks in chips from the Nedre Røssåga headrace tunnel is higher than in the chips from the AMR Project.

Chainage 1184

The detected cracks in the cut chips from chainage 1184 at the Nedre Røssåga headrace tunnel can be seen in Figure 5.52. In total, 37 cracks were documented on the nine cuts.

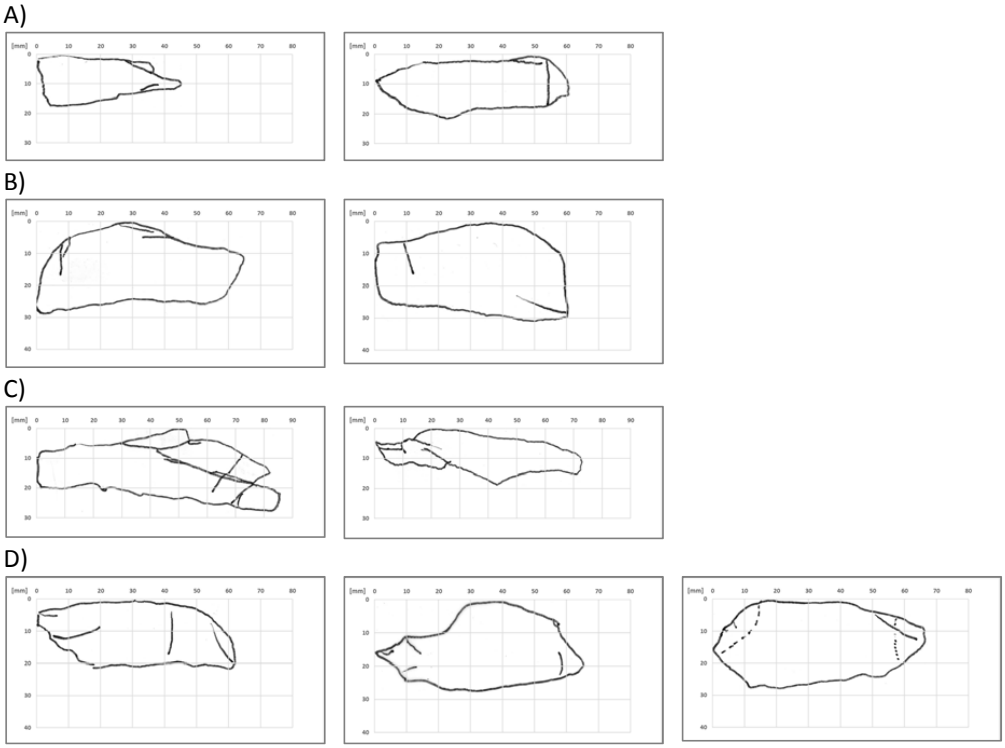

Figure 5.52: Detected cracks in cut chips from chainage 1184 at the Nedre Røssåga headrace tunnel A) R_1184_1-A-B and R_1184_1-B-C. B) R_1184_2-A-B and R_1184_2-B-C. C) R_1184_3-A-B and R_1184_3-B-C. D) R_1184_4-A-B, R_1184_4-B-C and R_1184_4-C-D.

Chainage 1440

The detected cracks in the cut chips from chainage 1440 at the Nedre Røssåga headrace tunnel can be seen in Figure 5.53. In total, 25 cracks were documented on the three cuts.

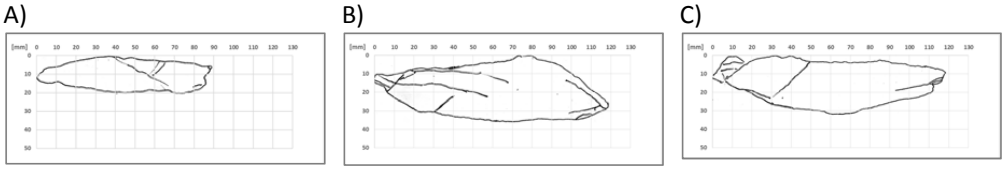

Figure 5.53: Detected cracks in cut chips from chainage 1440 at the Nedre Røssåga headrace tunnel. A) R_1440_1-A-B. B) R_1440_1-B-C. C) R_1440_1-C-D

Chainage 5437

The detected cracks in the cut chips from chainage 5437 at the Nedre Røssåga headrace tunnel can be seen in Figure 5.54. In total, 27 cracks were documented on the six cuts.

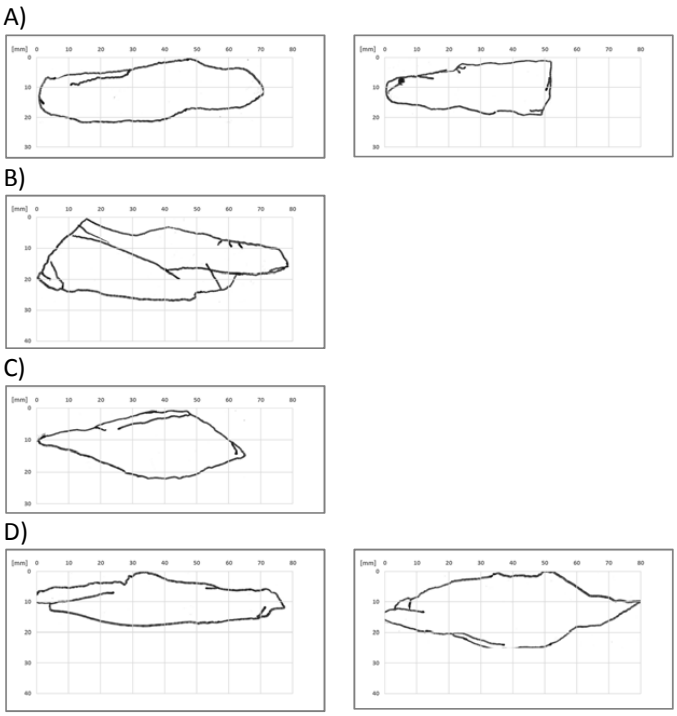

Figure 5.54: Detected cracks in cut chips from chainage 5437 at the Nedre Røssåga headrace tunnel. A) R_5437_1-A-B and A) R_5437_1-B-C. B) R_5437_2-A-B. C) R_5437_3-A-B. D) R_5437_4-A-B and R_5437_4-B-C.

6 Results and analysis of sound velocity measurements

6.1 Reference measurements of sound velocity

6.1.1 Repeatability and natural variation within the core samples

To check the validity of the measurements, the measuring procedure were repeated on the same core sample four times. The measured velocities from the four series in the 90-270 and the 0-180 direction are shown in Figure 6.1 and Figure 6.2. Note that the points in the graph represents the location of the center point of the 30 millimeters diameter transducers.

In both directions, all measurements were congruent, with a maximum deviation of 40 m/s. The average deviation was 22 m/s in the 0-180 direction and 26 m/s in the 90-270 direction.

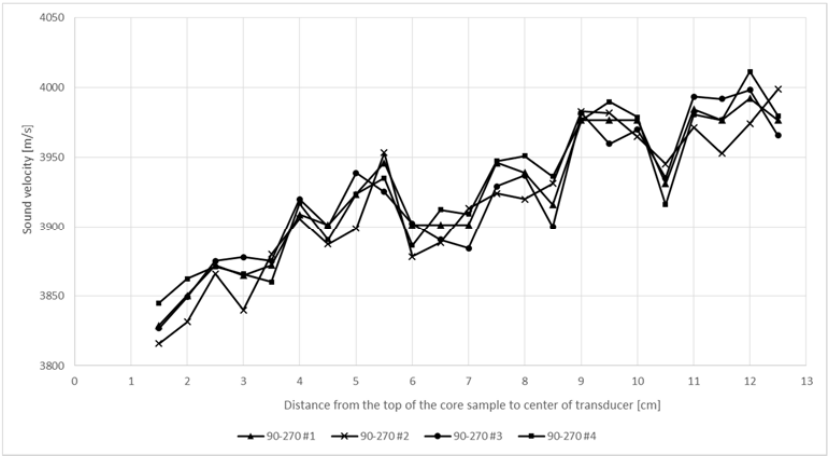

Figure 6.1: Four series of measured sound velocity in the 90-270 direction in core sample S_9-2 before crack initiation.

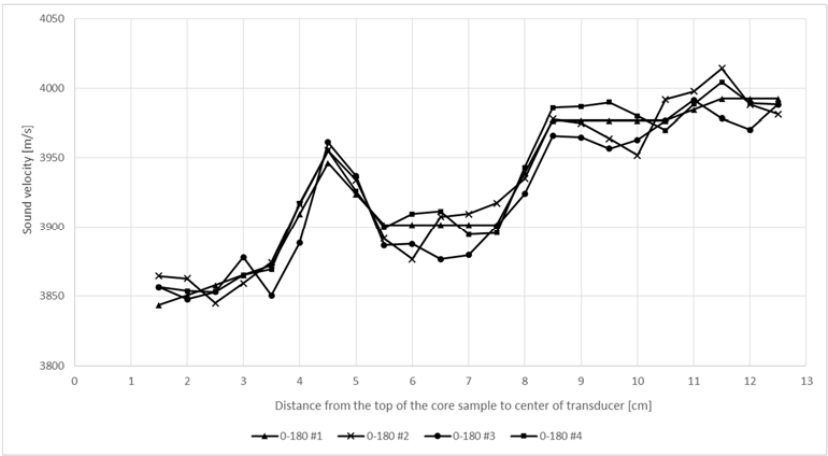

Figure 6.2: Four series of measured sound velocity in the 0-180 direction in core sample S_9-2 before crack initiation.

After crack initiation, another four series of sound velocity measurements were carried out in the 0-180 direction. The results are presented in Figure 6.3. Also after crack initiation, all measurements were congruent. The maximum deviation was 41 m/s, and the average deviation was 26 m/s. Note the difference in scale along the two y-axis.

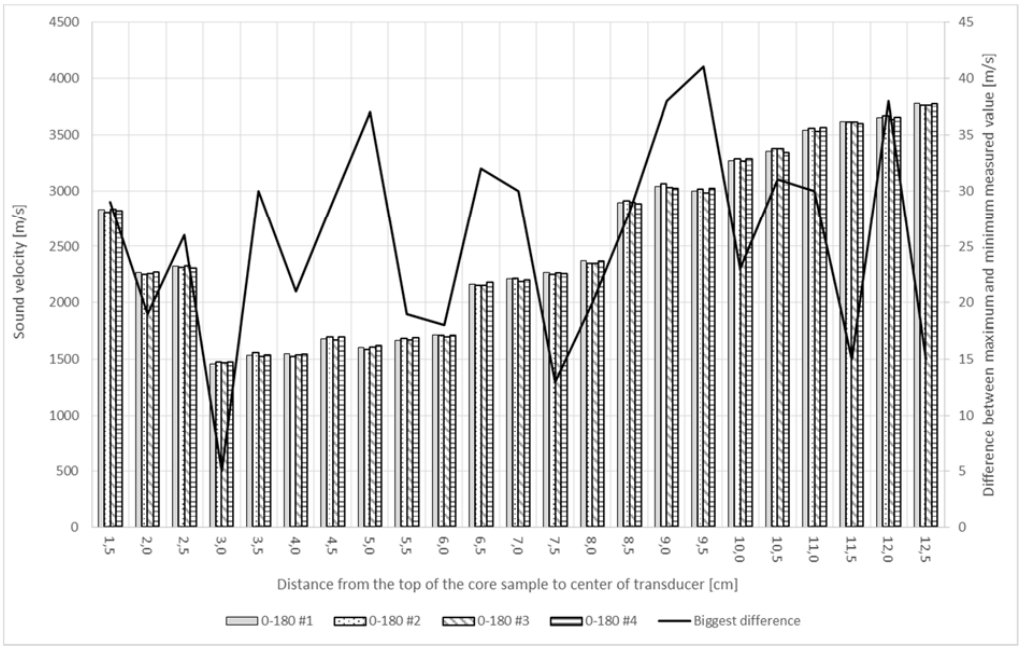

Figure 6.3: Four series of measured sound velocity in the 0-180 direction in core sample S_9-2 after crack initiation.

In order to check how much the sound velocity changes along an intact core sample from a homogenous rock mass, additional measurements were carries out on the remaining 14 core samples from the Trondhjemite quarry at Støren. The complete set of sound velocity measurements can be seen in Appendix F. In the following, all 15 core samples are included.

In total, 180 measuring in each measuring direction were carried out. These measurements show that there is a difference between the measured sound velocities in the two measuring directions, and that the sound velocity changes along the axis of the core samples. A summary of the sound velocity measurements can be seen in Table 6.1.

Table 6.1: Summary of the sound velocity measurements in the core samples from the Trondhjemite quarry at Støren.

	0-180 direction	90-270 direction	Both directions
Minimum difference within a core sample [m/s]	72	71	
Maximum difference within a core sample [m/s]	234	234	
Average difference within a core sample [m/s]	153	121	
Minimum difference from average sound velocity within a core sample [m/s]	2	3	
Maximum difference from average sound velocity within a core sample [m/s]	240	227	
Average difference from average sound velocity within a core sample [m/s]	65	51	
Minimum difference between measured sound velocity in a measuring point [m/s]			0
Maximum difference between measured sound velocity in a measuring point [m/s]			201
Average difference between measured sound velocity in a measuring point [m/s]			48

Looking at the distribution of differences in measured sound velocity between the two measuring directions, the average difference is 48 m/s, and 50 % of the measuring points have a difference of less than 44 m/s. In 23 % of the measuring points, the measured sound velocity is equal in the two directions and in 49 % of the measuring points, the measured sound velocity value is higher in the 90-270 direction than in the 0-180 direction. The distribution of differences between the two measuring directions can be seen in Figure 6.4.

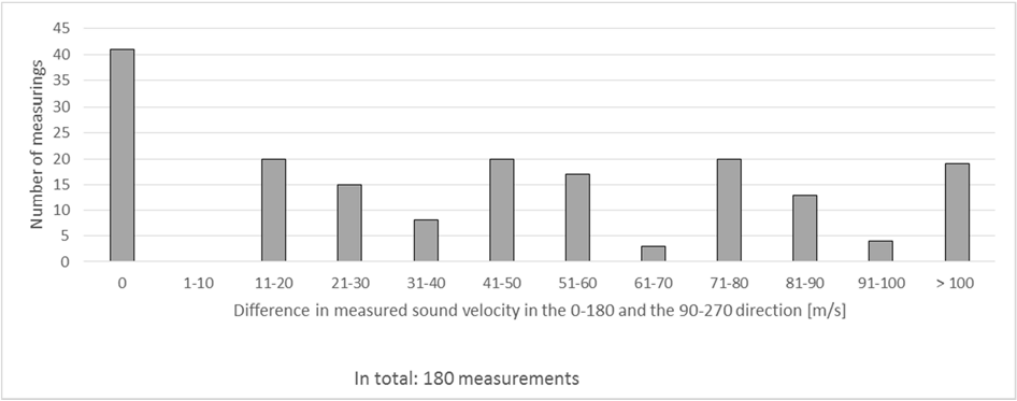

Figure 6.4: The distribution of differences between the two measuring directions in 15 core samples from the Trondhjemite quarry.

The average sound velocity in each direction is calculated individually for the 15 core samples, and the difference between the measured sound velocity and the calculated average sound velocity is calculated for each measuring point. Figure 6.5 shows the distribution of calculated differences between the measured sound velocity and the calculated average sound velocity in both directions. The figure shows that in 50 % of the measuring points, the difference from the calculated average sound velocity is less than 82 m/s in the 0-180 direction, and 48 m/s in the 90-270 direction.

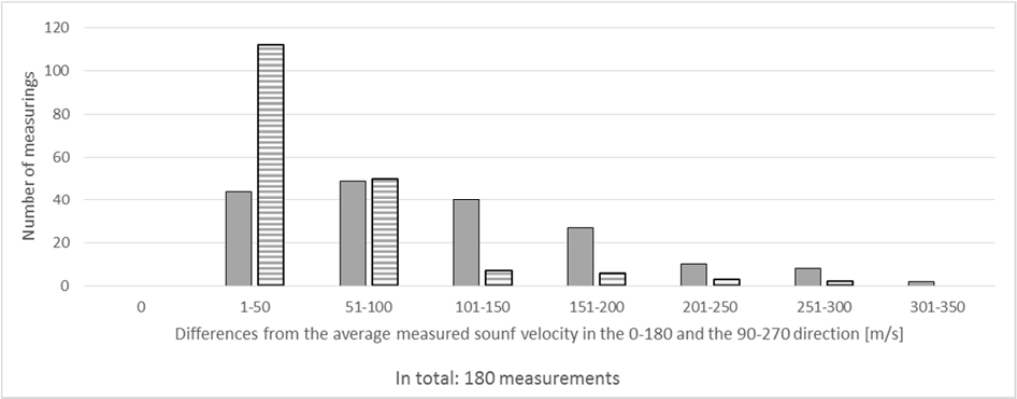

Figure 6.5: The distribution of differences from the average sound velocity in 15 core samples from the Trondhjemite quarry.

6.1.2 Sound velocity measurements after crack initiation

As described in chapter 4.4.3 *Reference measurements*, a crack was initiated in core sample S_9-2 after the initial measurements. This crack is measured to be 12 centimeters long, and the base of the core sample has no visual cracking. The core sample is 14 centimeters long. Ideally, using 30 millimeters probes, the crack should have been shorter, but it was not possible to control the length of the crack during the crack initiation. A visual inspection of the crack shows that the width of the crack decreases towards the bottom of the core sample. The width of the crack is approximately constant the first five centimeters. At five centimeters, the width of the crack decreases significantly, and then the width of the crack decreases gradually until 10,5 centimeters. At 10,5 centimeters, the width decreases significantly again, and from 10,5 to 12.1 centimeters the width of the crack decreases gradually. At 12 centimeters, the crack is no longer visible. The crack is schematically presented in Figure 6.6. As seen in Figure 4.22B, the crack is partly filled with crushed rock from the cutter ring during loading.

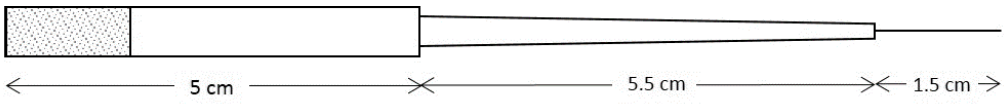

Figure 6.6: Schematically presentation of crack opening in S-9-2.

The measured sound velocities in core sample S_9-2 before and after crack initiation is presented in Figure 6.7. Note that the picture of the core sample and the crack with the measured sound velocity profile as the picture is slightly distorted due to the lens of the camera. In the 0-180 direction, the first three measuring points have a higher value than the fourth point, but from the fourth point, at three centimeters from the top of the core, the measured sound velocity increases towards the bottom of the core sample. In the last measuring point, the deviation between the measured sound velocity before and after cracking is 220 m/s.

Between six and six and a half centimeters, and between eight and eight and a half centimeter, the measured sound velocity increases significantly.

In the 90-270 direction, the measured sound velocities varies a lot along the core sample, and in five measuring points it was not possible to get any results at all. Towards the bottom of the core sample, the measured sound velocity increases significantly by 3012 m/s between 10,5 and 11,5 centimeters. From 11,5 to 12,5 centimeters the measured sound velocity still increases, but only by 590 m/s. In the last measuring point, the deviation between the measured sound velocity before and after cracking is 390 m/s.

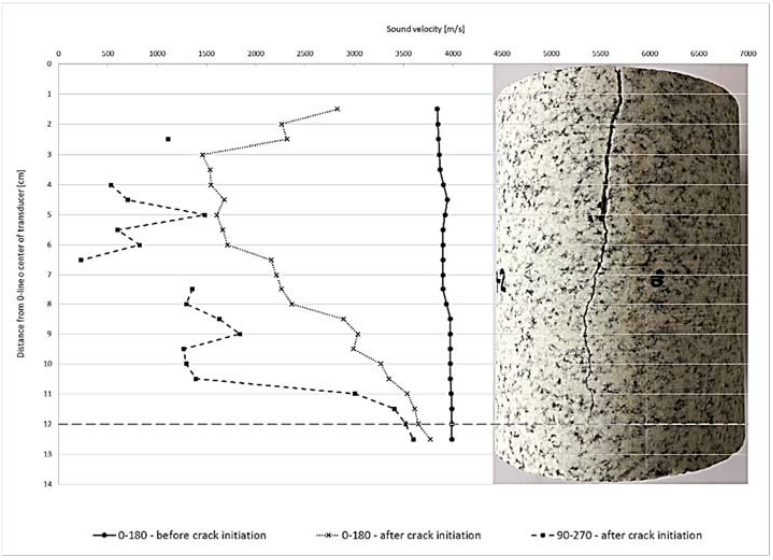

Figure 6.7: Measured sound velocities in core sample S_9-2 before and after crack initiation.

6.2 Sound velocity measurements and documented cracks

Sound velocity measurements were carried out on 20 core samples from the Nedre Røssåga headrace tunnel. The sound velocity profiles have been evaluated in relation to the two hypothesis presented in chapter 4.4.1 *Background for the choice of sound velocity measurements*. The velocity profiles have also been compared to the digitalized foldouts. A complete presentation of all the results can be seen in Appendix H *Sound velocity measurements and digital foldouts*.

Sound measurements and correlation with detected cracks

The sound velocity profiles are compared with the digitalized foldouts, and the correlation between the measured sound velocity profiles and the detected cracks are evaluated categorized in three different groups:

1.1 Good correlation; the measured sound velocity profiles correlates very well with the documented cracking
1.2 Medium correlation; the measured sound velocity profiles correlates to some extent with the documented cracking
1.3 Fair correlation; the measured sound velocity profiles does not correlate with the documented cracking

Table 6.2 shows the distribution of core samples within each category, and Figure 6.8 shows one example of sound velocity profiles in each category. A complete list that shows in which category each core samples is evaluated is presented in Appendix H *Sound velocity measurements and digital foldouts*.

Table 6.2: Classification of the core samples related to the correlation between the measured sound velocity profiles and the documented cracking.

	1.1	1.2	1.3
Number of core samples	8	8	4*

* in two of the core samples the correlation is good close to the 0-line

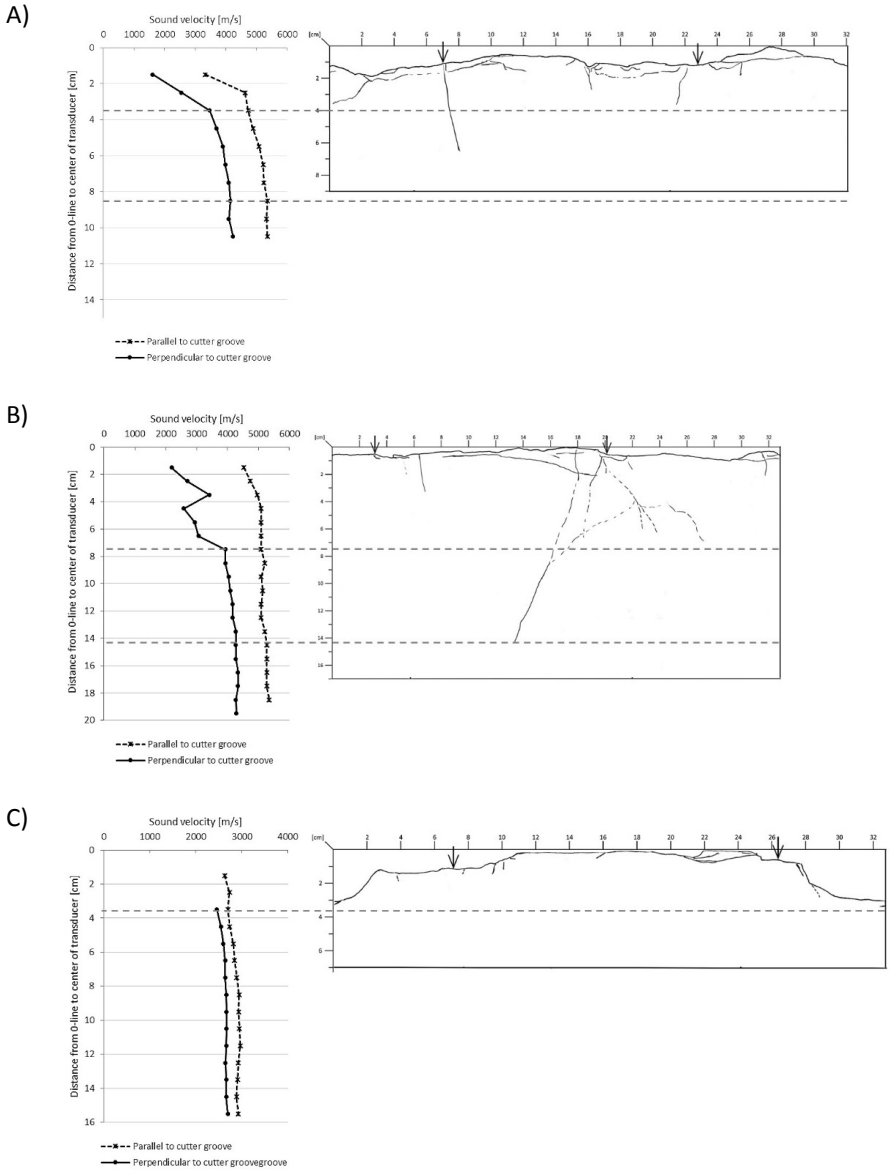

Figure 6.8: Measured sound velocities and digital foldouts for A) Core sample R_3112_4-2_22. B) Core sample R_3112_3-1_21. C) Core sample R_1184_1-5_25. Note that the arrows represents the cutter grooves.

Hypothesis 1

With the first hypothesis in mind, "The sound velocity will increase with increasing distance from the face, as the effect of the cutters on the TBM at a certain distance from face will be insignificant", the sound velocity profiles in the core samples are categorized in four different groups:

2.1 Gradually increasing sound velocity profile
2.2 Gradually increasing sound velocity profile, but with a pronounced change in sound velocity between two measuring points
2.3 Even sound velocity profile
2.4 Undulating sound velocity profile, but the average measured value increases when the distance from the face increases

Table 6.3 shows the distribution of core samples within each category, and Figure 6.9 shows one example of sound velocity profiles in each category. A complete list that shows in which category each core samples is evaluated is presented in Appendix H *Sound velocity measurements and digital foldouts*.

Table 6.3: Classification of the core samples related to the shape of the sound velocity profile.

	2.1	2.2	2.3	2.4
Number of core samples	5	10	2	3

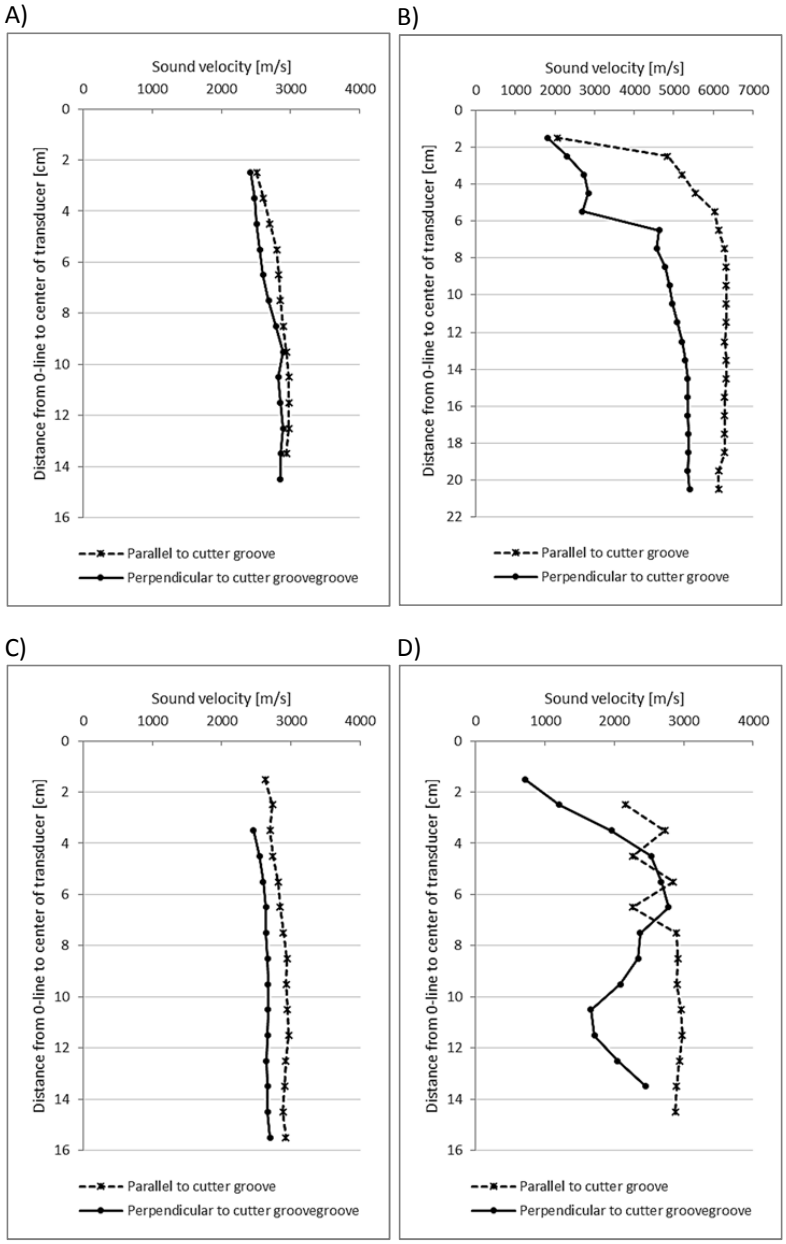

Figure 6.9: Measured sound velocities in A) Core sample R_1184_1-4_24. B) Core sample R_3112_3-2_22. C) Core sample R_1184_1-5_25. D) Core sample R_1184_1-1_21.

Hypothesis 2

With the second hypothesis and the concept model of rock breaking in mind, "*the sound velocity will be higher measured parallel to the cutter groove than measured perpendicular to it, given that the cracking is radial to the cutters*", the core samples are categorized in four different groups based on the differences between the sound velocity measurements parallel and perpendicular to the cutter grooves:

3.1 The measured sound velocity is higher parallel to the cutter groove than perpendicular to it, in all the measuring points
3.2 The measured sound velocity is higher parallel to the cutter groove than perpendicular to it, in all the measuring points except two
3.3 The measured sound velocity is more or less equal in the two measuring directions
3.4 The measured sound velocity is higher perpendicular to the cutter groove than parallel to it, in all the measuring points except two

Table 6.4 shows the distribution of core samples within each category, and Figure 6.10 shows one example of sound velocity profiles in each category. A complete list that shows the chosen categories for each core sample is presented in Appendix H *Sound velocity measurements and digital foldouts*.

Table 6.4: Classification of the core samples related to the sound velocity measurements parallel and perpendicular to the cutter groove.

	3.1	3.2	3.3	3.4
Number of core samples	15	3	1	1

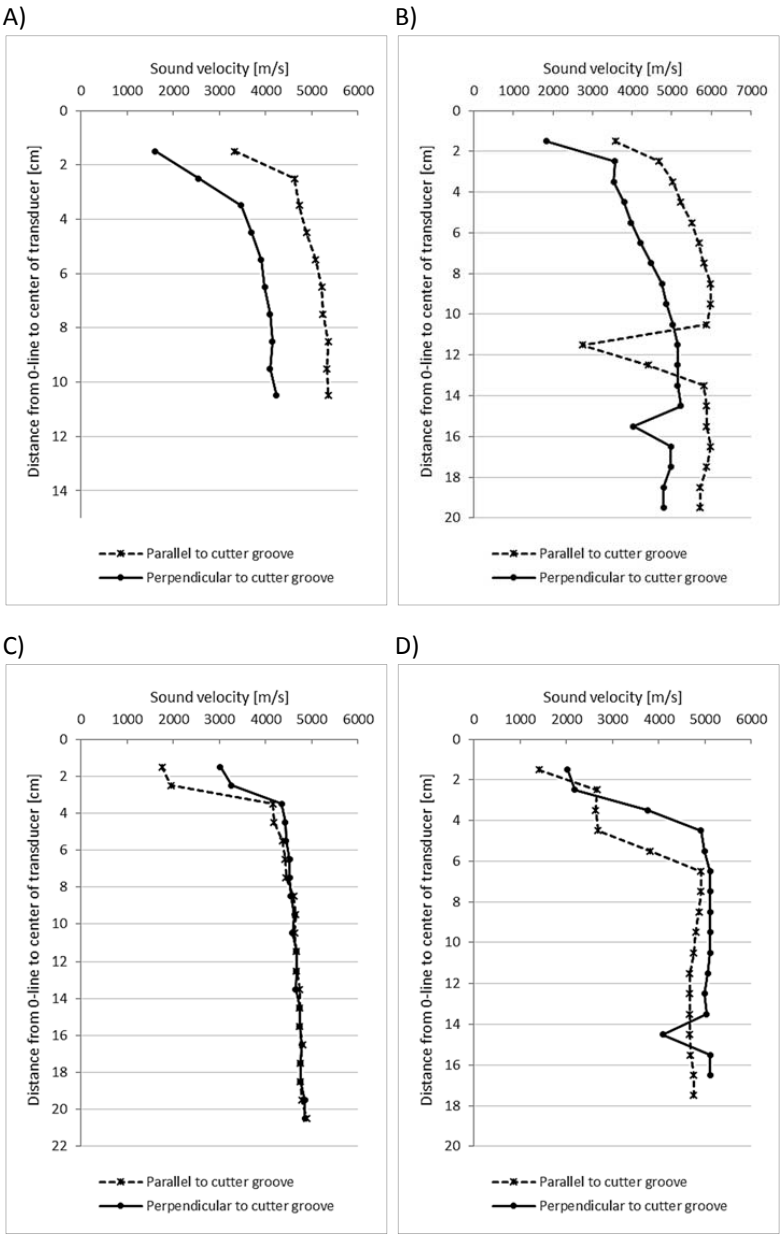

Figure 6.10: Measured sound velocities in A) Core sample R_3112_4-2_22. B) Core sample R_3112_3-3_23. C) Core sample R_3112_4-4_24. D) Core sample R_3112_4-3_23.

7 Discussion

7.1 On the methodology

As discussed in chapter 4.1 *Choice of sites* , there are both advantages and disadvantages by including samples from only two sites, but for this Ph.D.-study the advantages were considered bigger than the disadvantages. In retrospective, the advantage of getting to know the sites and the workers at site was found to be invaluable with respect to facilitation and knowledge about the TBM and the operation of the TBM. This has improved the quality of the decision related to choice of RPM as the preferable parameter to study, the choice of sampling chainages and the sampling itself.

When RPM was chosen as the preferable operational parameter to study, other parameters like thrust, torque and influence of the operator of the TBM were indirectly fixated in order to reduce the number of variable parameters. The effects of these parameters are not evaluated in this thesis. Most likely, these parameters affect the rock breaking under the disc cutters of a TBM to a variable extent. The findings in this study are only valid for the combinations of thrust, torque and TBM operator used in this study.

As discussed in chapter 4.2.1 *Sampling methods and procedures*, the advantages and disadvantages of core drilling as sampling method was evaluated before the decision was taken to use this as the main method. The available space and the need of a high number of samples were determining factors for the choice of core drilling.

The sylindrical shape of the core samples is not ideal with respect to direct measurements of the visualized cracks, as dip measurements only represents the apparent dip. For exact measurements, the sample should have been a rectangle or square box. The small diameter of the core samples gives a tolerable uncertainty regarding the dip of the cracks. In addition, the diameter of the core samples is constant, so the core samples can be compared directly without increasing the uncertainty.

The cracks are visualized on the surface of the core samples, and the propagation and orientation in the core is unknown. Consequently, all cracks are considered as two-dimensional lines and not three-dimensional planes. This simplification does not fully utilize the potential of the core samples, but enables the evaluation of many core samples in a short period. As mentioned, rock mass properties can change considerably over short distances, and a high number of samples is needed to achieve representative results for a given rock mass. The advantages of evaluating a high number of two-dimensional cracks was considered higher than the advantage of evaluating a low number of three-dimensional planes.

Because the cross-sections presented in chapter 5.2.1 *Digitalized foldouts* are flattened presentations of a curved surface, they have to be considered as simplified cross-sections. Still, they give a good visualization of the fracturing patterns.

The diameter of the core samples is 103-106 mm, and the cutter spacing at the Nedre Røssåga headrace tunnel was 72.3 mm. This implies that a core sample, if centered right over the cutter groove, covers slightly more than half the area between two cutters. With the chosen methods for sampling and crack visualization, it is not possible to determine whether the cracks in a core sample were initiated by the cutter cutting the cutter groove in the core sample or one of the cutters on each side. For cracks with point of origin close to the cutter groove and dip

away from the cutter groove, it is possible to assume that they are initiated by the cutter cutting the cutter groove. For cracks with point of origin further away from the cutter groove and cracks with low dip angles it is not possible to assume which cutter that initiated the cracks. Due to this great uncertainty, all cracks are evaluated with respect to their point of origin in relation to the cutter groove in each core sample.

All measured properties for the core samples are related to the 0-line and the cutter groove in each sample. As opposed to a global coordinate system in three dimensions, this reference is local and only valid for one core sample. In principle, these local references is problematic concerning direct comparisons of the core samples. Even though rock excavation with TBMs is a result of the interaction between all the cutters on the cutter head, the rock breaking under and between two disc cutters can be can be simplified to a two-dimensional process that takes place perpendicular to the cutter grooves, independent of position on the cross section of the tunnel. This enable the possibility of an individual reference system for each core sample, given that all references are related to the cutter groove. Individual reference systems exclude the possibility of documenting the possible correlation between dip angles and dip directions of the cracks in relation to the foliation, but due to folding of the rock mass this could have been challenging anyway.

All cracks are evaluated with respect to their point of origin. An evaluation of the same cracks in relation to their ending point could increase the understanding of the rock breaking, but this is not included in this study.

The study of the four different ratios describing the surface of the core sample shows that there are no correlation between the ratios within the core samples from the different sampling chainages or the two geologies. This lack of correlation shows that the core samples represent, the rock surface at different stages of the rock breaking, and that the documented cracks are representative findings from the sampling chainages.

Despite some simplifications, the chosen methods give a good basis for studies of rock breaking under disc cutters of a TBM.

All the findings and evaluations to be discussed in the following chapters are based on the choices the author has made concerning the methodology. The findings and evaluations are valid for those premises, and must be evaluated accordingly.

7.2 On the rock breaking at the AMR Project

Compared to the core samples from the Nedre Røssåga headrace tunnel, the core samples from the AMR Project contain a very low number of cracks that is likely to have been induced by the cutters of the TBM. An evaluation of rock breaking mechanisms and failure modes is not within the scopes of this study, but below is the authors' discussion about this.

From the operational parameters and the TBM performance, there are no obvious explanations to the low number of cracks. The thrust force, RPM and the penetration rate is within what is considered normal values.

Differences in wear on neighbor cutters can be a part of the explanation, as cutters with high wear might not transfer as much load as the neighbor cutters. For core sample AMR_11573_1-1_36 and AMR_11579_1-1_36, but is most likely not the case for the core samples. Cutter

wear can be found in appendix C. In addition, the chips from the AMR have a lower number of cracks per cut than the chips from the Nedre Røssåga headrace tunnel.

The monzo granite at the sampling chainages at the AMR Project have an extremely high estimated UCS, and a medium brittleness value. In addition, the monzo granite has a medium to coarse grain size. This combination of properties might also be a part of the explanation to the low number of cutter-induced cracks in the core samples and the chips. Due to the high UCS, the rock mass has a high resistance to the cutter load, and few cracks are induced previous to the failure. When failure occurs, it is a brittle failure with high energy, like failure of glass, and this may be a part of the explanation why there are so few cracks in the core samples.

Another possible explanation could be that some of the initiated cracks are opening or reopening of closed cracks and cracks with filling.

The findings from the AMR Project demonstrates that rock breaking under disc cutters is a complex process, and that the rock breaking is dependent of geology.

7.3 On the rock breaking at the Nedre Røssåga headrace tunnel

7.3.1 Cracking patterns and core sample surfaces

The study of digitalized foldouts and the cross sections from the Nedre Røssåga headrace tunnel shows a great variation of fracturing patterns and surfaces under the disc cutters, independent of RPM and geology.

The cracking patterns vary from patterns that are symmetric around cutter groove, like the concept model of rock breaking presented introductorily in this thesis, to patterns that appear as random combinations of cracks. In addition, there is an extensive variation in shapes of the surfaces of the core samples. Some of the surfaces are almost flat, and some have extensive variations in distances between the 0-line and the surface line.

From a visual evaluation of the cracking pattern and the surface of a core sample, it is not possible to determine which geology and RPM the core sample represents. This verifies that rock breaking under disc cutters of a TBM is a complex process, and that a generalization of the rock breaking process is difficult.

As discussed previously in this chapter, the choice of using individual reference systems for each core sample excluded the possibility to document any correlation between dip angles and dip directions of the cracks in relation to the foliation. At chainage 5458-5478 the angle between the foliation and the tunnel axis was approximately 30 °, and according to the NTNU prognosis model, geological formations have a low impact on the penetration when the angle between the tunnel axis and a geological formation is small. A visual evaluation of the cracks in relation to the foliation shows that, to a great extent, the foliation had a low influence on the fracturing patterns. This observation is in accordance with the NTNU prognosis model.

Given constant operating conditions, there is a considerable variation of fracture patterns, and the rock breaking under the cutters of a TBM is much more complex than presented in literature. The concept model of rock breaking under the cutters of a TBM can be considered

as a generalized and idealized presentation of the rock breaking, but is does not represent the great variety of fracture patterns and rock surfaces in front of a full size TBM.

7.3.2 The exclusion of cracks with dip less than 3 °

The share of cracks with dip less than 3 ° varies from 7.9 to 15.1 % in the five samling chainages from the Nedre Røssåga headrace tunnel. An exclusion of these cracks would affect the calculated average distanses between the cracks in the core samples. As default, the point of origin of all cracks with dip less than 3° have been defined at what appears as the left end of the crack on the digitalized foldouts. A manuell review of all cracks with dip less than 3 ° shows that 13 of the 144 cracks passes under the cutter groove, an that the default point of origin is almost evenly disributed on both sides of the cutter groove.This implies that the relative share of cracks with point of origin on the two sides of the core sample is unchanged even if these 13 cracks are excluded from the evaluations, and that cracks with dip less than 3 °could be included in the analysis, exept the 13 cracks described above.

Table 7.1: Share of cracks with dip less than 3° in the core samples from the five sampling chainages at the Nedre Røssåga headrace tunnel.

	R_3112	R_1184	R_5437	R_5478	R_5458
Number of cracks, dip < 3 °	45	13	29	22	35
Share of all cracks	13,9 %	15,1 %	7,9 %	14,1 %	11,0 %
Number of cracks outside the cutter groove, dip < 3°	21	6	13	13	22
Cracks on the center side of cutter groove, dip < 3 °	24	7	16	9	13
Number of cracks that passes under cutter groove from the center side towards the outside	1	1	1	1	2
Number of cracks that passes under cutter groove from the outside towards the center side	1	1	1	0	2

Table 7.1 shows the exact number and the share of cracks with dip less than 3° and the distribution of cracks with dip < 3 ° passing under the cutter groove in the core samples from the five sampling chainages at the Nedre Røssåga headrace tunnel.

For all other evaluations including point of origin in relation to the cutter groove, the cracks with a dip angle from the surface line of less than three degrees are excluded. As described in chapter 5 *Results and analysis of rock breaking*, this is due to the fact that it is not possible to determine the point of origin with the chosen methods. The share of cracks presented in these plots are based on the number of cracks with dip > 2°. The cracks with dip angle ≤ 2° can potentially intersect all other cracks. To a great extent, these cracks can affect the rock breaking and should, ideally, have been included in the analysis.

Due to the uncertainty regarding the point of origin, all cracks with dip less than 3 ° must be exluded from all evaluations that include point of origin, as long as the chosen methods are used to measure, and evauate the cracks. The only exeptions are the evaluations of average

area per crack and average distance between the cracks. To a great extent, these cracks can affect the rock breaking and should, ideally, have been included in the analysis.

In the following evaluations, the RPM of each test stroke will be used as the main reference.

7.3.3 Geology 1

The low number of core samples from sampling chainage R_1184 is a potential source of error for all the evaluations. This is due to that the documented cracks are evaluated in the same way as the other cracks, without any corrections or adjustments to compensate the low number of samples. Due to this, the findings from this sampling chainage have to be considered as an indication only of the rock breaking under the disc cutters. The comparison of the findings is done without any adjustments.

A summary of all the findings for geology 1 shows that:

- The average number of cracks is higher with a RPM of 5 than with a RPM of 7,5.
- The distribution of total length of cracks is more even with a RPM of 5 than with a RPM of 7,5.
- The distributions of vertical depths from both the surface line and the 0-line are more even with a RPM of 5 than with a RPM of 7,5.
- For all dip angles from 0-60 °, the calculated average total length of the cracks is highest when the RPM is 5, but for dip angles from 61-90 ° the calculated average length of cracks is higher when the RPM is 7,5.
- Independent of dip interval, he average calculated depths from the surface line and the 0-line is higher with a RPM of 5 than with a RPM of 7,5.
- There is a more even distribution of dip angles, both generally and by point of origin in relation to the cutter groove with a RPM of 5 than with a RPM of 7,5.
- The distribution of dip directions in relation to the cutter groove is more even with a RPM of 5 than with a RPM of 7,5.

A closer look at the cracks with dip between 60 and 90 ° shows that the share of cracks with dip in this interval is 31 and 30 % for the two sampling chainages. There is a higher share of cracks with dip angle between 60 and 70 ° in the core samples from R_1184 (RPM:7,5) than in the core samples from R_3112 (RPM:5), and consequently a lower share of cracks with dip between 70 and 90 °. Foliation could have been a possible explanation, but the foliation is only weakly pronounced in these core samples, and the cracks do not correlate with the foliation. Figure 7.1 shows, dip versus total length for cracks with dip between 60 and 90 ° from the two sampling chainages. As this plot shows, there is no obvious reasons for the high calculated average values for total length of cracks within the three dip intervals for the cracks in the core samples from R_3112, the author cannot explain this finding.

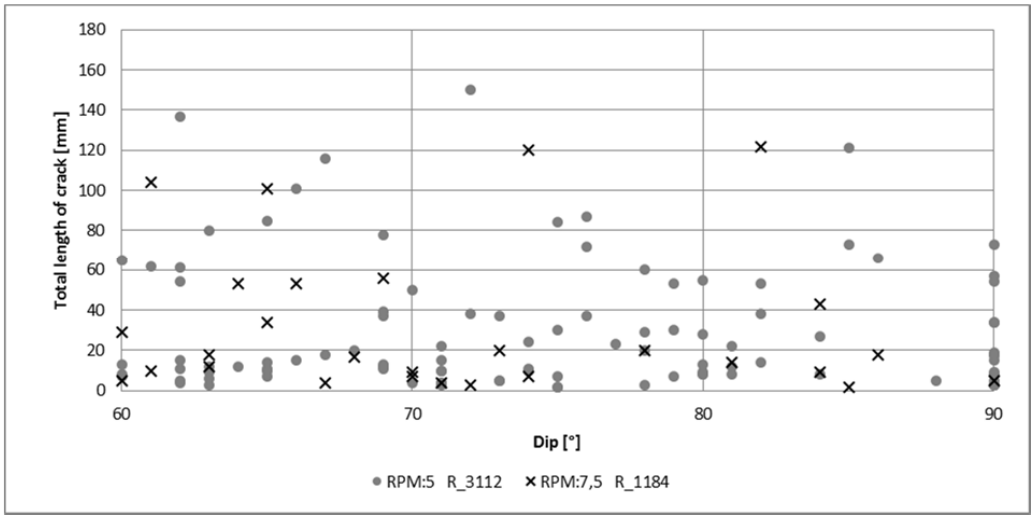

Figure 7.1: Dip versus total length for cracks with dip between 60 and 90 ° from the sampling chainages R_1184 and R_3112.

As described in chapter 2.5 *RPM as study parameter*, RPM was identified as an interesting parameter to study due to it's analogy to the loading rate and rock failure during uniaxial and triaxial compressive strength testing. Theory states that with an a high loading rate, the time to failure becomes shorter, and because of that the interaction between preexisting cracks gets weaker and less new cracks are generated. This results in smaller rock deformation, less weakening and a higher measured compressive strength than with lower strain rates. With a lower strain rate, the interaction between preexisting cracks gets stronger and more new cracks are generated. To a great extent, the findings in the core samples from geology 1 indicates that the analogy is valid for the rock breaking under the disc cutters of a TBM.

With a RPM of 5 versus a RPM of 7,5, the number of cracks is higher, the vertical depth of the cracks is higher and there is a better distribution of cracks, dip angles, and dip directions in reference to the cutter groove.

7.3.4 Geology 2

A summary of all the findings for geology 2 shows that:

- The average number of cracks is higher with a RPM of 3 than with a RPM of 6,5, but that the average number of cracks is lower with a RPM of 5 than with a RPM of 6,5.
- The distribution of total length of cracks is slightly more even with a RPM of 3 than with a RPM of 5 and 6,5, and the distribution is more even with a RPM of 5 than with a RPM of 6,5.
- The distribution of vertical depth from the surface line is slightly more even with a RPM of 3 than with a RPM of 5 and 6,5, but the distribution is more even with a RPM of 6,5 than with a RPM of 5.
- The distribution of vertical depth from the 0-line is more even with a RPM of 3 than with a RPM of 5 and 6,5, but the distribution is more even with a RPM of 6,5 than with a RPM of 5.
- For all cracks with dip angles above 20 °, the calculated average total length of the cracks is higher when the RPM is 3 than when it is 5 and 6,5, but there is no clear trend in the relation between the calculated average total lengths when the RPM is 5 versus 6,5.
- With small variances, the calculated average vertical depths from the surface and the 0-line is higher when the RPM is 3 than when it is 5 and 6,5, but it also higher when the RPM is 6,5 versus 5.
- There is a more even distribution of dip angles, both generally and by point of origin in relation to the cutter groove with a RPM of 3 than with a RPM of 5 and 6,5, but the distribution is more even with a RPM of 6,5 than with a RPM of 5.
- The distribution of dip directions in relation to the cutter groove is more even with a RPM of 3 than with a RPM of 6,5.

As for geology 1, the lowest RPM results in the highest number of cracks and vertical depth of the cracks, and the best distribution of cracks, dip angles, and dip directions in reference to the cutter groove.

A distinct difference to geology 1, is that the highest RPM does not result in the lowest number of cracks and vertical depth of the cracks, and the poorest distribution of cracks, dip angles, and dip directions in reference to the cutter groove. A RPM of 6,5 results in a higher number of cracks and vertical depth of the cracks, and a better distribution of cracks, dip angles, and dip directions in reference to the cutter groove compared to a RPM of 5. The only exception is the distribution of total length of cracks. Except the average number of cracks in the core samples from the two sampling strokes, the differences between the two RPM is not big, but compared to the findings in geology 1 and the findings for a RPM of 3 in geology 2 this is deviant findings.

Cutter wear could have been a possible explanation, but the difference in cutter wear was one millimeter for two of the cutters, so cutter wear cannot explain these findings. A difference in thrust force at the end of the sampling strokes coud have been another possible explanation, but the average thrust force during the sampling stroke with RPM of 6,5 was 15.500 kN, whereas it was 16.000 kN at the end of the sampling stroke with RPM of 5. By theory, this

difference should have caused more and deeper cracks in the core samples from the sampling strokes with RPM of 5, so thrust force cannot explain the deviant findings.

Despite a distance of only 20 meters between the two sampling chainages, differences in geology could have affected the rock breaking. A visual inspection of the core samples from the two sapling chainages shows that there were small crystals of garnet in six of the ten core samples from sampling chainage R_5478 (RPM:5). Like quartz, garnet is a hard mineral that can affect the rock breaking. This difference in geology has to be considered as the most possible explanation to the deviant findings.

With a RPM of 3 versus a RPM of 5 and 6,5, the number of cracks is higher, the vertical depth of the cracks is higher and there is a better distribution of cracks, dip angles, and dip directions in reference to the cutter groove. This is not the case with a RPM of 5 versus a RPM of 6,5, where the findings are contrary. Small differences in geology is the most possible explanation to these deviant findings.

7.3.5 All cracks

Independent of geology, the highest measured total length of a crack was 160 mm, and the highest vertical depth from the 0-line was 158 mm, but more than 80% of all cracks have a total length of less than 35 millimeters and a vertical depth from 0-line of less than 41 mm. This indicates that only a small increase in average vertical depth of the cracks can affect the penetration rate of the TBM.

The findings show that there are some trends, both between the different RPMs within a geology, but also between the two geologies. Within both geologies, the RPM affects the rock breaking, and the lowest RPMs generates the highest chipping potential in terms of number of cracks, length of cracks, vertical depth of the cracks and a distribution of cracks, dip angles, and dip directions in reference to the cutter groove. There are clear similarities between the distributions of the calculated average values of lengths and depths for the different RPMs and the two geologies. There are also similarities in the accumulative frequency distributions for the different properties, see Figure 7.2.

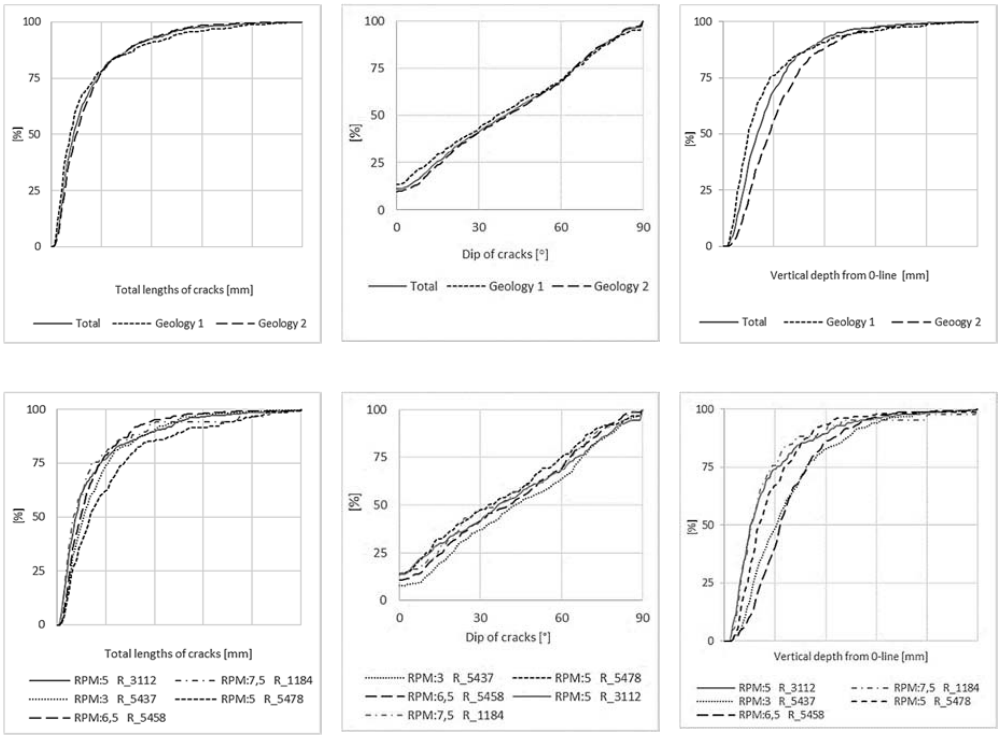

Figure 7.2: Comparison of accumulative frequency distributions, adjusted to the maximum value within the different series.

Both the average number of cracks, the average distance between cracks in relation to the cutter groove and to an imaginary line perpendicular to the cutter groove, and the average area per crack indicates that there is a small difference between the outside and the centerside of the cutter groove and that the density of cracks is higher on the outside of the cutter groove. One possible explanation can be that the cutters constantly are changing their direction, as opposed to a cutter of a linear cutter test, and that this torsion affects the rock breaking. Gravity could be another explanation. All the core samples in this study is from area between 150 and 210 degrees counted clockwise from the top of the face. In this area the cutters have a low angle in relation to a horizontal line, as opposed to the situation at 90 and 270 degrees from the top of the face. Core samples from these areas could increase the understanding of this difference in crack density on the two sides of the cutter groove.

As discussed above, the lowest RPM in each geology generated the most, longest, deepest and most evenly distributed cracks in relation to the cutter groove. This implies a higher chipping potential, as the probability of intersection of cracks increases. As mentioned earlier, there are no TBM performance data from sampling chainage R_3112, but the logged net excavation rate in mm/min for sampling stroke R_1184 in geology 1 and R_5437, R_5458 and R_5478 in geology 2 is presented in Figure 7.6. This figure clearly shows that the sampling strokes with low RPMs have a lower net excavation rate than the ones with higher RPMs. The net excavation rate measures in mm/min is very dependent of the RPM, and a low penetration

per revolution can be compensated by a high RPM to achieve a high penetration per minute. The penetration rate in mm/revolution is presented in Figure 7.4. This figure shows that the per revolution varies much more at a RPM of 3 than at a RPM of 5 and 6,5, and that the peaks of penetration rate is higher at a RPM of 3 than for a RPM of 5 and 6,5.

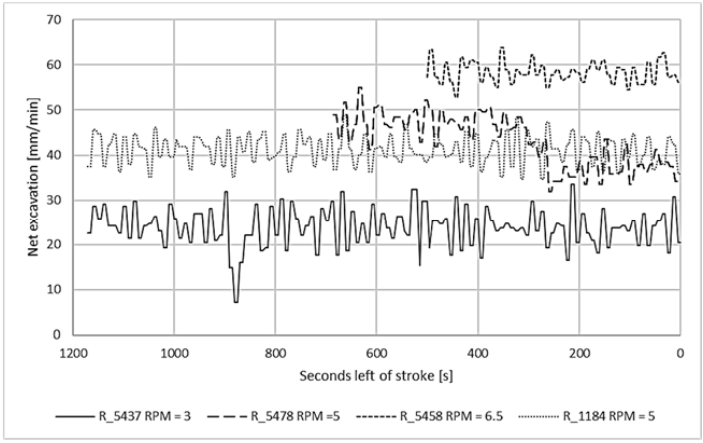

Figure 7.3: Logged net excavation rate in mm/ min for sampling stroke R_1184, R_5437, R_5458 and R_5478.

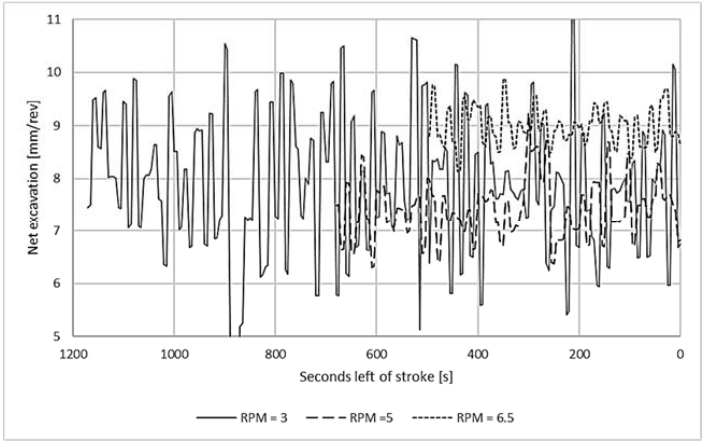

Figure 7.4: Logged net excavation rate in mm/revolution for sampling stroke R_5437, R_5458 and R_5478.

As discussed in chapter 2 *Technical background* the cutter life depends on rock and steel properties, cutter design, the operation of the TBM and geological conditions. When the geology, the rock and steel properties and the cutter design can be considered as constant, as for the sampling chainages within geology 2, the cutter life depends on the operation of the TBM. In this case, RPM is the only variable operational parameter. In the NTNU mode, the cutter life is estimated in meters per cutter, hours per cutter and cubic meters per cutter, and

with all other parameters constant this is directly related to the RPM. This implies that a low penetration rate for a low RPM, measured in millimeters per minute or hour, can be compensated for, by a higher cutter life due to the short rolling distance as long as the penetration per revolution is good. The findings from the core samples indicates that a higher chipping potential at lower RPMs and a high maximum values of the penetration rate per revolution. Based on these findings, it is not improbable that low RPMs indirectly can increase the efficiency of the cutters and thereby increase the cutter life. This possibility could not be proved or disapproved by the standard penetration tests, but require long term testing, possibly an entire tunnel.

Within both geologies, the cracking under the disc cutters is influenced by the RPM. There are some general trends across the two geologies, and between the distributions of crack properties for the different RPMs. Independent of geology, the lowest RPM generates the highest number of cracks, the highest vertical depth of the cracks and the best distribution of cracks, dip angles, and dip directions in reference to the cutter groove. From the available logged TBM performance, the lowest RPM generates the highest peaks of net penetration per revolution.

7.4 On the rock breaking in different geologies

As previous presented, the core samples from the Nedre Røssåga headrace tunnel represents two different geologies. In addition, the core samples from the AMR Project represents a third geology. Even though the geologies at the Nedre Røssåga headrace tunnel are more comparable than the geology at the AMR Project, both concerning mineralogy and UCS, some general comments about documented rock breaking should be discussed. The average measured UCS and number of cracks per core sample for each geology is summarized in Table 7.2.

Table 7.2: Summary of measured UCS and average number of cracks in the three geologies included in this thesis.

Site	UCS [MPa]	Average number of cracks per core sample
AMR Project	275-372	1,3
Nedre Røssåga headrace tunnel, Geology 1	62-139	18,3
Nedre Røssåga headrace tunnel, Geology 2	92-124	20,0

The average number of cracks in each core sample at the AMR Project is considerably lower than the average number of cracks in core samples from both geologies at the Nedre Røssåga headrace tunnel. At the same time, the UCS is considerably higher at the AMR Project than at the Nedre Røssåga headrace tunnel. From a rock mechanical point of view, the difference in number of cracks correlates with the difference in UCS, as rock masses with a high UCS has a higher resistance to the cutter load, and therefor fewer cracks are induced previous to the failure. At the Nedre Røssåga headrace tunnel, the difference in UCS in less, and as presented in the previous chapters, the number of cracks is related to the RPM. The samples from the AMR Project are from a sampling stroke with a RPM of 6. From the results from the Nedre Røssåga headrace tunnel, a higher number of samples could have been expected if the RPM had been lower.

From the results from the Nedre Røssåga headrace tunnel and the AMR Project, it is likely to think that a lowering of the RPM has an even higher influence on the rock breaking when the UCS is high.

7.5 On the rock breaking at the LCT

As discussed in chapter 5.3 *Rock breaking at the LCT*, there are some uncertainties concerning a direct comparison of the findings from the Nedre Røssåga headrace tunnel with the findings from the linear cutter test. Nevertheless, a comparison of the accumulative frequency distributions of dip angles, total lengths and vertical depths from the 0-line and the distribution of dip directions in relation to the cutter groove were evaluated as suitable properties for direct comparison, as these evaluations represents the trends within each group of samples. In addition, and a visual evaluation of the fracturing patterns was evaluated as a potential indications of similarities and differences between the rock breaking under the cutter of a LCT and the disc cutter of a full size TBM.

From a visual evaluation of the surfaces and the fracturing patterns, there are no obvious differences between the surfaces and the fracturing patterns in the core samples from the LCT and the core samples from the Nedre Røssåga headrace tunnel.

The comparison of the distribution of dip directions in reference to the cutter groove indicate that this distribution is congruent for the cracks from the LCT and from the full size TBM, but that the there is a higher share of cracks with low dip angles in the core samples from the LCT.

Despite a low number of documented cracks in the core samples from the LCT, the comparison of the distribution of total lengths of cracks indicates that the distribution of lengths, relative to the maximum length within both groups, is congruent.

The comparison of distributions of vertical depths from the 0-line, relative to the maximum depth from the 0-line within both groups, indicates that the distribution is incongruous, and that there is a more even distribution of measured vertical depths from the 0-line in the core samples form the LCT than in the core samples from the Nedre Røssåga headrace tunnel.

Due to a low number of samples, it is not possible to draw any distinct conclusions, but the findings show that the possibility of getting results that does not fully represents the conditions at the face of a full size TBM should be taken into account if a LCT is used to predict rock breaking under rolling disc cutters.

From the available data, the findings from the LCT indicates that there are some differences in the effects of the disc cutter on a TBM and a LCT, with respect to the distribution of dip angles and the relative distribution of vertical depths from the 0-line, relative to the maximum vertical depth from the 0-line in the core samples from the LCT and a full size TBM. The possibility of getting results that does not fully represents the conditions at the face of a full size TBM should be taken into account if a LCT is used to predict rock breaking under rolling disc cutters.

7.6 On the chip analyzes

The number of analyzed chips from the AMR Project and the Nedre Røssåga headrace tunnel is not high enough to draw any distinct conclusions about rock breaking under the disc cutters

at the two sites. Still, the number of documented cracks in the chips from the AMR Project and the Nedre Røssåga headrace tunnel support the findings in the core samples from the two sites, as the chips from the Nedre Røssåga headrace tunnel contains a higher number of cracks per chip than the chips from the AMR-project. Some of the chips from the AMR-project do not contain any cracks at all. As described in chapter 7.2 *On the rock breaking at the* AMR Project*,* operational parameters or difference in cutter wear cannot, solely, explain the low number of cracks in the core samples from the AMR-project. Because the collected chips were collected from the conveyor belt prior to core drilling, the chips are not directly related to the exact sampling chainage and the area of the core sampling. The uncertainties regarding operational parameters or difference in cutter wear are therefore considerably lowered. The fact that the chips also contains a very ow number of cracks increases the reliability of the findings in the core samples.

In the same way the high number of cracks in the chips from the Nedre Røssåga headrace tunnel supports the findings in the core samples, and increases the reliability of the findings in the core samples.

The number of analyzed chips from the AMR Project and the Nedre Røssåga headrace tunnel is not high enough to draw any distinct conclusions about rock breaking under the disc cutters at the two sites. Still, the number of documented cracks in the chips from the AMR Project and the Nedre Røssåga headrace tunnel support the findings in the core samples from the two sites.

7.7 On the sound velocity measurements

Note that the purpose of the measurements are to detect whether sound velocity measurements are suitable to detect cracking in core samples or not, and that the required accuracy of the results have to be seen in relation to the purpose.

7.7.1 Set up of test- and reference measurements

Reliability and suitability of the method

As described in chapter 4.4.3 *Reference measurements*, there were performed four series of measurements in each direction prior to crack initiation on core samples S_9-2 to check the repeatability of the measurements.

The reference measurement series have shown that the deviation between four measured series can be up to 41 m/s. Uncertainties related to the measuring equipment can cause a differences in velocity of about ± 15 m/s (Chryssanthakis & Tunbridge, 2004). In addition, there are some uncertainties related to the performance of the measurements. A deviation of 41 m/s make about 1 % of the average measured sound velocity of 3925 m/s for the entire core sample, and the deviation can be considered as low. This low deviation between the four series of sound velocity measurements, both before and after crack initiation, shows that the chosen set up provides repeatable and reliable results.

The measurements in the core samples from the Trondhjemite quarry at Støren, show that there is a difference between the measured sound velocities in the two measuring directions, and that the sound velocity changes along the axis of the core samples. This implies that the measuring method is sensitive to geological factors that are not visible to the naked eye, and

that there is a potential of natural variations within a core sample, even though the rock mass is considered as homogenous.

Despite the differences in the measured sound velocities in the two directions, the sound velocity profiles are congruent. In addition, the measured sound velocity profiles can be considered as variations of straight lines, with minor variations in some measuring points, see Figure 6.4. This indicate that the variations in measured sound velocities are caused by minor geological differences or uncertainties related to the measuring equipment and measuring performance rather than cracks.

The congruency of the measured values in the two measuring directions, and the fact that the sound velocity profiles are variations of straight lines shows that the core samples are suitable for reference measurements, despite the differences in the two directions and within the core samples.

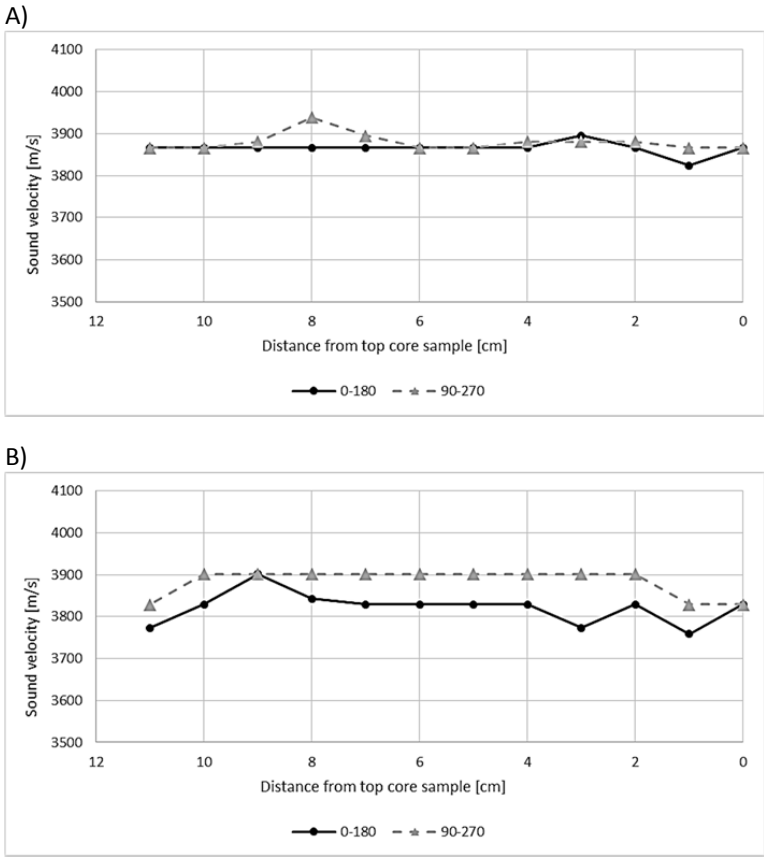

Figure 7.5: A) Sound velocity profile in core sample S_2-1. B) Sound velocity profile in core sample S_7-2.

These results show that the chosen set up provides repeatable and reliable results and that the core samples from the Trondhjemite quarry at Støren are suitable for reference measurements.

Accuracy of sound velocity measurements

90-270 direction

After crack initiation, the measured sound velocity profile along the 90-270° direction varies a lot. In some measuring points it was not possible to achieve any results at all. The most likely explanation is that the straight line between the transducers in these points, fully or partially, runs along the open crack. The transducers can not measure sound velocity through air and therefore, measurements in these points can not be done.

The significant increase in measured sound velocity between a depth of 10,5 and 11,5 centimeters from the top of the core sample, correlates well with the observed closing of the crack the depth of 10,5 centimeters.

To a great extent, this shows how much an open crack can influence the measured sound velocity if the measurements are carried out parallel to the crack.

0-180 direction

In the 0-180 direction, the measured sound velocities are higher close to the top of the core sample than they are three centimeters into the core sample, see Figure 6.7. As seen in Figure 4.22B, the crack is partly filled with crushed rock from the cutter ring during loading. This crushed rock ensure better conditions for sound wave propagation across the crack than the width of the crack could indicate, and is probably the explanation to the relatively high sound velocities measured in the upper three measuring points in the 0-180 direction. The Author tried to remove the crushed rock by water and compressed air before measuring, but it was not possible to remove everything without destroying the core. The thickness of the layer of crushed rock is unknown, but it is at least one centimeter thick.

From three to 12,5 centimeters, the measured sound velocity increases from 1459 m/s to 3773 m/s. The increase in measured sound velocity from one measuring point to another is less from three to six centimeters and from 10,5 to 12,5 centimeters than it is from six to 10,5 centimeters. In addition, there is a significant increase in the measured sound velocity between six and six and a half centimeters, and between eight and eight and a half centimeter. These points do not directly correlate with any observations of shape or thickness of the observed crack. This significant increases in measured sound velocity might be due to relations inside the core or uncertainties concerning the measuring equipment and the measuring performance.

In this specific case, the width and the length of the crack was visible by observation. In order to evaluate whether the method was suitable to detect cracks and evaluate the length of a crack if no cracks are visible, the sensitivity of the measurements was evaluated by calculation. By polynomial regression, a fourth degree polynomial representing the measured sound velocity profile was crated. This regression is presented in Figure 7.6 and formula [7.1]. Note that this regression only represents this specific set of measurements.

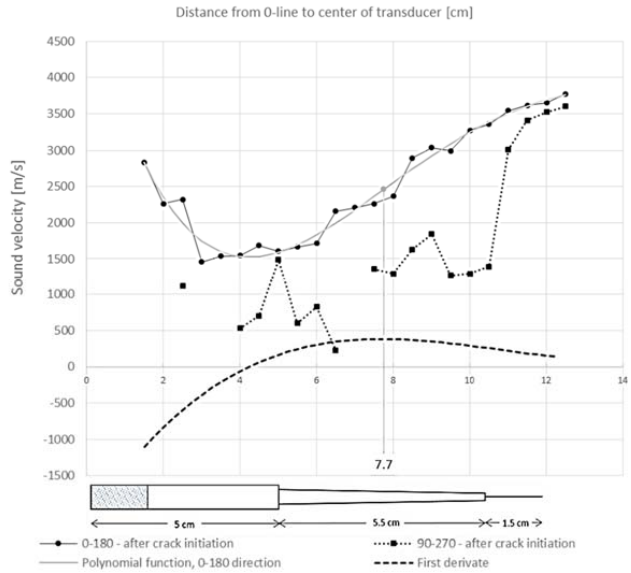

$$y = 0{,}6199x^4 - 26{,}847x^3 + 399{,}81x^2 - 2130{,}1x + 5215{,}7 \qquad [7.1]$$
$$R^2 = 0{,}9731$$

Figure 7.6: Changes in measured sound velocity from one measuring point to another in core sample S_9-2.

By solving the fourth degree equation that represents the first derivative of the function, the point of inflexion was found to be at 7,7 centimeters. This point represents the point on the curve where the curve is steepest, which means where the rate of change of the sound velocity profile is highest. This means, that in this specific case, the crack has less influence of the measured sound velocity when the width of the crack is equal to or less than the width at 7,7 centimeters. If more measuring points could have been included in the polynomial regression it could have been possible to calculate at what width the crack have a negligible influence on the measured velocity. At 12,5 centimeters, the rate of change is about 137 m/s per 0,5 centimeters. This relatively high rate of change indicates that the crack still influence the measures sound velocity in this point. Unfortunately, it was not possible to do any more measurements along the core due to the 30 millimeters diameter of the transducer. At this point, the visible end of the crack is almost straight under the center of the transducer, and the measured sound velocity represents both the sound velocity across the crack and in intact rock mass. The lack of measurements in the last 1,5 centimeters of the core makes a considerable uncertainty. This might explain the relatively high rate of change in this point. In addition, the crack might be longer inside the core than it is on the surface of the core sample.

At the bottom of the core sample, the measured sound velocities in both directions deviates from the measurements before crack initiation. The deviation was about 390 m/s in the 90-270 direction and 220 m/s in the 0-180 direction. A part of the deviation of can be due to uncertainties in the measuring equipment and uncertainties related to the performance of the measurements, as described above. AS described above, the last measuring point was at 12,5 millimeters due to the 30 millimeters diameter of the transducer. At this point, the visible

end of the crack is almost straight under the center of the transducer, and the measured sound velocity represents both the sound velocity across the crack and in intact rock mass. The lack of measurements in the last 1,5 centimeters of the core makes a considerable uncertainty. In addition, some of the deviation might be due to cracking inside the core, not visible by visual inspection of the core the crack might be longer inside the core than it is on the surface of the core.

A difference of 220 m/s is not very high compared to the average sound velocity in the intact core sample. If the rate of change decreases to 100 m/s per 0,5 centimeters in measuring point 13,5, the calculated sound velocity would be around 20 m/s in the 0-18 direction. This would have been within the uncertainty of the measurements of 40 m/s. In the 90-270 direction the deviation of 390 m/s considerably higher. As discussed above, the measured sound velocity can be considerably influenced if the measurements are carried out parallel to the crack. This might explain some of the deviation.

To a great extent, the measured sound velocity profile in core sample S_9-2 after crack initiation shows how a crack influences the measured sound velocity, even though there is an uncertainty towards the end of the crack.

These reference measurements show that it is possible to get reliable and repeatable results with the chosen equipment and set up. They also show that it is possible to detect cracks by sound velocity measurements, and that there is a good correlation between measured sound velocity and the length and width of a crack, as long as there is only one crack. The method is suitable as a check for potential cracking in the core samples. The accuracy of the method would most likely be better with a smaller diameter of the transducers.

7.7.2 Sound velocity measurements and detected cracks

Sound velocity measurements and correlation with the digitalized foldouts

The core samples from the Nedre Røssåga headrace tunnel were categorized in three groups, based on the correlation with the digitalized foldouts. The reference measurements show that it is difficult to define a specific rule or formula to calculate the exact correlation between the measured sound velocity and the visually observed cracks. The purpose of these measurements was to check if there were any cracking in the core samples or not, and to some extent how deep the cracking was. With this in mind, there has been no attempt to define a formula or rule to categorize the core samples. The categorization is there for solely based on a visual comparison and the author's personal opinion.

All the ten core samples with an increasing sound velocity profile with a pronounced increase in measured sound velocity between two measuring points, show good or medium correlation with the detected cracking. In the four cases where the correlation is medium, the digital foldouts show a cluster of cracks close to the 0-line in combination with one crack that goes deeper into the core samples. The pronounced change in sound velocity correlates good with the cluster of cracks near the 0-line, and then the measured sound velocity increases gradually until the sound velocity profile is more or less constant. If the depth of the crack is known, it is possible to see some correlation with the measured sound velocity near the end of the crack, but with unknown length of the crack the correlation is not pronounced enough to conclude with the length of the crack. An example of this is shown in Figure 7.7. This figure also show how the measured sound velocity measured parallel to the cutter groove is affected at depth

of 10,5 centimeters from the 0-line, when the straight line between the transducers runs parallel the detected crack.

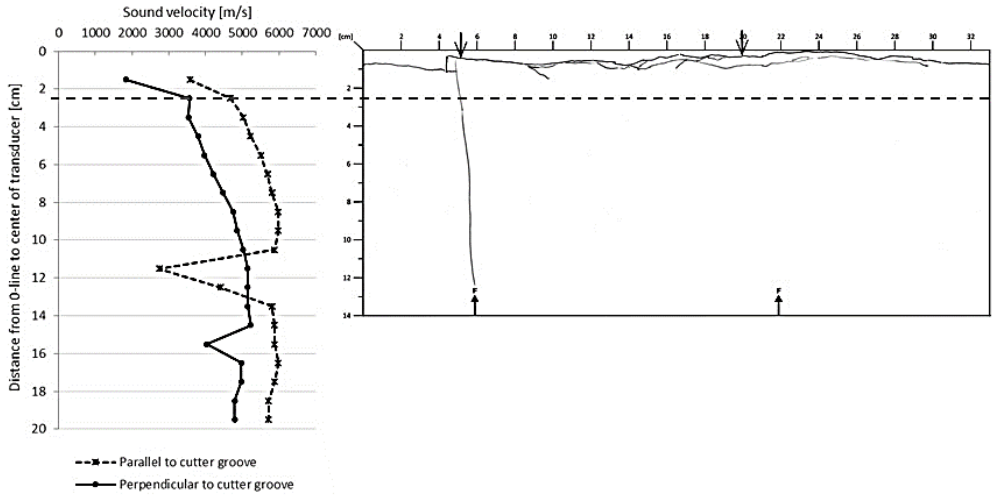

Figure 7.7: Sound velocity profiles and digitalized foldout for core sample R_3112_3-3_23.

A visual comparison of the four core samples with a gradually increasing sound velocity profile, without a pronounced change in measured sound velocity, shows that for all the core samples, the correlation between the sound velocity and the detected cracking is medium. These measured sound velocity profiles have a curved shape, where the measured sound velocity is more or less constant at the bottom of the core sample.

In addition, one core sample with an even sound velocity profile and one with an undulating sound velocity profile show good or medium correlation.

The results from the preliminary measurements on the core samples from the Trondhjemite quarry stated that, despite geological related variations along the core samples, the sound velocity profiles were variations of straight lines, with minor deviations from the average values. Only two of the core samples from the Nedre Røssåga headrace tunnel are straight lines, and in those two core samples, there are no detected cracks. The combination between these two observations indicate that a curved shaped measured sound velocity profile most likely is related to cracking.

The comparison of measured sound velocity profiles and the detected cracks in the core samples from the Nedre Røssåga headrace tunnel, shows that sound velocity measurements correlates best with the measured sound velocity under two conditions;

1) When there are many cracks
2) When there is one pronounced crack

For the 16 core samples in category 1.1 Good correlation and 1.2 Medium correlation, the measured sound velocities indicates that the cracking is 0-1 centimeters deeper than the

observed cracking. Most likely, this can be explained by the use of 30 millimeters diameter transducers. As described in chapter 4.4.2 *Equipment and set-up*, the measured sound velocity represents the sound velocity in the 30 millimeters thick area between the two transducer, but that the conditions under the center of the transducer has the highest impact in the recorded pulse. This means that a crack can affect the measured sound velocity in a measuring point as far as 1,5 centimeters away from the crack. Transducers with a smaller diameter would probably increase the accuracy of the measurements. Some of the miscorrelation might be due to geological factors and / or not detected cracking inside the core samples. No investigations have been done to verify / disprove this.

As for the reference measurements on core sample S_9-2 after crack initiation, the measured sound velocity profiles for the core samples from the Nedre Røssåga headrace tunnel show that it is challenging to detect exactly at what depth one single, closed crack, ends. Using transducers with a smaller diameter and/or measurements every 0,5 centimeters could probably have improved the accuracy.

As for core sample S_9-2 a polynomial regression was made for core sample R_1184_1-2_22. The fourth degree polynomial representing the measured sound velocity profile is presented in Figure 7.8 and formula [7.2]. Note that this regression only represents this specific set of measurements.

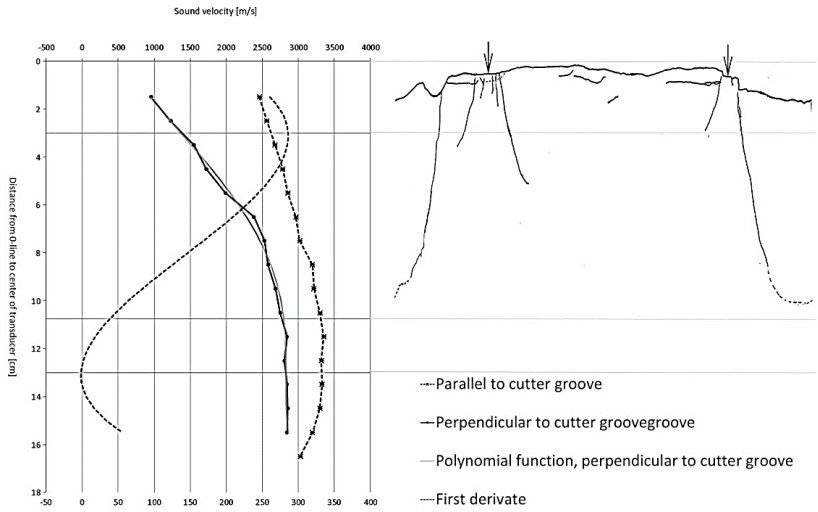

$$y = 0{,}1448x^4 - 4{,}6975x^3 + 35{,}533 + 183{,}9x + 615{,}89 \qquad [7.2]$$
$$R^2 = 0{,}9945$$

Figure 7.8: Changes in measured sound velocity from one measuring point to another in core sample R_1184_1-2_22.

By solving the fourth degree equation that represents the first derivative of the function, the points of inflexion was found to be at a depth of three and 13 centimeters. At three centimeters the rate of change of the sound velocity profile is highest. This correlates well with the observed cracks. At 13 centimeters, the rate of change is lowest, and this point does

not correlate very good with the observed end of the crack. At this point, the rate of change is 4 m/s per centimeter. This is far less than the Uncertainty in the measurements of 40 m/s, discussed earlier. The rate of change is 40 m/s per centimeter at 10,75. This correlates very well with the observed cracking. This shows that it is possible to estimate the end of a crack from a measures velocity profile by regression. In this study, no other regressions have been done,

From the measured sound velocity profiles, it is not possible to tell whether there are one or many cracks in the core samples. Nevertheless, the method gives a good indication to whether there are cracks in a core sample and to a great extent at what distance from the 0-line the rock in the core samples have been affected by the disc cutters of the TBM.

Hypothesis 1

The core samples from the Nedre Røssåga headrace tunnel were categorized in four groups, based on the shape of the measured sound velocity profiles. A common characteristic for the 18 core samples in group 2.1, 2.2 and 2-4 is that the sound velocity increases with increasing distance from the 0-line. For the two core samples in category 2.3 the measured sound velocity is more or less constant through the core samples. In addition, the measured sound velocity profile in the 0-180 direction in core sample S_9-2 after crack initiation have an increasing sound velocity profile towards the bottom of the core sample.

To a great extent, this results verify the first hypothesis; The sound velocity will increase with increasing distance from the face, as the effect of the cutters on the TBM at a certain distance from face will be insignificant.

Hypothesis 2

The core samples from the Nedre Røssåga headrace tunnel were categorized in four groups, based on the differences between the sound velocity measurements parallel and perpendicular to the cutter groove. The results show that 15 out of 20 core samples can be placed in category 3.1; having a higher measured sound velocity parallel to the cutter groove then perpendicular to the cutter groove in the entire core sample.

The three core samples in category 3.2 show the same trend, but in each core sample, two of the measured velocities parallel to the cutter groove is lower than the measured velocity perpendicular to the cutter groove. A comparison of the sound velocity profiles with the digitalized foldouts, shows that in core sample R_3112_3-3_23, the measurements parallel to the cutter groove at 11,5 and 12,5 centimeters most likely are influenced by one crack that runs parallel the measuring direction, see Figure 7.7. In core sample R_3112_5-3_27, there are many cracks directly under the cutter groove. These cracks most likely affects the measuring, and causes an undulating sound velocity profile in both directions. These two core samples correlates to the core samples in category 3.1. In core sample R_1184_1-1_21, there are no visible explanations to why the measure sound velocity is higher perpendicular to the cutter groove than parallel to it in two of the measuring points.

Looking at core sample R_3112_4-4_24 in category 3.3 and core sample R_3112_4-3_23 there are no visible explanations to why the measured sound velocity is higher perpendicular to the cutter groove than parallel to it in two of the measuring points.

After the comparison with the digitalized foldouts, only three core samples differ from the hypothesis. To a great extent, this results verify the sound hypothesis; velocity will be higher measured parallel to the cutter groove than measured perpendicular to it.

7.8 On loose ends

All the sampling, investigations and evaluations are done within the scopes and limitations of this Ph.D.-study, and are based on the available information and knowledge at the different stages of the process. New knowledge gives new basis and opportunities to raise new questions for further research and analysis.

In the following, some suggestions, based on lessons learned in this Ph.D.-study are provided. These suggestions are believed to further improve the understanding of the rock breaking:

- All cracks are evaluated with respect to their point of origin. An evaluation of the same cracks in relation to their ending point could increase the understanding of the rock breaking.
- Including core samples from other location of the face could improve the understanding of the difference in observed cracking on the two sides of the cutter groove.
- Long term testing of low RPMs in a tunnel could prove the effect of lowering the RPM in relation to cutter life and a long term penetration rate.

8 Conclusions

The aim of this Ph.D. study has been to **increase the understanding of the rock breaking under a disc cutter of a full size TBM** by answering nine research questions and fulfilling three objectives.

Objective 1

Establish an economical and time efficient method to detect and document the rock breaking under the disc cutters of a full size TBM in hard rock in order to verify, disprove or differentiates the interpretation of rock breaking under disc cutters.

1.1 How can a high number of useful samples be collected from the face of a TBM tunnel, in a cost and time efficient way, without influencing the excavation of the tunnel unnecessary?

- *Core drilling at the tunnel face during TBM-idle is a cost and time efficient way to collect representative samples, both in number and location from a TBM tunnel without interfering the excavation unnecessary.*

1.2 How can the effect of disc cutters be detected and documented in a cost and time efficient way?

- *Sound velocity measurements is a cost and time efficient way to get a qualified indication of whether there are cracks in the core or not, and how deep into the face the rock is affected by the cutters .*

- *Dye penetrant is a cost and time efficient way to visualize cracks that are not visible to the naked eye. It doesn´t require any laboratory facilities and can be used at site.*

- *Digitalized foldouts, cross sections and measurements of crack properties is a cost and time efficient way to document the effect of disc cutters*

All of which provides relevant information on the crack initiation and distribution caused by the rolling disc cutters of a TBM excavating in hard rock.

1.3 How deep into the rock mass is the rock mass affected by the cutters?

- *Independent of geology, the highest measured total length of a crack was 160 mm, and the highest vertical depth from the 0-line was 158 mm, but more than 80% of all cracks have a total length of less than 35 millimeters and a vertical depth from 0-line of less than 41 mm. Consequently, the depth of influence on rock breaking is quite limited.*

1.4 Can the concept model of rock breaking under the cutters of a TBM be verified, or would the findings lead to a revision or differentiation of the drawing?

- *The concept model of rock breaking under the cutters of a TBM can be considered as a generalized and idealized presentation of this situation. However, the great variety of fracture patterns, and rock chipping caused by the rolling cutters in front of a full size TBM are by far fully represented in this idealized concept model .*

1.5 Is there any correlation between cracks found in chips compared to those in the core samples?

- *Due to a small number of chips, it is not possible to draw a distinct conclusion on rock breaking under the disc cutters at the two sites, but to some extent, the number of documented cracks in the chips from the AMR Project and the Nedre Røssåga headrace tunnel support the findings in the core samples from the two sites.*

Through these questions and answers, the first objective of this study is fulfilled.

Objective 2

Document the effect of different RPMs concerning rock breaking under the disc cutters of a full size TBM in hard rock

2.1 Is it possible to identify different responses of disc cutters using different RPMs within the same geology?

The data collected for this Ph.D.-study indicates that RPM has an influence on rock breaking in the following aspects:

- *RPM influences the number of cracks*
- *RPM influences the total length of the cracks*
- *RPM influences the vertical depth of cracks, both from the surface line and the 0-line*
- *RPM influences the dip and dip direction of the cracks*
- *RPM influences the allocation of cracks between the cutter grooves*

2.2 Is it possible to identify similar responses of disc cutters in two different geologies?

- *Within both geologies included in this study, the lower RPM generates the highest chipping potential in terms of; a higher number of cracks, longer cracks, higher vertical depth of the cracks and a better distribution of cracks, dip angles, and dip directions in reference to the cutter groove.*

2.3 Does the RPM affect the shape of the surface lines of the core samples?

- *In this Ph.D.-Study there is no indication that RPM affects the shape of the surface lines of the core samples.*

Through these questions and answers, the second objective of this study is fulfilled.

Objective 3

Detect and document the rock breaking under the disc cutter in a linear cutter, and compare this with the results from a full size TBM in order to document any similarities or differences in the effect of a disc cutter in a LCT and on a full size TBM.

3.1 Is it possible to identify similar effects of disc cutters on a TBM and in a LCT?

- *From a visual evaluation of the surfaces and the fracturing patterns, there are no obvious differences between the surfaces and the fracturing patterns in the core samples from the LCT and the core samples from the Nedre Røssåga headrace tunnel.*

- *The comparison of the distribution of dip directions in reference to the cutter groove indicate that this distribution is congruent for the cracks from the LCT and from the full size TBM, but that the there is a higher share of cracks with low dip angles in the core samples from the LCT.*

- *Despite a small number of documented cracks in the core samples from the LCT, the comparison of the distribution of total lengths of cracks indicates that the distribution of lengths, relative to the maximum length within both groups, is congruent.*

- *The comparison of distributions of vertical depths from the 0-line, relative to the maximum depth from the 0-line within both groups, indicates that the distribution is incongruous, and that there is a more even distribution of measured vertical depths from the 0-line in the core samples form the LCT than in the core samples from the Nedre Røssåga headrace tunnel.*

The possibility of getting results that does not fully represents the conditions at the face of a full size TBM should be taken into account if a LCT is used to predict rock breaking under rolling disc cutters.

Through this question and answer, the third objective of this study is fulfilled, but due to the low number of samples, these findings can only be considered as indications.

Final remarks

The findings presented in this thesis represents the actual conditions at the two selected sites. The findings must not be considered as universal for all types of rock masses and different TBMs, but as a contribution to a better understanding of the rock breaking under a disc cutter of a full size TBM. By these findings, the author fulfils the aim of this Ph.D.-study.

9 References

Aalberg, A., April 2013. *Identification of micro cracks in curing concrete by use of methylated spirit.* Trondheim, Norway: Personal communication April 2013: Concrete engineer, Norwegian Public Roads Administration.

ABROCK Reseach Project, 2013. *http://www.uibk.ac.at/abrock/.* [Internett] Available at: http://www.uibk.ac.at/abrock/organisation.html

Alvarez, M. G., Bruines, P. & Verhoef, P., 2000. Modelling Tunnel Boring Machine Performance by Neuro-Fuzzy Methods. *Tunneling and Underground Space Technology*, No 3 Vol 15, pp. 259-269.

Balchi, C., 2008. Correlation of rock cutting tests with field performance of a TBM in a highly fractured rock formation: A case study in Kozyatagi-Kadikoy metro tunnel, Turkey. *Tunnelling and Underground Space Technology*, Vol 24, pp. 423-435.

Barton, N., 2000. *TBM Tunneling in Jointed and Faulted Rock.* s.l.:A. A. Balkema.

Bilgin, N. et al., 2005. The performance of a full face tunnel boring machine (TBM) in Tarabya (Istanbul). I: Y. Erdem & T. Solak, red. *Underground Space Use. Analysis of the Past and Lessons for the Future Vol 1&2.* s.l.:A.A. Balkema, pp. 821-826.

Bjerkgård, T., Larsen, R. & Marker, M., 1995. *95.153 Regional geology of the Okstindene area, the Rödingsfjäll nappe complex, Nordland, Norway,* Trondheim: NGU (Geological Survey of Norway).

Blindheim, O. T., 1979. *Doctoral thesis; Boreability predictions for tunneling,* Trondheim: The Norwegian Institute of Technology, Department of Geological Engineering.

Blindheim, T. O. & Bruland, A., 1998. Boreability Testing. I: *Publication 11: Norwegian TBM Tunneling.* s.l.:NFF - Norwegian Tunnelling Society, pp. 21-27.

Boniface, A., 2000. Tunnel Boring Machine Performance in Basalts of the Lesotho Formation. *Tunneling and Underground Space Technology*, Vol 15, pp. 49-54.

Brady, B. & Brown, E. T., 2006. *Rock Mechanics for underground mining,.* 3rd red. New York, Boston, Dordrech, London, Moscow: Kluwer Academic Publishers.

Broch, E. & Franklin, J., 1972. The point load strength test. *International Journal of Rock Mechanics and Mining Sciences,* Volume 9, Volum 9, pp. 669-697.

Bruland, A., 2000. *Doctoral thesis; Hard Rock Tunnel Boring,* Trondheim: Norwegian Univeristy of Science and Technology, Department of Civil and Transport Engineering.

Büchi, E., 1984. *Einfluss geologisher Parameter auf die Vortriebsleitung einer Tunnelbohrmachine.* Diss. Universität Bern: Self-Published.

Bycotest AB, January 2007. *Product data sheet BYCOTEST RP20.* Karlstad, Sweden: Bycotest AB.

Cho, J.-W., Jeon, S., Jeong, H.-Y. & Chang, S.-H., 2013. Evaluation of cutting efficiency during TBM disc cutter excavation within a Korean granitic rock using linear-cutting-machine testing

and photogrammetric measurement. *Tunnel and Underground Space Technology*, Vol 35, pp. 37-54.

Cho, J.-W., Jeon, S., Yu, S.-H. & Chang, S.-H., 2009. Optimum spacing of TBM disc cutters: A numerical simulation using the three-dimensional dynamic fracturing method. *Tunneling and Underground Space Technology*, Vol 25, pp. 230-244.

Christiansson, R., Lehtimäki, T., Pettersson, . S. & Olsson, M., 2013. *R-13-06 - Studie av vajersågning för deponeringstunnlar,* Stockholm: Svensk Kärnbränslehantering AB.

Chryssanthakis, P. & Tunbridge, L., 2004. *Forsmark site investigation - Determination of P-wave velocity, transverse borehole core,* Stockholm: Svensk Kärnbränslehantering AB.

Dahl, F., 2015. *Laboratory testing Trondhjemite and Iddefjord granite.* Trondheim, Norway: Personal communication 10.03.2015: laboratory manager at SINTEF Geological Engineering Laboratory.

Dahl, F. et al., 2011. Classifications of properties influencing the drillability of rocks, based on the NTNU/SINTEF test method. *Tunneling and Underground Space Technology*, pp. 150-158.

Dieter, G. E. & Bacon, D., 1988. *Mechanical Metallurgy, SI Metric Edition.* s.l.:McGraw-Hill Book Company.

Eide, L. N. R., 2014. *TBM Tunneling at the Stillwater Mine,* Trondheim: Norwegian University of Science and Technology, Department of Civil and Transport Engineering.

Eitzenberger, A., 2002. *IPR-03-17: Determination of the Degree of Anisotropy on Cores from Äspö HRL,* Stockholm: :Äspö Hard Rock Laboratory - Svensk Kärnbränslehantering AB .

Eitzenberger, A., 2012. *Doctoral thesis; Wave Propagation in Rock and the Influence of Discontinuities,* Luleå, Sweden: Division of Mining and Geotechnical Engineering Department of Civil, Environmental and Natural Resources Engineering Luleå University of Technology Luleå University of Technology.

Eitzenberger, A. & Nordlund, E., 2002. Detection of Anisotropy by Diametrical Measurements of Longituinal Wave Velocities on Rock. I: *Proceedings of the 5th North American Rock Mechanics Symposium and the 17th Tunnelling Association of Canada Conference: NARMS-TAC 200.* 2, Toronto, Ontario, Canada: s.n., p. 7p.

Entacher, M., Schuller, E. & Galler, R., 2014. Rock Failure and Crack Propagation Beneath Disc Cutters. *Rock Mechanics & Rock Engineering*, Volume 48, pp. 1559-1572.

Entacher, M. et al., 2012. Cutter force measurement on tunnel boring machines - System design. *Tunneling and Underground Space Technology*, Vol 31, pp. 97-106.

FAST-Tunn, 2011. *Project description FAST-Tunn.* s.l.:s.n.

FAST-Tunn, 2013. *Revised Project description FAST-Tunn.* s.l.:s.n.

Gertsch, R., Gertsch, L. & Rostami, J., 2007. Disc cutting tests in Colorado Red Granite: Implications for TBM performance prediction. *International Journal of Rock Mechanics and Mining Sciences*, Vol 44, pp. 238-246.

Gong, Q. M. et al., 2012. Rock burst and slabbing failure and its influence on TBM excavation at headrace tunnels in Jinping II hydropower station. *Engineering Geology*, Vol 124, pp. 98-108.

Gong, Q. M. & Zhao, J., 2008. Developement of a rock mass characteristics model for TBM penetration rate prediction. *Internaional Journal of Rock MEchanics & Mining Sciences*, Vol 46, pp. 8-18.

Graham, P. C., 1976. Rock exploration for machine manufacturers. I: Z. T. Bieniawski, red. *Exploration for rock engineering.* Johannesburg: Balkema, pp. 173-180.

Grøv, E., 2014. FAST-Tunn, a research program to develop steel quality for hard rock TBM-cutters. I: A. Negro, M. O. Cecilio Jr. & W. Bilfinger, red. *Proceedings of the World Tunnel Congress 2014 - Iguassu Falls - Brazil.* Sao Paolo: s.n., pp. Paper 181, 8p.

Hajiabdolmajid, V., Kaiser, P. K. & Martin, C. D., 2002. Modelling brittle failure of rock. *Rock Mechanics and Mining Science*, Volume 39 april, pp. 731-741.

Hannestad, E., 2015. *Use of indentation tests to study the rock breaking mechanisms,* Trondheim: IGB, NTNU.

Hansen, A., 2017. Norwegian TBM Tunneling - machines for hard, though and abrasive rock conditions. I: *Publication 26 The principles of Norwegian Tunneling.* s.l.:Norwegian Tunnelling Society NFF, pp. 55-65.

Hansen, A. M., 1998. The history of TBM tunneling in Norway. I: *Publication 11: Norwegian TBM Tunneling.* s.l.:NFF - Norwegian Tunnelling Society, pp. 11-19.

Hashiba, K., Okubo, S. & Fukui, K., 2006. *International Journal of Rock Mechanics & Mining Sciences,* Volum 43, No 6, pp. 894-904.

Haugen, M. K., 2015. *Petrographic analysis of rock samples from the specified chainages at Røssåga.* Trondheim: Personal communication 10.12.2015: Senior research scientist SINTEF building and infrastructure departement of architecture, materials and structures.

Hjelmer, A. & Matern, N. v., 1943. *Försök med pågrus ("Test with Chippings"),* Stockholm: Statens väginstitut, Medelande 65, 65p (English summary, pp. 56-60).

Innaurato, N. & Oreste, P., 2011. Theoretical Study on the TBM Tool-Rock Interaction. *Geotechnical and Geological Engineering*, vol 29, pp. 297-305.

International Tunnelling and Underground Space Association, 2011. *http://www.ita-aites.org.* [Internett]
Available at: http://www.ita-aites.org/index.php?id=348&tx_ttnews%5Btt_news%5D=1005&cHash=ebe08edfe57f8196e1ca9b5215ff76fa

ISRM, 1978. Suggested Method for Determining Sound Velocity. *International Journal of Rock Mechanics and Mining Sciences & Geomechanics, Abstr. Vol. 15*, pp. 53-58.

Johannessen, S., Askilsrud, O. G. & Bruland, A., 1998. The Meråker Project - 10 km of tunnel in 12 months. I: *NFF Publication no11 - Norwegian TBM Tunneling.* s.l.:NFF, pp. 85 - 89.

Jung, H.-S.et al., 2011. Causes of reduction in shield TBM performance – A case study in Seoul. *Tunneling and Underground Space Technology*, Vol 26, pp. 453-461.

KICT, K. I. o. C. E. a. B. T., 2015. *A Project for Linear Cutting Machine (LCM) Tests with Norwegian Granite,* Seoul: s.n.

Kou, S., Xiangchum, T. & Lindqvist, P.-A., 1997. *R-99-11 - Modelling of excavation depth and fractures in rock caused by tool indentation,* Stockholm: Swedish Nuclear Fuel and Waste Management Co.

Laughton, C., 1998. *Doctoral theses;Evaluation and Prediction of Tunnel Boring Machine Performance in Variable Rock Masses,* Austin: University of Texas, Austin USA.

Leonhard Nilsen & Sønner AS, 2013. *lns.no.* [Internett] Available at: http://lns.no/Nyheter/LNS-og-Robbins-med-TBM-avtale [Funnet 25 January 2013].

Macias, F. J., 2016. *Doctoral thesis; Hard Rock Tunnel Boring - Performance predictions and cutter life assessments,* Trondheim: Norwegian Univeristy of Science and Technology, Department of Civil and Transport Engineering.

Macias, F. J., Andersson, T. & Eide, L. N., 2017. Project control by using the NTNU model methodology: The new Ulriken Tunnel. *Proceedings of the World Tunnel Congress 2017* , p. ID: 14999.

Macias, F. J., Dahl, F. & Bruland, A., 2016. New rock abrasivity test method for tool life assessments on hard rock unnel boring. The Rolling Indentation Abrasion Test (RIAT). *Rock Mechanics and Rock Engineering*, No 5 Vol 49, pp. 1679-1693.

Maidl, B., Schmid, L., Ritz, W. & Herrenknecht, M., 2008. *Hardrock Tunnel Boring Machines.* Germany: Ernst & Son.

Martin, C. D. & Chandler, N. A., 1994. The Progressive Fracture of Lac du Bonnet Granite. *International Journal of Rock Mechanics and Mining Sciences & Geomechanics Abstracts,* Volum 31, No 6, pp. 643-659.

NGU, 2017. *Geological map of Norway,* s.l.: Geological Survey of Norway.

Nilsen, O., Corfu, F. & Roberts, D., 1987. Silurian gabbro-diorite-trondhjemite plutons in the Trondheim Nappe Complex, Caledonides, Norway: petrology and U-Pb geochronology. *Norwegian Journal of Geology*, Vol 3, pp. 329-342.

Norconsult, 2013. *Technical geological report Nedre Røssåga Power Plant,* s.l.: s.n.

NTH, 1976. *Hard Rock Tunnel Boring, Projet Report 1-79.* 1976 red. Trondheim: Norwegian Institute of Technology, Div. of Construction Engineering, Trondheim, Norway.

NTH, 1983. *Hard Rock Tunnel Boring, Project Report 1-83..* 1983 red. Trondheim: Norwegian Institute of Technology, Div. of Construction Engineering, Trondheim, Norway.

Okubo, S., Nishimatsu, Y. & He, C., 1990. Loading rate dependence of class II rock behaviour in uniaxial and triaxial compression tests - an application of a proposed new control method. *International Journal of Rock Mechanics & Mining Sciences,* Volum 27, No.6, pp. 559-562.

Olsson, M., 2014. *The use of dye penetrant to visualize cracks.* Stockholm: Personal communication 28.04.2014: MSc in blasting and mining and founder of EDZ-consulting.

Olsson, M., Markström, I., Pettersson, A. & Sträng, M., 2009. *R-09-39 - Examination of the Excavation Damaged Zone in the TASS tunnel, Äspö HRL,* Stockholm: Swedish Nuclear Fuel and Waste Management Co.

Onur, A. H., Bakraç , S. & Karakuş, D., 2012. Ultrasonic Waves in Mining Application. I: D. Santos, red. *Ultrasonic Waves.* s.l.:InTech, pp. 189-210.

Ozdemir, L. & Nilsen, B., 1999. Recommended laboratory rock testing for TBM projects. *AUA news*, Vol 14, pp. 21-35.

Pedersen, S. & Maaløe, S., 1990. The Iddefjord granite: geology and age. *Geological Survey of Norway Bulletin (NGU Bulletin)*, Vol 417, pp. 55-64.

Proceq, 2014. *Operating Instructions Pundit Lab Ultrasonic Instrument.* Switzerland: Proceq.

Rinne, M., 2008. *TKK Dissertation 128: Fracture mechanics and subcritical crack growth approach to model time-dependent failure in brittle rock.* Helsinki: Helsinki University of Technology.

Rostami, J., 1997. Developement of a Force Estimation Model for Rock Fragmentation with Disc Cutters through Teoretical Modeling and Physical Measurement of Crushed Zone Preassure. *PhD-thesis Colorado School of Mines*, p. 249.

Rostami & Ozdemir, 1993. A new model for performance prediction of haard rock TBM. I: *Rapid Excavation and Tunneling Conference.* s.l.:Bowerman, L.D. et al, pp. 793-809.

Scialpi, M., Comis, S. & Clarck, J., 2012. System Efficiency in one of the World´s Longest TBM Tunnels. I: N. &. B. T. Phienwej, red. *Proceedings of the World Tunnel Congress 2012 - Bangkok - Thailand.* Bangkok: Engineering Institute of Thailand, pp. Paper ID: 0155 , 9p.

Selmer-Olsen, R. & Blindheim, O. T., 1970. On the drillability of rock by percussive drilling. I: *Proceedings 2nd Congress of IRSM.* Belgrade: s.n.

Selmer-Olsen, R. & Lien, R., 1960. Bergartens borbarhet og sprengbarhet (Boreability and blastiability of rocks). *Teknisk ukeblad*, Vol 34, pp. 3-11.

Seo, Y., 2016. *Linear Cutter Test at KICT* [Intervju] (February 2016).

Sievers, H., 1950. Die Bestimmung des Bohrwiderstandes von Gesteinen. *Glückauf*, 86:37/38, pp. 776-784.

SINTEF, 2013. *13029IG - Test report Drillability,* Trondheim: SINTEF.

Sänger, B., 2006. History of disc cutters. *Felsbau 24*, Vol 6, pp. 46-51.

TBM operators AMR project, February 2013. *TBM operation philosophy.* AMR Project, India: Personal communication Februar 2013: TBM operators at the AMR Project, India.

TBM operators Nedre Røssåga headrace tunnel, April 2014 - December 2015. *TBM operation philosophy.* Nedre Røssåga head race tunnel, Norway: Personal communication April 2014 - December 2015: TBM operators Nedre Røssåga head race tunnel, Norway.

The Norwegian National Rail Administration, 2012. *jbv.no.* [Internett] Available at: http://www.jernbaneverket.no/no/Nyheter/Pressemeldinger/2012/Follobanens-tunnel-skal-drives-med-tunnelboremaskiner/
[Funnet 30 October 2012].

The Norwegian National Rail Administration, 2012. *jbv.no.* [Internett] Available at: http://www.jernbaneverket.no/no/Nyheter/Pressemeldinger/2012/Vurderer-bruk-av-tunnelboremaskin-i-Bergen/

The Norwegian National Rail Administration, 2014. *http://www.jernbaneverket.no.* [Internett] Available at: http://www.jernbaneverket.no/Prosjekter/prosjekter/Arna---Bergenx/Nyhetsarkiv/TBM-kontrakt-pa-nye-Ulriken-tunnel-signert/

The Robbins Company, 2012. *Time consuption report AMR, TBM 317, sept-oct 2012* [Intervju] (October 2012).

Tunneling Journal, oct/nov 2011. Inside disc cutter R&D. *Tunneling Journal,* pp. 36-39.

Tunnels & Tunneling, 2009. Life on the cutting edge: Dick Robbins. *Tunnels & Tunneling,* May 2009(5), pp. 23-25.

Vassenden, 2016. Rock breaking under disc cutters of a TBM – A part of the research project FAST-Tunn . I: *Fjellsprengningskonferansen 2016.* s.l.: Norwegian Tunneling Society, pp. 4.1 - 4.12.

Vassenden, S. & Grøv, E., 2013. FAST-Tunn; a research project to increase the TBM cutter efficiency with 25 %. I: *Fjellsprengningskonferansen 2013.* s.l.:Norwegian tunneling Society, pp. 6.1 - 6.7.

Vassenden, S. & Grøv, E., 2017. *Rock Breaking Under the Disc Cutters of a TBM – a Part of the Research Project FAST-Tunn.* Bergen, Proceedings of the World Tunnel Congress 2017 – Surface challenges – Underground solutions. Bergen, Norway.

Vutkuri, V., Lama, R. & Saluja, S., 1978. *Handbook on Mechanical Properties of Rocks..* 2nd Edition red. Switzerland: Trans Tech Publications.

Wittaker, B. N., Singh, R. N. & Sun, G., 1992. *Rock Fracture Mechanics. Principles, Design and Applications. Developments in Geotechnical Engineering.* Amsterdam: Elsevier.

Yang, J., 2015. Effect of Displacement Loading Rate on Mechanical Properties of Sandstone. *The Electronic Journal of Geotechnical Engineering,* Volum 20, No.2, pp. 591-602.

Yilmaz, I., 2009. A new testing method for indirect determination of the unconfined compressive strenght of rocks. *International Journal of Rock Mechanics & Mining Sciences*, Vol 46, pp. 1349-1357.

Yin, L. J. et al., 2014. Use of indentation tests to study the influence of confining stress on rock fragmentation by a TBM cutter. *International Journal of Rock Mechanics & Mining Science*, Vol 72, pp. 261-276.

Appendix A

APPENDIX A
OPERATIONAL PARAMETERS AND TBM PERFORMANCE

List of contents

List of figures

A1 Logged data during sampling strokes

Operational parameters and TBM performance were logged continuously during boring at both the AMR Project and the Nedre Røssåga headrace tunnel. In addition, the operators provided manually logged data for the last 50 cm of every sampling stroke. This manually logged data is presented in Table A1.1.

Table A1.1: Manually logged average performance of the TBM during boring of sampling strokes.

	The AMR project		The Nedre Røssåga headrace tunnel				
Chainage [m]	11573	11579	1184	3112	5437	5458	5478
Date of sampling	25.02.2013	25.02.2013	14.07.2014	10.02.2015	21.07.2015	22.07.2015	23.07.2015
RPM	5.9	5.5	7.5	5	3	6.5	5
Thrust force [kN]	16000	16000	14000	14000	16000	15500	16000
Torque [kNm]	No data	No data	2100	No data	2100	2200	2200
Pressure [bar]	No data	No data	220	220	240	240	250
Cutter load [tonn/disc]	No data	No data	26	26	28	28	29
Penetration [mm/min]	25	27	40	No data	26	60	43
Penetration [mm/rev]	No data	No data	5.5	No data	8	9	8.6
Penetration [m/h]	1.50	1.60	2.48	1.70	1.60	3.50	2.50

In the following, continuously logged data for each sampling stroke is presented. At chainage 3112 at the Nedre Røssåga headrace tunnel the data logger suffered from some technical problems, but the operator was aware of this and manually logged average data. Al data is provided by Robbins and LNS. The notations corresponds to the notations in the data logger. Table A1.2 gives an overview of available data.

Table A1.2: Available data for each sampling stroke

	The AMR project		The Nedre Røssåga headrace tunnel				
Chainage [m]	11573	11579	1184	3112	5437	5458	5478
Stroke position]mm]	+	+	+	-	+	+	+
Chainage [m]	+	+	+	-	+	+	+
Cutter head thrust force [kN]	+	+	+	-	+	+	+
Cutter head RPM [rev/min]	+	+	+	-	+	+	+
Net excavation [mm/min]	+	+	+	-	+	+	+
Net excavation [mm/rev]	-	-	-	-	+	+	+
Cutter head torque [kNm]	-	-	+	-	+	+	+

A1.1 The AMR Project

Logged values every ten seconds.

Chainage 11573

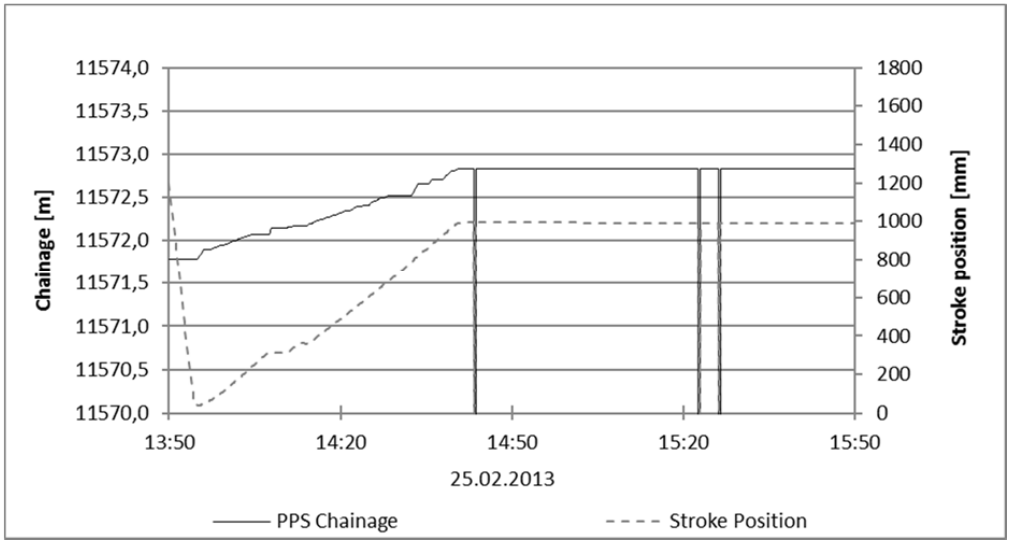

Figure A1.1: Increasing chainage and stroke position before sampling at chainage 11572.8.

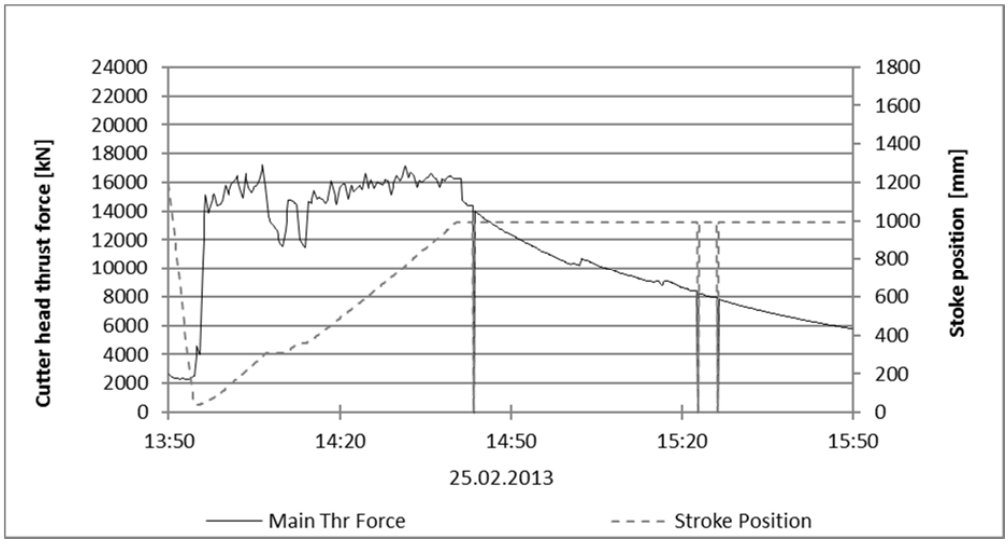

Figure A1.2: Thrust force at the cutter head and stroke position before sampling at chainage 11572.8.

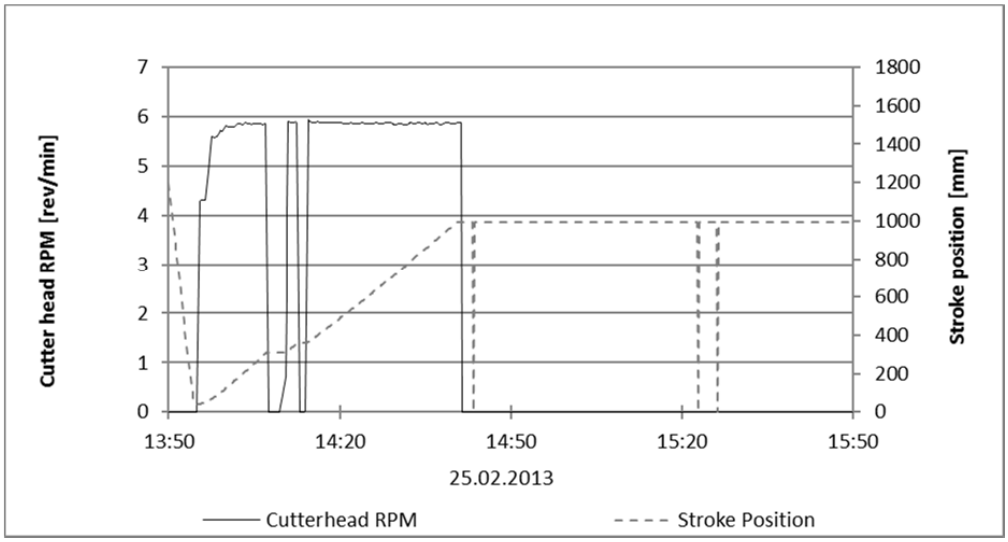

Figure A1.3: Cutter head RPM and stroke position before sampling at chainage 11572.8.

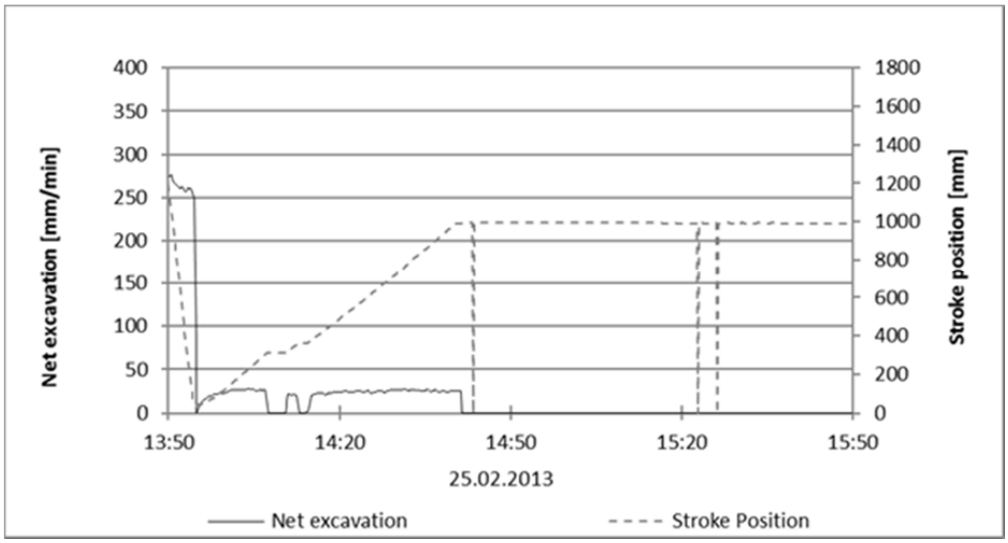

Figure A1.4: Net excavation rate and stroke position before sampling at chainage 11572.8.

Penetration rate in millimeters per minute. The high peaks is caused by repositioning of the cutter head, and is not related to boring.

Chainage 11579

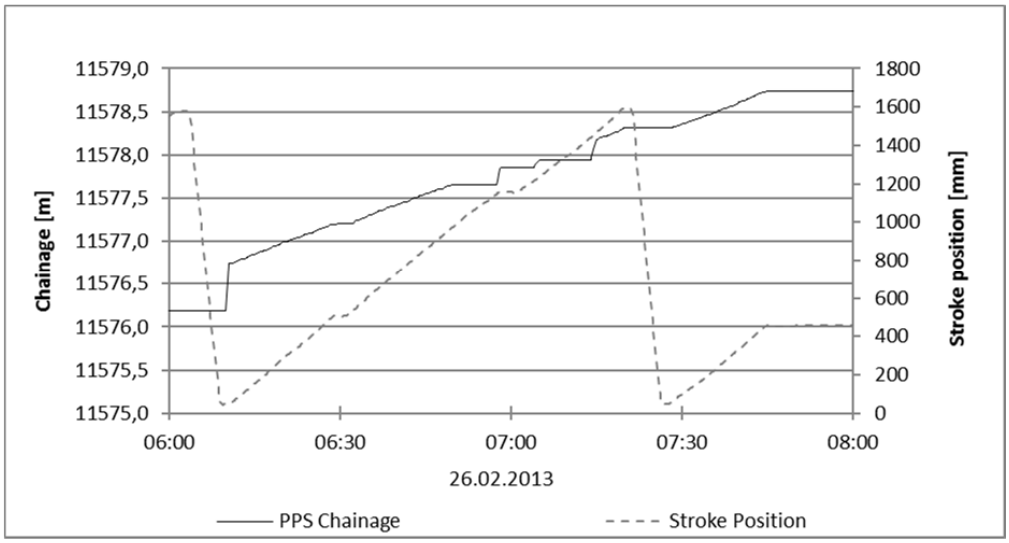

Figure A1.5: Increasing chainage and stroke position before sampling at chainage 11578.8.

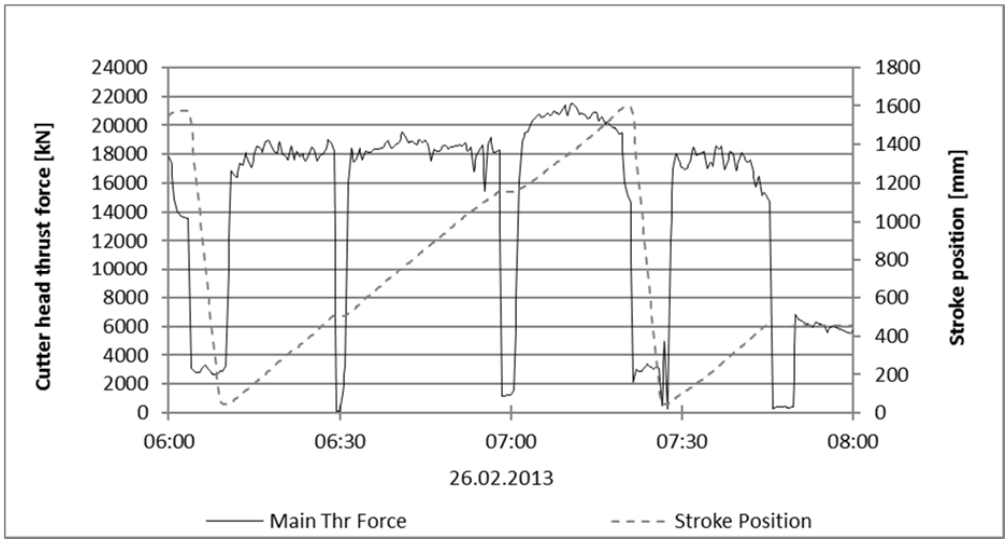

Figure A1.6: Thrust force at the cutter head and stroke position before sampling at chainage 11578.8.

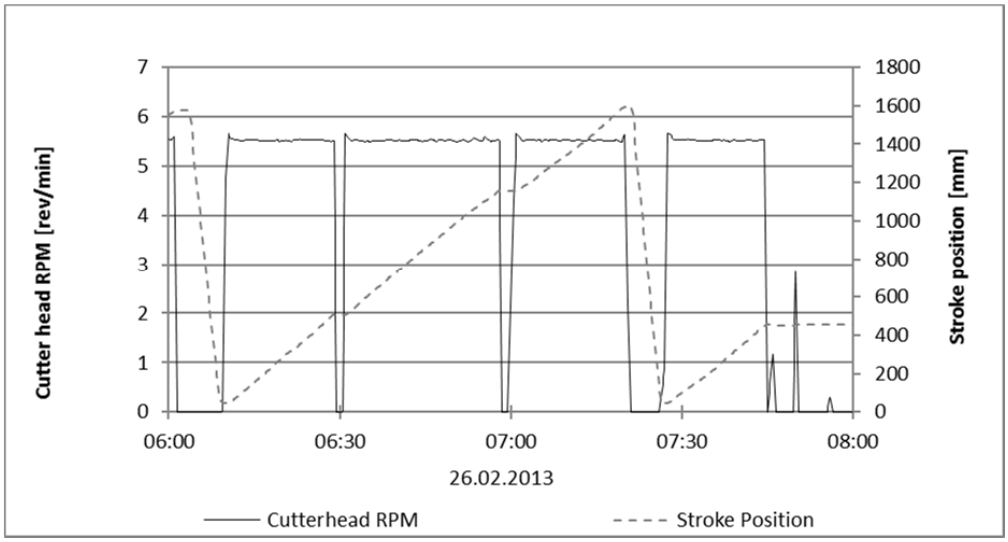

Figure A1.7: Cutter head RPM and stroke position before sampling at chainage 11578.8.

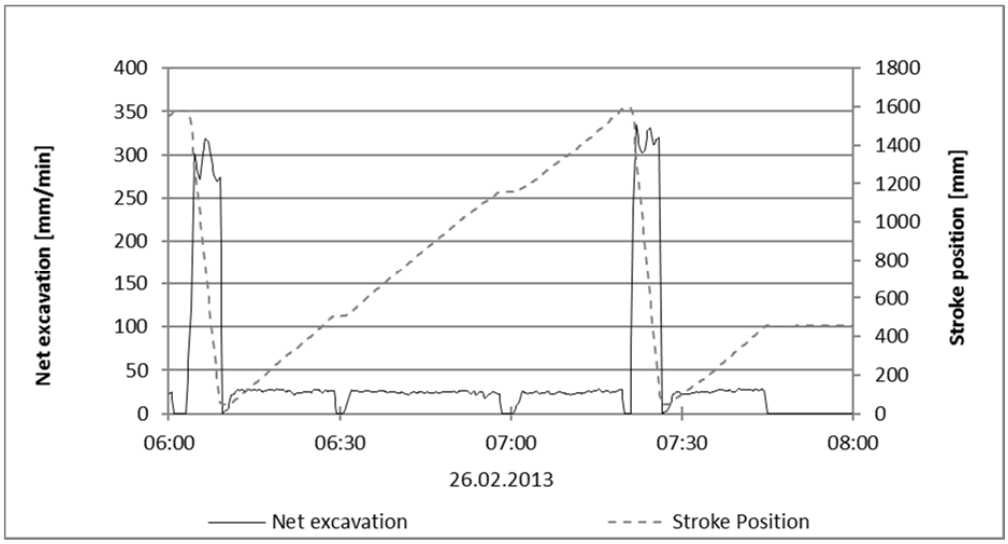

Figure A1.8: Net excavation rate and stroke position before sampling at chainage 11578.8.

Penetration rate in millimeters per minute. The high peaks is caused by repositioning of the cutter head, and is not related to boring.

A1.2 The Nedre Røssåga headrace tunnel

Logged values every five seconds.

Chainage 1184

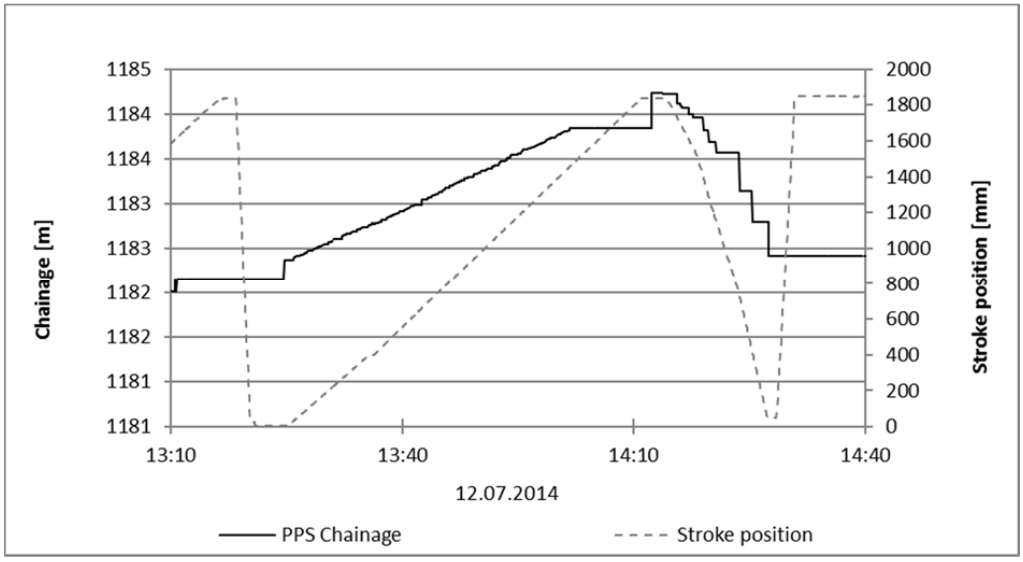

Figure A1.9: Increasing chainage and stroke position before sampling at chainage 1184.2.

The continuously increasing stroke positioning indicates that there are some values missing for the logged chainage.

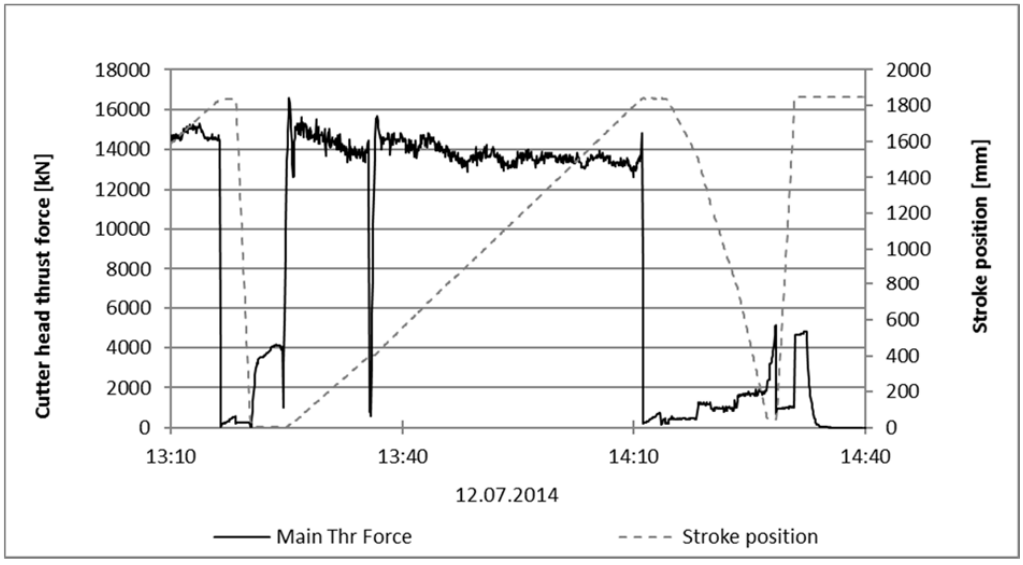

Figure A1.10: Thrust force at the cutter head and stroke position before sampling at chainage 1184.2.

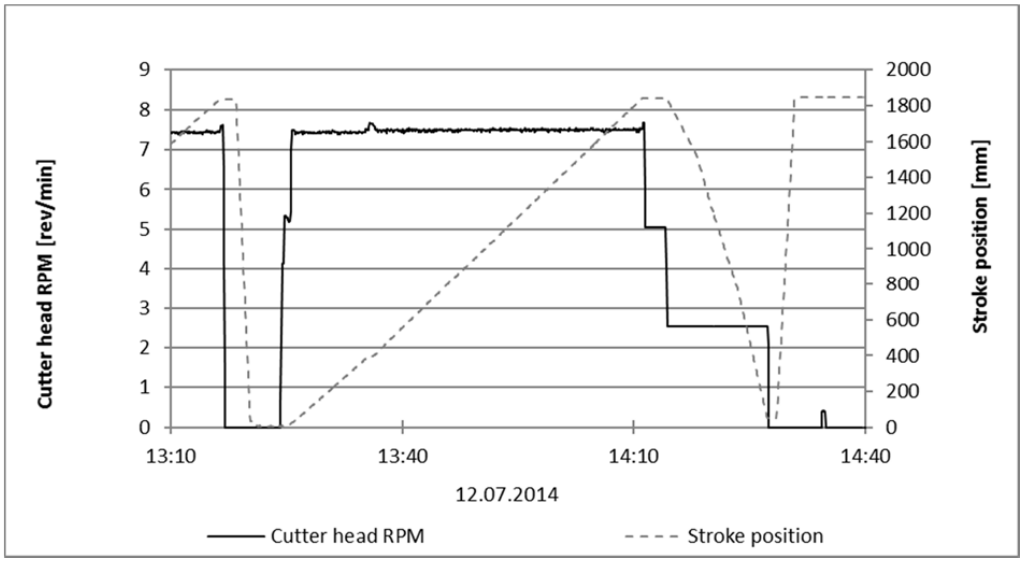

Figure A1.11: Cutter head RPM and stroke position before sampling at chainage 1184.2.

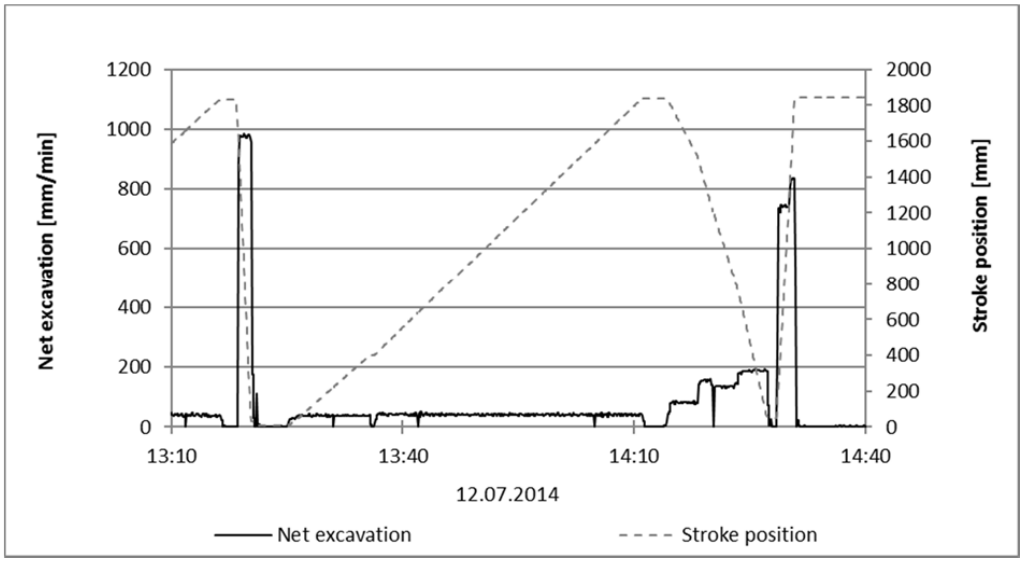

Figure A1.12: Net excavation rate and stroke position before sampling at chainage 1184.2.

Penetration rate in millimeters per minute. The high peaks is caused by repositioning of the cutter head, and is not related to boring.

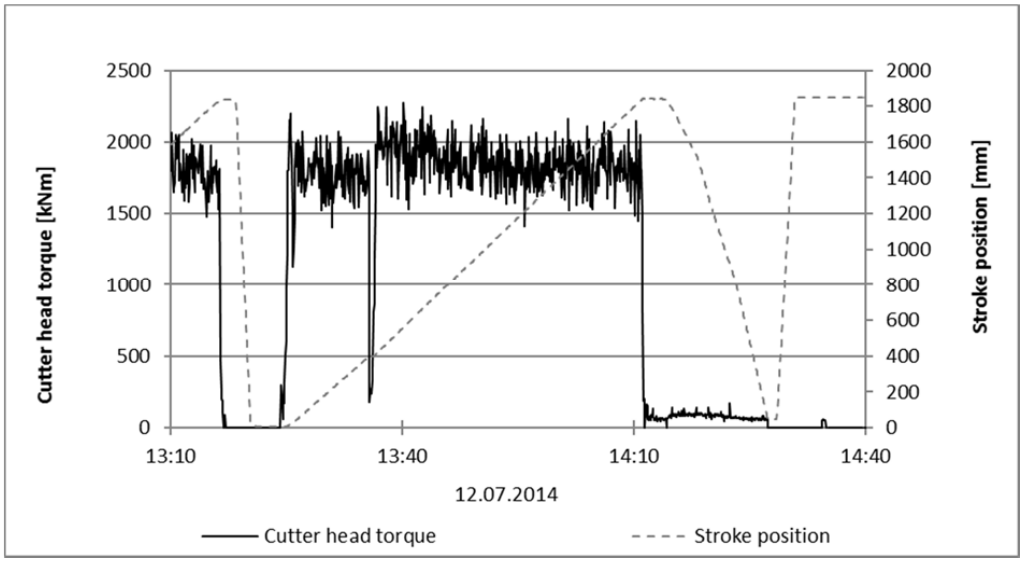

Figure A1.13: Cutter head torque and stroke position before sampling at chainage 1184.2.

Chainage 3112

No available data logg. The values below are provided by the operator.

Table A1.3: Average logged performance of the TBM during sampling stroke at chainage 3112.6.

Chainage [m]	3112.6
Date of sampling	10.02.2015
RPM	5
Thrust force [kN]	14000
Preassure[bar]	220
Cutter load [tonn/disc]	26
Penetration [mm/min]	No data
Penetration [mm/rev]	No data
Penetration [m/h]	1.70

Chainage 5437

No available data before 21.07.2015 18:15:00.

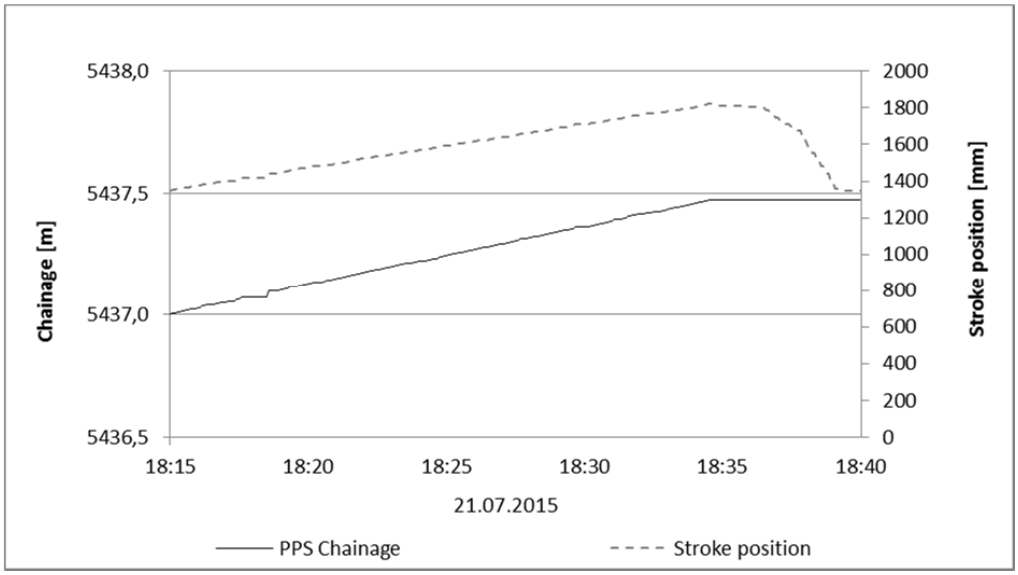

Figure A1.14: Increasing chainage and stroke position before sampling at chainage 5437.5.

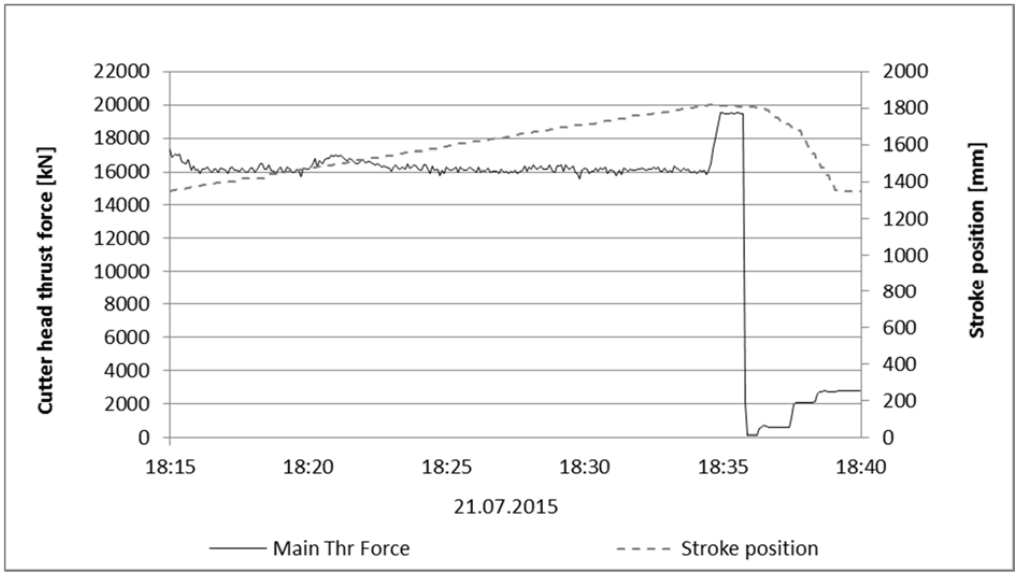

Figure A1.15: Thrust force at the cutter head and stroke position before sampling at chainage 5437.5.

The increased logged thrust force towards the end of the stroke is caused by the pressure in the stuffing box in the hydraulic cylinder. This increased pressure in the cylinders is not transferred to the cutters.

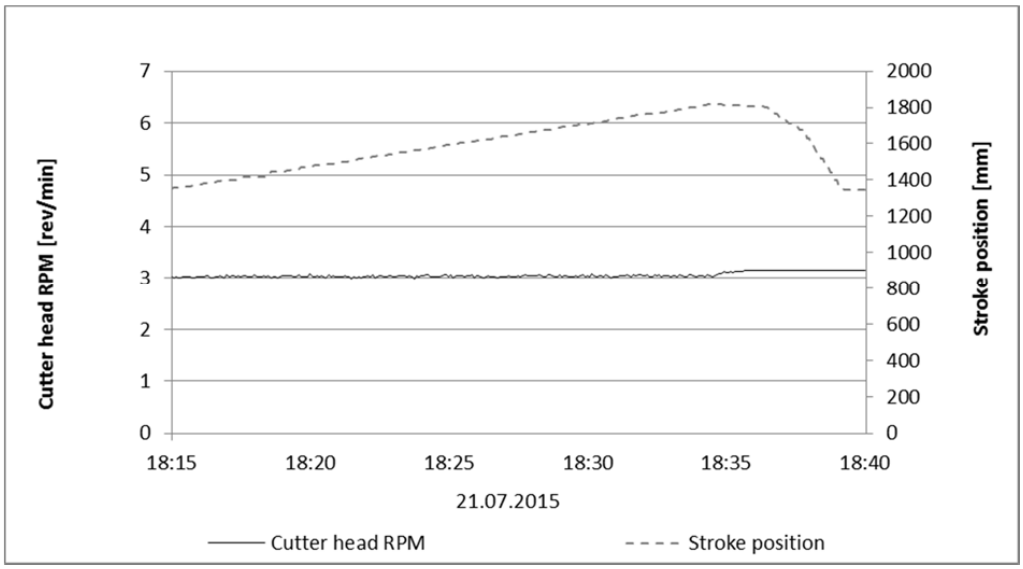

Figure A1.16: Cutter head RPM and stroke position before sampling at chainage 5437.5.

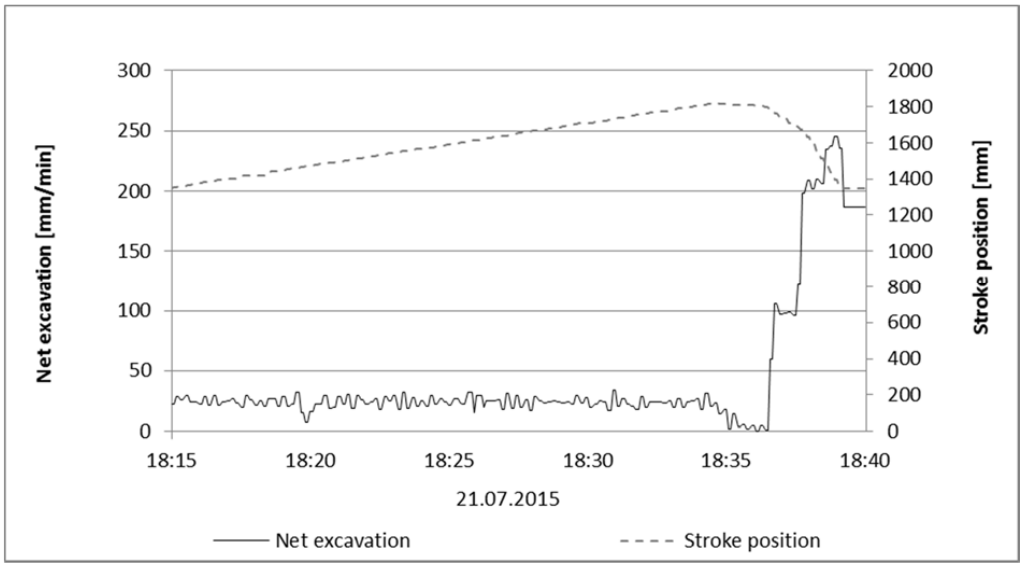

Figure A1.17: Net excavation rate in millimeter per minute and stroke position before sampling at chainage 5437.5.

Penetration rate in millimeters per minute. The high peaks is caused by repositioning of the cutter head, and is not related to boring.

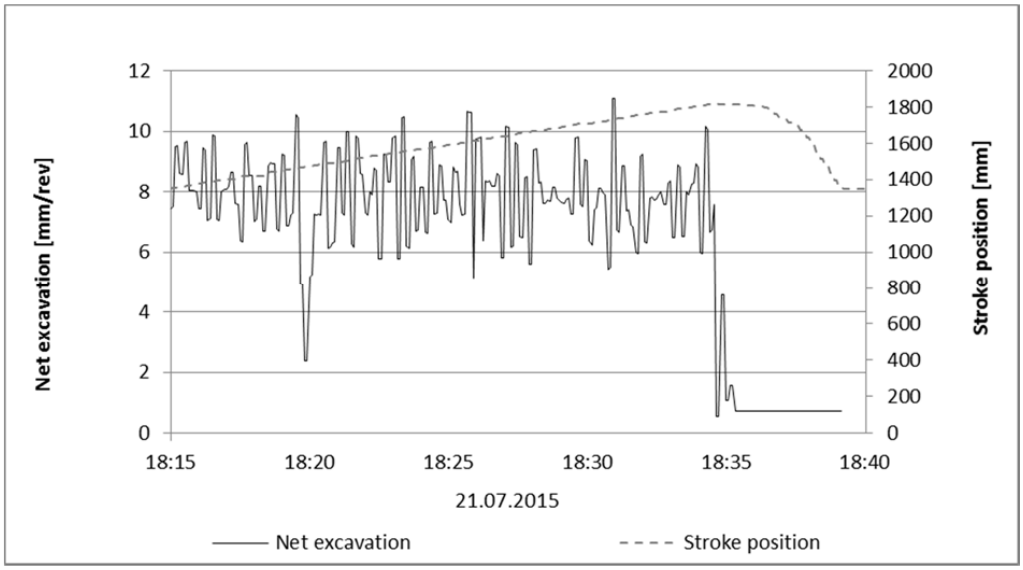

Figure A1.18: Net excavation rate in millimeter per revolution and stroke position before sampling at chainage 5437.5.

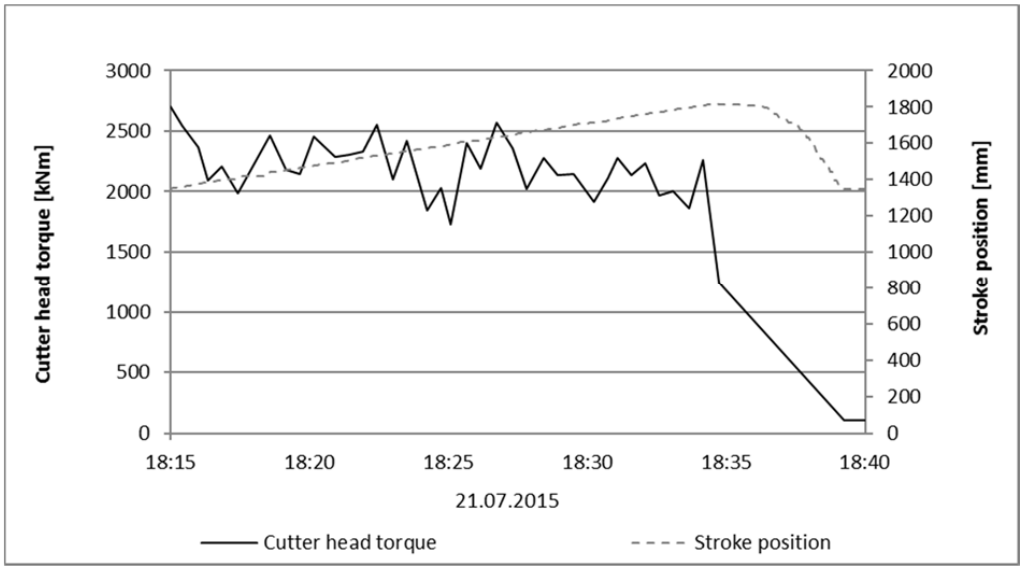

Figure A1.19: Cutter head torque and stroke position before sampling at chainage 5437.5.

Chainage 5458

No available data before 22.07.2015 18:25:00.

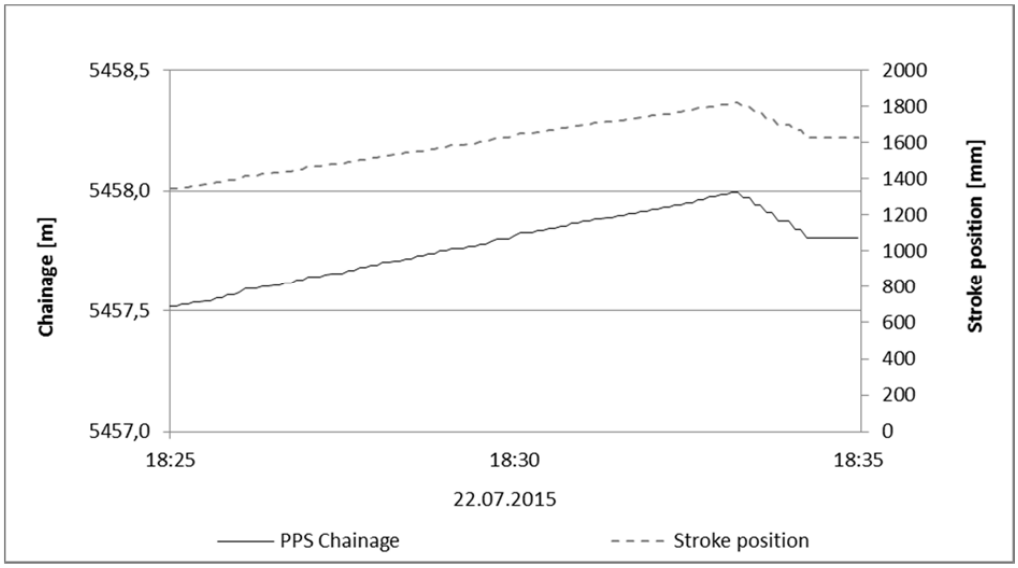

Figure A1.20: Increasing chainage and stroke position before sampling at chainage 5458.0.

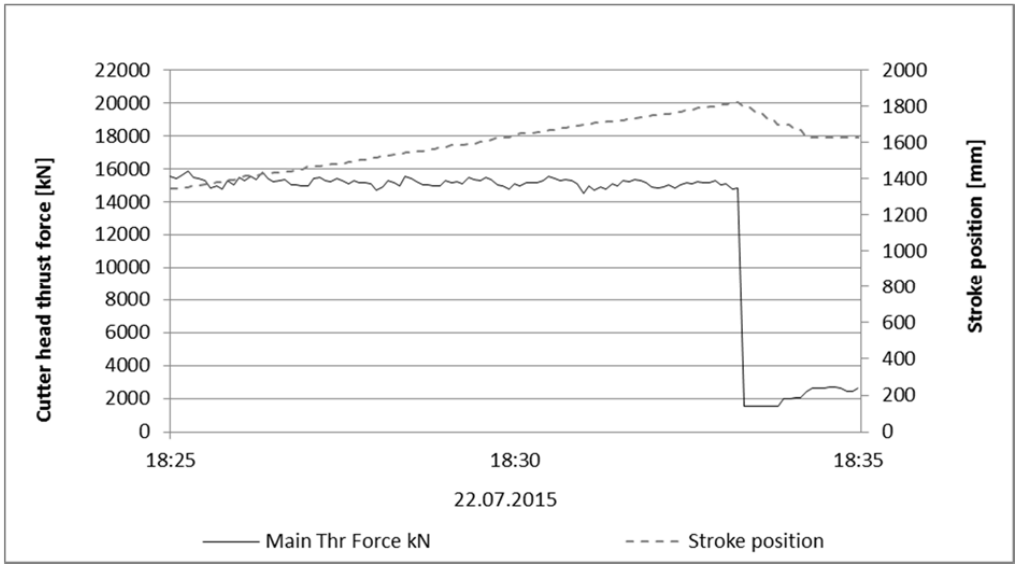

Figure A1.21: Thrust force at the cutter head and stroke position before sampling at chainage 5458.0.

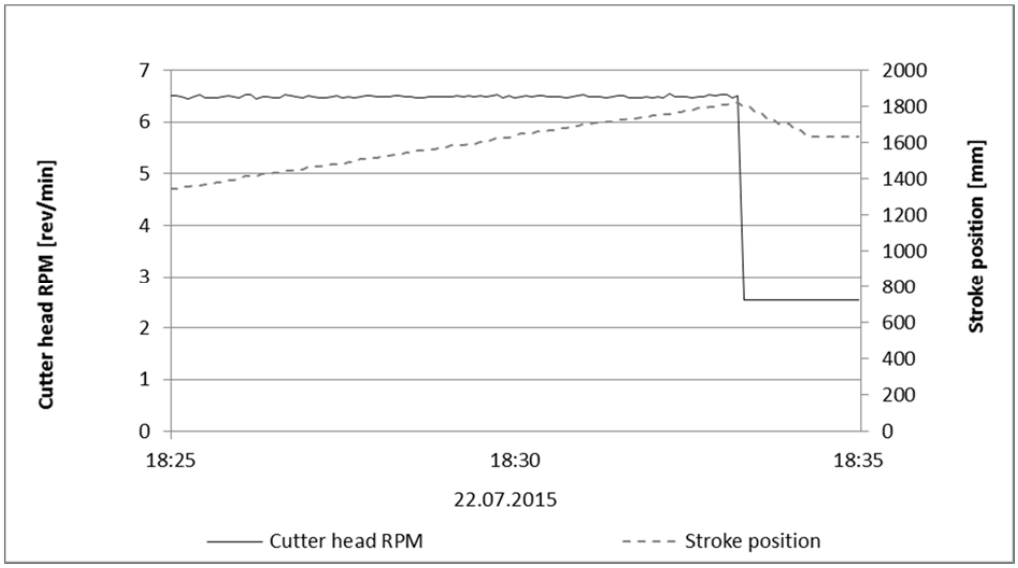

Figure A1.22: Cutter head RPM and stroke position before sampling at chainage 5458.0.

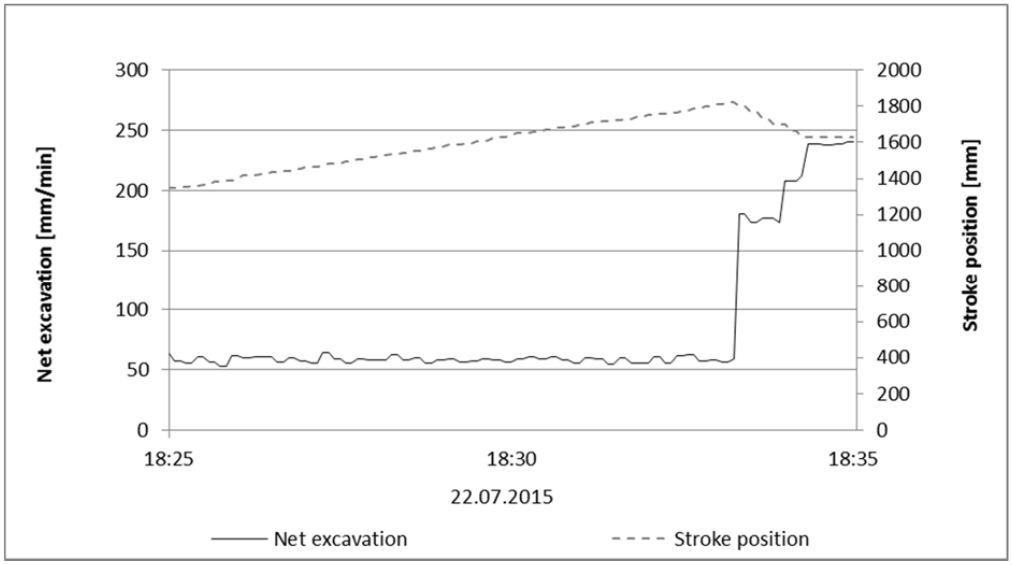

Figure A1.23: Net excavation rate in millimeters per minute and stroke position before sampling at chainage 5458.0.

Penetration rate in millimeters per minute. The high peaks is caused by repositioning of the cutter head, and is not related to boring.

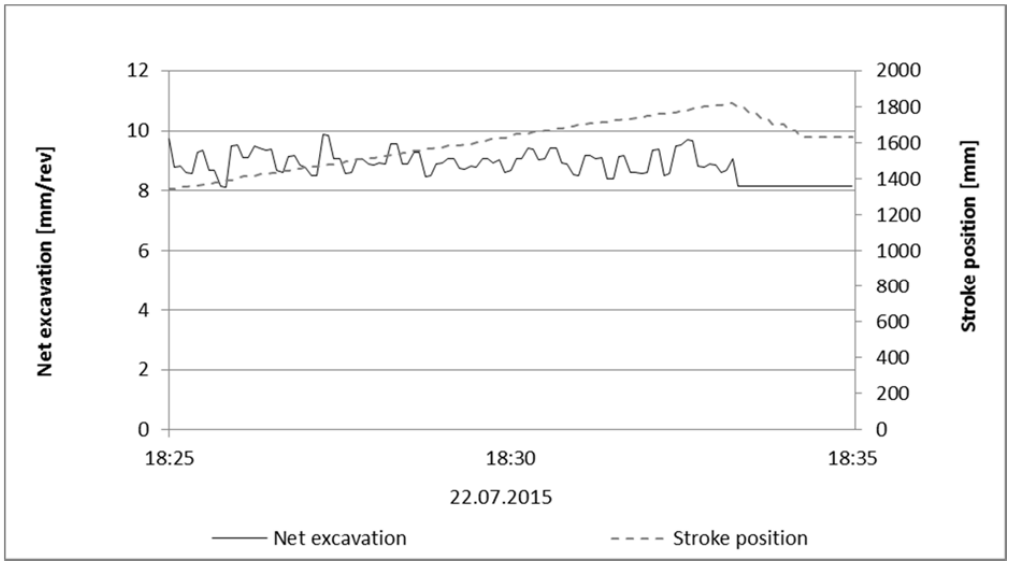

Figure A1.24: Net excavation rate in millimeters per revolution and stroke position before sampling at chainage 5458.0.

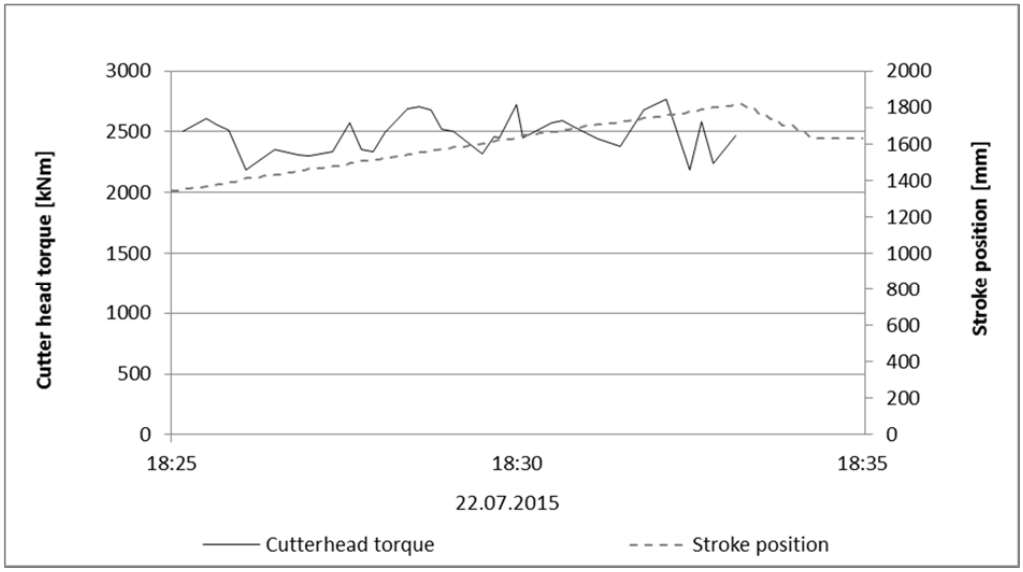

Figure A1.25: Cutter head torque and stroke position before sampling at chainage 5458.0.

Chainage 5478

No available data before 23.07.2015 18:17:00.

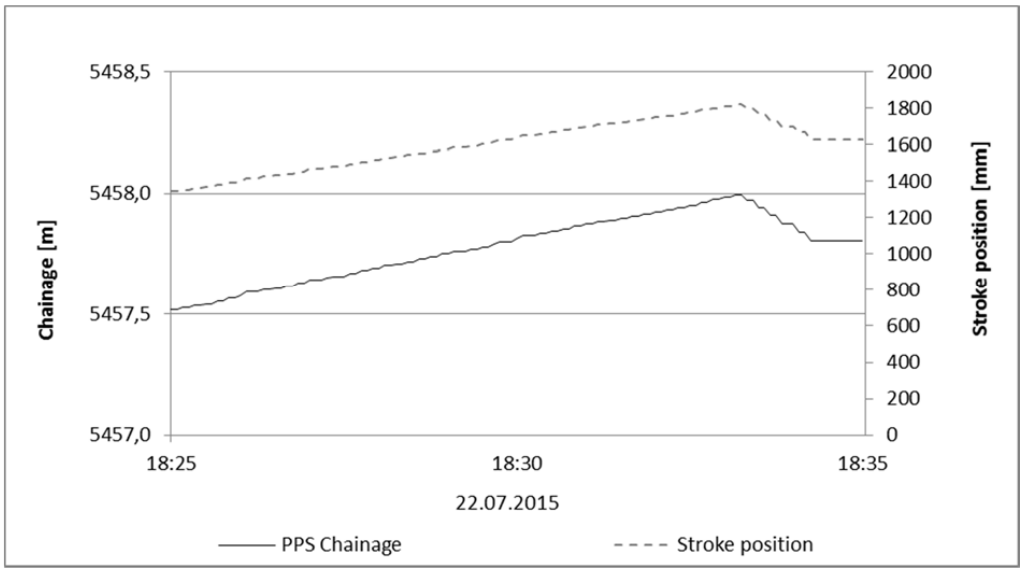

Figure A1.26: Increasing chainage and stroke position before sampling at chainage 5478.0.

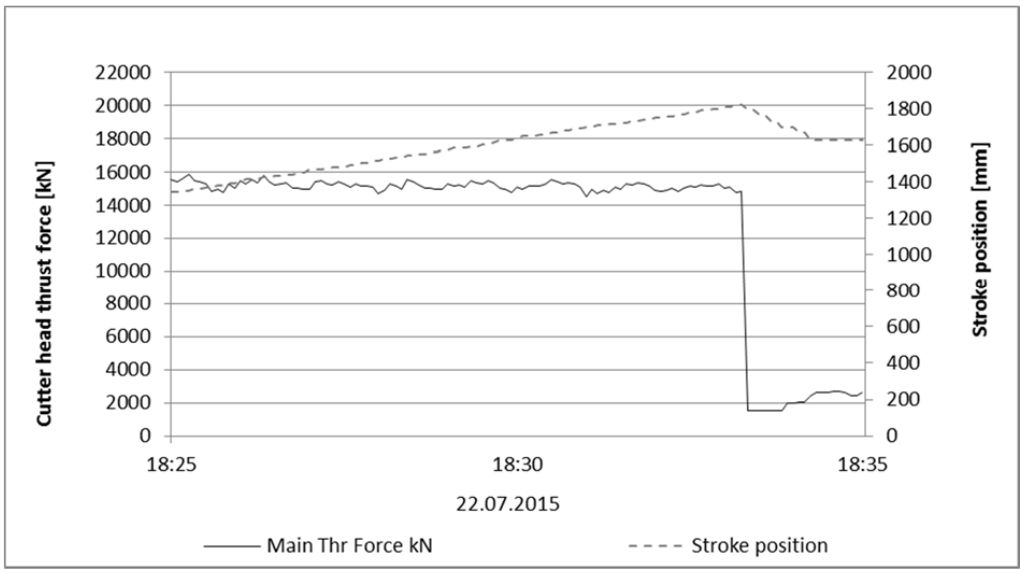

Figure A1.27: Thrust force at the cutter head and stroke position before sampling at chainage 5478.0.

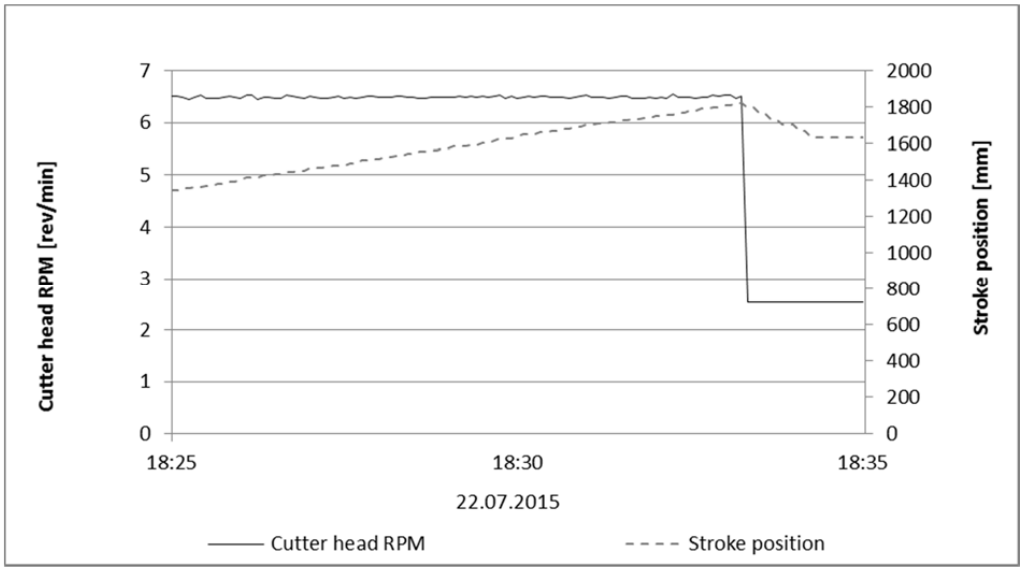

Figure A1.28: Cutter head RPM and stroke position before sampling at chainage 5478.0.

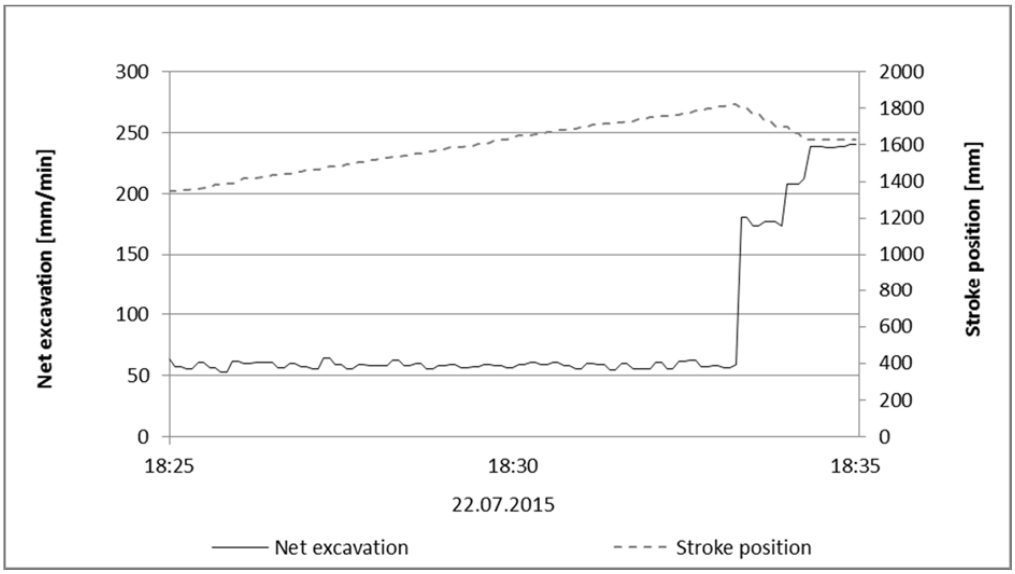

Figure A1.29: Net excavation rate in millimeters per minute and stroke position before sampling at chainage 5478.0.

Penetration rate in millimeters per minute. The high peaks is caused by repositioning of the cutter head, and is not related to boring.

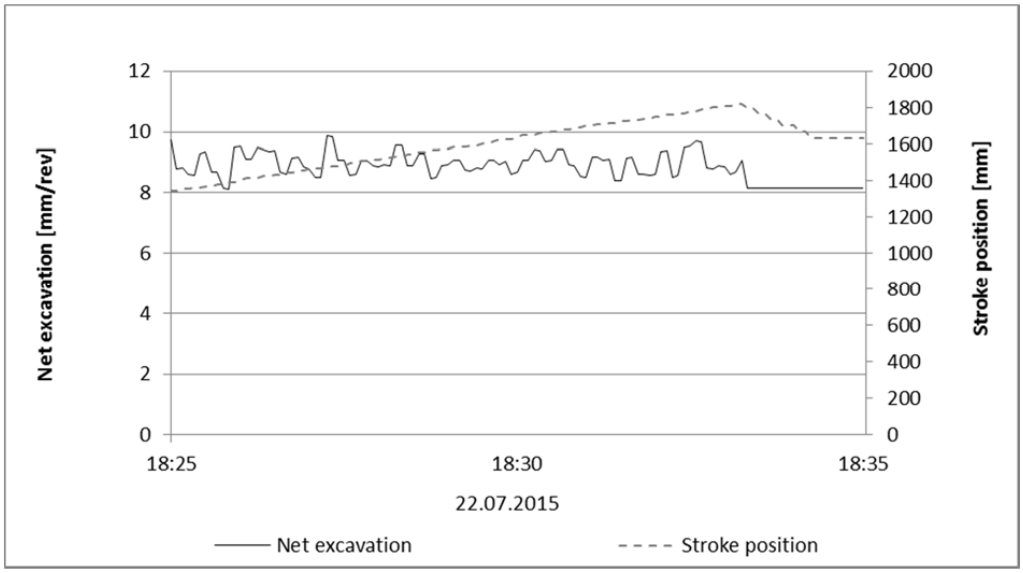

Figure A1.30: Net excavation rate in millimeters per revolution and stroke position before sampling at chainage 5478.0.

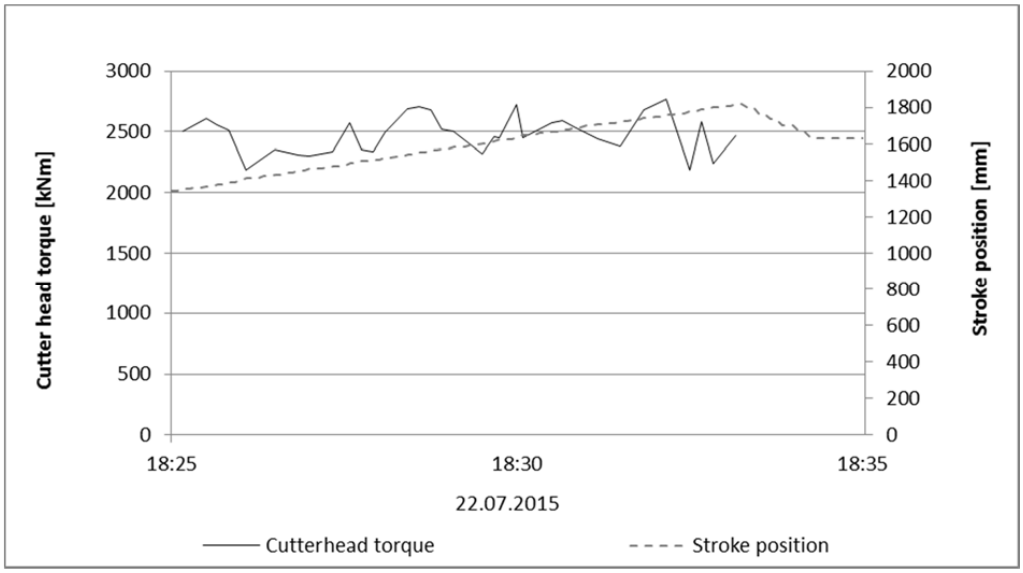

Figure A1.31: Cutter head torque and stroke position before sampling at chainage 5478.0.

A2 Comparison of logged data for different groups sampling strokes

Comparison of the operational parameters the last 1200 seconds of each sampling stroke

A2.1 Sampling strokes at the AMR Project

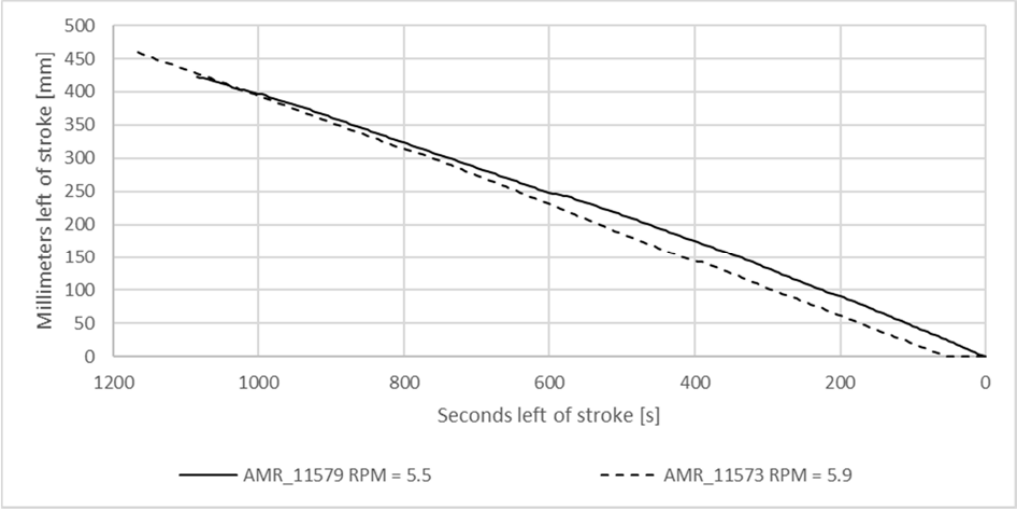

Figure A2.1: Millimeters left of strokes during the last 1200 seconds of the sampling strokes.

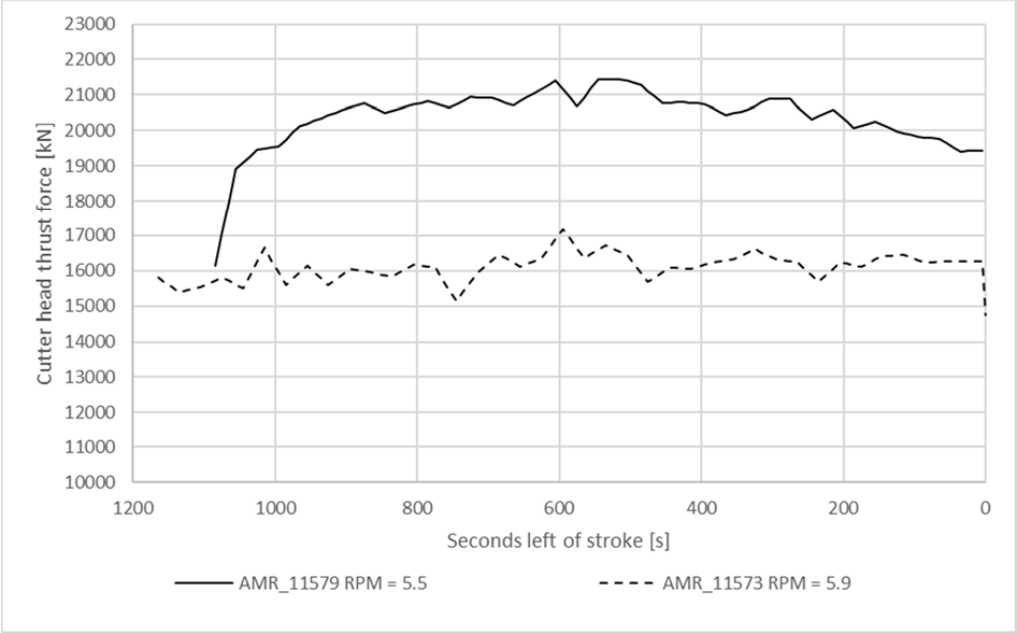

Figure A2.2: Cutter head thrust during the last 1200 seconds of the sampling strokes.

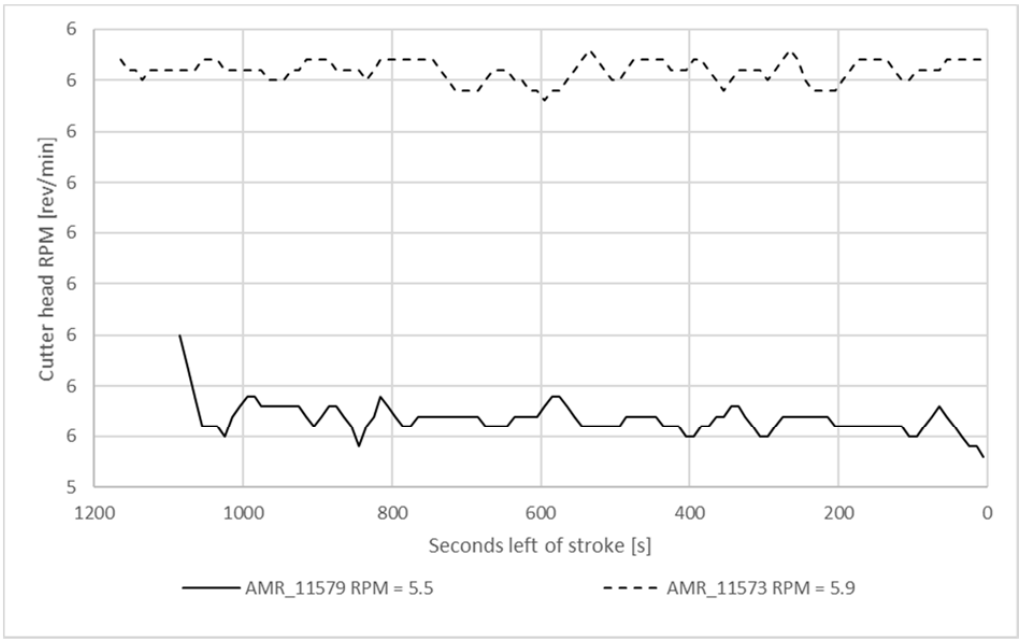

Figure A2.3: Cutter head RPM during the last 1200 seconds of the sampling strokes.

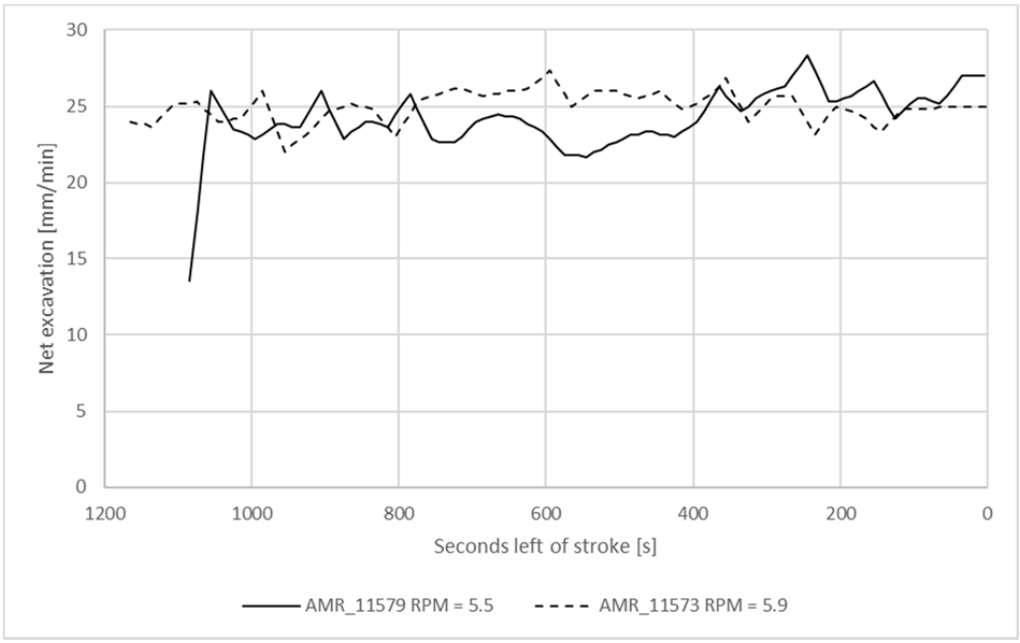

Figure A2.4: Net excavation in millimeters per minute during the last 1200 seconds of the sampling strokes.

A2.2 Sampling strokes at the Nedre Røssåga headrace tunnel

Chainages 5437, 5458 and 5478

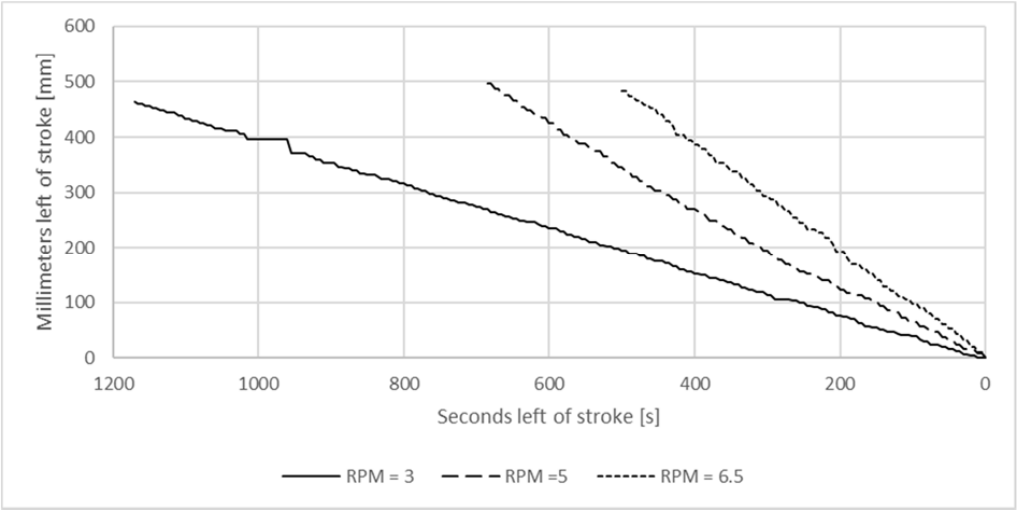

Figure A2.5: Millimeters left of strokes during the last 1200 seconds of the sampling strokes.

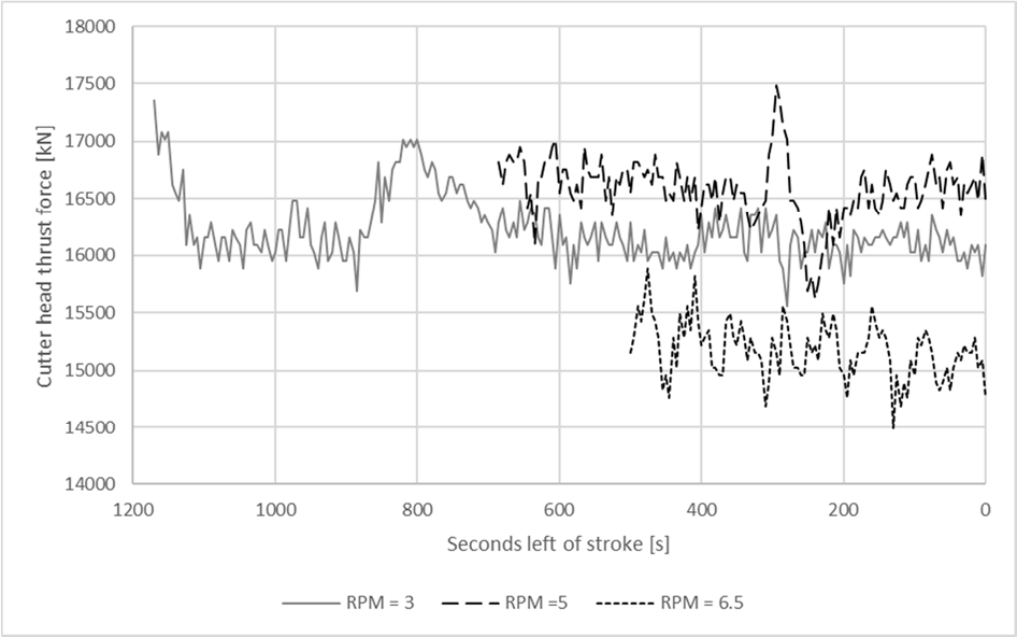

Figure A2.6: Cutter head thrust during the last 1200 seconds of the sampling strokes.

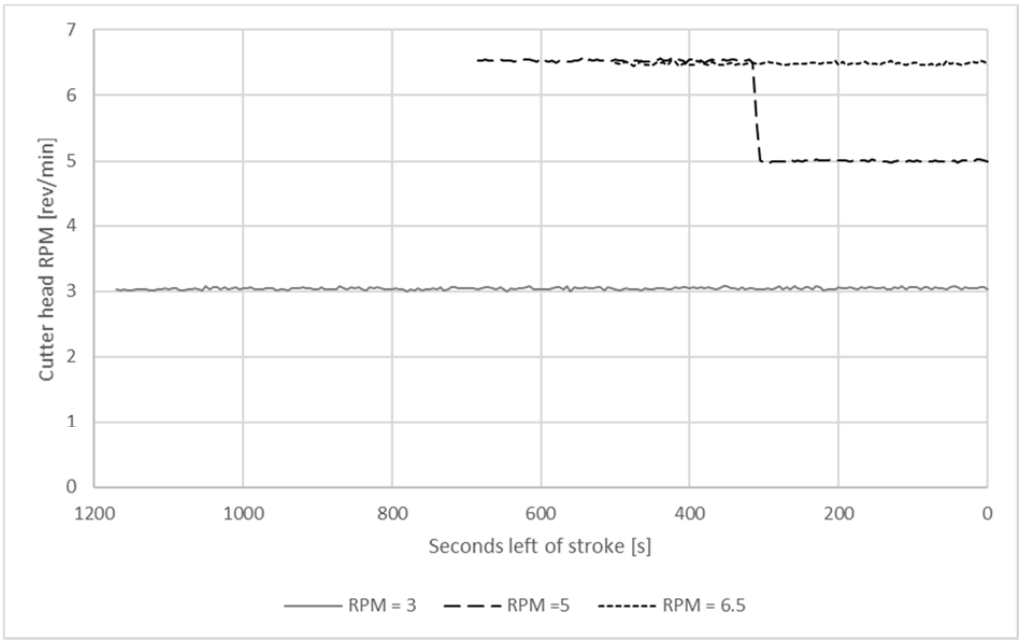

Figure A2.7: Cutter head RPM during the last 1200 seconds of the sampling strokes.

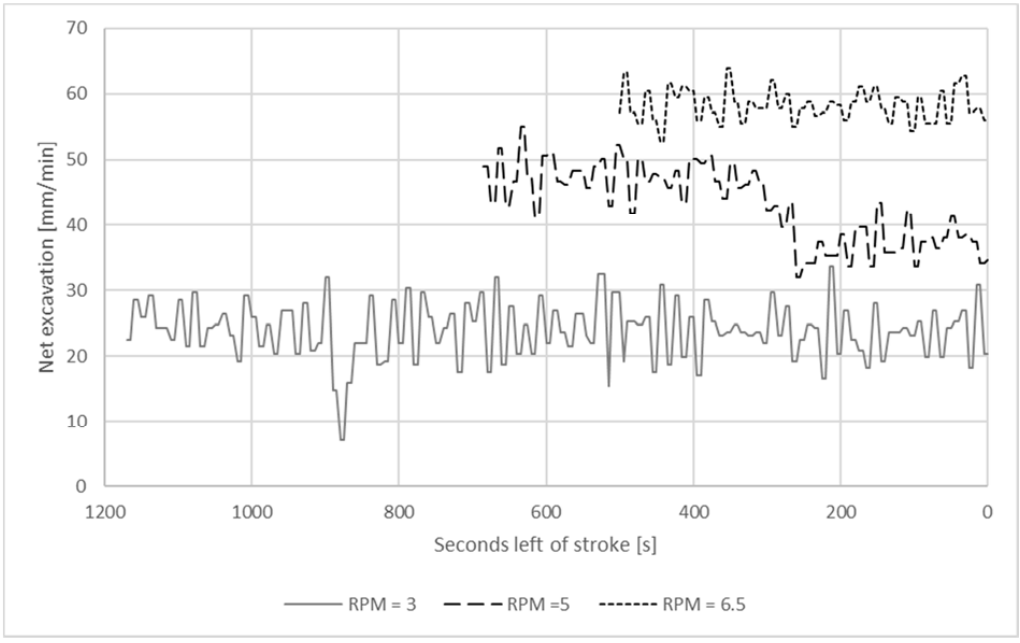

Figure A2.8: Net excavation in millimeters per minute during the last 1200 seconds of the sampling strokes.

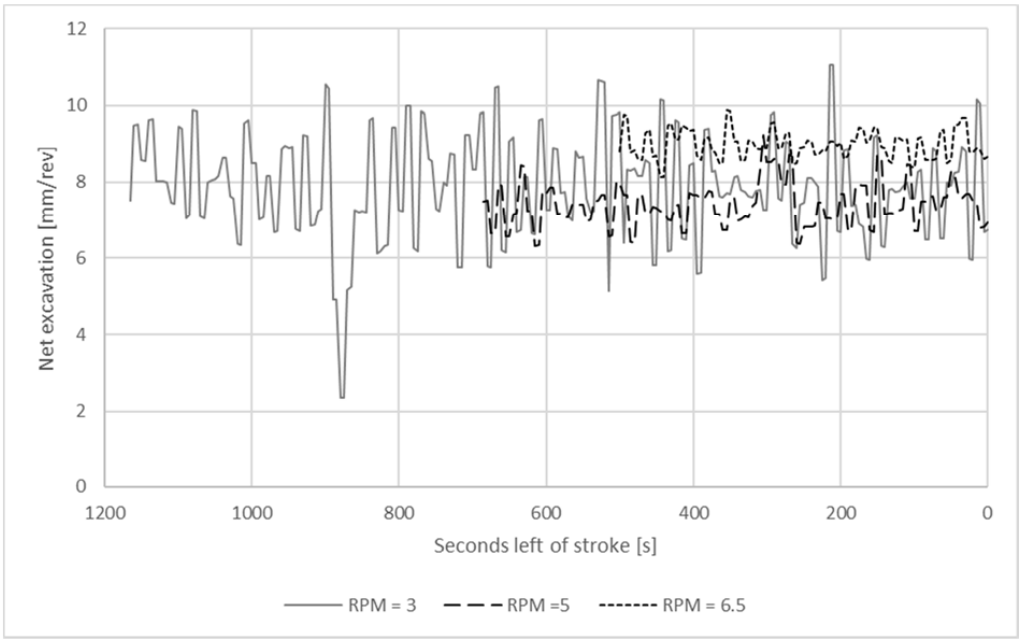

Figure A2.9: Net excavation in millimeters per revolution during the last 1200 seconds of the sampling strokes.

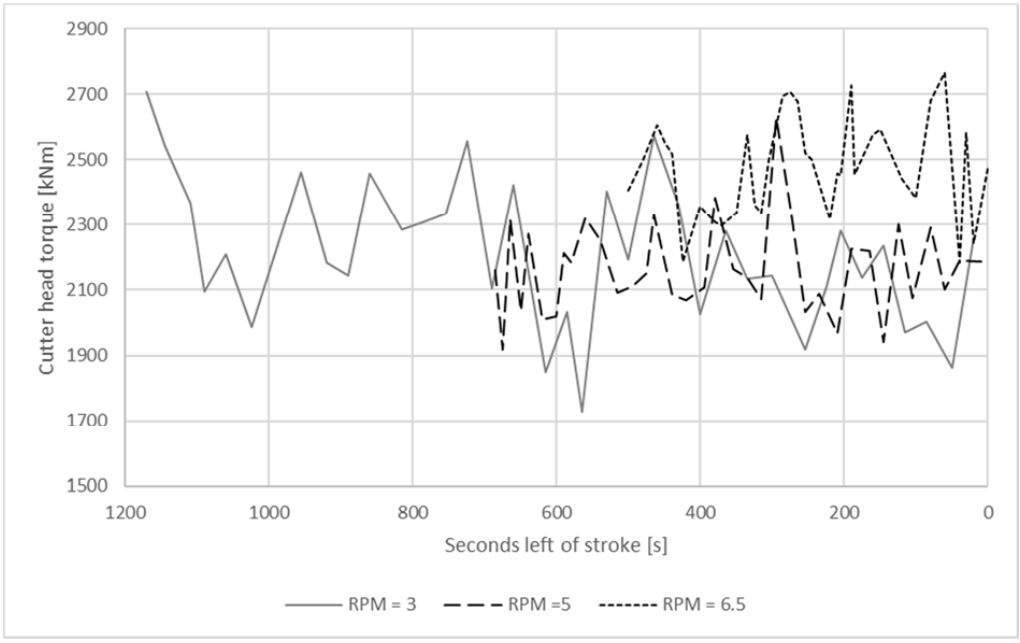

Figure A2.10: Cutter head torque during the last 1200 seconds of the sampling strokes.

Chainages 1184, 5437, 5458 and 5478

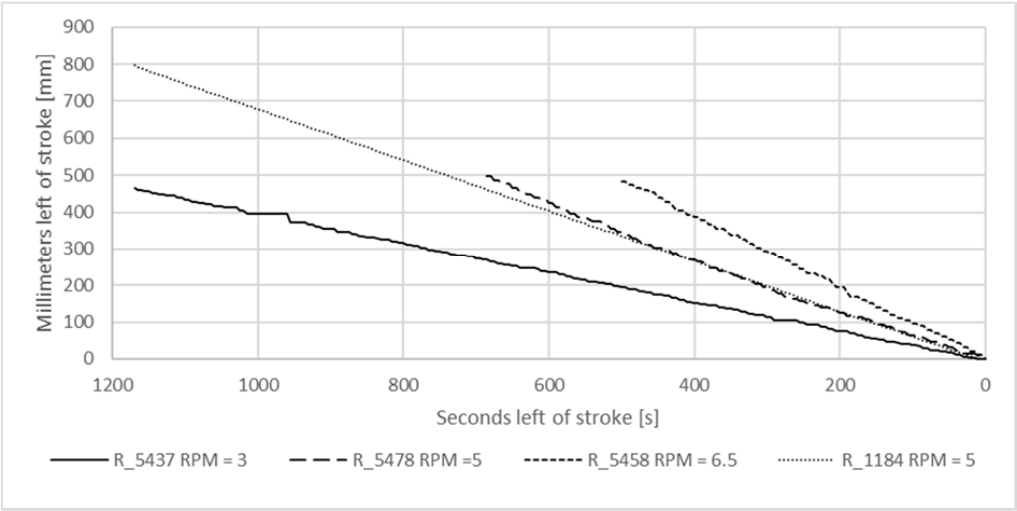

Figure A2.11: Millimeters left of strokes during the last 1200 seconds of the sampling strokes.

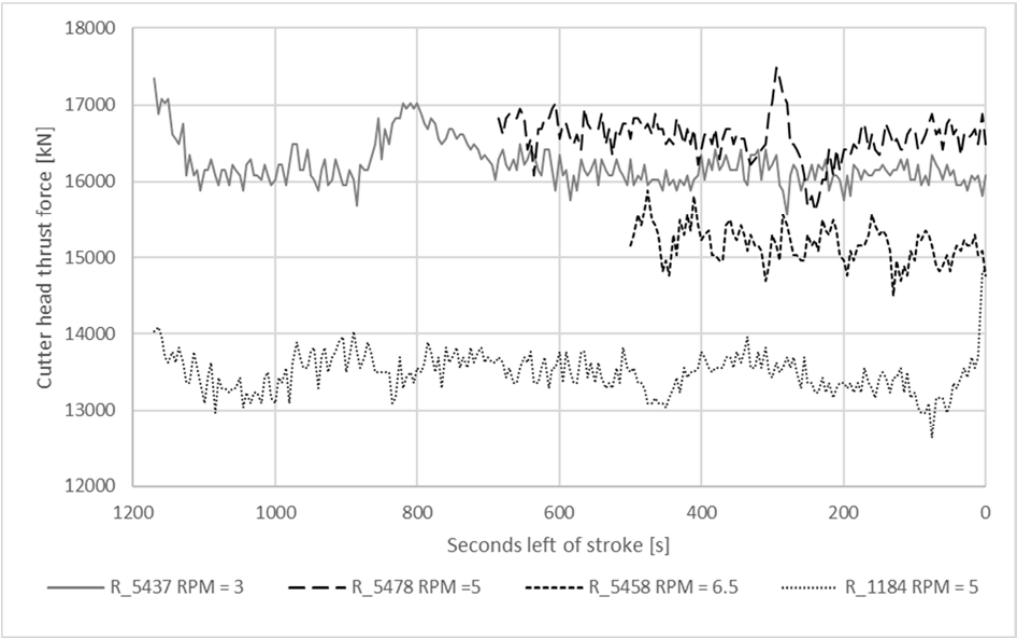

Figure A2.12: Cutter head thrust during the last 1200 seconds of the sampling strokes.

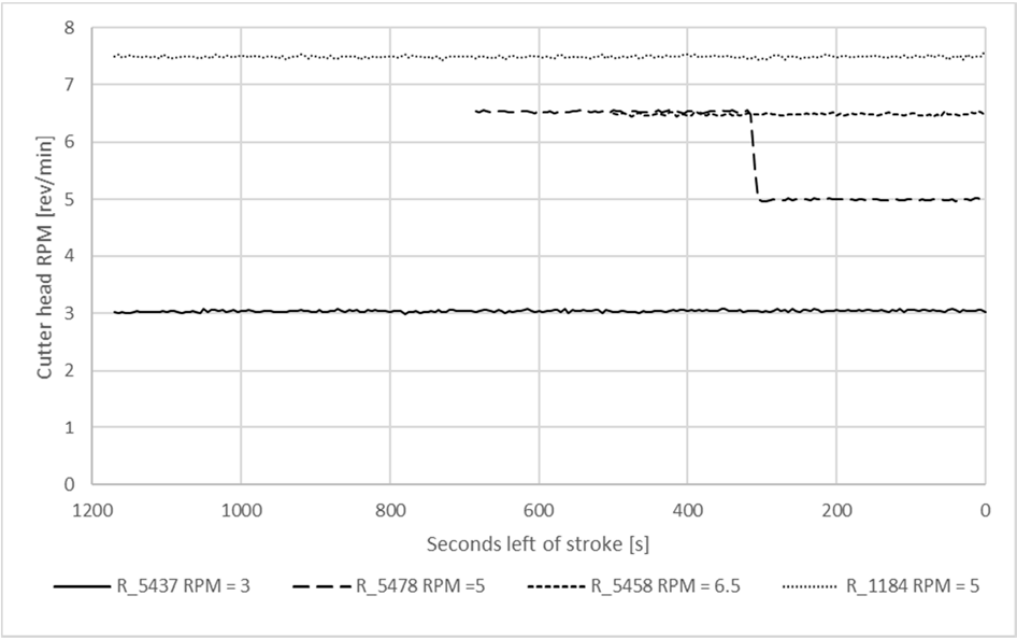

Figure A2.13: Cutter head RPM during the last 1200 seconds of the sampling strokes.

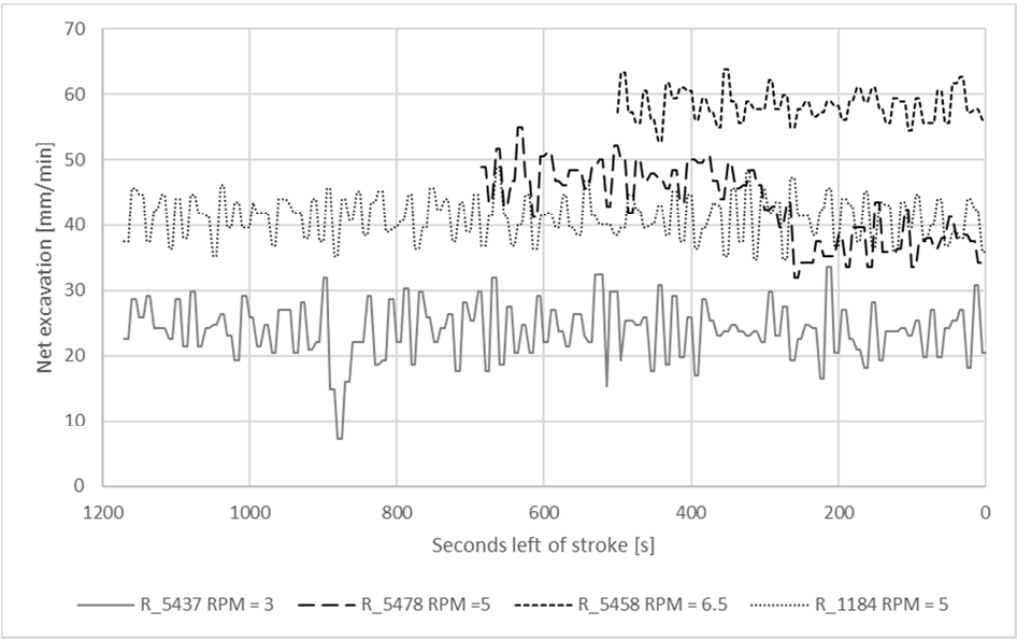

Figure A2.14: Net excavation in millimeters per minute during the last 1200 seconds of the sampling strokes.

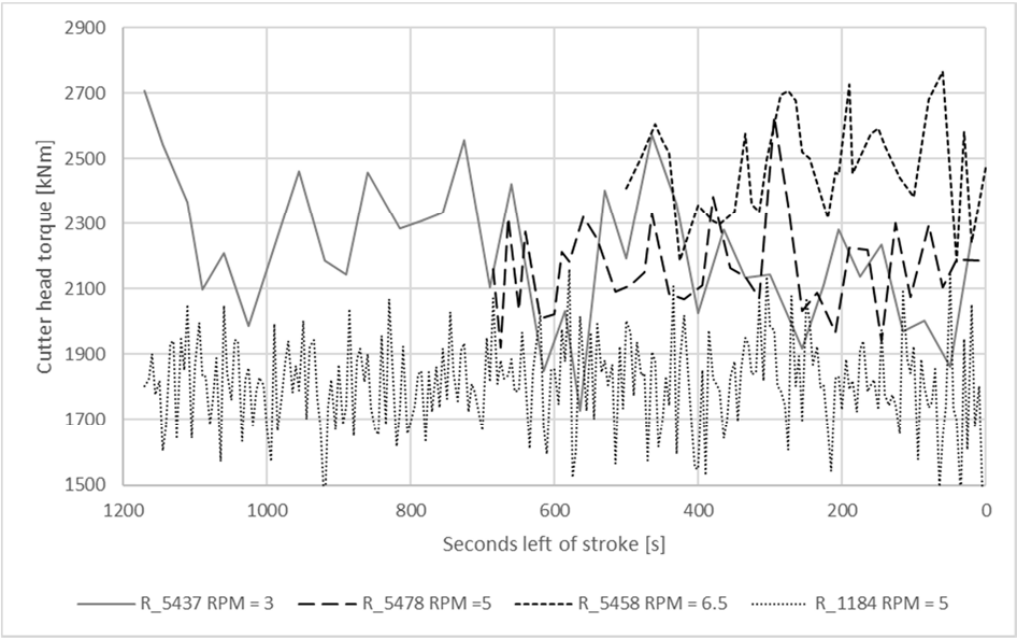

Figure A2.15: Torque during the last 1200 seconds of the sampling strokes.

A2.3 All sampling strokes

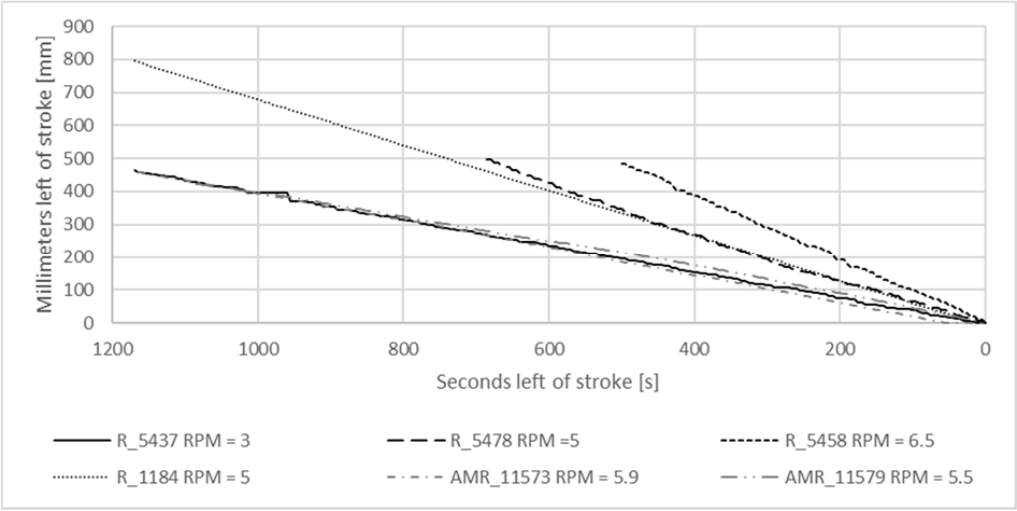

Figure A2.16: Millimeters left of strokes during the last 1200 seconds of the sampling strokes.

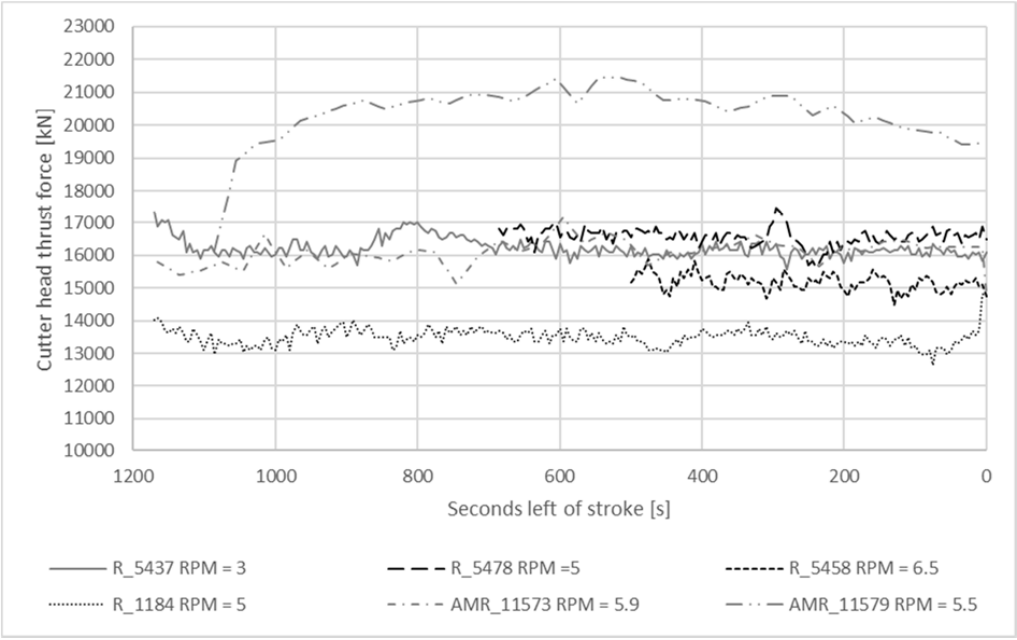

Figure A2.17: Cutter head thrust during the last 1200 seconds of the sampling strokes.

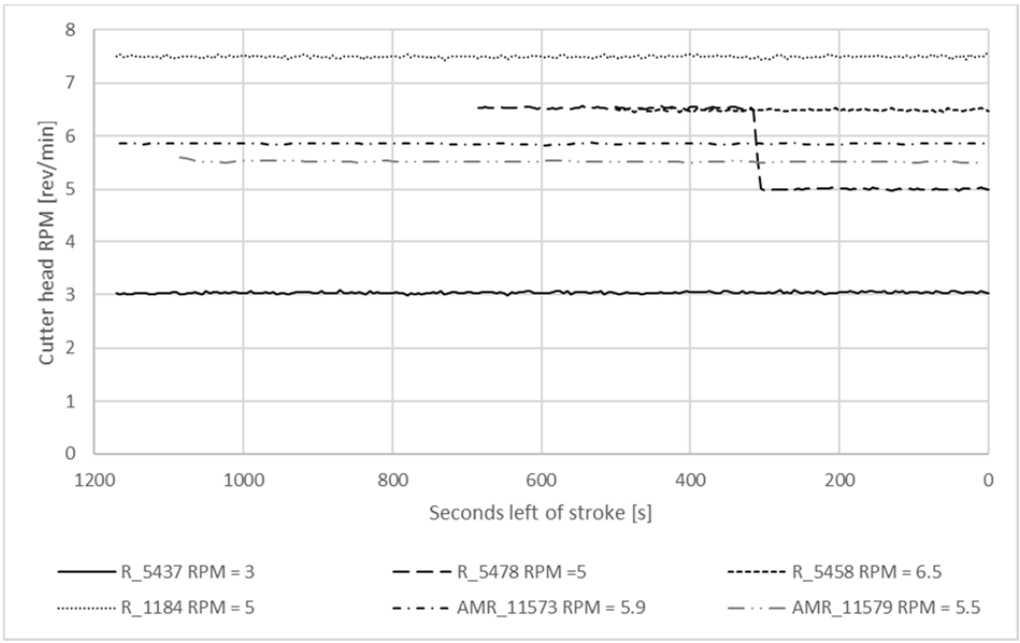

Figure A2.18: Cutter head RPM during the last 1200 seconds of the sampling strokes.

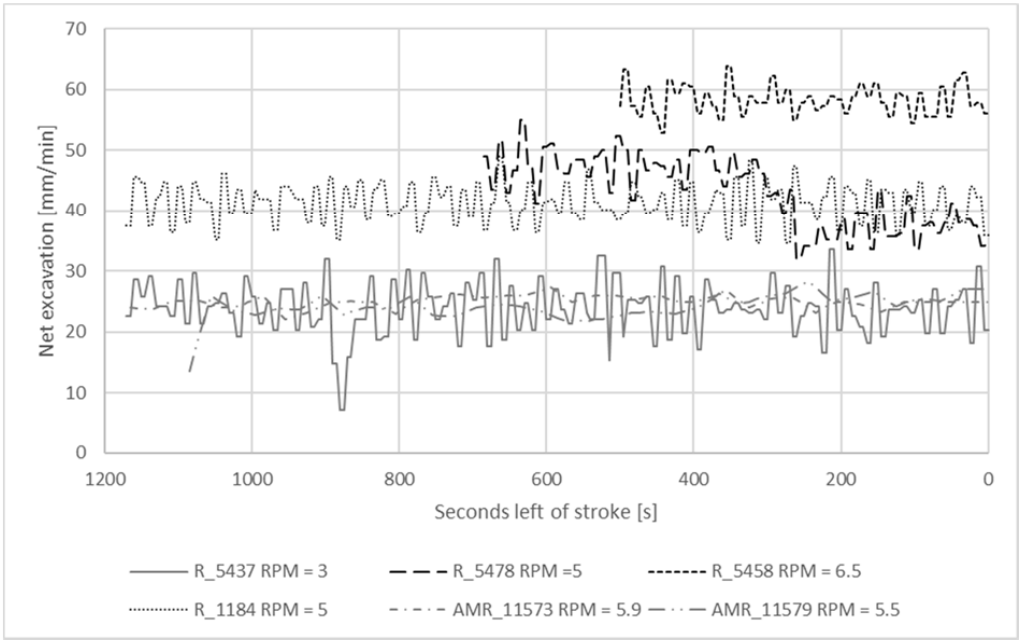

Figure A2.19: Net excavation in millimeters per minute during the last 1200 seconds of the sampling strokes.

Appendix B

APPENDIX B
GEOLOGICAL MAPPING

List of contents

List of figures

B1 Geological mapping of sampling strokes

An extensive geological mapping was carried out at both tunnel sites. At the AMR project, concrete lining was set up continuously, and the only accessible rock surface was at the face of the tunnel. Because of limited access to the face, some observations from outside the tunnel was also implemented. At the Nedre Røssåga headrace tunnel, no lining or shotcrete were installed, and the entire tunnel was accessible during the construction time. This accessibility gave good premise for geological mapping, and made it possible to ensure representative sampling strokes.

At both sites, a detailed mapping of the face was carried out during the core drilling.

B1.1 The AMR Project

Mapping done in front of the cutter head.

Chainage 11573

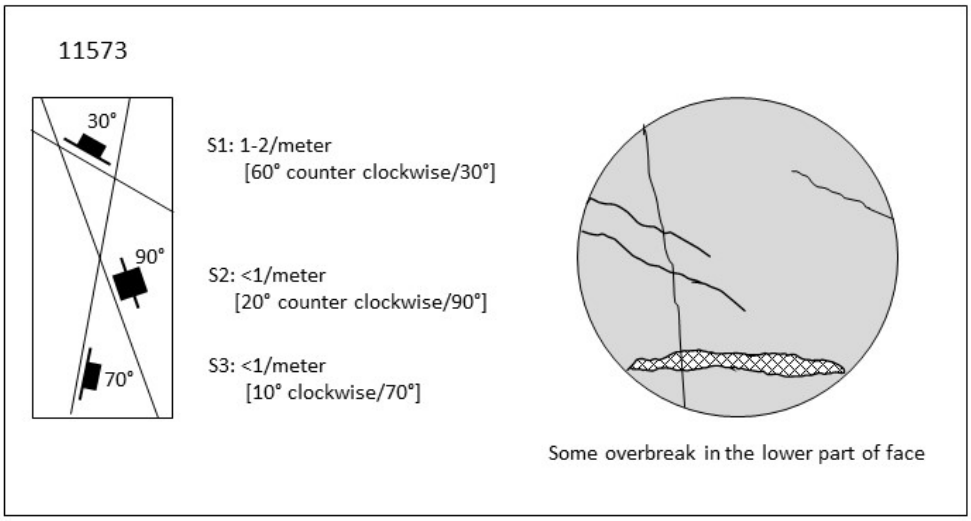

Figure B1.1: Geological mapping at the face at chainage 11573.

Chainage 11579

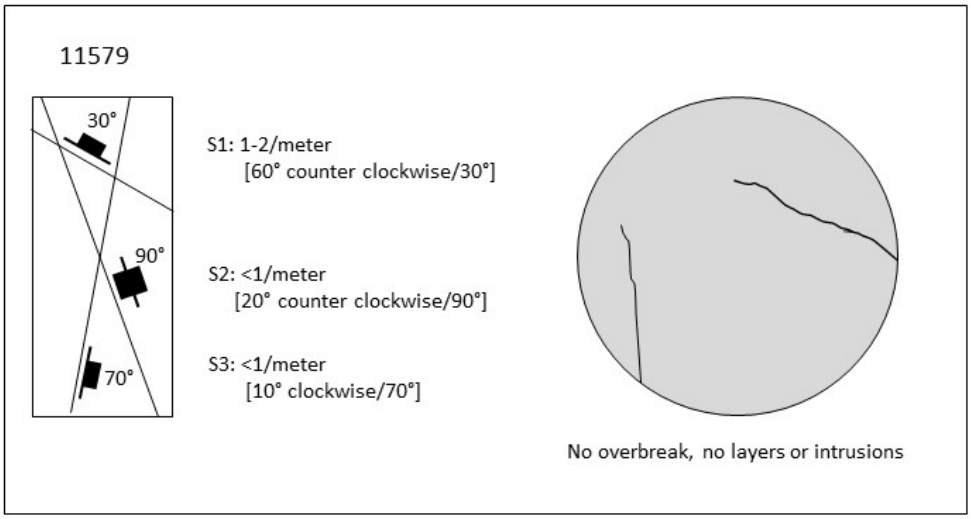

Figure B1.2: Geological mapping at the face at chainage 11579.

B1.2 The Nedre Røssåga headrace tunnel

Chainage 1184

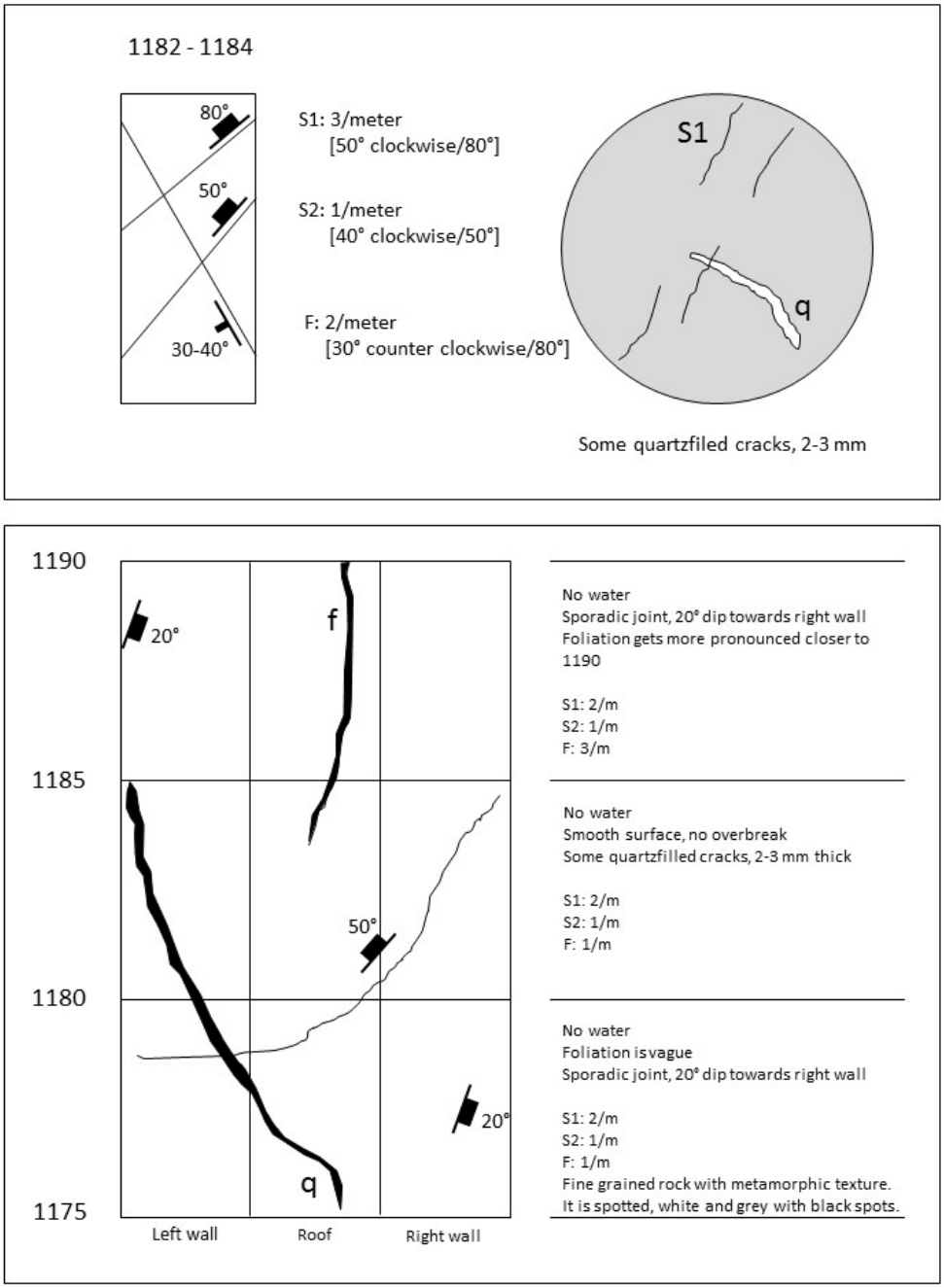

Figure B1.3: Geological mapping prior to and at the face at chainage 1184.

Chainage 3112

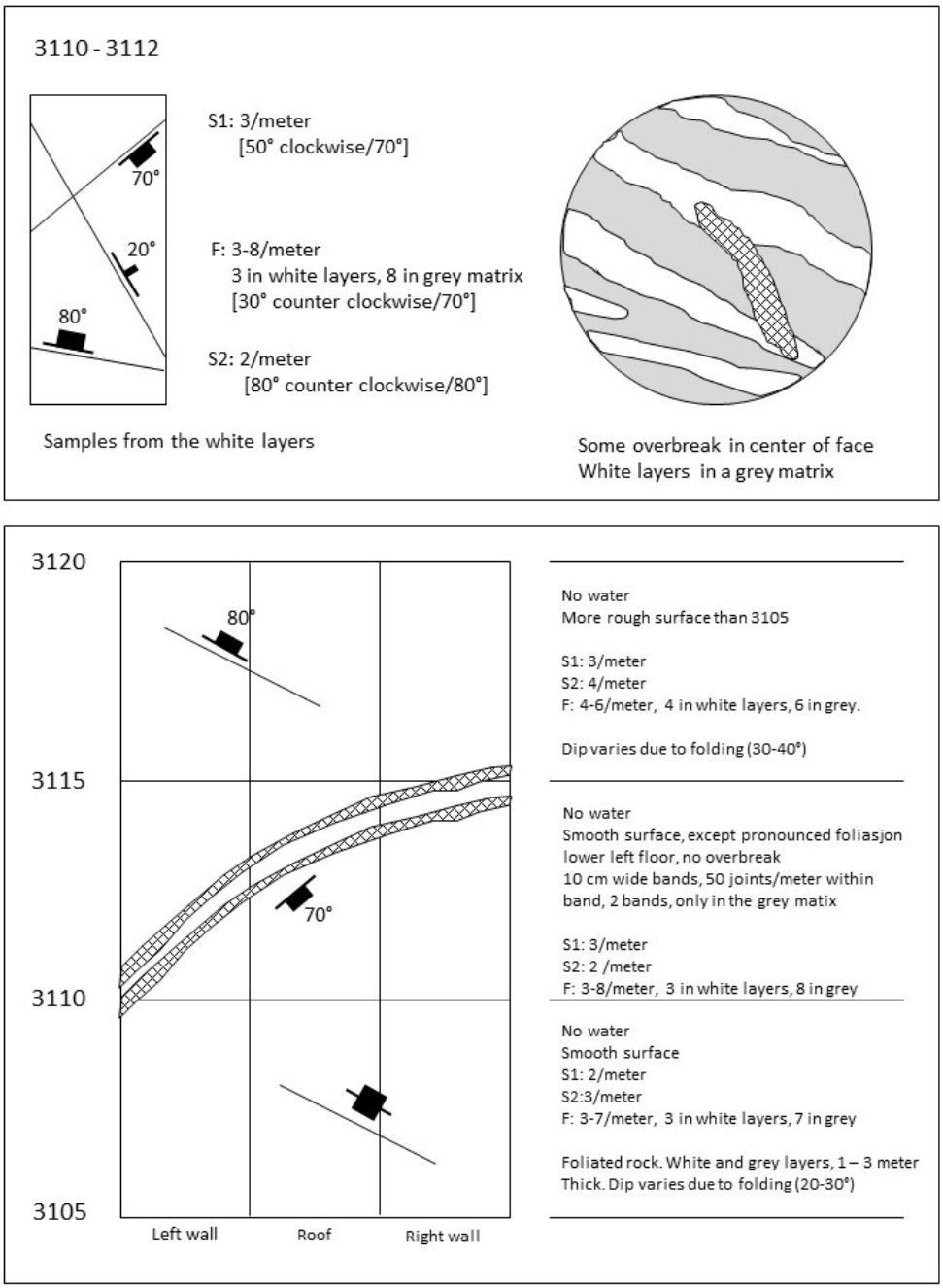

Figure B1.4: Geological mapping prior to and at the face at chainage 3112.

Chainage 5437

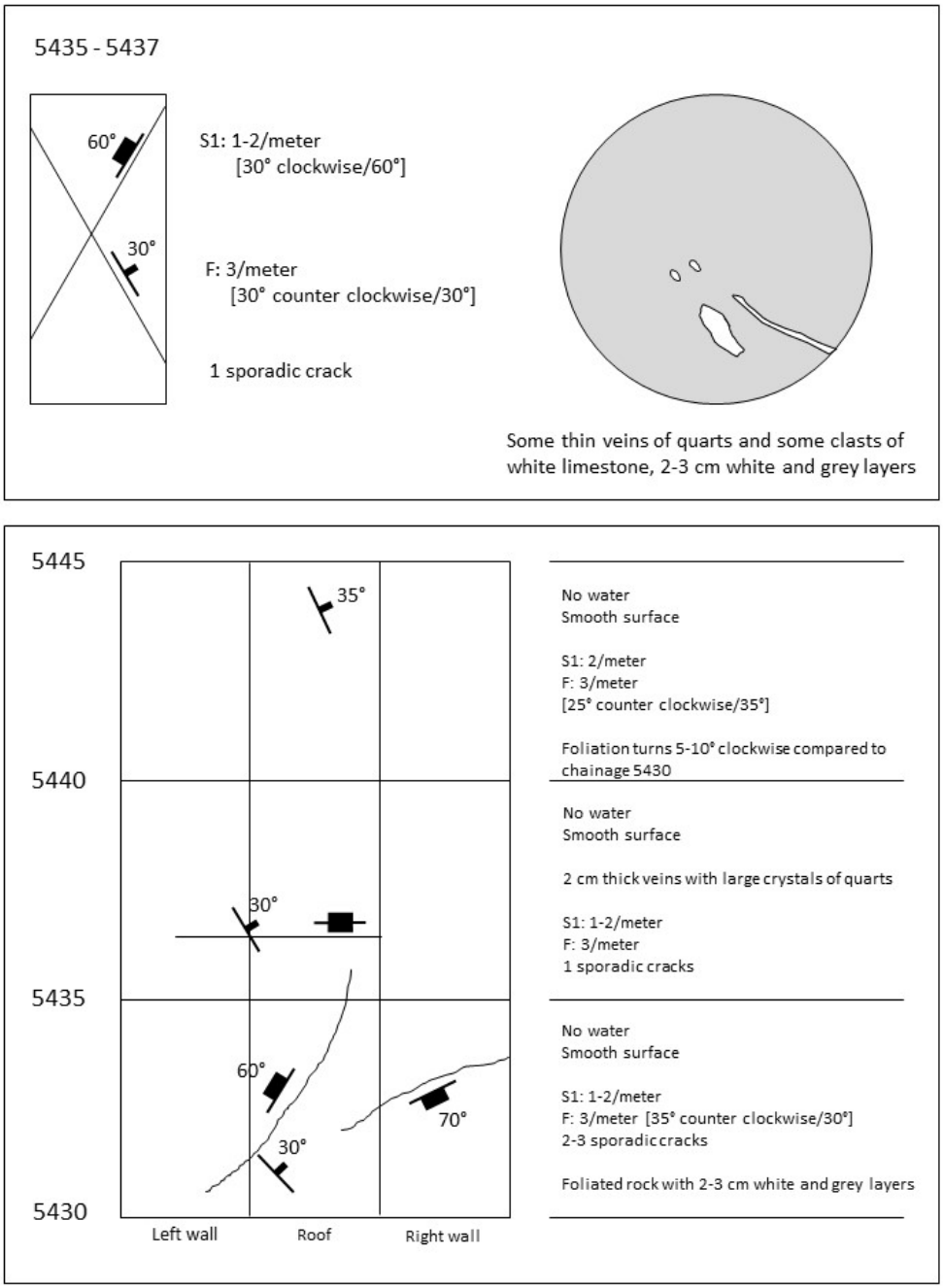

Figure B1.5: Geological mapping prior to and at the face at chainage 5437.

Chainage 5458

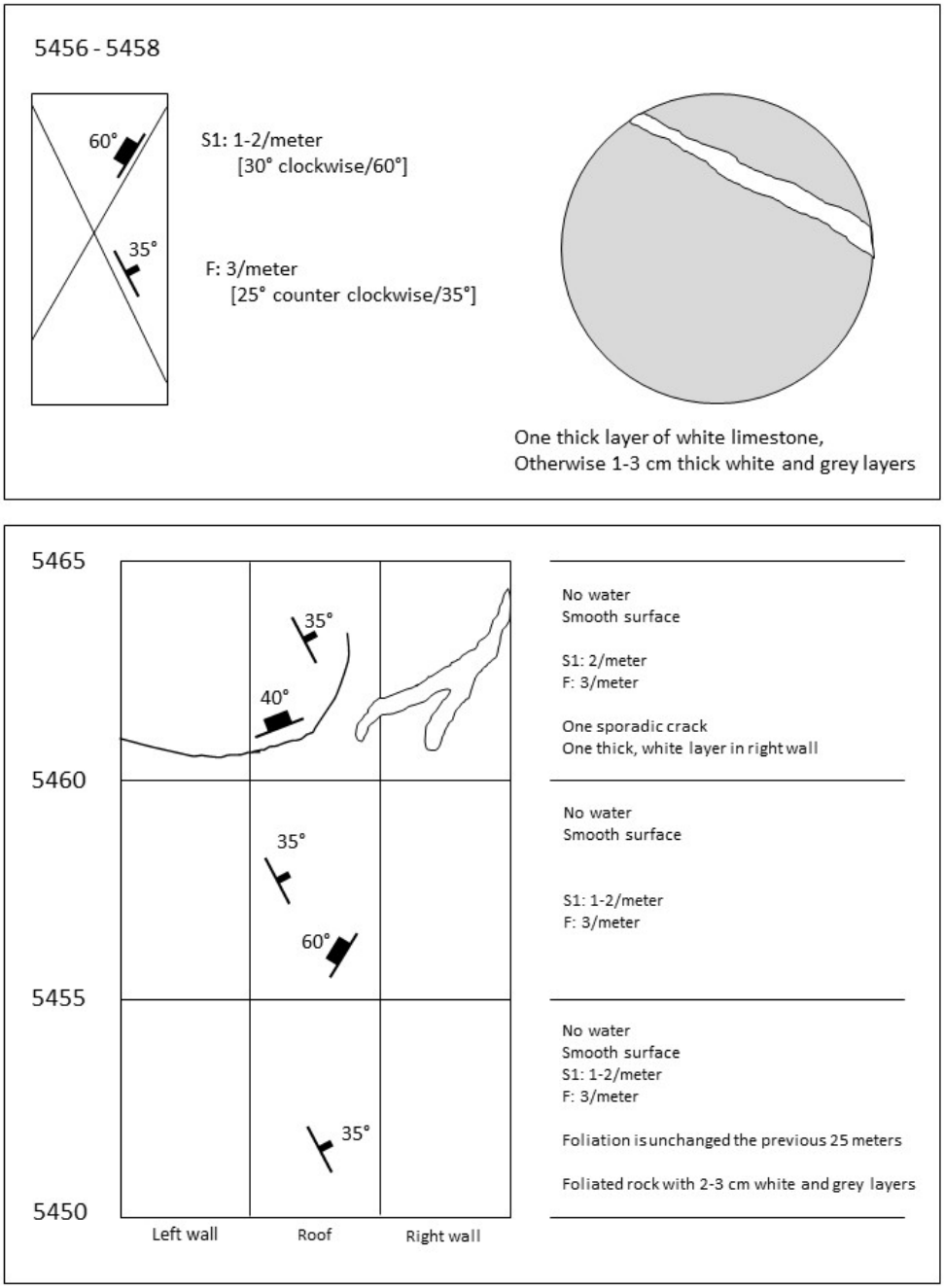

Figure B1.6: Geological mapping prior to and at the face at chainage 5458.

Chainage 5478

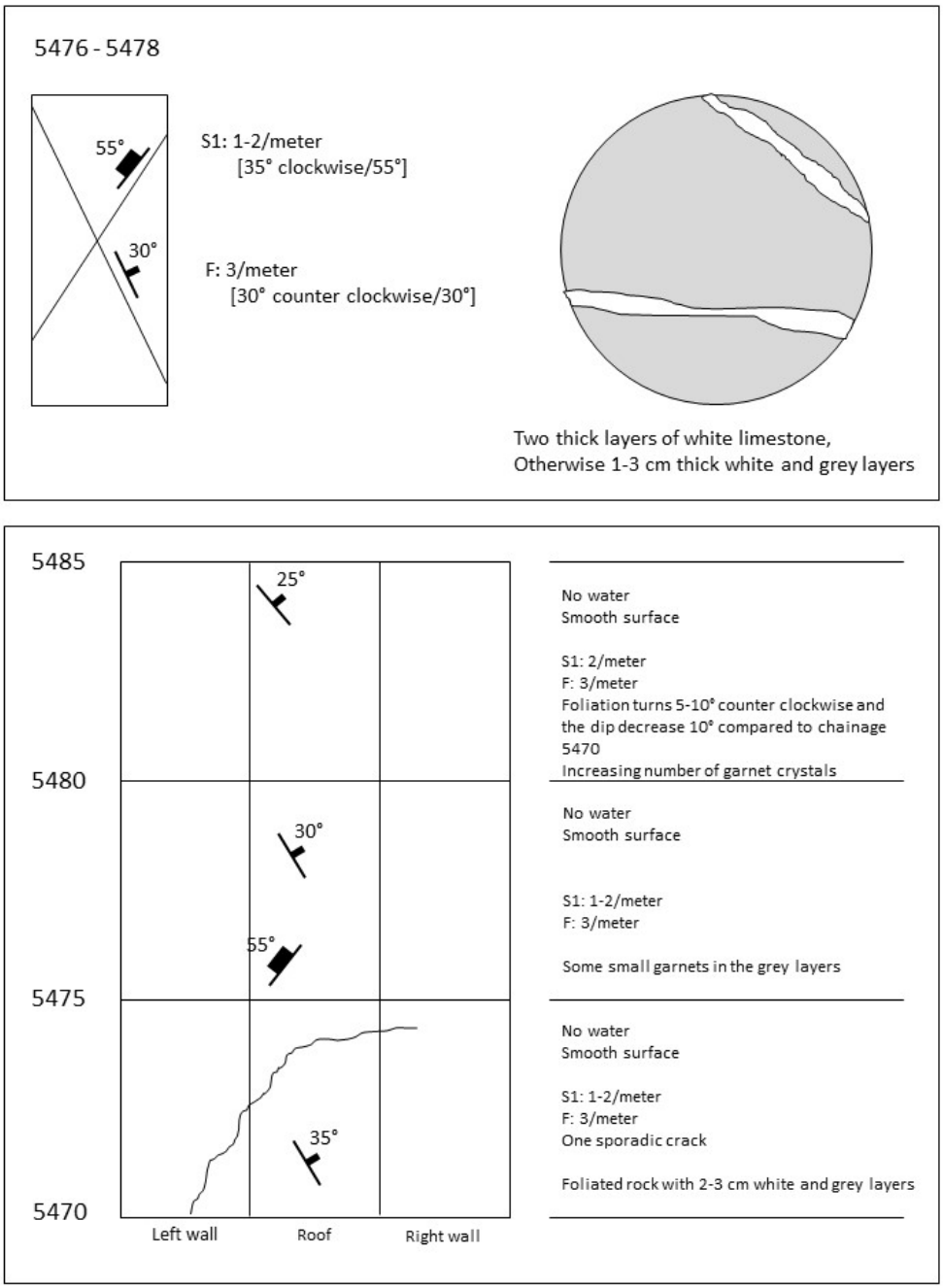

Figure B1.7: Geological mapping prior to and at the face at chainage 5478.

Appendix C

APPENDIX C
CORE SAMPLES FROM THE AMR PROJECT

List of contents

List of figures

C1 Core samples

In total, six core samples from two different test strokes were collected at the AMR project. Table C1.1 shows number of core samples from each test stroke.

Table C1.1: Number of samples from the two chainages at the AMR Project

Chainage	Number of samples
11573	1
11579	5

C1.1 Chainage 11573

Date:	25.02.2013
Chainage	11572.9
Average RPM:	5.9
Average thrust:	16 000 kN
Average tonn/disc:	No data
Average pressure:	220 bar
Penetration:	25 mm/min
	1.5 m/h
Average torque:	No available information
Number of cores:	1

Rock type:	Monzo granite
σ_c:	275-372 MPa
SJ:	3.3 – 3.7 (very high)
S_{20}:	47.5 – 50.9 (medium)
DRI:	43-45 (medium)

Additional information:
All cutters where 20” cutters, with a cutter width of 3/4”.

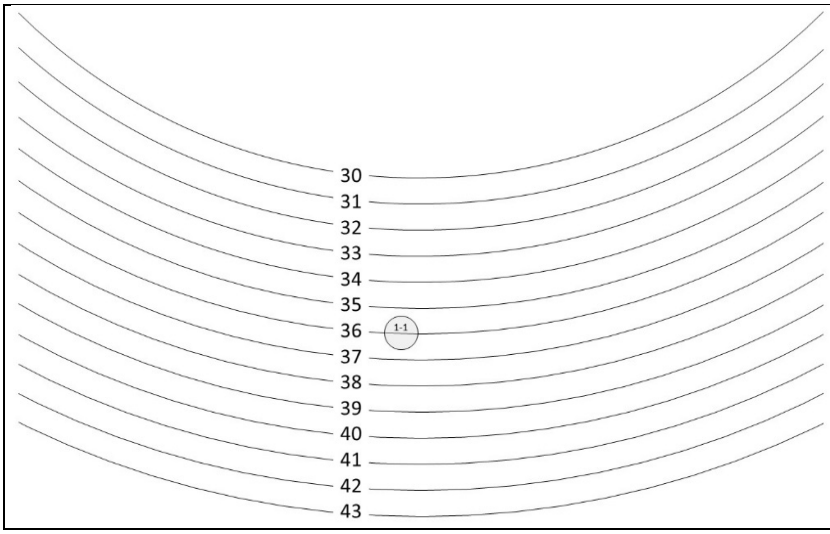

Cutter wear:
30: 25
31: 40
32: 5
33: 30
34: 36
35: 16
36: 28
37: 11
38: 38
39: 35
40: 21
41: 36

Figure C1.1: Sampling at AMR_11573.

AMR_11573-_1-1_38

Circumference:	314 mm
Number of cracks:	0
Number of cracks with dip < 3°:	0

Additional information:
No additional information

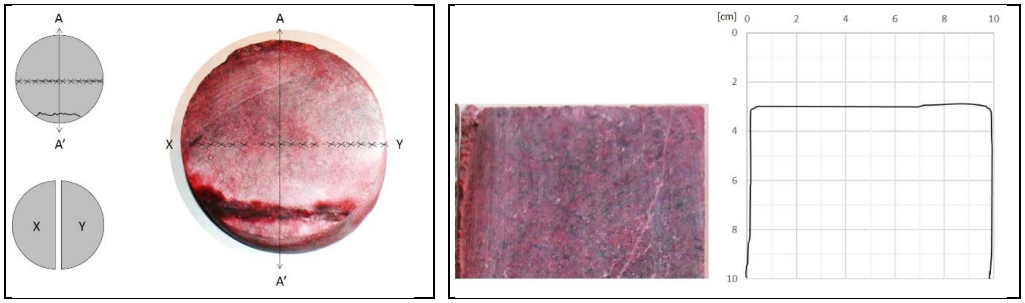

Figure C1.2: Core sample AMR_11573_1-1.

C1.2 Chainage 11579

Date:	26.02.2013
Chainage	11578.8
Average RPM:	5.5
Average thrust:	16 000 kN
Average tonn/disc:	No data
Average pressure:	220 bar
Penetration:	27 mm/min
	1.6 m/h
Average torque:	No available information
Number of cores:	1

Rock type:	Monzo granite
σ_c:	275-372 MPa
SJ:	3.3 – 3.7 (very high)
S_{20}:	47.5 – 50.9 (medium)
DRI:	43-45 (medium)

Additional information:
All cutters where 20” cutters, with a cutter width of 3/4”.

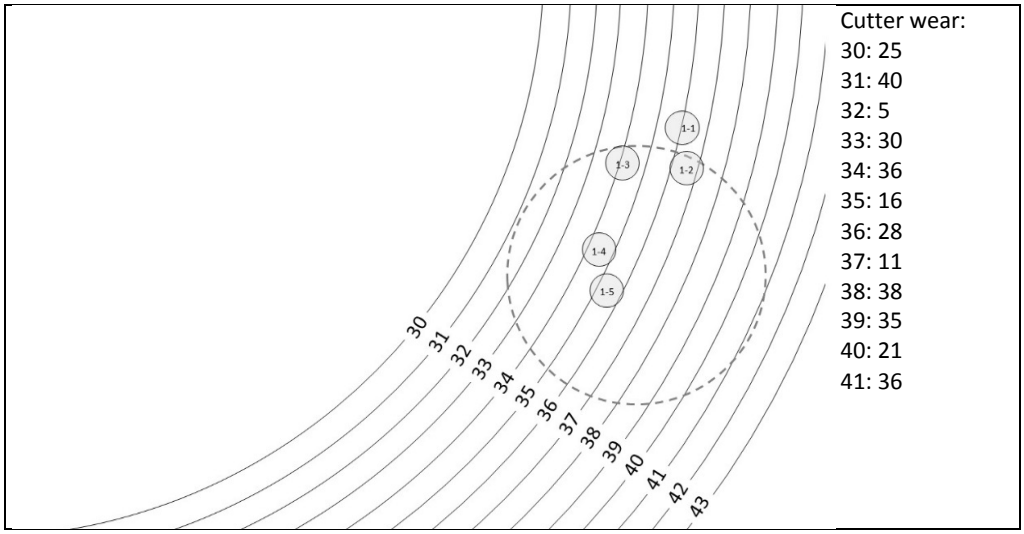

Figure C1.3: Sampling at AMR_11579.

AMR_11579-_1-1_36

Circumference:	313 mm
Number of cracks:	2
Number of cracks with dip < 3°:	0

Additional information:
A lot of open pre-existing cracks

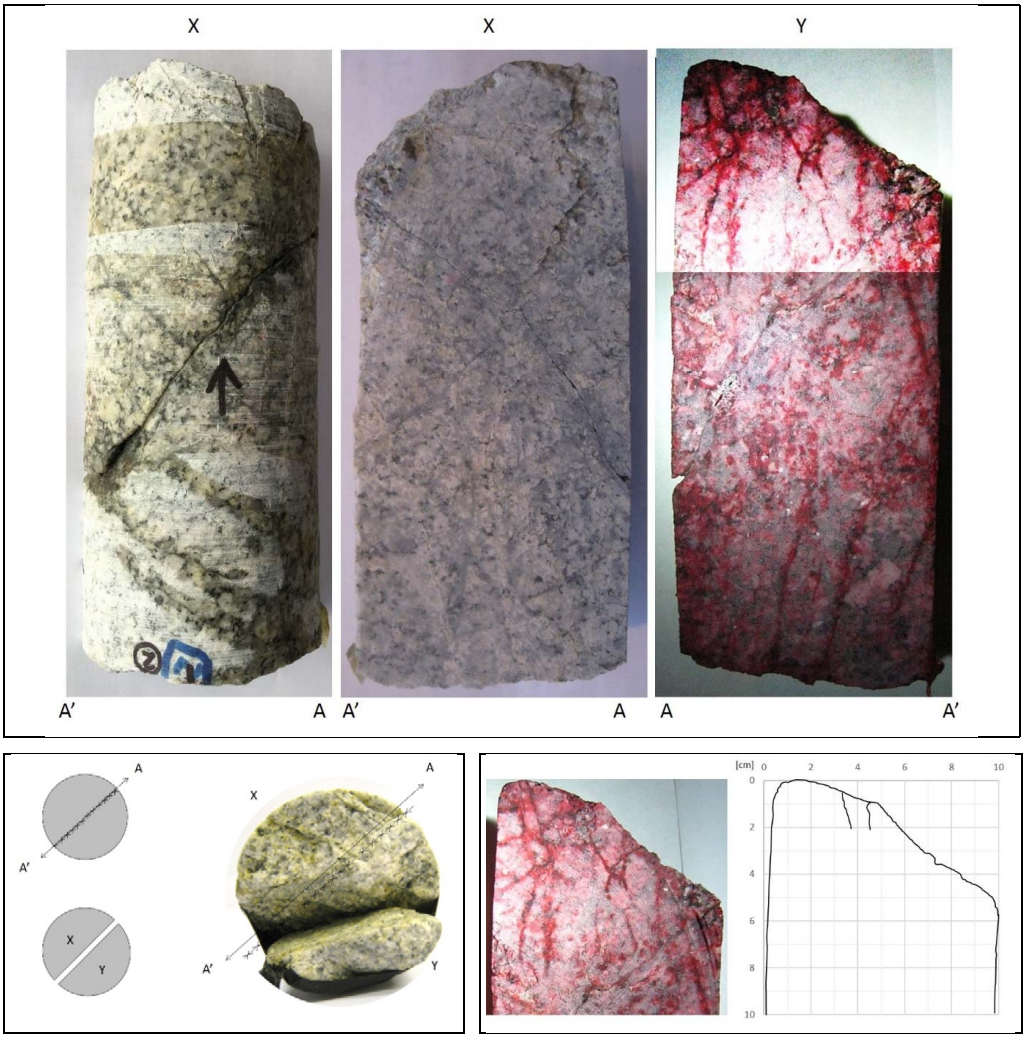

Figure C1.4: Core sample AMR_11579_1-1.

AMR_11579-_1-2_37-38

Circumference:	314 mm
Number of cracks:	3
Number of cracks with dip < 3°:	1

Additional information:
No additional information

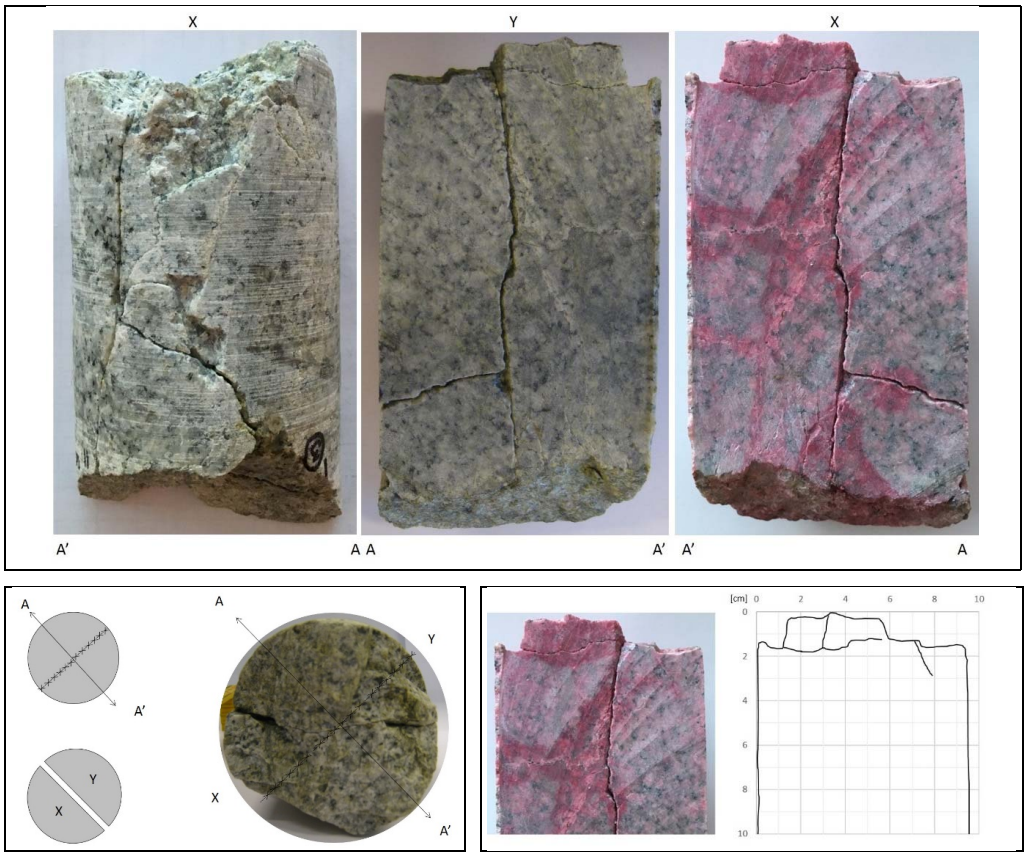

Figure C1.5: Core sample AMR_11579_1-2.

AMR_11579-_1-3_34

Circumference:	312 mm
Number of cracks:	0
Number of cracks with dip < 3°:	0

Additional information:
No additional information

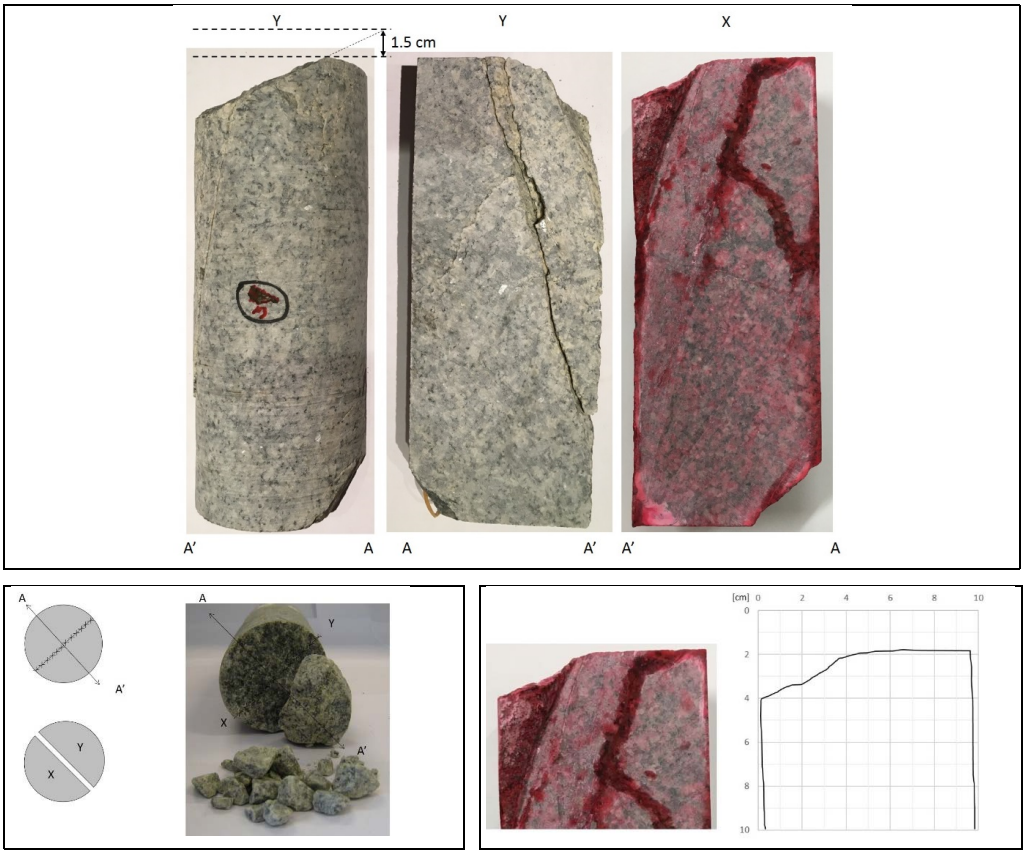

Figure C1.6: Core sample AMR_11579_1-3.

AMR_11579-_1-4_34-35

Circumference:	313 mm
Number of cracks:	13
Number of cracks with dip < 3°:	2

Additional information:
No additional information

Figure C1.7: Core sample AMR_11579_1-4.

AMR_11579-_1-5_35

Circumference:	314 mm
Number of cracks:	2
Number of cracks with dip < 3°:	1

Additional information:
No additional information

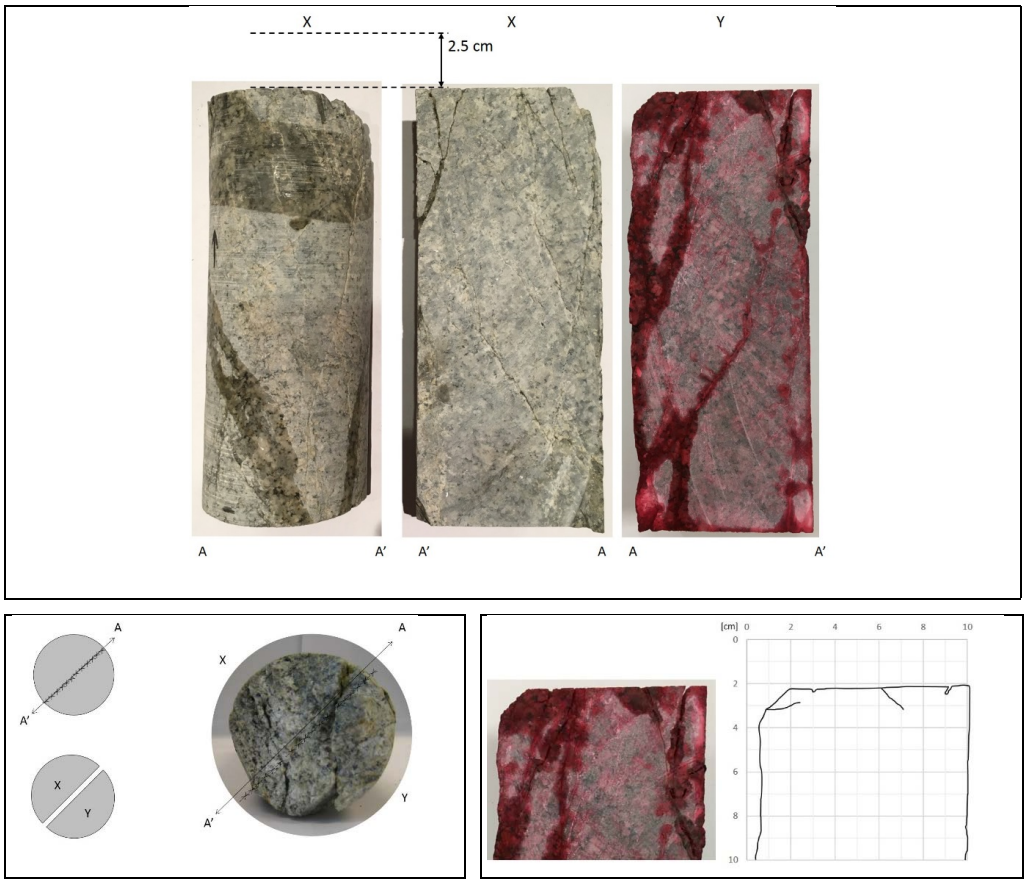

Figure C1.8: Core sample AMR_11579_1-5

Appendix D

APPENDIX D
CORE SAMPLES FROM THE NEDRE RØSSÅGA HEADRACE TUNNEL

List of contents

List of figures

D1 Core samples

In total, 68 core samples from five different test strokes were collected at the Nedre Røssåga headrace tunnel. Table D1.1 shows number of core samples from each test stroke. Note that three of the cores from chainage 3112 not are included in the analysis. At chainage 5478, one of the core samples are used for laboratory testing. These cores will not be presented in this appendix.

Table D1.1: Number of samples from the test strokes at the Nedre Røssåga headrace tunnel.

Chainage	Number of samples
1184	5
3112	17 + 3
5437	16
5458	16
5478	10 + 1

D1.1 Chainage 1184

Date:	14.07.2014
Chainage	1184.2
Average RPM:	7.5
Average thrust:	14 000 kN
Average tonn/disc:	26 tonn/disc
Average pressure:	220 bar
Penetration:	5.5 mm/rev 40 mm/min 2.48 m/h
Average torque:	1 800 kNm
Number of cores:	5

Rock type:	Granodioritic gneiss with layers of mica schist
σ_c:	62 - 92 MPa
SJ:	2,3 - 2.3 (extremely to very low)
S_{20}:	51 - 53 (medium to high)
DRI:	45-51 (medium)

Additional information:
All cutters where 19” cutters, with a cutter width of 7/8”.

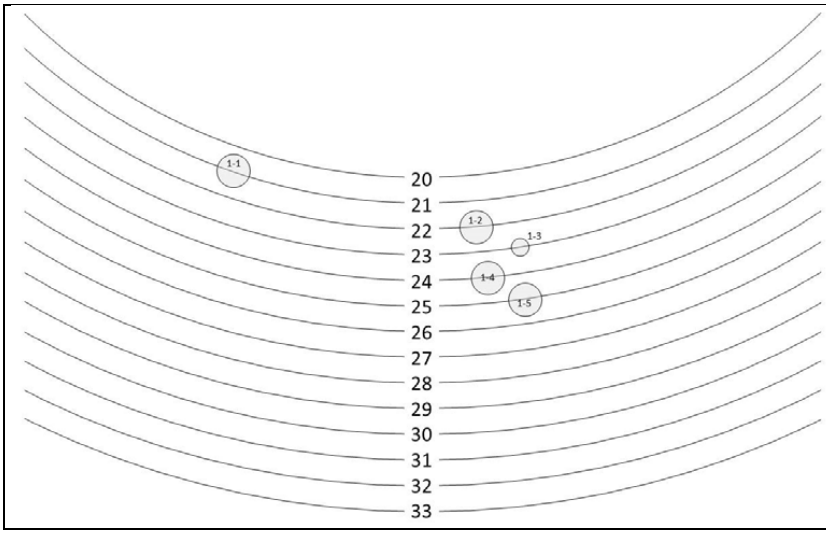

Cutter wear:
20: 10
21: 10
22: 10
23: 10
24: 7
25: 10
26: 10

Figure D1.1: Sampling at R_1184.

R_1184_1-1_21

Circumference:	328 mm
Number of cracks:	13
Number of cracks with dip < 3°:	2

Distance from 0-line to lowest point on surface:	19 mm
Area between 0-line and surface:	22.4 cm^2

Additional information:
The longest crack propagates through the entire core, but was not observed further in the borehole.

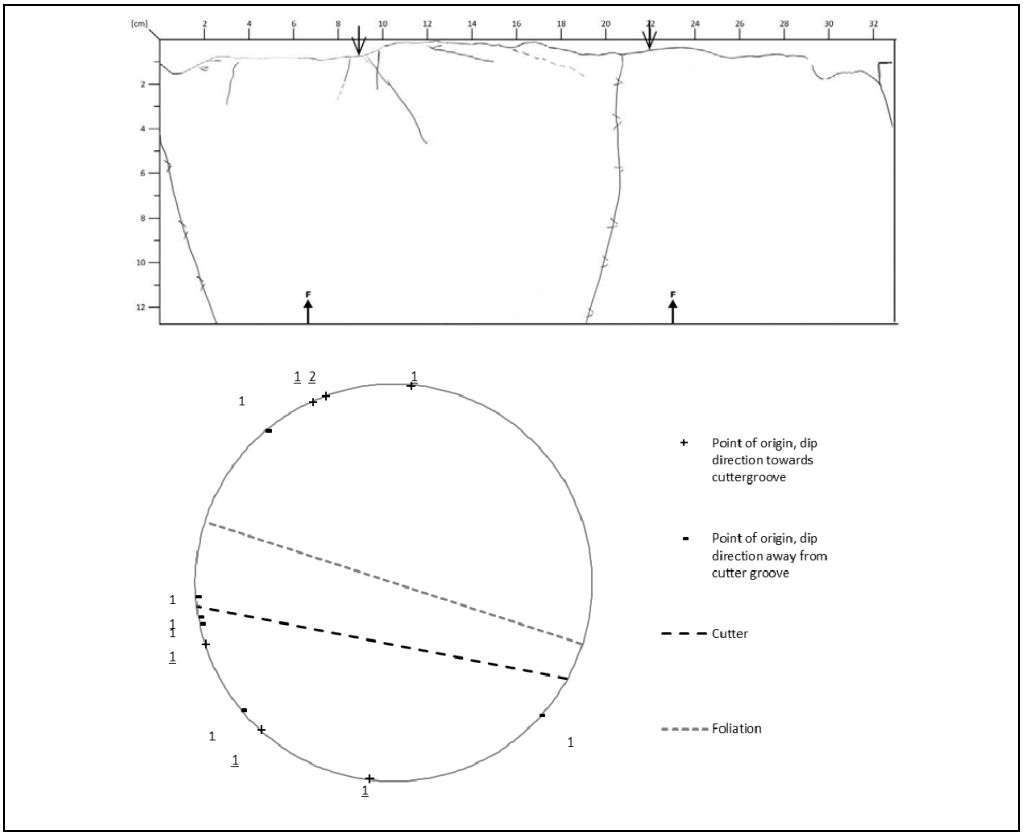

Figure D1.2: Core sample R_1184_1-1_21.

R_1184_1-2_22

Circumference:	325 mm
Number of cracks:	16
Number of cracks with dip < 3°:	3

Distance from 0-line to lowest point on surface:	16 mm
Area between 0-line and surface:	19.3 cm^2

Additional information:
No pictures of core before colouring with penetrant

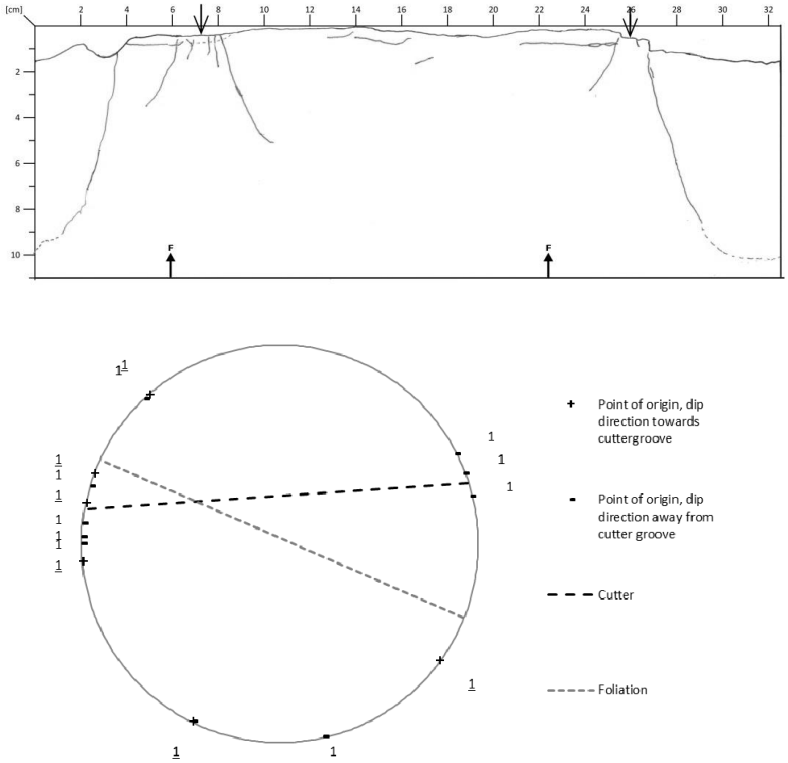

Figure D1.3: Core sample R_1184_1-2_22.

R_1184_1-3_23

Circumference:	176 mm
Number of cracks:	13
Number of cracks with dip < 3°:	0

Distance from 0-line to lowest point on surface:	11 mm
Area between 0-line and surface:	12.7 cm^2

Additional information:
The only core with a circumference less than 320 mm

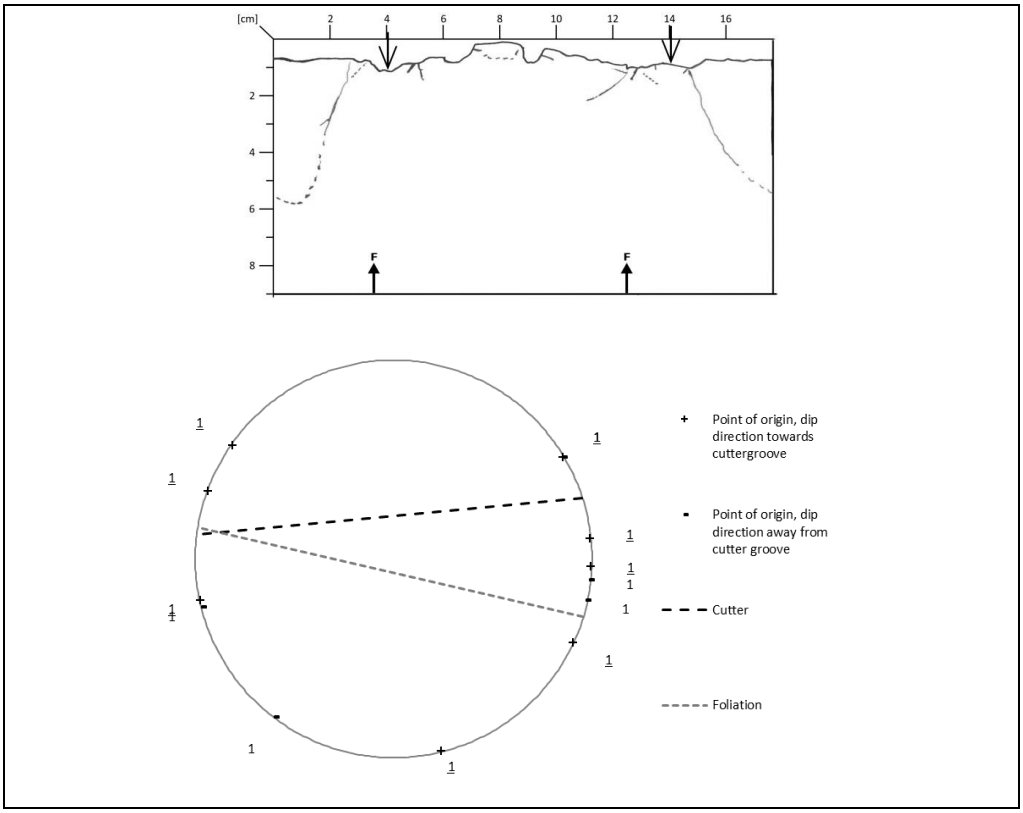

Figure D1.4: Core sample R_1184_1-3_23.

R_1184_1-4_24

Circumference:	328 mm
Number of cracks:	30
Number of cracks with dip < 3°:	6

Distance from 0-line to lowest point on surface:	18 mm
Area between 0-line and surface:	27.6 cm^2

Additional information:
No additional information

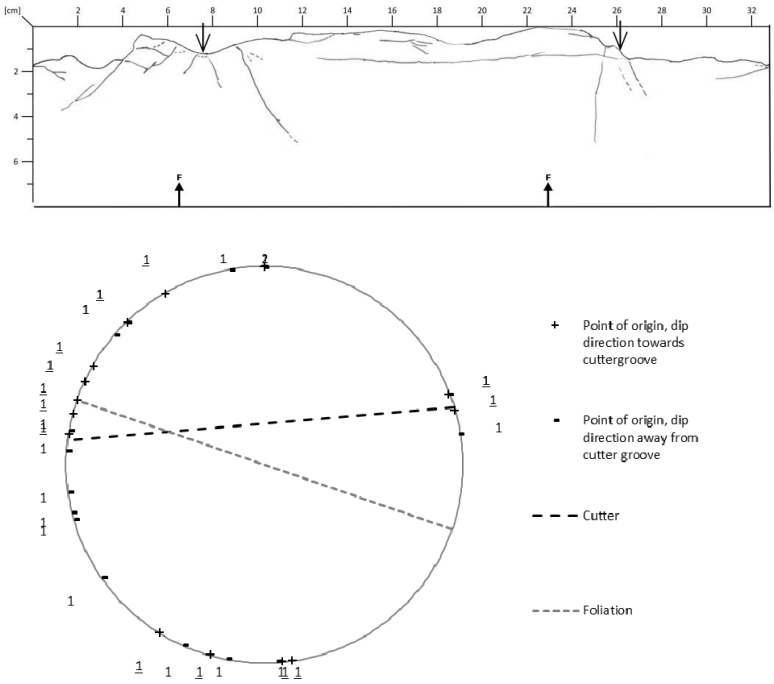

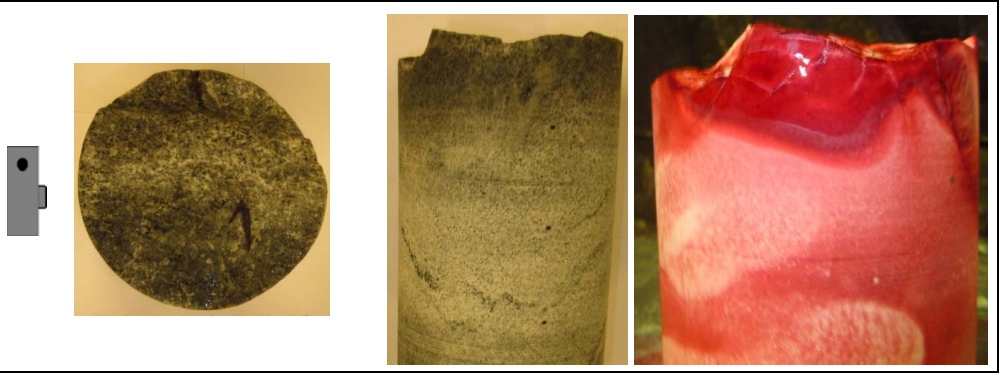

Figure D1.5: Core sample R_1184_1-4_24.

R_1184_1-5_25

Circumference:	326 mm
Number of cracks:	14
Number of cracks with dip < 3°:	2

Distance from 0-line to lowest point on surface:	31 mm
Area between 0-line and surface:	35.5 cm^2

Additional information:
No additional information

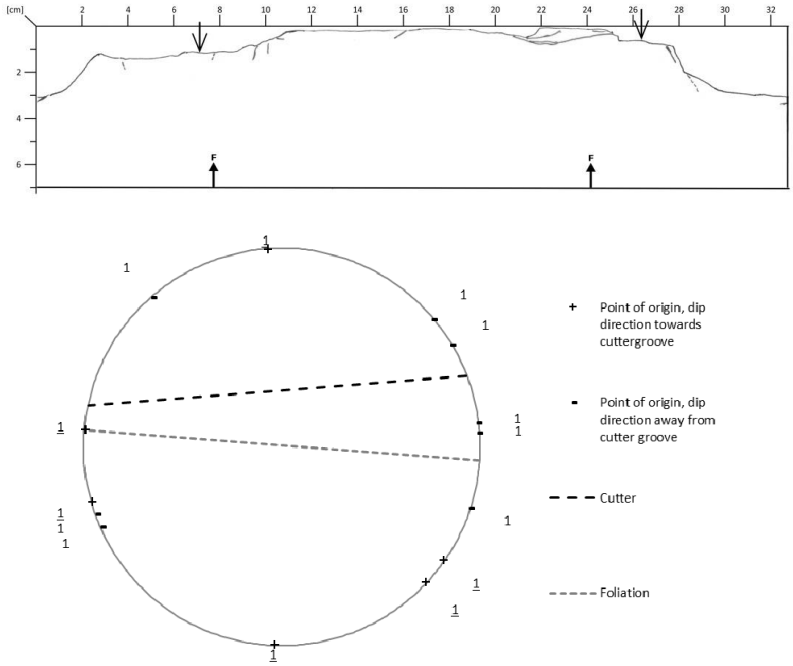

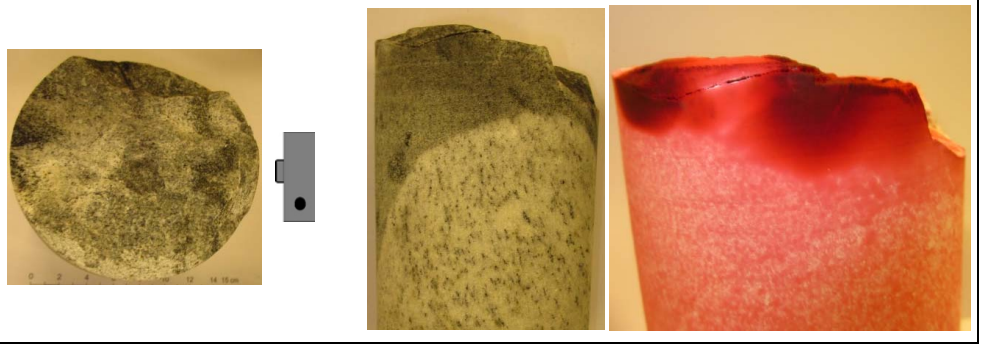

Figure D1.6: Core sample R_1184_1-5_25.

D1.2 Chainage 3112

Date:	10.02.2015	Rock type:	Calcareous rock with biotite and a high quarts content
Chainage	3112.6		
Average RPM:	5	σ_c:	65 – 139 MPa
Average thrust:	14 000 kN /	SJ:	1.9 – 3.8 (extremely to very low)
Average tonn/disc:	26 tonn/cutter		
Average Pressure:	220 bar	S_{20}:	45 - 57 (medium to high)
Penetration:	No available information No available information 1.7 m/h	DRI:	38 -40 (low)
Average torque:	No available information		
Number of cores:	17 +3		

Additional information:
All cutters where 19” cutters, with a cutter width of 3/4”. Samping serie 3 is not included in this study.

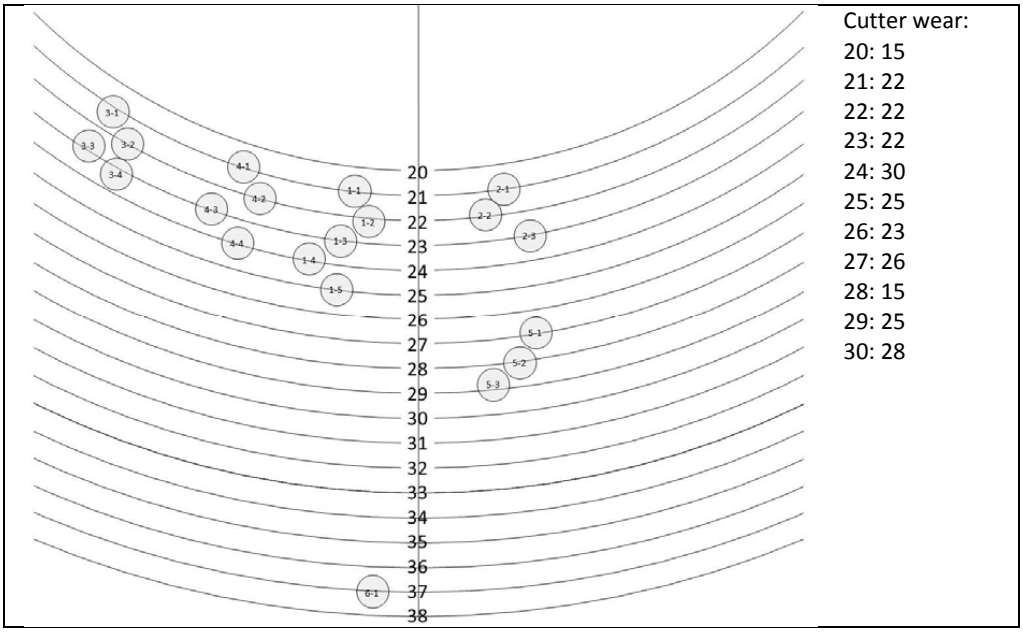

Cutter wear:
20: 15
21: 22
22: 22
23: 22
24: 30
25: 25
26: 23
27: 26
28: 15
29: 25
30: 28

Figure D1.7: Sampling at R_3112.

R_3112_1-1_21

Circumference:	328 mm
Number of cracks:	12
Number of cracks with dip < 3°:	1

Distance from 0-line to lowest point on surface:	16 mm
Area between 0-line and surface:	35.5 cm^2

Additional information:
No additional information

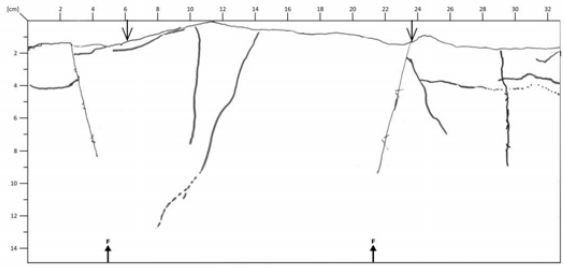

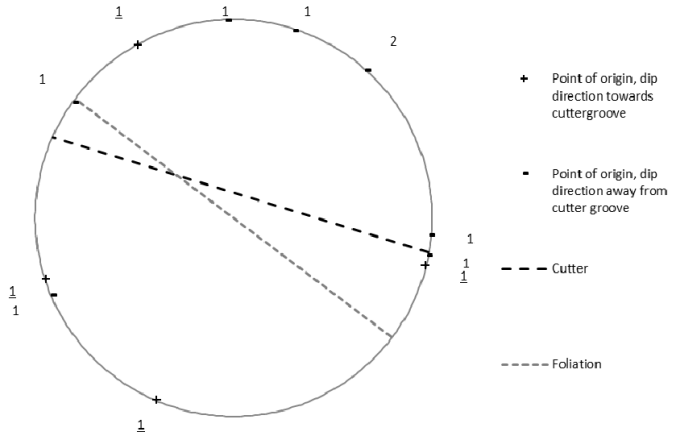

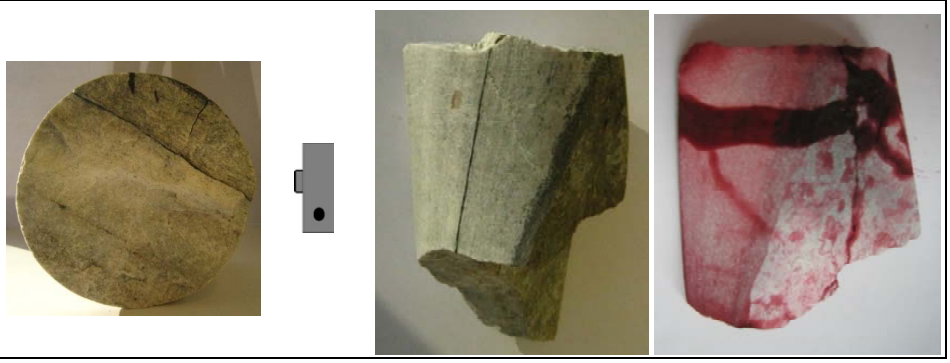

Figure D1.8: Core sample R_3112_1-1_21.

R_3112_1-2_22

Circumference:	328 mm
Number of cracks:	12
Number of cracks with dip < 3°:	2

Distance from 0-line to lowest point on surface:	14 mm
Area between 0-line and surface:	18.5 cm^2

Additional information:
No additional information

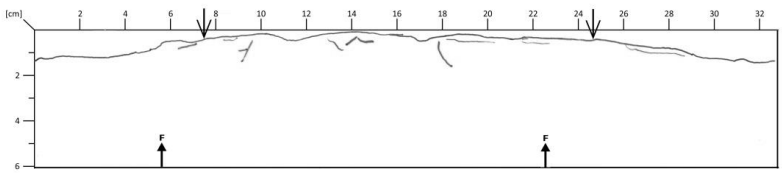

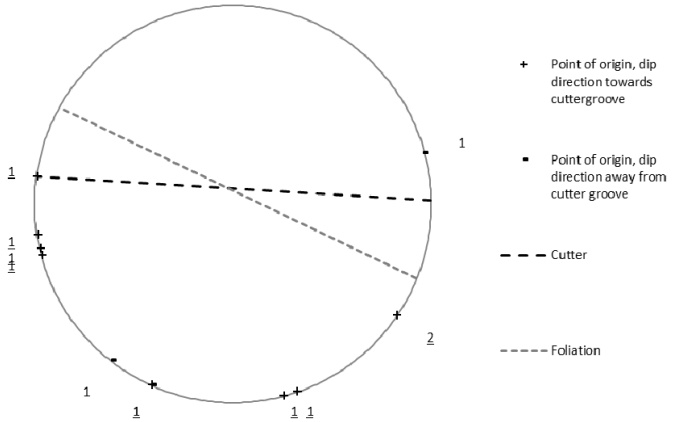

Figure D1.9: Core sample R_3112_1-2_22.

R_3112_1-3_23

Circumference:	328 mm
Number of cracks:	11
Number of cracks with dip < 3°:	1

Distance from 0-line to lowest point on surface:	22 mm
Area between 0-line and surface:	35.1 cm^2

Additional information:
No additional information

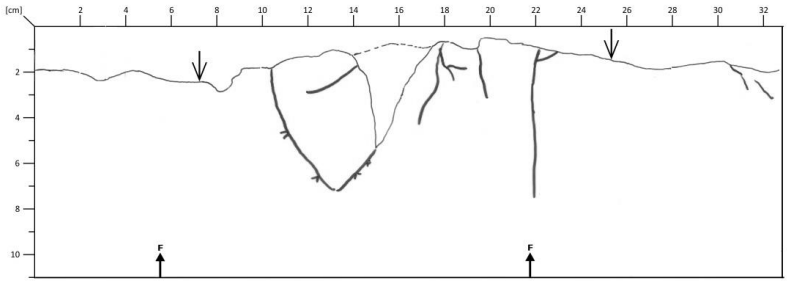

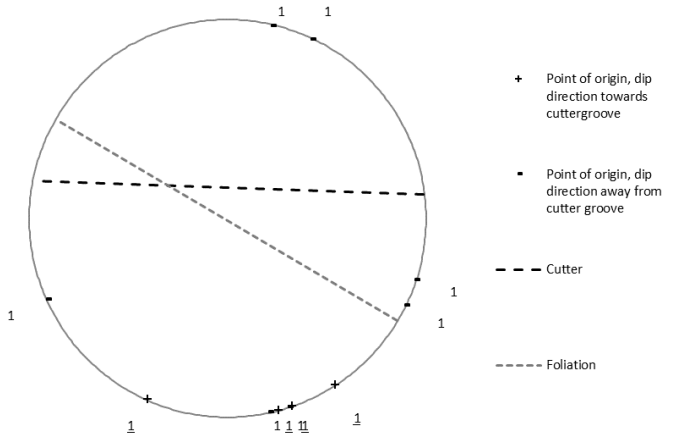

Figure D1.10: Core sample R_3112_1-3_23.

R_3112_1-4_24

Circumference:	327mm
Number of cracks:	13
Number of cracks with dip < 3°:	1

Distance from 0-line to lowest point on surface:	10 mm
Area between 0-line and surface:	16.1 cm^2

Additional information:
No additional information

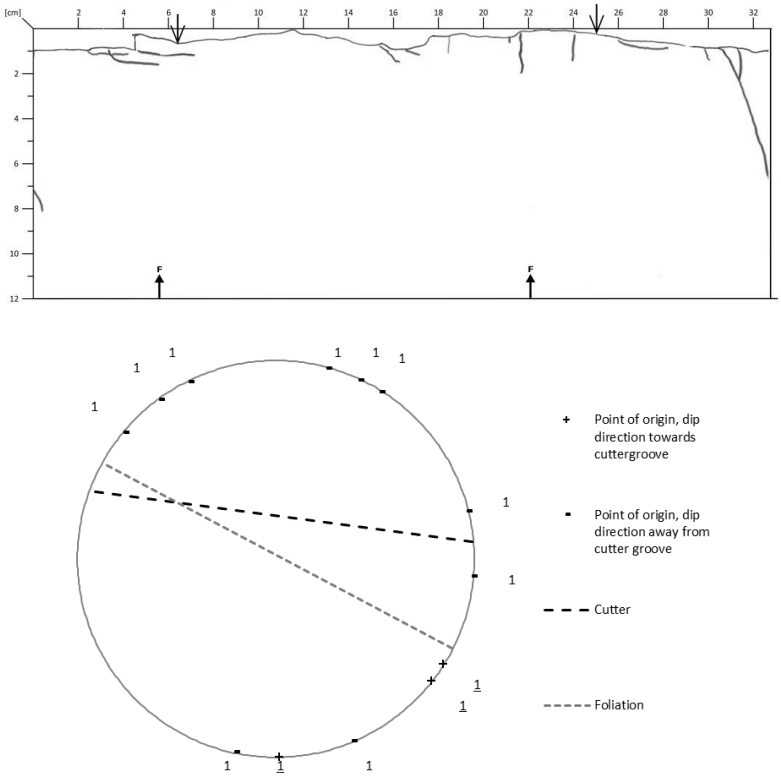

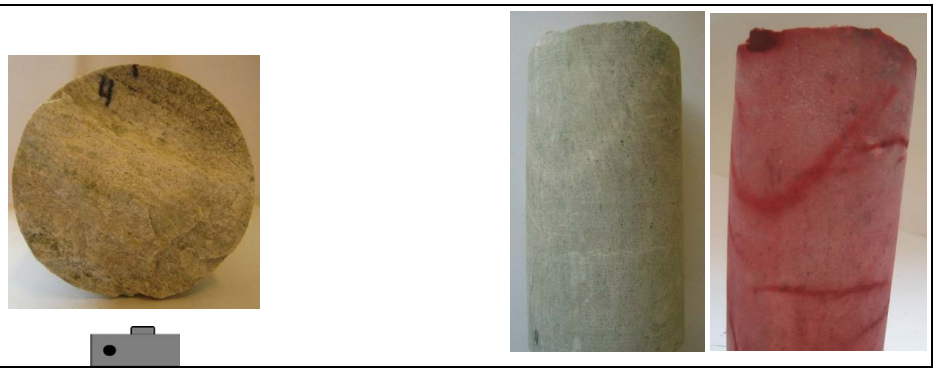

Figure D1.11: Core sample R_3112_1-4_24.

R_3112_1-5_25

Circumference:	326 mm
Number of cracks:	14
Number of cracks with dip < 3°:	0

Distance from 0-line to lowest point on surface:	10 mm
Area between 0-line and surface:	19.8 cm^2

Additional information:
No additional information

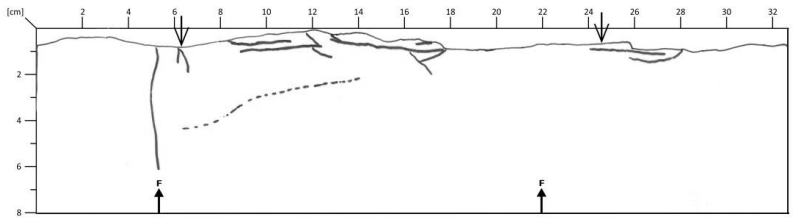

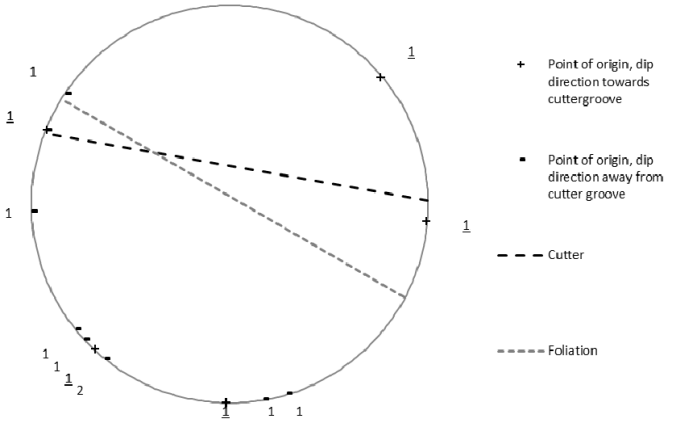

Figure D1.12: Core sample R_3112_1-5_25.

R_3112_2-1_21

Not included in study, due to low quality of core sample.

R_3112_2-2_22

Not included in study, due to low quality of core sample.

R_3112_2-3_23

Not included in study, due to low quality of core sample.

R_3112_3-1_21

Circumference:	328 mm
Number of cracks:	22
Number of cracks with dip < 3°:	4

Distance from 0-line to lowest point on surface:	10 mm
Area between 0-line and surface:	15.1 cm^2

Additional information:
No additional information

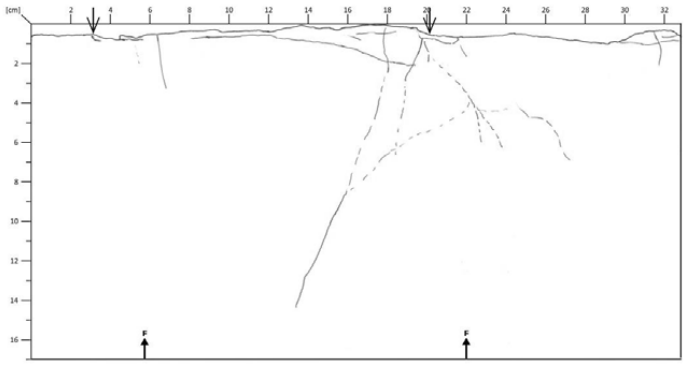

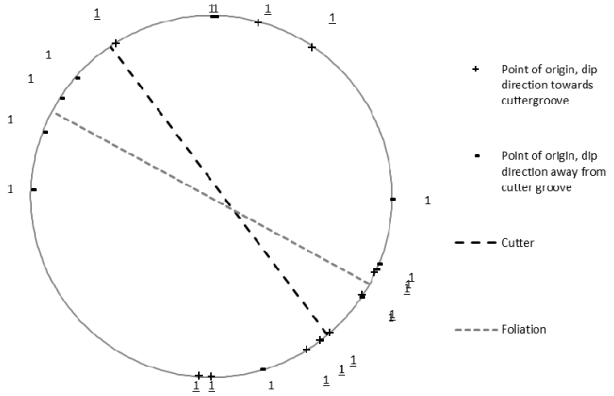

Figure D1.13: Core sample R_3112_3-1_21.

R_3112_3-2_22

Circumference:	329 mm
Number of cracks:	18
Number of cracks with dip < 3°:	0

Distance from 0-line to lowest point on surface:	11 mm
Area between 0-line and surface:	17.6 cm^2

Additional information:
No additional information

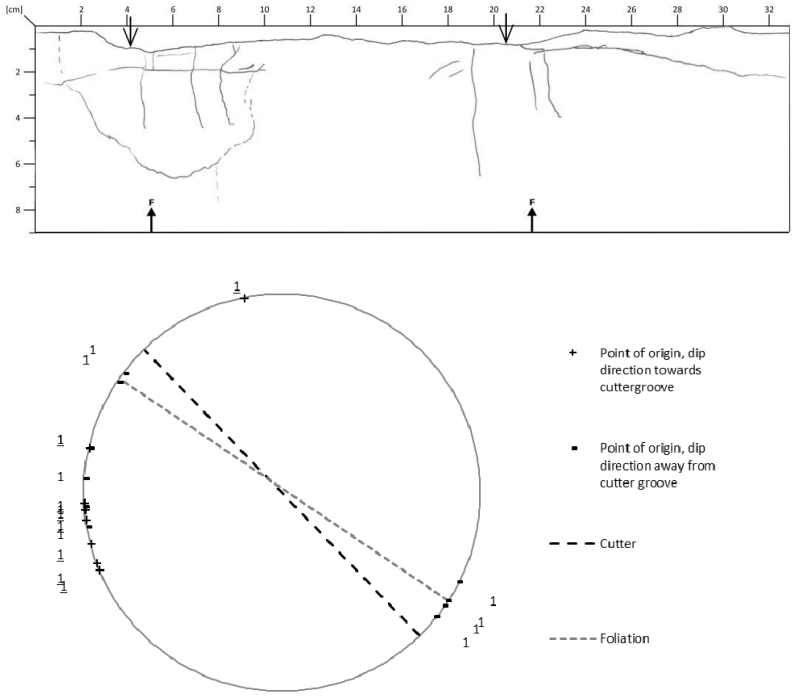

Figure D1.14: Core sample R_3112_3-2_22.

R_3112_3-3_23

Circumference:	329 mm
Number of cracks:	12
Number of cracks with dip < 3°:	2

Distance from 0-line to lowest point on surface:	11 mm
Area between 0-line and surface:	15.9 cm^2

Additional information:
No additional information

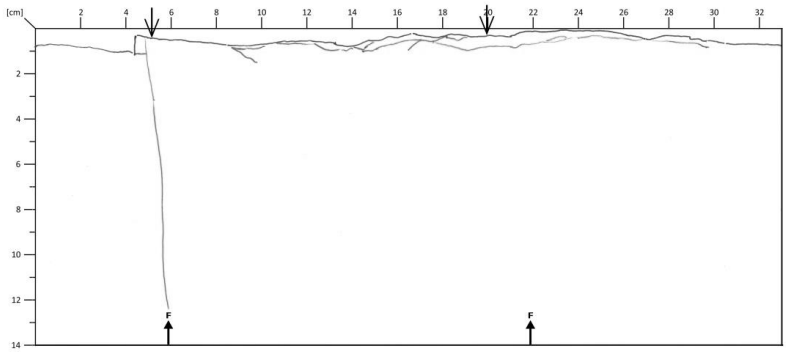

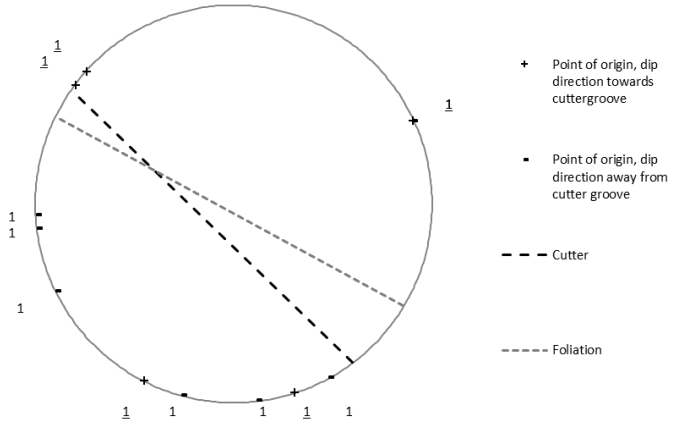

Figure D1.15: Core sample R_3112_3-3_23.

R_3112_3-4_23

Circumference:	322 mm
Number of cracks:	13
Number of cracks with dip < 3°:	2

Distance from 0-line to lowest point on surface:	11 mm
Area between 0-line and surface:	15.4 cm^2

Additional information:
No additional information

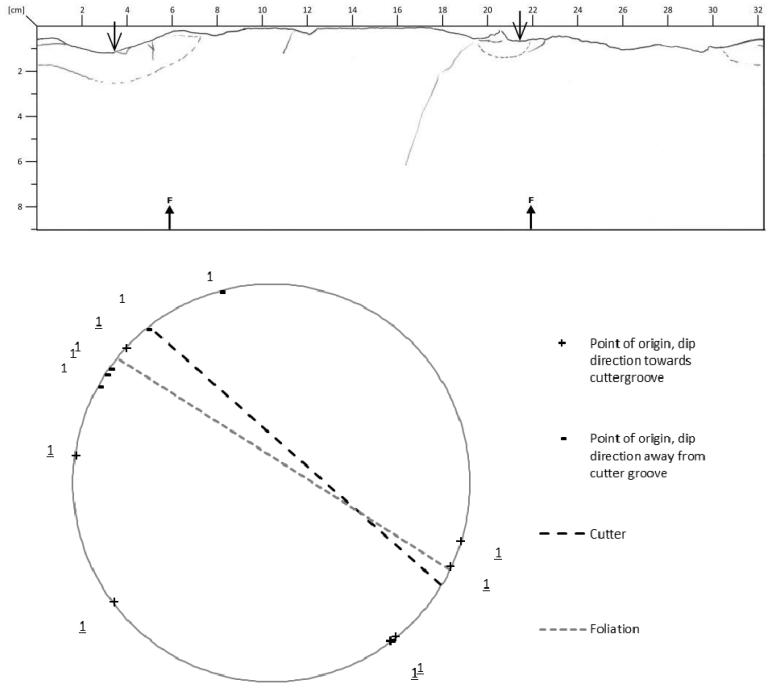

Figure D1.16: Core sample R_3112_3-4_23.

R_3112_4-1_21

Circumference:	321 mm
Number of cracks:	17
Number of cracks with dip < 3°:	3

Distance from 0-line to lowest point on surface:	13 mm
Area between 0-line and surface:	17.7 cm^2

Additional information:
No additional information

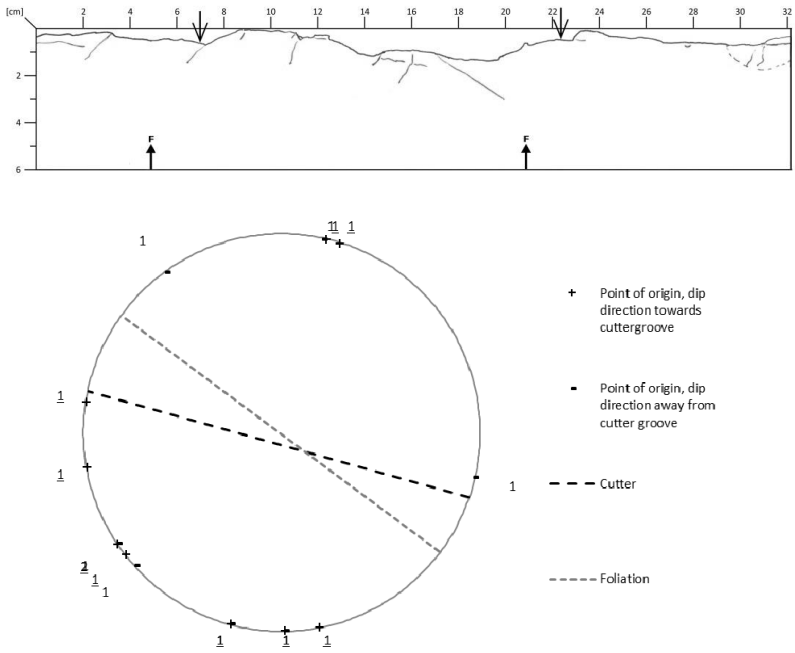

Figure D1.17: Core sample R_3112_4-1_21.

R_3112_4-2_22

Circumference:	320 mm
Number of cracks:	26
Number of cracks with dip < 3°:	5

Distance from 0-line to lowest point on surface:	19 mm
Area between 0-line and surface:	30.1 cm^2

Additional information:
No additional information

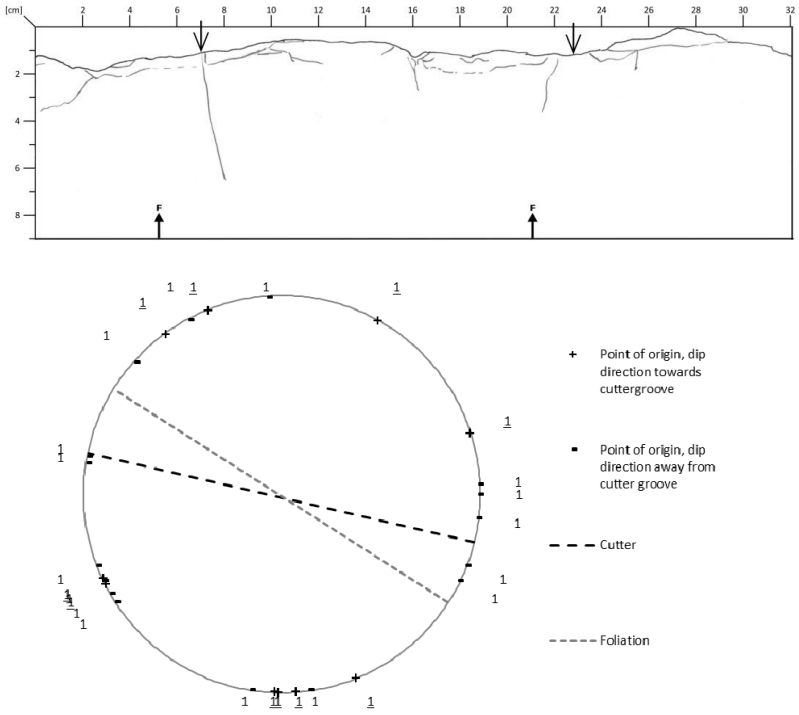

Figure D1.18: Core sample R_3112_4-2_22.

R_3112_4-3_23

Circumference:	321 mm
Number of cracks:	25
Number of cracks with dip < 3°:	3

Distance from 0-line to lowest point on surface:	6 mm
Area between 0-line and surface:	13.5 cm^2

Additional information:
No additional information

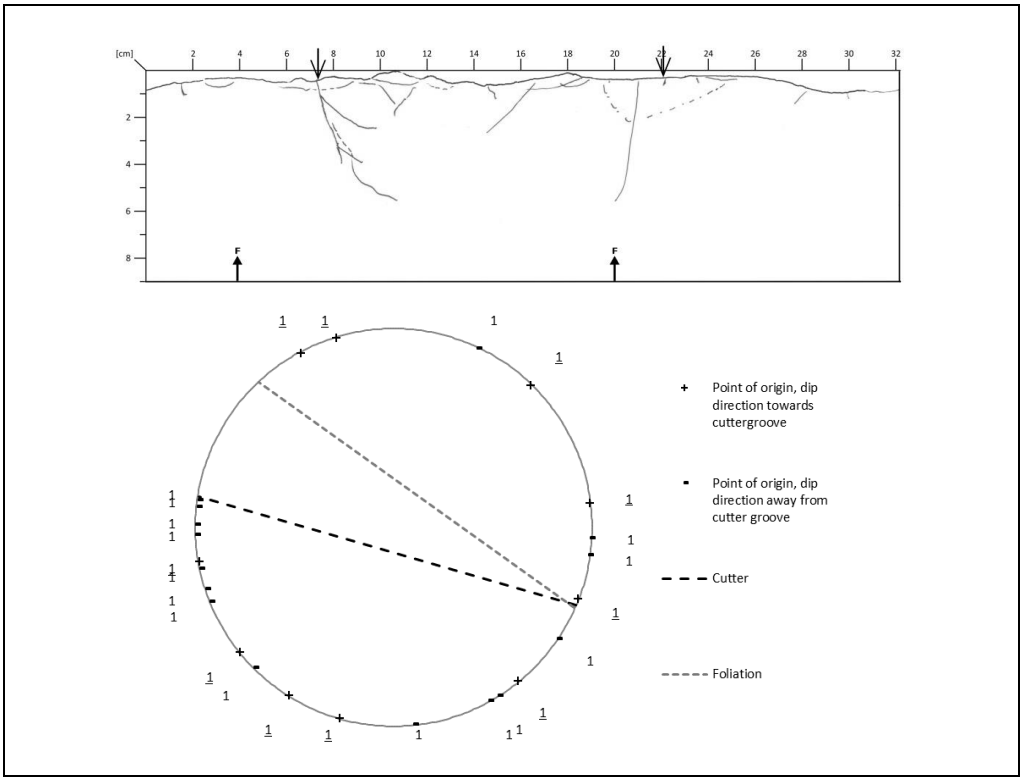

Figure D1.19: Core sample R_3112_4-3_23.

R_3112_4-4_24

Circumference:	321 mm
Number of cracks:	18
Number of cracks with dip < 3°:	4

Distance from 0-line to lowest point on surface:	15 mm
Area between 0-line and surface:	16.6 cm^2

Additional information:
No additional information

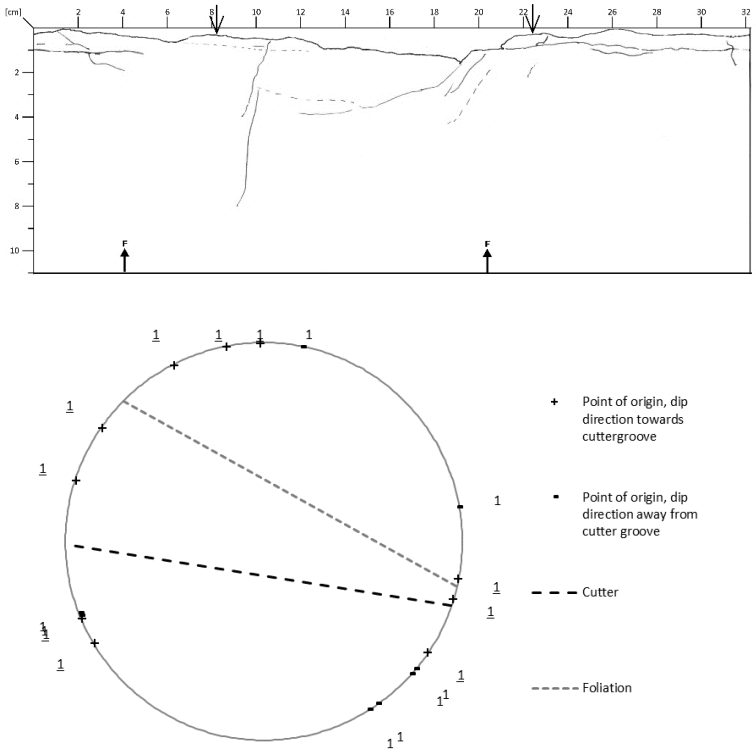

Figure D1.20: Core sample R_3112_4-4_24.

R_3112_5-1_27

Circumference:	328 mm
Number of cracks:	26
Number of cracks with dip < 3°:	3

Distance from 0-line to lowest point on surface:	21 mm
Area between 0-line and surface:	31.4 cm^2

Additional information:
No additional information

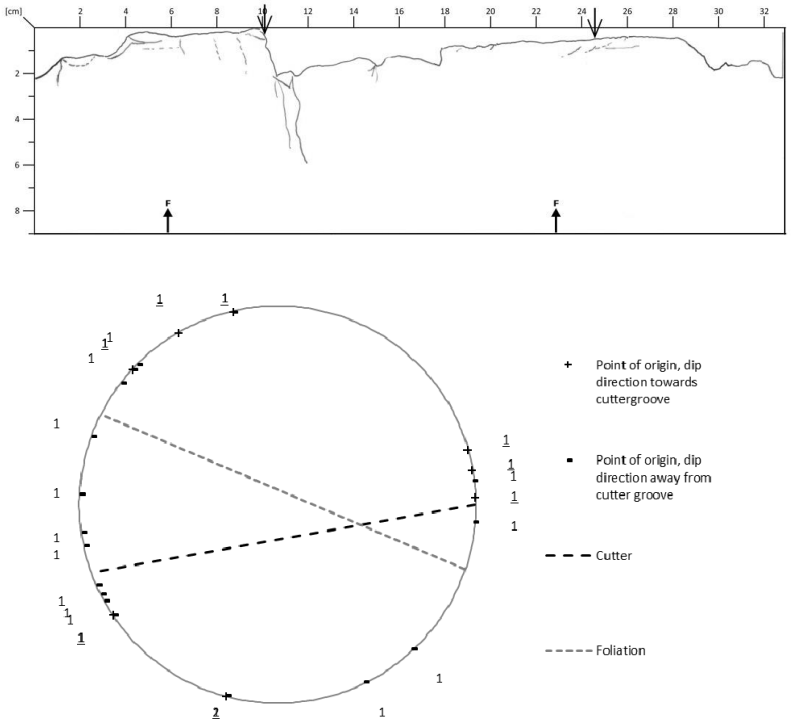

Figure D1.21: Core sample R_3112_5-1_27.

R_3112_5-2_28

Circumference:	327 mm
Number of cracks:	26
Number of cracks with dip < 3°:	4

Distance from 0-line to lowest point on surface:	19 mm
Area between 0-line and surface:	37.5 cm^2

Additional information:
No additional information

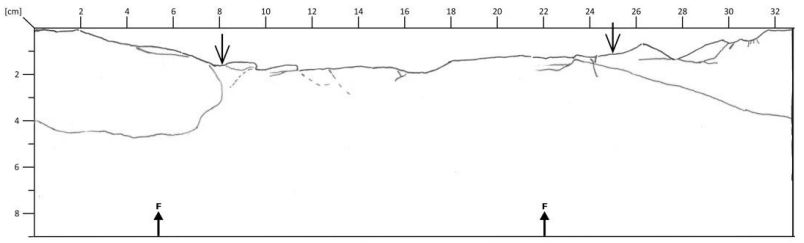

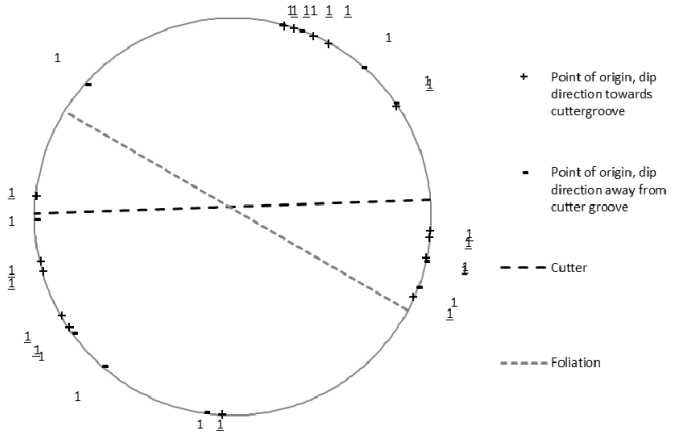

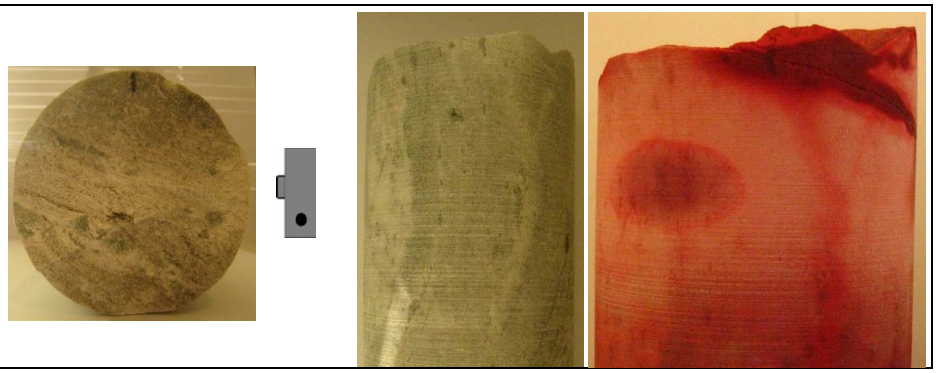

Figure D1.22: Core sample R_3112_5-2_28.

R_3112_5-3_29

Circumference:	327 mm
Number of cracks:	27
Number of cracks with dip < 3°:	4

Distance from 0-line to lowest point on surface:	54 mm
Area between 0-line and surface:	666 cm^2

Additional information:
No additional information

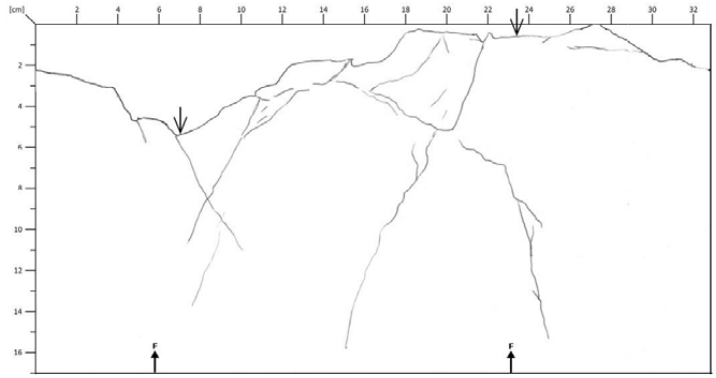

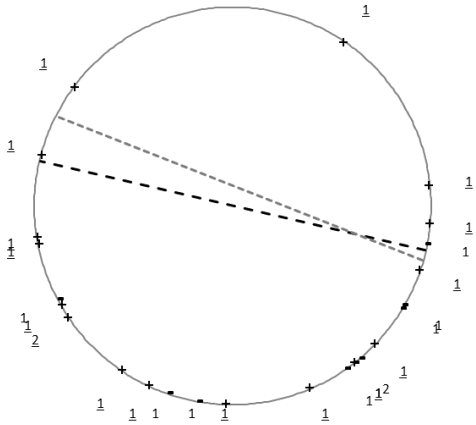

Figure D1.23: Core sample R_3112_5-3_29.

R_3112_6-1_37

Circumference:	319 mm
Number of cracks:	24
Number of cracks with dip < 3°:	5

Distance from 0-line to lowest point on surface:	30 mm
Area between 0-line and surface:	45.5 cm^2

Additional information:
No additional information

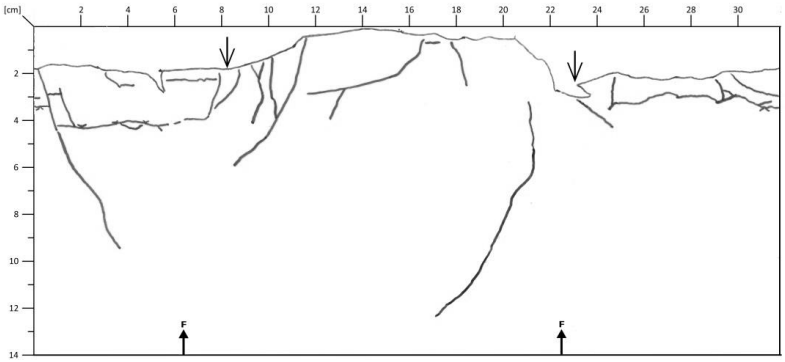

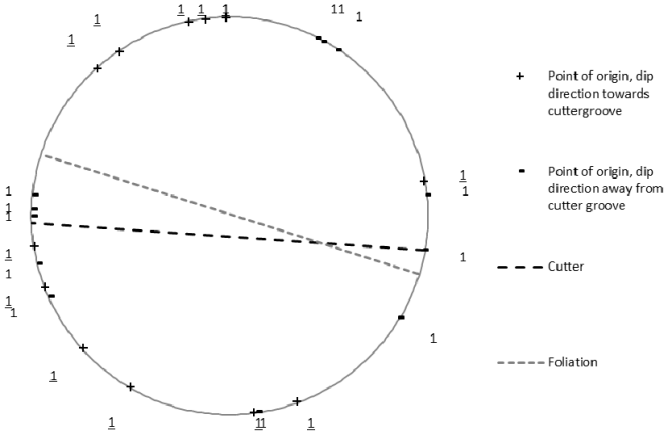

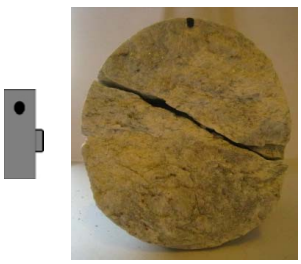

Figure D1.24: Core sample R_3112_6-1_37.

D1.3 Chainage 5437

Date:	21.07.2015
Chainage	5437.5
Average RPM:	3.0
Average thrust:	16 000 kN
Average tonn/disc:	28 tonn/disc
Average Pressure:	240 bar
Penetration:	8 mm/rev
	26 mm/min
	1.6 m/h
Average torque:	2 100 kNm
Number of cores:	16

Rock type:	Gneiss with garnet and some lime
σ_c:	92 - 124 MPa
SJ:	1.7 (Extremely low)
S_{20}:	48 - 54 (Medium to high)
DRI:	45 (Medium)

Additional information:
All cutters where 19” cutters, with a cutter width of 3/4”.

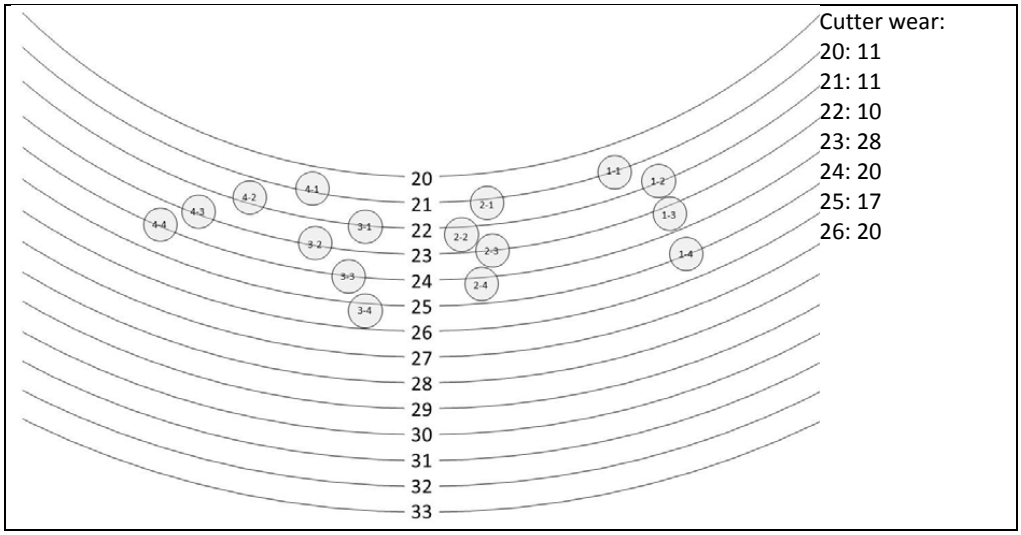

Figure D1.25: Sampling at R_5437.

R_5437_1-1_21

Circumference:	328 mm
Number of cracks:	21
Number of cracks with dip < 3°:	2

Distance from 0-line to lowest point on surface:	23 mm
Area between 0-line and surface:	36.5 cm^2

Additional information:
No additional information

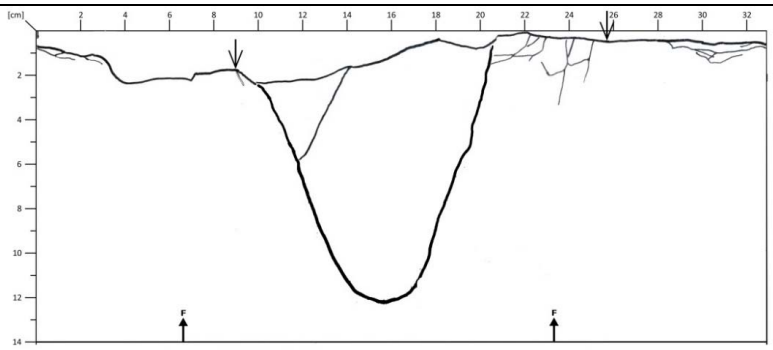

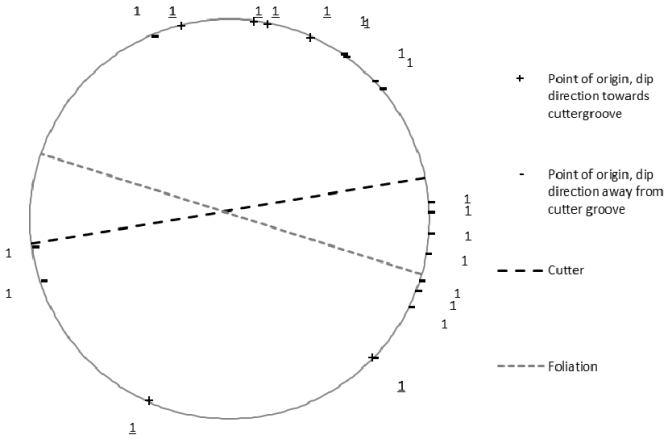

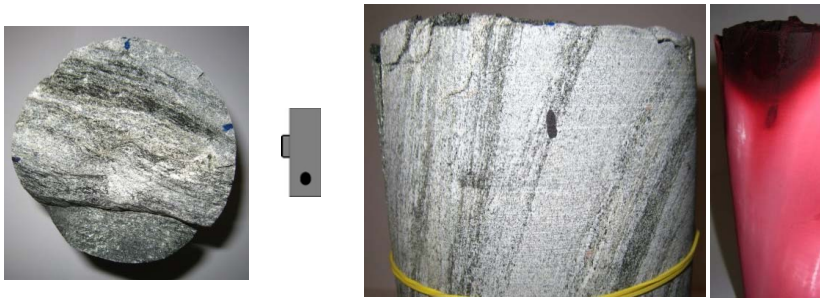

Figure D1.26: Core sample R_5437_1-1_21.

R_5437_1-2_22

Circumference:	329 mm
Number of cracks:	41
Number of cracks with dip < 3°:	5

Distance from 0-line to lowest point on surface:	43 mm
Area between 0-line and surface:	83.7 cm^2

Additional information:
No additional information

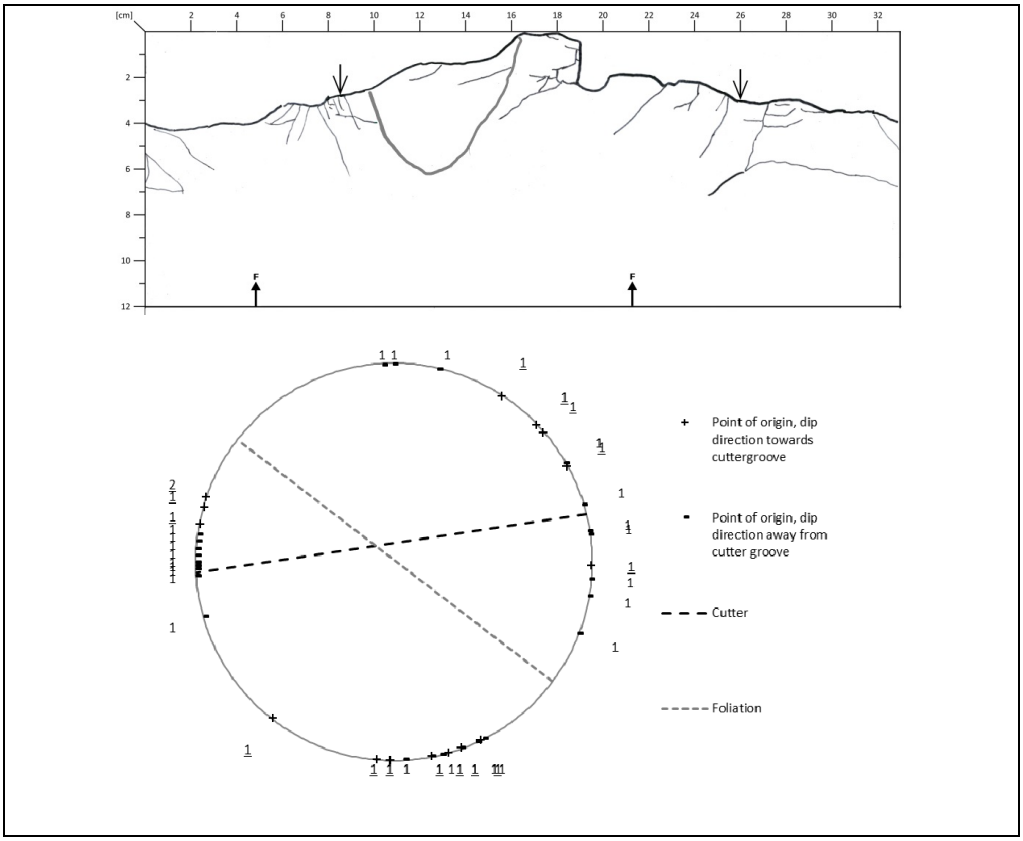

Figure D1.27: Core sample R_5437_1-2_22.

R_5437_1-3_23

Circumference:	328 mm
Number of cracks:	16
Number of cracks with dip < 3°:	1

Distance from 0-line to lowest point on surface:	24 mm
Area between 0-line and surface:	37.4 cm^2

Additional information:
No additional information

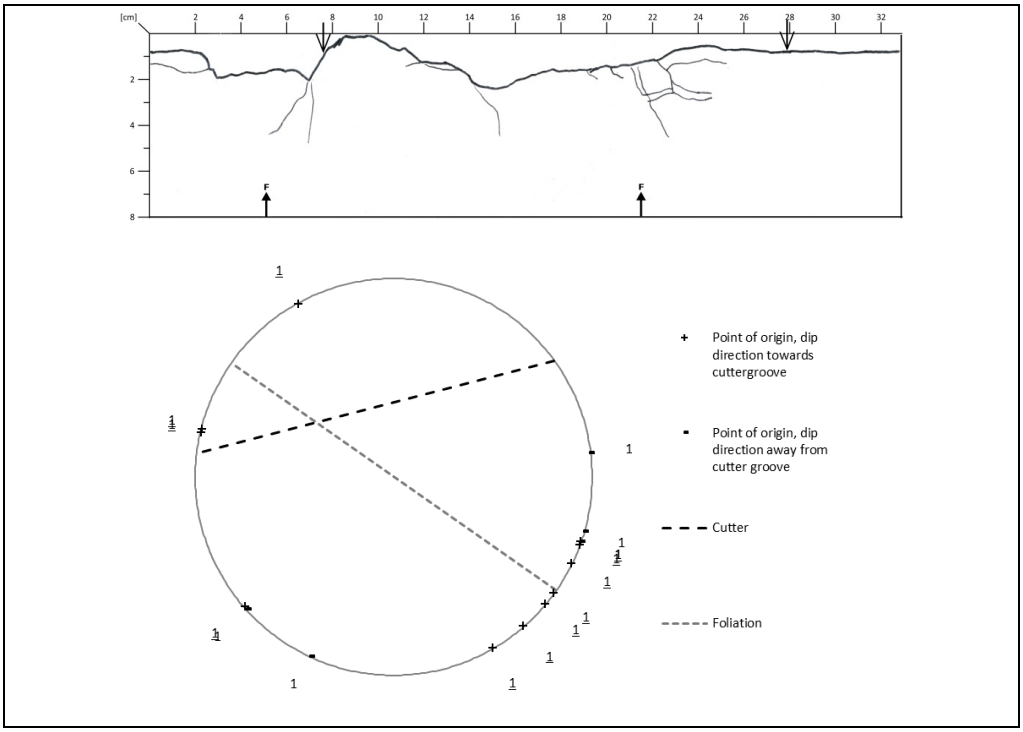

Figure D1.28: Core sample R_5437_1-3_23.

R_5437_1-4_25

Circumference:	328 mm
Number of cracks:	29
Number of cracks with dip < 3°:	3

Distance from 0-line to lowest point on surface:	16 mm
Area between 0-line and surface:	24.6 cm^2

Additional information:
No additional information

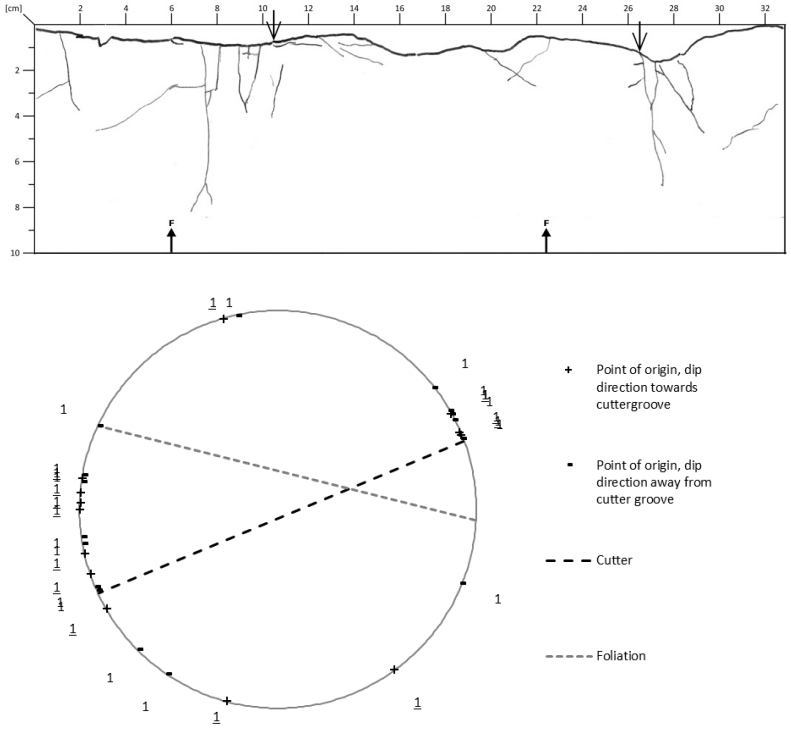

Figure D1.29: Core sample R_5437_1-4_25.

R_5437_2-1_21

Circumference:	329 mm
Number of cracks:	37
Number of cracks with dip < 3°:	4

Distance from 0-line to lowest point on surface:	11 mm
Area between 0-line and surface:	17.5 cm^2

Additional information:
No additional information

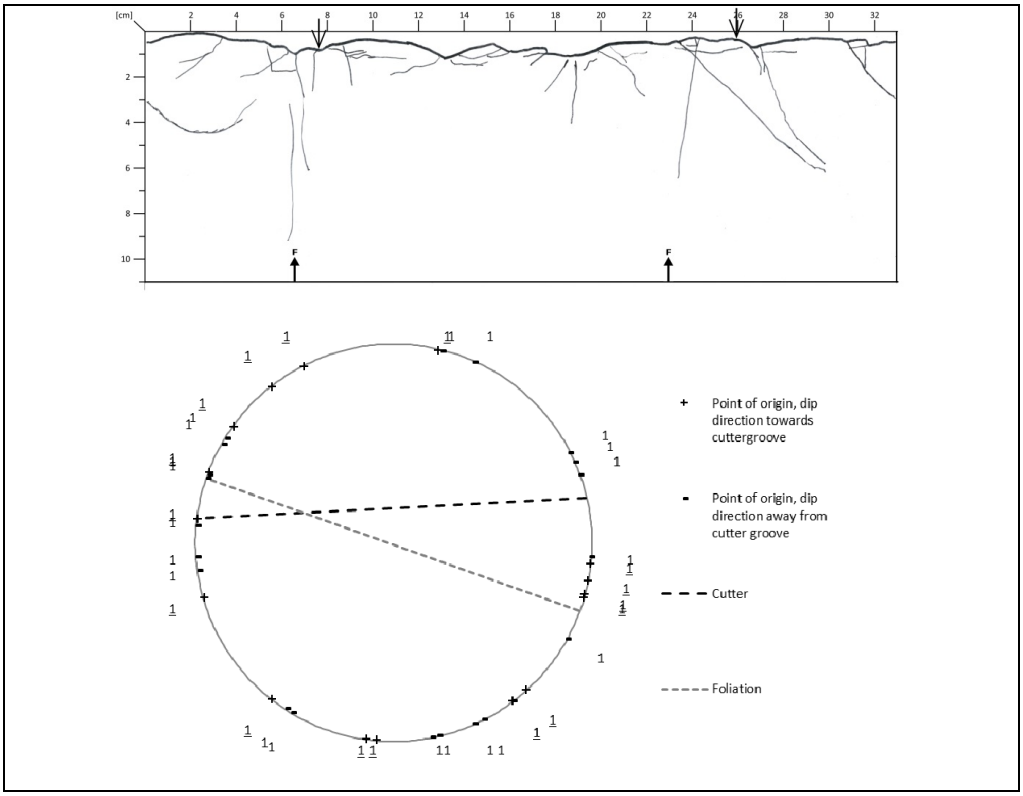

Figure D1.30: Core sample R_5437_2-1_21.

R_5437_2-2_22

Circumference:	329 mm
Number of cracks:	9
Number of cracks with dip < 3°:	1

Distance from 0-line to lowest point on surface:	16 mm
Area between 0-line and surface:	Not relevant

Additional information:
This core is not included in all evaluations. This is commented when relevant.

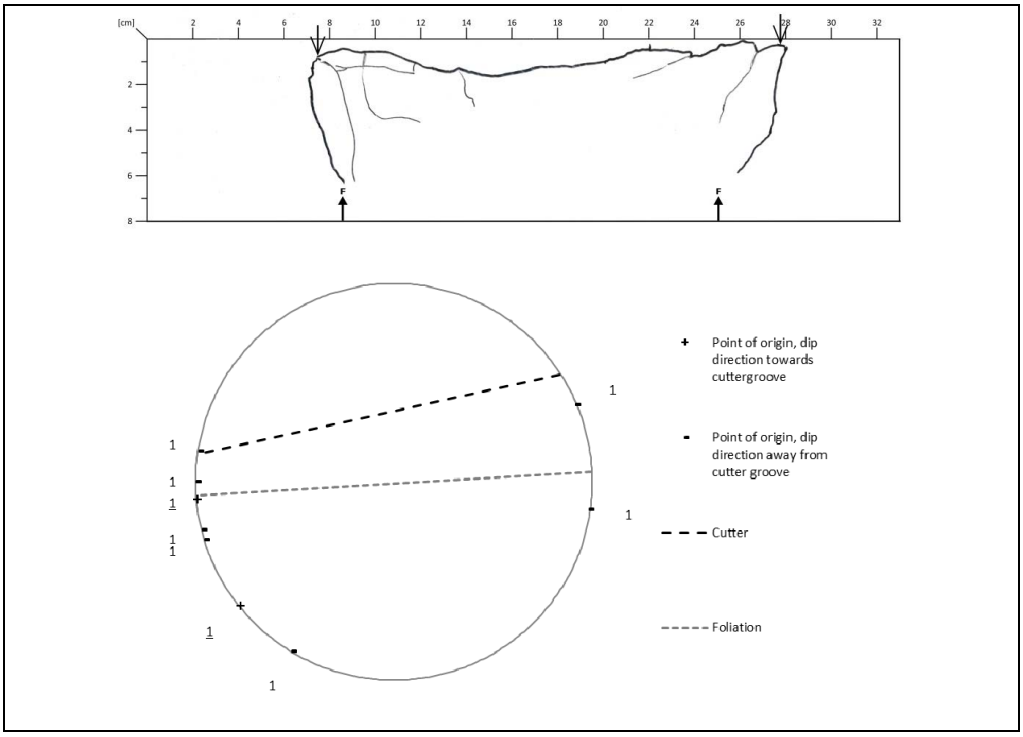

Figure D1.31: Core sample R_5437_2-2_22.

R_5437_2-3_23

Circumference:	328 mm
Number of cracks:	12
Number of cracks with dip < 3°:	1

Distance from 0-line to lowest point on surface:	25 mm
Area between 0-line and surface:	41.4 cm^2

Additional information:
No additional information

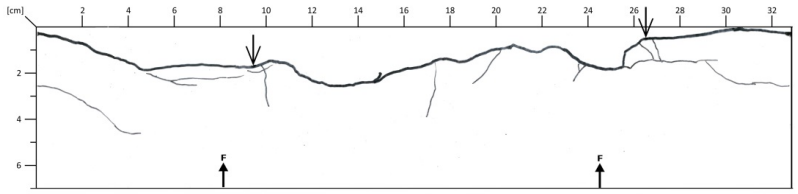

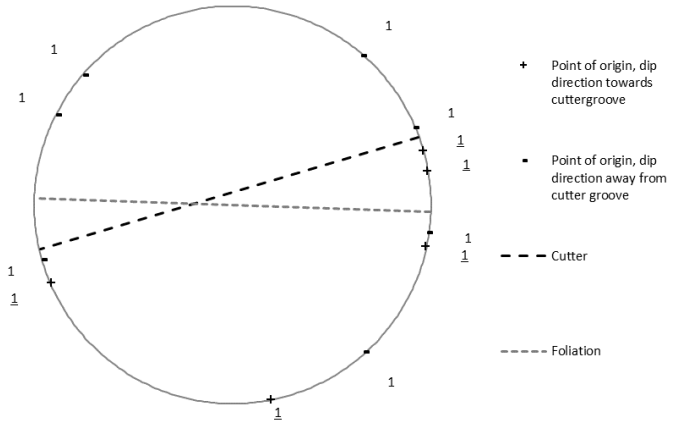

Figure D1.32: Core sample R_5437_2-3_23.

R_5437_2-4_24

Circumference:	329 mm
Number of cracks:	21
Number of cracks with dip < 3°:	0

Distance from 0-line to lowest point on surface:	20 mm
Area between 0-line and surface:	36.6 cm^2

Additional information:
No additional information

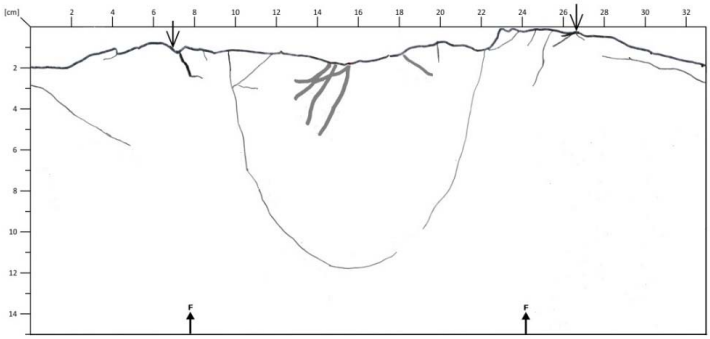

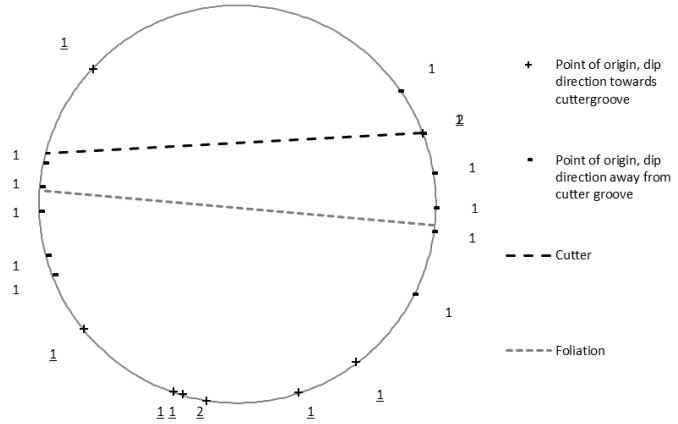

Figure D1.33: Core sample R_5437_2-4_24.

R_5437_3-1_22

Circumference:	330 mm
Number of cracks:	18
Number of cracks with dip < 3°:	0

Distance from 0-line to lowest point on surface:	22 mm
Area between 0-line and surface:	38.7 cm^2

Additional information:
No additional information

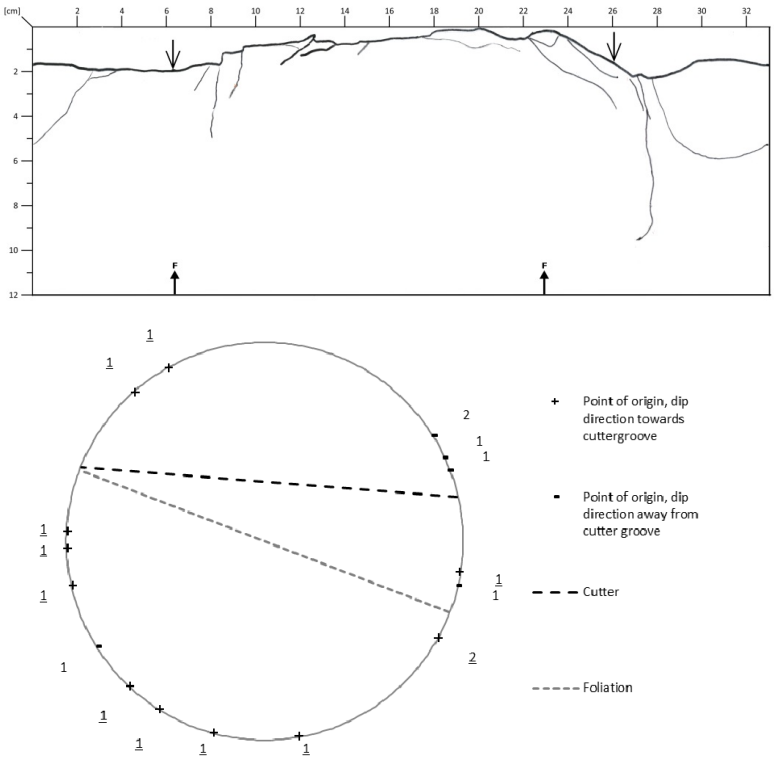

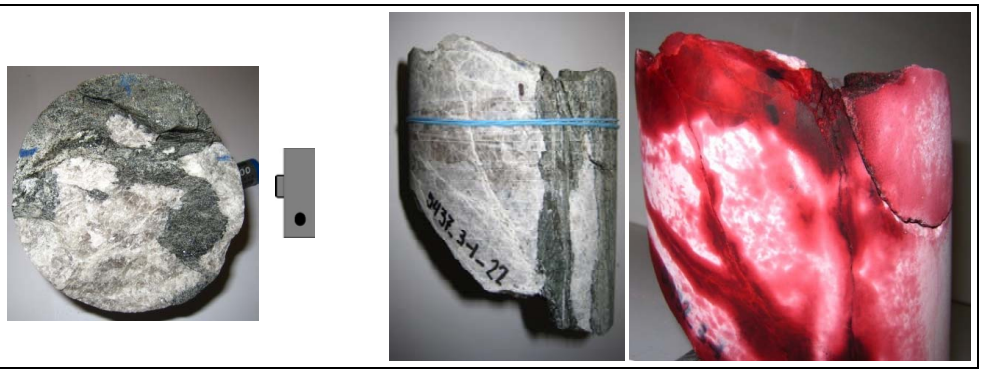

Figure D1.34: Core sample R_5437_3-1_22.

R_5437_3-2_23

Circumference:	330 mm
Number of cracks:	10
Number of cracks with dip < 3°:	1

Distance from 0-line to lowest point on surface:	35 mm
Area between 0-line and surface:	50.9 cm^2

Additional information:
No additional information

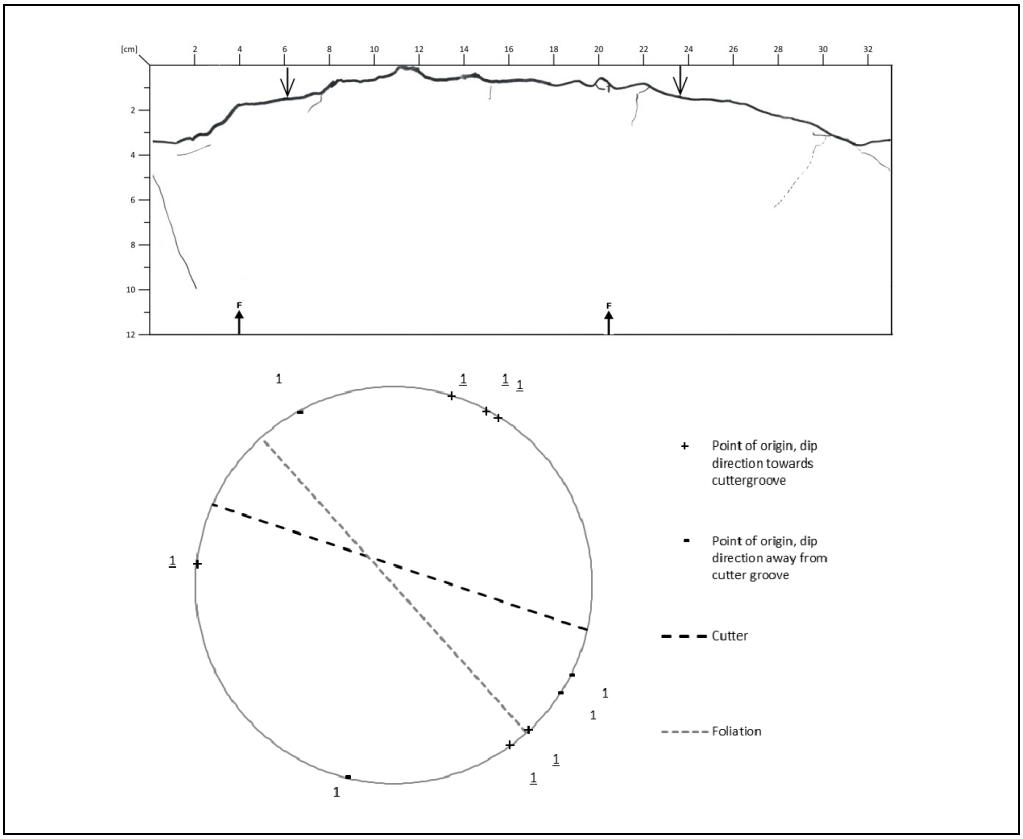

Figure D1.35: Core sample R_5437_3-2_23.

R_5437_3-3_24

Circumference:	332 mm
Number of cracks:	21
Number of cracks with dip < 3°:	1

Distance from 0-line to lowest point on surface:	44 mm
Area between 0-line and surface:	51.4 cm^2

Additional information:
No additional information

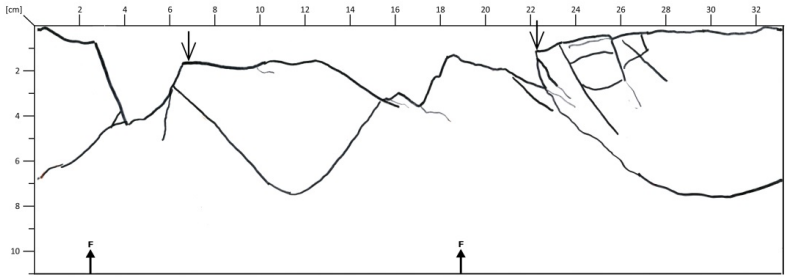

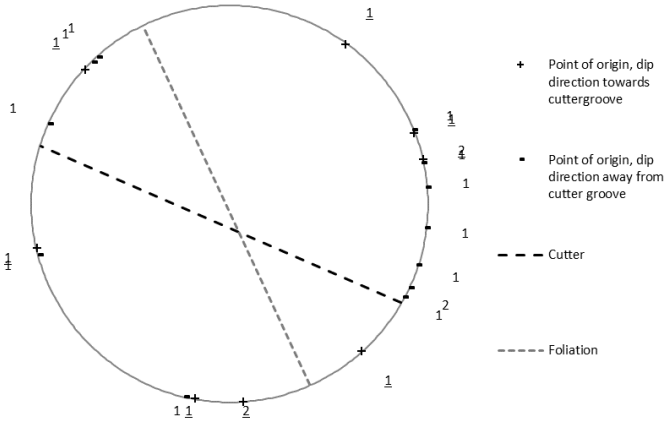

Figure D1.36: Core sample R_5437_3-3_24.

R_5437_3-4_25

Circumference:	331 mm
Number of cracks:	26
Number of cracks with dip < 3°:	0

Distance from 0-line to lowest point on surface:	41 mm
Area between 0-line and surface:	62.9 cm^2

Additional information:
No additional information

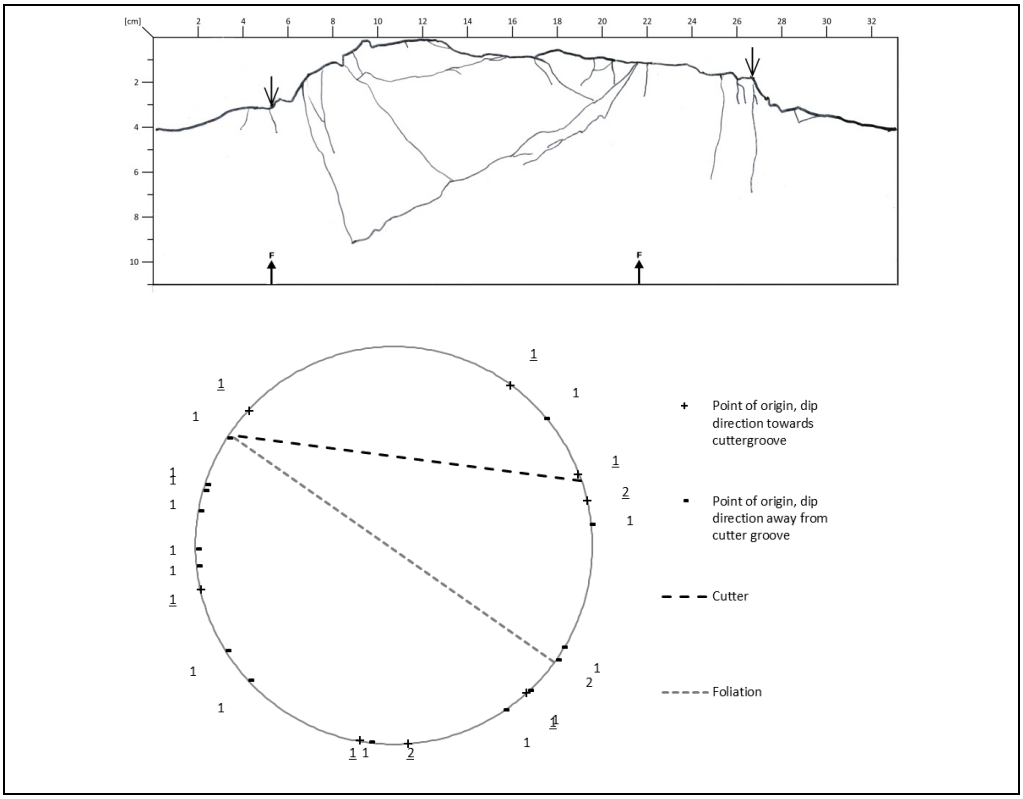

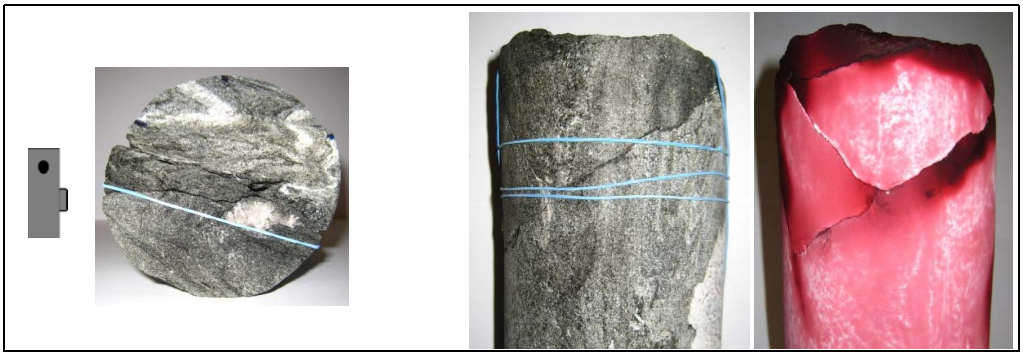

Figure D1.37: Core sample R_5437_3-4_25.

R_5437_4-1_21

Circumference:	329 mm
Number of cracks:	24
Number of cracks with dip < 3°:	1

Distance from 0-line to lowest point on surface:	14 mm
Area between 0-line and surface:	13.3 cm^2

Additional information:

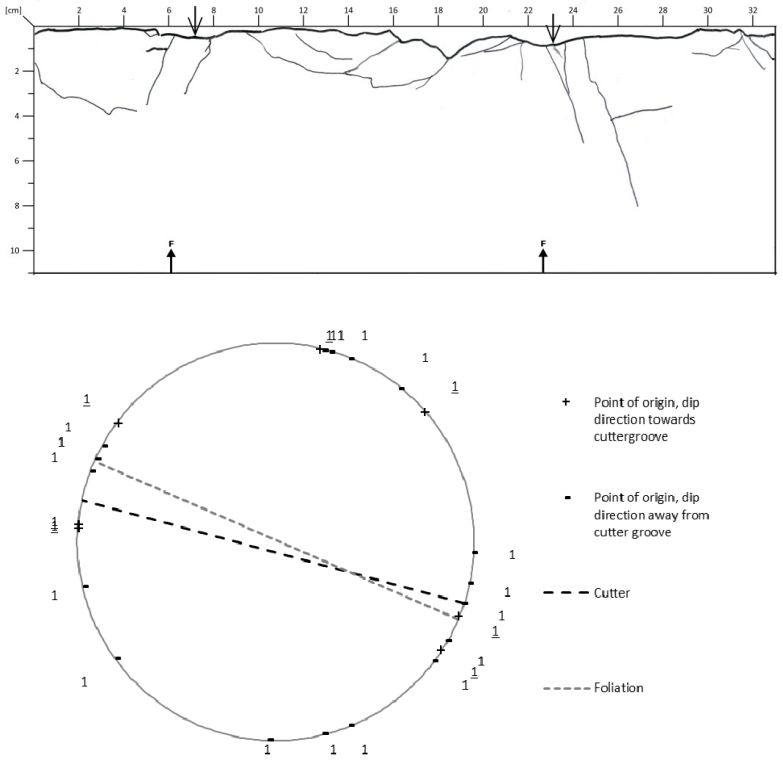

Figure D1.38: Core sample R_5437_4-1_21.

R_5437_4-2_22

Circumference:	329 mm
Number of cracks:	28
Number of cracks with dip < 3°:	2

Distance from 0-line to lowest point on surface:	20 mm
Area between 0-line and surface:	27.6 cm^2

Additional information:
No additional information

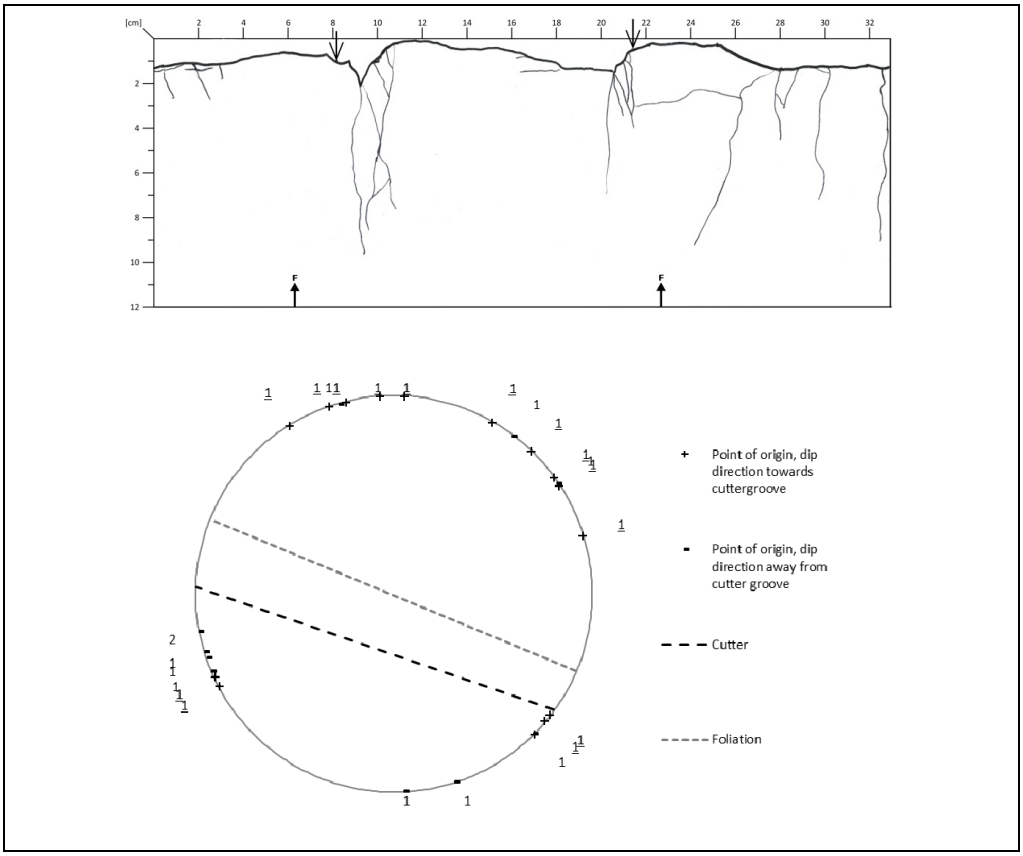

Figure D1.39: Core sample R_5437_4-2_22.

R_5437_4-3_23

Circumference:	331 mm
Number of cracks:	20
Number of cracks with dip < 3°:	5

Distance from 0-line to lowest point on surface:	20 mm
Area between 0-line and surface:	30.9 cm^2

Additional information:
No additional information

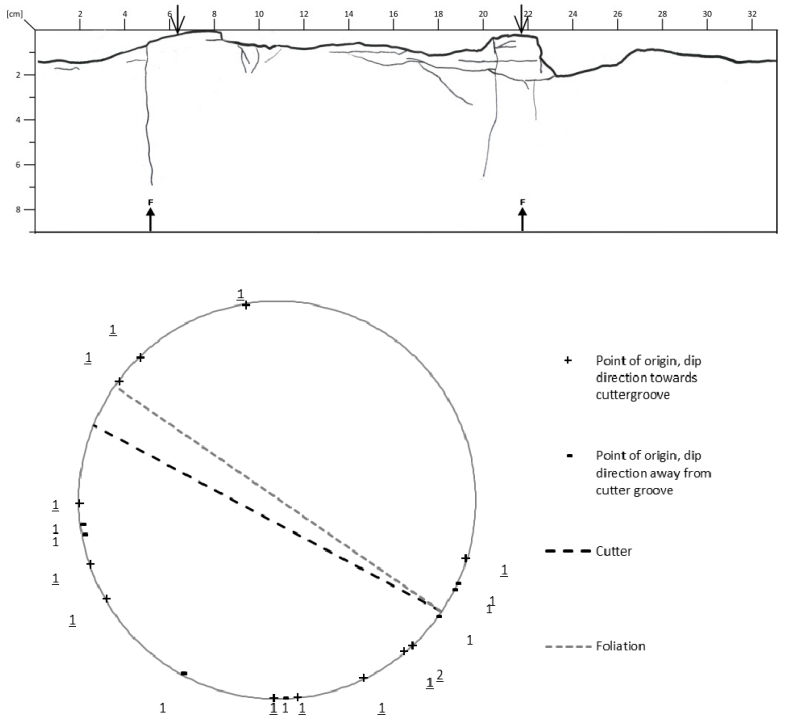

Figure D1.40: Core sample R_5437_4-3_23.

R_5437_4-4_24

Circumference:	330 mm
Number of cracks:	35
Number of cracks with dip < 3°:	2

Distance from 0-line to lowest point on surface:	26 mm
Area between 0-line and surface:	36.4 cm^2

Additional information:
No additional information

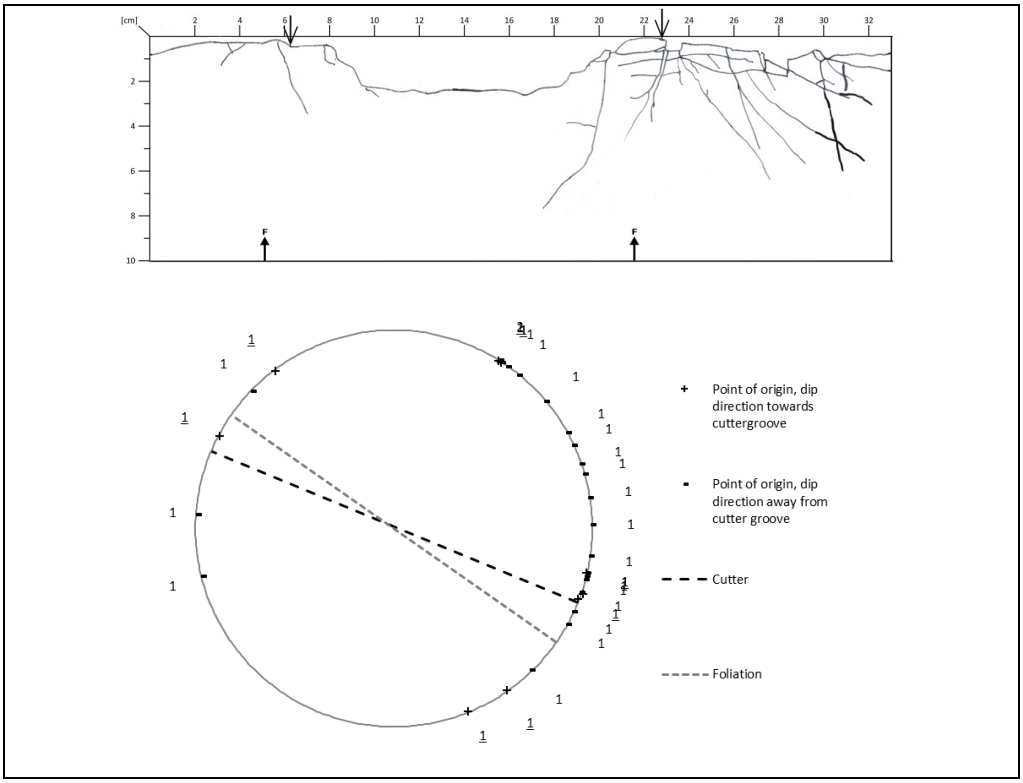

Figure D1.41: Core sample R_5437_4-4_24.

D1.4 Chainage 5458

Date:	22.07.2015
Chainage	5458.0
Average RPM:	6.5
Average thrust:	15 500 kN
Average tonn/disc:	28 tonn/disc
Average pressure:	240 bar
Penetration:	9 mm/rev
	26 mm/min
	3.5 m/h
Average torque:	2 200 kNm
Number of cores:	16

Rock type:	Gneiss with garnet and some lime
σ_c:	92 - 124 MPa
SJ:	1.7 (Extremely low)
S_{20}:	48 - 54 (Medium to high)
DRI:	45 (Medium)

Additional information:
All cutters where 19” cutters, with a cutter width of 3/4”.

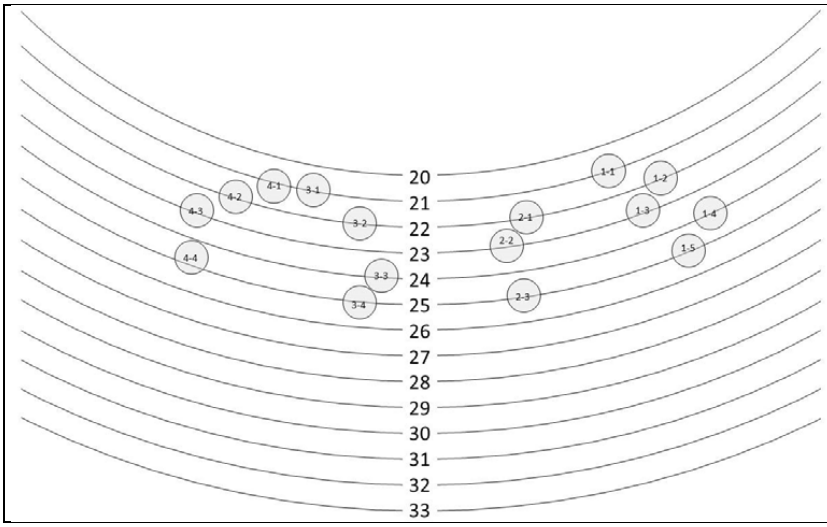

Cutter wear:
20: 12
21: 12
22: 11
23: 28
24: 20
25: 18
26: 20

Figure D1.42: Sampling at R_5458.

R_5458_1-1_21

Circumference:	329 mm
Number of cracks:	25
Number of cracks with dip < 3°:	2

Distance from 0-line to lowest point on surface:	19 mm
Area between 0-line and surface:	25.8 cm^2

Additional information:
No additional information

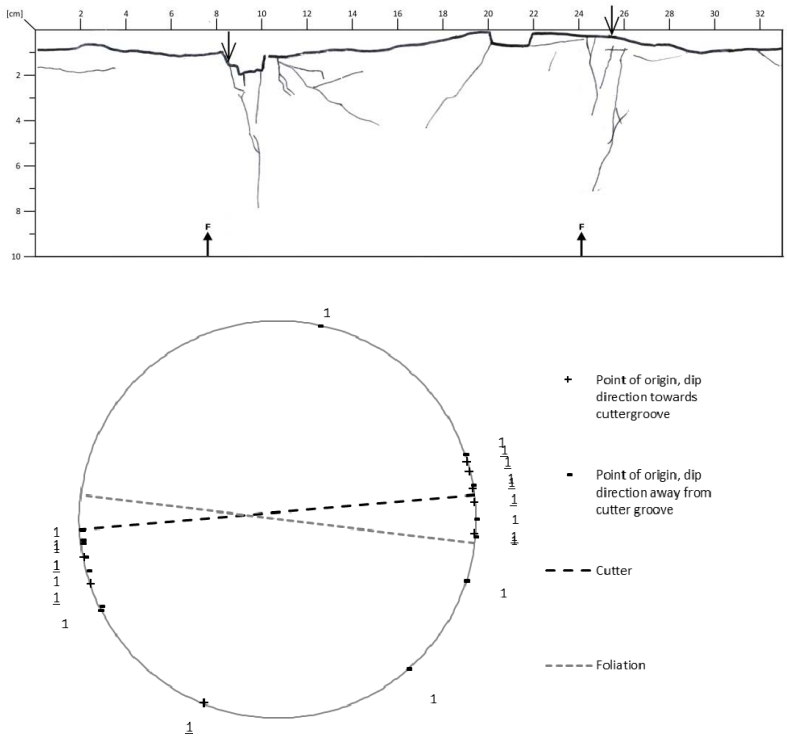

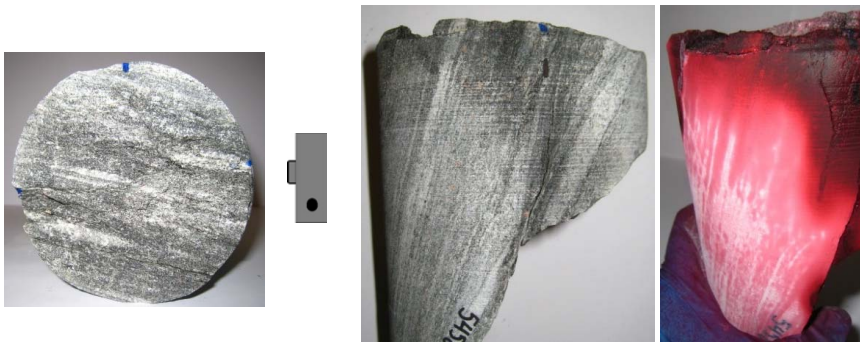

Figure D1.43: Core sample R_5458_1-1_21.

R_5458_1-2_22

Circumference:	330 mm
Number of cracks:	28
Number of cracks with dip < 3°:	5

Distance from 0-line to lowest point on surface:	23 mm
Area between 0-line and surface:	43.8 cm^2

Additional information:
No additional information

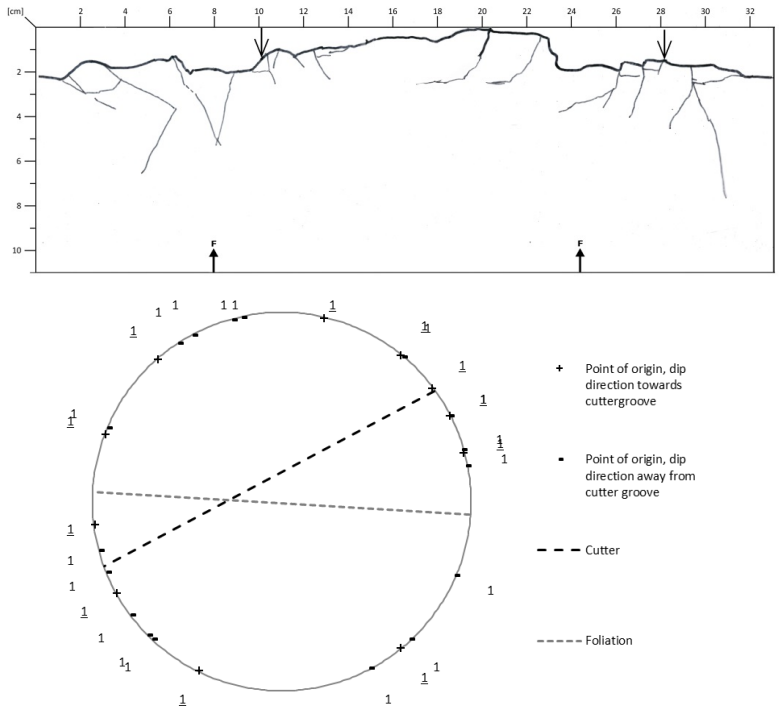

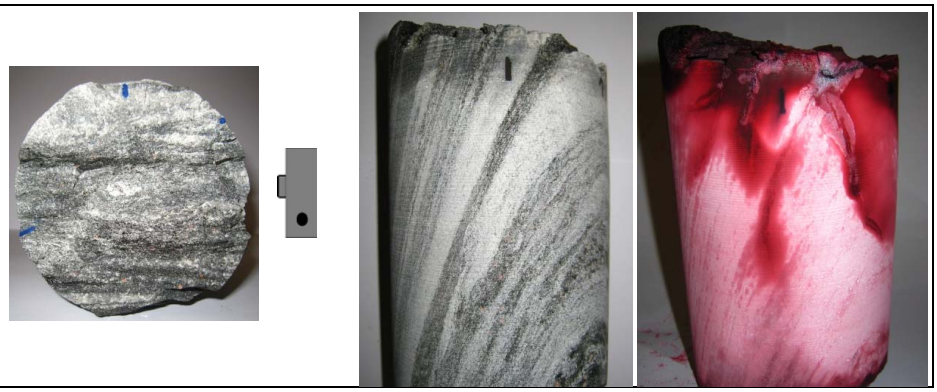

Figure D1.44: Core sample R_5458_1-2_22.

R_5458_1-3_23

Circumference:	330 mm
Number of cracks:	20
Number of cracks with dip < 3°:	1

Distance from 0-line to lowest point on surface:	19 mm
Area between 0-line and surface:	24.7 cm^2

Additional information:
No additional information

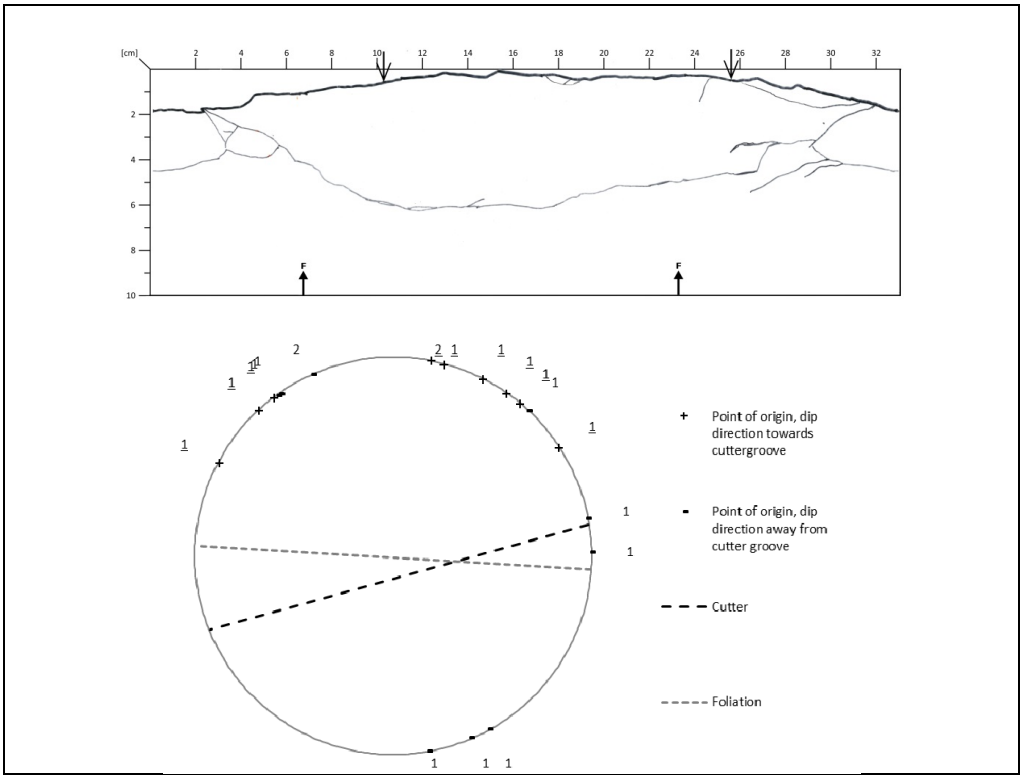

Figure D1.45: Core sample R_5458_1-3_23.

R_5458_1-4_24

Circumference:	330 mm
Number of cracks:	26
Number of cracks with dip < 3°:	0

Distance from 0-line to lowest point on surface:	23 mm
Area between 0-line and surface:	33.9 cm^2

Additional information:
No additional information

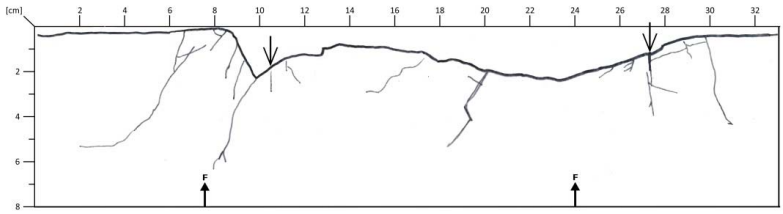

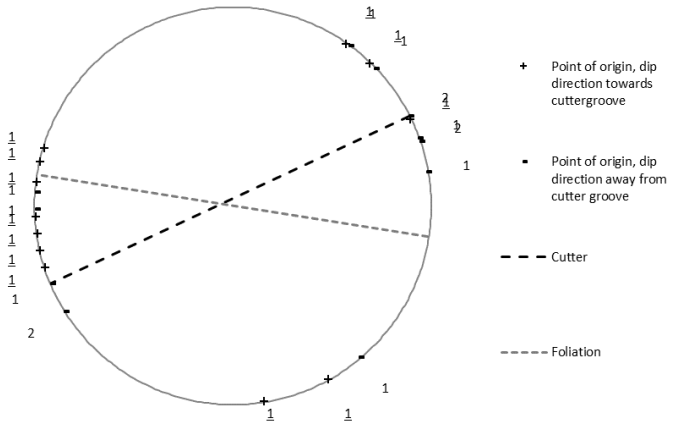

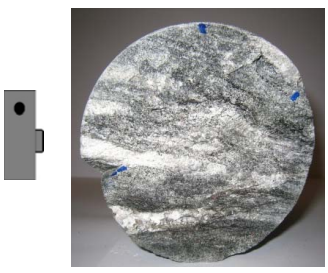

Figure D1.46: Core sample R_5458_1-4_24.

R_5458_1-5_25

Circumference:	332 mm
Number of cracks:	31
Number of cracks with dip < 3°:	5

Distance from 0-line to lowest point on surface:	37 mm
Area between 0-line and surface:	56.8 cm^2

Additional information:
No additional information

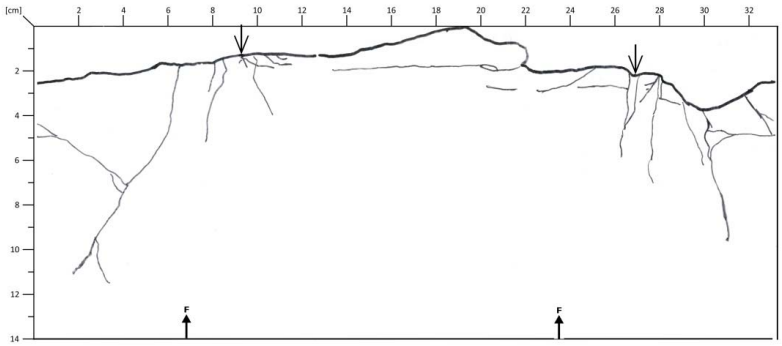

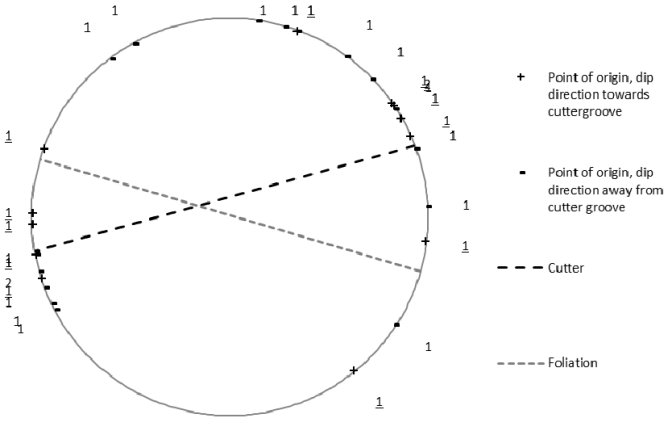

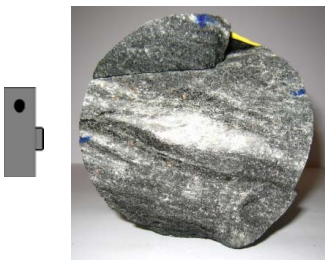

Figure D1.47: Core sample R_5458_1-5_25.

R_5458_2-1_22

Circumference:	330 mm
Number of cracks:	14
Number of cracks with dip < 3°:	2

Distance from 0-line to lowest point on surface:	20 mm
Area between 0-line and surface:	44.7 cm^2

Additional information:
No additional information

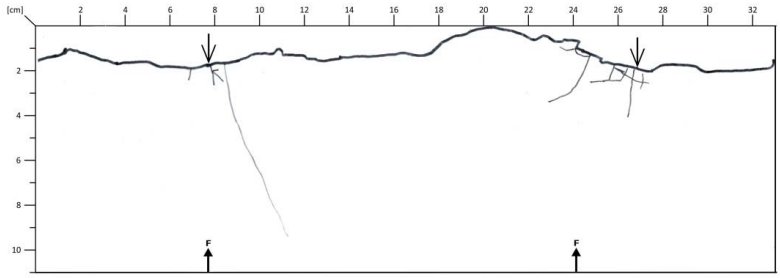

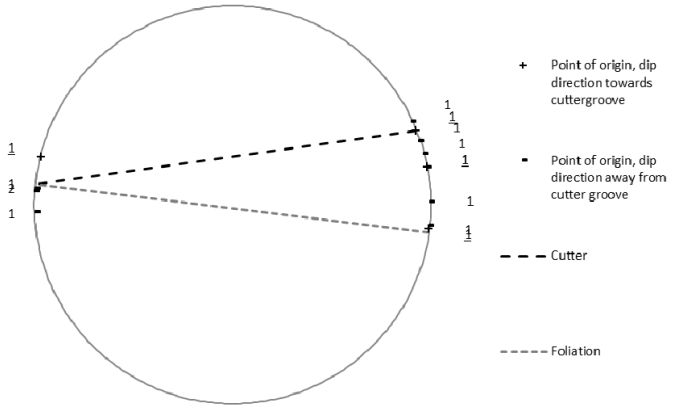

Figure D1.48: Core sample R_5458_2-1_22.

R_5458_2-2_23

Circumference:	331 mm
Number of cracks:	5
Number of cracks with dip < 3°:	1

Distance from 0-line to lowest point on surface:	14 mm
Area between 0-line and surface:	25.5 cm^2

Additional information:
No additional information

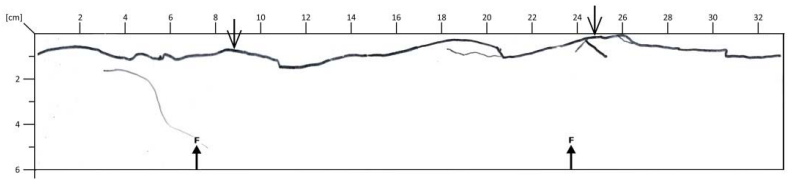

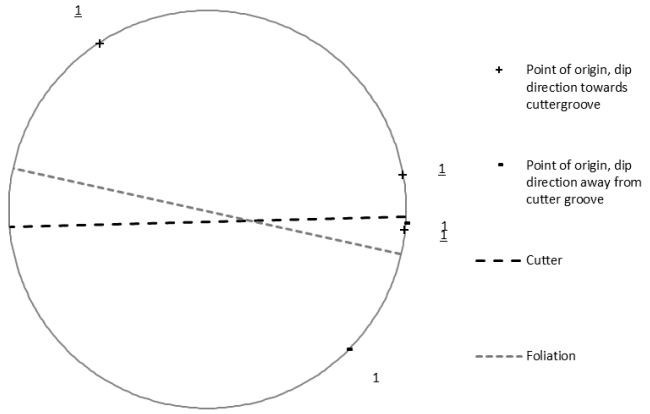

Figure D1.49: Core sample R_5458_2-2_23.

R_5458_2-3_25

Circumference:	329 mm
Number of cracks:	14
Number of cracks with dip < 3°:	2

Distance from 0-line to lowest point on surface:	20 mm
Area between 0-line and surface:	33.1 cm^2

Additional information:
No additional information

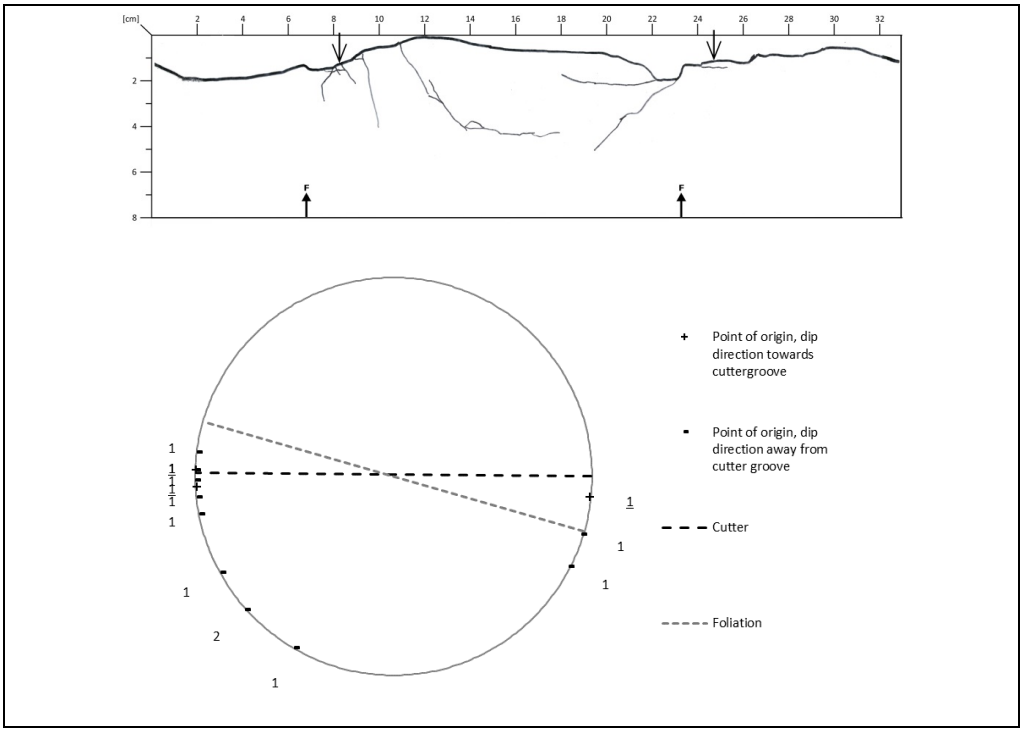

Figure D1.50: Core sample R_5458_2-3_25.

R_5458_3-1_21

Circumference:	330 mm
Number of cracks:	21
Number of cracks with dip < 3°:	4

Distance from 0-line to lowest point on surface:	26 mm
Area between 0-line and surface:	42.6 cm^2

Additional information:
No additional information

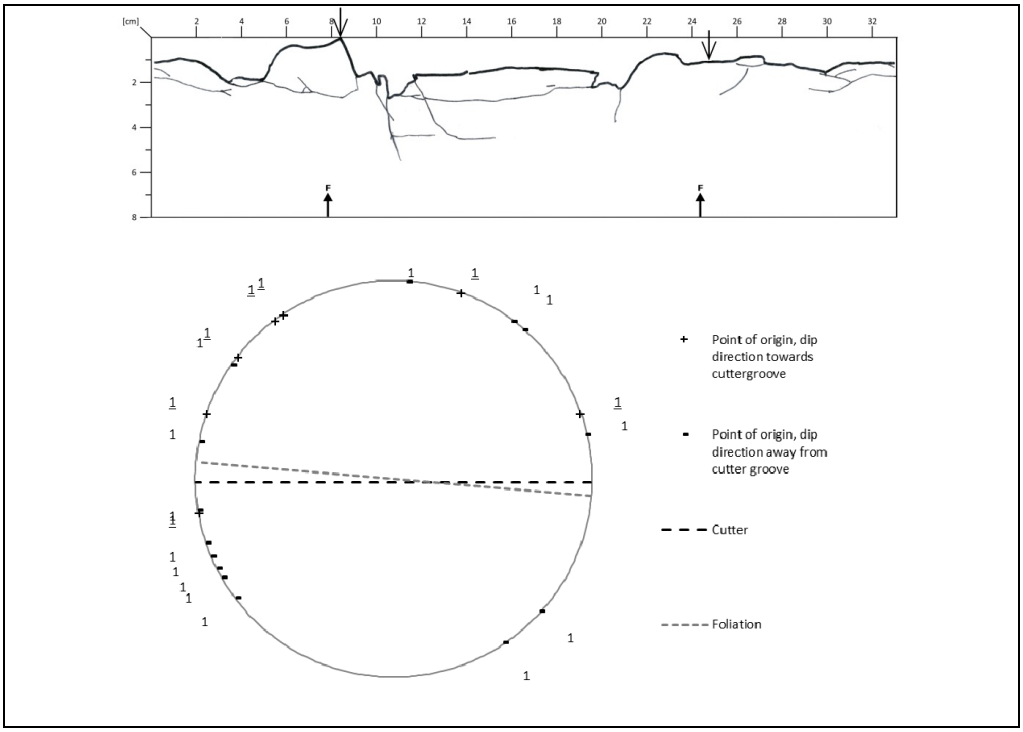

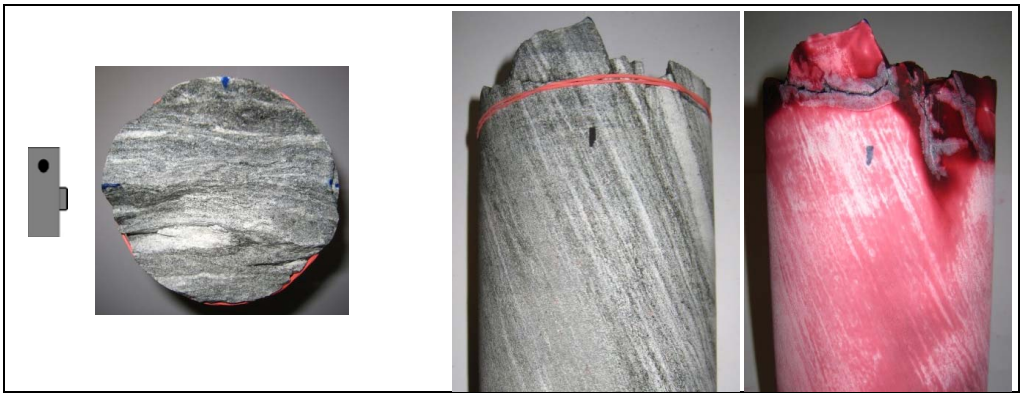

Figure D1.51: Core sample R_5458_3-1_21.

R_5458_3-2_22

Circumference:	330 mm
Number of cracks:	33
Number of cracks with dip < 3°:	4

Distance from 0-line to lowest point on surface:	17 mm
Area between 0-line and surface:	23.2 cm^2

Additional information:
No additional information

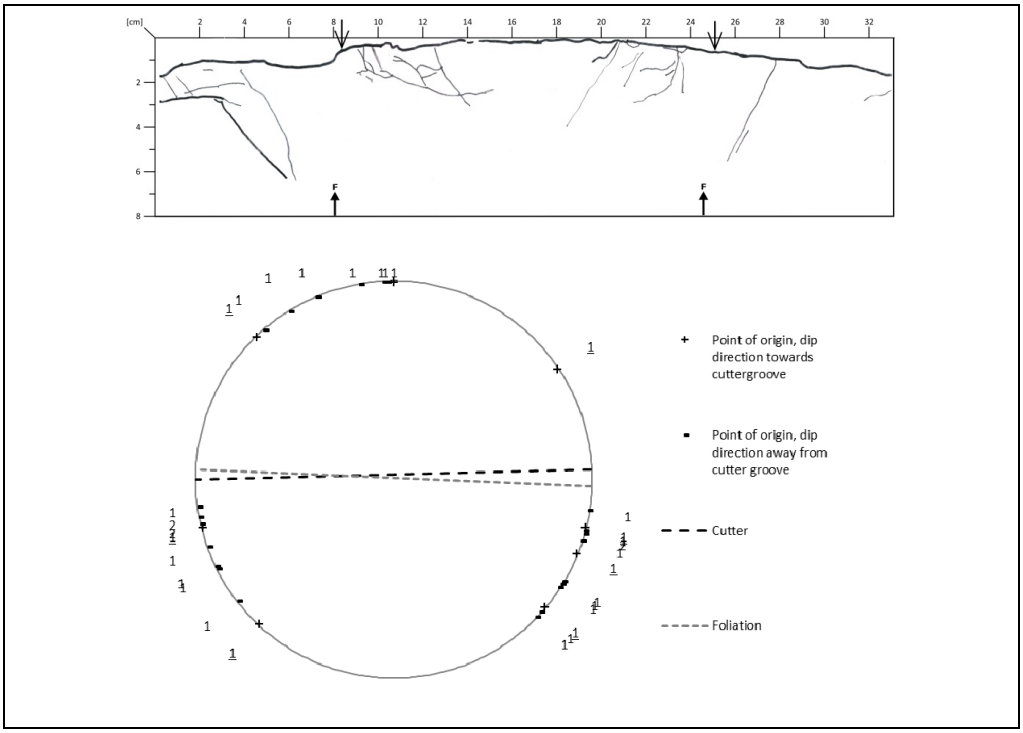

Figure D1.52: Core sample R_5458_3-2_22.

R_5458_3-3_24

Circumference:	332 mm
Number of cracks:	22
Number of cracks with dip < 3°:	1

Distance from 0-line to lowest point on surface:	26 mm
Area between 0-line and surface:	46.6 cm^2

Additional information:
No additional information

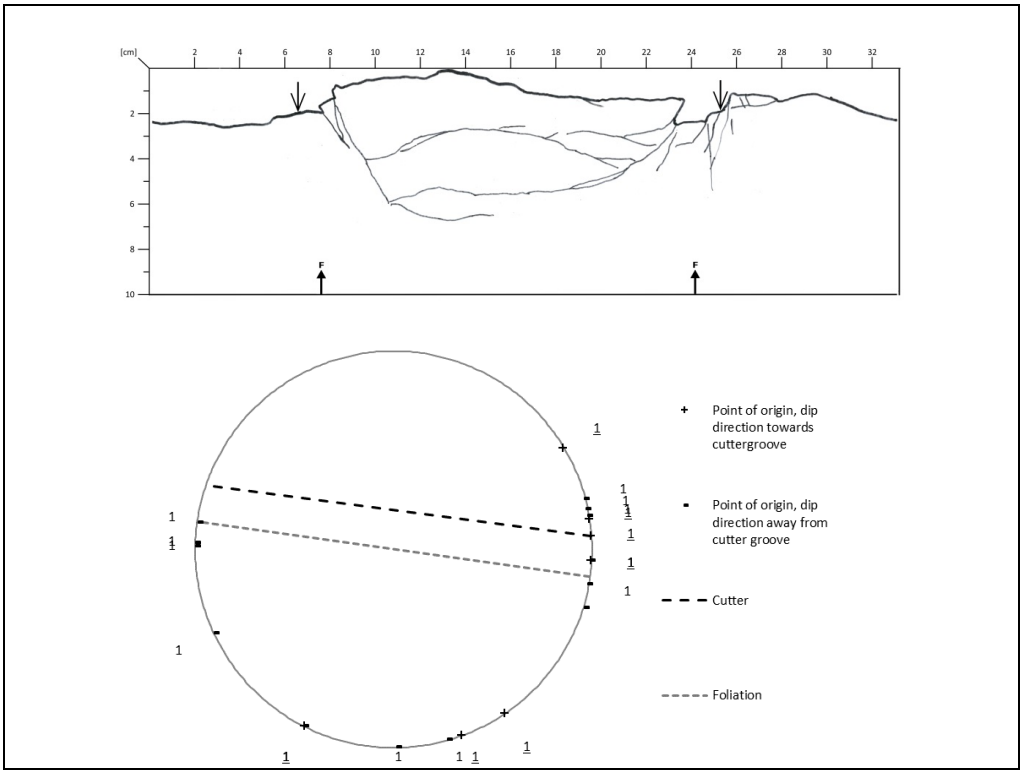

Figure D1.53: Core sample R_5458_3-3_24.

R_5458_3-4_25

Circumference:	330 mm
Number of cracks:	7
Number of cracks with dip < 3°:	0

Distance from 0-line to lowest point on surface:	16 mm
Area between 0-line and surface:	24.8 cm^2

Additional information:
No additional information

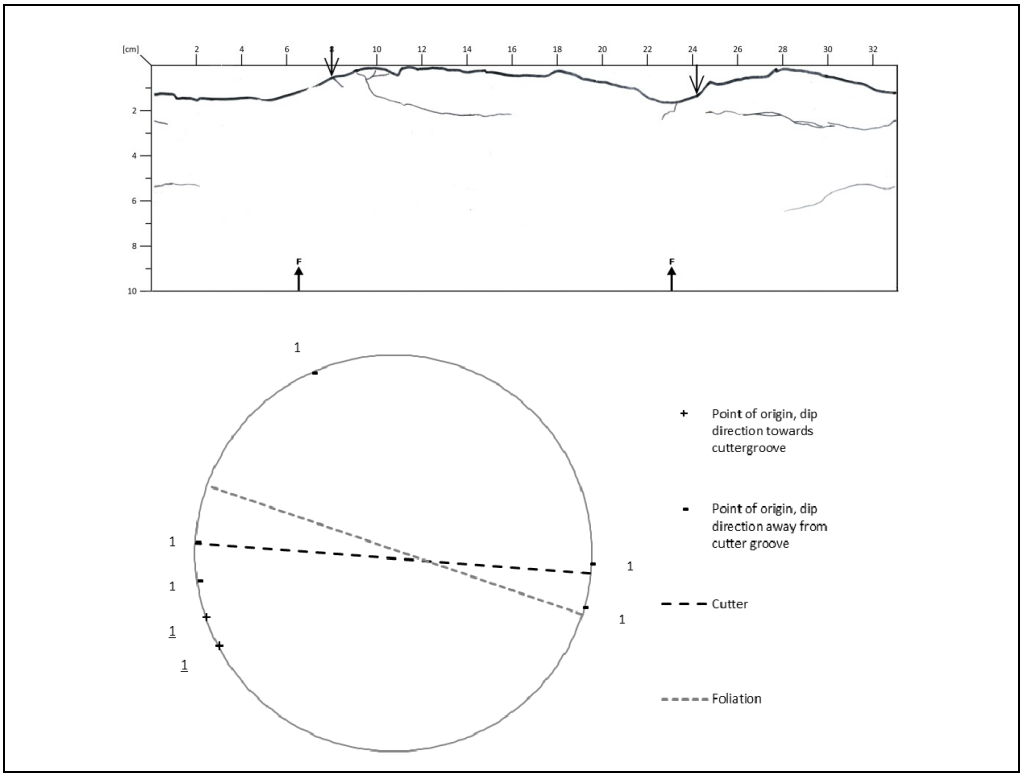

Figure D1.54: Core sample R_5458_3-4_25.

R_5458_4-1_21

Circumference:	332 mm
Number of cracks:	18
Number of cracks with dip < 3°:	0

Distance from 0-line to lowest point on surface:	27 mm
Area between 0-line and surface:	44.9 cm^2

Additional information:
No additional information

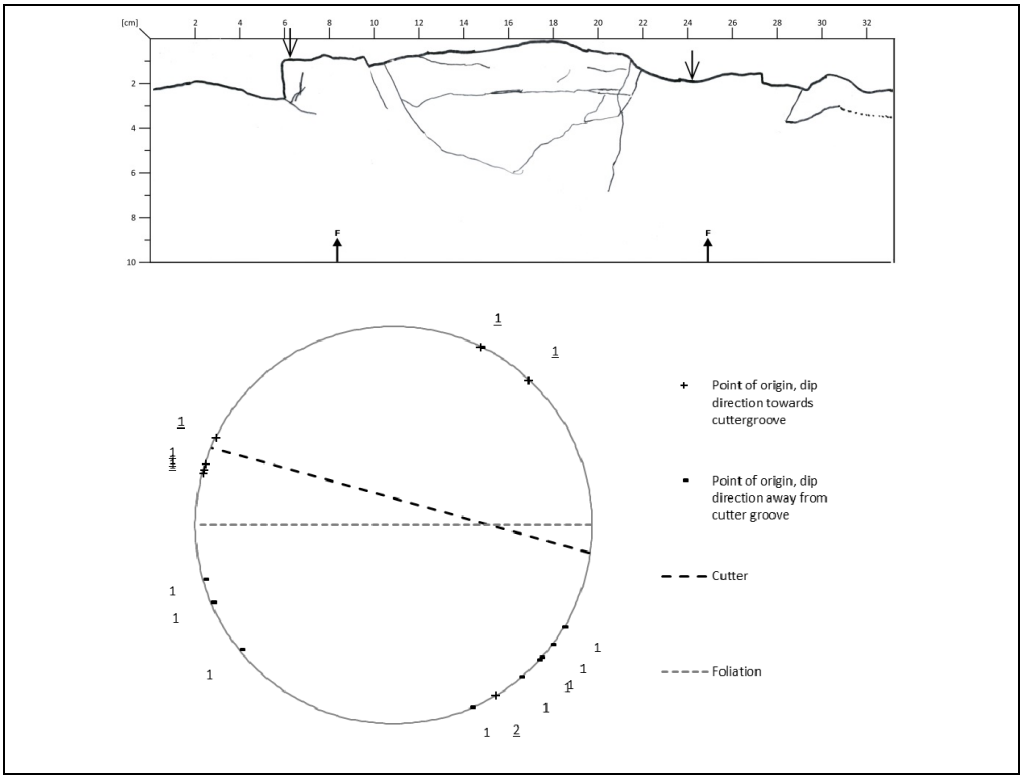

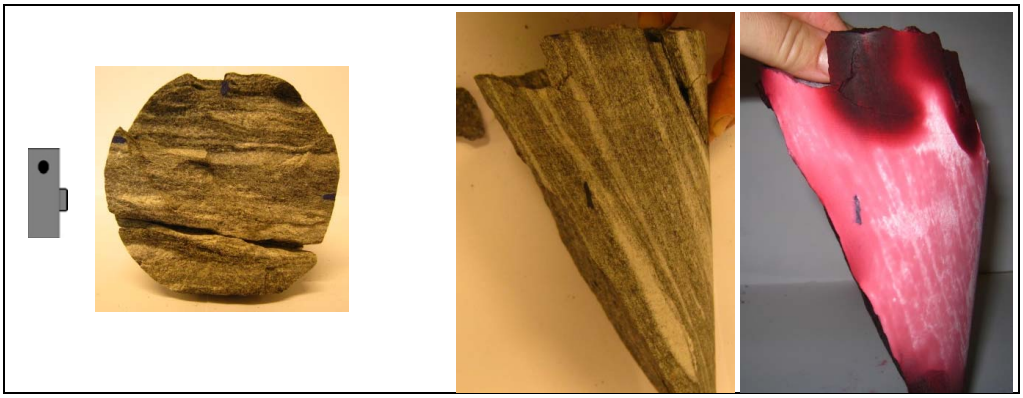

Figure D1.55: Core sample R_5458_4-1_21.

R_5458_4-2_22

Circumference:	331 mm
Number of cracks:	27
Number of cracks with dip < 3°:	4

Distance from 0-line to lowest point on surface:	15 mm
Area between 0-line and surface:	21.3 cm^2

Additional information:
No additional information

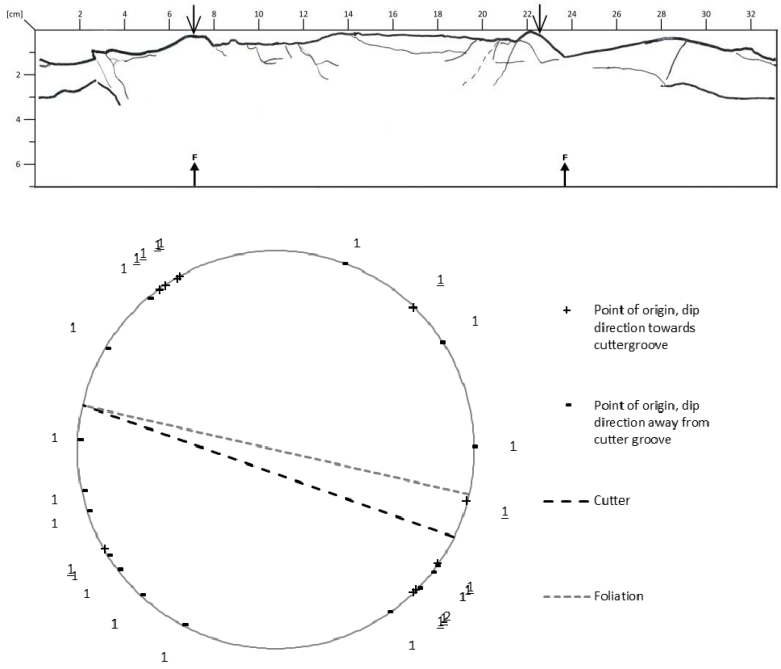

Figure D1.56: Core sample R_5458_4-2_22.

R_5458_4-3_23

Circumference:	332 mm
Number of cracks:	8
Number of cracks with dip < 3°:	4

Distance from 0-line to lowest point on surface:	32 mm
Area between 0-line and surface:	61.7 cm^2

Additional information:
No additional information

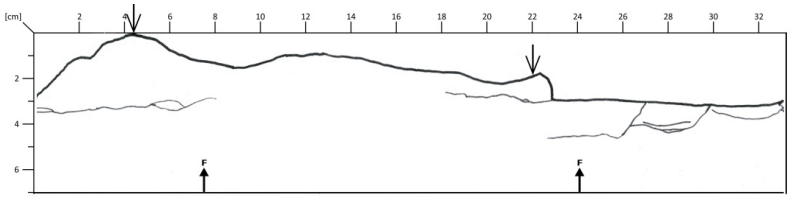

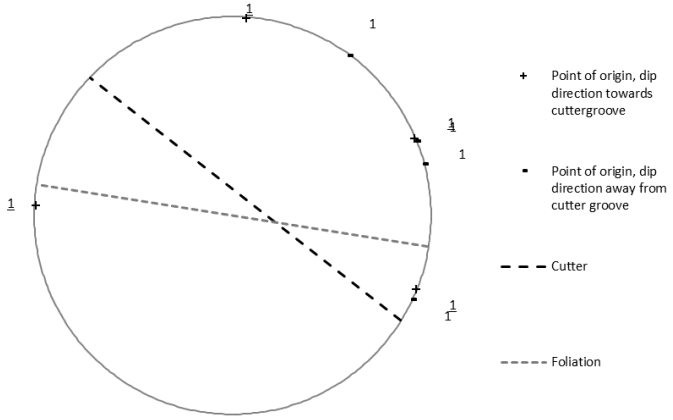

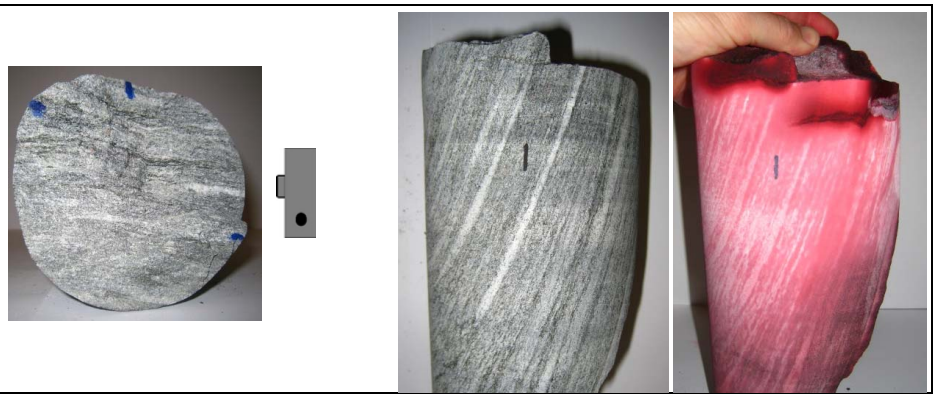

Figure D1.57: Core sample R_5458_4-3_23.

R_5458_4-4_25

Circumference:	331 mm
Number of cracks:	18
Number of cracks with dip < 3°:	0

Distance from 0-line to lowest point on surface:	32mm
Area between 0-line and surface:	39.6 cm^2

Additional information:
No additional information

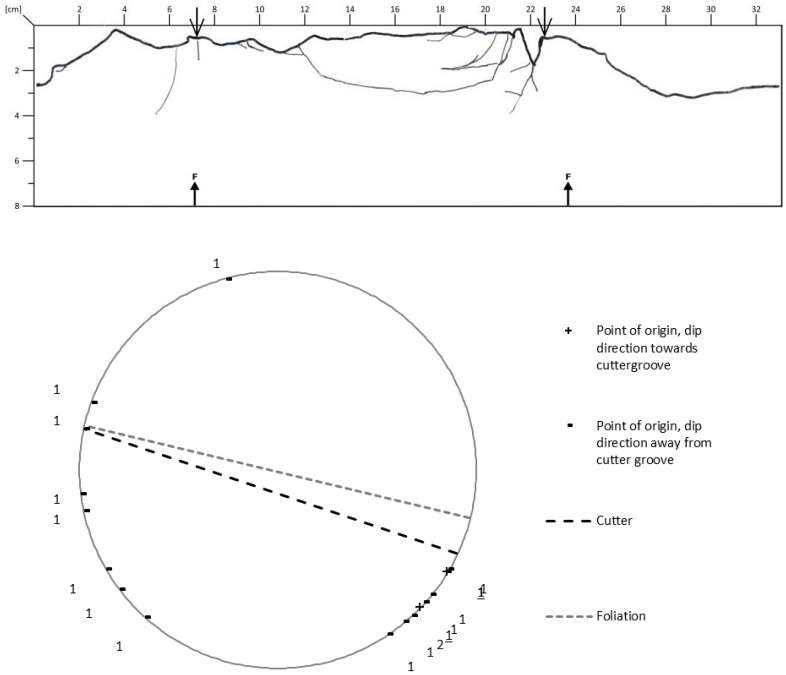

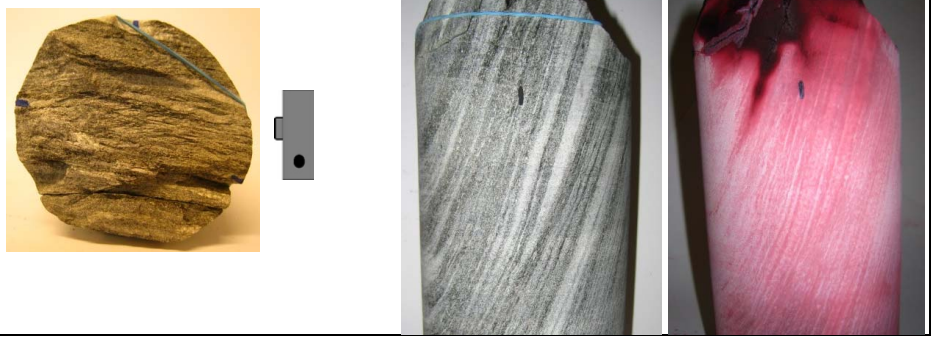

Figure D1.58: Core sample R_5458_4-4_25.

D1.5 Chainage 5478

Date:	23.07.2015
Chainage	5478.0
Average RPM:	5
Average thrust:	16 000 kN
Average tonn/disc:	29 tonn/disc
Average pressure:	250 bar
Penetration:	8.6 mm/rev
	43 mm/min
	2.5 m/h
Average torque:	2 200 kNm
Number of cores:	10+1

Rock type:	Gneiss with garnet and some lime
σ_c:	92 - 124 MPa
SJ:	1.7 (Extremely low)
S_{20}:	48 - 54 (Medium to high)
DRI:	45 (Medium)

Additional information:
All cutters where 19” cutters, with a cutter width of 3/4”. The “ref”-core was used for laboratory test.

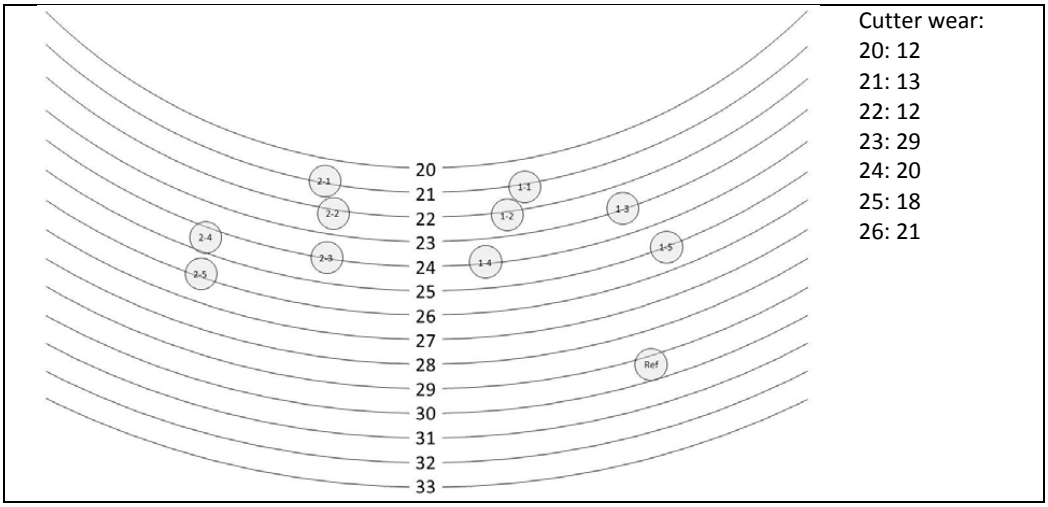

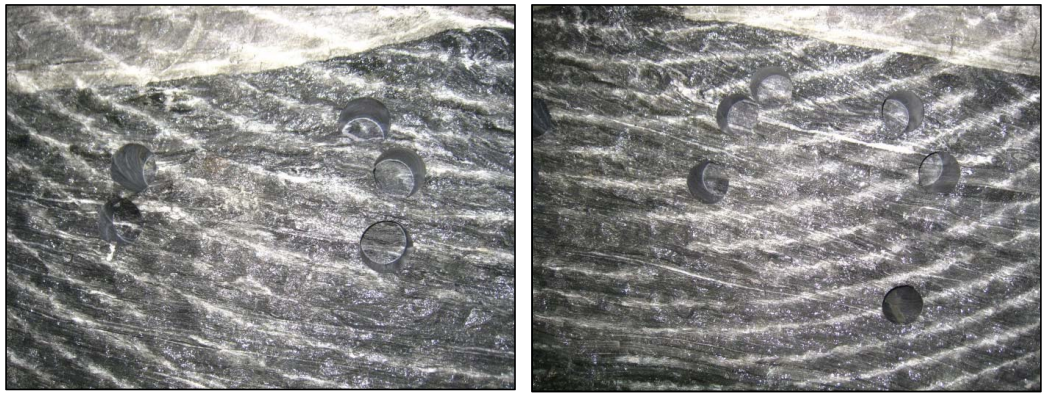

Figure D1.59: Sampling at R_5478.

R_5478_1-1_21

Circumference:	329 mm
Number of cracks:	19
Number of cracks with dip < 3°:	2

Distance from 0-line to lowest point on surface:	45 mm
Area between 0-line and surface:	83.1 cm^2

Additional information:
No additional information

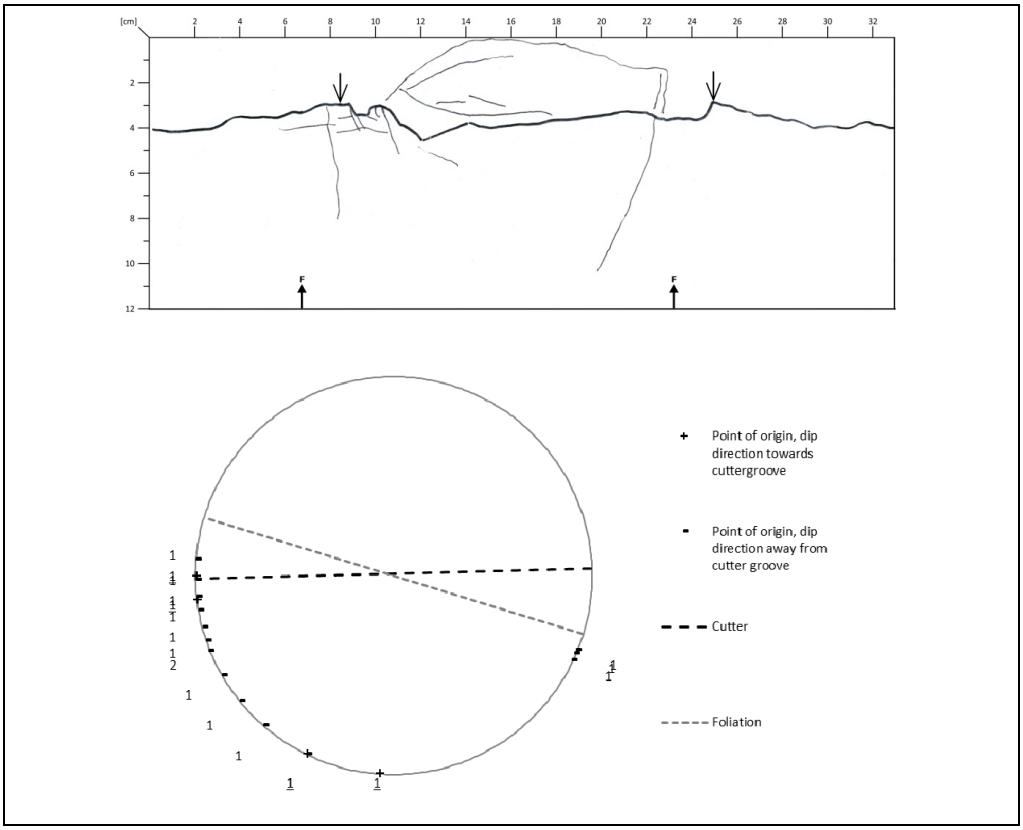

Figure D1.60: Core sample R_5478_1-1_21.

R_5478_1-2_22

Circumference:	331 mm
Number of cracks:	22
Number of cracks with dip < 3°:	1

Distance from 0-line to lowest point on surface:	63 mm
Area between 0-line and surface:	39.3 cm^2

Additional information:
No additional information

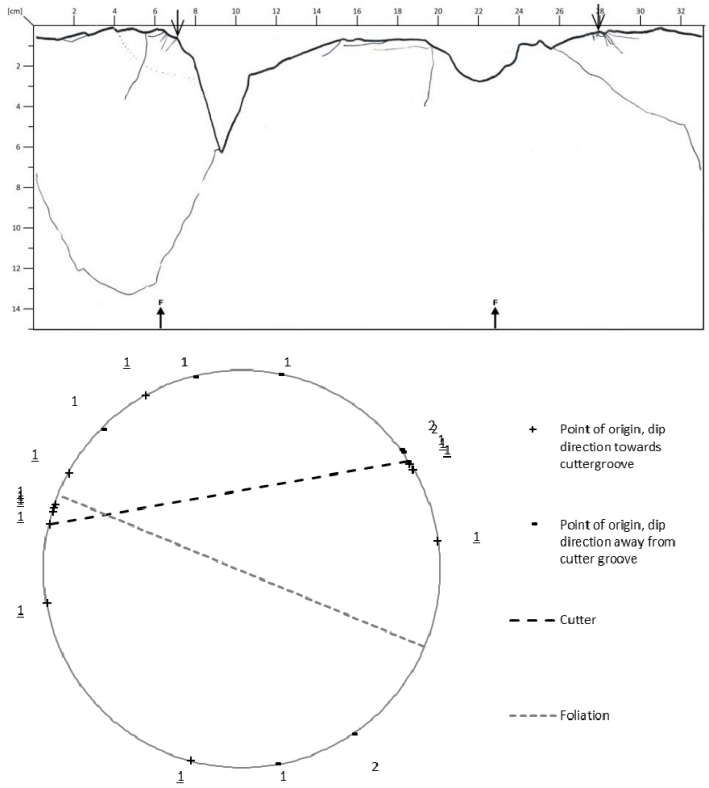

Figure D1.61: Core sample R_5478_1-2_22.

R_5478_1-3_23

Circumference:	330 mm
Number of cracks:	5
Number of cracks with dip < 3°:	0

Distance from 0-line to lowest point on surface:	18 mm
Area between 0-line and surface:	28.6 cm^2

Additional information:
No additional information

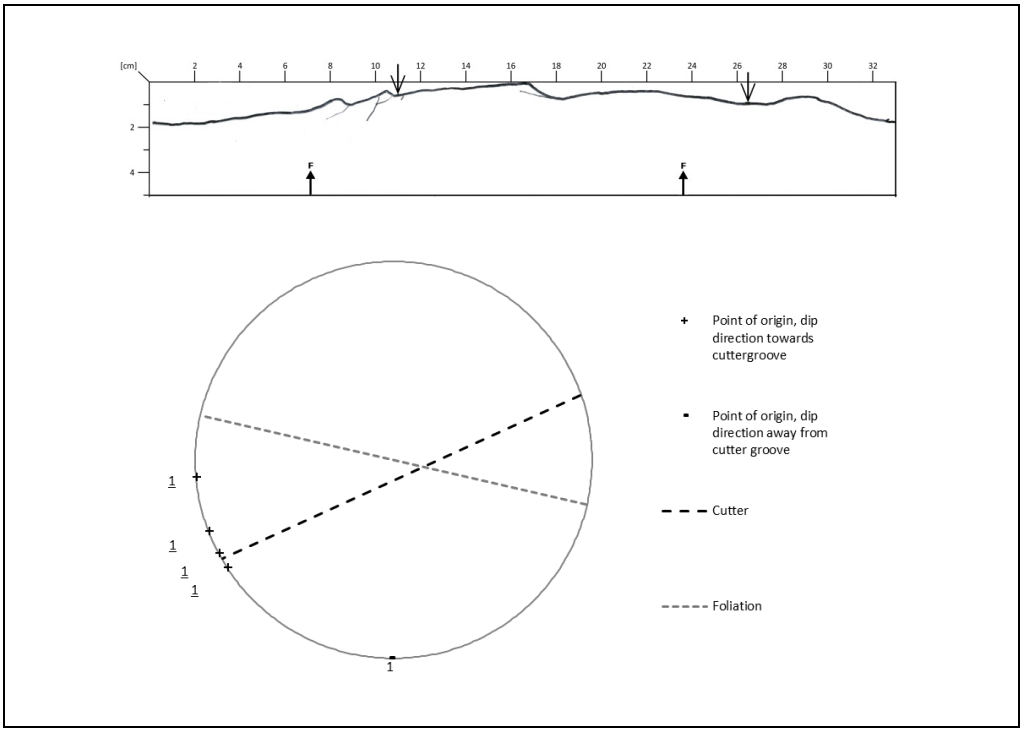

Figure D1.62: Core sample R_5478_1-3_23.

R_5478_1-4_24

Circumference:	330 mm
Number of cracks:	20
Number of cracks with dip < 3°:	4

Distance from 0-line to lowest point on surface:	19 mm
Area between 0-line and surface:	29 cm^2

Additional information:
No additional information

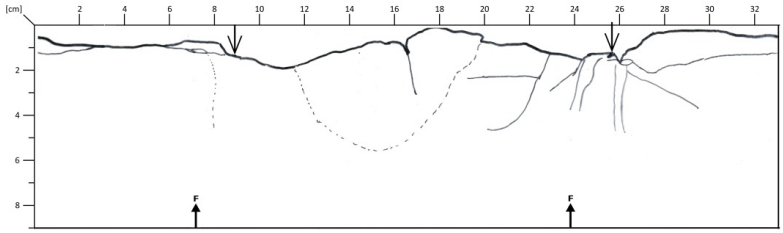

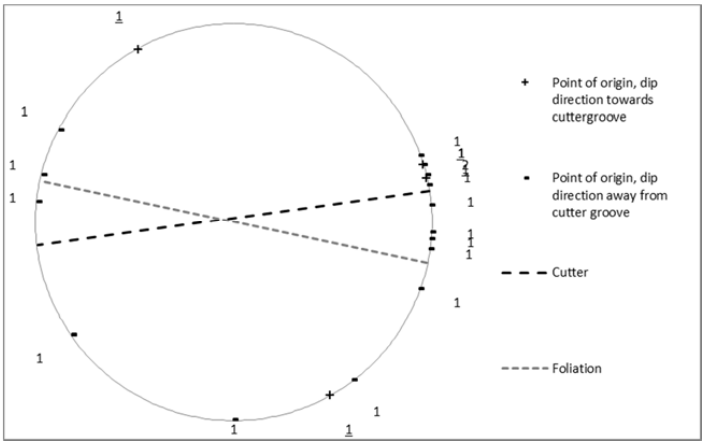

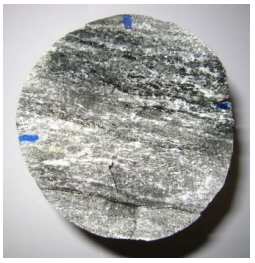

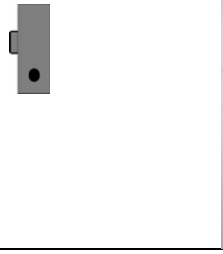

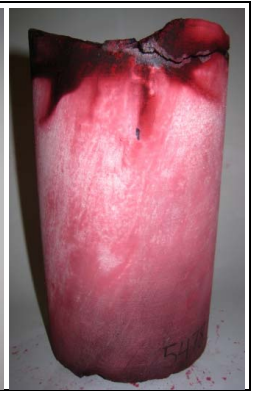

Figure D1.63: Core sample R_5478_1-4_24.

R_5478_1-5_25

Circumference:	329 mm
Number of cracks:	16
Number of cracks with dip < 3°:	5

Distance from 0-line to lowest point on surface:	14 mm
Area between 0-line and surface:	20.7 cm^2

Additional information:
No additional information

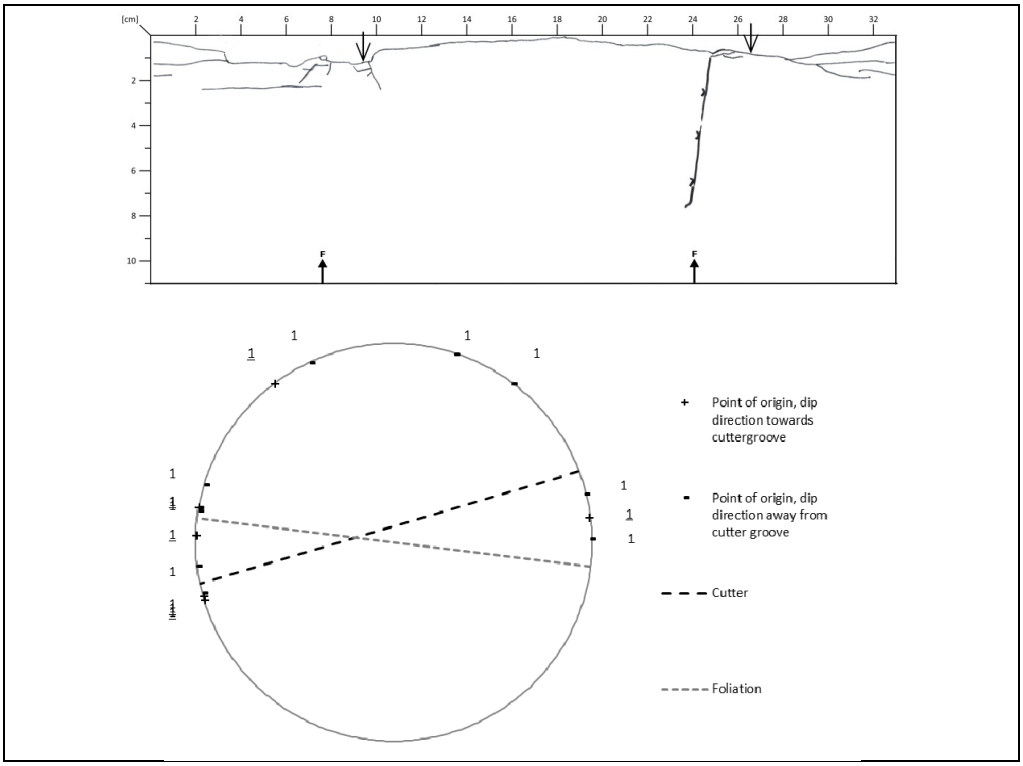

Figure D1.64: Core sample R_5478_1-5_25.

R_5478_2-1_21

Circumference:	330 mm
Number of cracks:	8
Number of cracks with dip < 3°:	1

Distance from 0-line to lowest point on surface:	20 mm
Area between 0-line and surface:	42.9 cm^2

Additional information:
No additional information

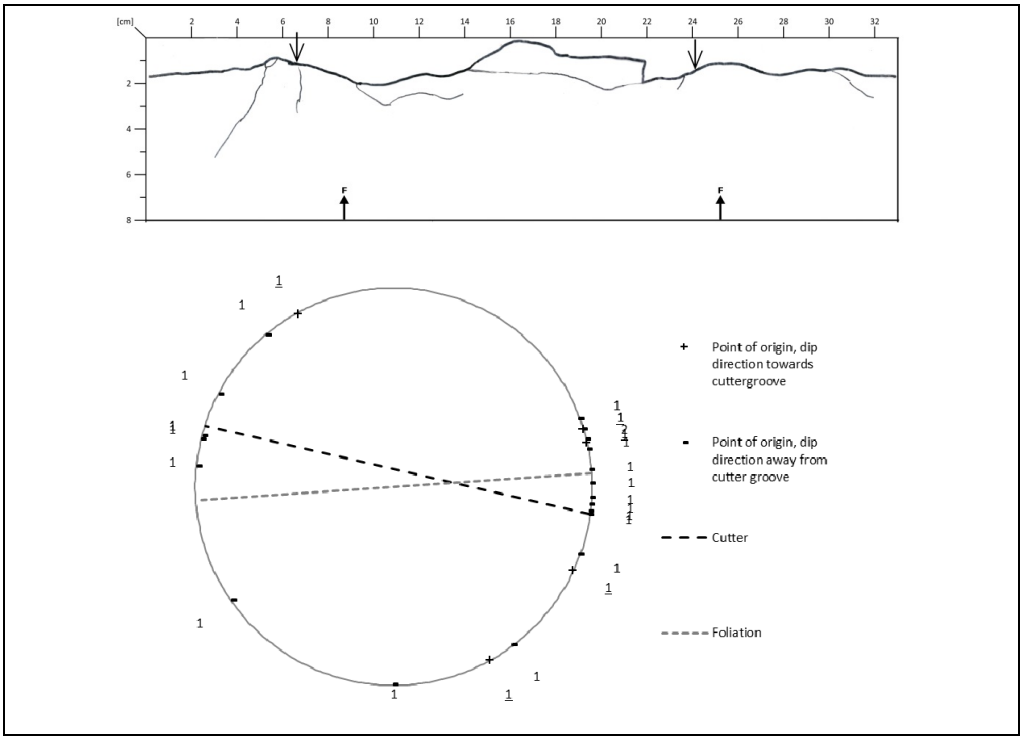

Figure D1.65: Core sample R_5478_2-1_21.

R_5478_2-2_22

Circumference:	330 mm
Number of cracks:	16
Number of cracks with dip < 3°:	3

Distance from 0-line to lowest point on surface:	26mm
Area between 0-line and surface:	38.3 cm^2

Additional information:
No additional information

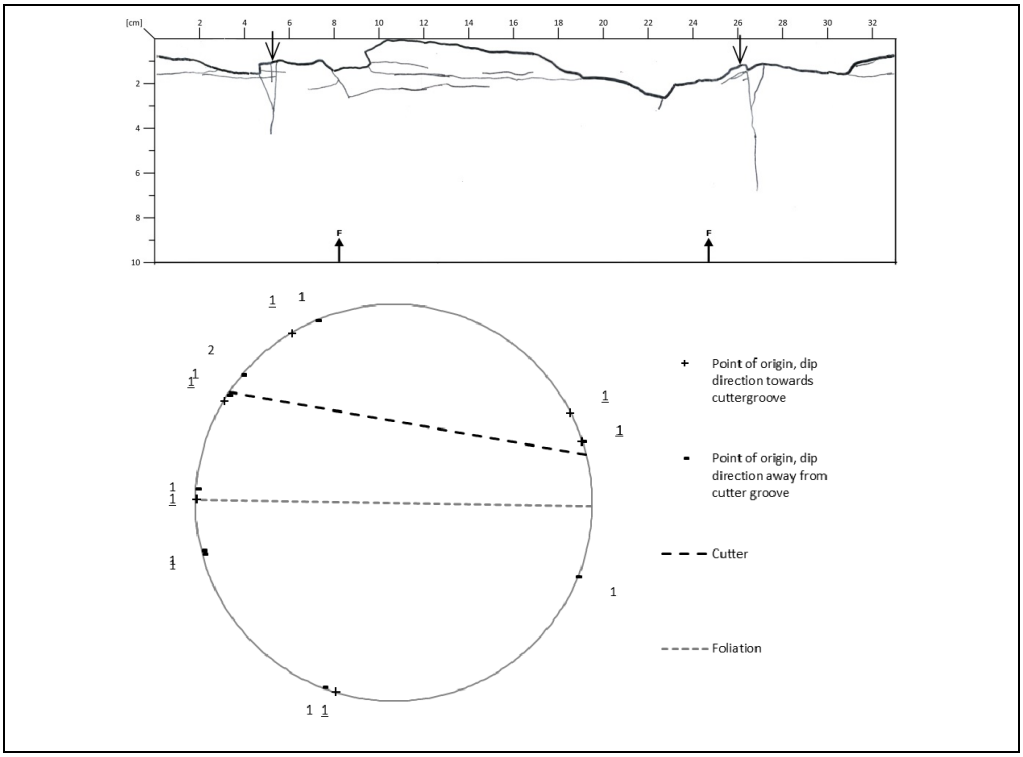

Figure D1.66: Core sample R_5478_2-2_22.

R_5478_2-3_24

Circumference:	330 mm
Number of cracks:	11
Number of cracks with dip < 3°:	0

Distance from 0-line to lowest point on surface:	16 mm
Area between 0-line and surface:	26.1 cm^2

Additional information:
No additional information

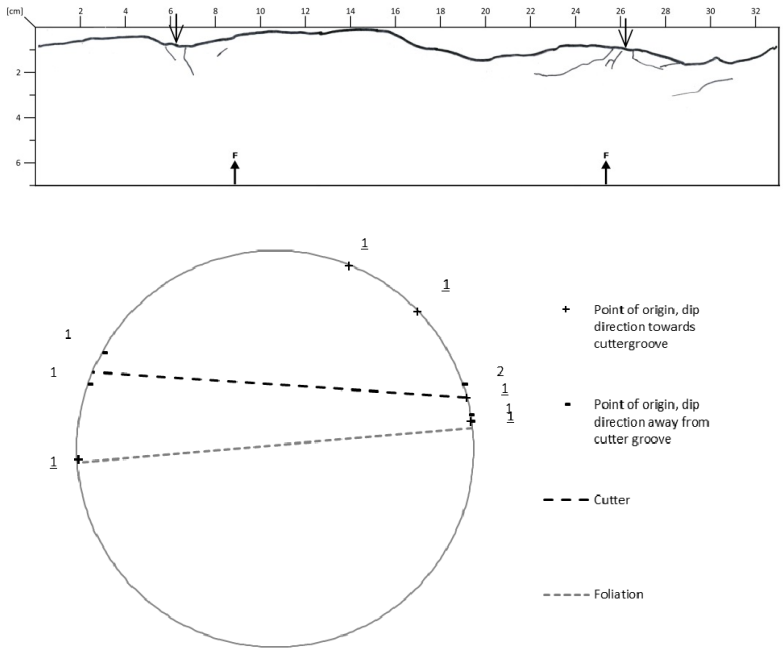

Figure D1.67: Core sample R_5478_2-3_24.

R_5478_2-4_24/25

Circumference:	330 mm
Number of cracks:	27
Number of cracks with dip < 3°:	1

Distance from 0-line to lowest point on surface:	13 mm
Area between 0-line and surface:	19.5 cm^2

Additional information: This core is not included in all evaluations because it is drilled in between two cutter grooves. This is commented when relevant.

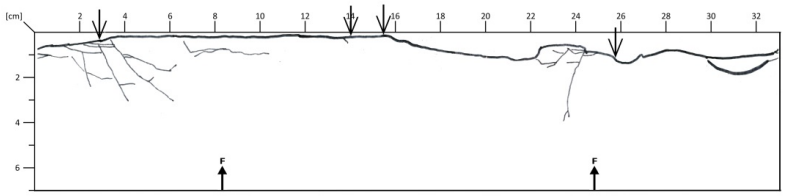

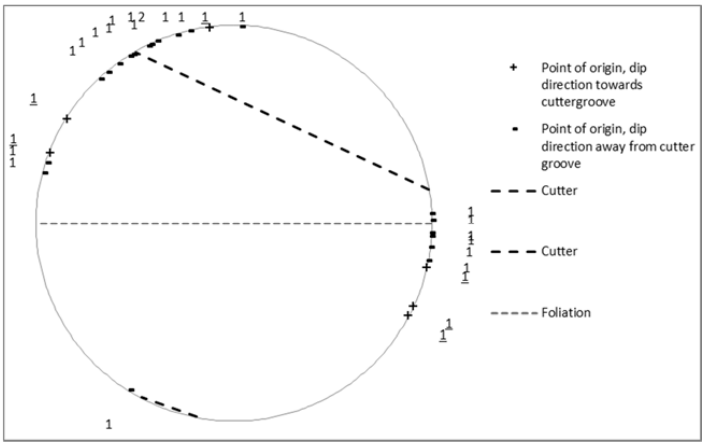

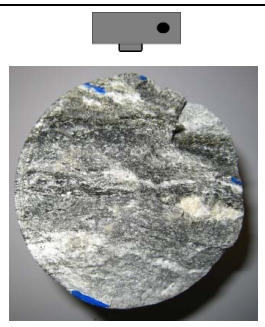

Figure D1.68: Core sample R_5478_2-4_24/25.

R_5478_2-5_26

Circumference:	329 mm
Number of cracks:	12
Number of cracks with dip < 3°:	0

Distance from 0-line to lowest point on surface:	43 mm
Area between 0-line and surface:	47.5 cm^2

Additional information:
No additional information

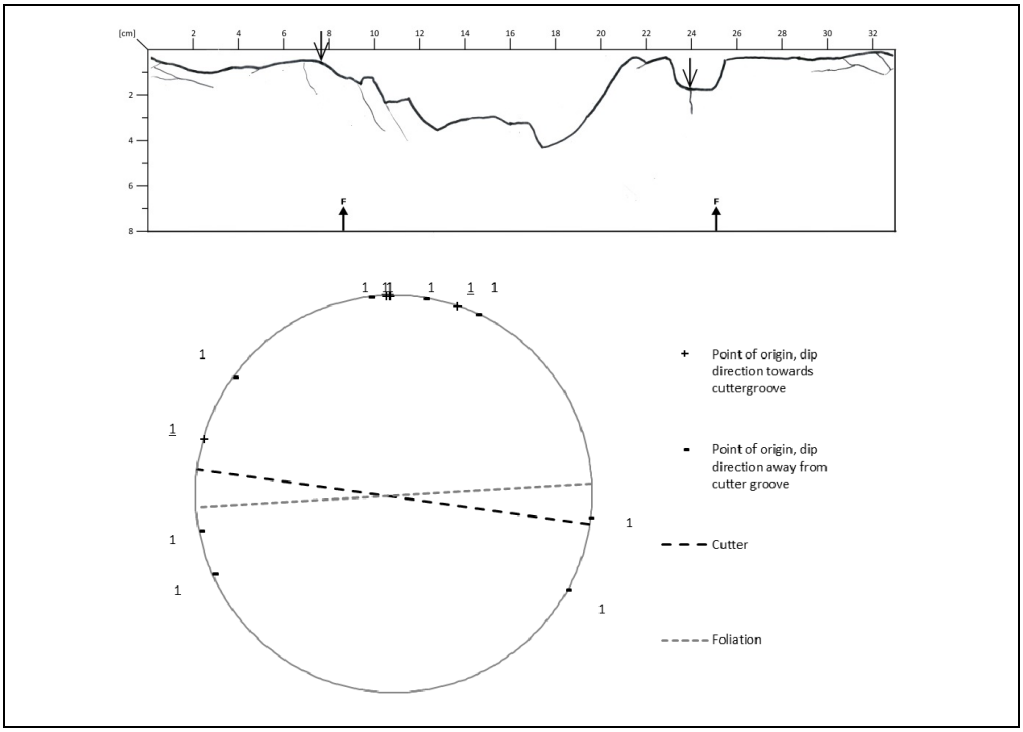

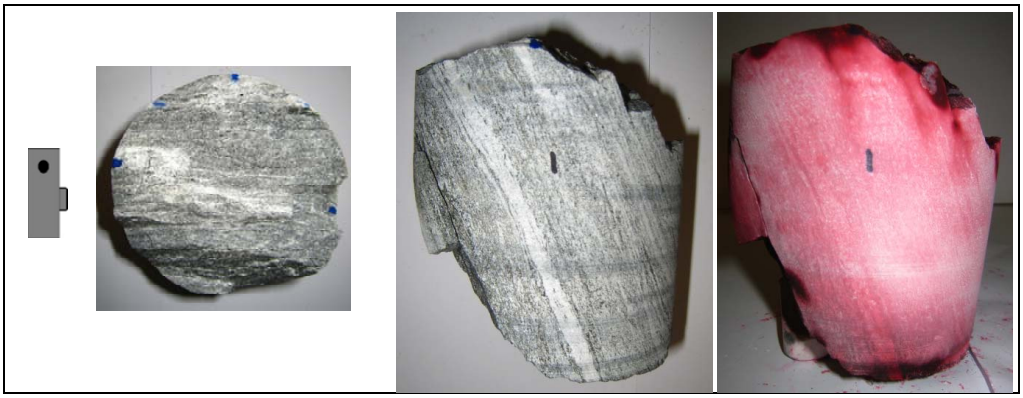

Figure D1.69: Core sample R_5478_2-5_26.

R_5478_ref

Used for laboratory testing and is not included in the analysis.

Appendix E

APPENDIX E
CORE SAMPLES FROM THE LINEAR CUTTER TEST

List of contents

List of figures

E1 Core samples

In total, eight core samples from two different set ups were collected from the rock block used at the linear cutter test performed at KIT. Table E1.1 shows number of core samples from each set up.

Table E1.1: Number of samples from the two set ups used at the linear cutter test.

Cutter spacing	Number of samples	
	Over cutter groove	Between cutter grooves
80 mm	2	2
100 mm	2	2

E1.1 Cutter spacing 80 mm

Date:	Nov./ Dec. 2014	Rock type:	Granite
Average load on cutter:	27,7 t	σ_c:	188 Mpa (very high)
Cutting method:	Sequential	SJ:	5.0 (low)
Penetration depth:	4 mm	S_{20}:	61.9 (very high)
Number of cutting lines	7	DRI:	58 (high))
Number of cores:	4		

Additional information:
19” cutter

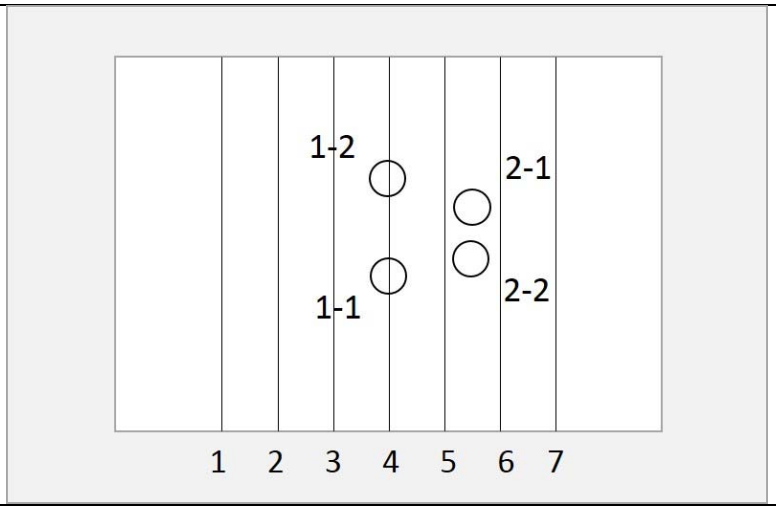

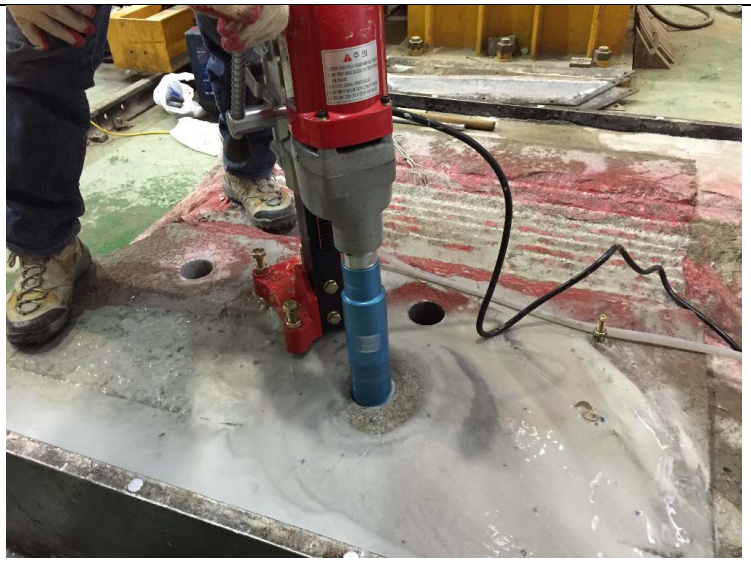

(photo: Yongbem Seo).

Figure E1.1: Sampling after linear cutter test with cutter spacing 80 mm. Note that the sampling was done from the bottom of the specimen

LCT_80_1-1

Circumference:	174 mm
Length of surface:	198 mm
Number of cracks:	12
Number of cracks with dip < 3°:	2

Distance from 0-line to lowest point on surface:	12 mm
Area between 0-line and surface:	771 mm^2

Additional information:
No additional information

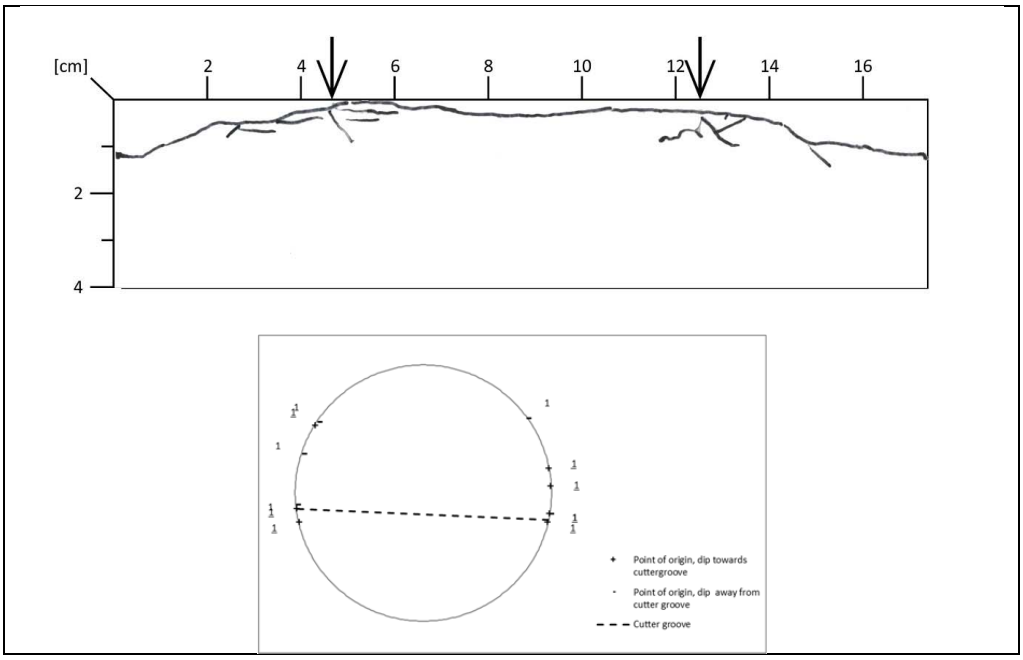

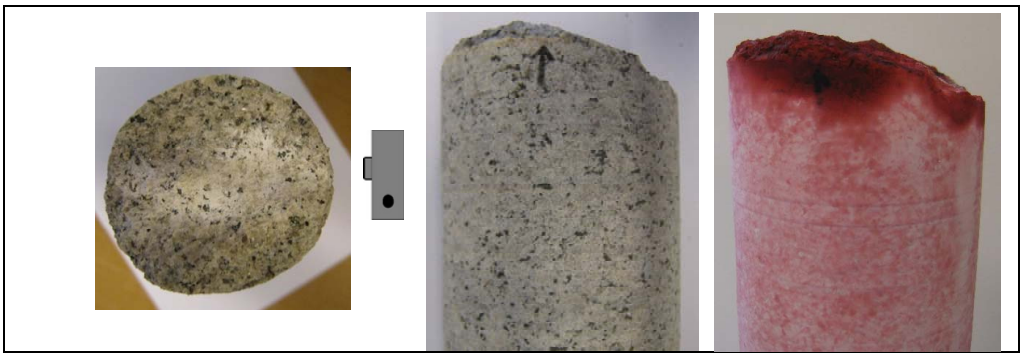

Figure E1.2: Core sample LCT_80_1-1.

LCT_80_1-2

Circumference:	173 mm
Length of surface:	192 mm
Number of cracks:	9
Number of cracks with dip < 3°:	1

Distance from 0-line to lowest point on surface:	6 mm
Area between 0-line and surface:	574 mm^2

Additional information:
No additional information

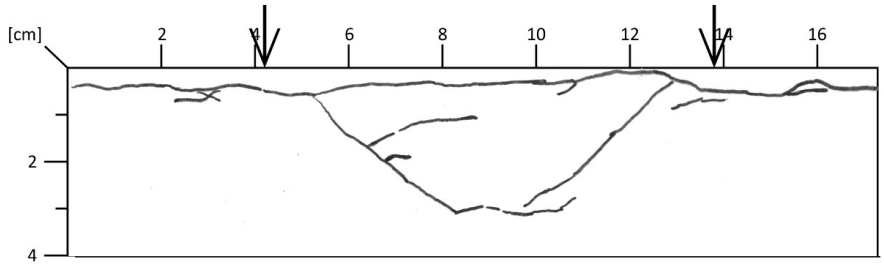

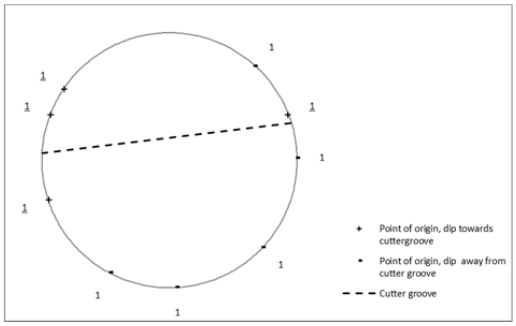

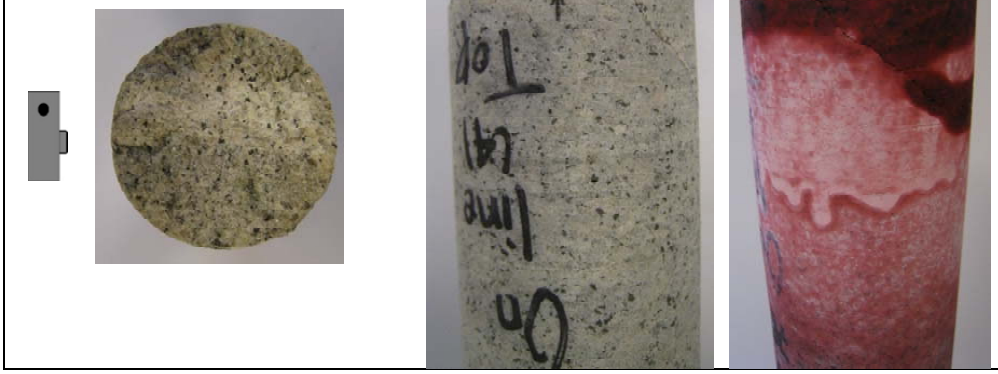

Figure E1.3: Core sample LCT_80_1-2.

LCT_80_2-1

Circumference:	173 mm
Length of surface:	No data
Number of cracks:	3
Number of cracks with dip < 3°:	0

Distance from 0-line to lowest point on surface:	No data
Area between 0-line and surface:	No data

Additional information:
No mapping from the upper 1.5 cm of the core because of an uneven surface. Dotted line is a small damage to the core. Not counted as crack.

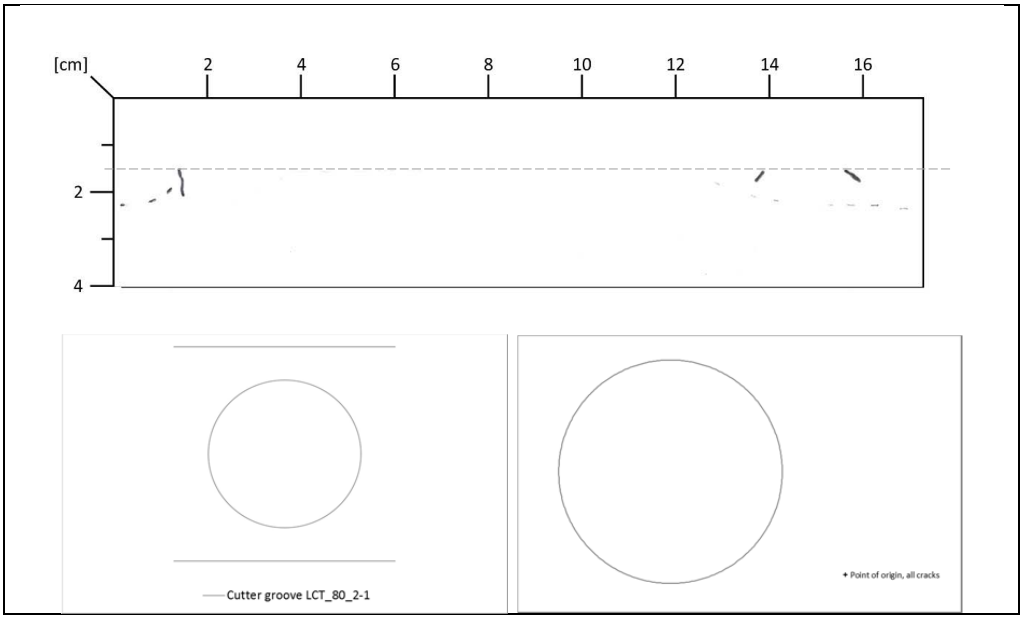

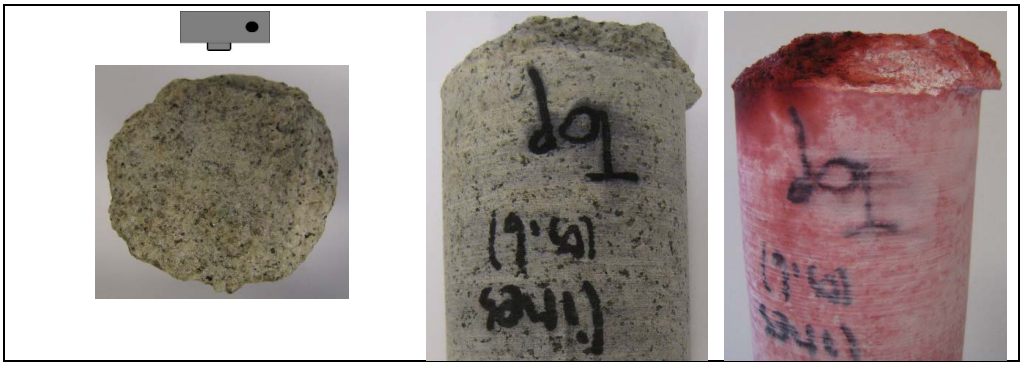

Figure E1.4: Core sample LCT_80_2-1

LCT_80_2-2

Circumference:	176 mm
Length of surface:	209 mm
Number of cracks:	7
Number of cracks with dip < 3°:	1

Distance from 0-line to lowest point on surface:	7 mm
Area between 0-line and surface:	725 mm^2

Additional information:
No additional information

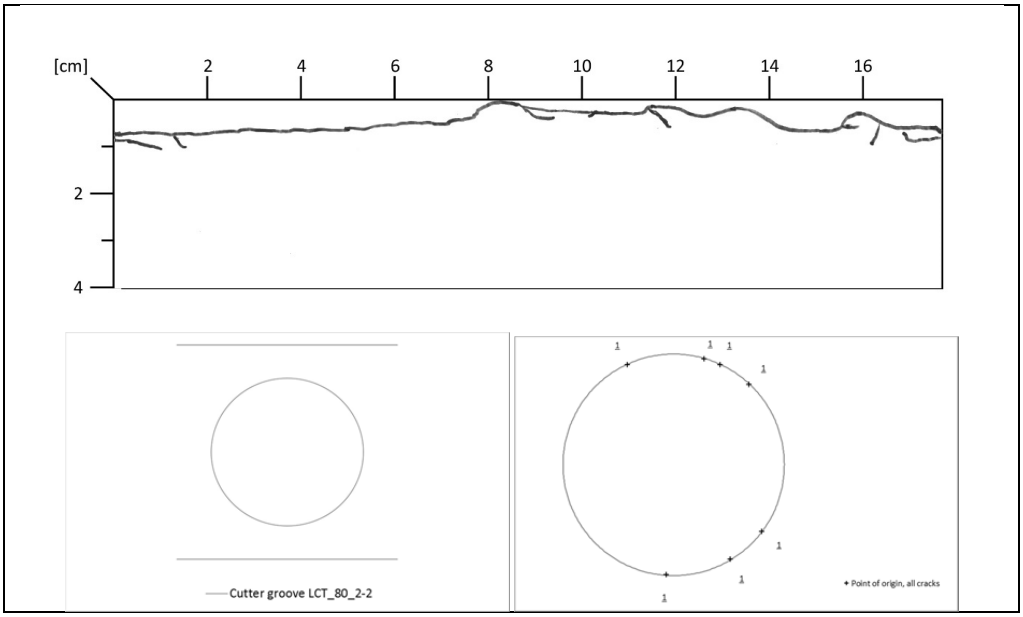

Figure E1.5: Core sample LCT_80_2-2.

E1.2 Cutter spacing 100 mm

Date:	Nov./ Dec. 2014	Rock type:	Granite
Average load on cutter:	22 t	σ_c:	188 Mpa (very high)
Cutting method:	Sequential	SJ:	5.0 (low)
Penetration depth:	4 mm	S_{20}:	61.9 (very high)
Number of cutting lines	7	DRI:	58 (high))
Number of cores:	4		

Additional information:
19” cutter

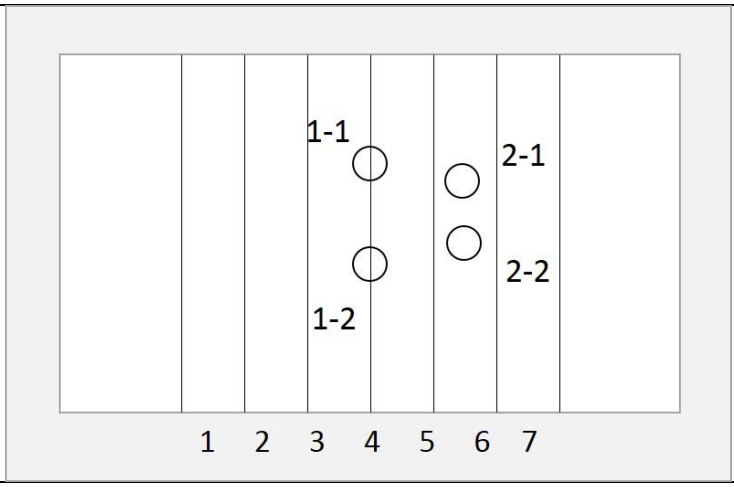

(photo: Yongbem Seo)

Figure E1.6: Sampling after linear cutter test with cutter spacing 100 mm. Note that the sampling was done from the bottom of the specimen.

LCT_100_1-1

Circumference:	175 mm
Length of surface:	307 mm
Number of cracks:	4
Number of cracks with dip < 3°:	0

Distance from 0-line to lowest point on surface:	8 mm
Area between 0-line and surface:	787 mm^2

Additional information:
No additional information

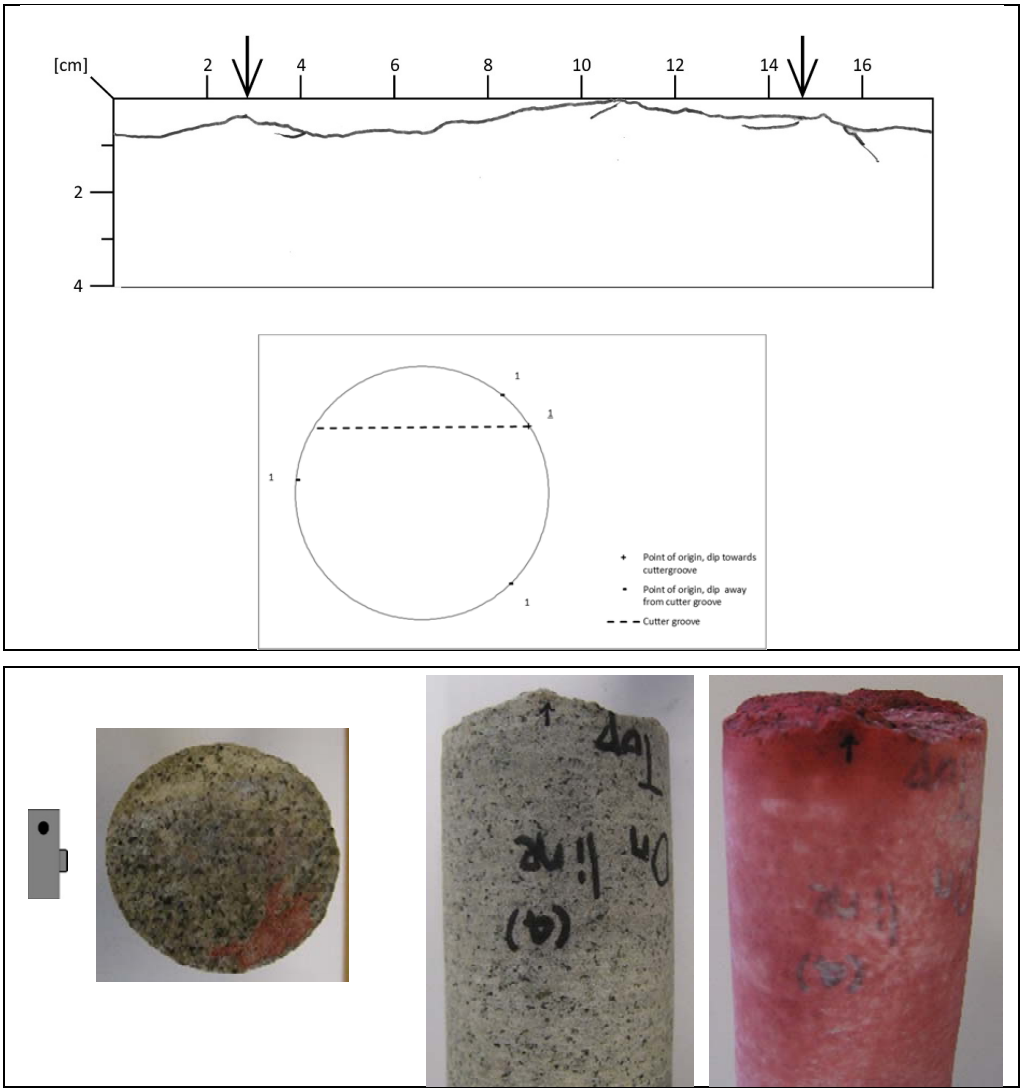

Figure E1.7: Core sample LCT_100_1-1.

LCT_100_1-2

Circumference:	175 mm
Length of surface:	196
Number of cracks:	5
Number of cracks with dip < 3°:	0

Distance from 0-line to lowest point on surface:	8 mm
Area between 0-line and surface:	610 cm^2

Additional information:
No additional information

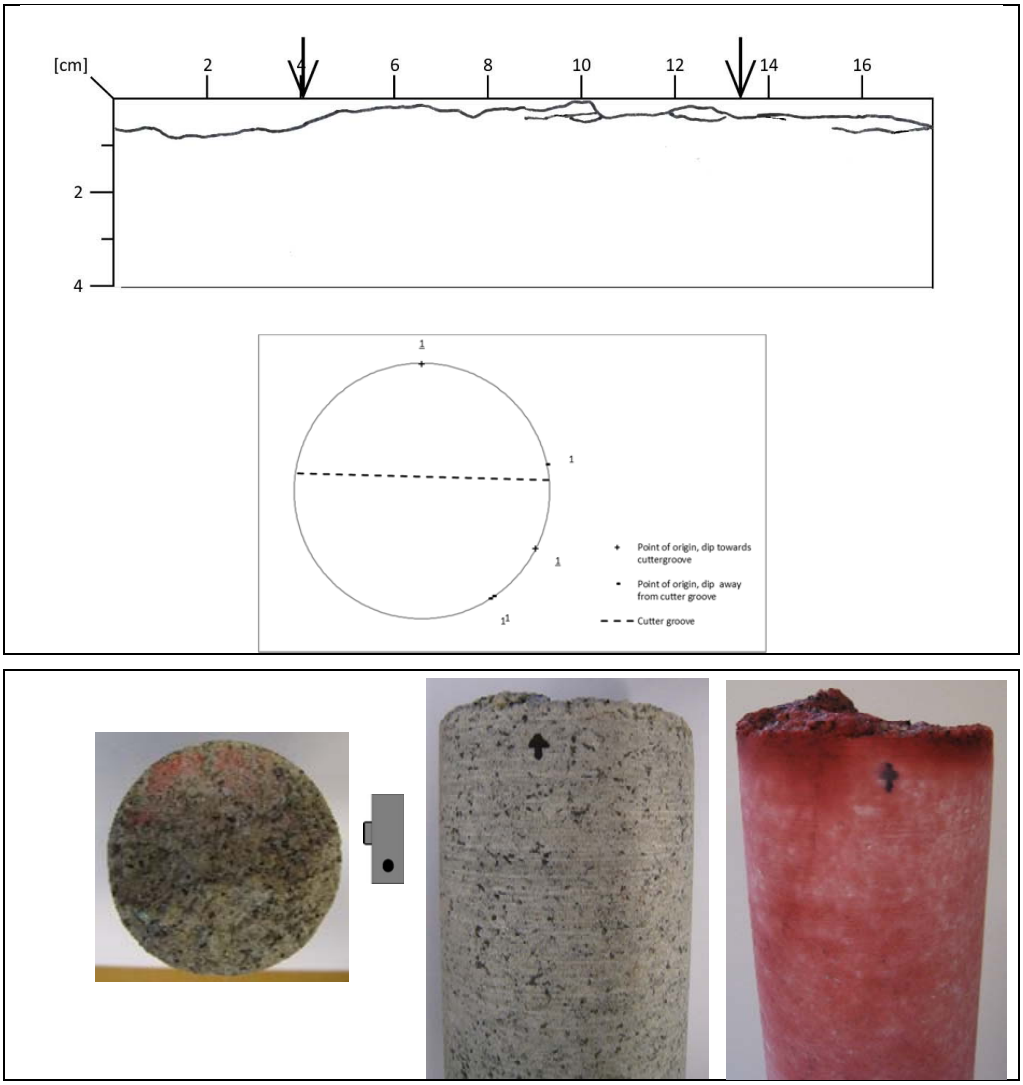

Figure E1.8: Core sample LCT_100_1-2.

LCT_100_2-1

Circumference:	176 mm
Length of surface:	200 mm
Number of cracks:	7
Number of cracks with dip < 3°:	2

Distance from 0-line to lowest point on surface:	9 mm
Area between 0-line and surface:	780 cm^2

Additional information:
No additional information

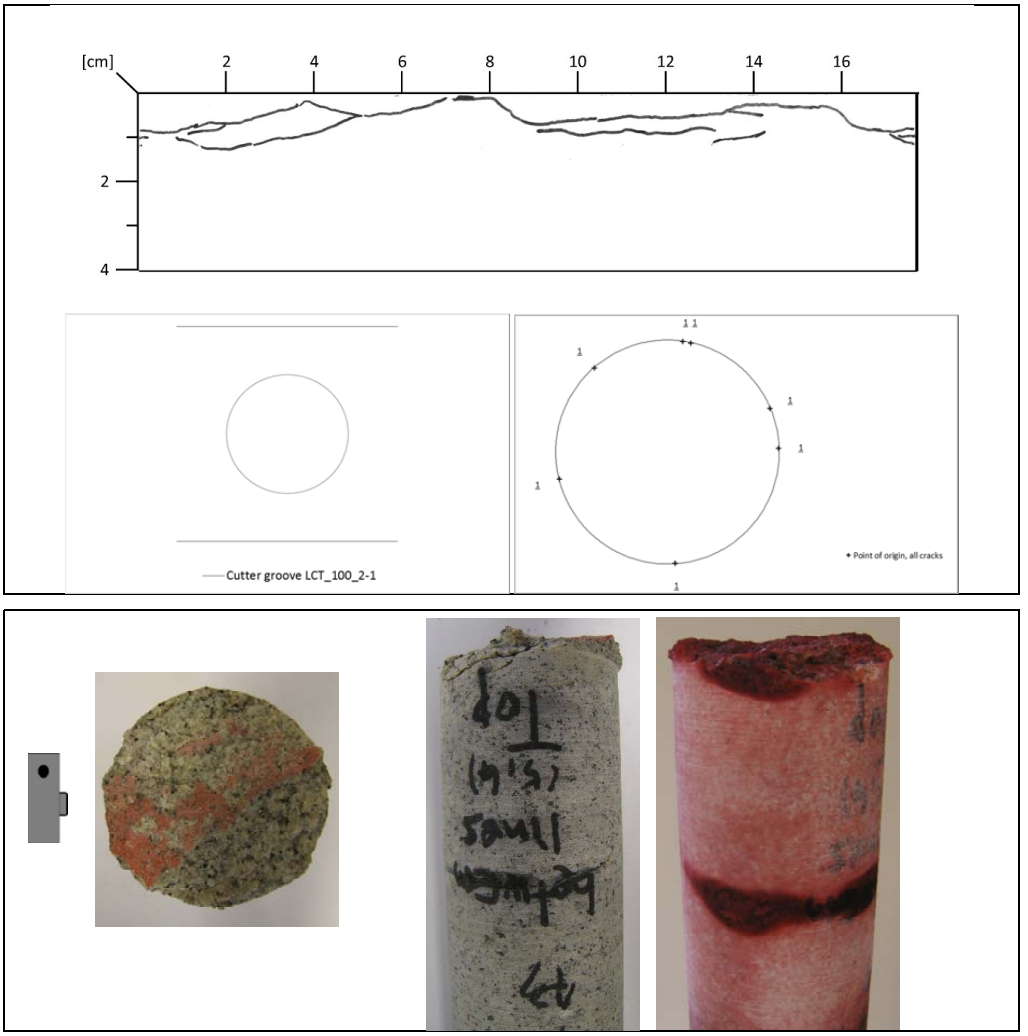

Figure E1.9: Core sample LCT_100_2-1.

LCT_100_2-2

Circumference:	174 mm
Length of surface:	202 mm
Number of cracks:	4
Number of cracks with dip < 3°:	1

Distance from 0-line to lowest point on surface:	13 mm
Area between 0-line and surface:	653 mm^2

Additional information:
No additional information

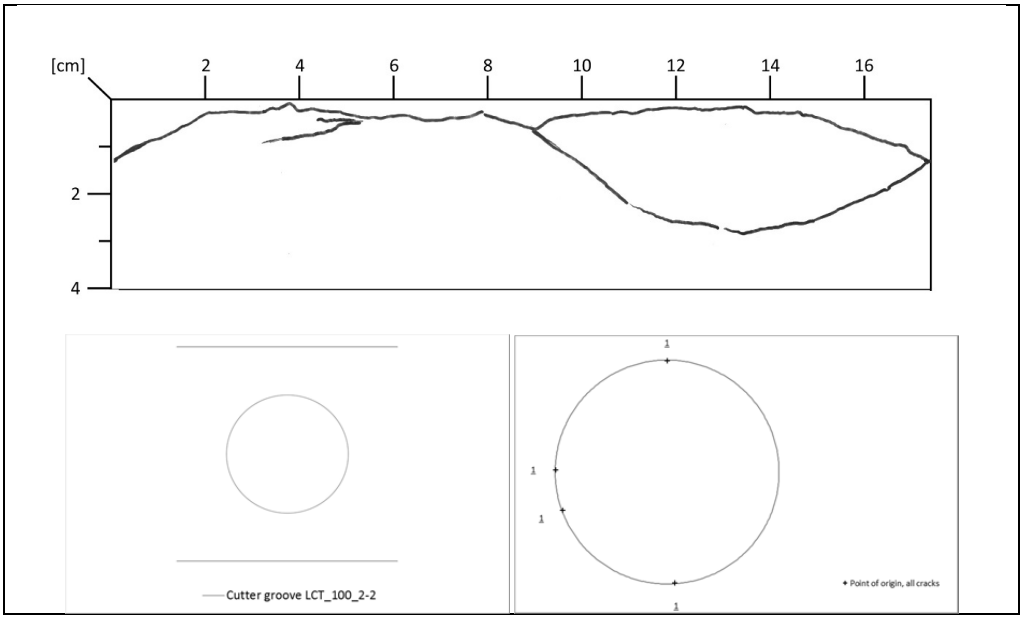

Figure E1.10: Core sample LCT_100_2-2.

Appendix F

APPENDIX F
CORE SAMPLES FROM THE TRONDHJEMITE QUARRY AT STØREN

List of contents

List of figures

F1 Core samples

In total, nine core from one location at the Trondhjemite quarry were collected. The cores were cut in two equally sized core samples, except core 1 and 8. The total number of samples from the Trondhjemite quarry were 16. Table F1.1 shows an overview of the samples. Note that only one core sample was cloved and used for a second round of sound velocity measurements. The other samples were used for other laboratory purposes after the sound velocity measurements.

Table F1.1: Number of samples from the Trondhjemite quarry at Støren.

Sample number	Core samples
1	1
2	2
3	2
4	2
5	2
6	2
7	2
8	1
9	2

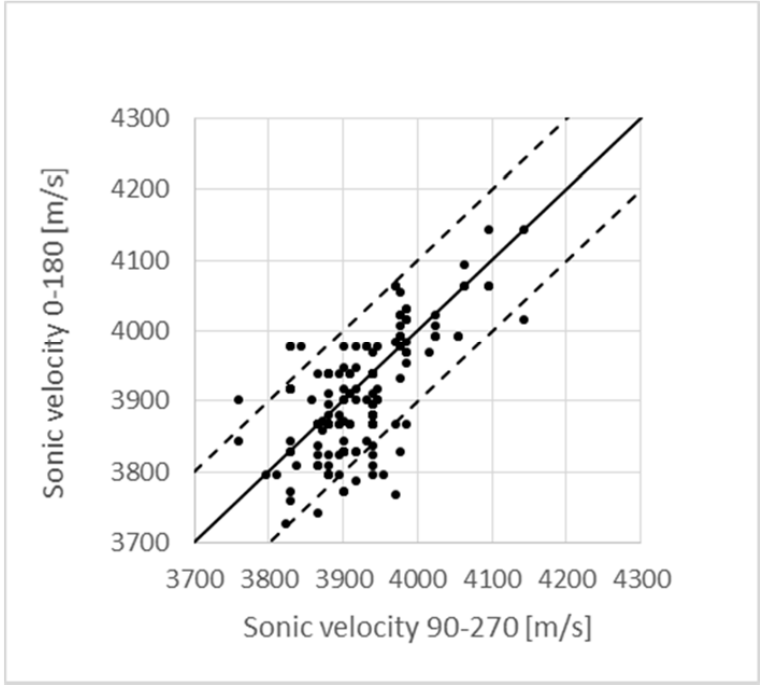

Figure F1.1: Distribution of measured sound velocity measurements in the two directions, all core samples.

F1.1 Location

Date:	27.02.2015	Rock type:	Quartz diorite (trondhjemite)
Number of cores:	9	σ_c:	1196 MPa (very high)
Number of samples:	16	SJ:	3.6 (very low)
		S_{20}:	56.1 (very high)
		DRI:	51 (medium)

Additional information:
No additional information

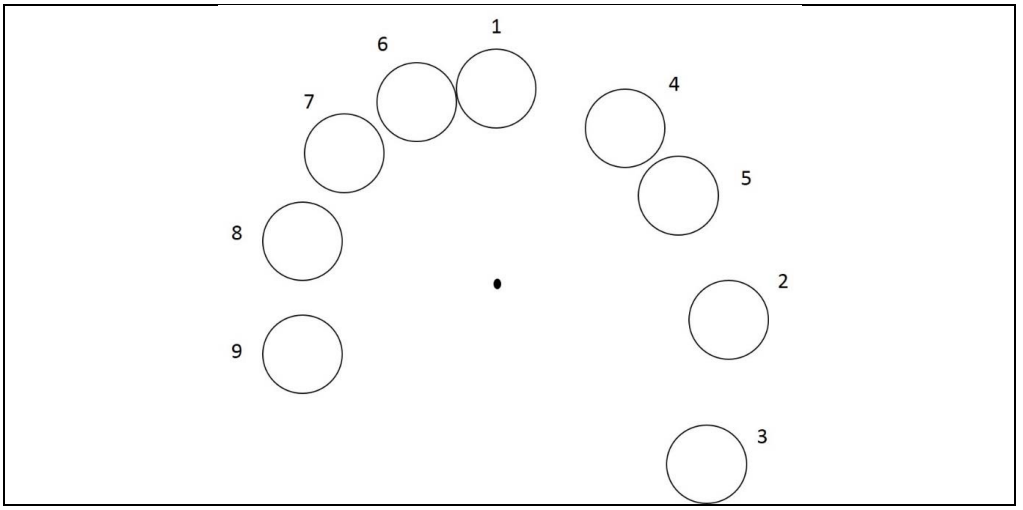

Figure F1.2: Sampling at the Trondhjemite quarry.

S_1-1

Diameter:	104 mm

Additional information:
No additional information

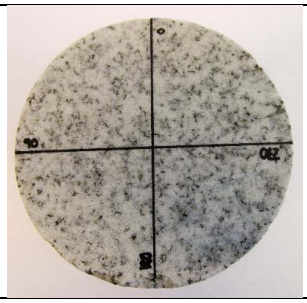

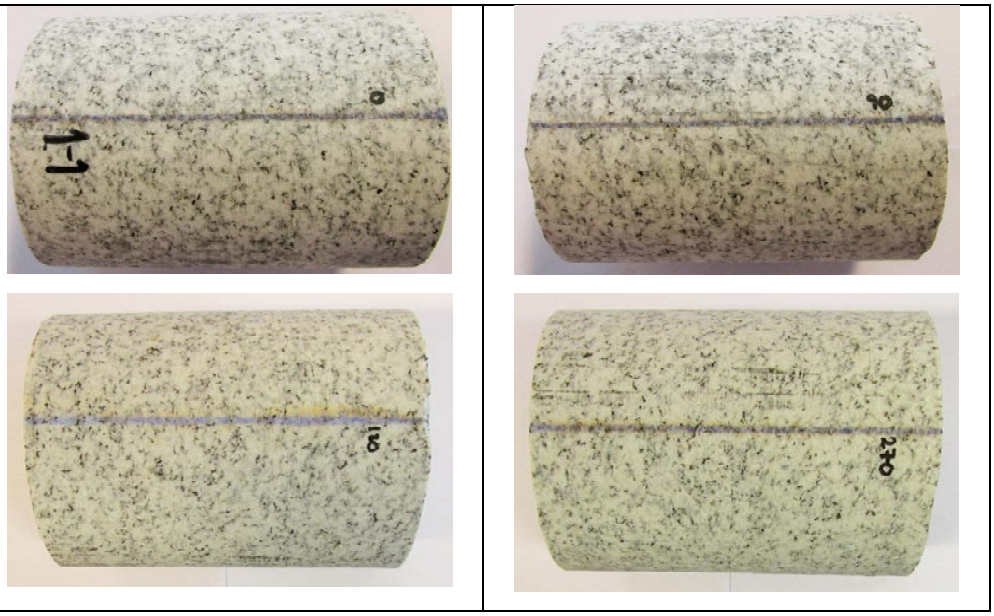

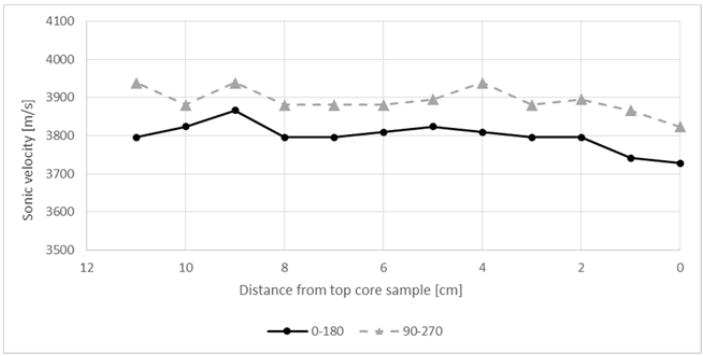

Figure F1.3: Core sample S_1-1.

S_2-1

Diameter: 104 mm	

Additional information:
No additional information

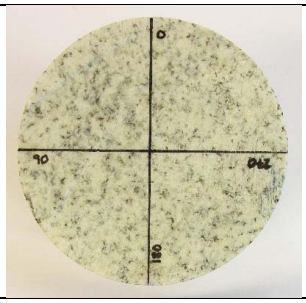

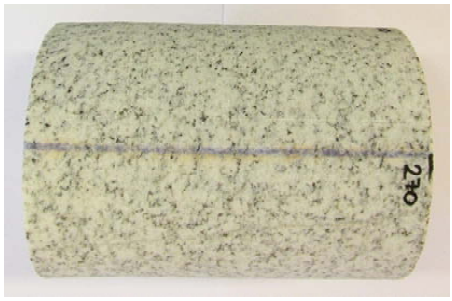

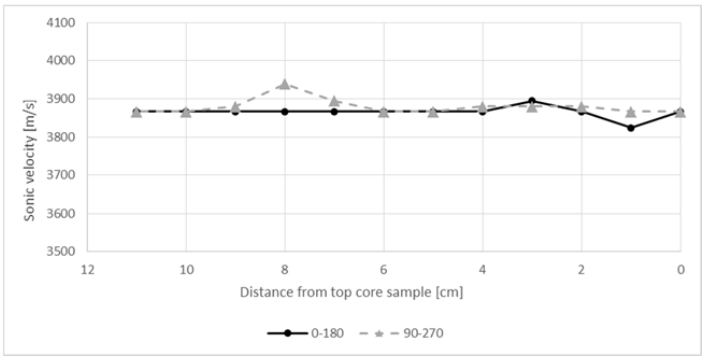

Figure F1.4: Core sample S_2-1.

S_2-2

Diameter:	104 mm	

Additional information:
No additional information

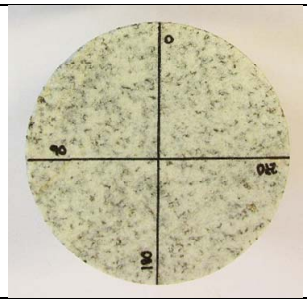

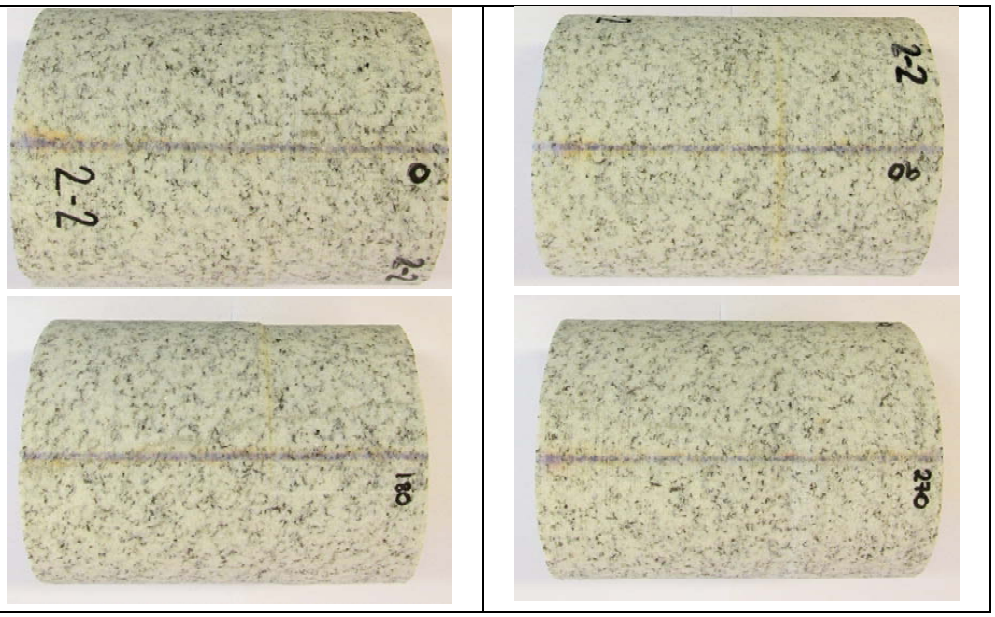

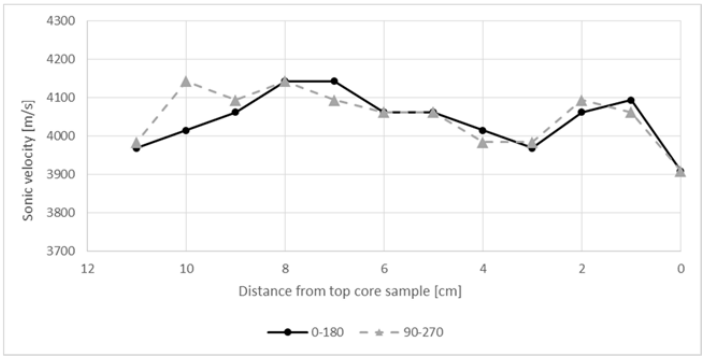

Figure F1.5: Core sample S_2-2.

S_3-1

Diameter:	104 mm

Additional information:
No additional information

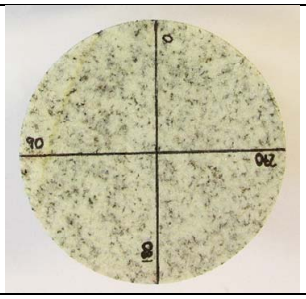

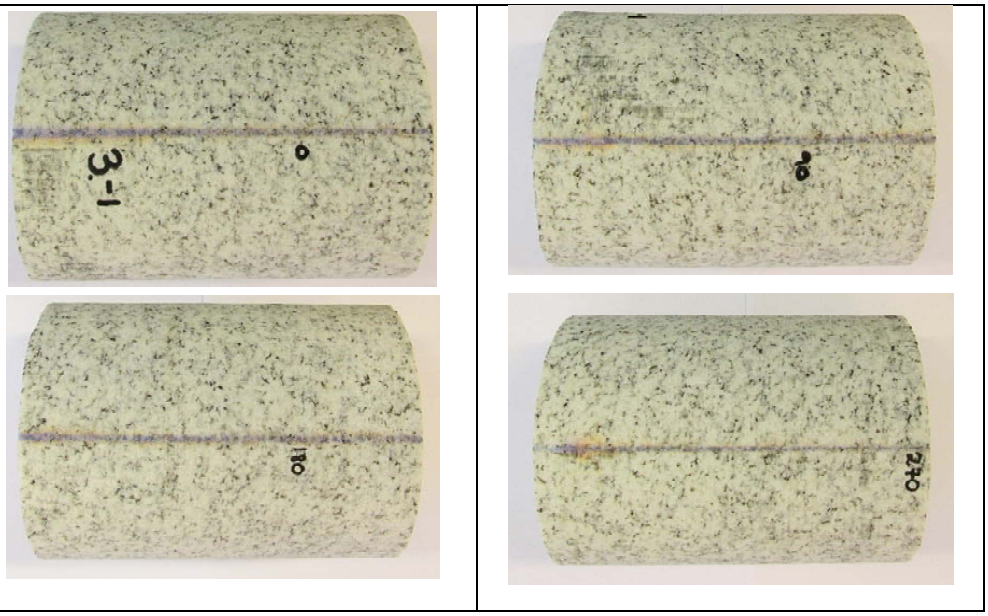

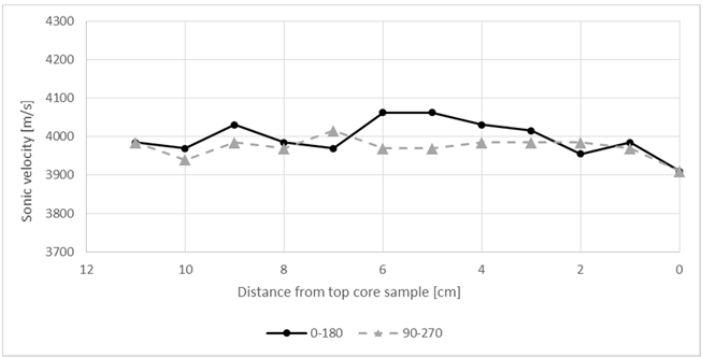

Figure F1.6: Core sample S_3-1.

S_3-2

Diameter:	104 mm

Additional information:
No additional information

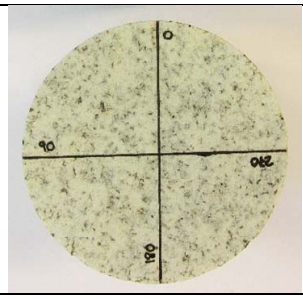

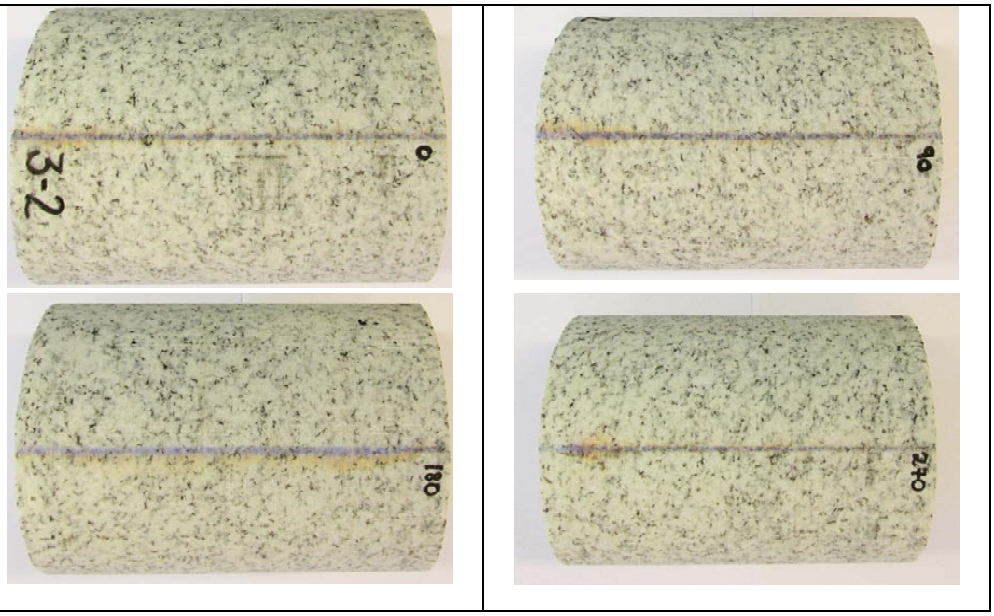

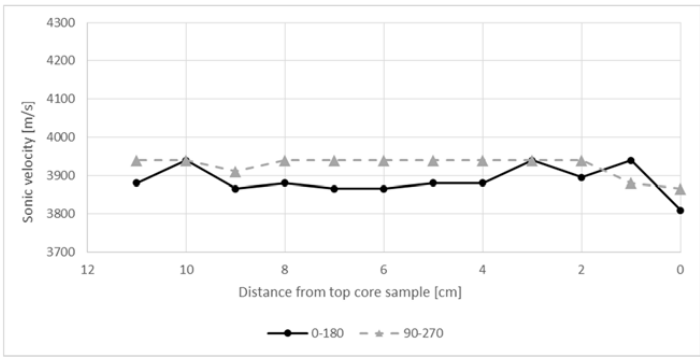

Figure F1.7: Core sample S_3-2.

S_4-1

Diameter:	104 mm

Additional information:
No additional information

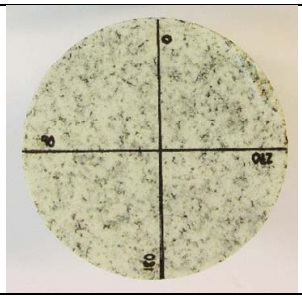

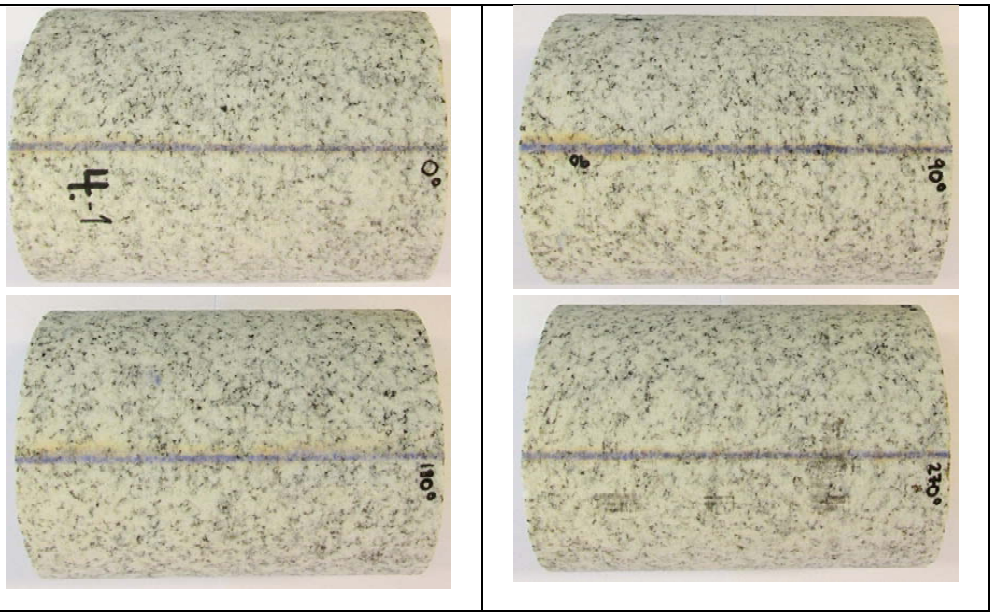

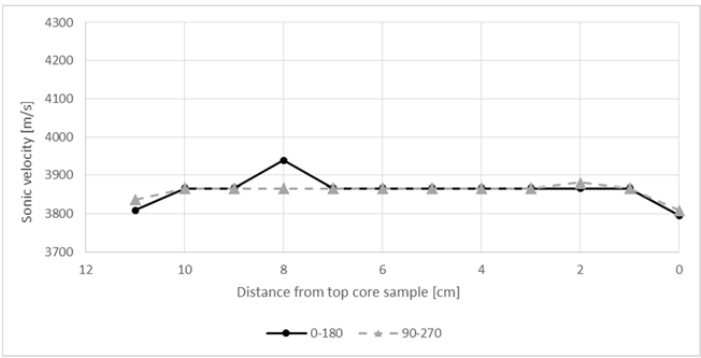

Figure F1.8: Core sample S_4-1.

S_4-2

Diameter:	104 mm

Additional information:
No additional information

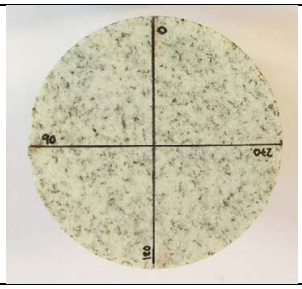

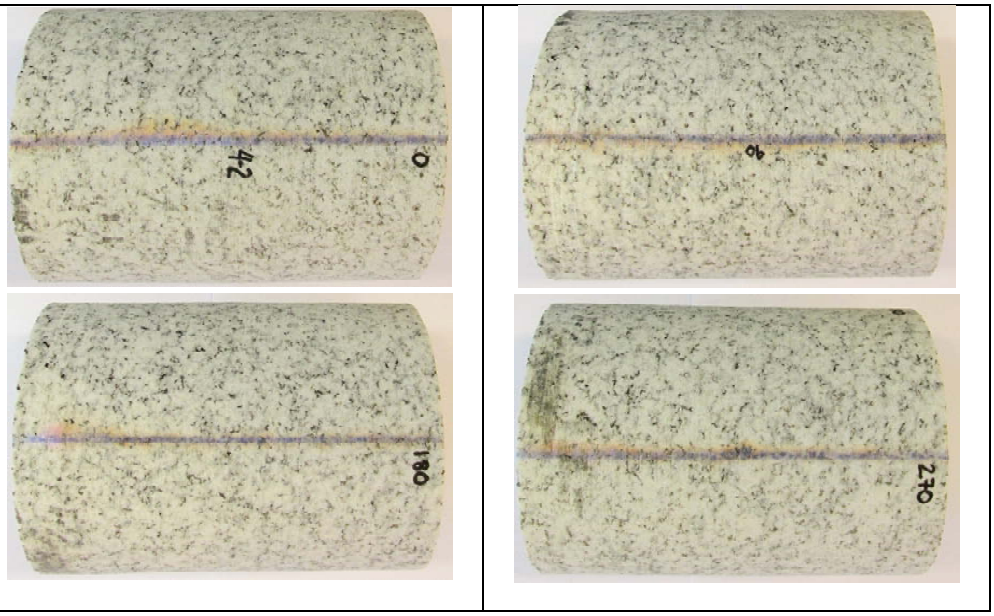

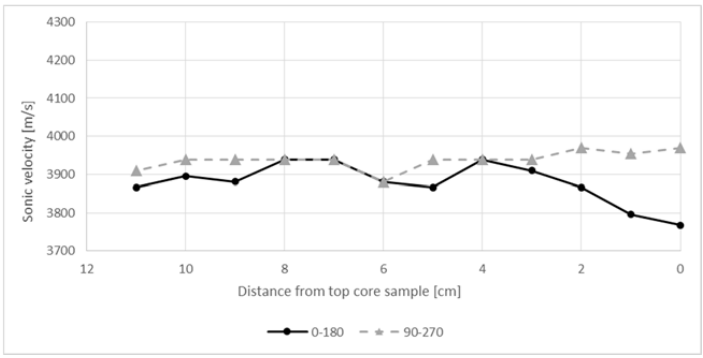

Figure F1.9: Core sample S_4-2.

S_5-1

Diameter: 104 mm	

Additional information:
No additional information

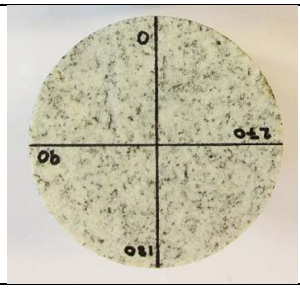

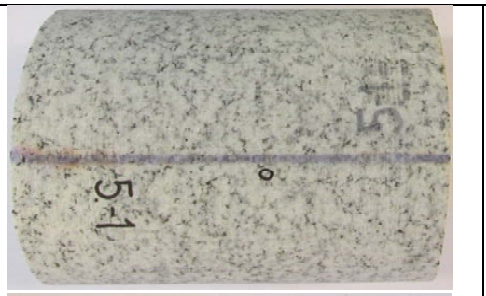

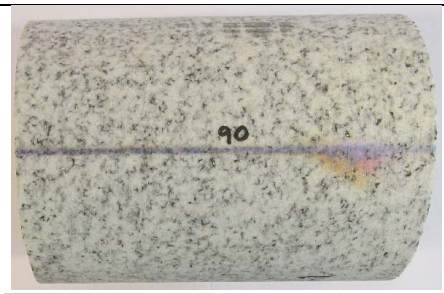

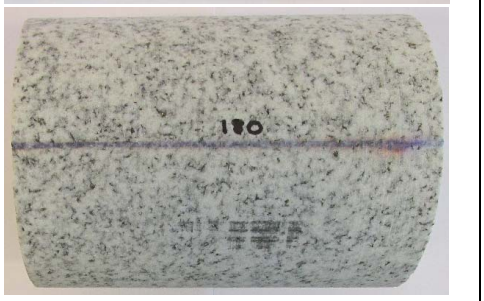

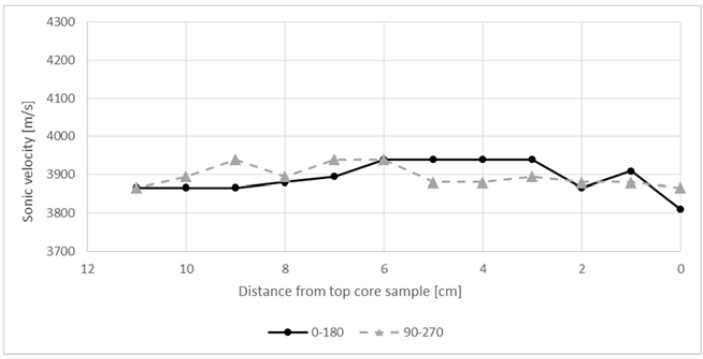

Figure F1.10: Core sample S_5-1.

S_5-2

Diameter:	104 mm	

Additional information:
No additional information

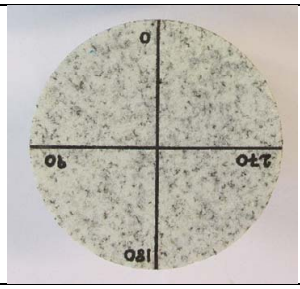

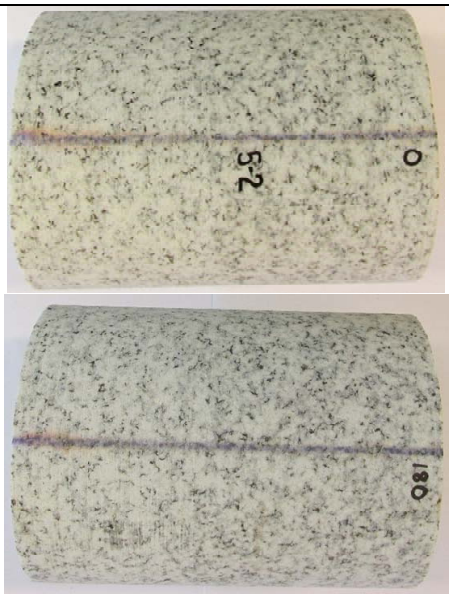

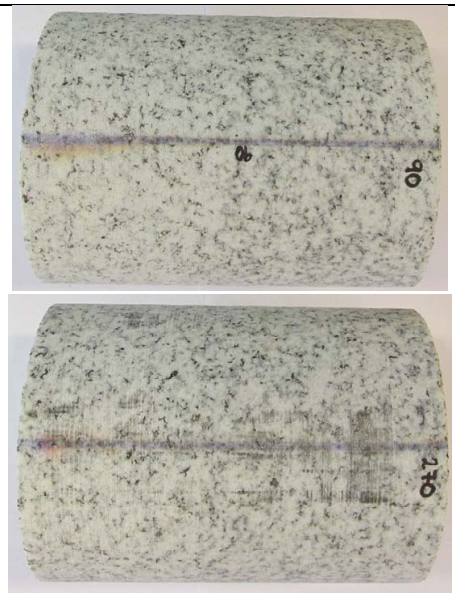

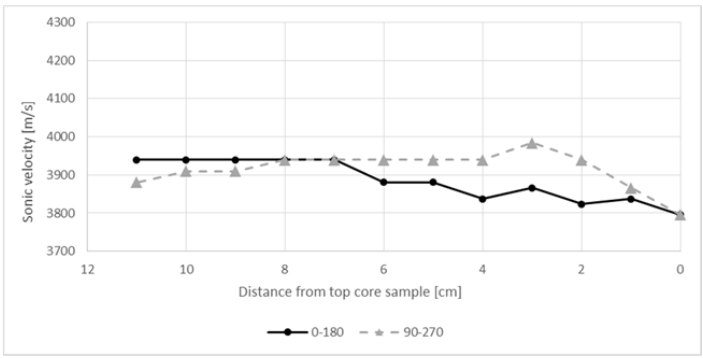

Figure F1.11: Core sample S_5-2.

S_6-1

Diameter:	104 mm	

Additional information:
The core is only 8 cm long, and was used for laboratory purpose. No sound velocity measurements were carried out..

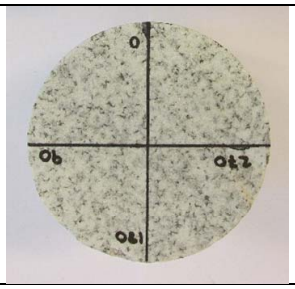

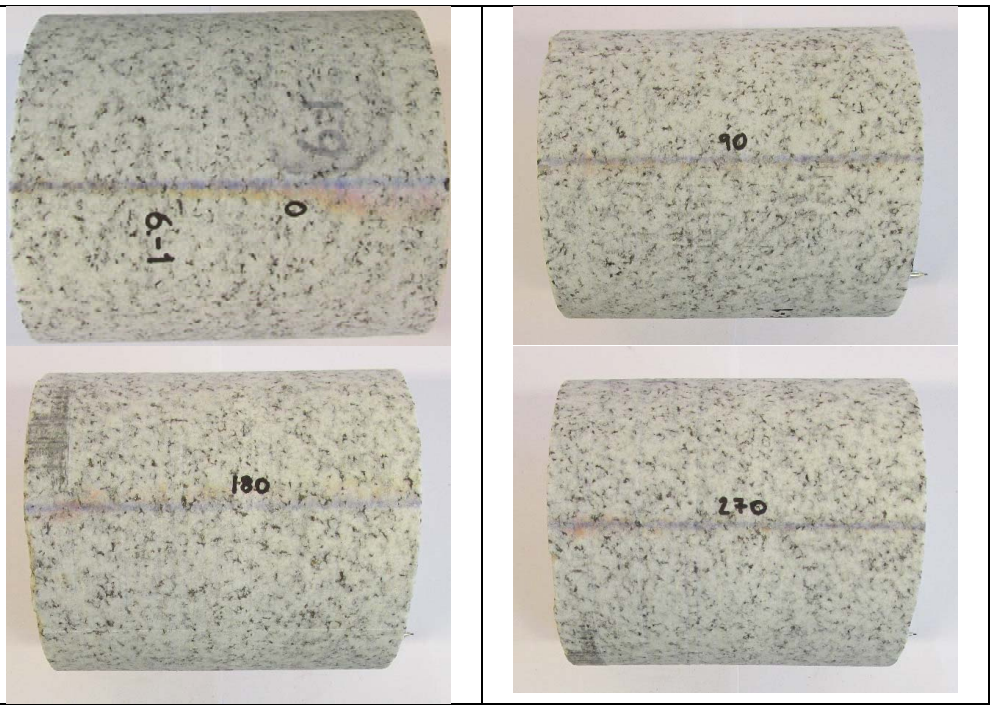

Figure F1.12: Core sample S_6-1.

S_6-2

Diameter:	103 mm	

Additional information:
No additional information

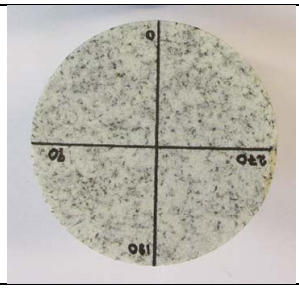

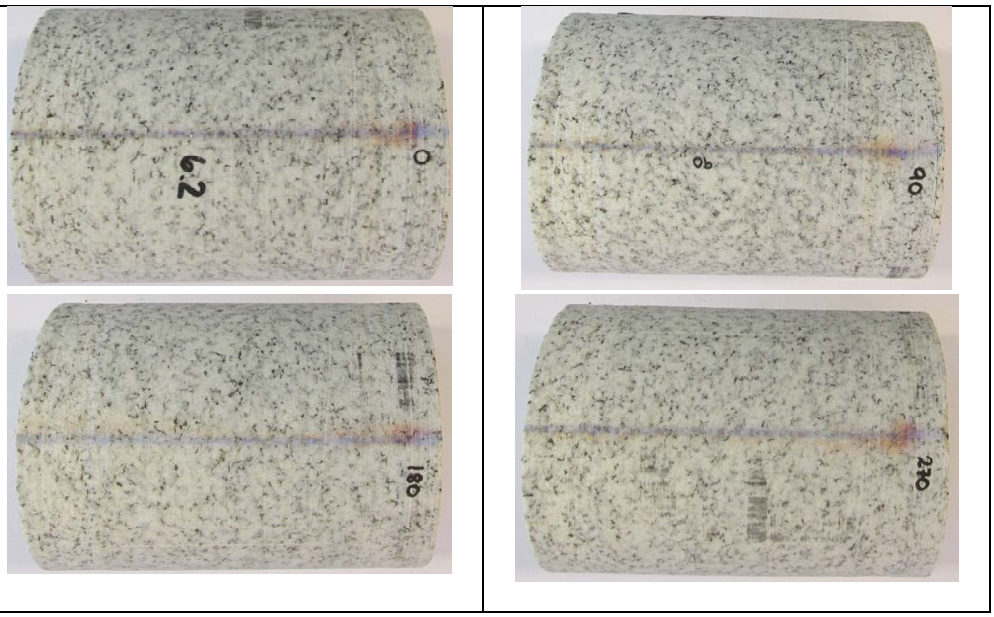

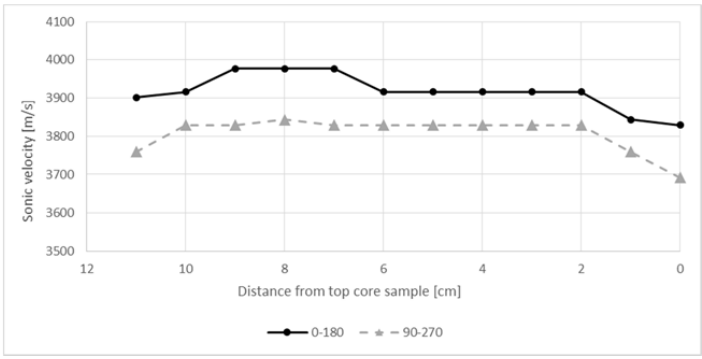

Figure F1.13: Core sample S_6-2.

S_7-1

Diameter:	103 mm	

Additional information:
No additional information

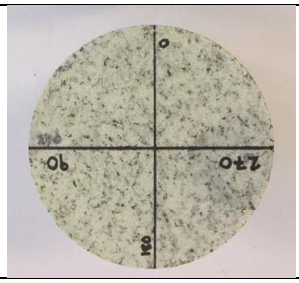

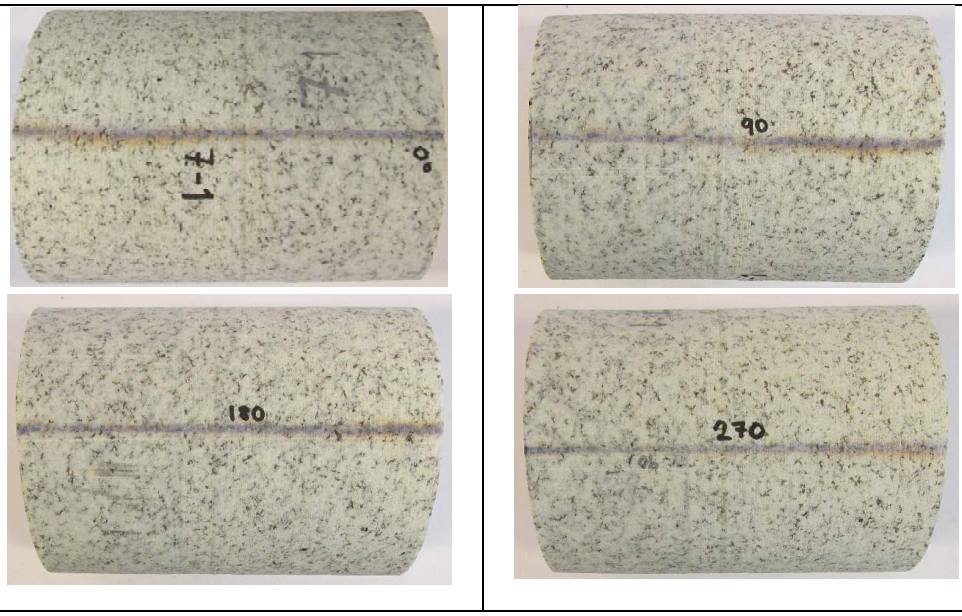

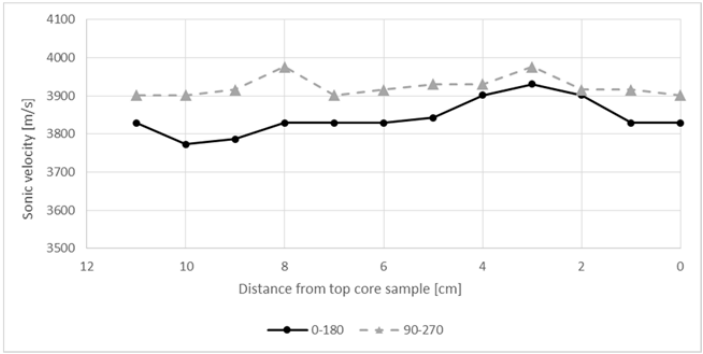

Figure F1.14: Core sample S_7-1.

S_7-2

Diameter: 103 mm	

Additional information:
No additional information

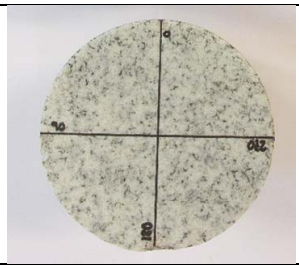

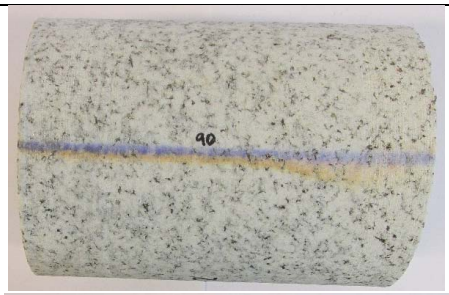

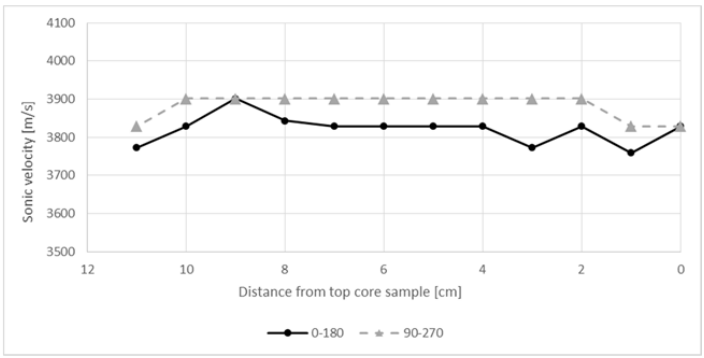

Figure F1.15: Core sample S_7-2.

S_8-1

Diameter:	103 mm

Additional information:
No additional information

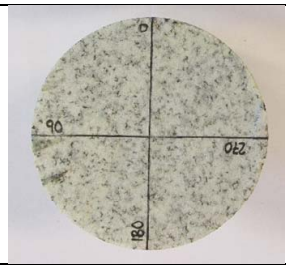

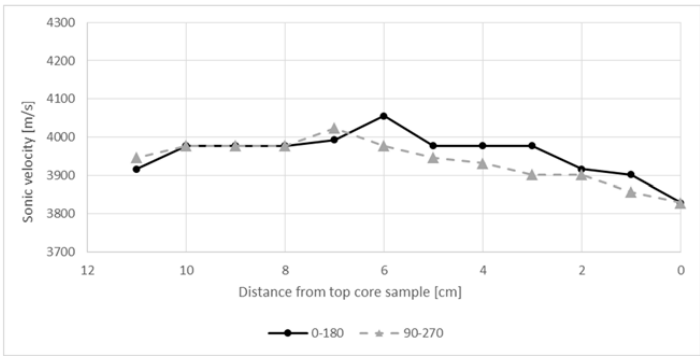

Figure F1.16: Core sample S_8-1.

S_9-1

Diameter:	103 mm

Additional information:
No additional information

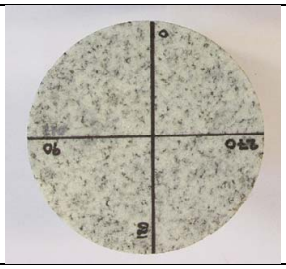

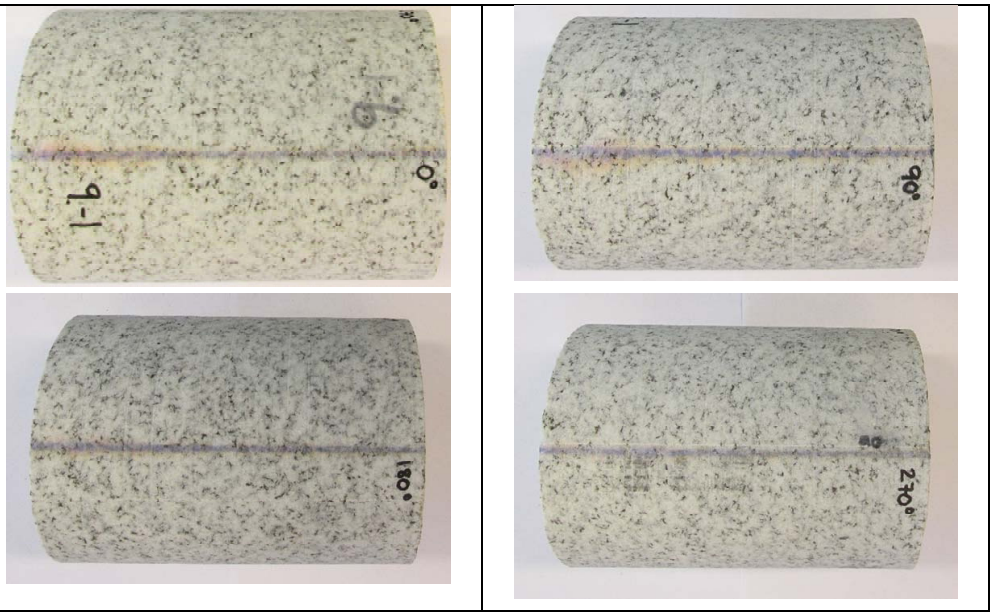

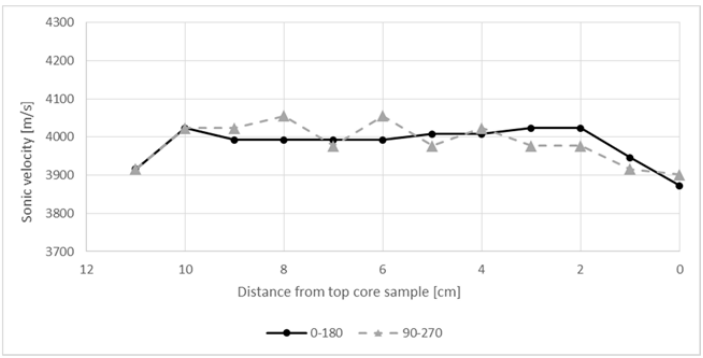

Figure F1.17: Core sample S_9-1.

S_9-2

Diameter: 103 mm	

Additional information:
Used for sound velocity measurements before and after initiation of cracks.

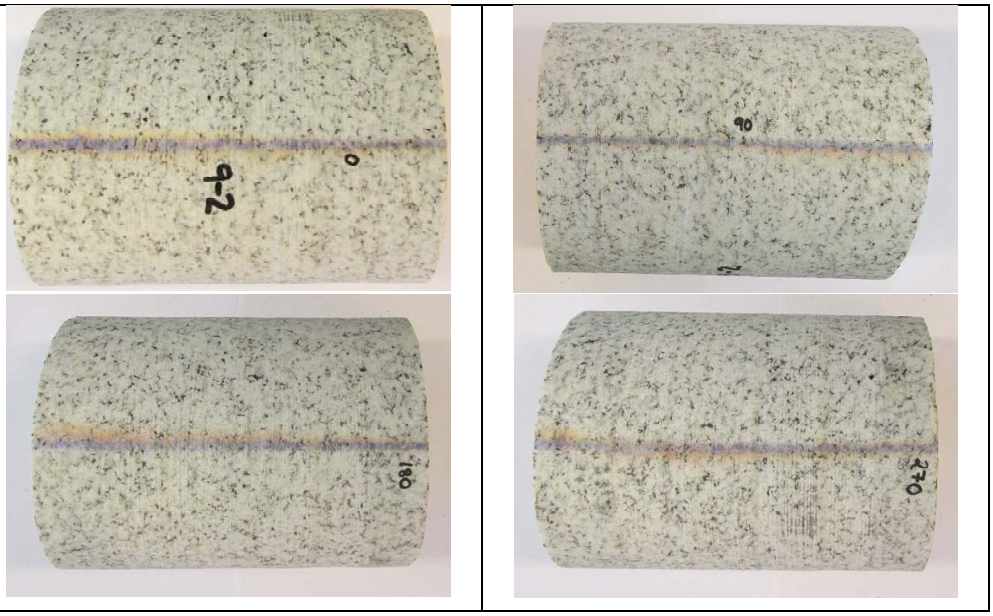

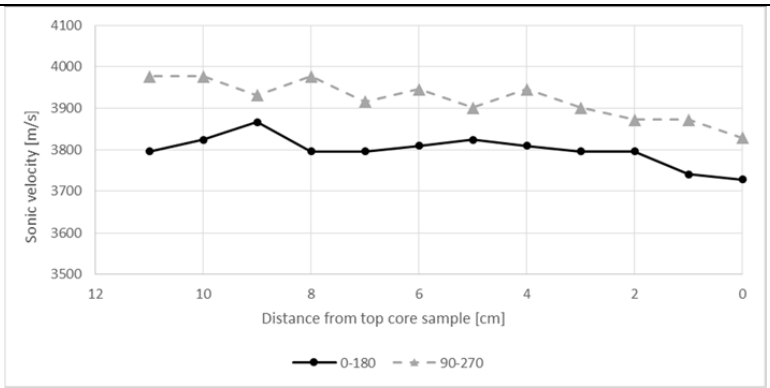

Figure F1.18: Core sample S_9-2.

Appendix G

APPENDIX G
CHIPS

List of contents

List of figures

G1 Cracks in chip samples

In total, 12 chips samples from four chainages close to, or directy at, the sample strokes were collected at the AMR project and the Nedre Røssåga headrace tunnel. Table G1.1 presents the number of chip samples from each chainage and Figure G1.1 shows a picture of all the sample chips before cutting.

Table G1.1: Number of samples from the sampling chainages at the AMR Project and the Nedre Røssåga headrace tunnel.

Chainage	Number of samples
AMR_11573	3
R_1184	4
R_1440	1
R_5437	4

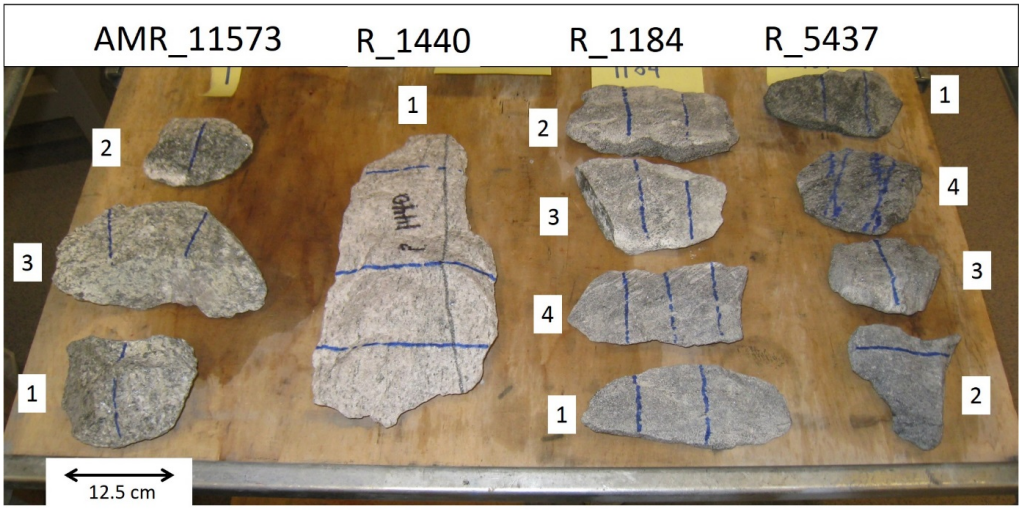

Figure G1.1: Chip samples from the AMR Project and the Nedre Røssåga headrace tunnel before cutting. The blue lines mark how the chips were cut before inspection.

G1.1 The AMR Project

Chainage 11573

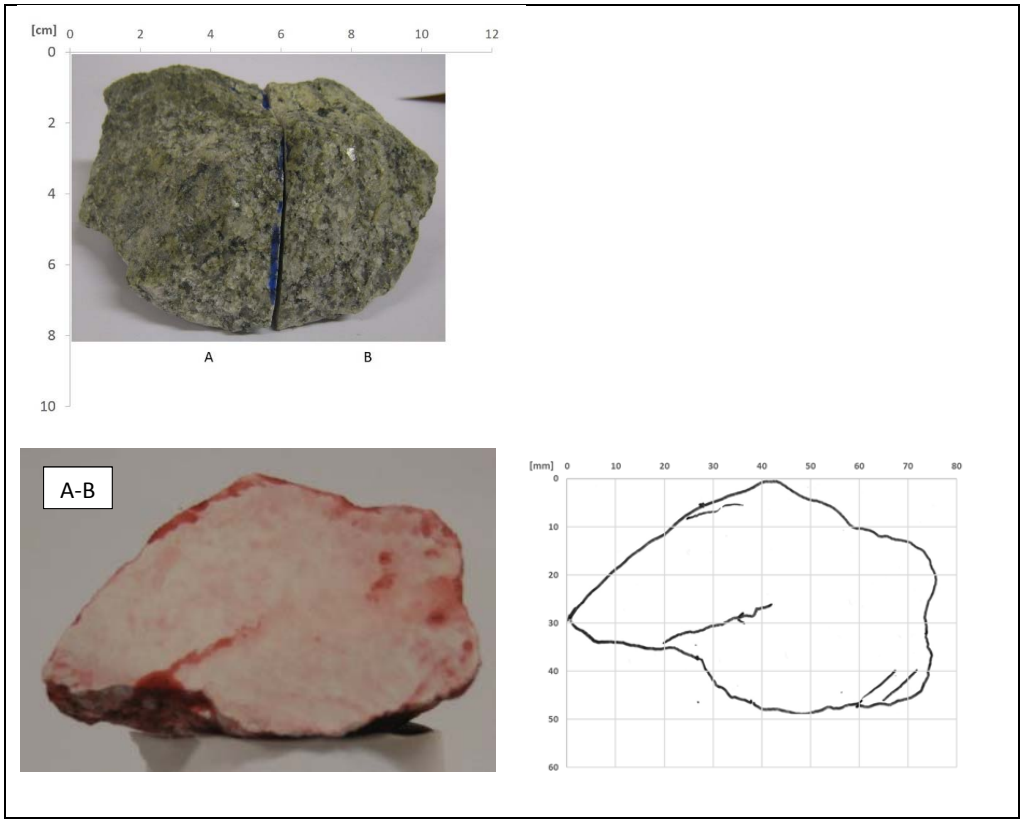

Figure G1.2: Chip AMR_11573_1.

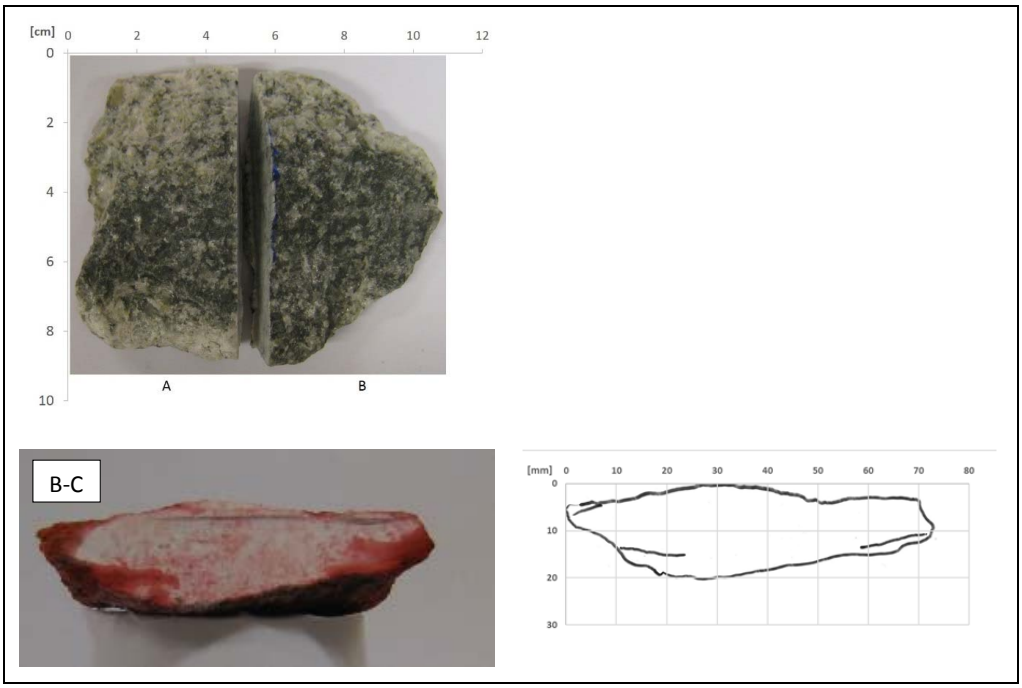

Figure G1.3: Chip AMR_11573_2.

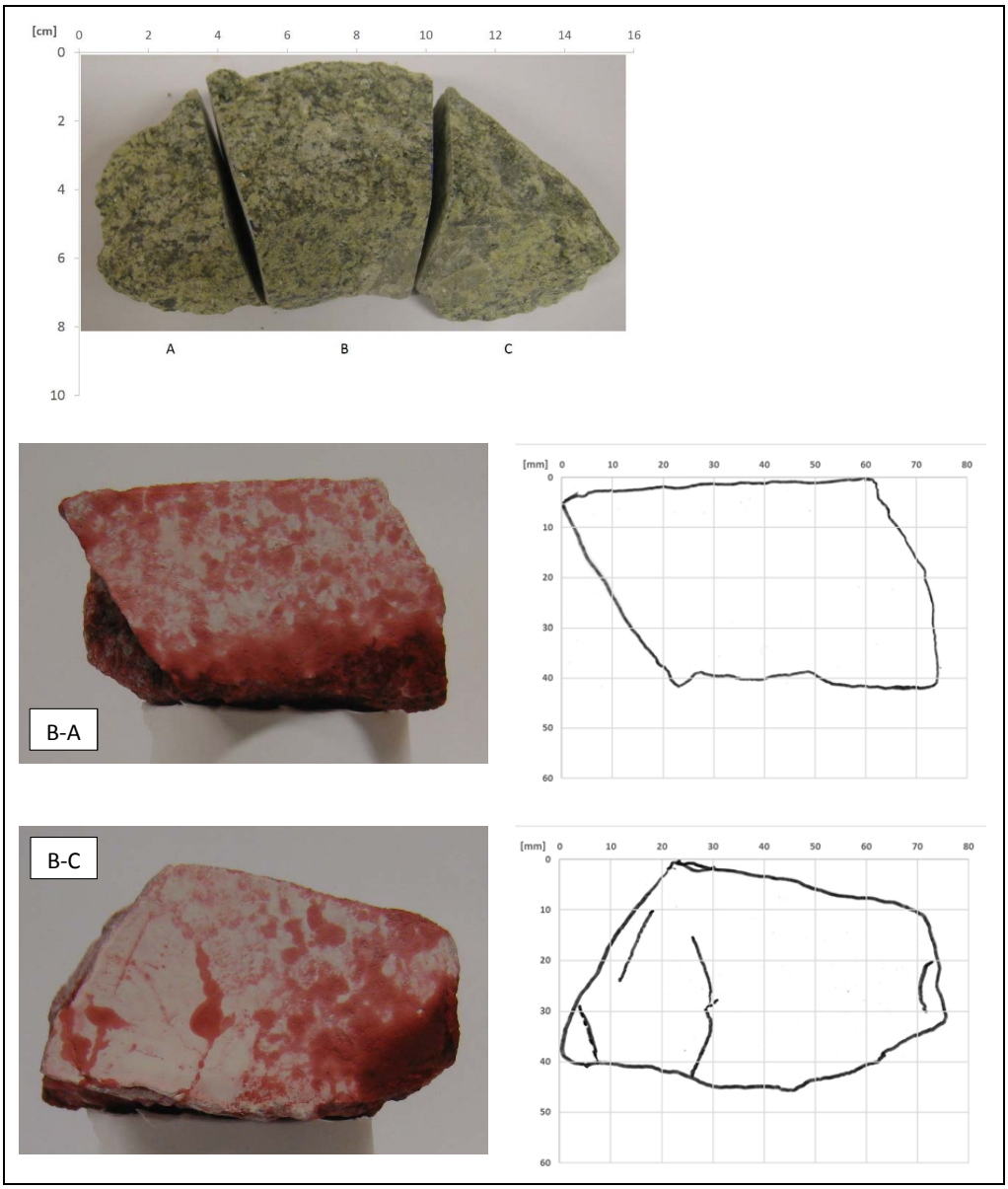

Figure G1.4: Chip AMR_11573_3.

G1.2 The Nedre Røssåga headrace tunnel

Chainage 1184

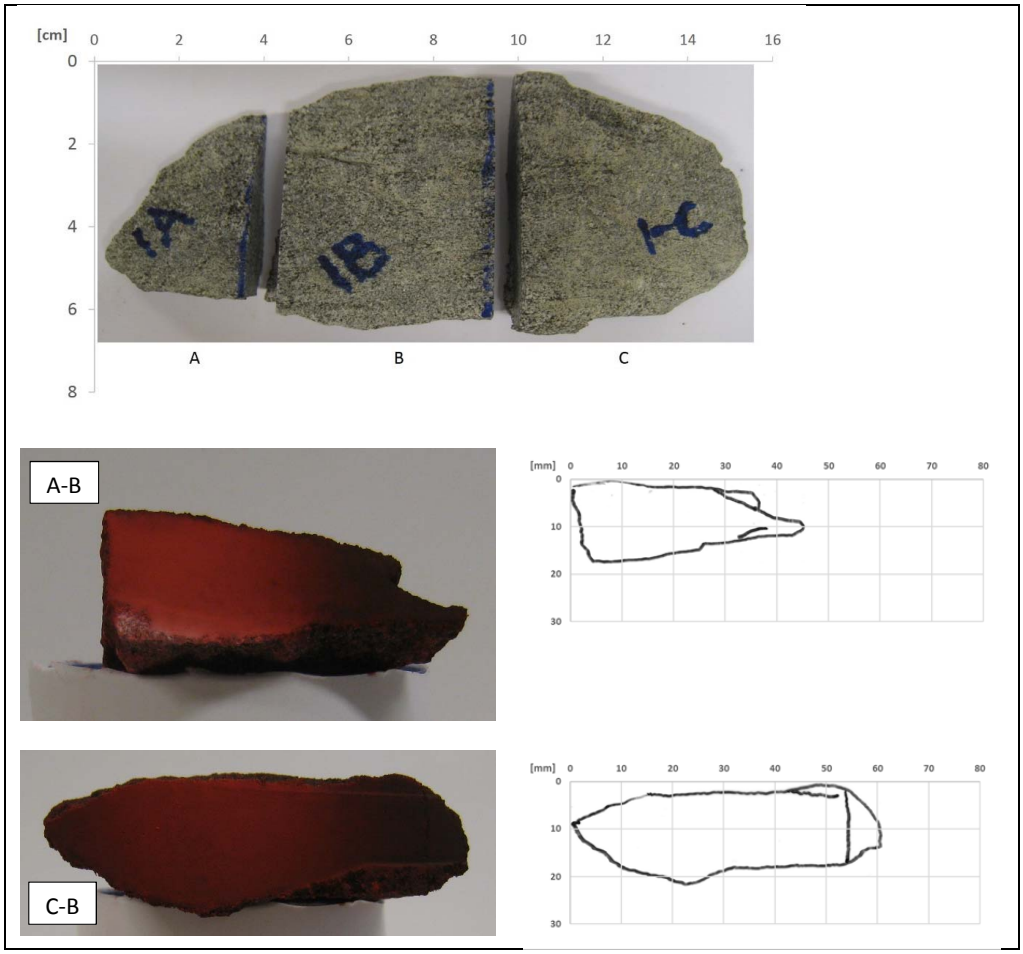

Figure G1.5: Chip R_1184_1.

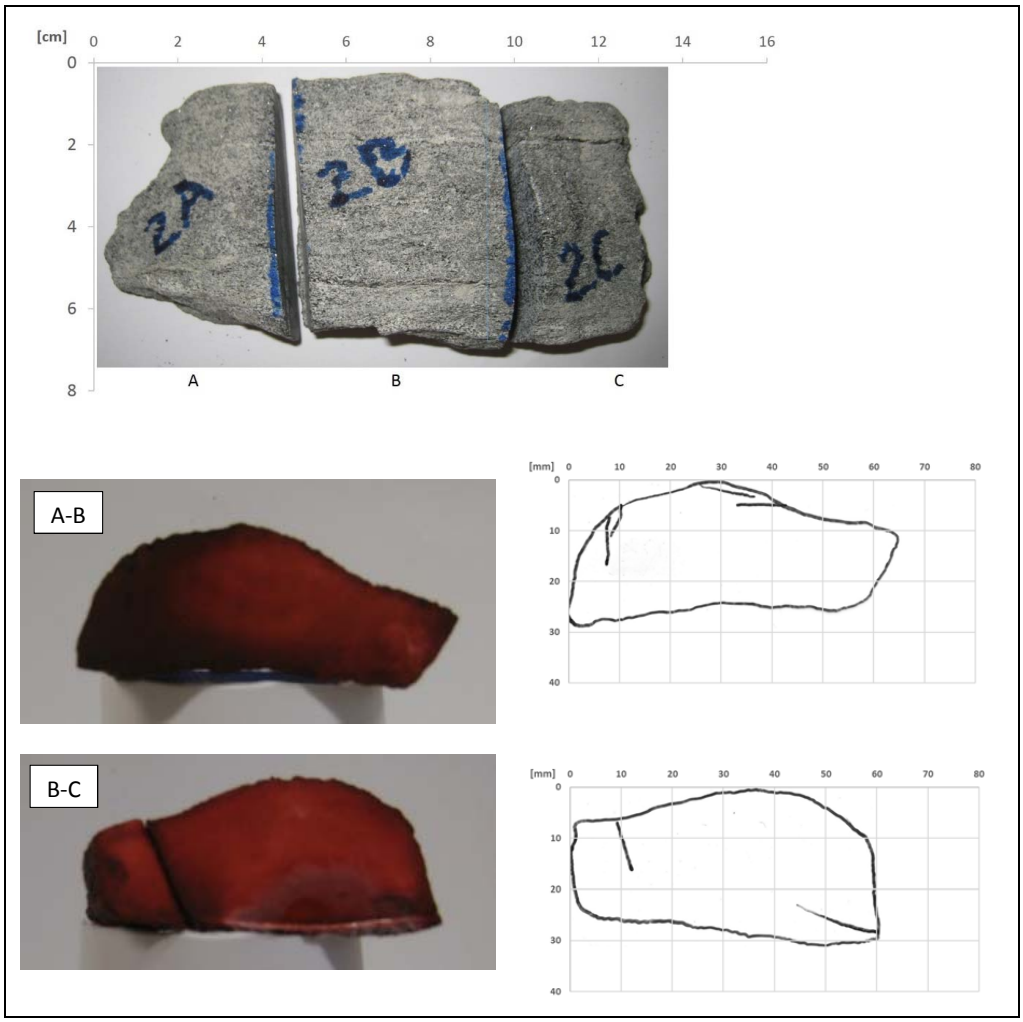

Figure G1.6: Chip R_1184_2.

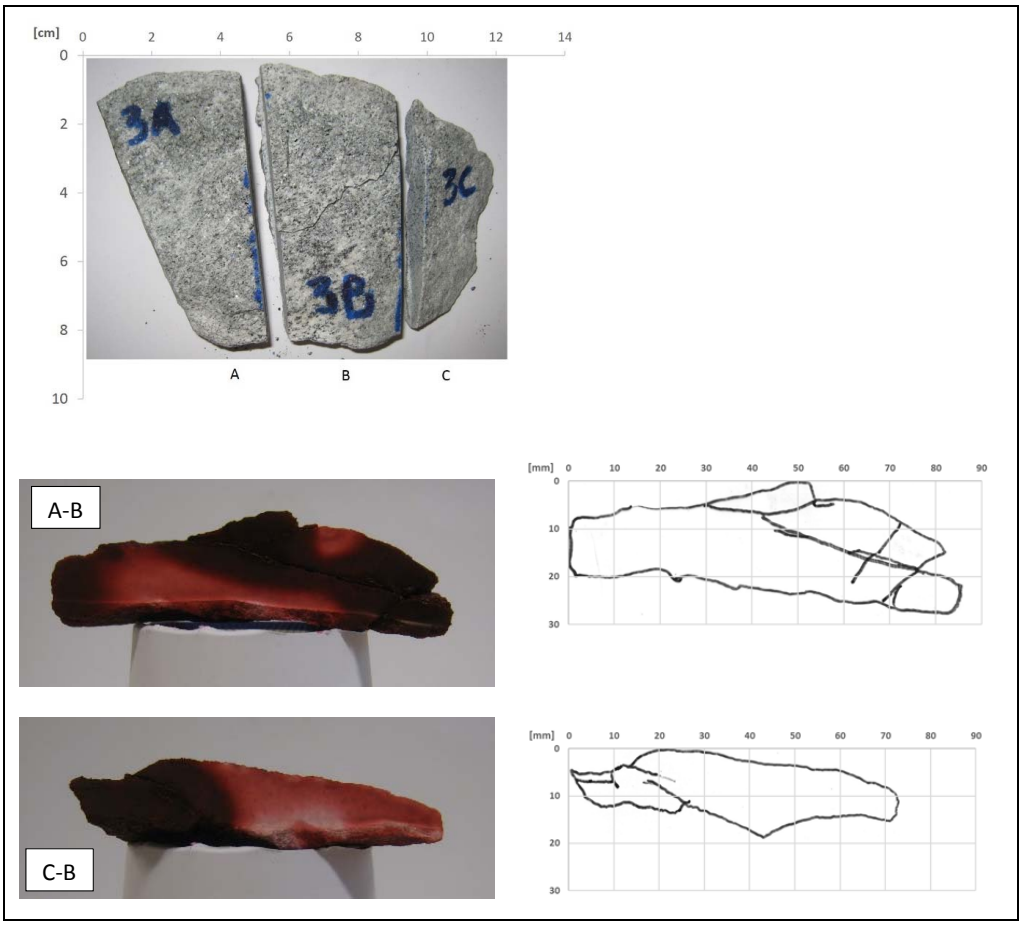

Figure G1.7: Chip R_1184_3.

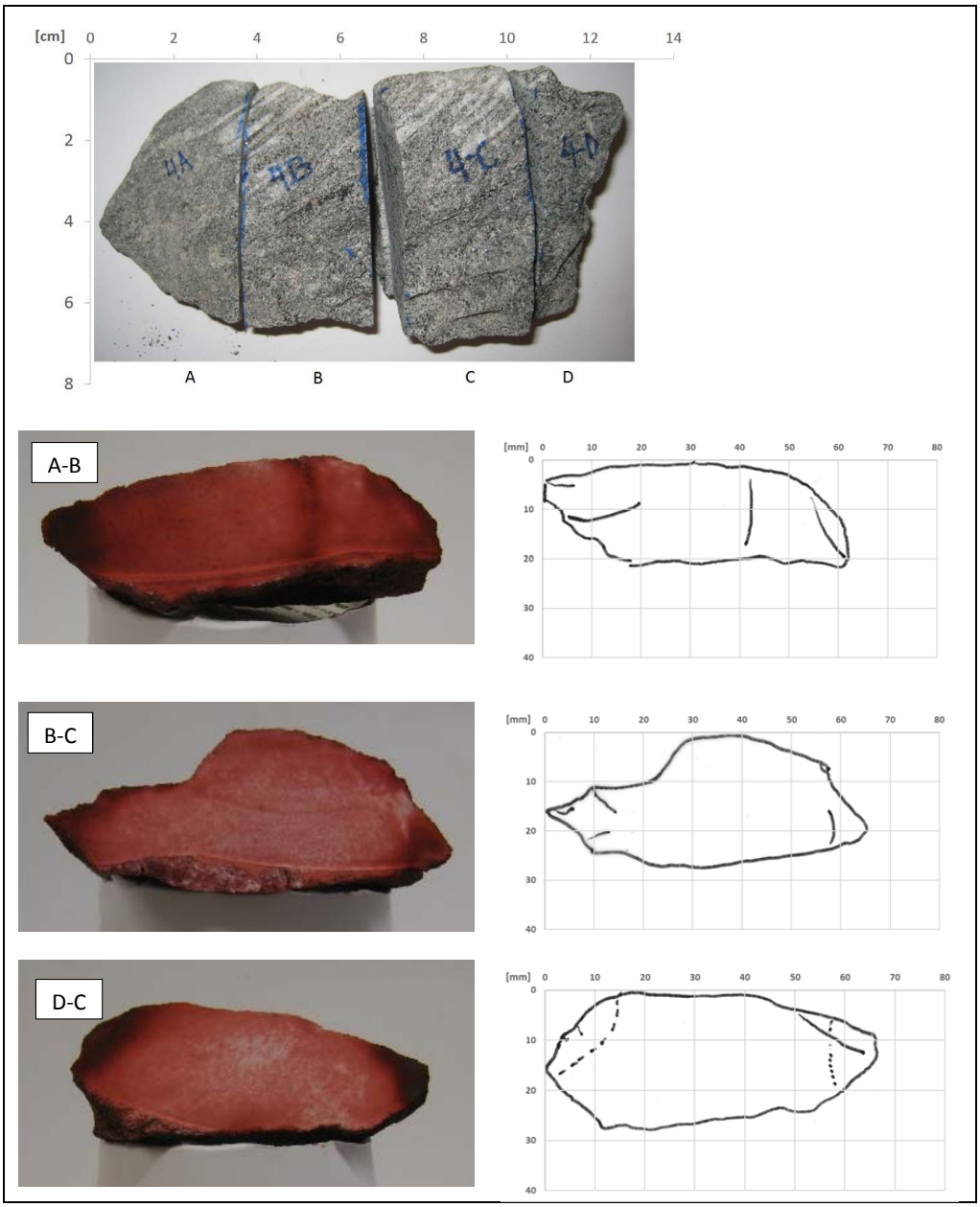

Figure G1.8: Chip R_1184_4.

Chainage 1440

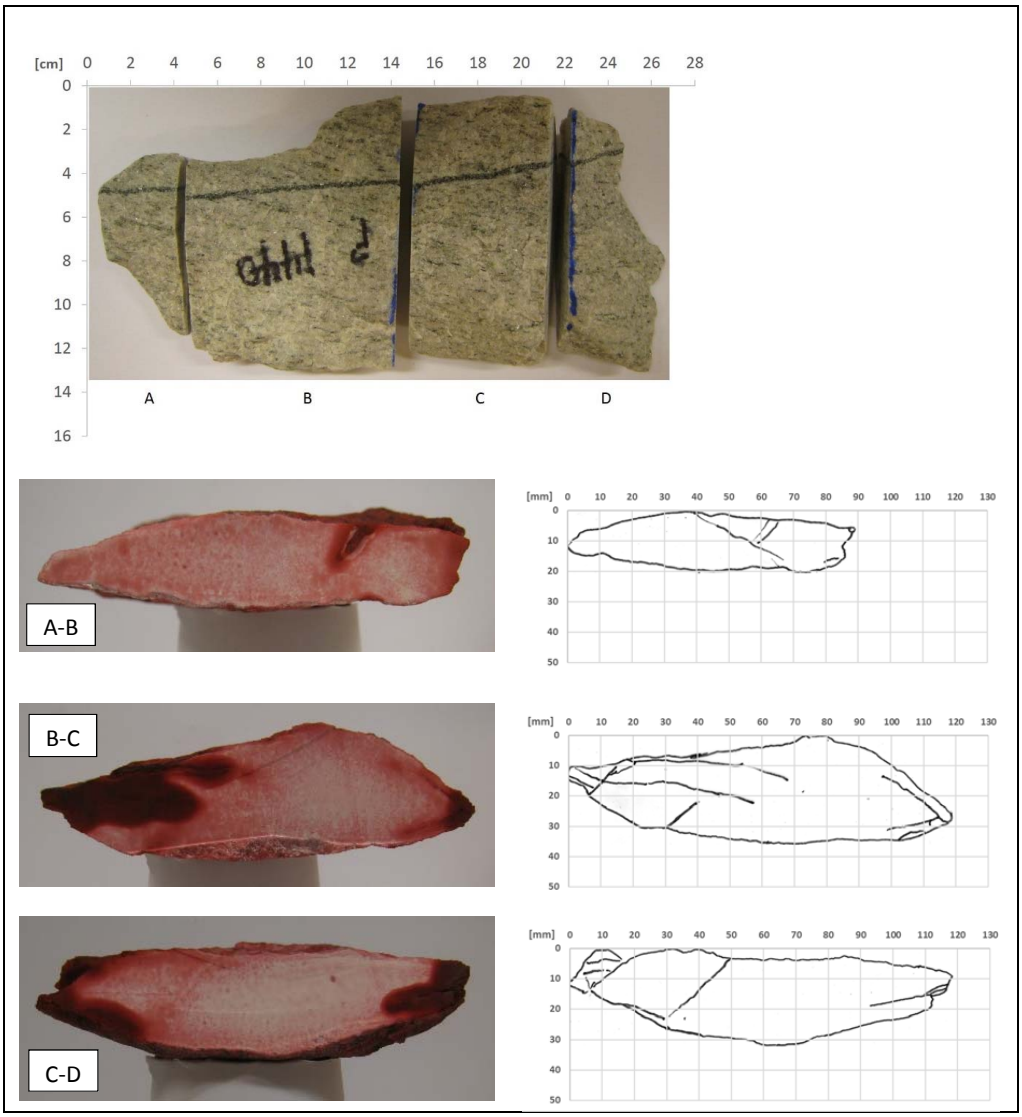

Figure G1.9: Chip R_1440_1.

Chainage 5437

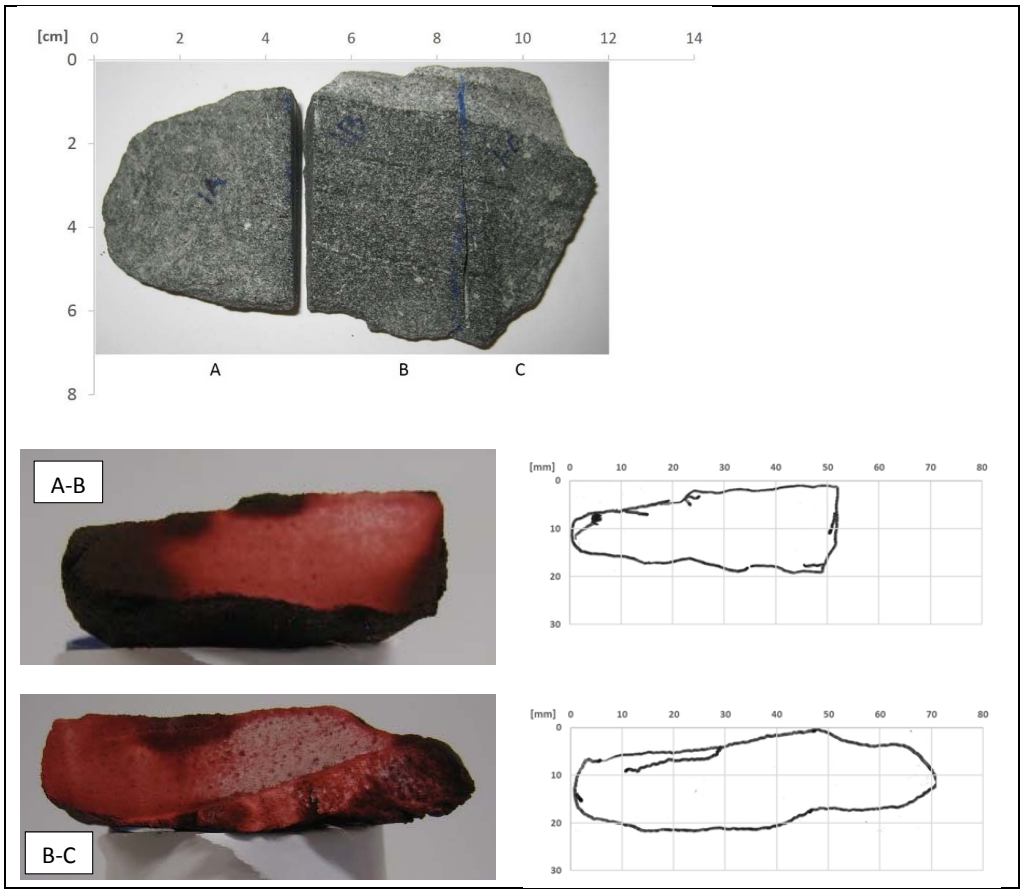

Figure G1.10: Chip R_5437_1.

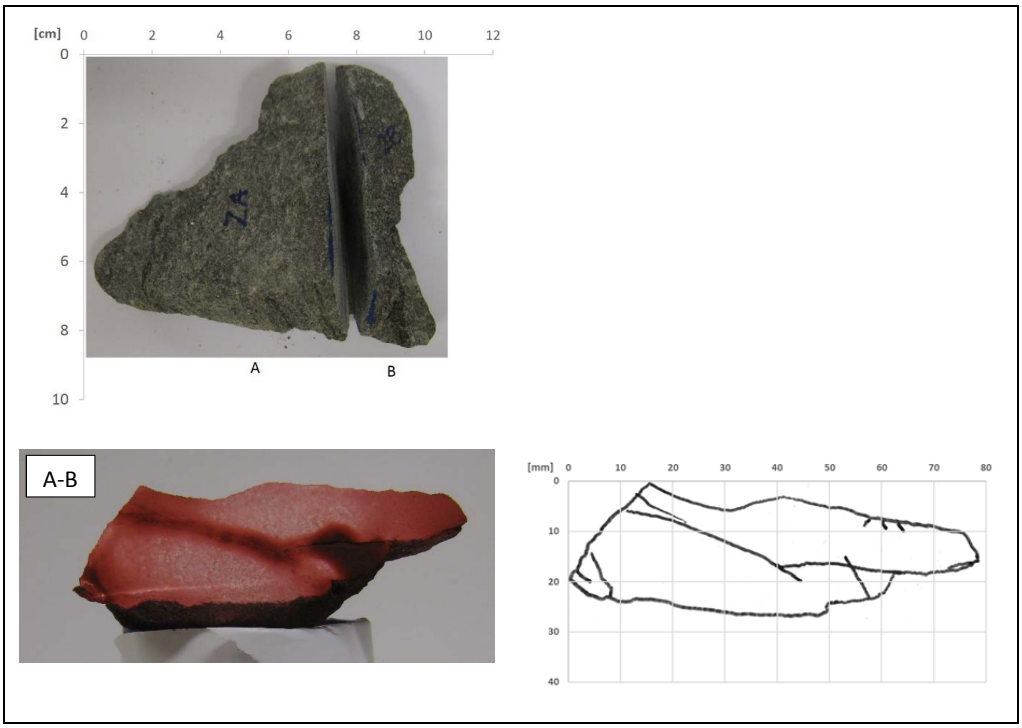

Figure G1.11: Chip R_5437_2.

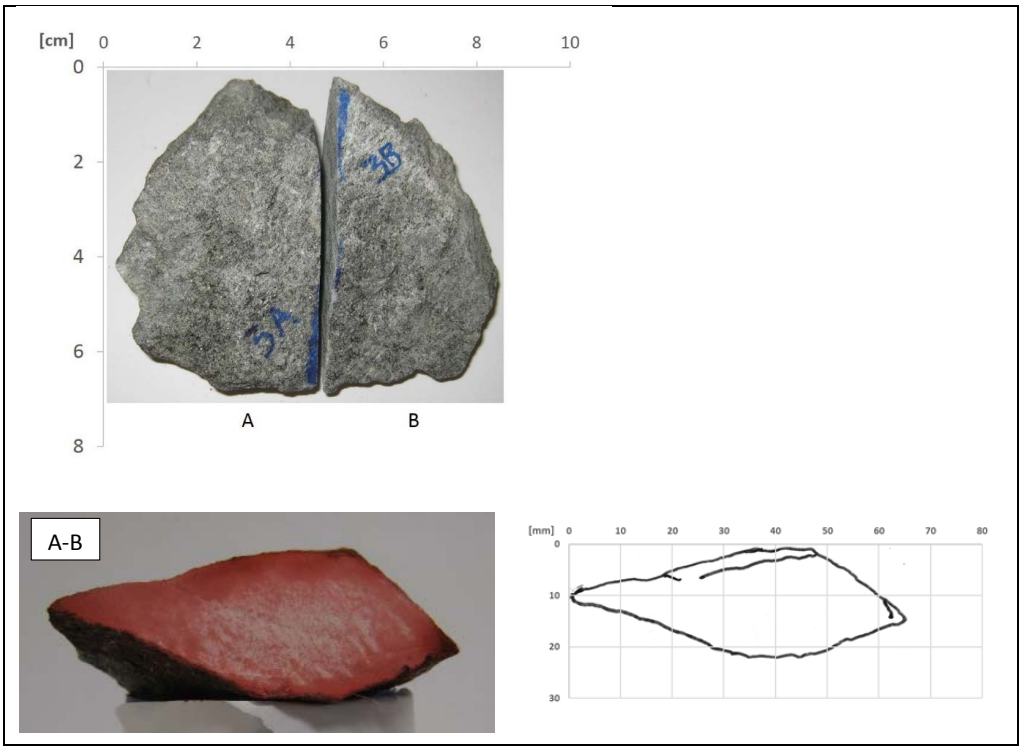

Figure G1.12: Chip R_5437_3.

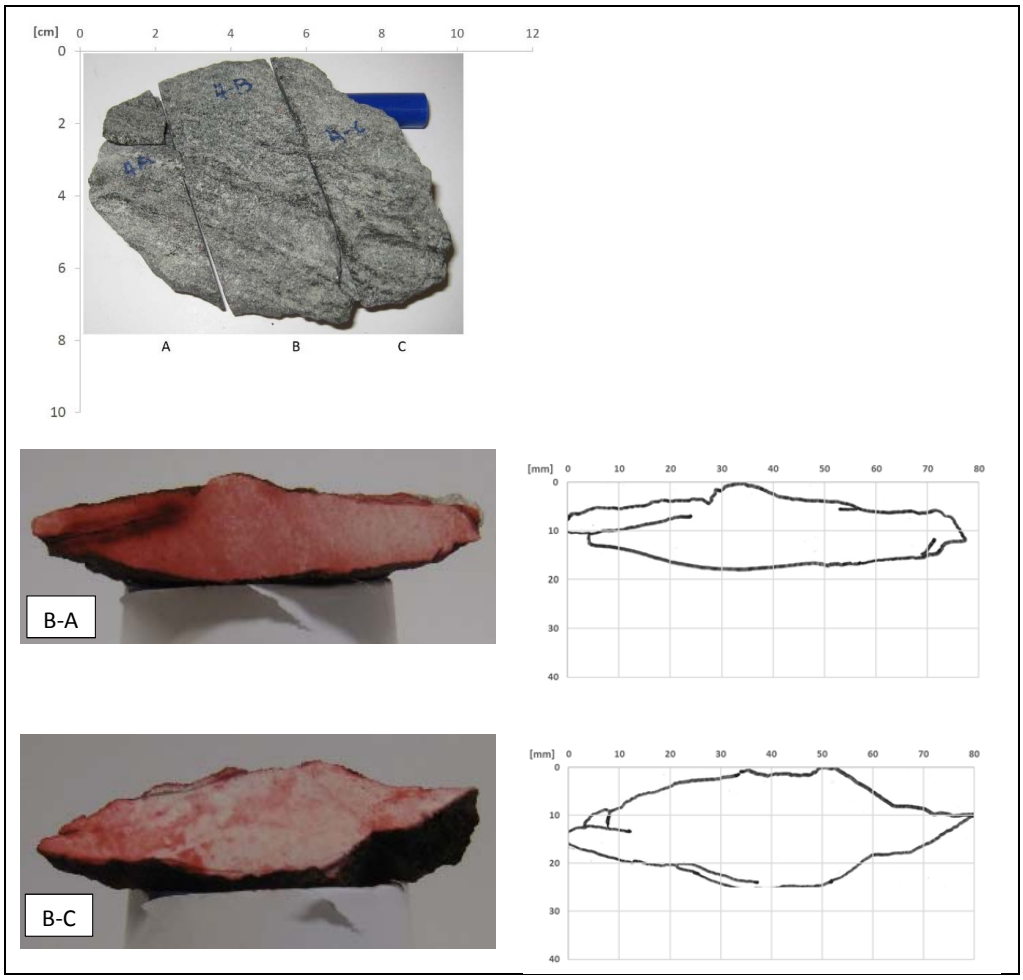

Figure G1.13: Chip R_5437_4.

Appendix H

APPENDIX H
SOUND VELOCITY MEASUREMENTS AND DIGITALIZED FOLDOUTS

List of contents

List of figures

H1 The Nedre Røssåga headrace tunnel

Sound velocity measurements have been performed on 20 cores from the Nedre Røssåga headrace tunnel. Five core samples from chainage 3112 are not included, due to cloved cores. Table H1.1 presents the number of core samples at each sample chainage.

Table H1.1: Number of samples from the sampling chainages at the Nedre Røssåga headrace tunnel.

Chainage	Number of samples
R_1184	5
R_3112	15

The sound velocity profiles are compared with the digitalized foldouts, and the correlation between the measured sound velocity profiles and the detected cracks are evaluated categorized in three different groups:

1.1 Good correlation; the measured sound velocity profiles correlates very well with the documented cracking
1.2 Medium correlation; the measured sound velocity profiles correlates to some extent with the documented cracking
1.3 Fair correlation; the measured sound velocity profiles does not correlate with the documented cracking

The core samples are categorized in four groups based on the shape of the sound velocity profiles:

2.1 Gradually increasing sound velocity profile
2.2 Gradually increasing sound velocity profile, but with a pronounced change in sound velocity between two measuring points
2.3 Even sound velocity profile
2.4 Undulating sound velocity profile, but the average measured value increases when the distance from the face increases

The core samples are categorized in four groups based on the differences between the sound velocity measurements parallel and perpendicular to the cutter groove:

3.1 The measured sound velocity is higher parallel to the cutter groove than perpendicular to it, in all the measuring points
3.2 The measured sound velocity is higher parallel to the cutter groove than perpendicular to it, in all the measuring points, except two
3.3 The measured sound velocity is more or less equal in the two measuring directions
3.4 The measured sound velocity is higher perpendicular to the cutter groove than parallel to it, in all the measuring points, except two

Table H1.2 show how the different core samples are classified.

Table H1.2: Classification of core samples.

	Category based on the correlation between the sound velocity profiles and the documented cracking			Category based on the shape of the sound velocity profiles				Category based on the differences between the sound velocity measurements parallel and perpendicular to the cutter groove			
	1.1	1.2	1.3	2.1	2.2	2.3	2.4	3.1	3.2	3.3	3.4
R_1184_1-1_21	x						x		x		
R_1184_1-2_22		x		x				x			
R_1184_1-3_23	x				x			x			
R_1184_1-4_24		x			x			x			
R_1184_1-5_25			x			x		x			
R_3112_1-2_22			x	x				x			
R_3112_1-3_23		x			x			x			
R_3112_1-4_24	x				x			x			
R_3112_1-5_25		x		x				x			
R_3112_3-1_21		x		x				x			
R_3112_3-2_22	x				x			x			
R_3112_3-3_23		x			x				x		
R_3112_3-4_24			x*				x	x			
R_3112_4-1_21	x				x			x			
R_3112_4-2_22	x				x			x			
R_3112_4-3_23	x				x						x
R_3112_4-4_24	x				x					x	
R_3112_5-1_27		x				x		x			
R_3112_5-2_28		x		x				x			
R_3112_5-3_29			x*				x		x		

*) the correlation is good close to the 0-line

H1.1 Chainage 1184

R_1184_1-1_21

Category based on correlation between the measured sound velocity profiles and the detected cracks:	1.1
Category based on the shape of the sound velocity profiles:	2.4
Category based on the differences between the sound velocity measurements parallel and perpendicular to the cutter groove:	3.2
Additional information: No additional information	

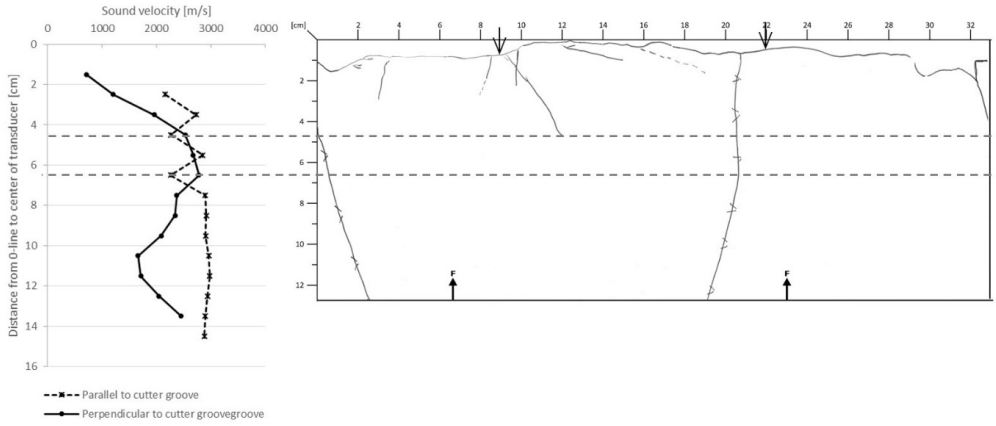

Figure H1.1: Sound velocity measurements and digital foldout of R_1184_1-1_21.

R_1184_1-2_22

Category based on correlation between the measured sound velocity profiles and the detected cracks:	1.2
Category based on the shape of the sound velocity profiles:	2.1
Category based on the differences between the sound velocity measurements parallel and perpendicular to the cutter groove:	3.1
Additional information: No additional information	

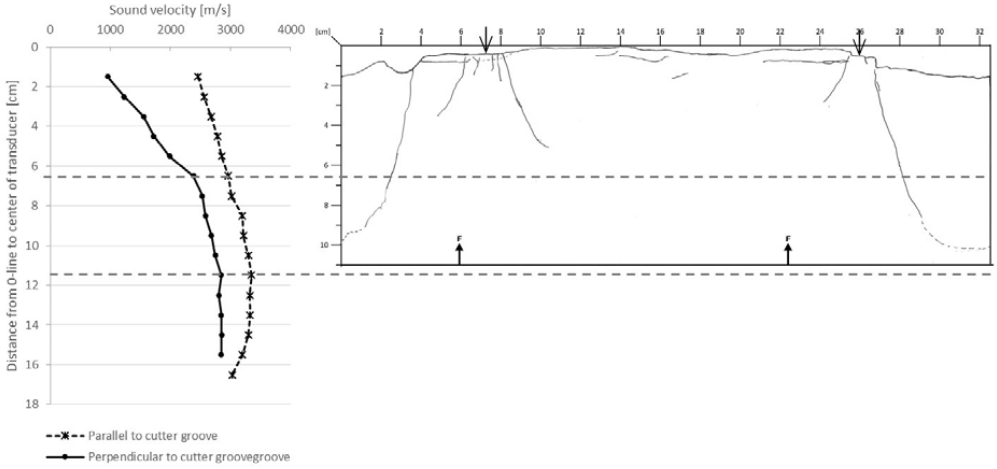

Figure H1.2: Sound velocity measurements and digital foldout of R_1184_1-2_22.

R_1184_1-3_23

Category based on correlation between the measured sound velocity profiles and the detected cracks:	1.1
Category based on the shape of the sound velocity profiles:	2.2
Category based on the differences between the sound velocity measurements parallel and perpendicular to the cutter groove:	3.1
Additional information: There is a change in geology at 6.5 cm. Low measured sound velocities compared to the other cores.	

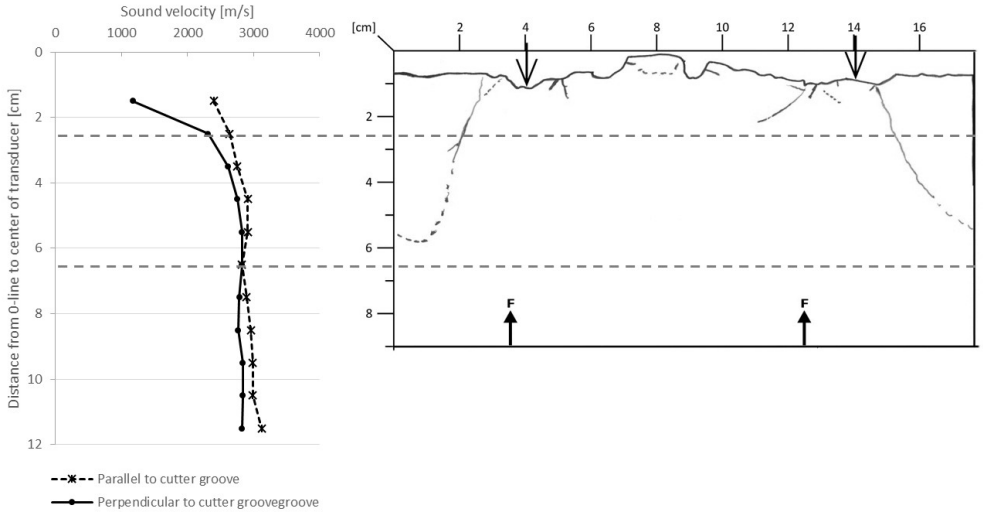

Figure H1.3: Sound velocity measurements and digital foldout of R_1184_1-3_23.

R_1184_1-4_24

Category based on correlation between the measured sound velocity profiles and the detected cracks:	1.2
Category based on the shape of the sound velocity profiles:	2.2
Category based on the differences between the sound velocity measurements parallel and perpendicular to the cutter groove:	3.1
Additional information: Low measured sound velocities compared to the other cores.	

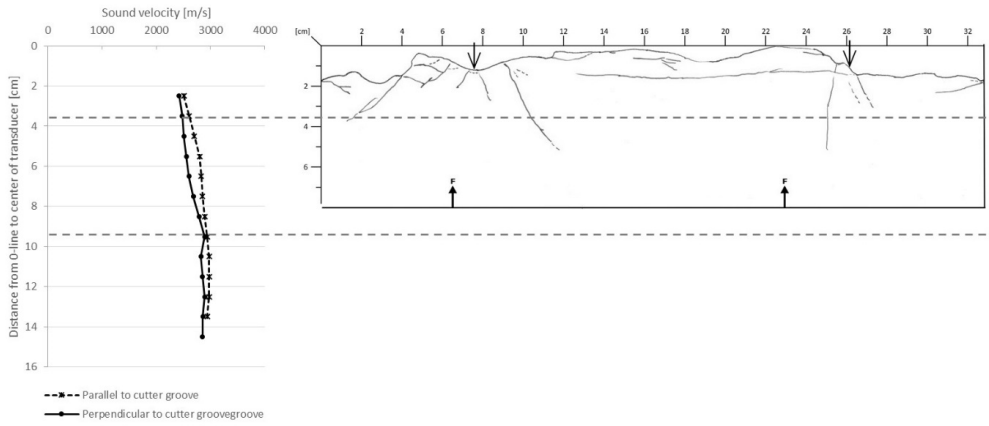

Figure H1.4: Sound velocity measurements and digital foldout of R_1184_1-4_24.

R_1184_1-5_25

Category based on correlation between the measured sound velocity profiles and the detected cracks:	1.3
Category based on the shape of the sound velocity profiles:	2.3
Category based on the differences between the sound velocity measurements parallel and perpendicular to the cutter groove:	3.1
Additional information: Not possible to measure perpendicular to the cutter groove in the upper three centimeters due to uneven surface of the core sampel. p	

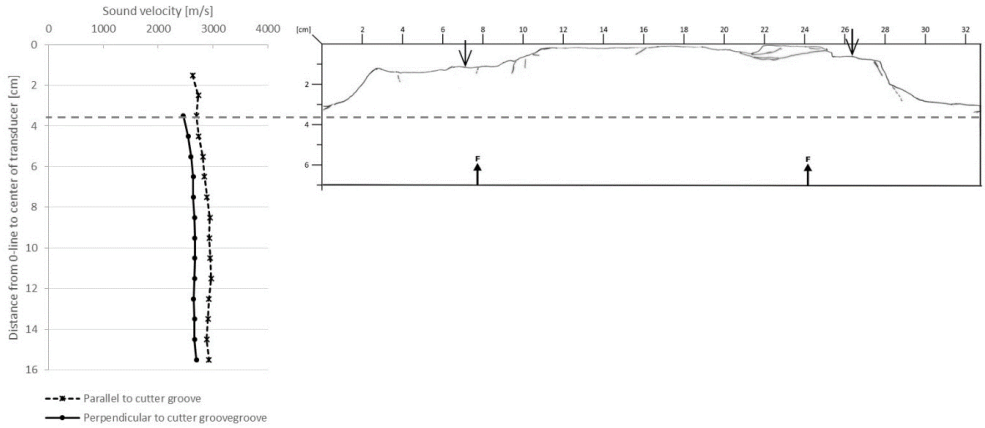

Figure H1.5: Sound velocity measurements and digital foldout of R_1184_1-5_25.

H1.2 Chainage 3112

R_3112_1-2_22

Category based on correlation between the measured sound velocity profiles and the detected cracks:	1.3
Category based on the shape of the sound velocity profiles:	2.1
Category based on the differences between the sound velocity measurements parallel and perpendicular to the cutter groove:	3.1
Additional information: No additional information	

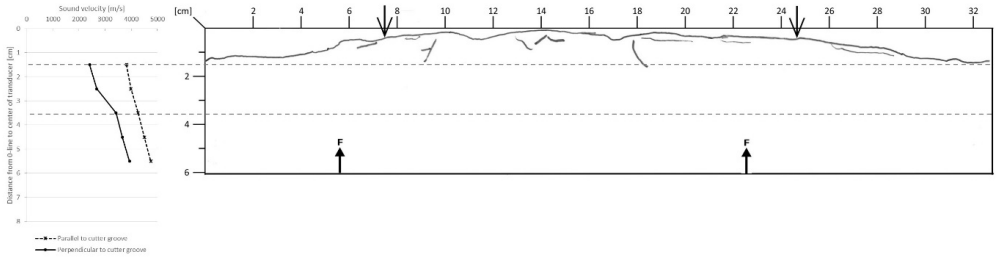

Figure H1.6: Sound velocity measurements and digital foldout of R_3112_1-2_22.

R_3112_1-3_23

Category based on correlation between the measured sound velocity profiles and the detected cracks:	1.2
Category based on the shape of the sound velocity profiles:	2.2
Category based on the differences between the sound velocity measurements parallel and perpendicular to the cutter groove:	3.1
Additional information: No additional information	

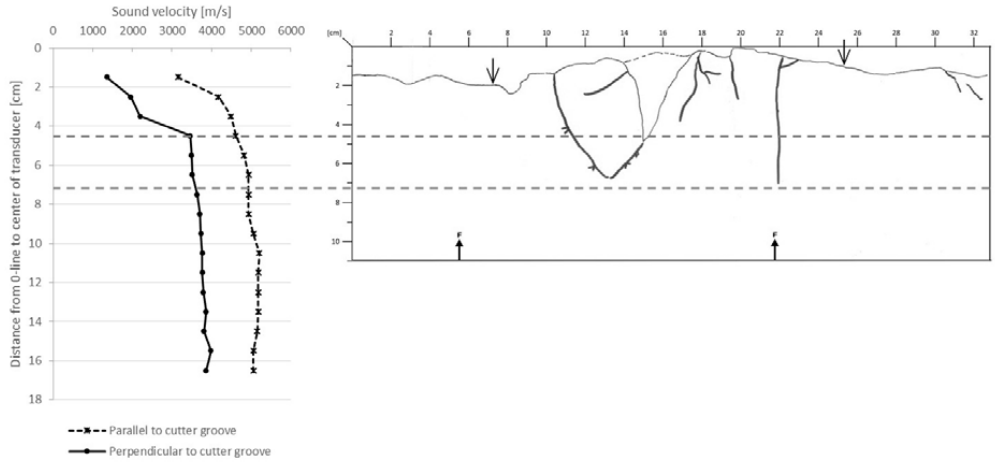

Figure H1.7: Sound velocity measurements and digital foldout of R_3112_1-3_23.

R_3112_1-4_24

Category based on correlation between the measured sound velocity profiles and the detected cracks:	1.1
Category based on the shape of the sound velocity profiles:	2.2
Category based on the differences between the sound velocity measurements parallel and perpendicular to the cutter groove:	3.1
Additional information: No additional information	

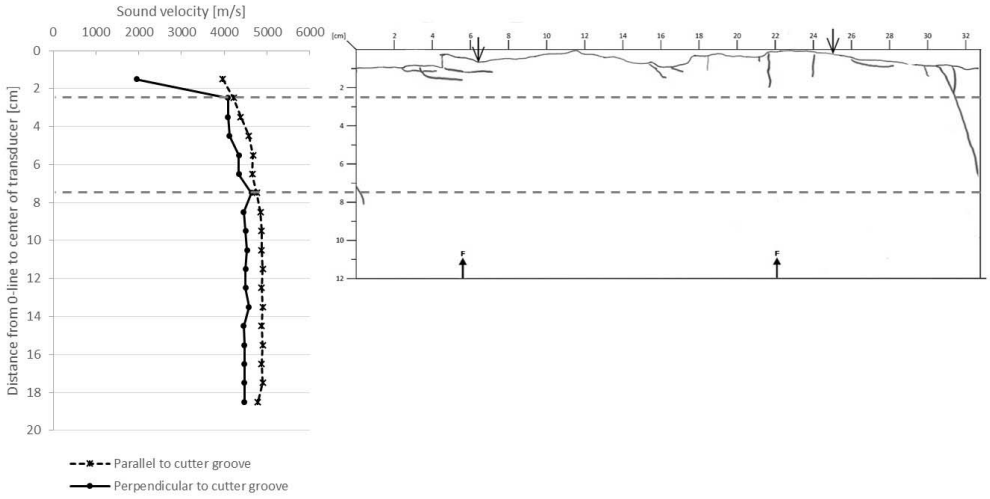

Figure H1.8: Sound velocity measurements and digital foldout of R_3112_1-4_24.

R_3112_1-5_25

Category based on correlation between the measured sound velocity profiles and the detected cracks:	1.2
Category based on the shape of the sound velocity profiles:	2.1
Category based on the differences between the sound velocity measurements parallel and perpendicular to the cutter groove:	3.1
Additional information: No additional information	

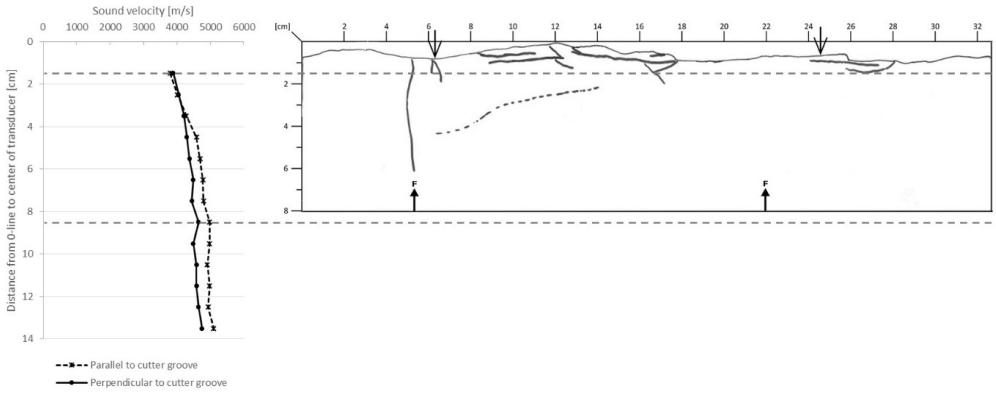

Figure H1.9: Sound velocity measurements and digital foldout of R_3112_1-5_25.

R_3112_3-1_21

Category based on correlation between the measured sound velocity profiles and the detected cracks:	1.2
Category based on the shape of the sound velocity profiles:	2.1
Category based on the differences between the sound velocity measurements parallel and perpendicular to the cutter groove:	3.1
Additional information: No additional information	

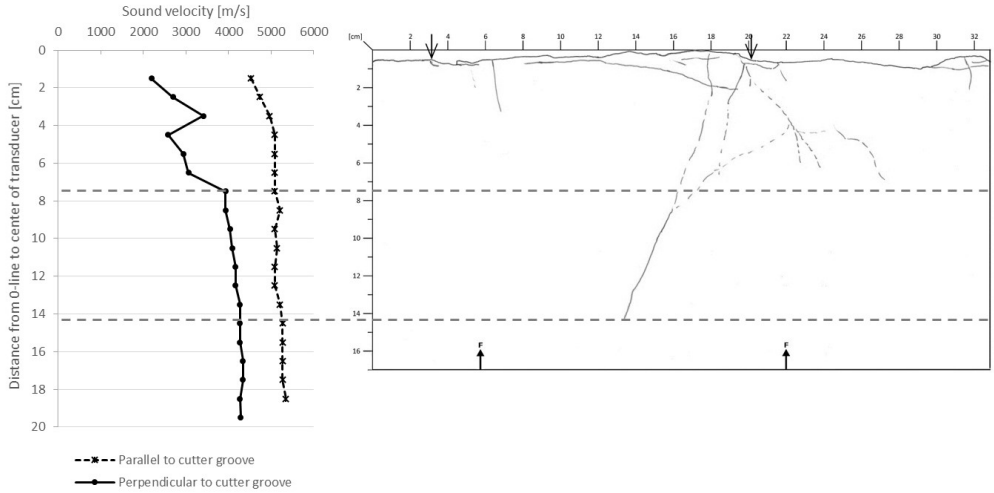

Figure H1.10: Sound velocity measurements and digital foldout of R_3112_3-1_21.

R_3112_3-2_22

Category based on correlation between the measured sound velocity profiles and the detected cracks:	1.1
Category based on the shape of the sound velocity profiles:	2.2
Category based on the differences between the sound velocity measurements parallel and perpendicular to the cutter groove:	3.1
Additional information: No additional information	

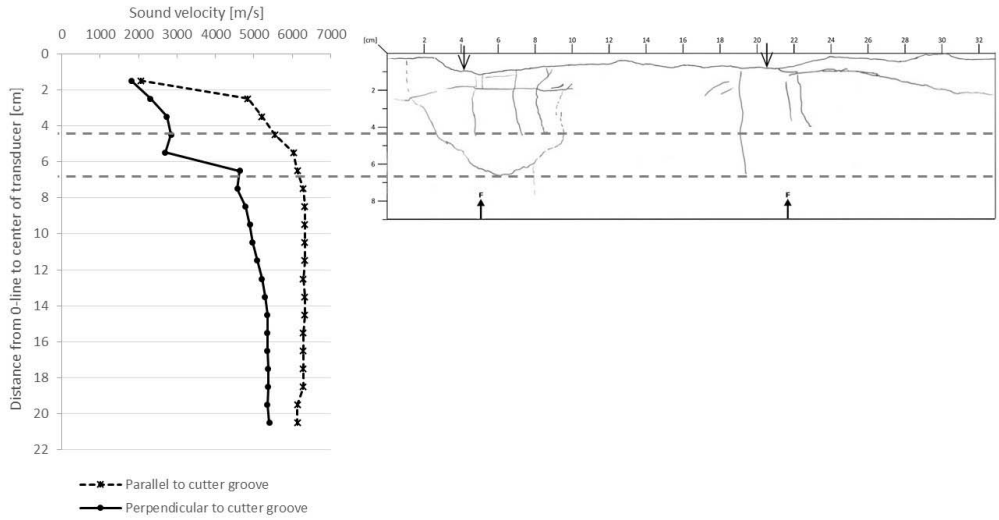

Figure H1.11: Sound velocity measurements and digital foldout of R_3112_3-2_22.

R_3112_3-3_23

Category based on correlation between the measured sound velocity profiles and the detected cracks:	1.2
Category based on the shape of the sound velocity profiles:	2.2
Category based on the differences between the sound velocity measurements parallel and perpendicular to the cutter groove:	3.2
Additional information: No additional information	

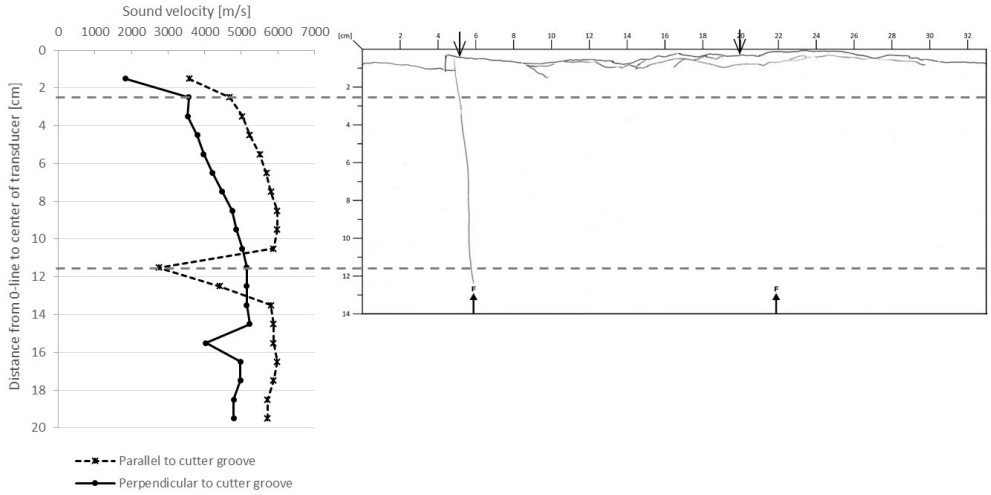

Figure H1.12: Sound velocity measurements and digital foldout of R_3112_3-3_23.

R_3112_3-4_24

Category based on correlation between the measured sound velocity profiles and the detected cracks:	1.3
Category based on the shape of the sound velocity profiles:	2.4
Category based on the differences between the sound velocity measurements parallel and perpendicular to the cutter groove:	3.1
Additional information: Good correlation in the top of the core sample	

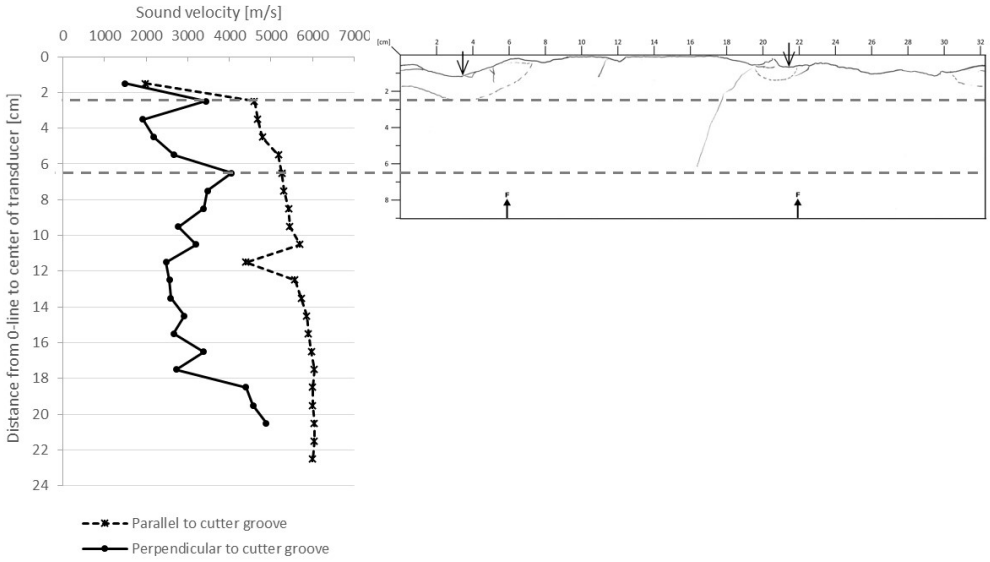

Figure H1.13: Sound velocity measurements and digital foldout of R_3112_3-4_24.

R_3112_4-1_21

Category based on correlation between the measured sound velocity profiles and the detected cracks:	1.1
Category based on the shape of the sound velocity profiles:	2.2
Category based on the differences between the sound velocity measurements parallel and perpendicular to the cutter groove:	3.1
Additional information: No additional information	

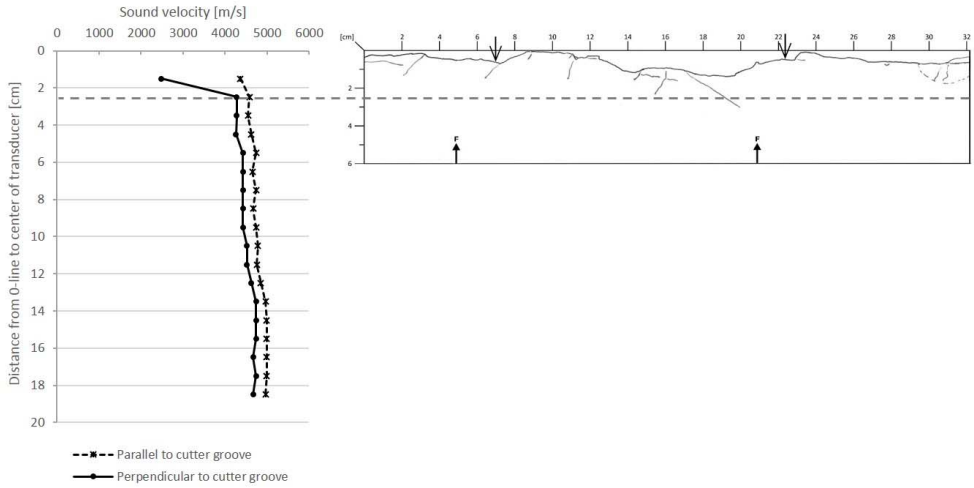

Figure H1.14: Sound velocity measurements and digital foldout of R_3112_4-1_21.

R_3112_4-2_22

Category based on correlation between the measured sound velocity profiles and the detected cracks:	1.1
Category based on the shape of the sound velocity profiles:	2.2
Category based on the differences between the sound velocity measurements parallel and perpendicular to the cutter groove:	3.1
Additional information: No additional information	

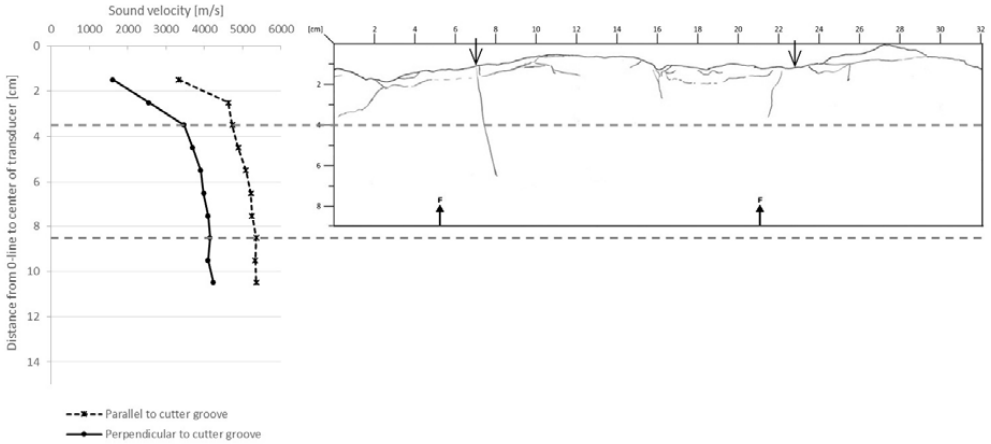

Figure H1.15: Sound velocity measurements and digital foldout of R_3112_4-2_22.

R_3112_4-3_23

Category based on correlation between the measured sound velocity profiles and the detected cracks:	1.2
Category based on the shape of the sound velocity profiles:	2.2
Category based on the differences between the sound velocity measurements parallel and perpendicular to the cutter groove:	3.4
Additional information: No additional information	

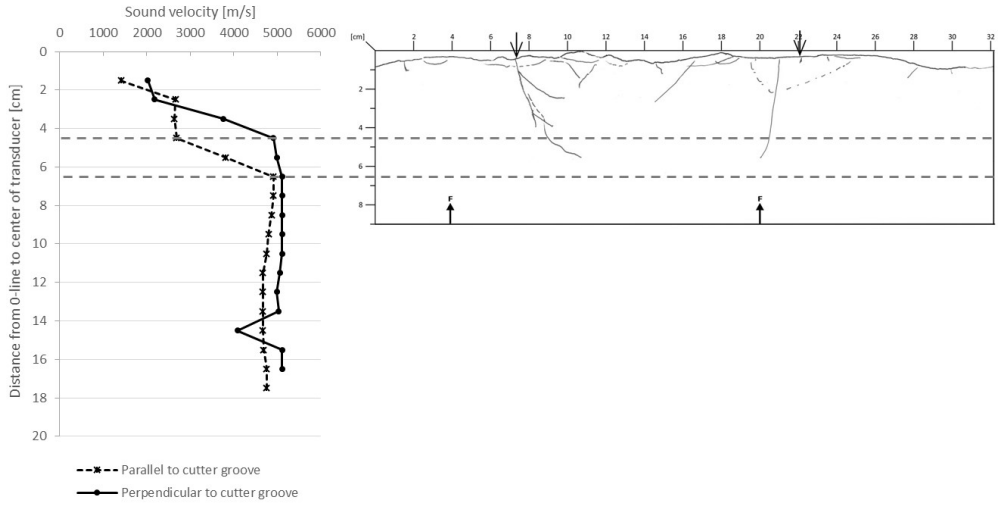

Figure H1.16: Sound velocity measurements and digital foldout of R_3112_4-3_23.

R_3112_4-4_24

Category based on correlation between the measured sound velocity profiles and the detected cracks:	1.1
Category based on the shape of the sound velocity profiles:	2.2
Category based on the differences between the sound velocity measurements parallel and perpendicular to the cutter groove:	3.3
Additional information: No additional information	

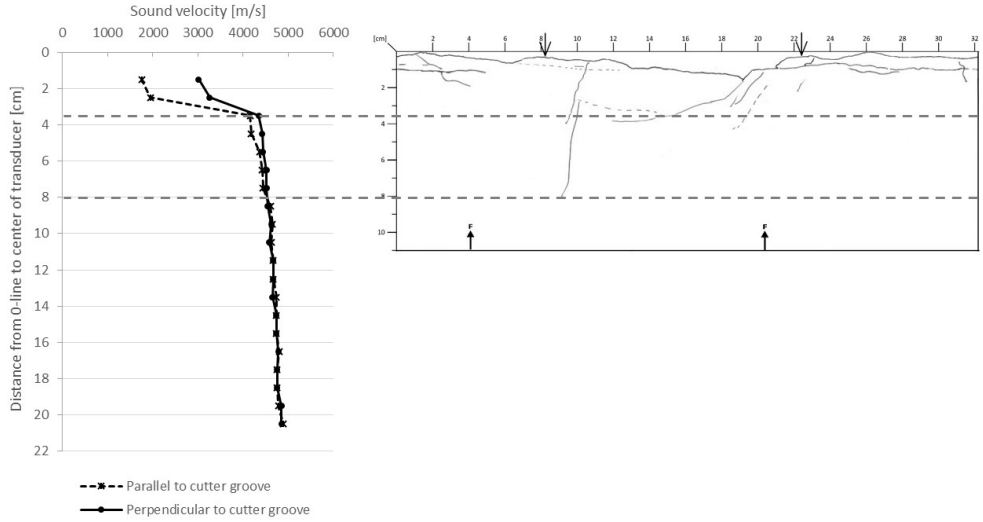

Figure H1.17: Sound velocity measurements and digital foldout of R_3112_4-4_24.

R_3112_5-1_27

Category based on correlation between the measured sound velocity profiles and the detected cracks:	1.2
Category based on the shape of the sound velocity profiles:	2.3
Category based on the differences between the sound velocity measurements parallel and perpendicular to the cutter groove:	3.1
Additional information: Correlation is good in the top of the core sample	

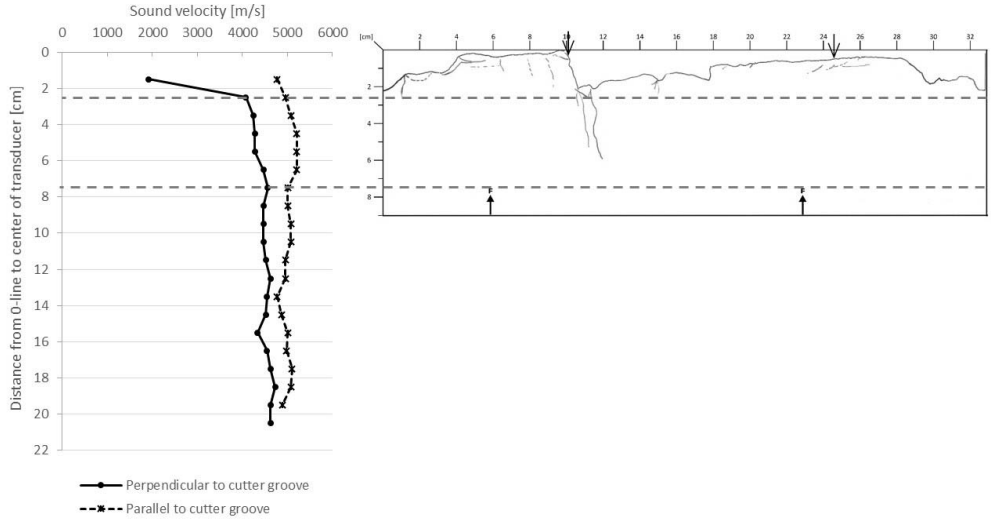

Figure H1.18: Sound velocity measurements and digital foldout of R_3112_5-1_27.

R_3112_5-2_28

Category based on correlation between the measured sound velocity profiles and the detected cracks:	1.2
Category based on the shape of the sound velocity profiles:	2.1
Category based on the differences between the sound velocity measurements parallel and perpendicular to the cutter groove:	3.1
Additional information: No additional information	

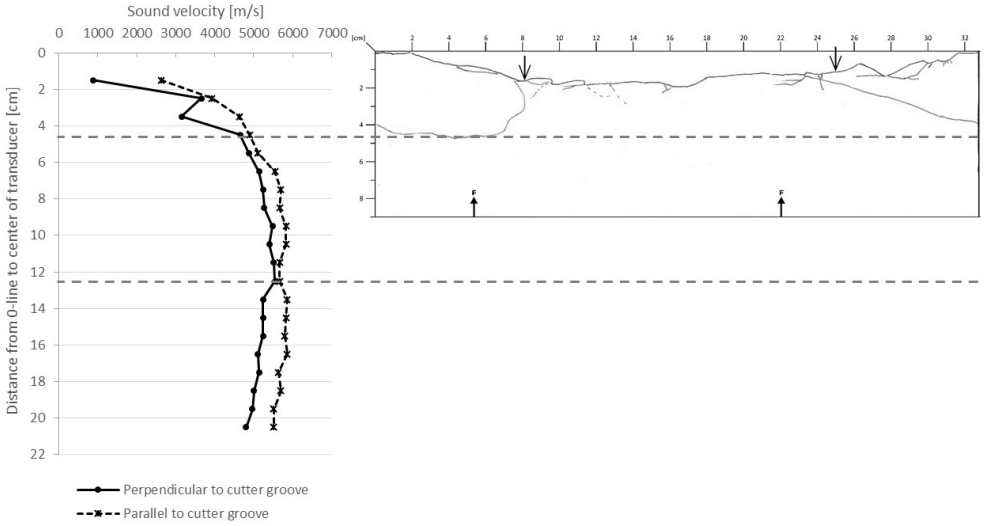

Figure H1.19: Sound velocity measurements and digital foldout of R_3112_5-2_28.

R_3112_5-3_29

Category based on correlation between the measured sound velocity profiles and the detected cracks:	1.3
Category based on the shape of the sound velocity profiles:	2.4
Category based on the differences between the sound velocity measurements parallel and perpendicular to the cutter groove:	3.3
Additional information: No additional information	

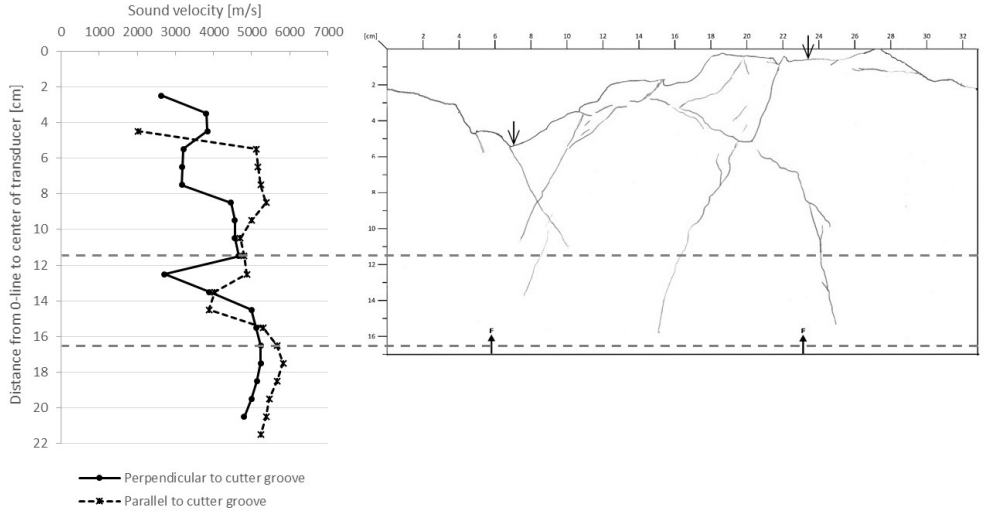

Figure H1.20: Sound velocity measurements and digital foldout of R_3112_5-3_29.

Appendix I

APPENDIX I
SURFACES AND CRACK PATTERNS IN THE CORE SAMPLES FROM THE NEDRE RØSSÅGA HEADRACE TUNNEL

List of contents

List of figures

I1 Surfaces

The digitalized foldouts are the basis for a sectioning that shows the cracking pattern and the surface of the core sample in relation to the cutter groove.

All sections are seen counter the direction of rotation.

I1.1 Chainage 1184

R_1184_1-1_21

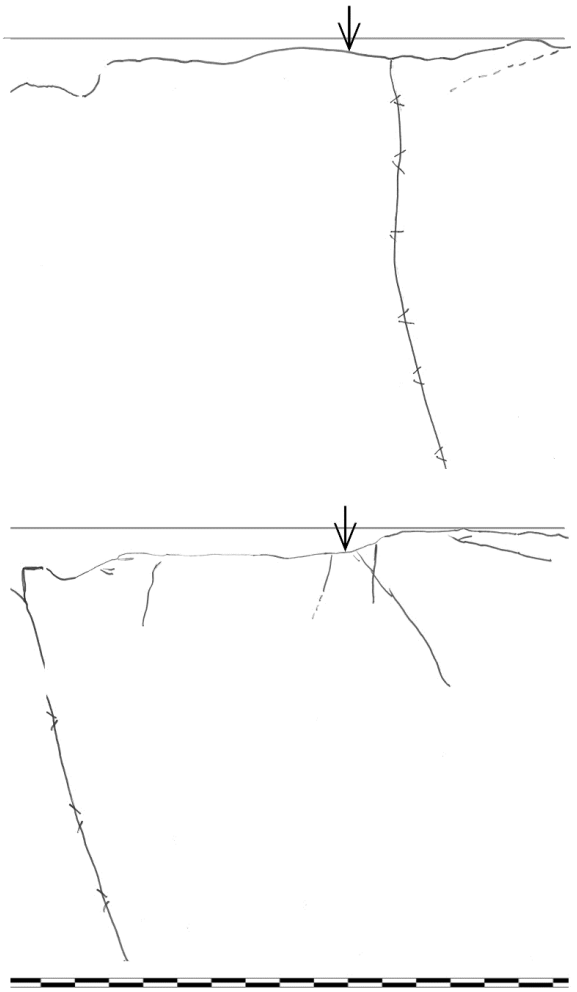

Figure I1.1: Surface and crack pattern under the cutter groove in core sample R_1184_1-1_21.

R_1184_1-2_22

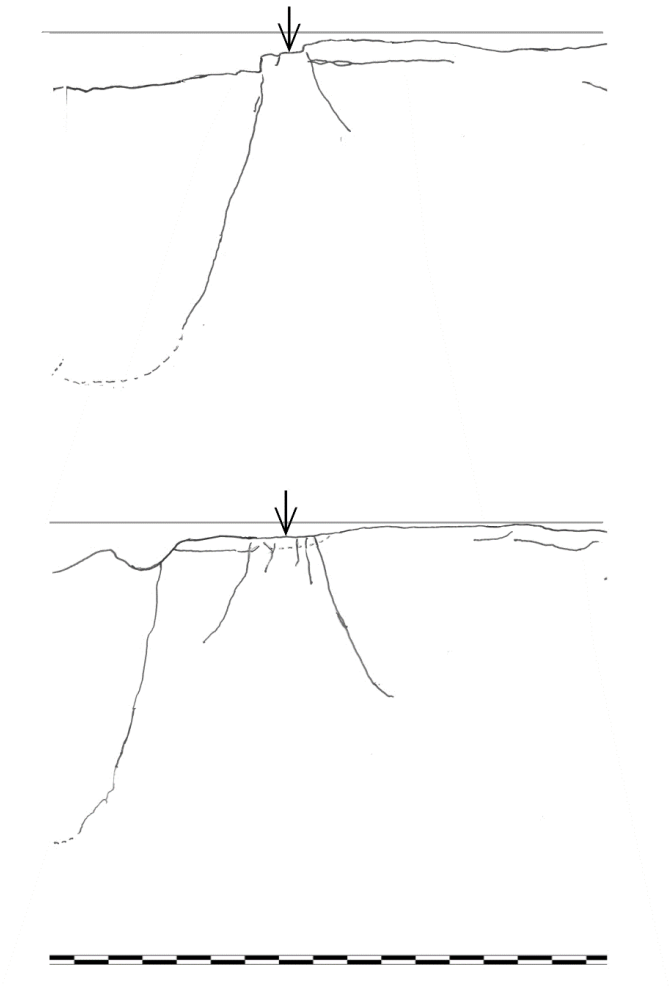

Figure I1.2: Surface and crack pattern under the cutter groove in core sample R_1184_1-2_22.

R_1184_1-3_23

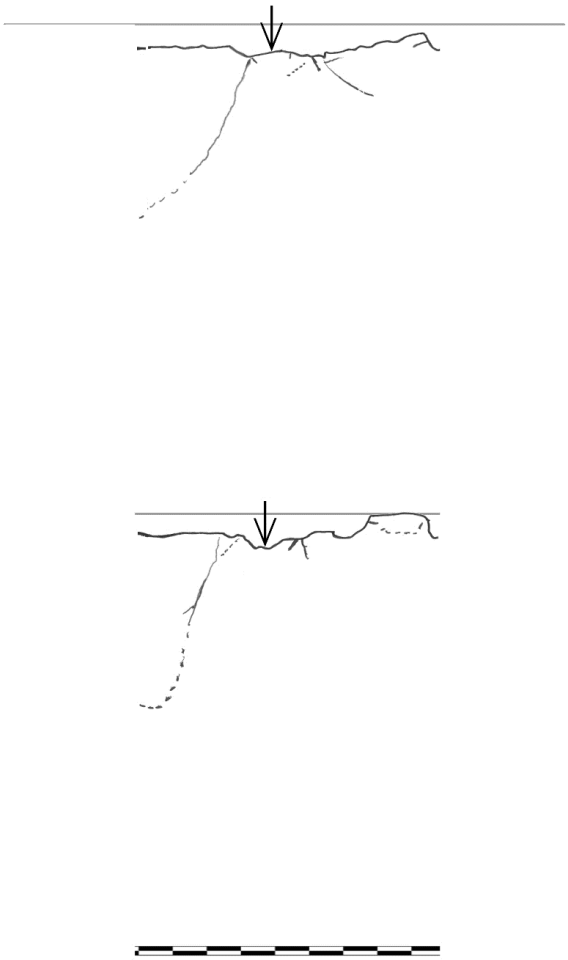

Figure I1.3: Surface and crack pattern under the cutter groove in core sample R_1184_1-3_23.

R_1184_1-4_24

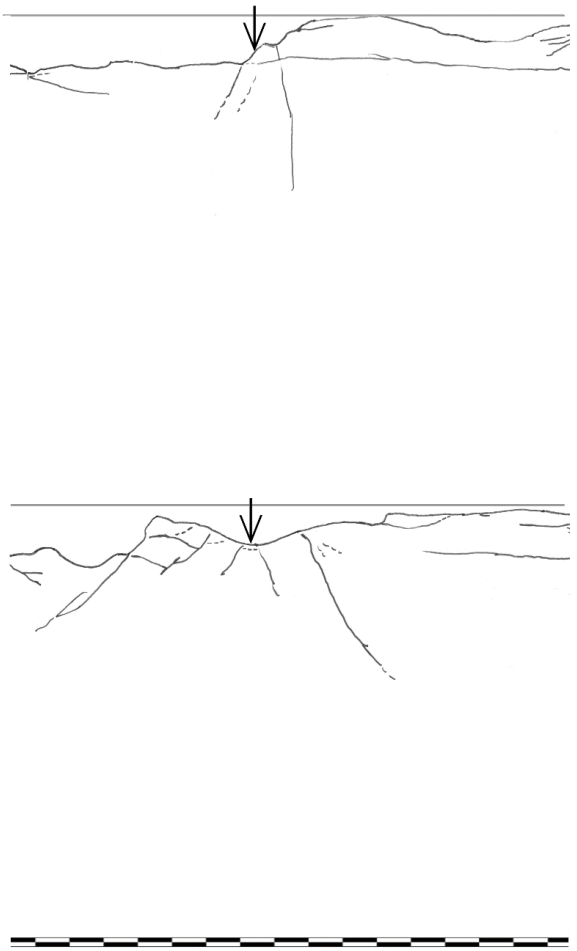

Figure I1.4: Surface and crack pattern under the cutter groove in core sample R_1184_1-4_24.

R_1184_1-5_25

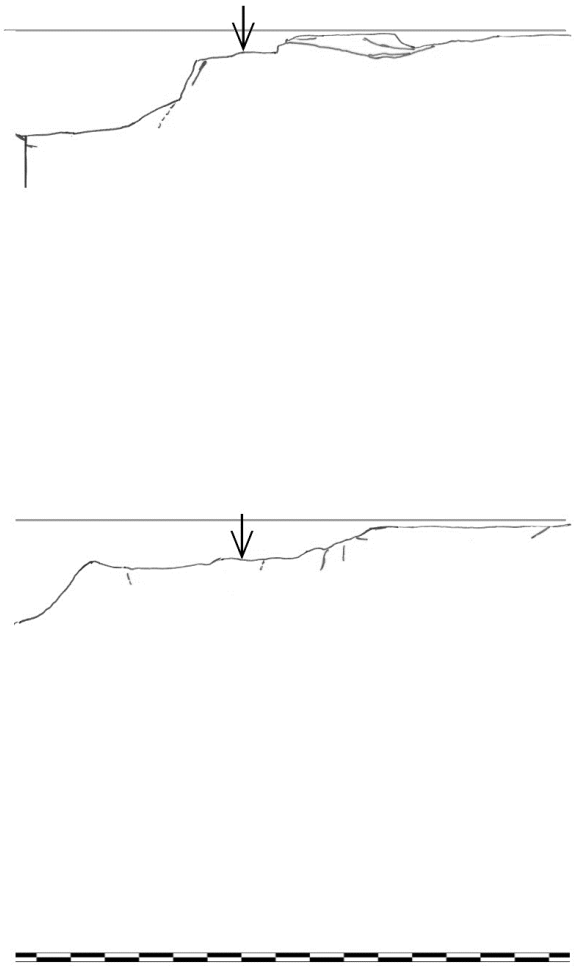

Figure I1.5: Surface and crack pattern under the cutter groove in core sample R_1184_1-5_25.

I1.2 Chainage 3112

R_3112_1-1_21

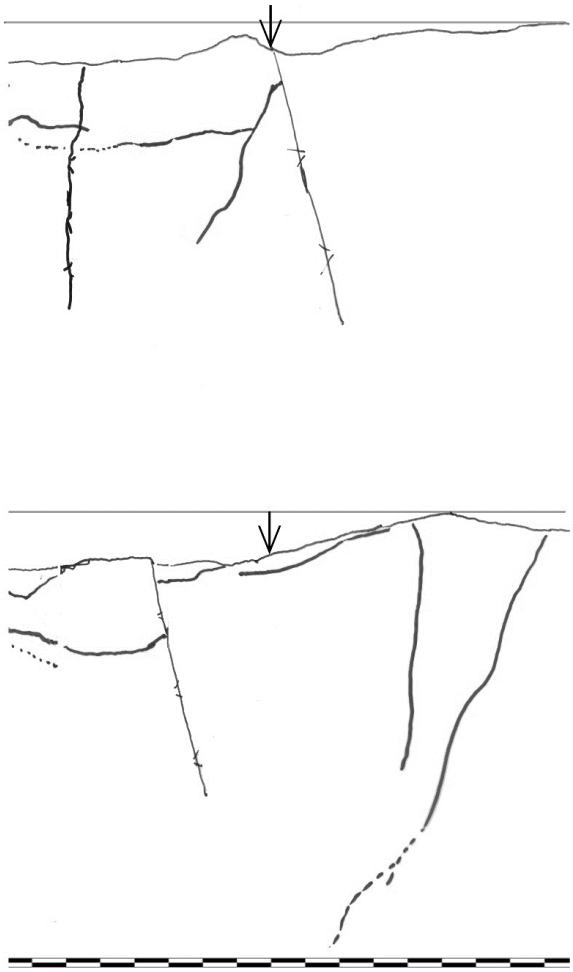

Figure I1.6: Surface and crack pattern under the cutter groove in core sample R_3112_1-1_21.

R_3112_1-2_22

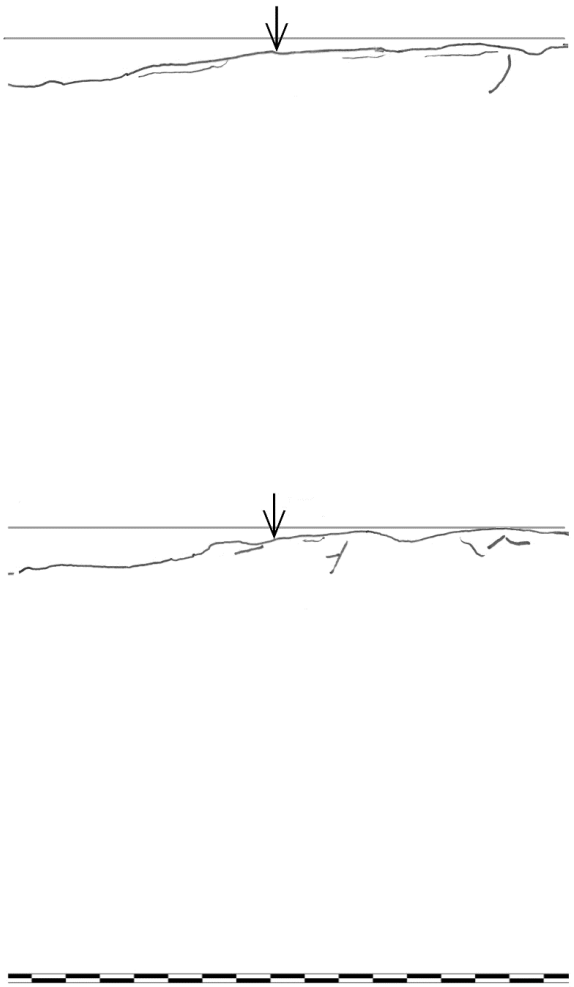

Figure I1.7: Surface and crack pattern under the cutter groove in core sample R_3112_1-2_22.

R_3112_1-3_23

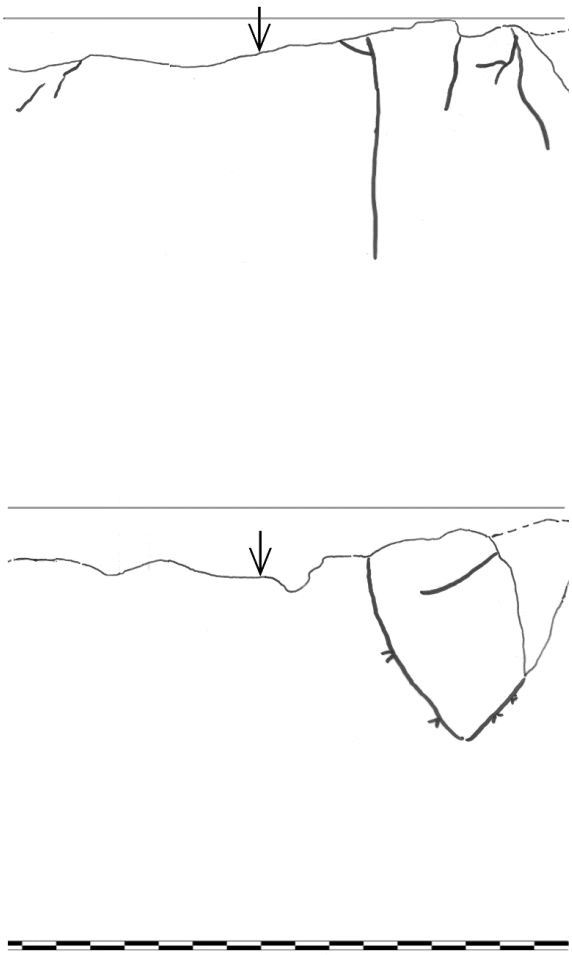

Figure I1.8: Surface and crack pattern under the cutter groove in core sample R_3112_1-3_23.

R_3112_1-4_24

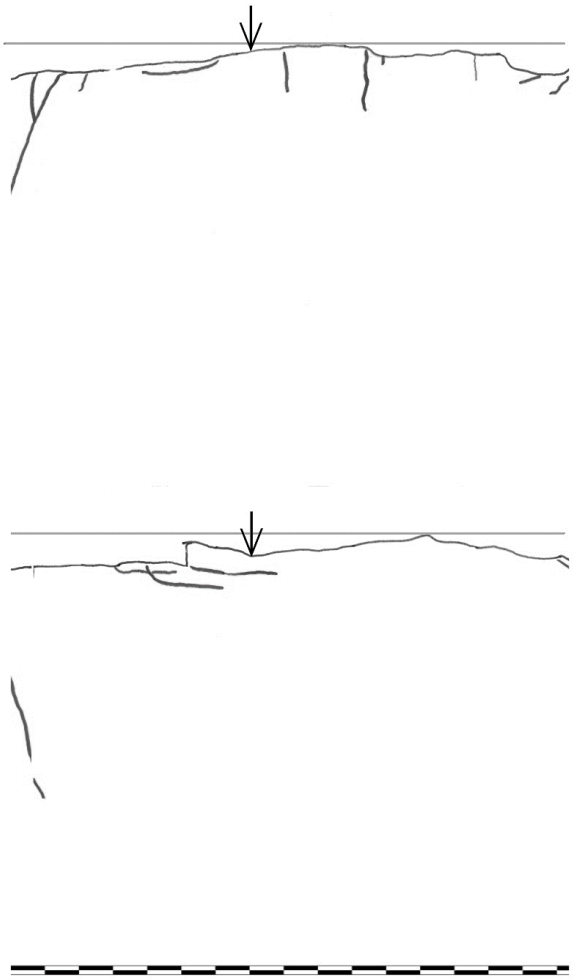

Figure I1.9: Surface and crack pattern under the cutter groove in core sample R_3112_1-4_24.

R_3112_1-5_25

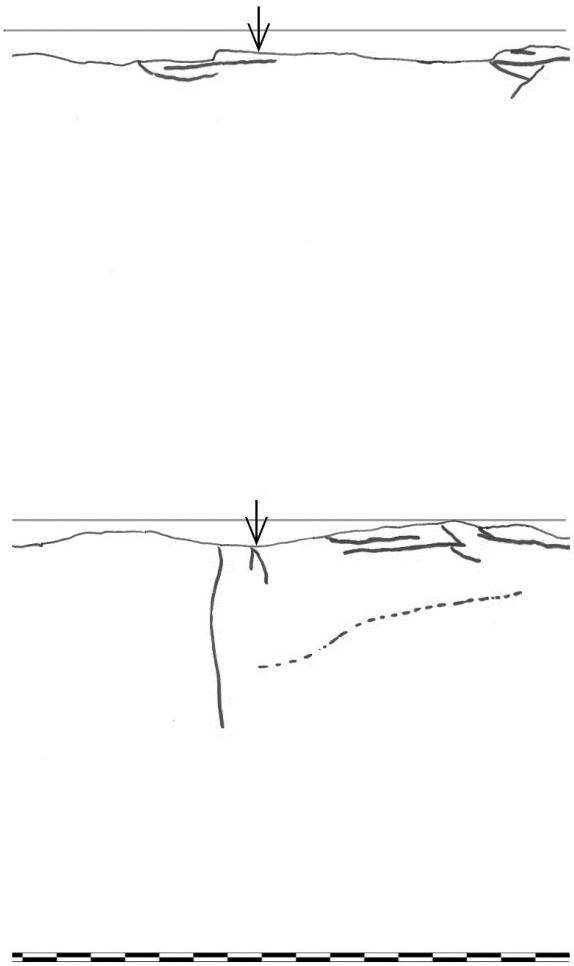

Figure I1.10: Surface and crack pattern under the cutter groove in core sample R_3112_1-5_25.

R_3112_3-1_21

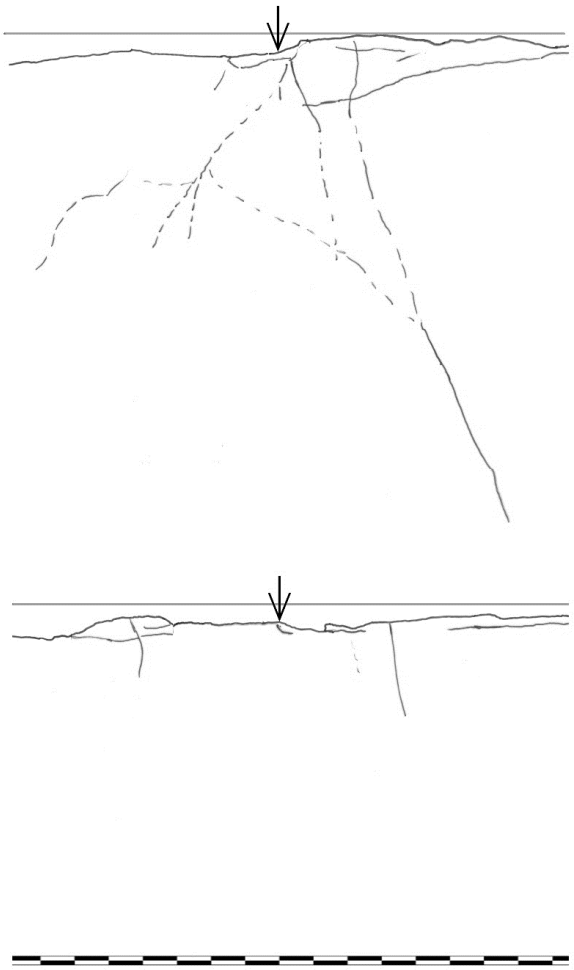

Figure I1.11: Surface and crack pattern under the cutter groove in core sample R_3112_3-1_21.

R_3112_3-2_22

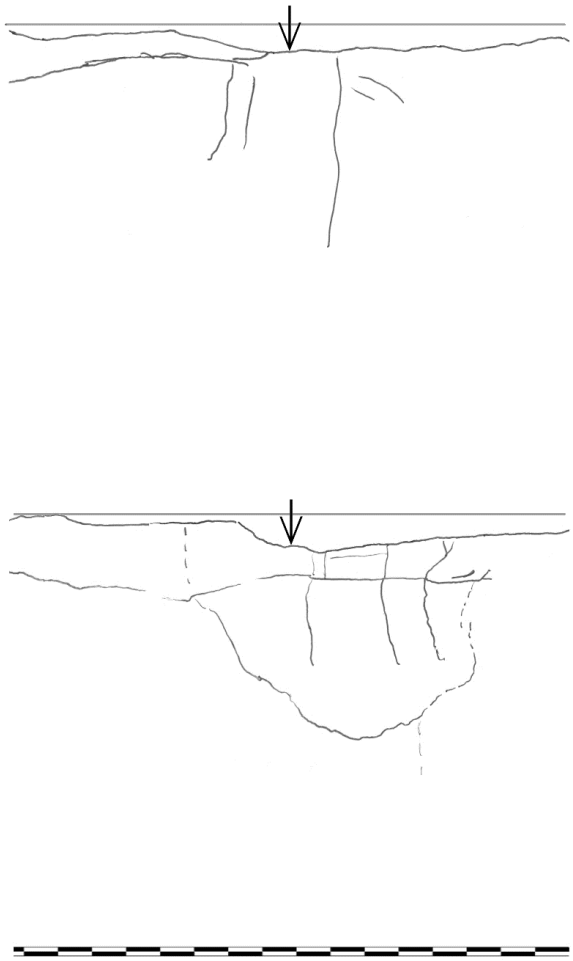

Figure I1.12: Surface and crack pattern under the cutter groove in core sample R_3112_3-2_22.

R_3112_3-3_23

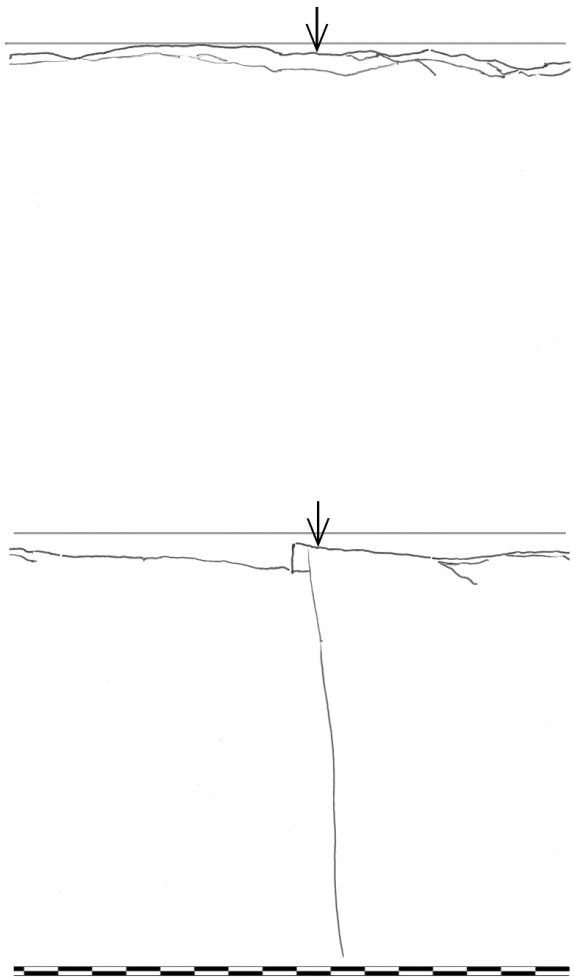

Figure I1.13: Surface and crack pattern under the cutter groove in core sample R_3112_3-3_23.

R_3112_3-4_23

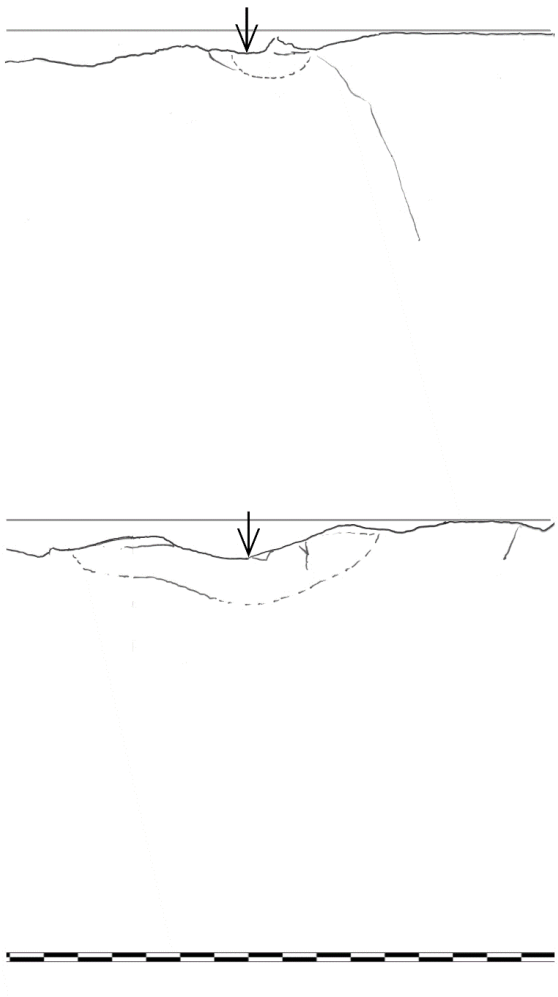

Figure I1.14: Surface and crack pattern under the cutter groove in core sample R_3112_3-4_23.

R_3112_4-1_21

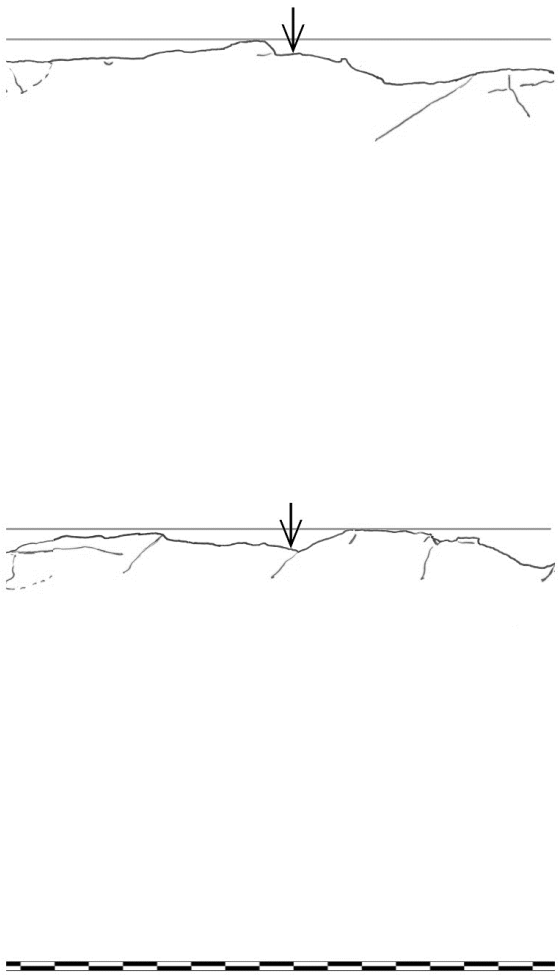

Figure I1.15: Surface and crack pattern under the cutter groove in core sample R_3112_4-1_21.

R_3112_4-2_22

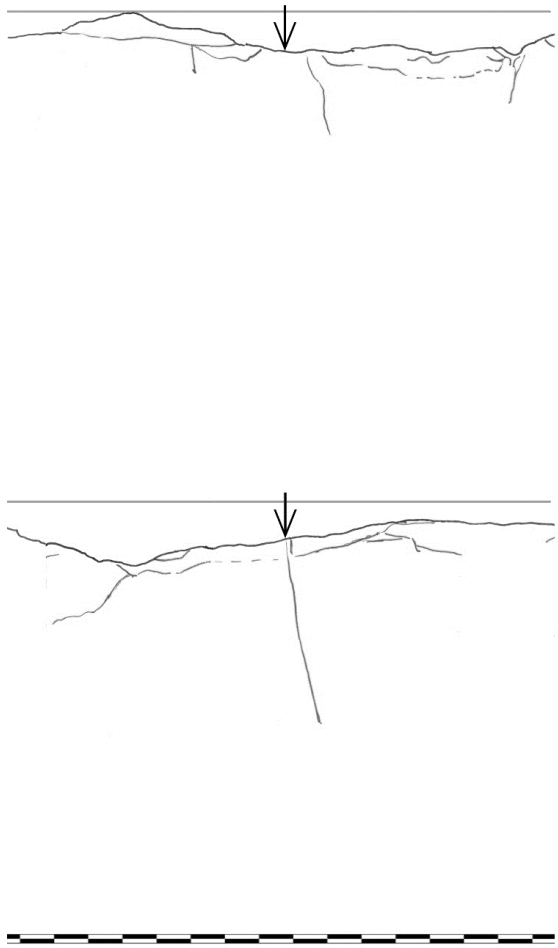

Figure I1.16: Surface and crack pattern under the cutter groove in core sample R_3112_4-2_22.

R_3112_4-3_23

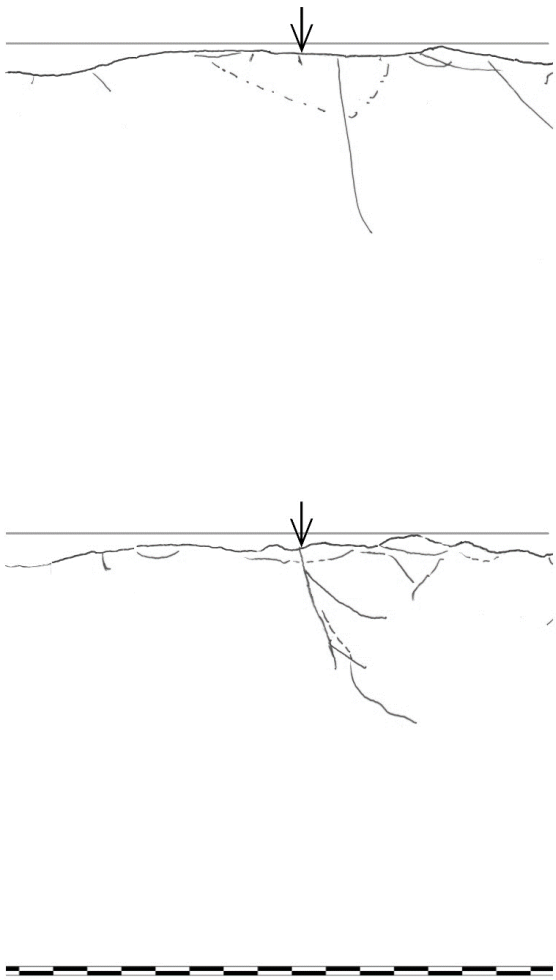

Figure I1.17: Surface and crack pattern under the cutter groove in core sample R_3112_4-3_23.

R_3112_4-4_24

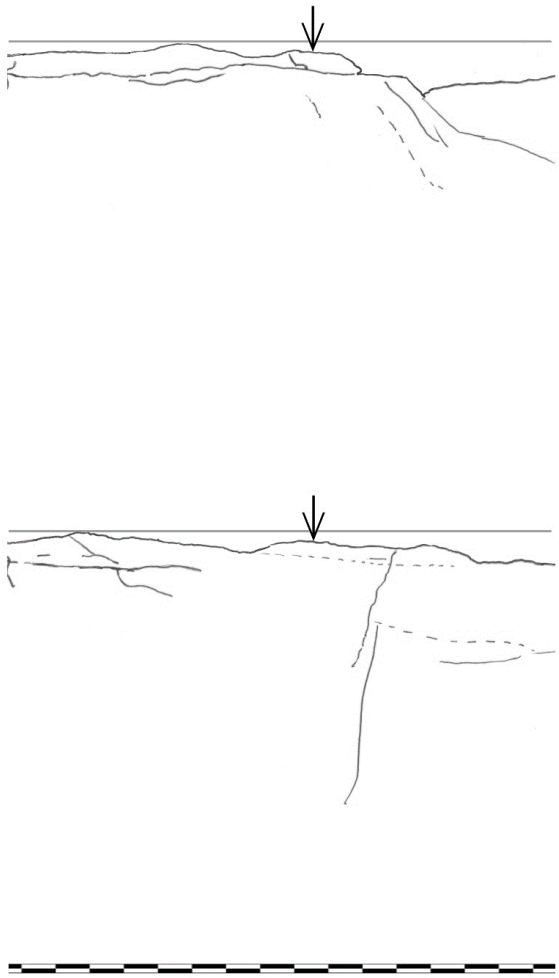

Figure I1.18: Surface and crack pattern under the cutter groove in core sample R_3112_4-4_24.

R_3112_5-1_27

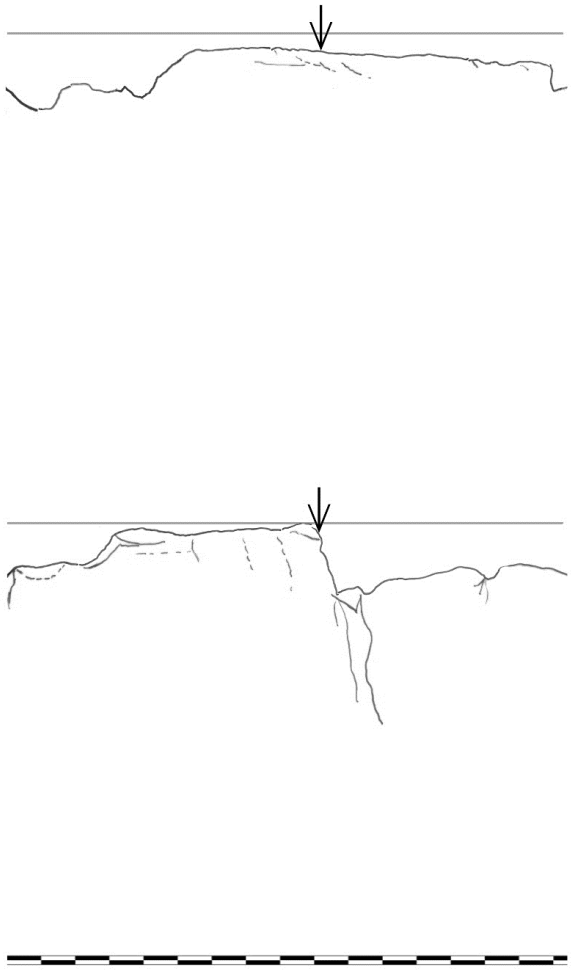

Figure I1.19: Surface and crack pattern under the cutter groove in core sample R_3112_5-1_27.

R_3112_5-2_28

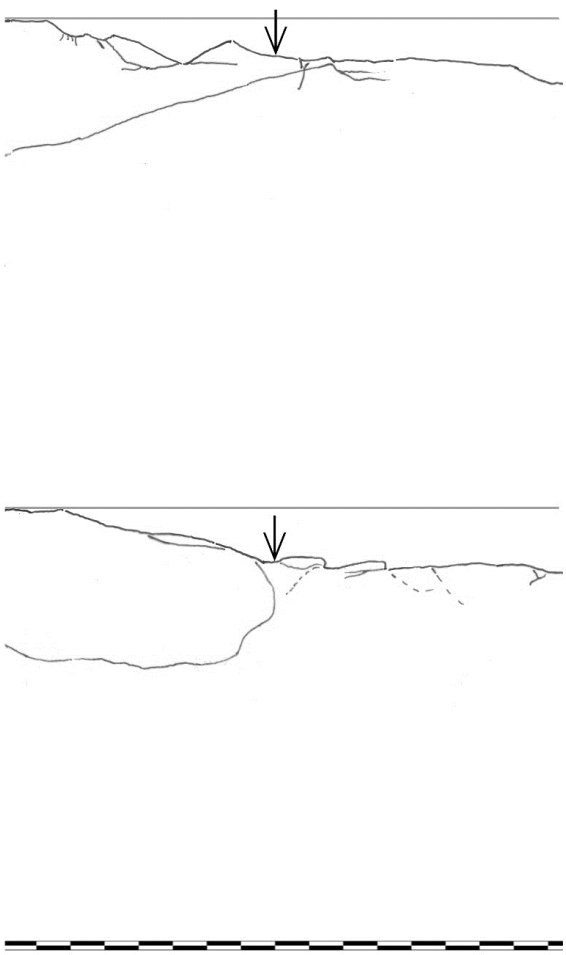

Figure I1.20: Surface and crack pattern under the cutter groove in core sample R_3112_5-2_28.

R_3112_5-3_29

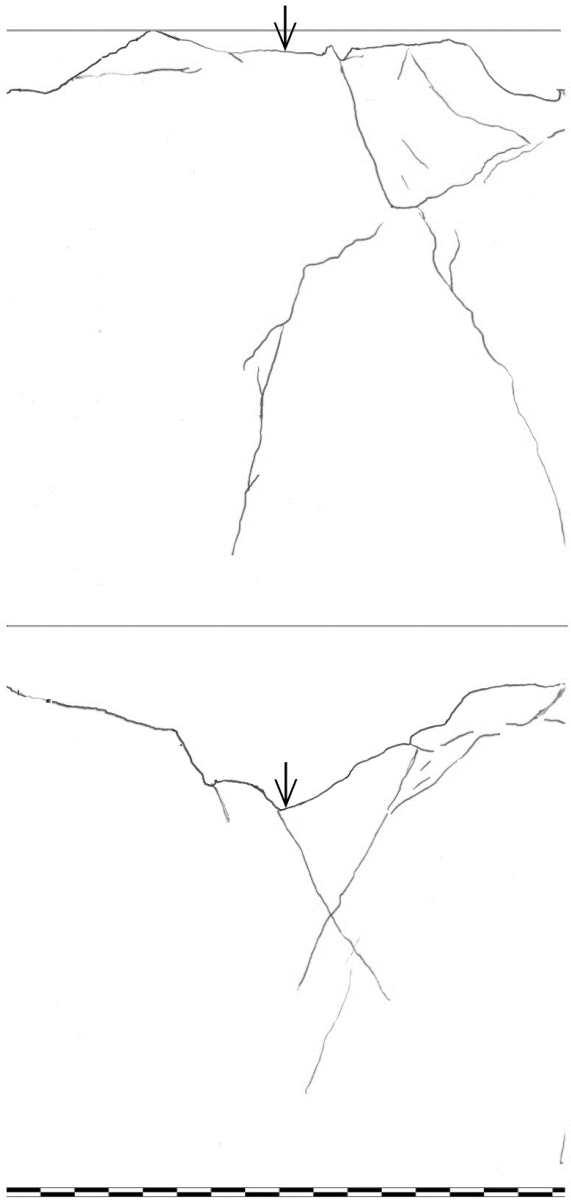

Figure I1.21: Surface and crack pattern under the cutter groove in core sample R_3112_5-3_29.

R_3112_6-1_37

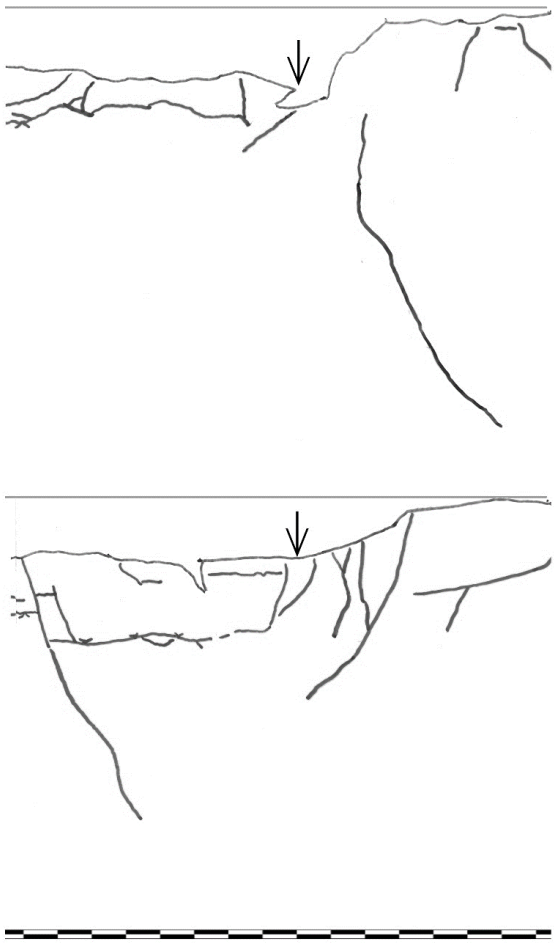

Figure I1.22: Surface and crack pattern under the cutter groove in core sample R_3112_6-1_37.

I1.3 Chainage 5437

R_5437_1-1_21

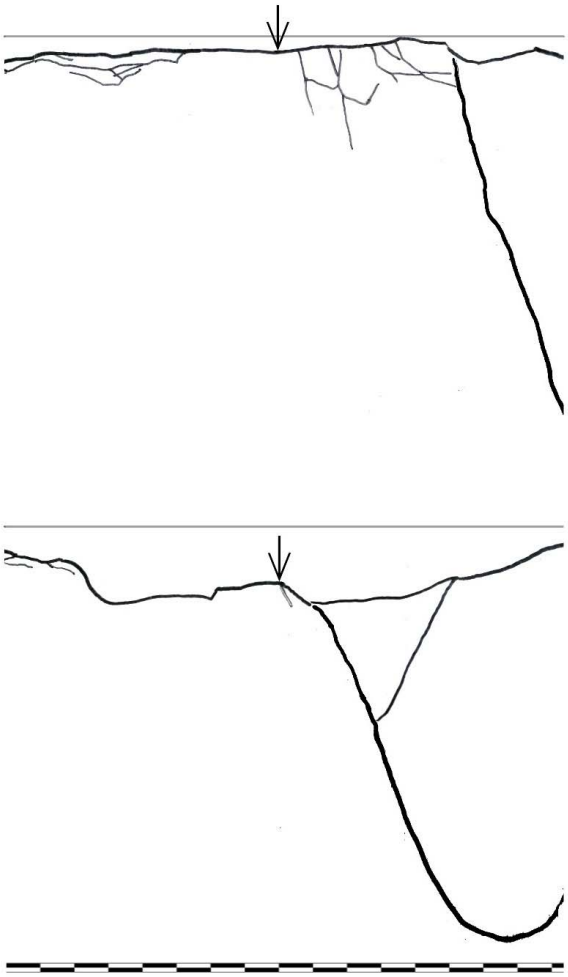

Figure I1.23: Surface and crack pattern under the cutter groove in core sample R_5437_1-1_21.

R_5437_1-2_22

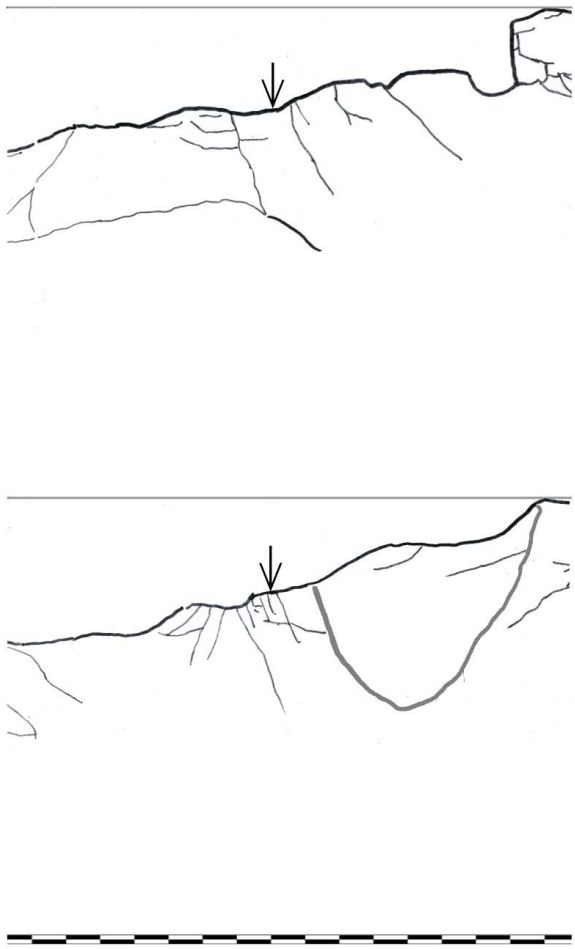

Figure I1.24: Surface and crack pattern under the cutter groove in core sample R_5437_1-2_22.

R_5437_1-3_23

Figure I1.25: Surface and crack pattern under the cutter groove in core sample R_5437_1-3_23.

R_5437_1-4_25

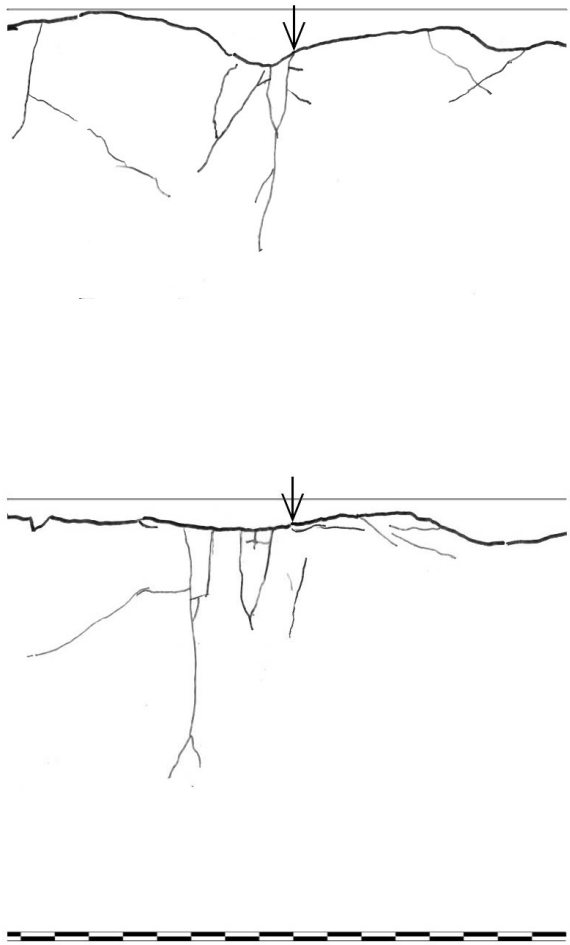

Figure I1.26: Surface and crack pattern under the cutter groove in core sample R_5437_1-4_25.

R_5437_2-1_21

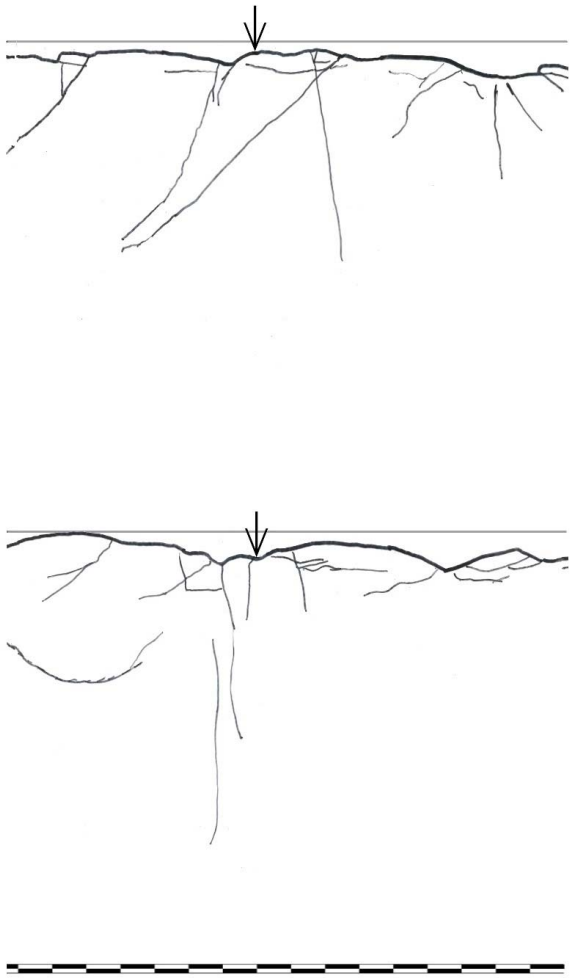

Figure I1.27: Surface and crack pattern under the cutter groove in core sample R_5437_2-1_21.

R_5437_2-2_22

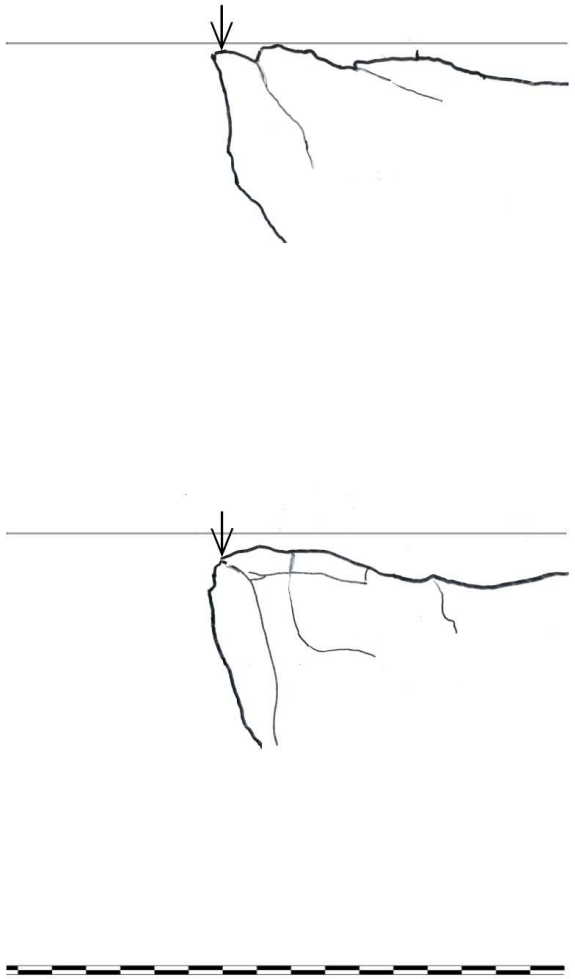

Figure I1.28: Surface and crack pattern under the cutter groove in core sample R_5437_2-2_22.

R_5437_2-3_23

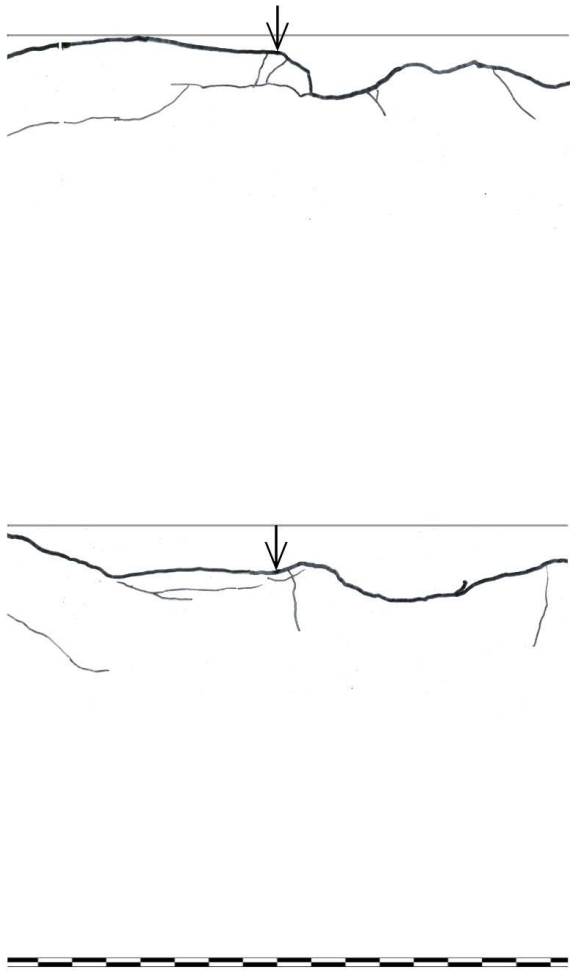

Figure I1.29: Surface and crack pattern under the cutter groove in core sample R_5437_2-3_23.

R_5437_2-4_24

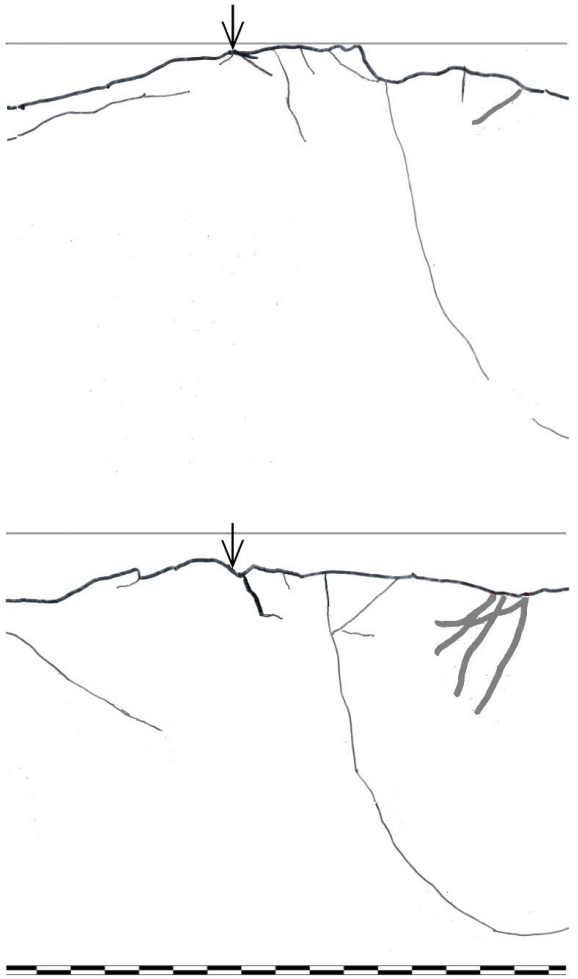

Figure I1.30: Surface and crack pattern under the cutter groove in core sample R_5437_2-4_24.

R_5437_3-1_22

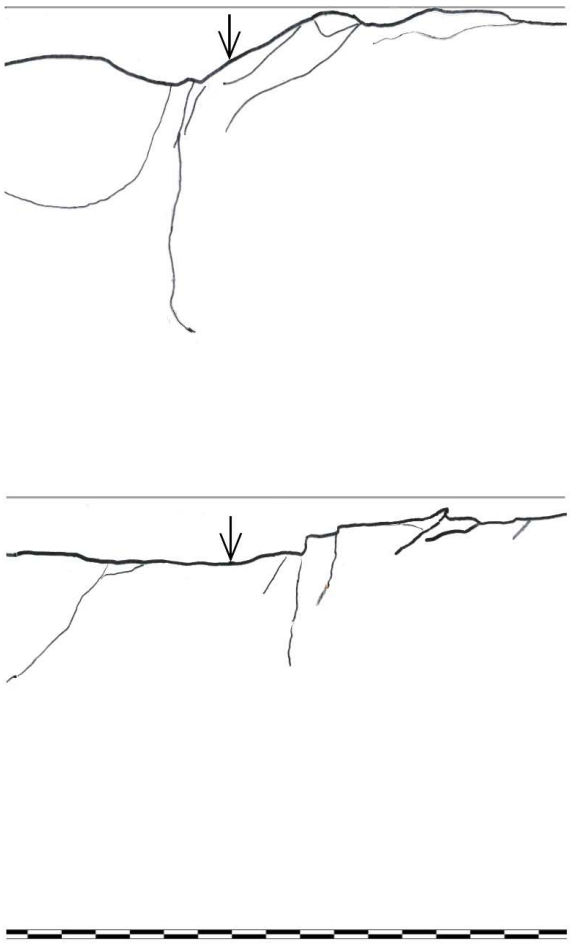

Figure I1.31: Surface and crack pattern under the cutter groove in core sample R_5437_3-1_22.

R_5437_3-2_23

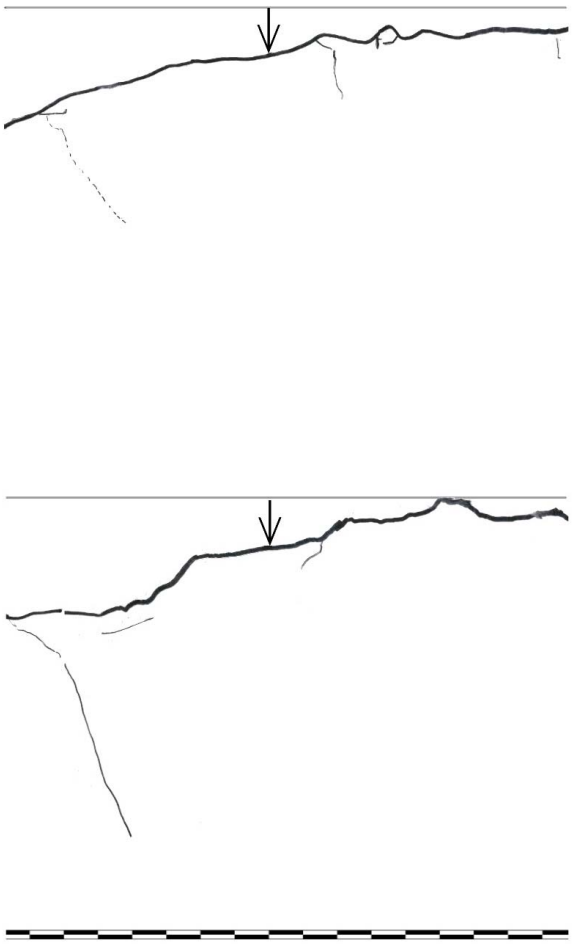

Figure I1.32: Surface and crack pattern under the cutter groove in core sample R_5437_3-2_23.

R_5437_3-3_24

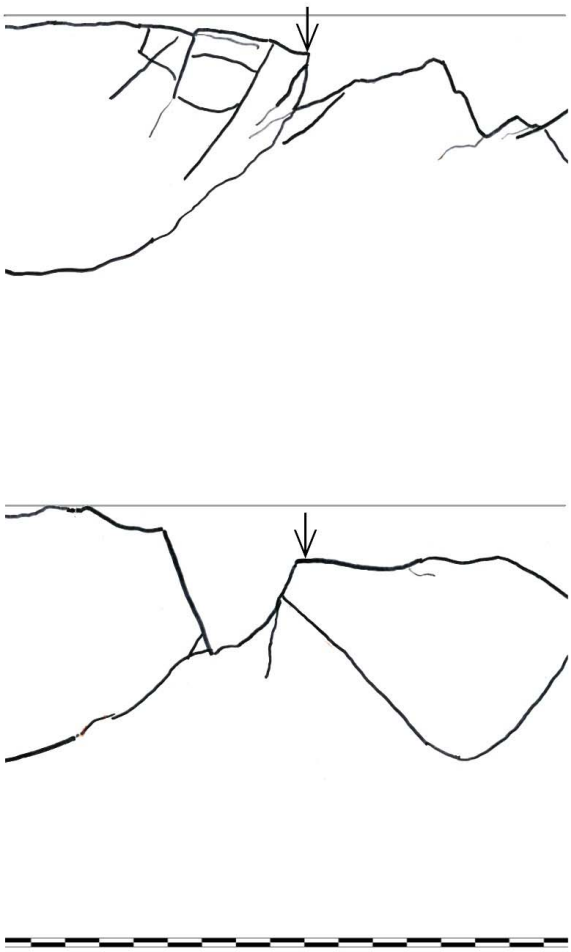

Figure I1.33: Surface and crack pattern under the cutter groove in core sample R_5437_3-3_24.

R_5437_3-4_25

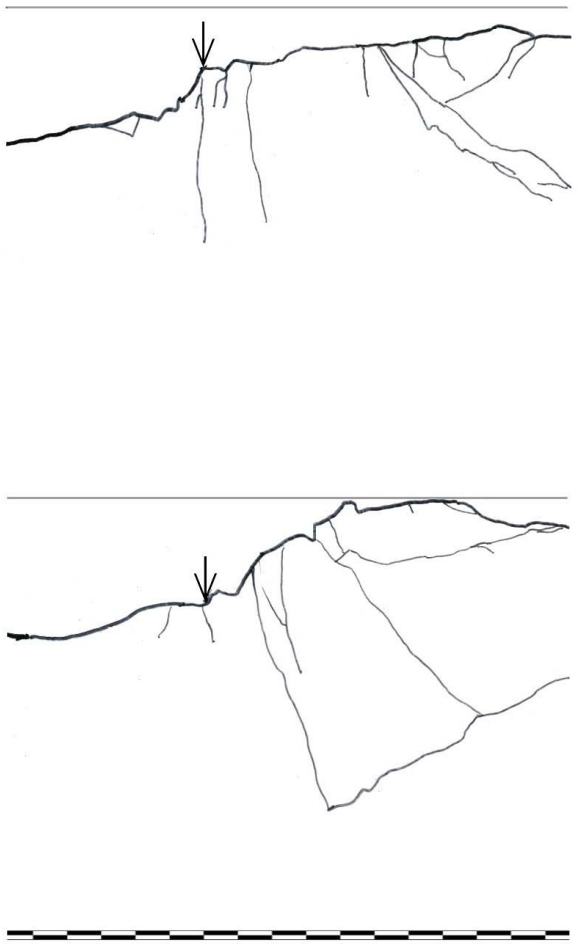

Figure I1.34: Surface and crack pattern under the cutter groove in core sample R_5437_3-4_25.

R_5437_4-1_21

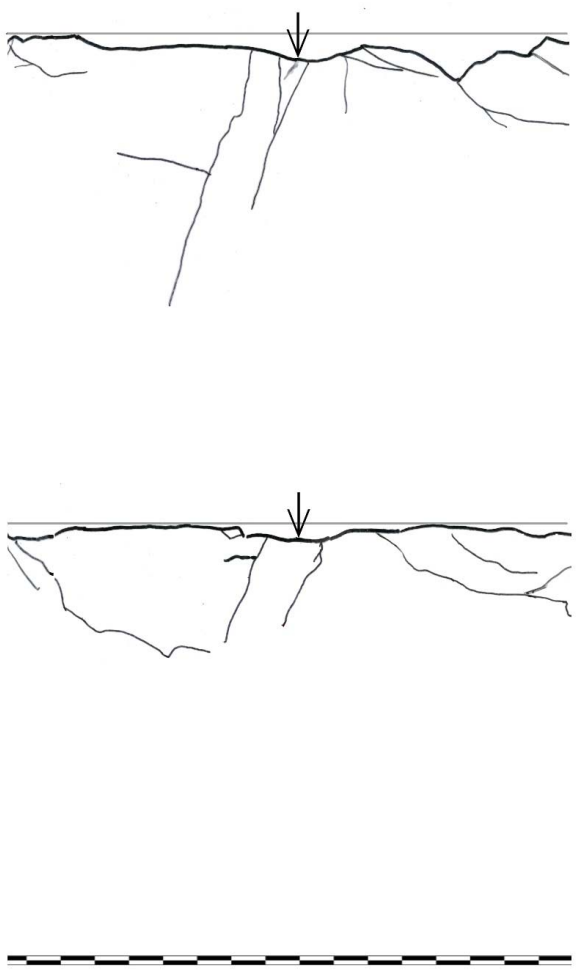

Figure I1.35: Surface and crack pattern under the cutter groove in core sample R_5437_4-1_21.

R_5437_4-2_22

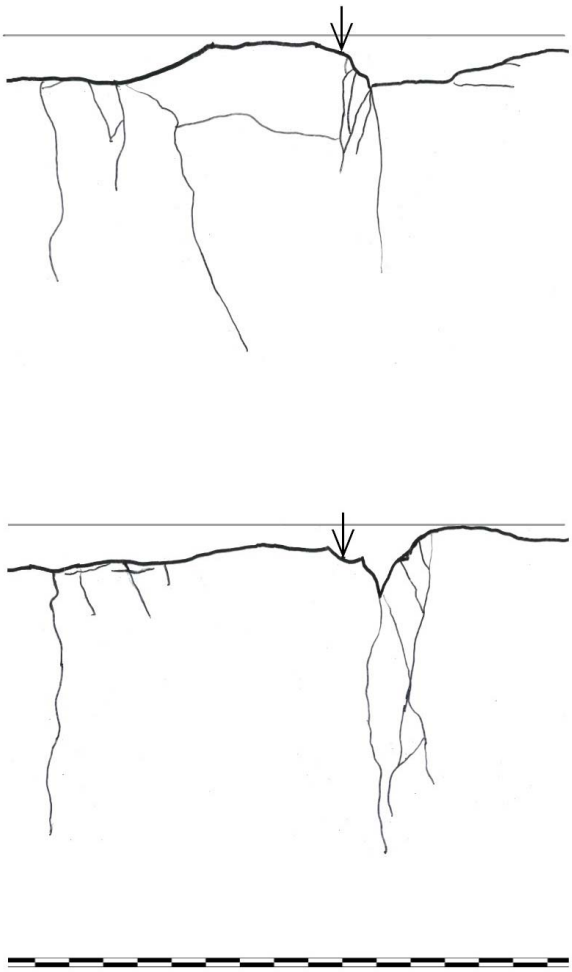

Figure I1.36: Surface and crack pattern under the cutter groove in core sample R_5437_4-2_22.

R_5437_4-3_23

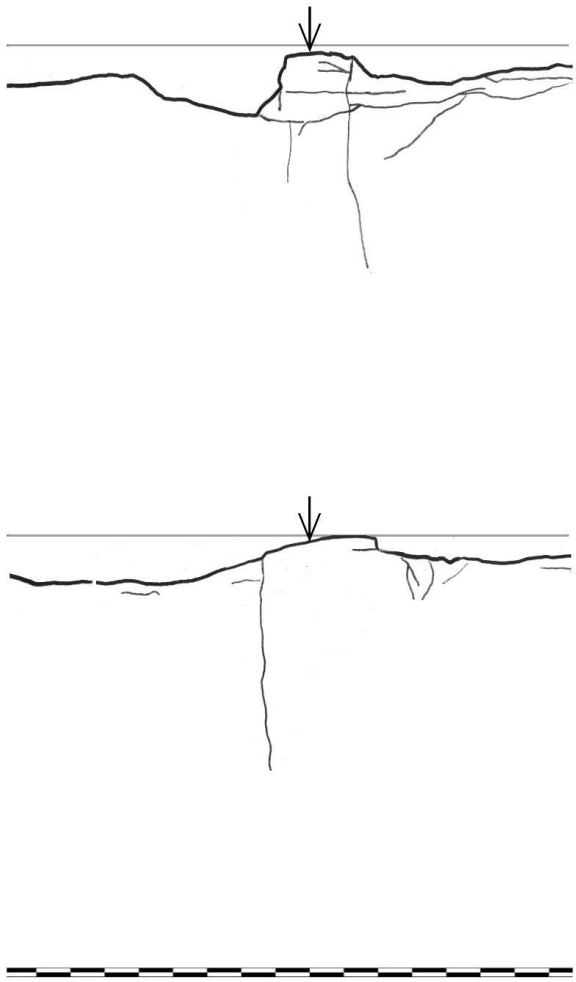

Figure I1.37: Surface and crack pattern under the cutter groove in core sample R_5437_4-3_23.

R_5437_4-4_24

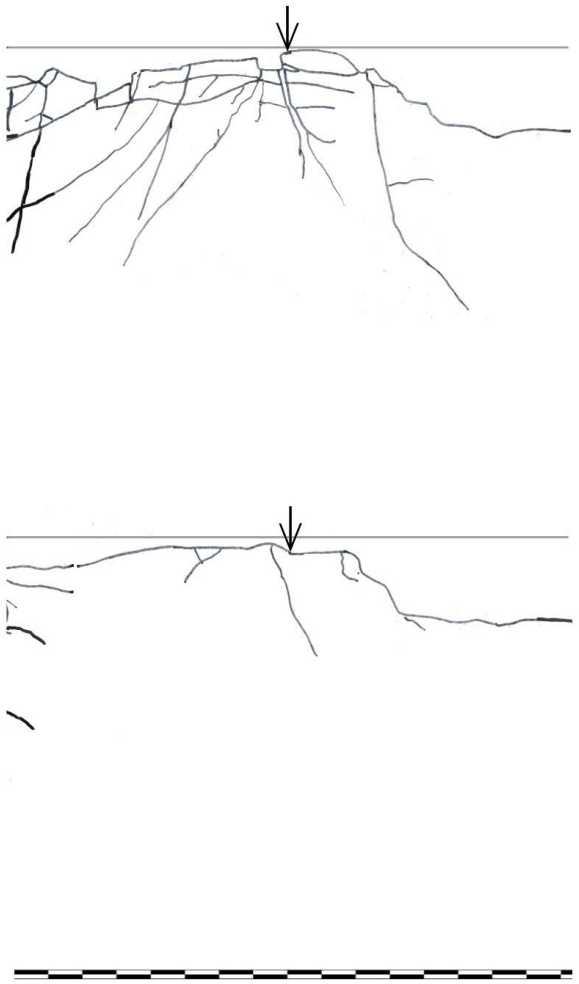

Figure I1.38: Surface and crack pattern under the cutter groove in core sample R_5437_4-4_24.

I1.4 Chainage 5458

R_5458_1-1_21

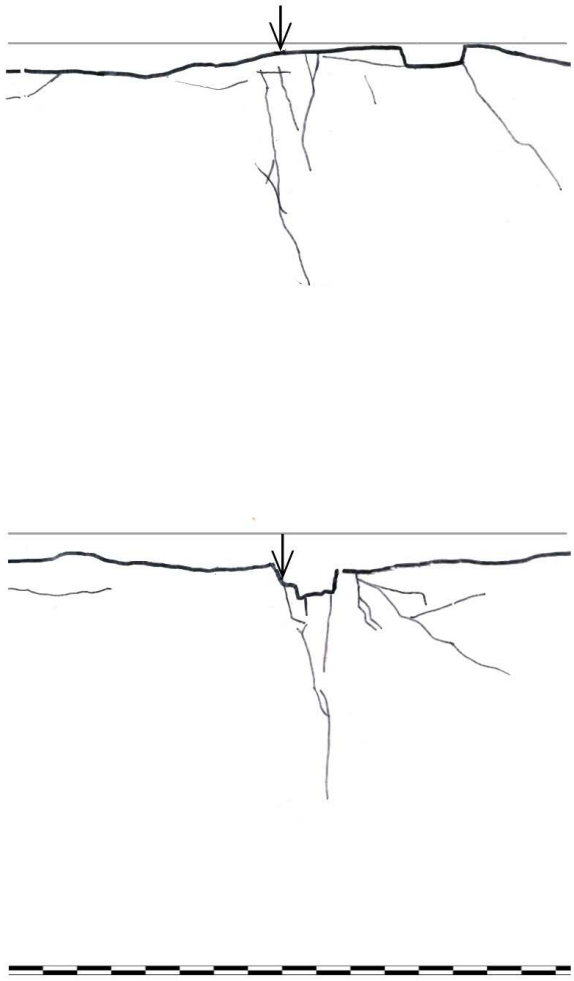

Figure I1.39: Surface and crack pattern under the cutter groove in core sample R_5458_1-1_21.

R_5458_1-2_22

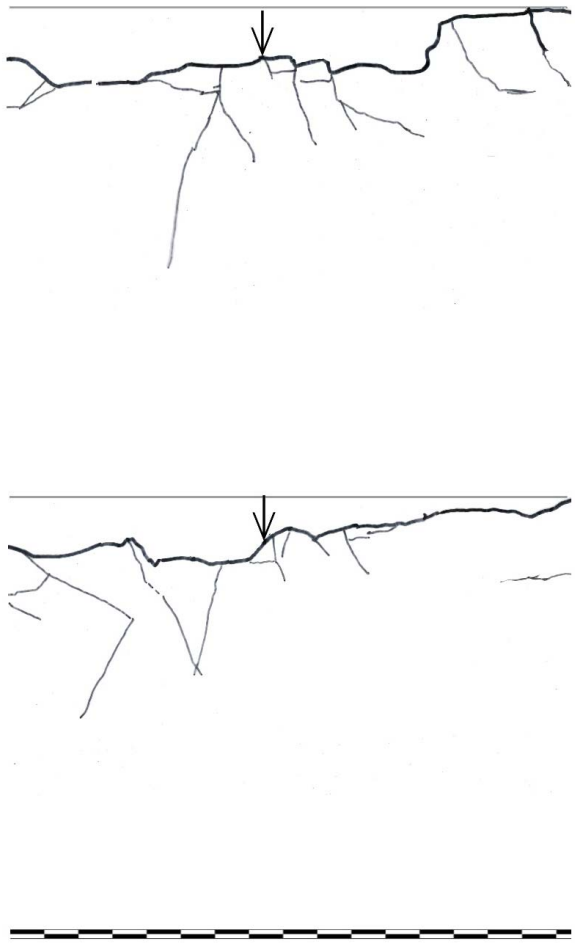

Figure I1.40: Surface and crack pattern under the cutter groove in core sample R_5458_1-2_22.

R_5458_1-3_23

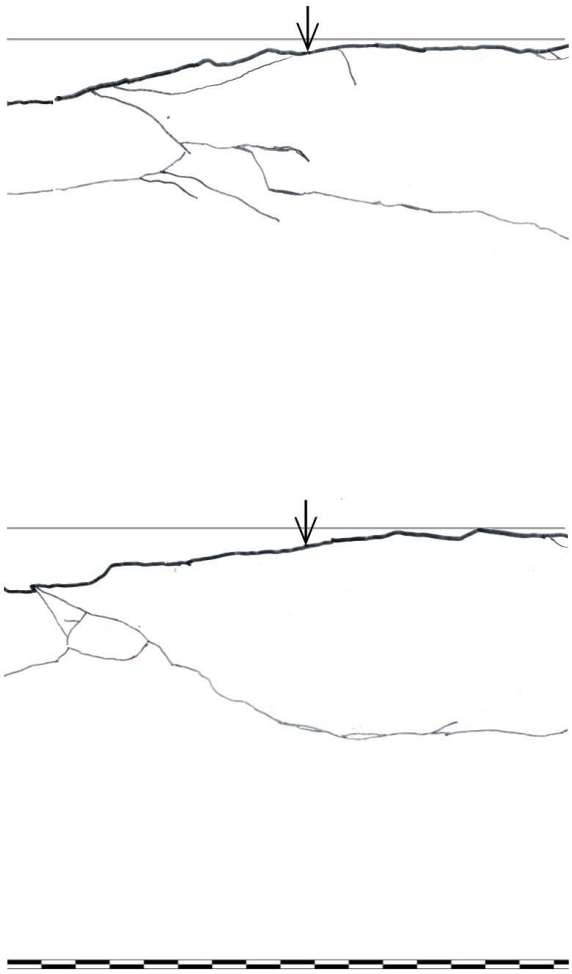

Figure I1.41: Surface and crack pattern under the cutter groove in core sample R_5458_1-3_23.

R_5458_1-4_24

Figure I1.42: Surface and crack pattern under the cutter groove in core sample R_5458_1-4_24.

R_5458_1-5_25

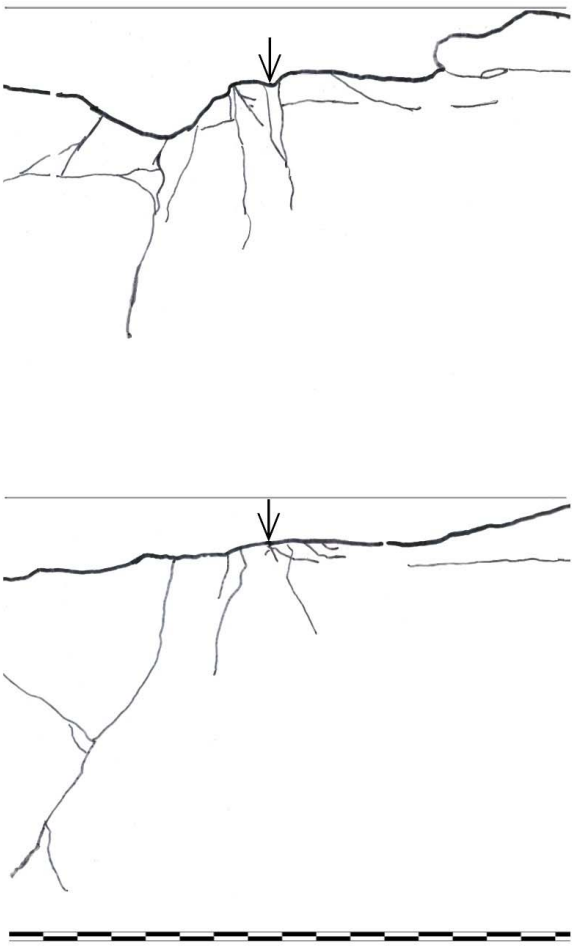

Figure I1.43: Surface and crack pattern under the cutter groove in core sample R_5458_1-5_25.

R_5458_2-1_22

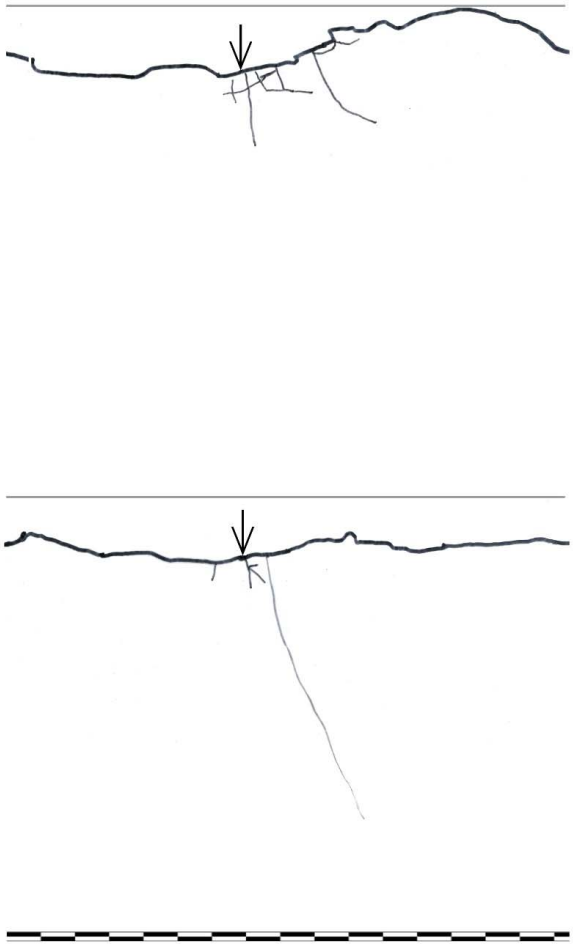

Figure I1.44: Surface and crack pattern under the cutter groove in core sample R_5458_2-1_22.

R_5458_2-2_23

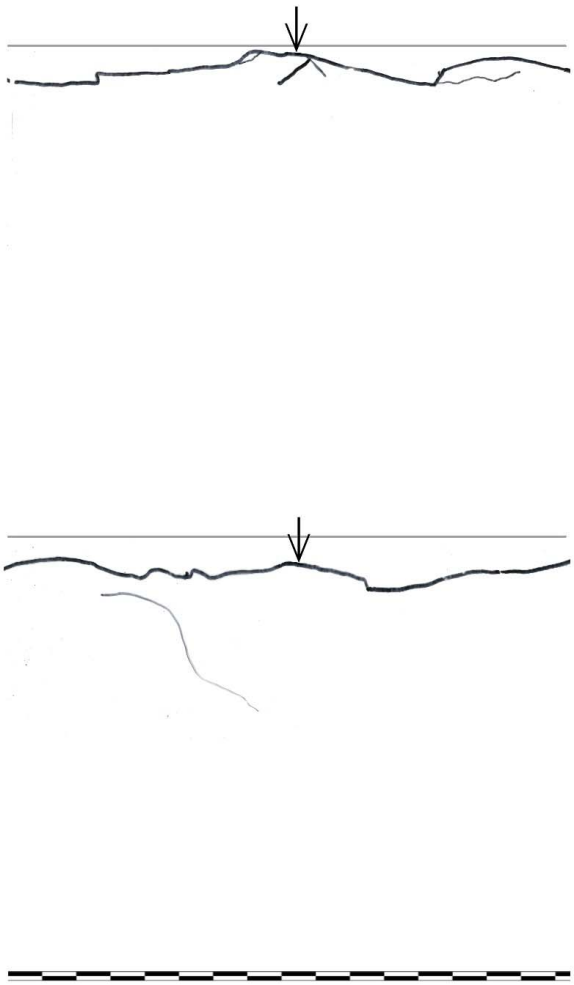

Figure I1.45: Surface and crack pattern under the cutter groove in core sample R_5458_2-2_23.

R_5458_2-3_25

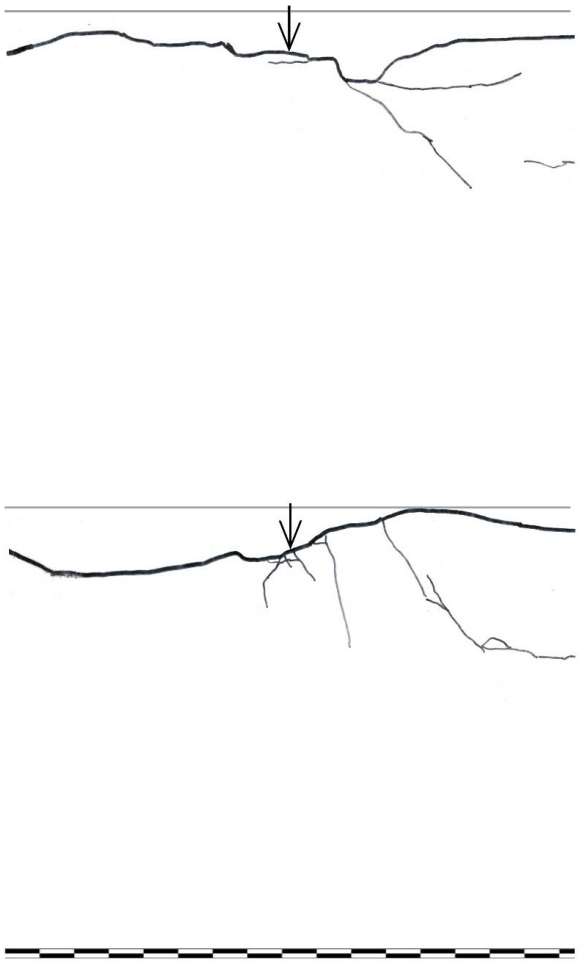

Figure I1.46: Surface and crack pattern under the cutter groove in core sample R_5458_2-3_25.

R_5458_3-1_21

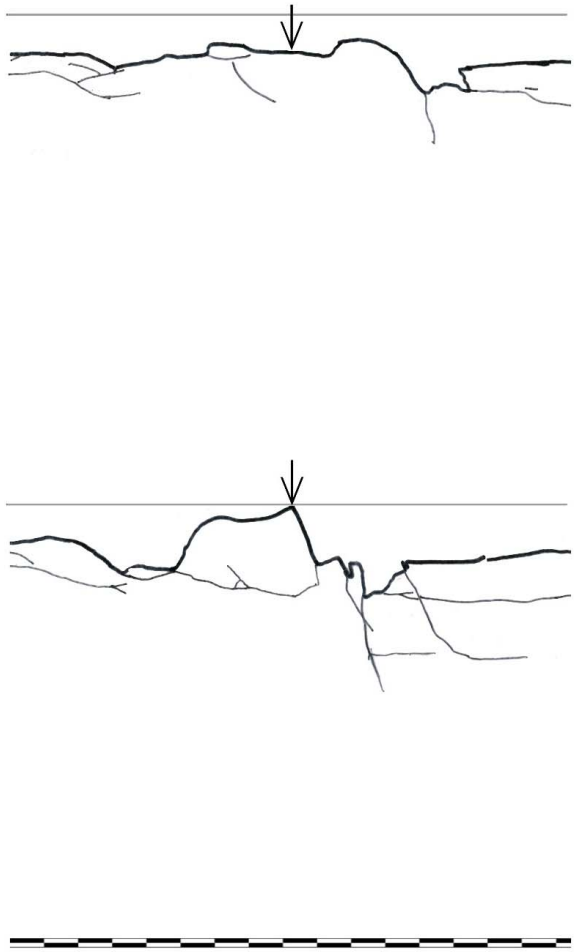

Figure I1.47: Surface and crack pattern under the cutter groove in core sample R_5458_3-1_21.

R_5458_3-2_22

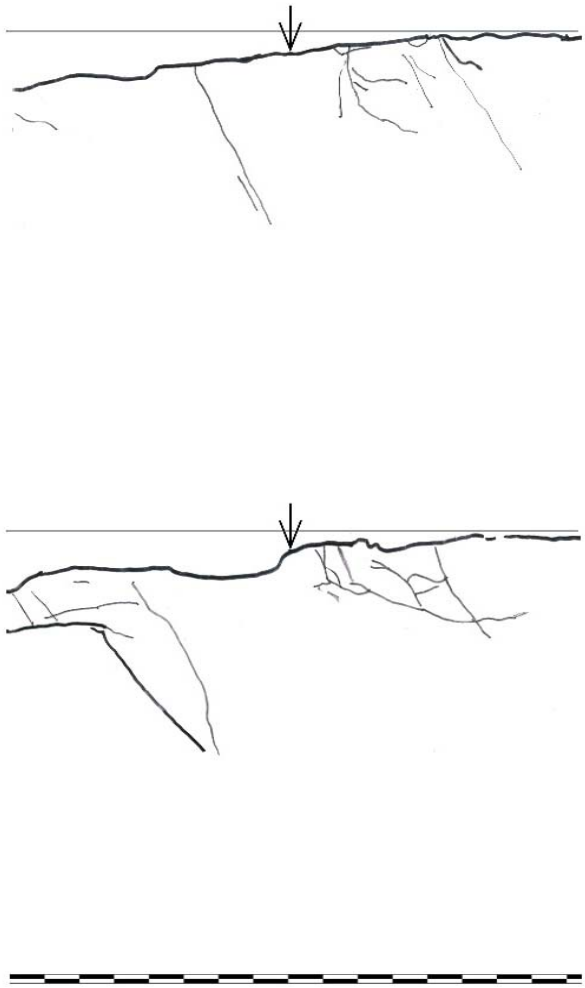

Figure I1.48: Surface and crack pattern under the cutter groove in core sample R_5458_3-2_22.

R_5458_3-3_24

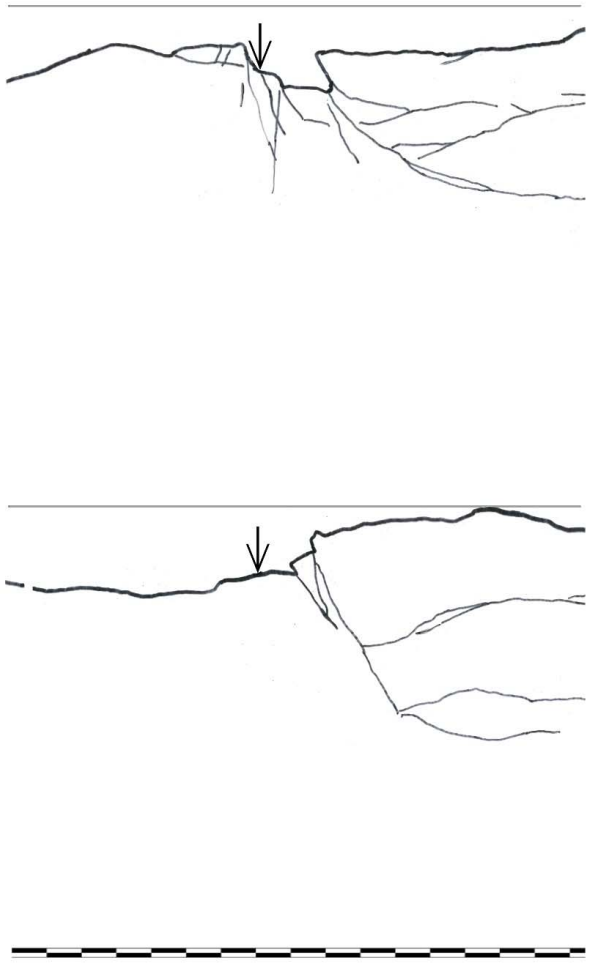

Figure I1.49: Surface and crack pattern under the cutter groove in core sample R_5458_3-3_24.

R_5458_3-4_25

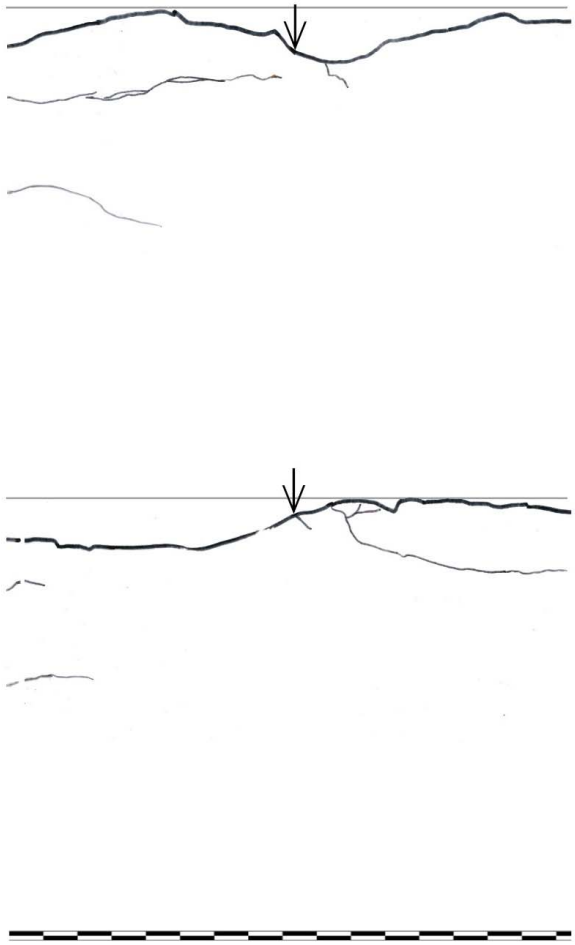

Figure I1.50: Surface and crack pattern under the cutter groove in core sample R_5458_3-4_25.

R_5458_4-1_21

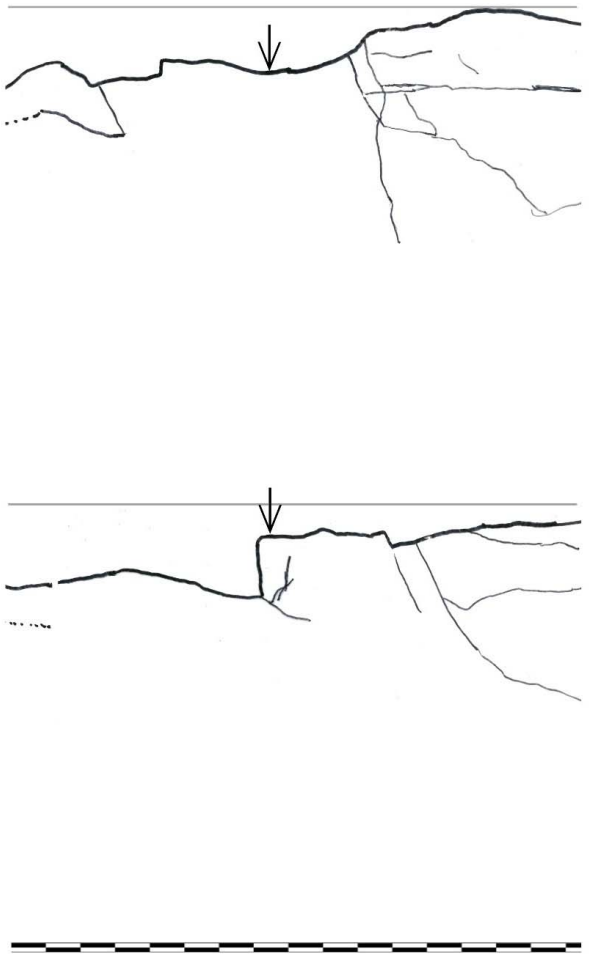

Figure I1.51: Surface and crack pattern under the cutter groove in core sample R_5458_4-1_21.

R_5458_4-2_22

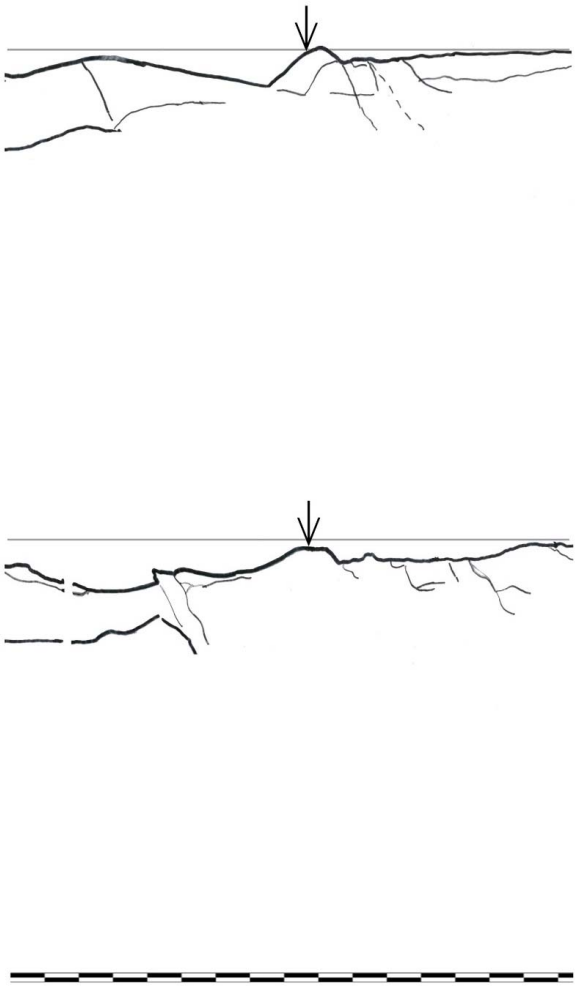

Figure I1.52: Surface and crack pattern under the cutter groove in core sample R_5458_4-2_22.

R_5458_4-3_23

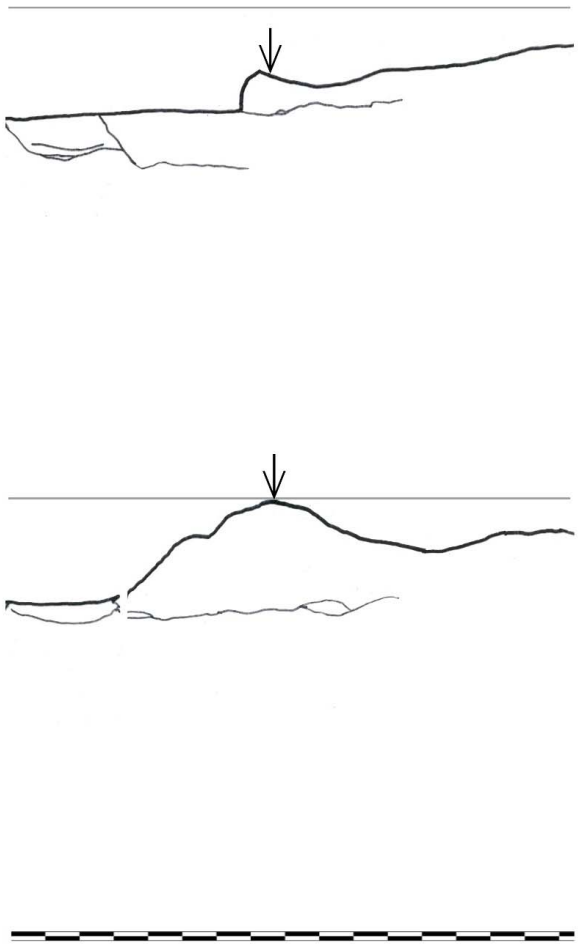

Figure I1.53: Surface and crack pattern under the cutter groove in core sample R_5458_4-3_23.

R_5458_4-4_25

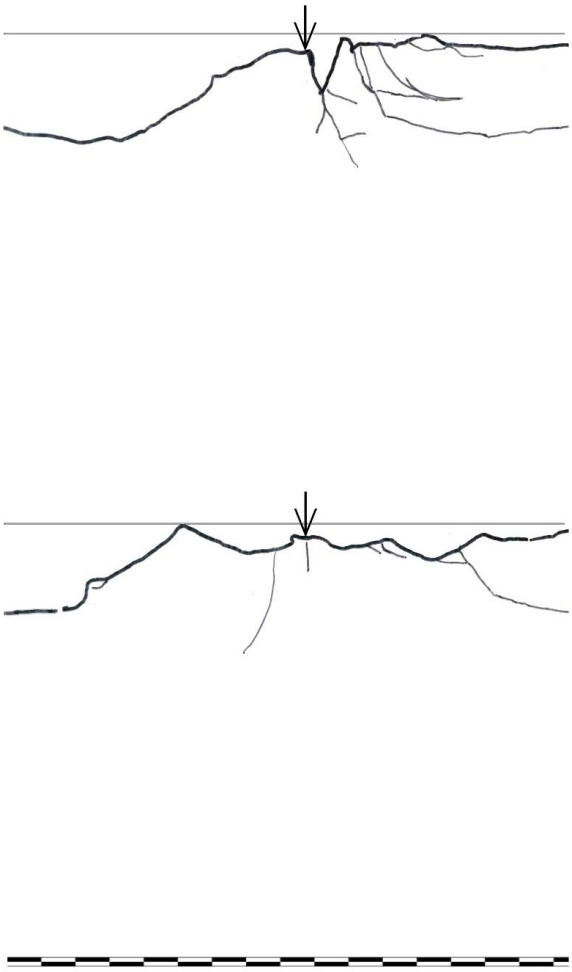

Figure I1.54: Surface and crack pattern under the cutter groove in core sample R_5458_4-4_26.

I1.5 Chainage 5478

R_5478_1-1_21

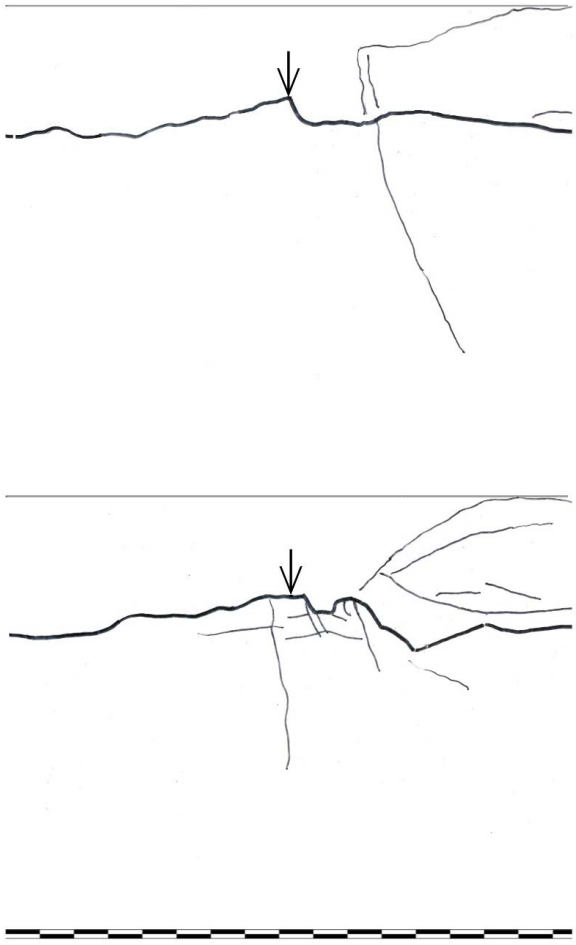

Figure I1.55: Surface and crack pattern under the cutter groove in core sample R_5478_1-1_21.

R_5478_1-2_22

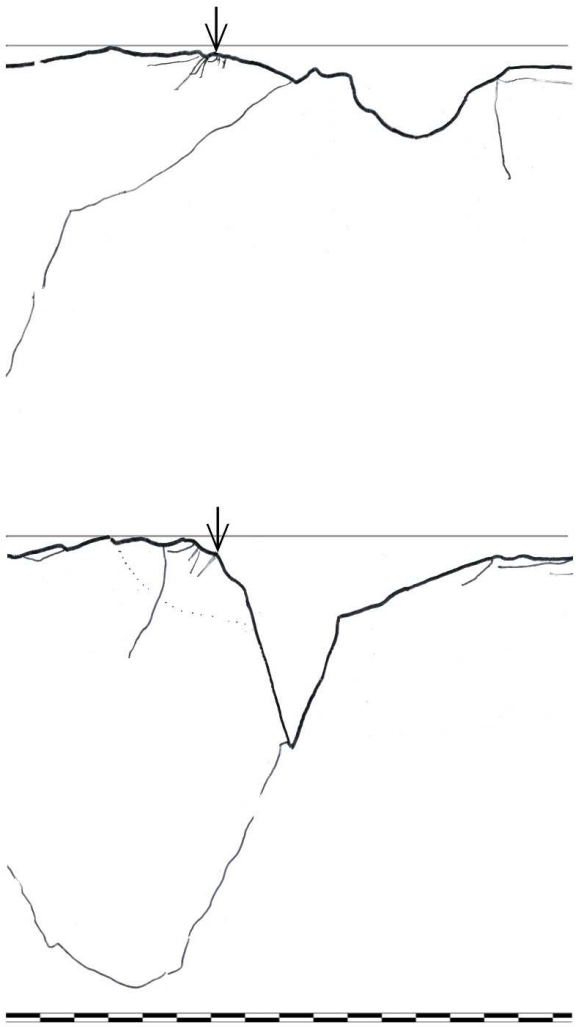

Figure I1.56: Surface and crack pattern under the cutter groove in core sample R_5478_1-2_22.

R_5478_1-3_23

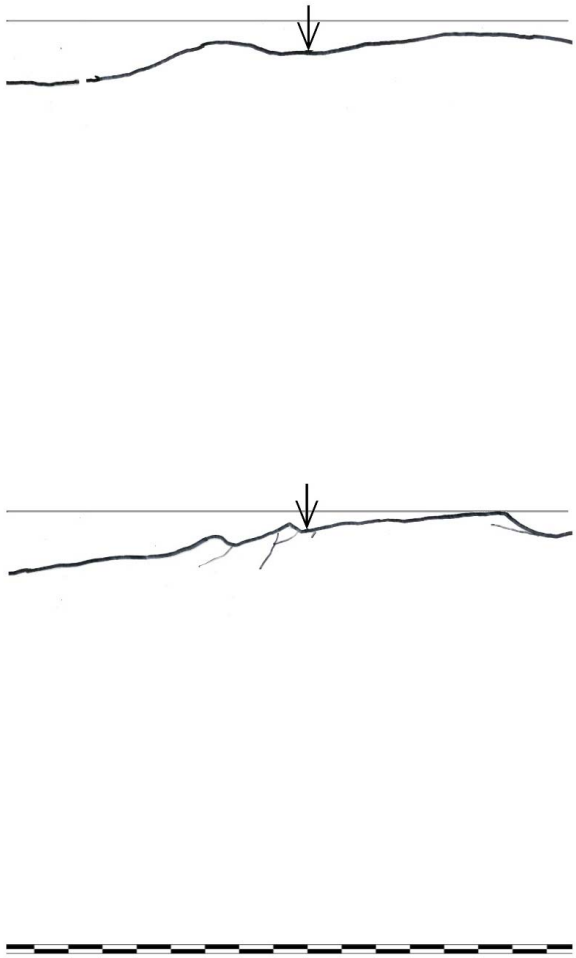

Figure I1.57: Surface and crack pattern under the cutter groove in core sample R_5478_1-3_23.

R_5478_1-4_24

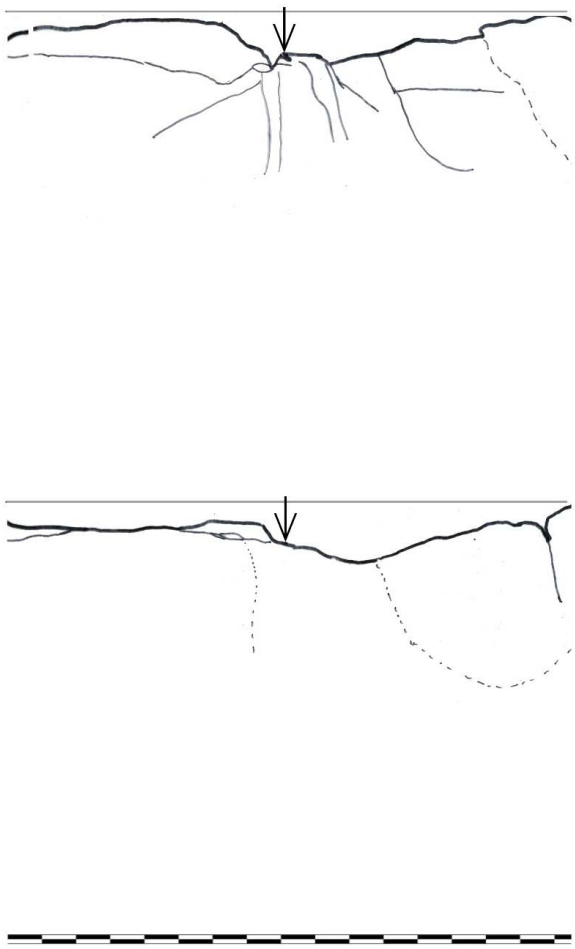

Figure I1.58: Surface and crack pattern under the cutter groove in core sample R_5478_1-4_24.

R_5478_1-5_25

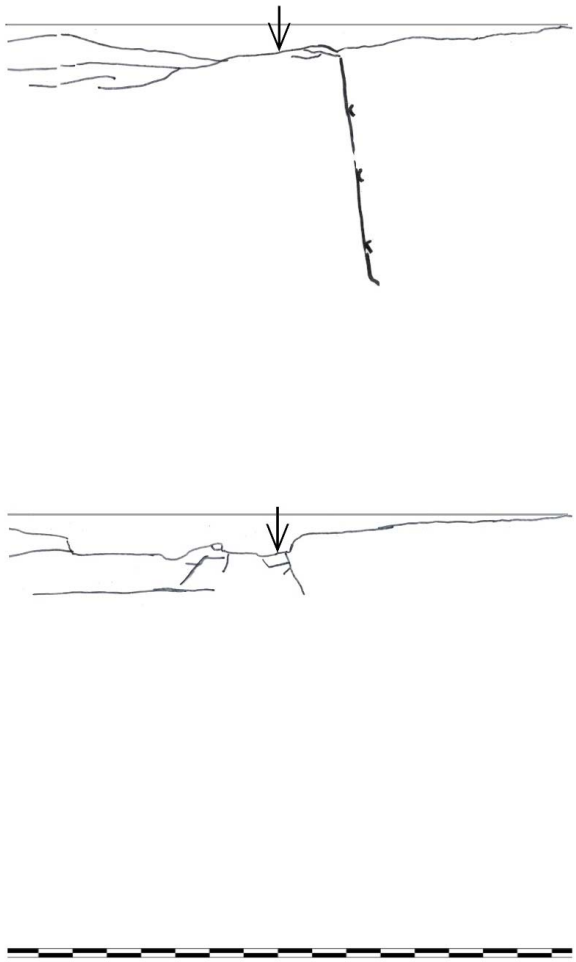

Figure I1.59: Surface and crack pattern under the cutter groove in core sample R_5478_1-5_25.

R_5478_2-1_21

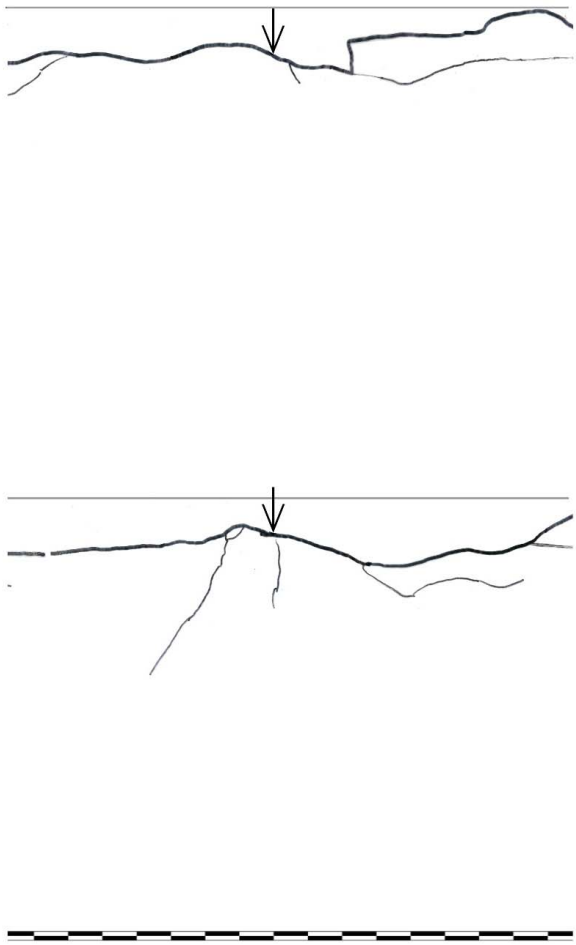

Figure I1.60: Surface and crack pattern under the cutter groove in core sample R_5478_2-1_21.

R_5478_2-2_22

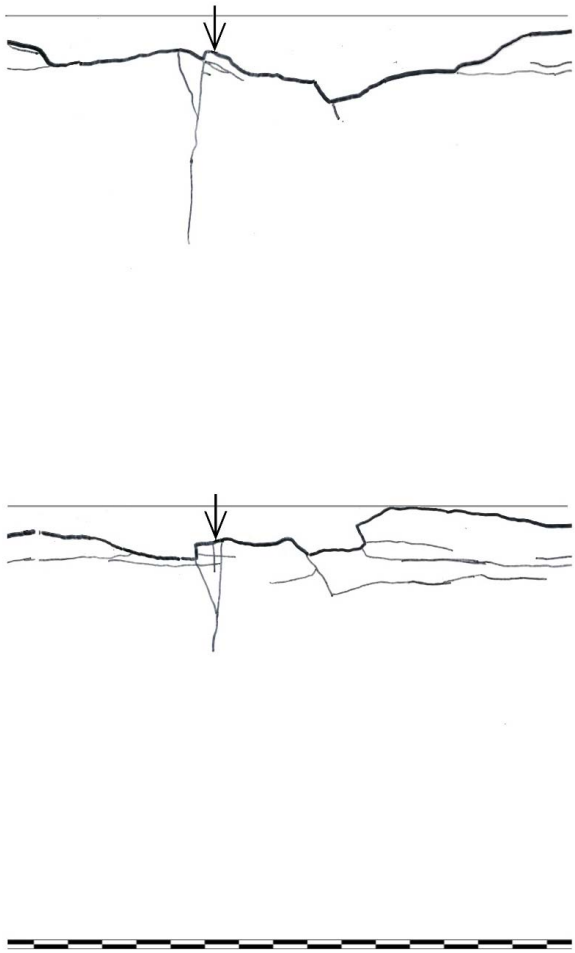

Figure I1.61: Surface and crack pattern under the cutter groove in core sample R_5478_2-2_22.

R_5478_2-3_24

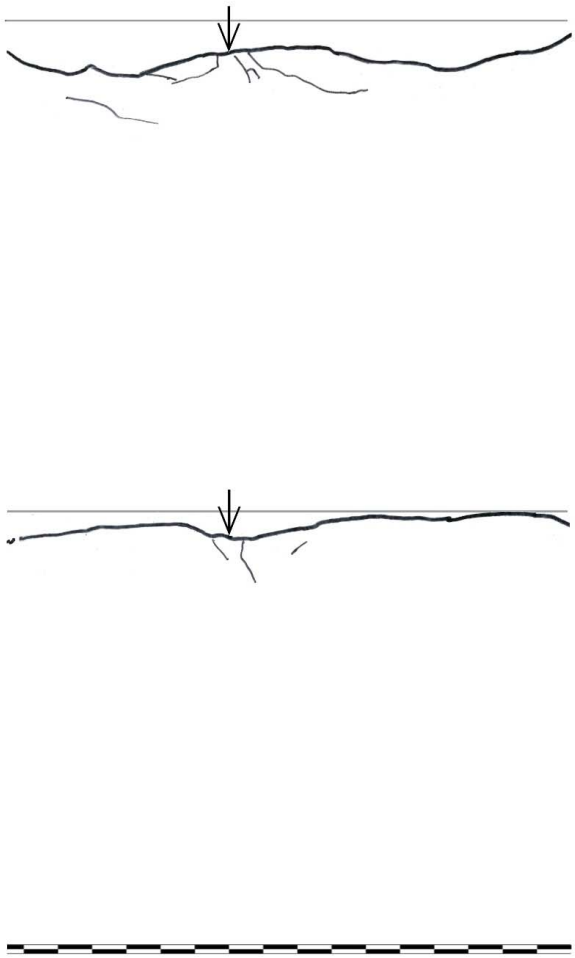

Figure I1.62: Surface and crack pattern under the cutter groove in core sample R_5478_2-3_24.

R_5478_2-4_24/25

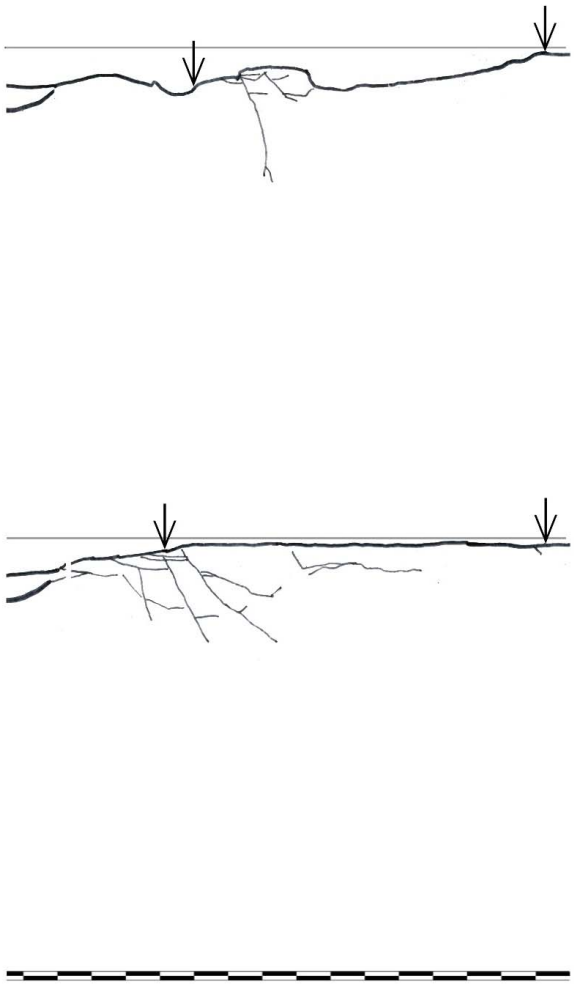

Figure I1.63: Surface and crack pattern under the cutter groove in core sample R_5478_2-4_24/25.

R_5478_2-5_26

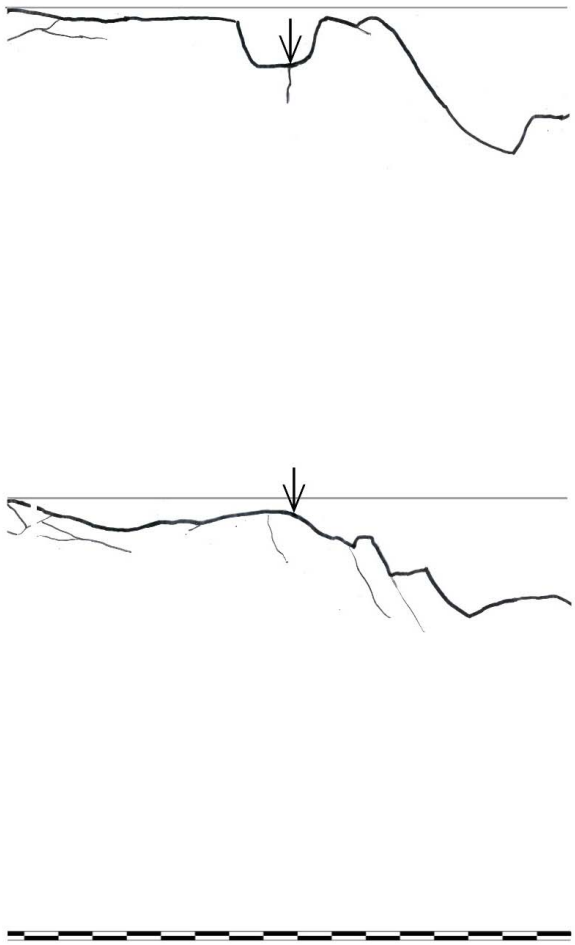

Figure I1.64: Surface and crack pattern under the cutter groove in core sample R_5478_2-5_26.

Appendix J

APPENDIX J
DATA ANALYSIS OF CRACKS FROM THE NEDRE RØSSÅGA HEADRACE TUNNEL

List of contents

List of figures

J1 Data analysis

This appendix presents the detailed data analysis for the cracks documented in the core samples from the Nedre Røssåga headrace tunnel. The order of the subjects is the same as in the thesis. The order of the results within each subject is:

- Sample chainage R_3112
- Sample chainage R_1184
- Sample chainage R_5437
- Sample chainage R_5478
- Sample chainage R_5458
- Geology 1 (Sample chainage R_3112 and R_1184)
- Geology 2 (Sample chainage R_5437, R_5478, and R_5458)
- Total, all cracks

Unless commented, all cracks and core samples are included in the analysis.

J1.1 Number of cracks

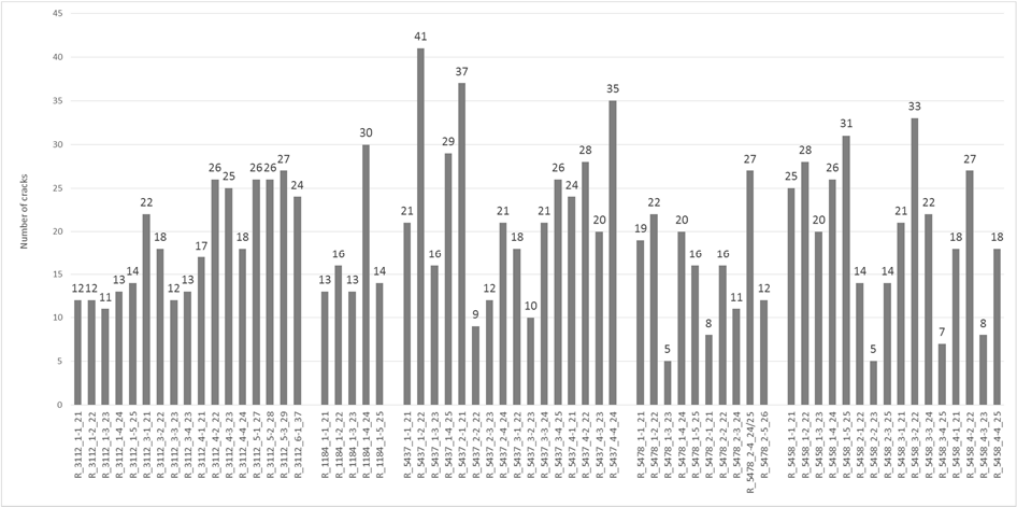

Figure J1.1: Number of documented cracks in each of the core sample.

J1.2 Distribution of the dip angles and dip directions

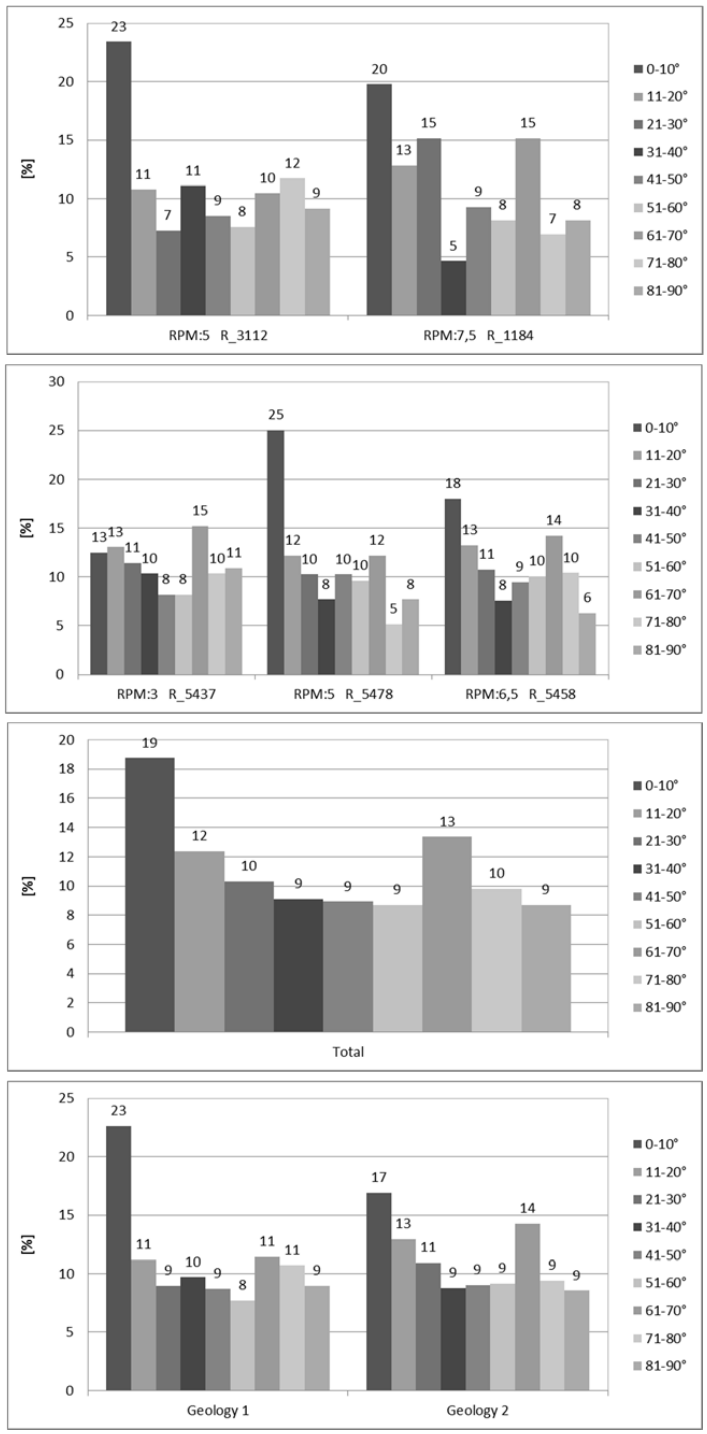

Figure J1.2: Distribution of dip angles.

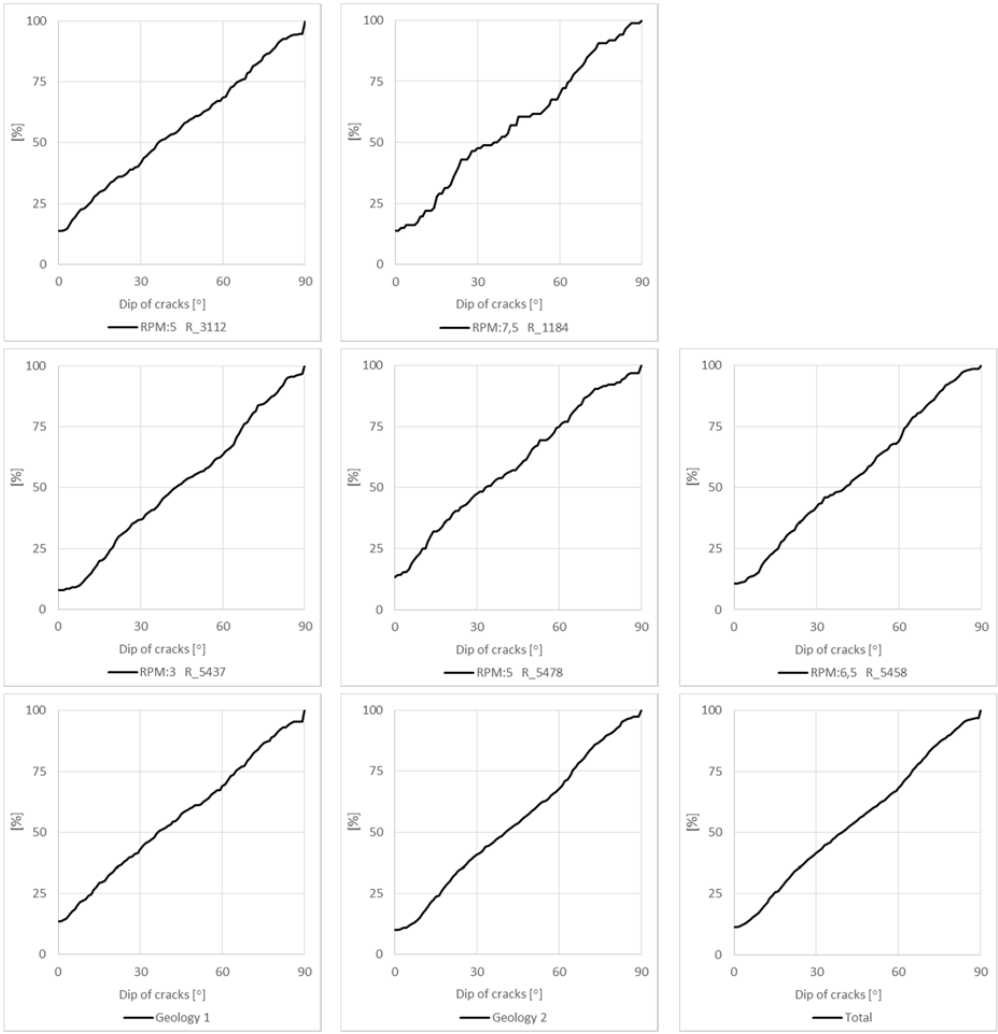

Figure J1.3: Accumulative frequency distribution of dip angles.

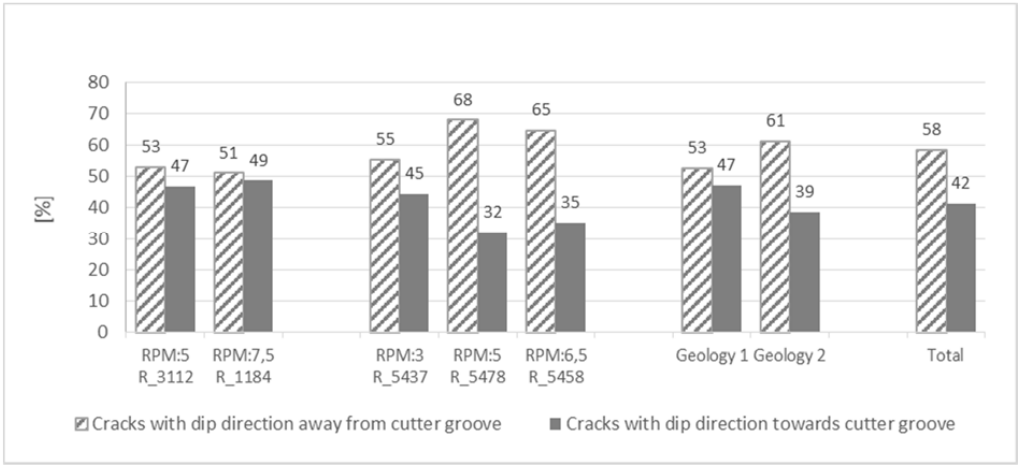

Figure J1.4: Distribution of dip directions in relation to cutter groove.

J1.3 Distribution of the horizontal lengths of cracks

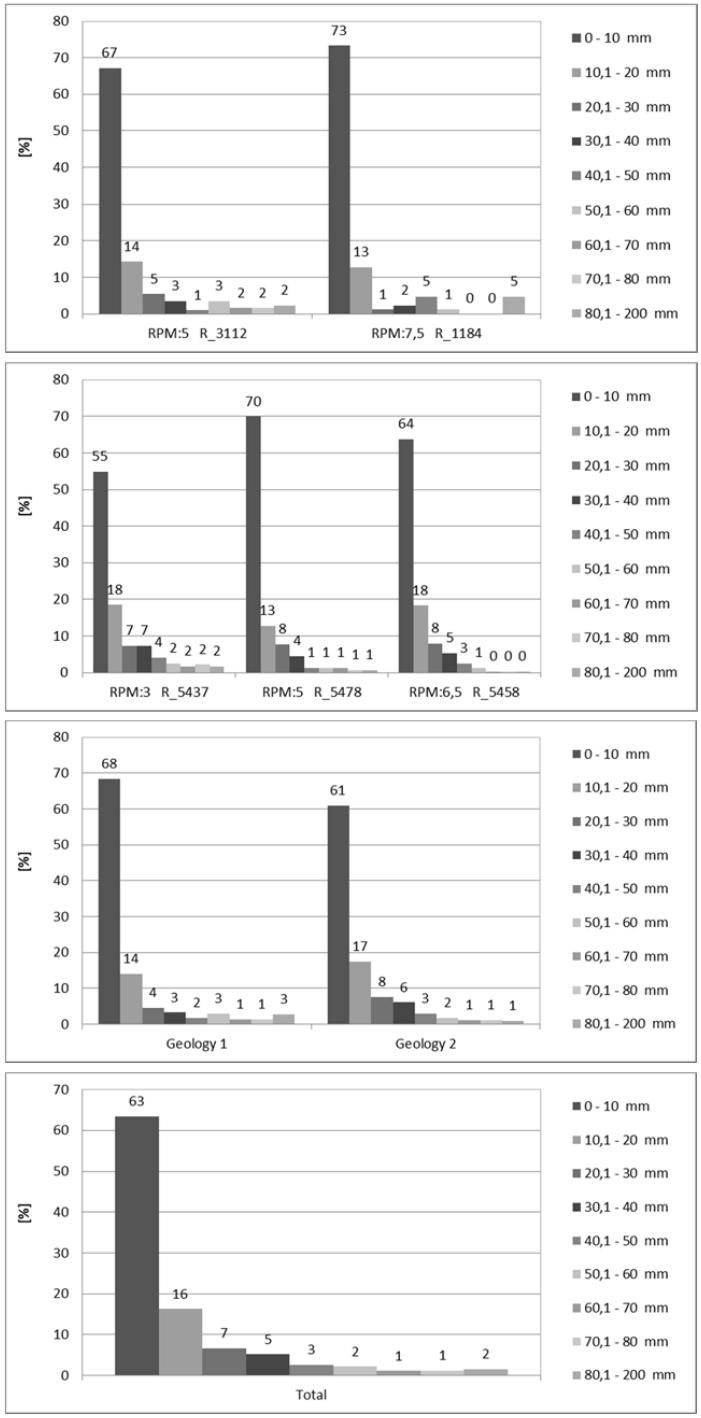

Figure J1.5: Distribution of horizontal lengths of cracks.

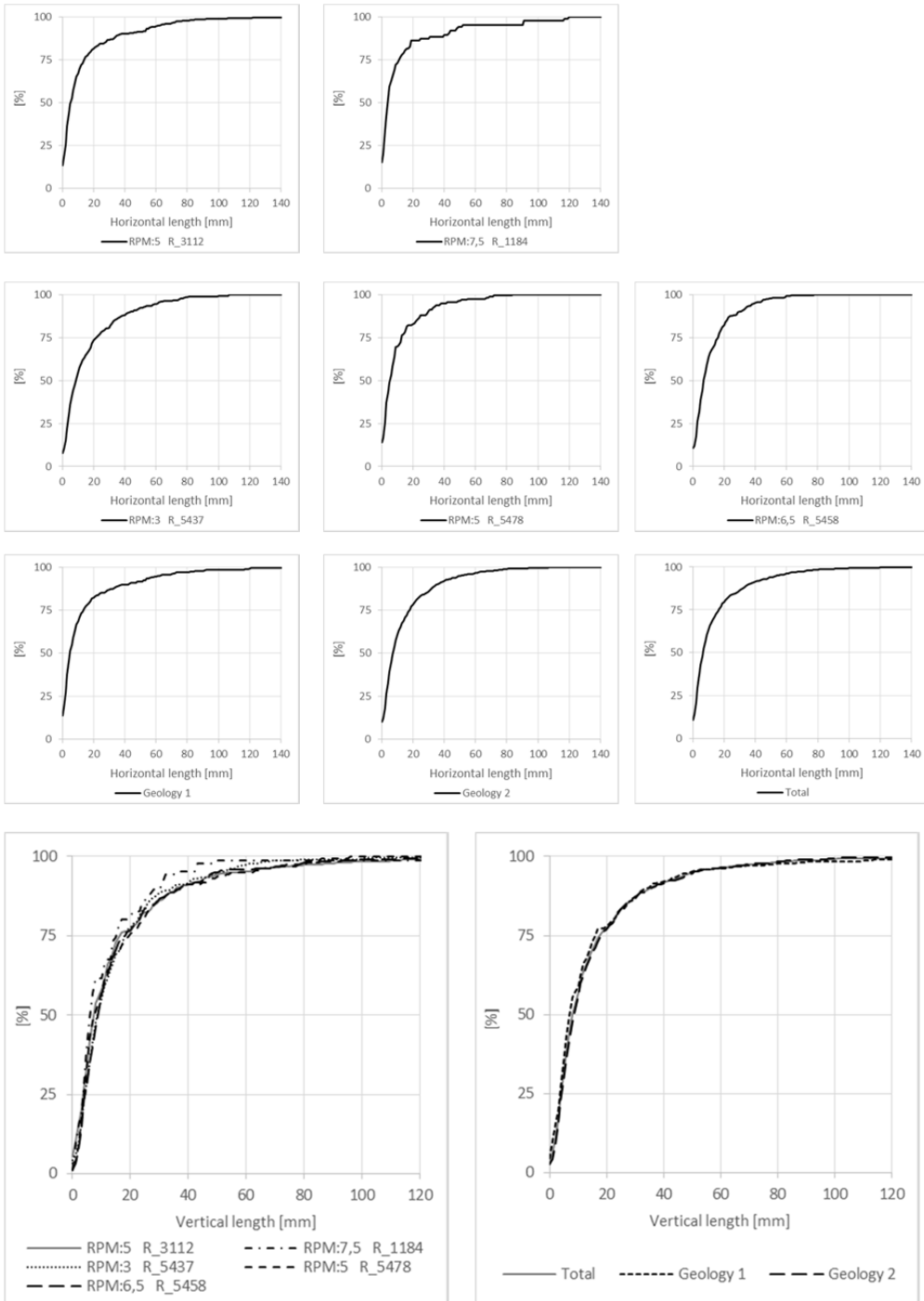

Figure J1.6: Accumulative frequency distribution of horizontal lengths of cracks.

J1.4 Distribution of the vertical lengths of cracks

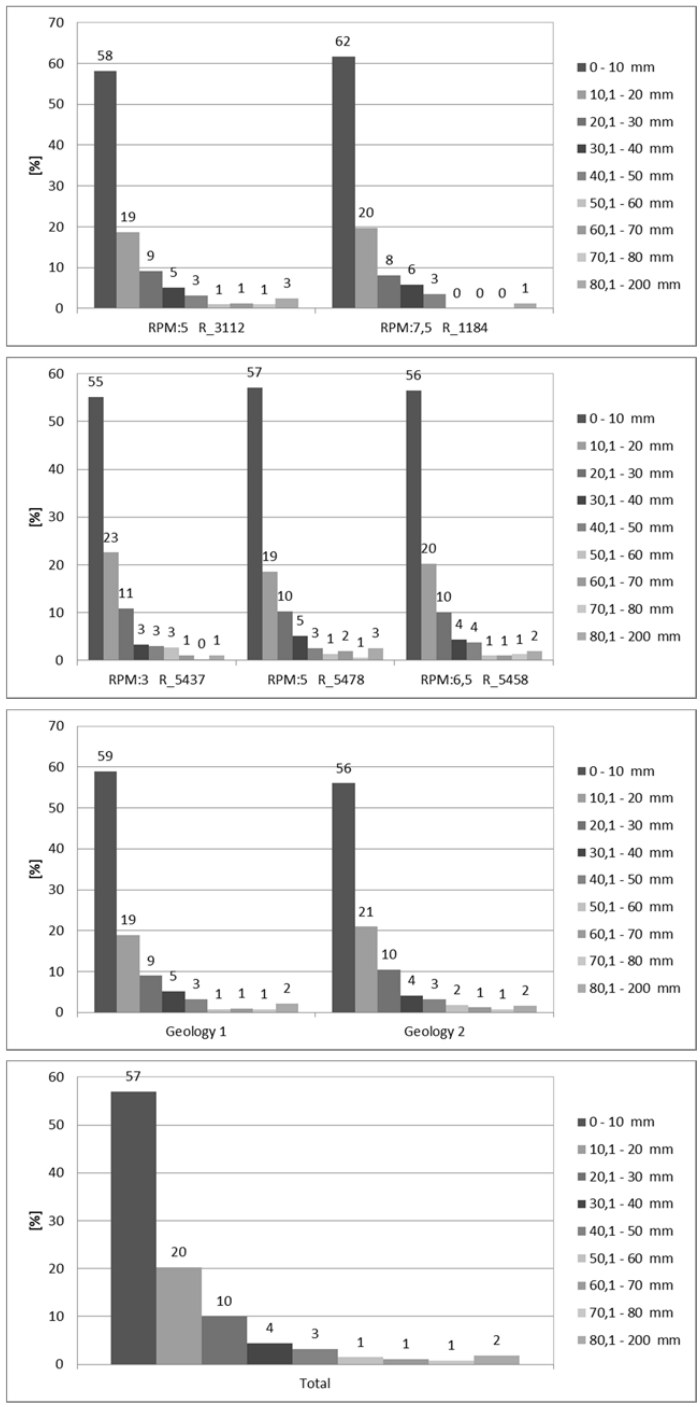

Figure J1.7: Distribution of vertical lengths of cracks.

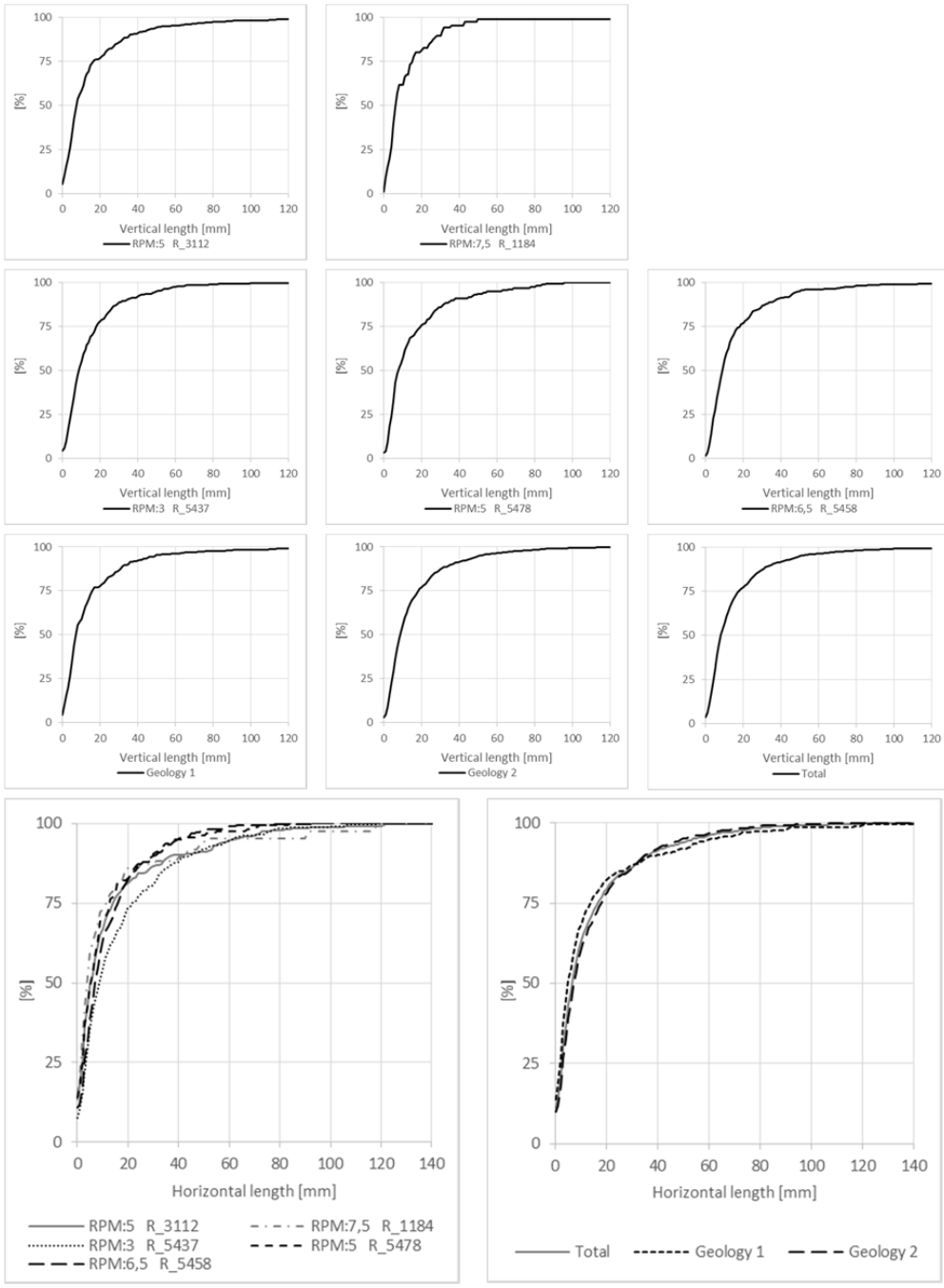

Figure J1.8: Accumulative frequency distribution of vertical lengths of cracks.

J1.5 Distribution of the total lengths of cracks

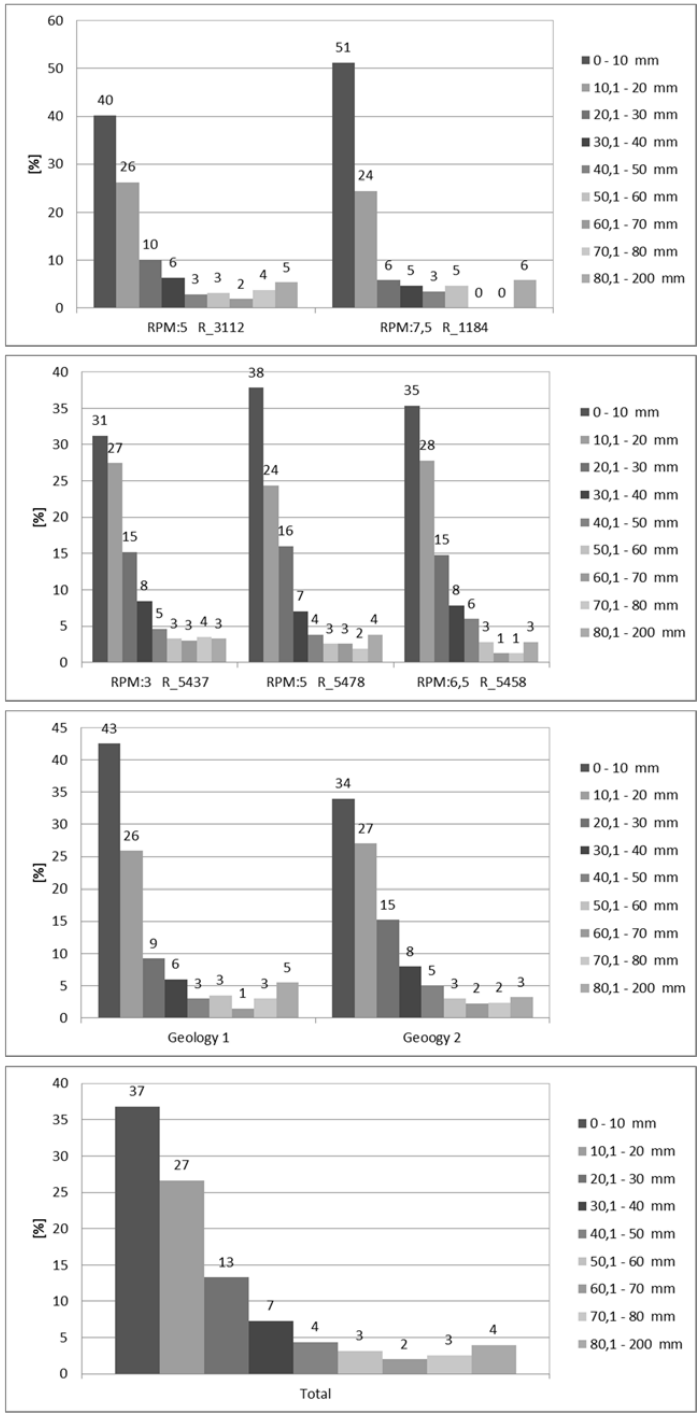

Figure J1.9: Distribution of total lengths of cracks.

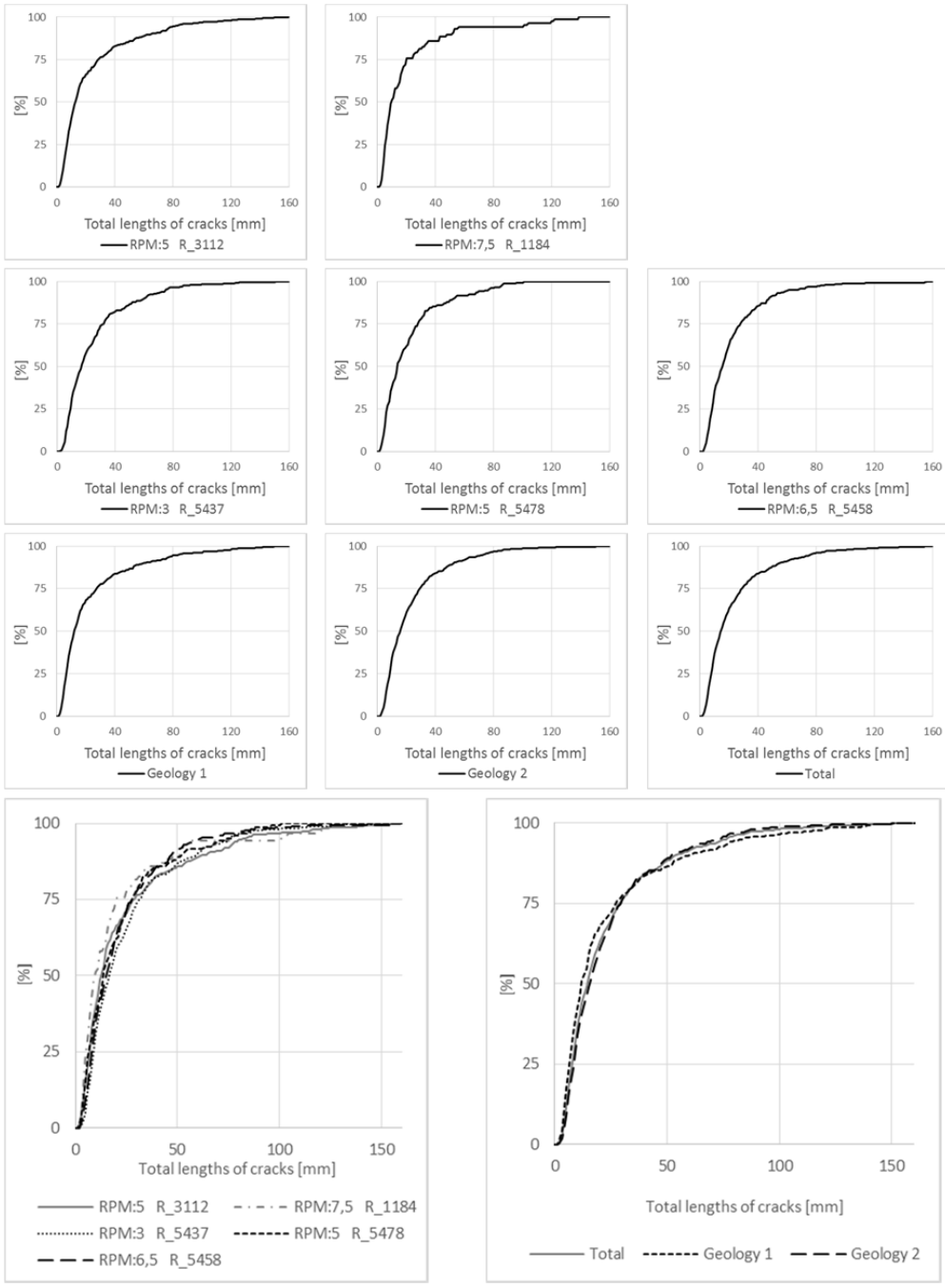

Figure J1.10: Accumulative frequency distribution of total lengths of cracks.

J1.6 Distribution of vertical distance from surface to crack end

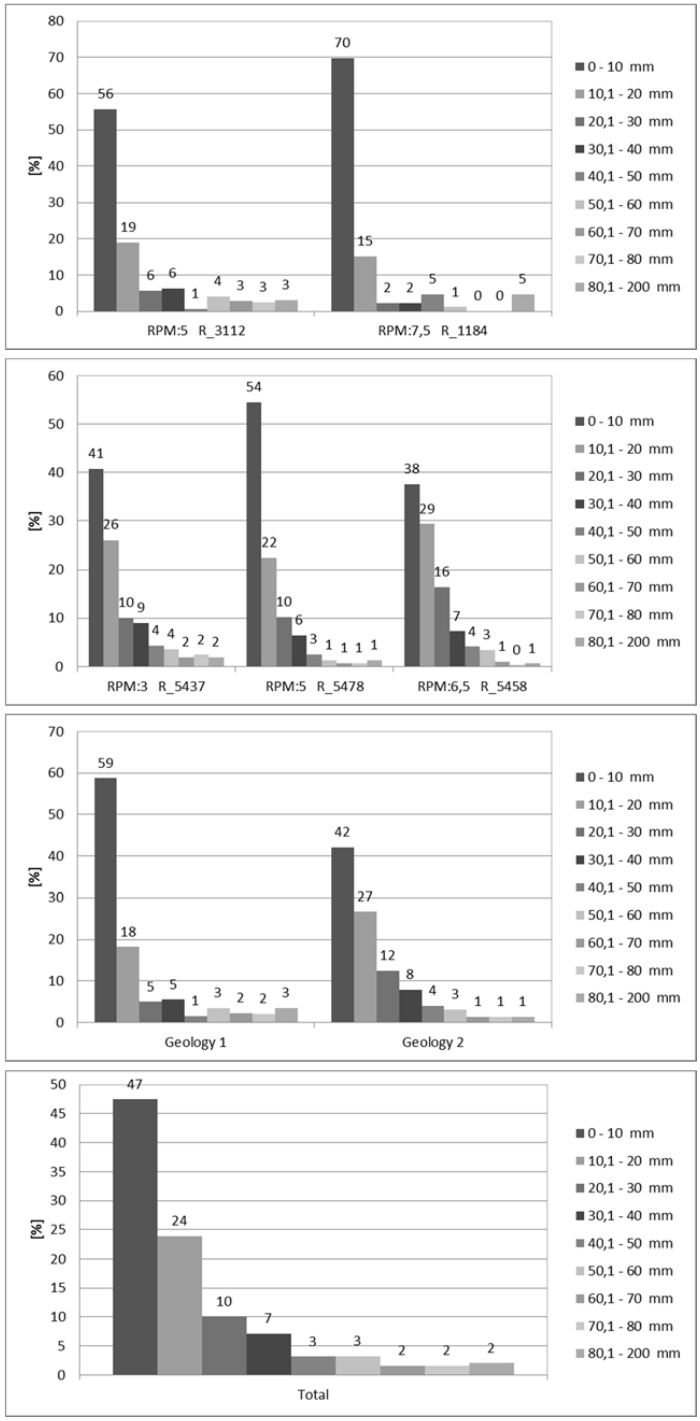

Figure J1.11: Distribution of vertical distances from the surface line to end of cracks for all cracks.

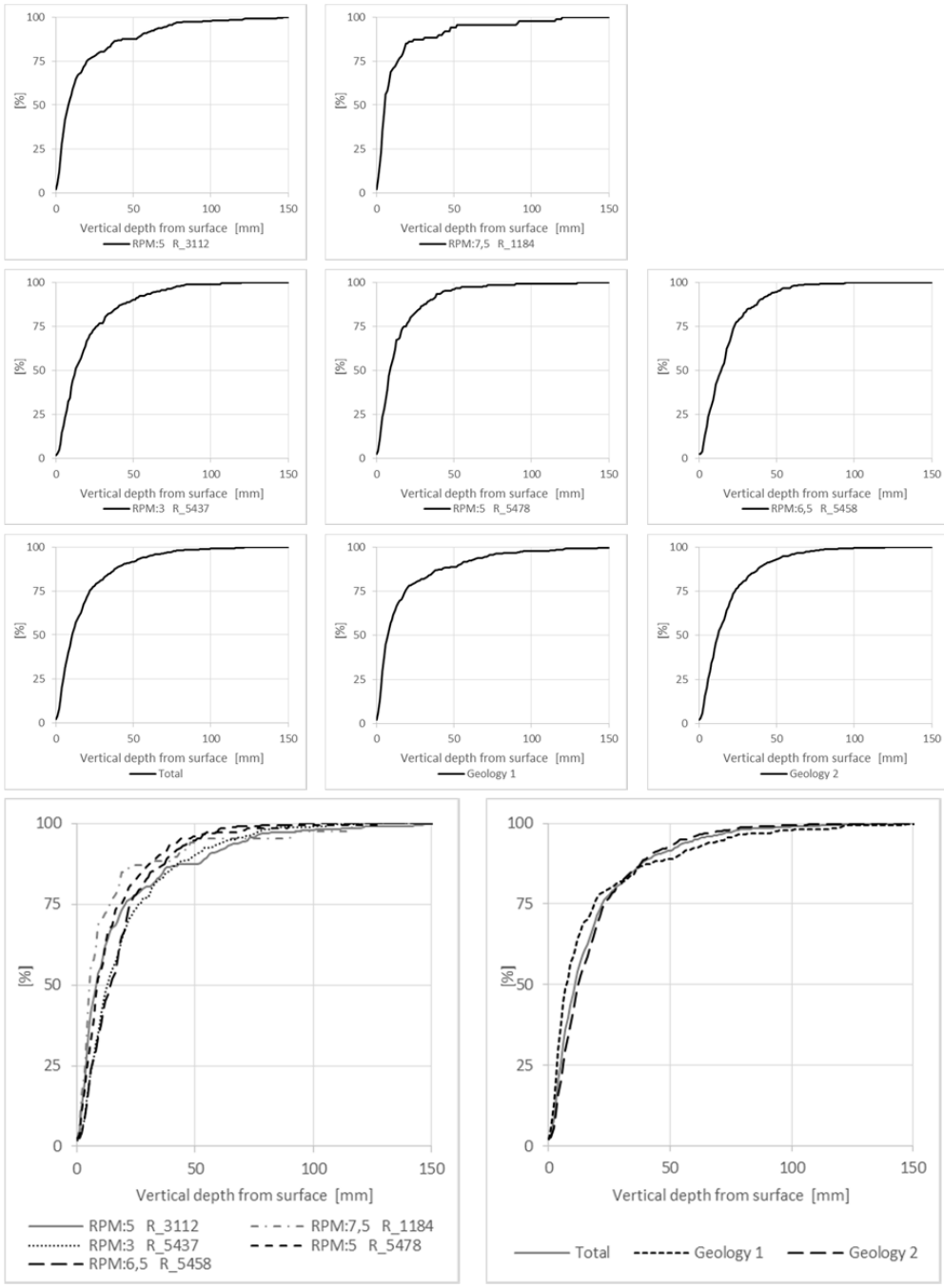

Figure J1.12: Accumulative frequency distribution of vertical distances from the surface line to end of cracks for all cracks.

J1.7 Distribution of vertical distance from 0-line to crack end

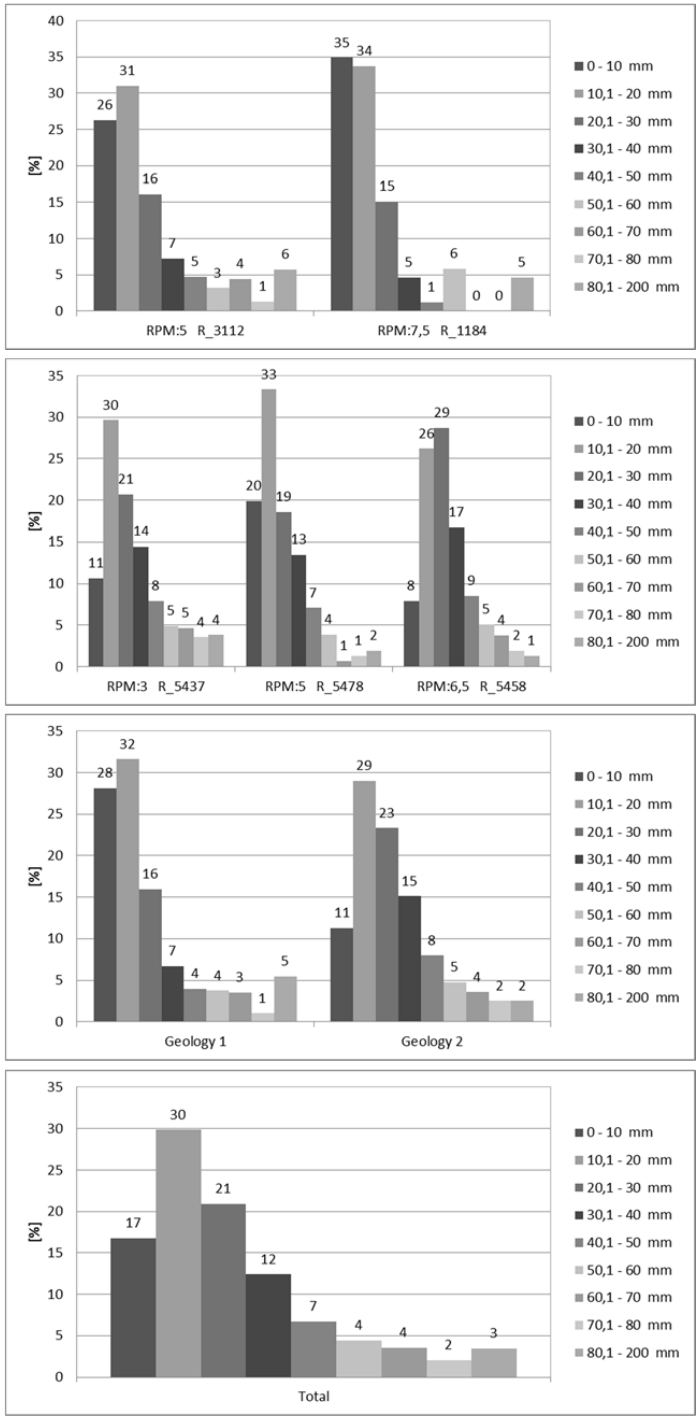

Figure J1.13: Distribution of vertical distances from the 0-line to the end of cracks for all cracks.

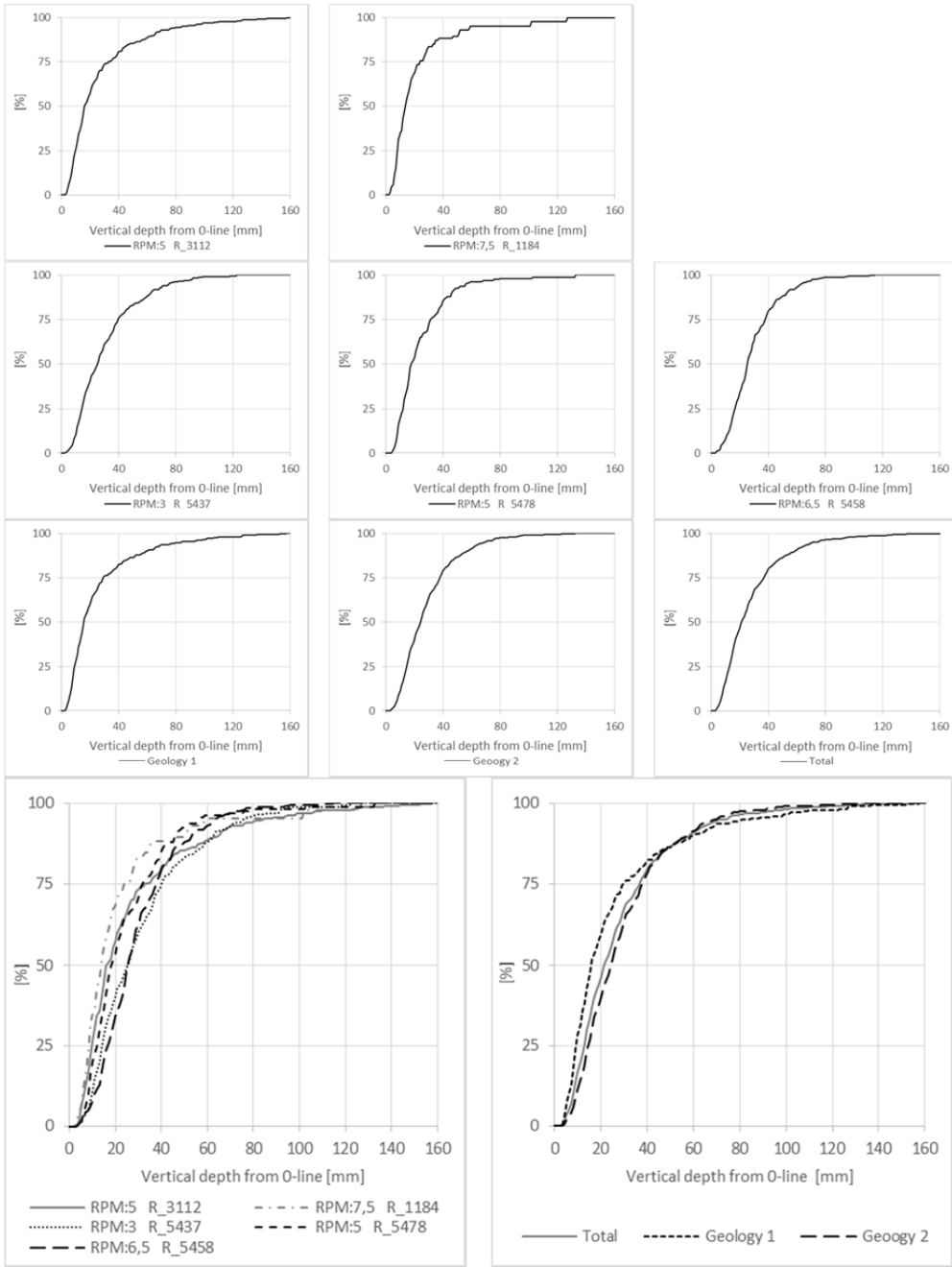

Figure J1.14: Accumulative frequency distribution of vertical distances from the 0-line to the end of cracks for all cracks.

J1.8 Distribution of horizontal distance from the point of origin to the cutter groove

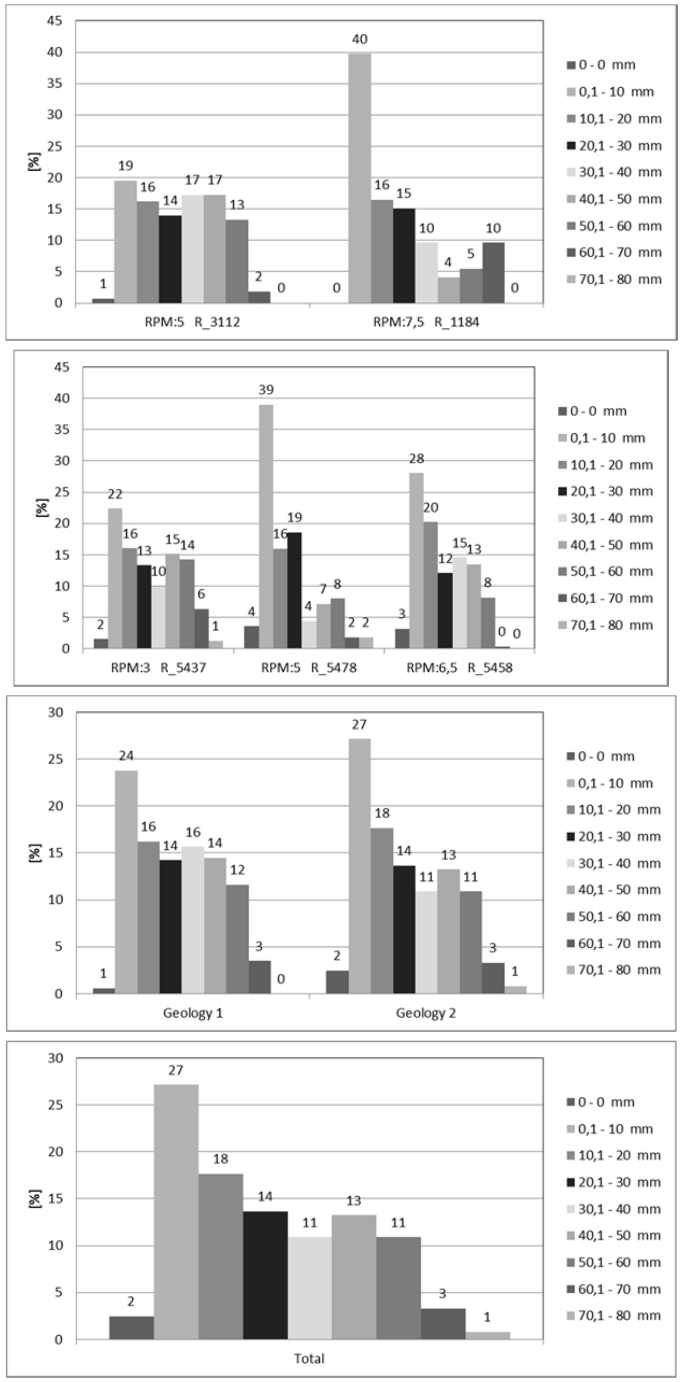

Figure J1.15: Distribution of horizontal distances from point of origin to the cutter groove for all cracks with dip >3°.

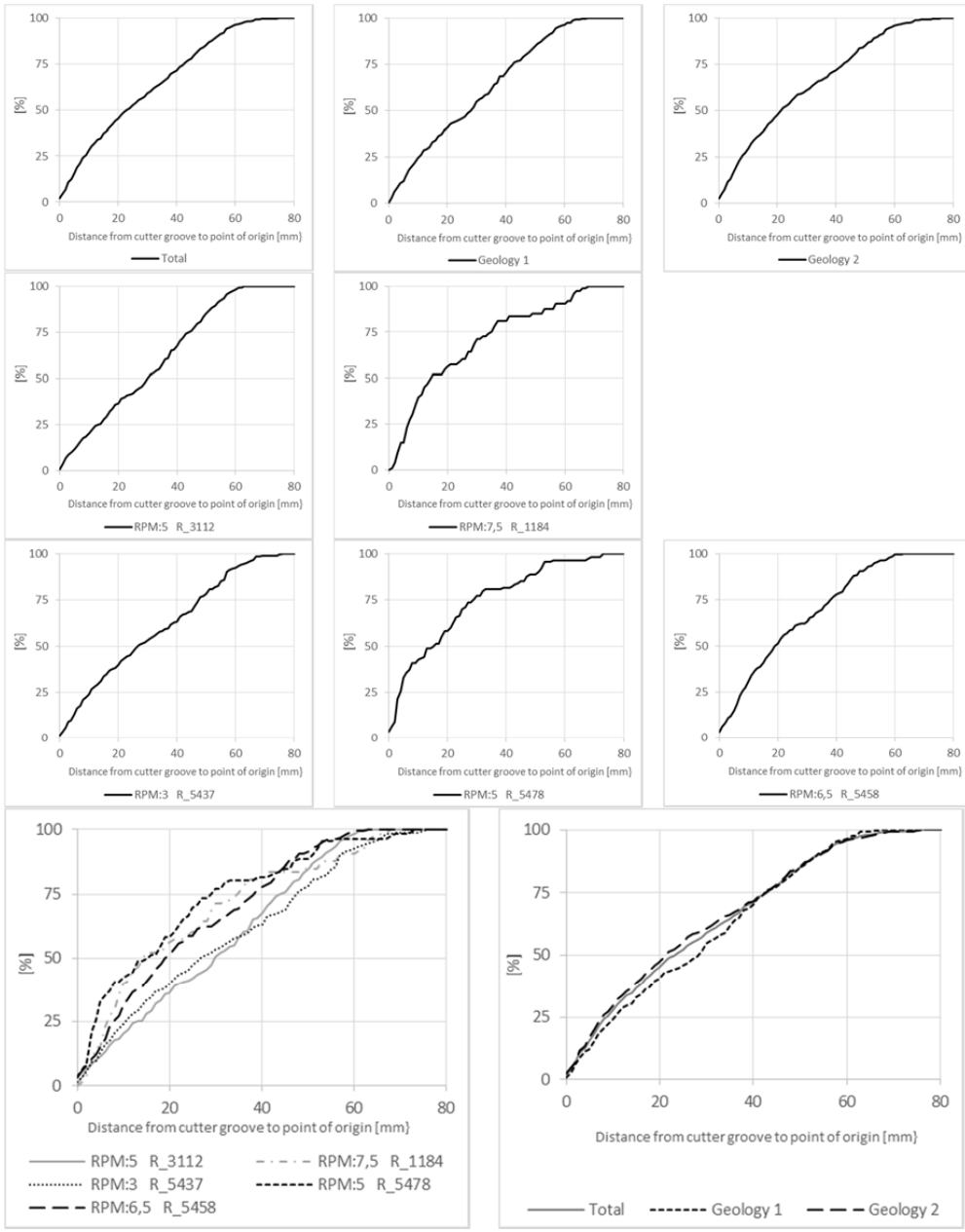

Figure J1.16: Accumulative frequency distribution of horizontal distances from point of origin to the cutter groove for all cracks with dip >3°.

J1.9 Distribution of number of cracks on the two sides of the cutter groove

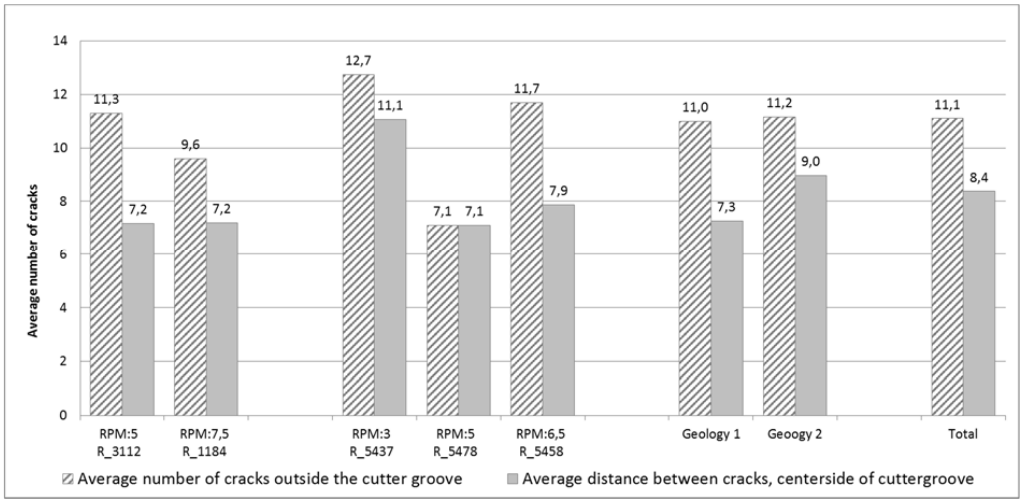

Figure J1.17: Average number of cracks on the outside and the centerside of the cutter groove. Cracks with dip >3°are not included.

J1.10 Distribution of cracks perpendicular and parallel to the cutter groove

Cracks with dip <3° are not included. Cross-marks cracks with dip way from the cutter groove, and dot marks cracks with dip towards the cutter groove.

Perpendicular to cutter groove

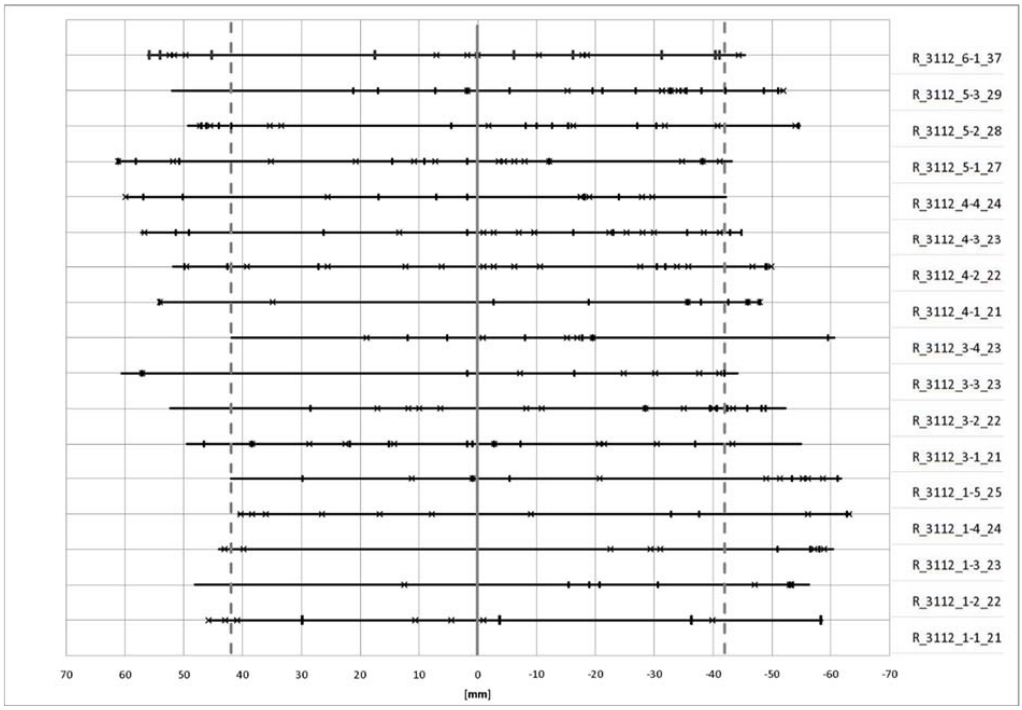

Figure J1.18: Projection of cracks from circumference to a line perpendicular to the cutter groove for the core samples from R_3112.

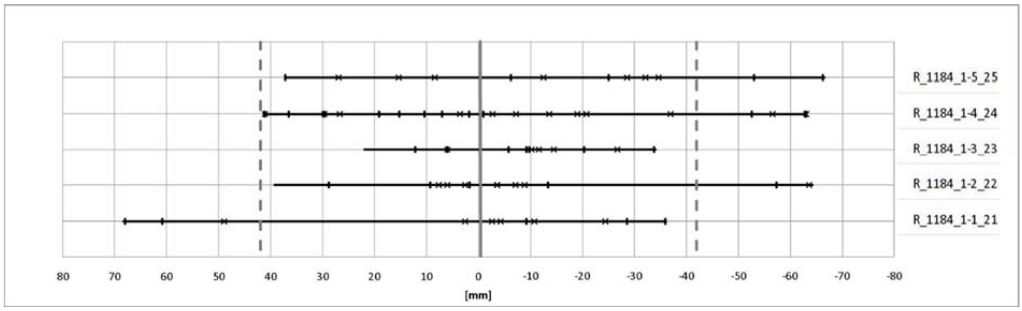

Figure J1.19: Projection of cracks from circumference to a line perpendicular to the cutter groove for the core samples from R_1184.

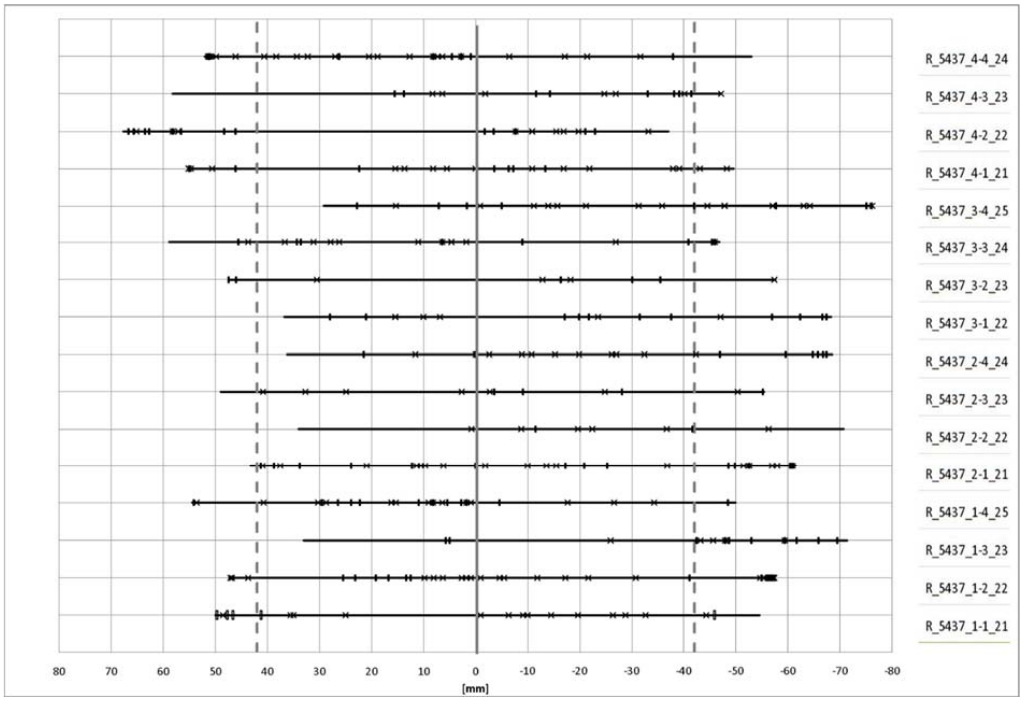

Figure J1.20: Projection of cracks from circumference to a line perpendicular to the cutter groove for the core samples from R_5437.

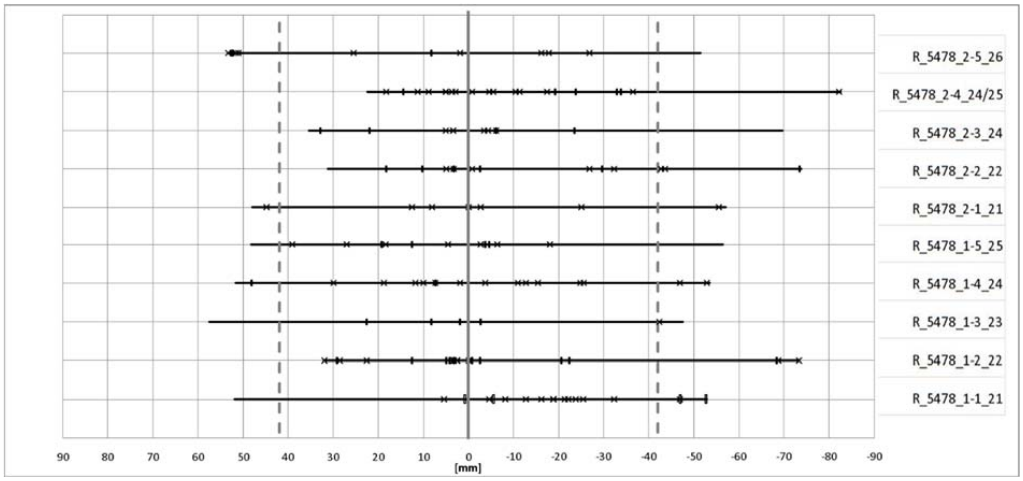

Figure J1.21: Projection of cracks from circumference to a line perpendicular to the cutter groove for the core samples from R_5478.

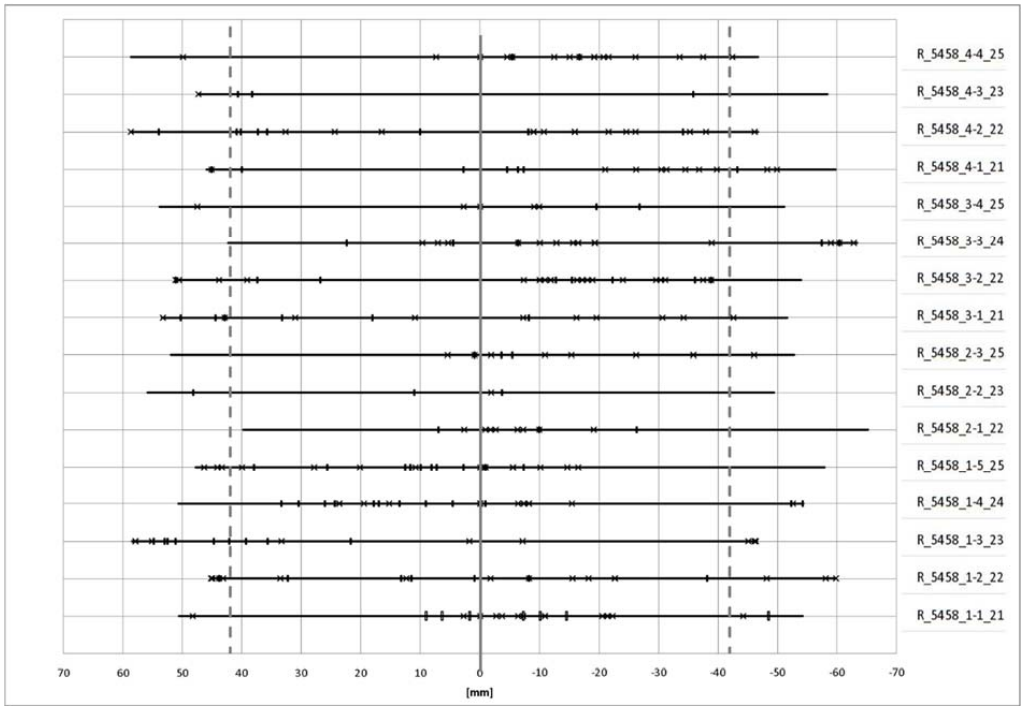

Figure J1.22: Projection of cracks from circumference to a line perpendicular to the cutter groove for the core samples from R_5458.

Parallel to cutter groove

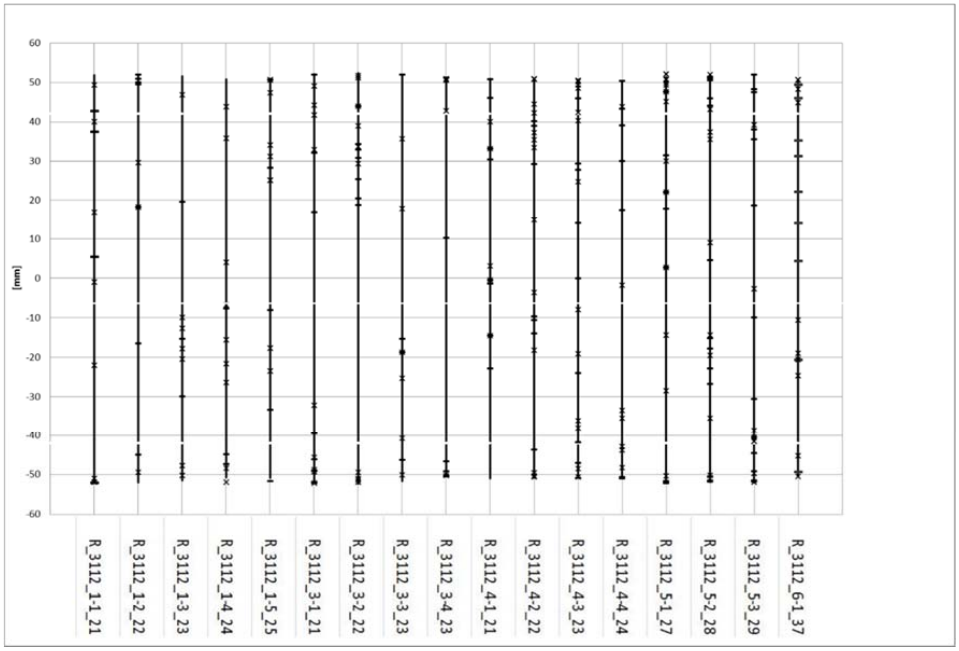

Figure J1.23: Projection of cracks from circumference to the cutter groove for the core samples from R_3112.

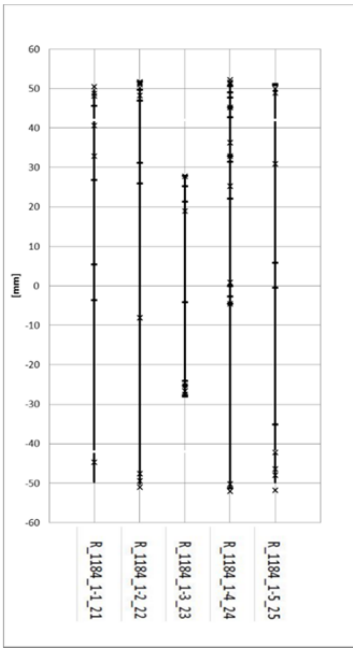

Figure J1.24: Projection of cracks from circumference to the cutter groove for the core samples from R_1184.

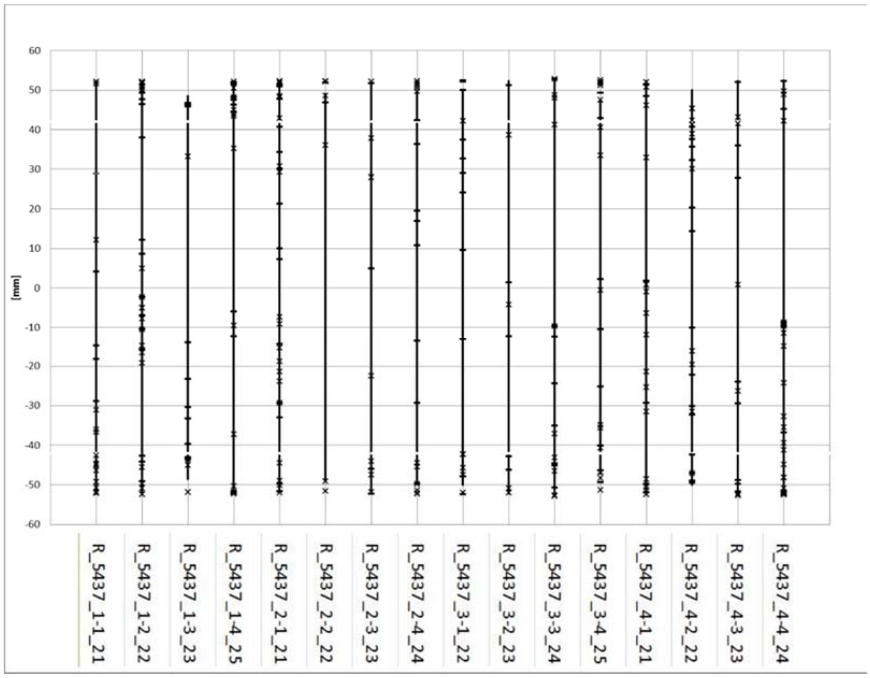

Figure J1.25: Projection of cracks from circumference to the cutter groove for the core samples from R_5437.

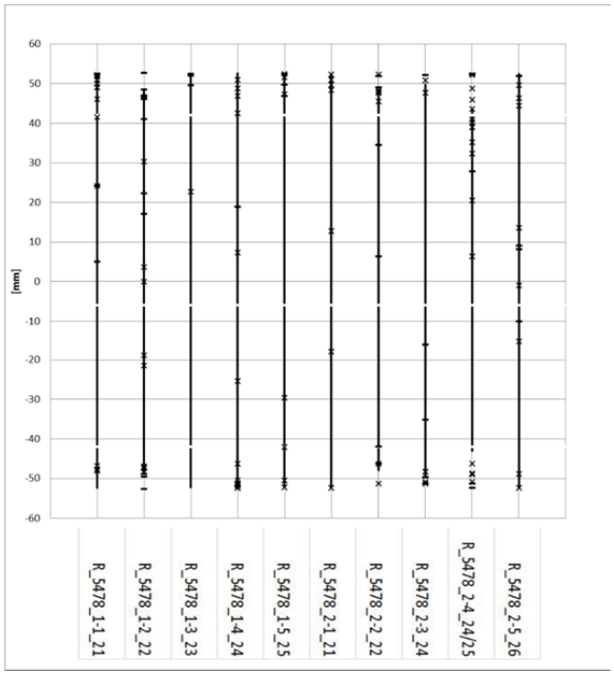

Figure J1.26: Projection of cracks from circumference to the cutter groove for the core samples from R_5478.

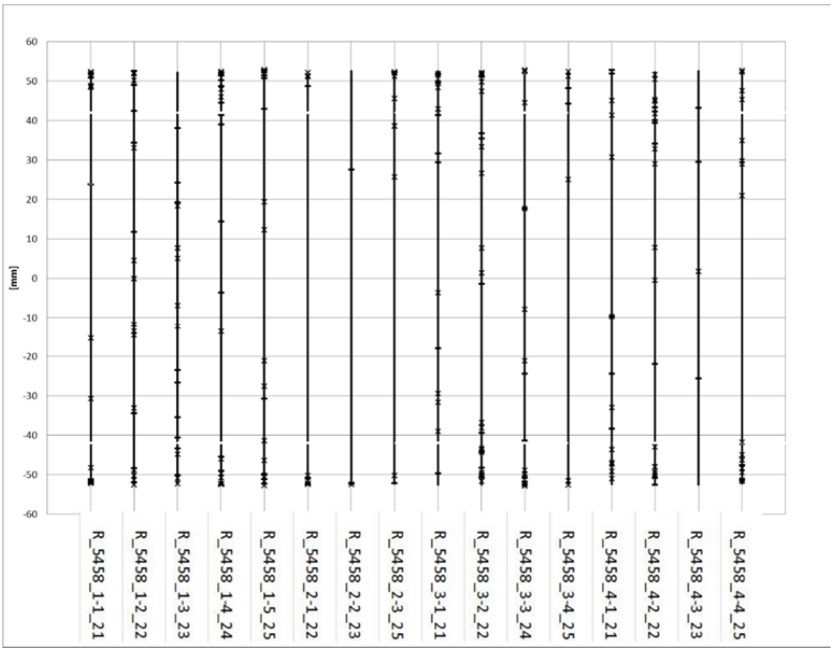

Figure J1.27: Projection of cracks from circumference to the cutter groove for the core samples from R_5458.

J1.11 Dip of crack versus average horizontal length of cracks

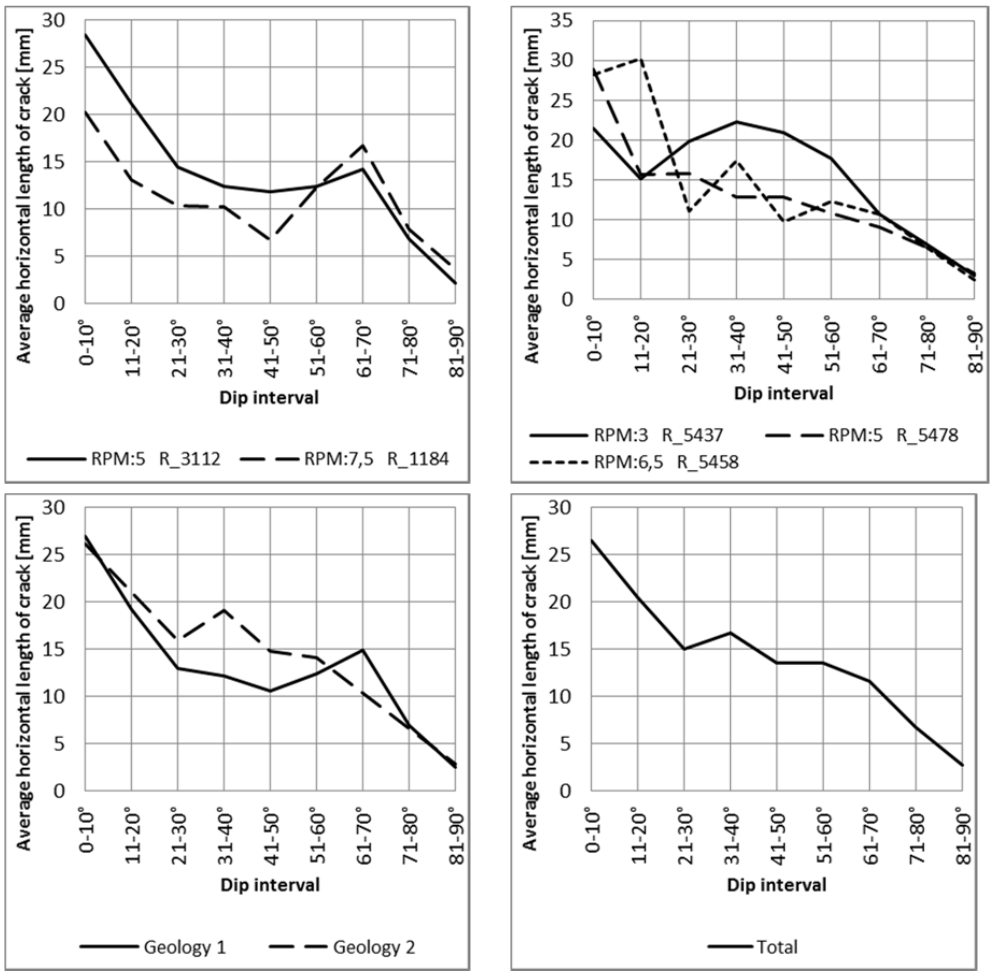

Figure J1.28: Calculated average horizontal lengths of cracks with dips within intervals of 10 ° in the core samples.

J1.12 Dip of crack versus average vertical length of cracks

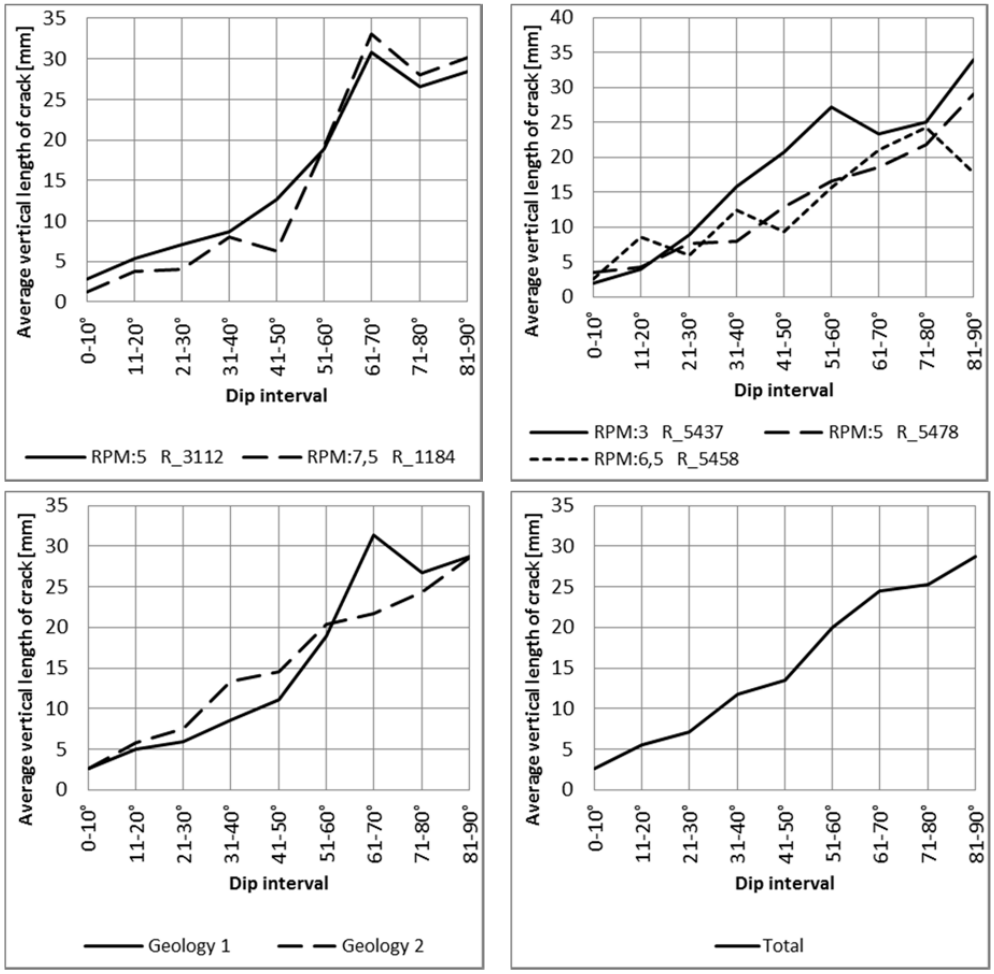

Figure J1.29: Calculated average vertical lengths of cracks with dips within intervals of 10 ° in the core samples.

J1.13 Dip of crack versus average total length of cracks

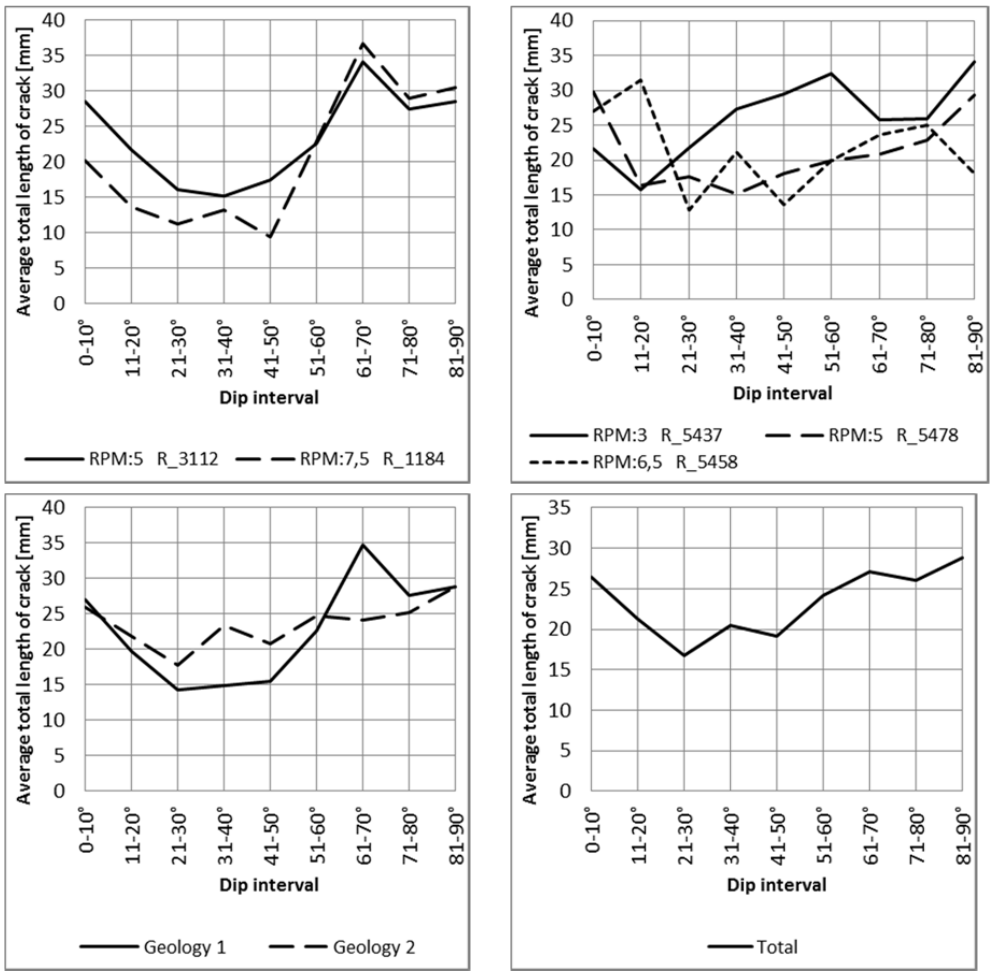

Figure J1.30: Calculated average total lengths of cracks with dips within intervals of 10 ° in the core samples.

J1.14 Dip of cracks versus average vertical distance from surface line to crack end

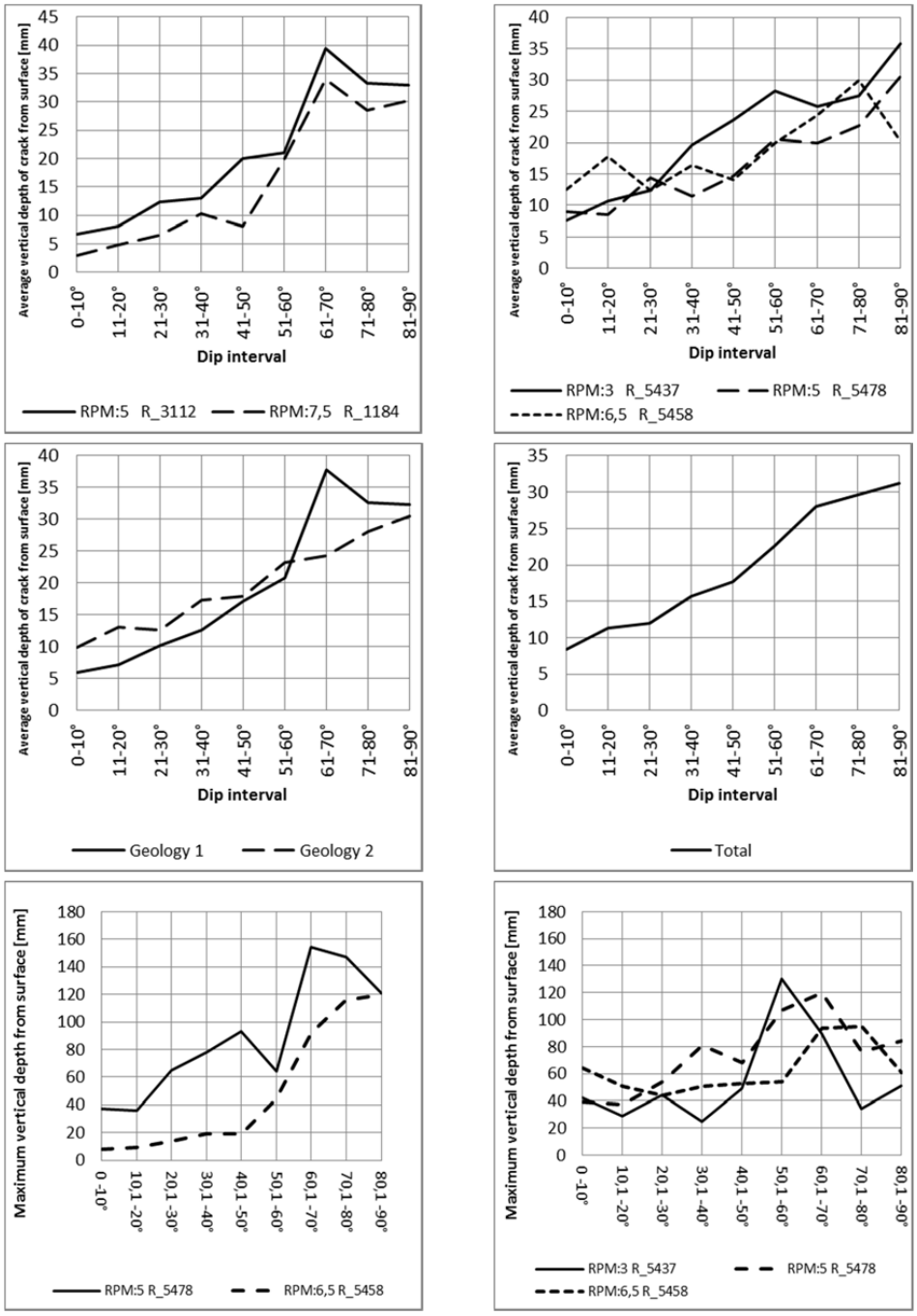

Figure J1.31: Calculated average vertical depths from the surface line of cracks with dips within intervals of 10 ° in the core samples.

J1.15 Dip of crack versus average vertical distance from 0-line to crack end

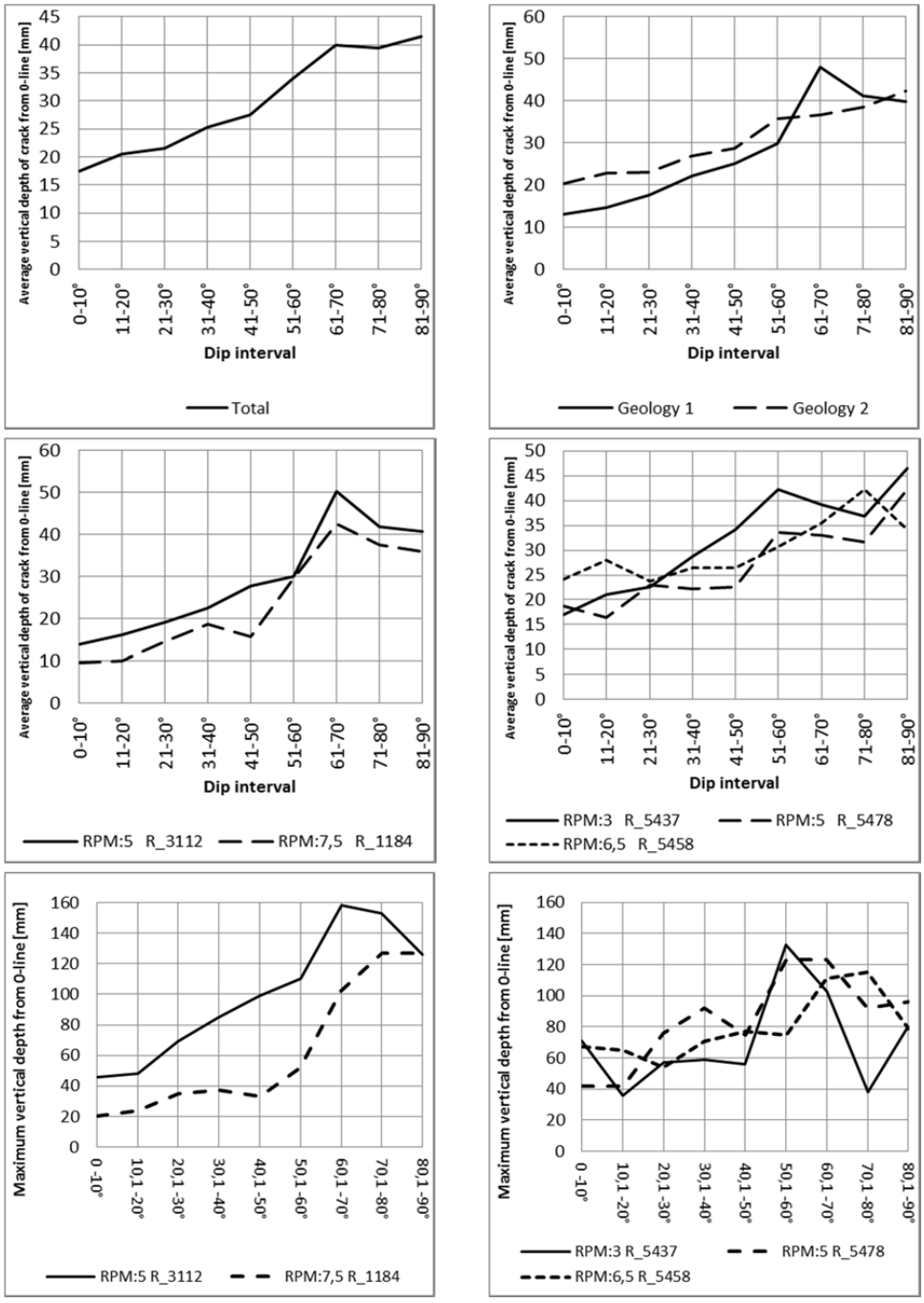

Figure J1.32: Calculated average vertical depths from the 0-line of cracks with dips within intervals of 10 ° in the core samples.

J1.16 Dip of cracks versus horizontal distance from the point of origin to the cutter groove

a)

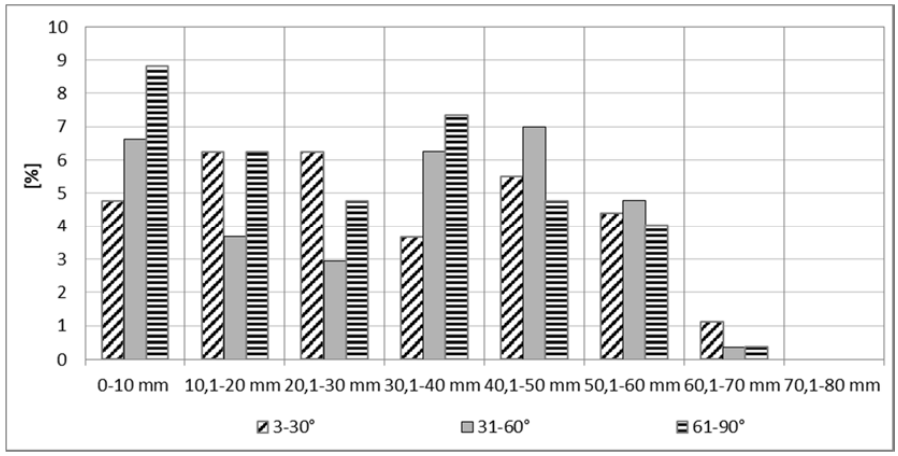

b)

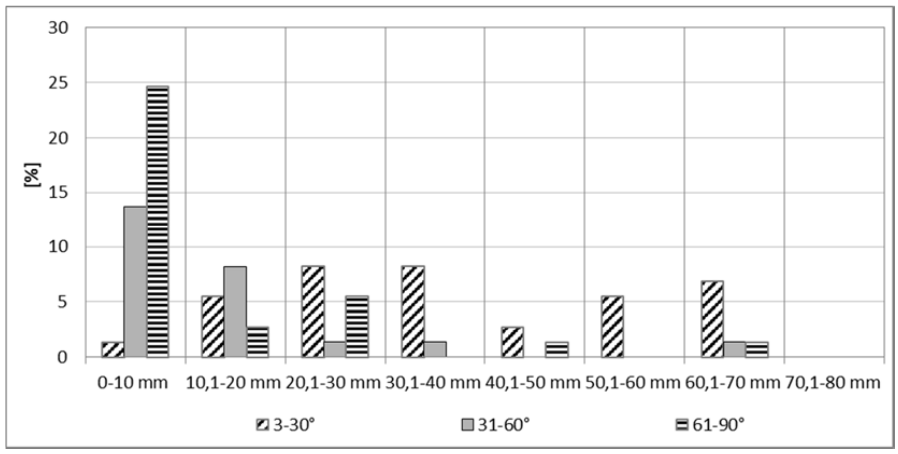

Figure J1.33: Distribution of dip of cracks versus horizontal distance from the point of origin to the cutter groove
for the core samples. Cracks with dip < 3 ° are not included. A) R_3112. B) R_1184.

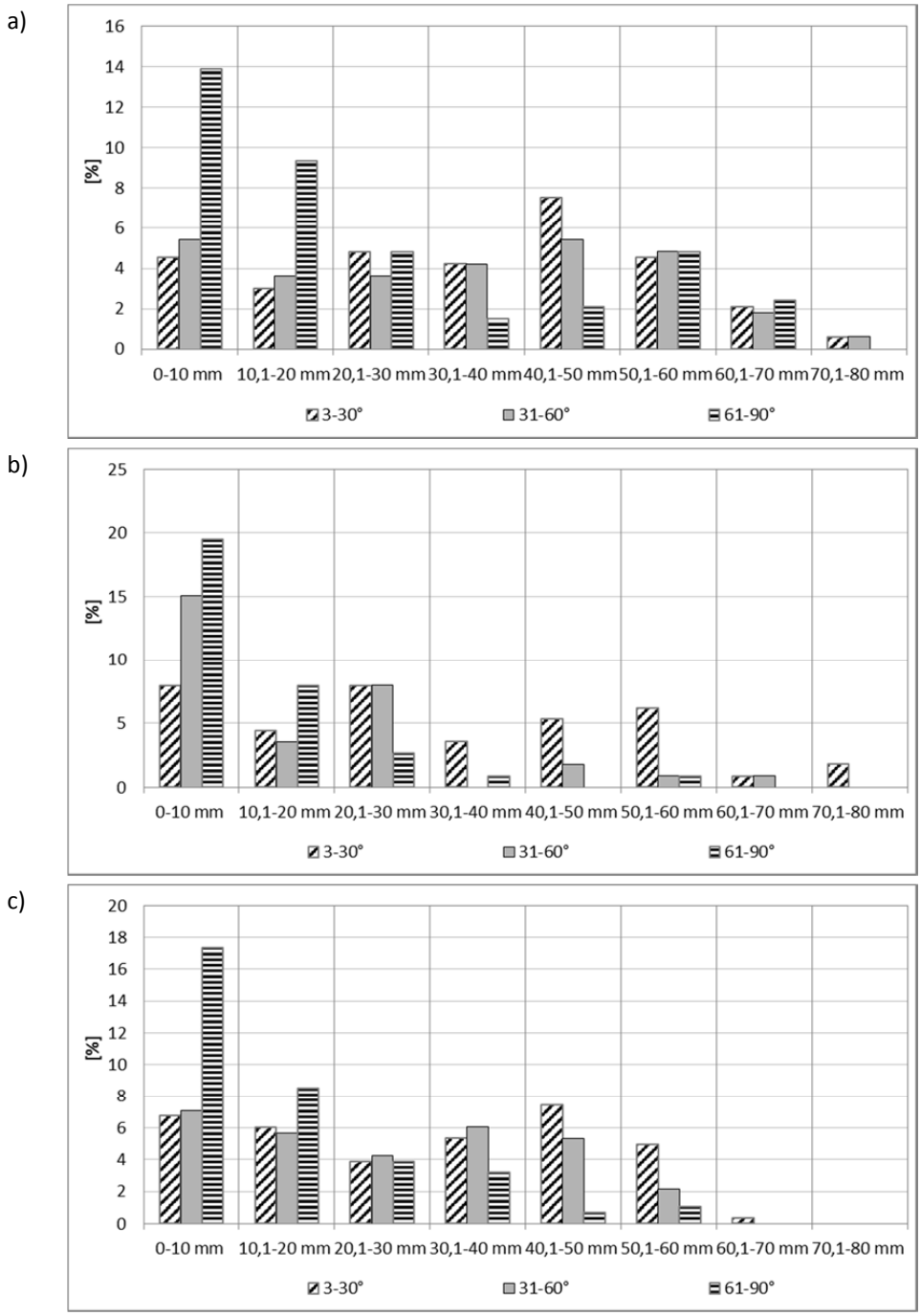

Figure J1.34: Distribution of dips related to the point of origin in relation to the cutter groove for the core samples. Cracks with dip < 3 ° are not included. A) R_5437. B) R_5478. C) R_5458.

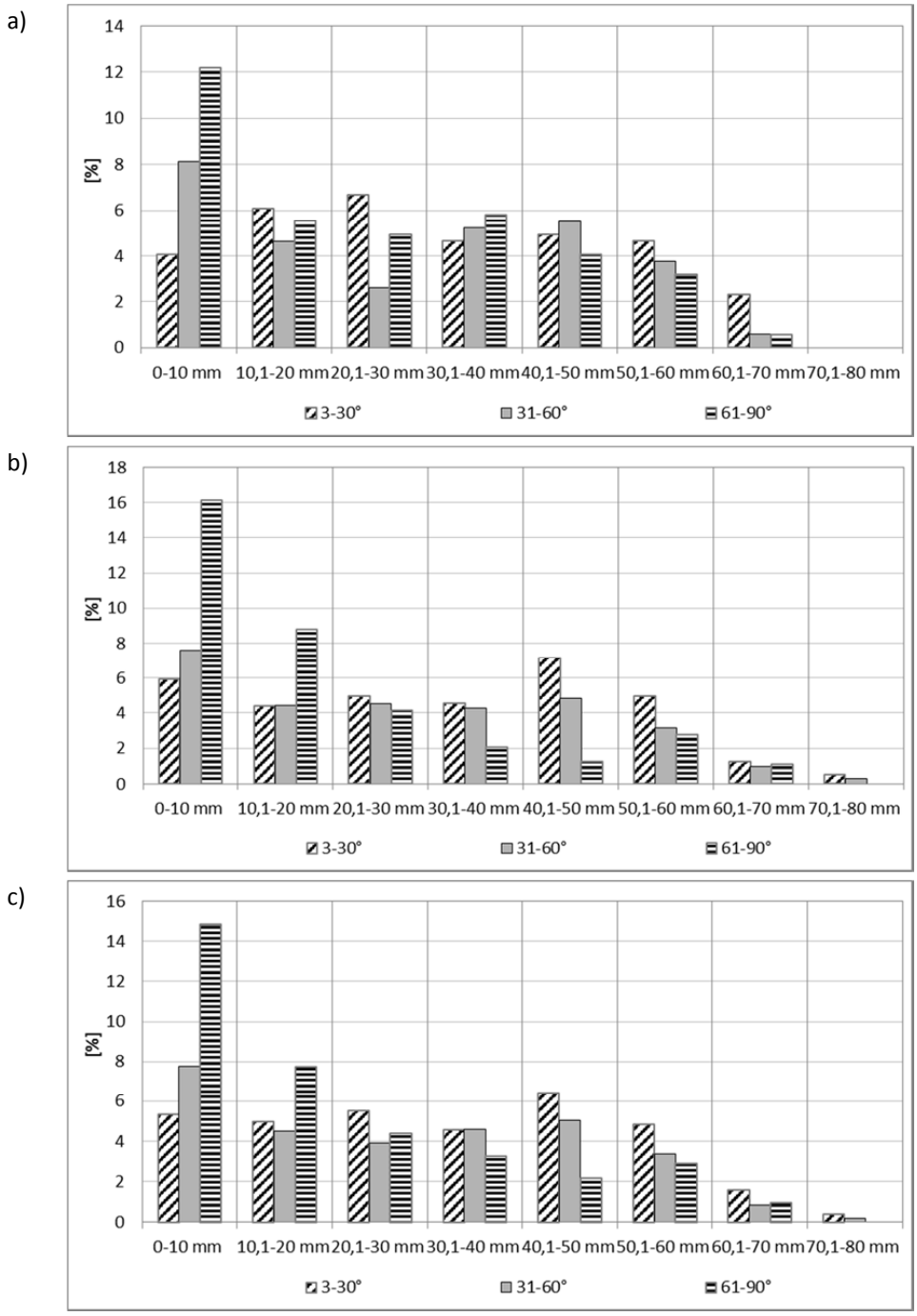

Figure J1.35: Distribution of dips related to the point of origin in relation to the cutter groove for the core samples. Cracks with dip < 3 ° are not included. A) Geology 1. B) Geology 2. C) All cracks

J1.17 Horizontal distance from point of origin to cutter groove versus dip angles and dip direction of crack

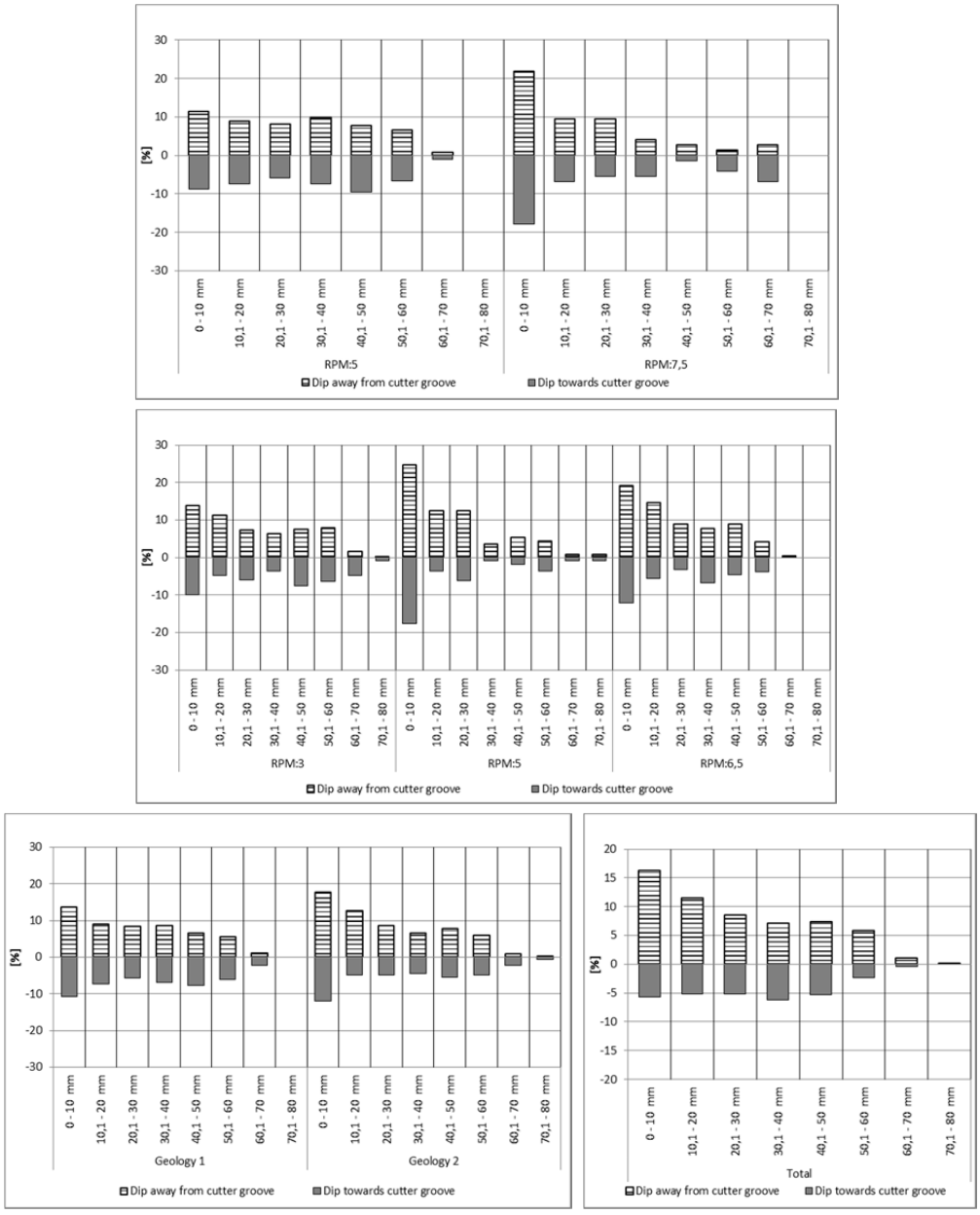

Figure J1.36: Distribution of dip directions related to the point of origin in relation to the cutter groove for the core samples. Cracks with dip < 3 ° are not included.

a)

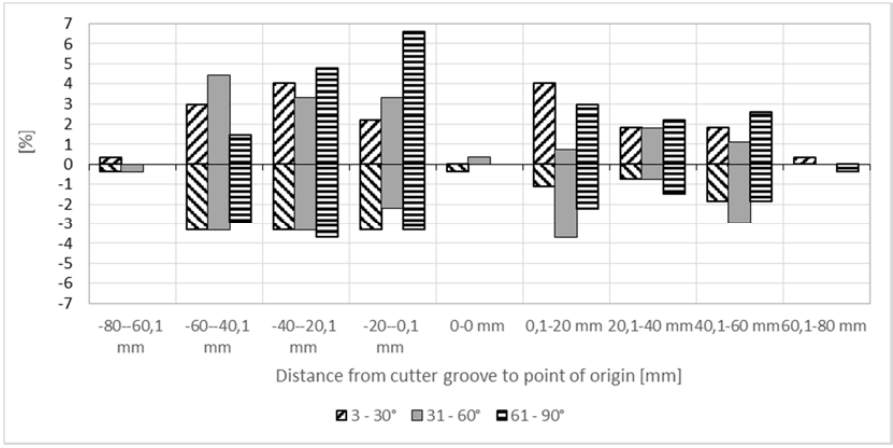

b)

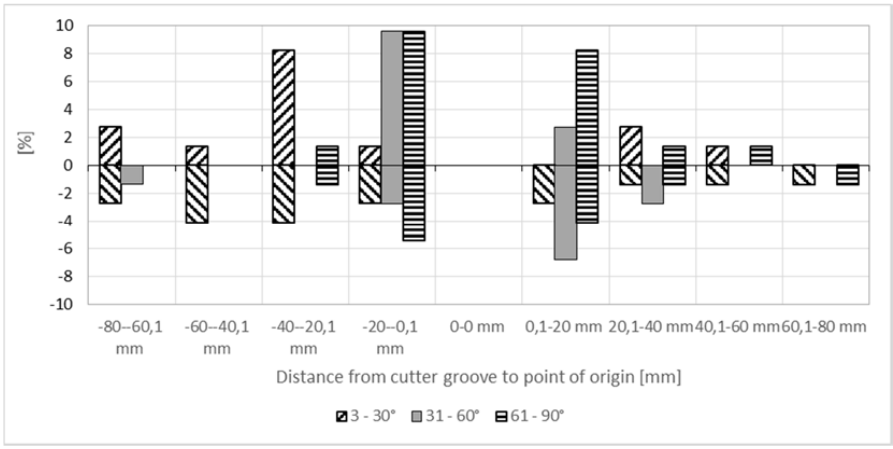

Figure J1.37: Distribution of dips and dip directions related to the point of origin in relation to the cutter groove for the core samples. Cracks with dip < 3 ° are not included. A) R_3112. B) R_1184.

a)

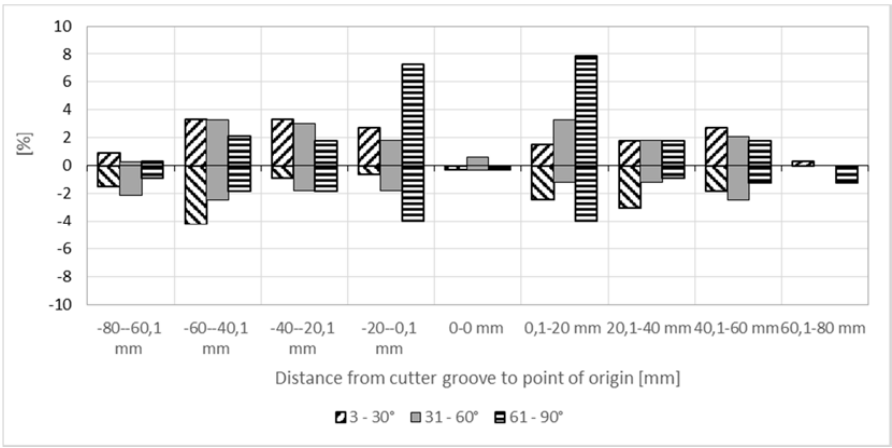

b)

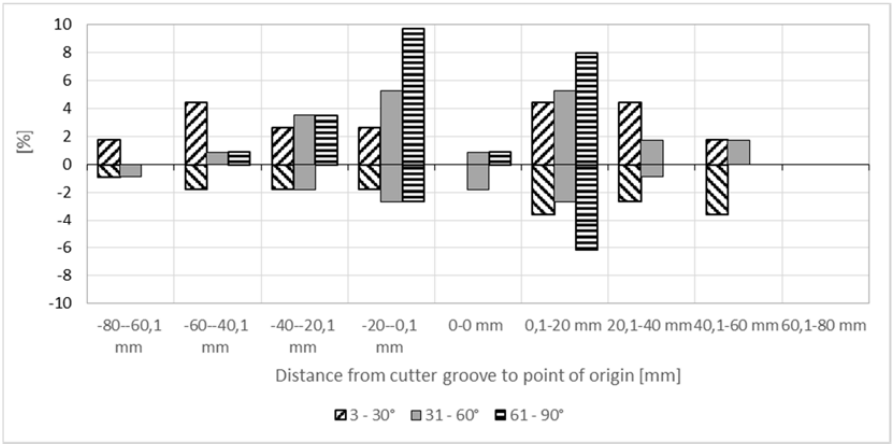

c)

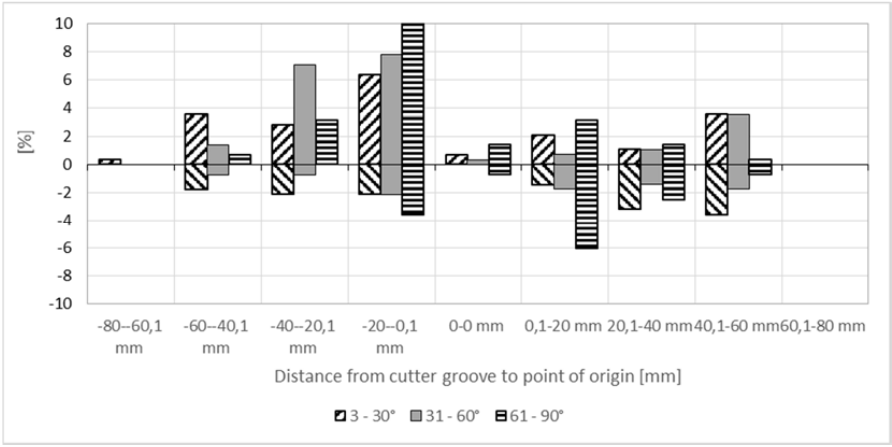

Figure J1.38: Distribution of dip and dipdirections related to the point of origin in relation to the cutter groove for the core samples. Cracks with dip < 3 ° are not included.A) R_5437. B) R_5478. C) R_5458.

a)

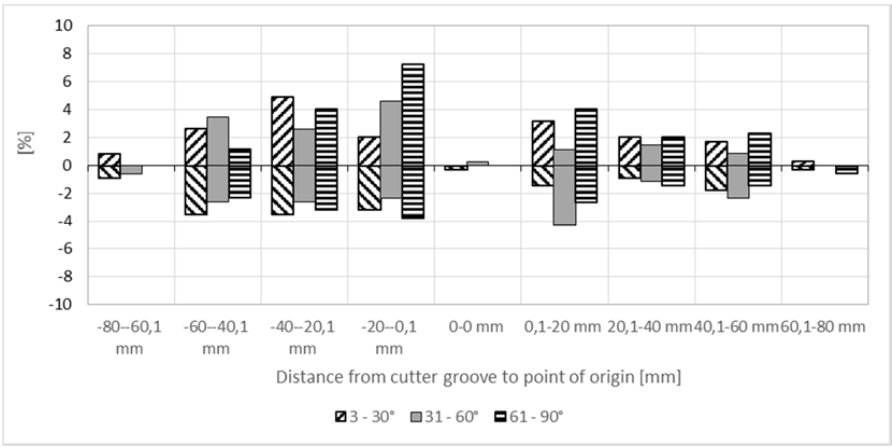

b)

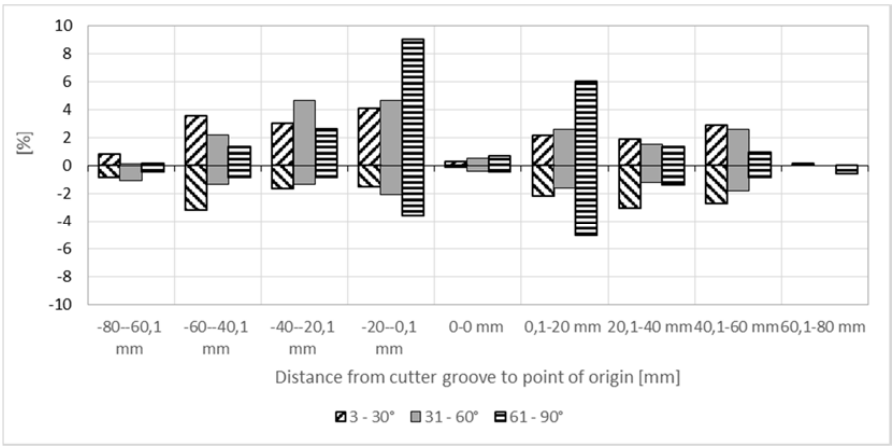

c)

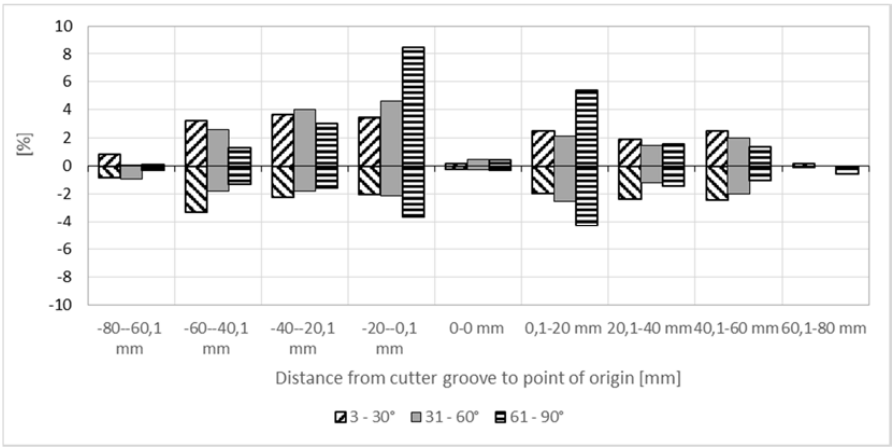

Figure J1.39: Distribution of dip and dipdirections related to the point of origin in relation to the cutter groove for the core samples. Cracks with dip < 3 ° are not included.A) Geology 1. B) Geology 2. C) All cracks

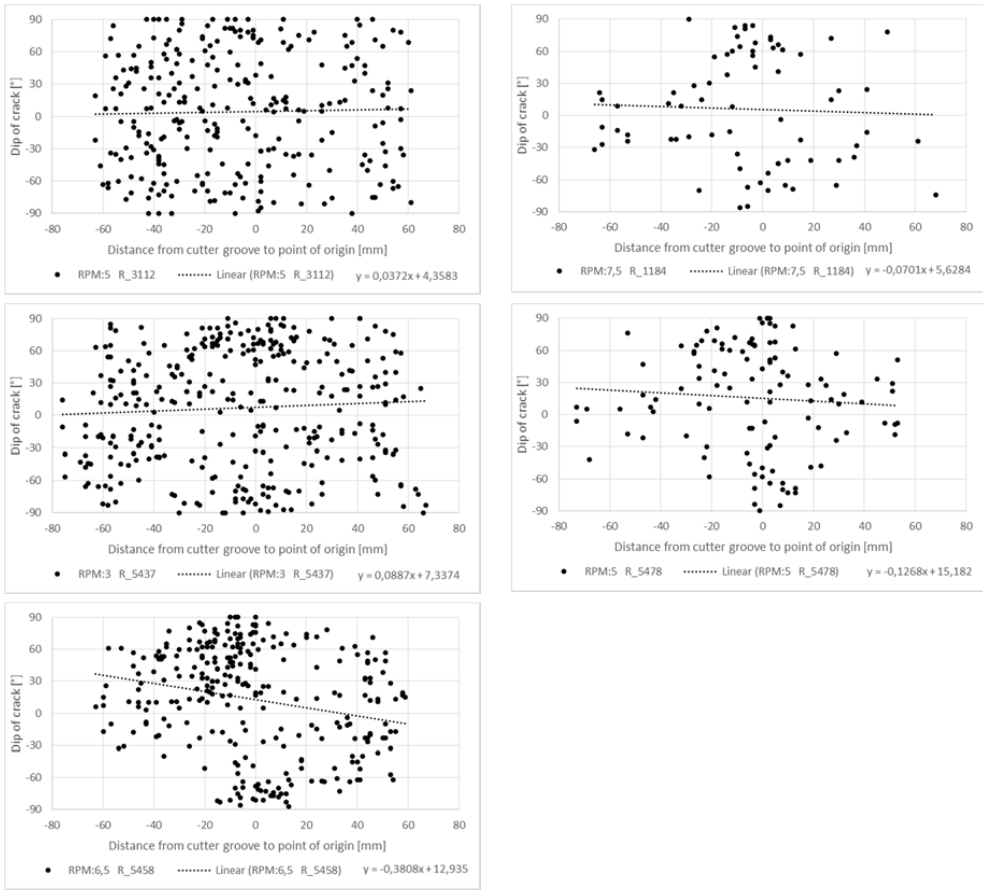

Figure J1.40: Dip values, dip direction and exact point of origin in relation to the cutter groove for all cracks with dip >3° in the core samples.

J1.18 Horizontal distance from point of origin to cutter groove versus total length of crack

a)

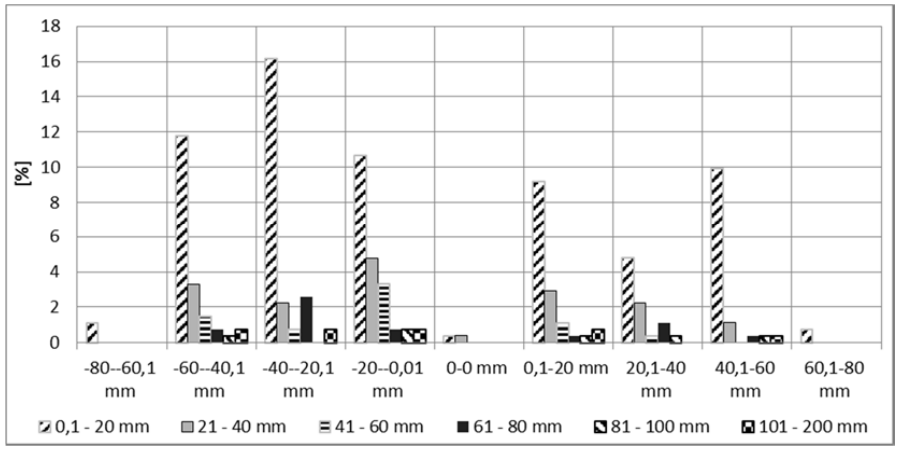

b)

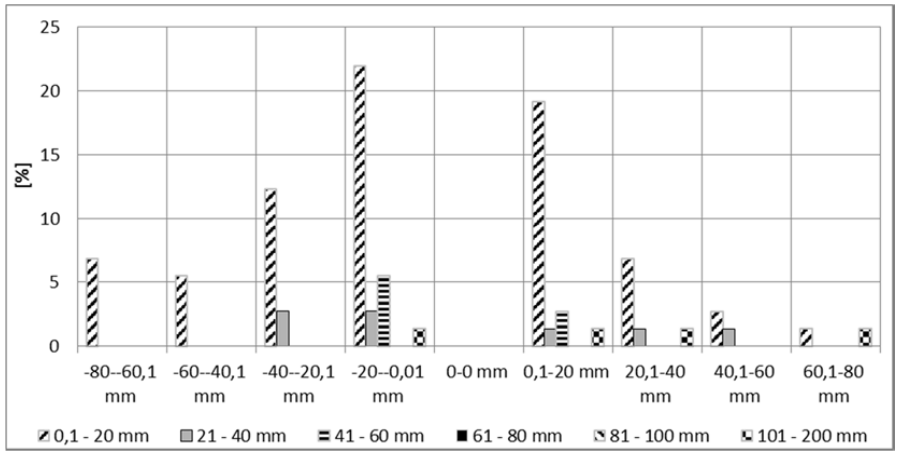

Figure J1.41: Distribution of total lenghs of crack related to the point of origin in relation to the cutter groove for the core samples. Cracks with dip < 3 ° are not included. A) R_3112. B) R_1184.

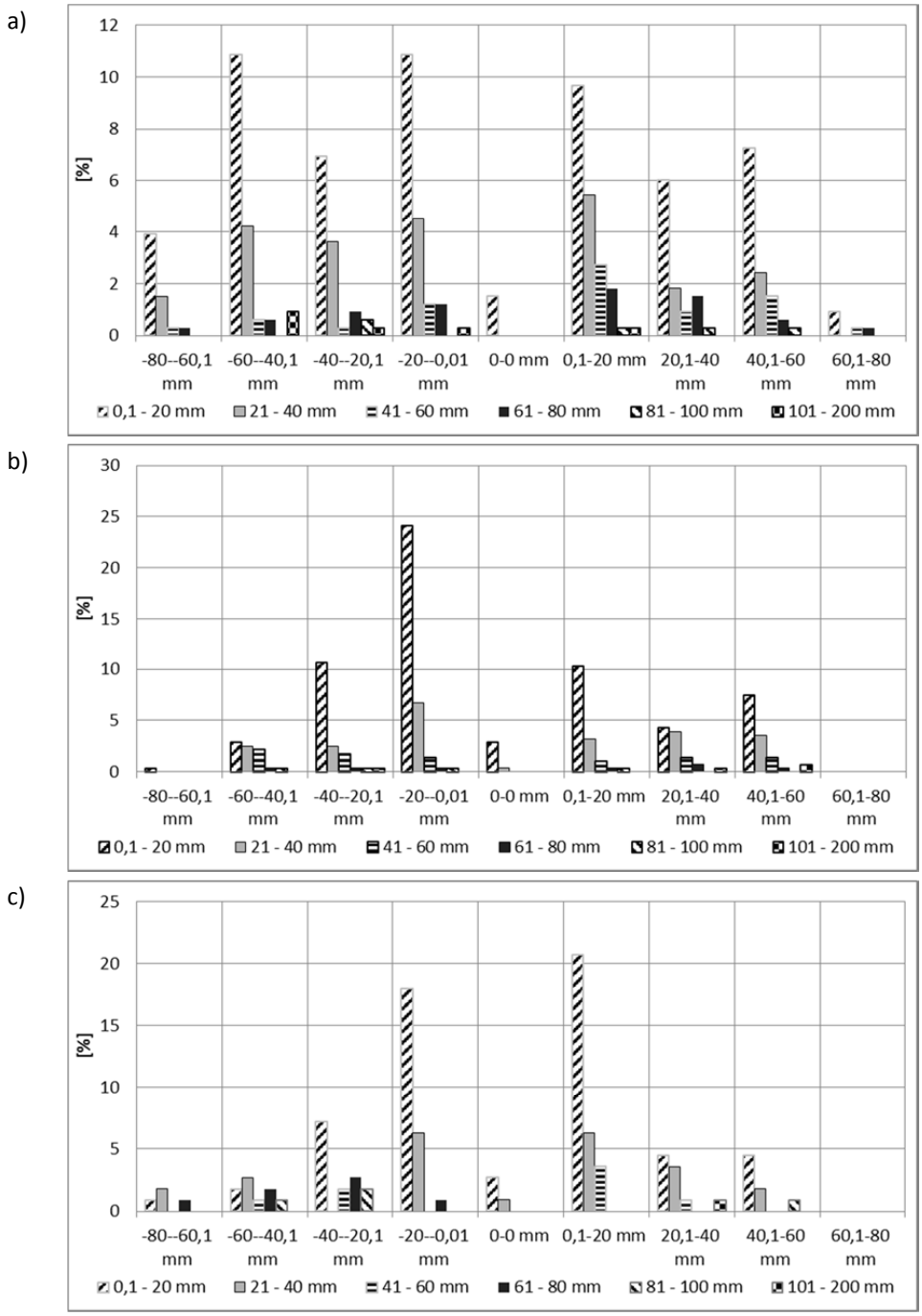

Figure J1.42: Distribution of total lenghs of crack related to the point of origin in relation to the cutter groove for the core samples. Cracks with dip < 3 ° are not included. A) R_5437. B) R_5478. C) R_5458.

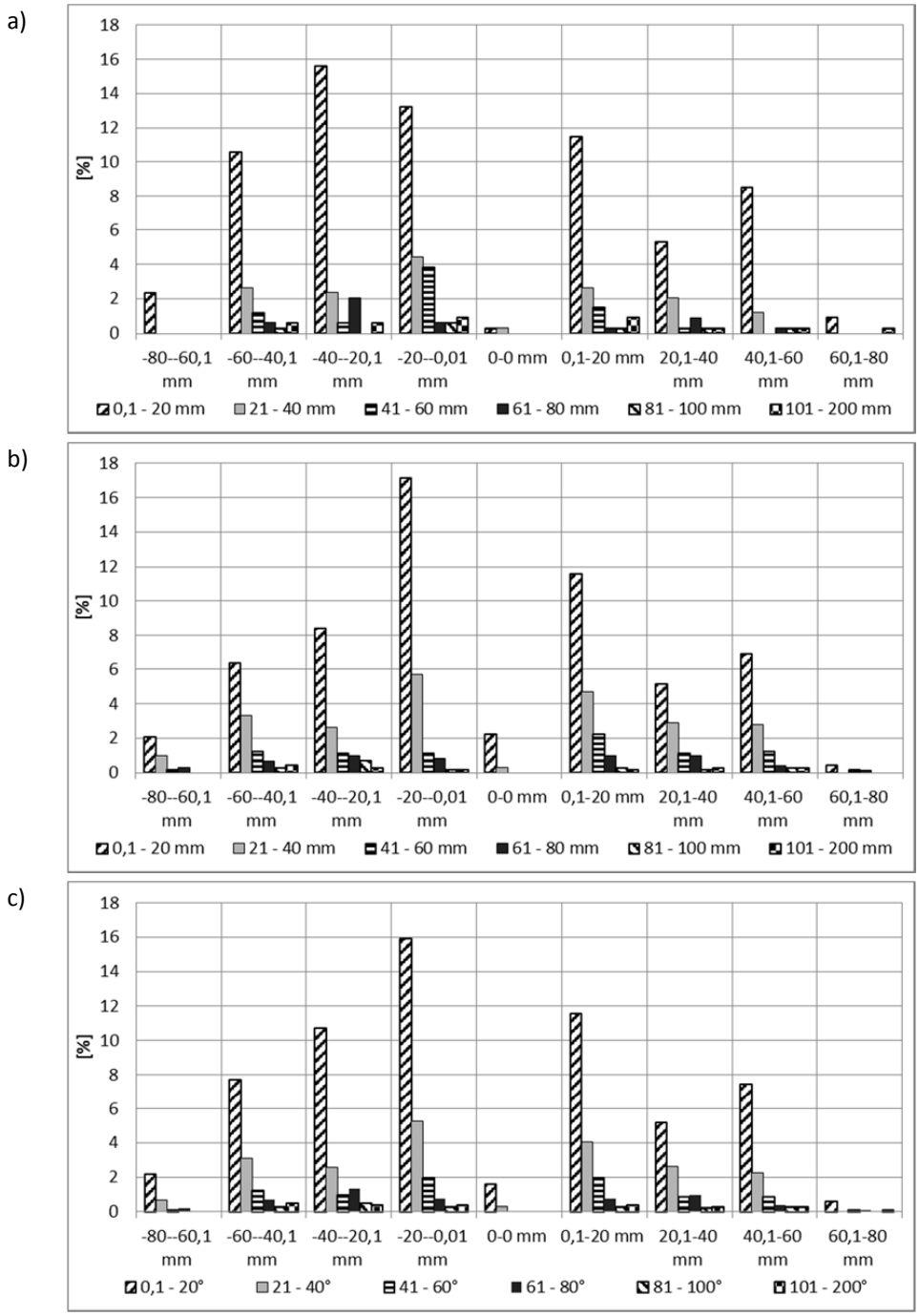

Figure J1.43: Distribution of total lenghs of crack related to the point of origin in relation to the cutter groove for the core samples. Cracks with dip < 3 ° are not included. A) Geology 1. B) Geology 2. C) All cracks.

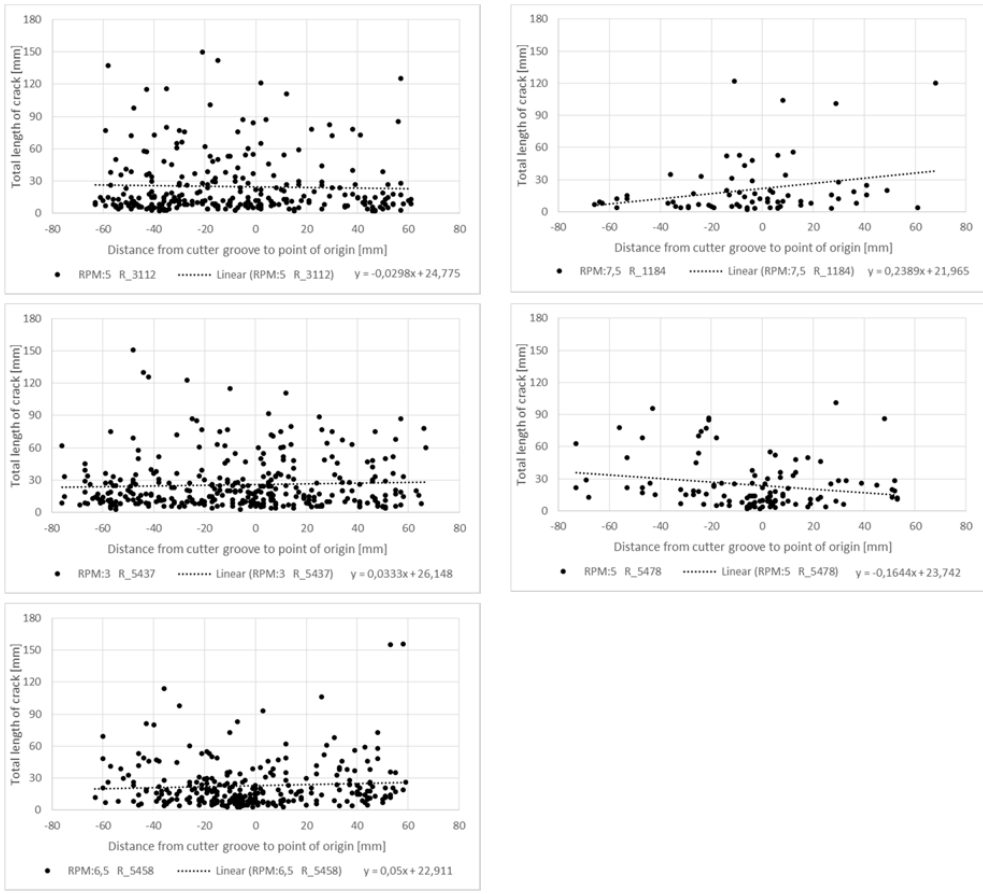

Figure J1.44: Total lengths of cracks and exact point of origin in relation to the cutter groove for all cracks with dip >3° in the core samples.

J1.19 Horizontal distance from point of origin to cutter groove versus vertical distance from surface line to end of crack

a)

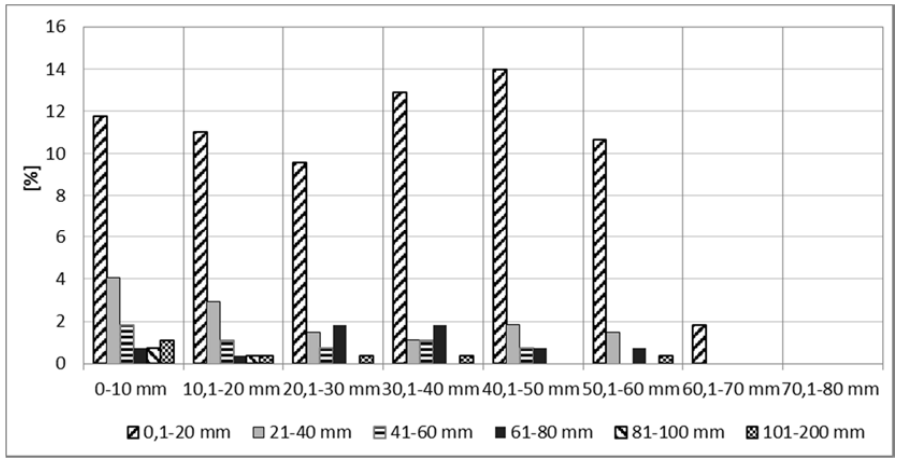

b)

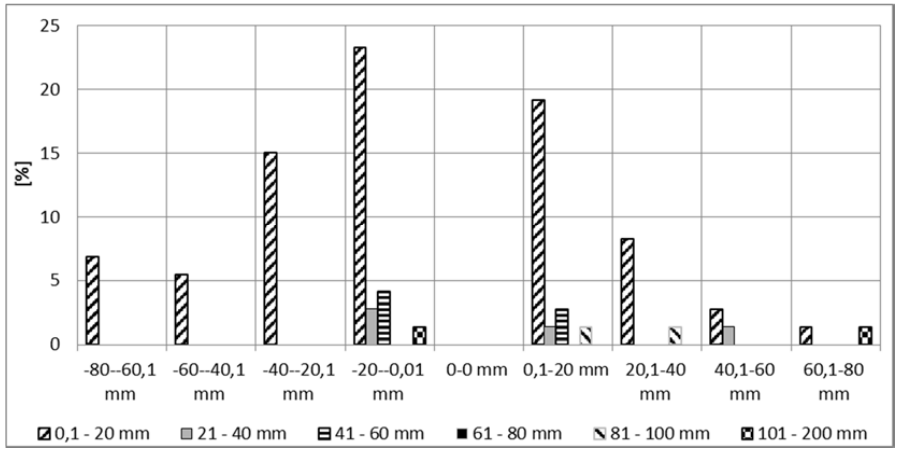

Figure J1.45: Distribution verticl depth from surface lines related to the point of origin in relation to the cutter groove for the core samples. Cracks with dip < 3 ° are not included. A) R_3112. B) R_1184.

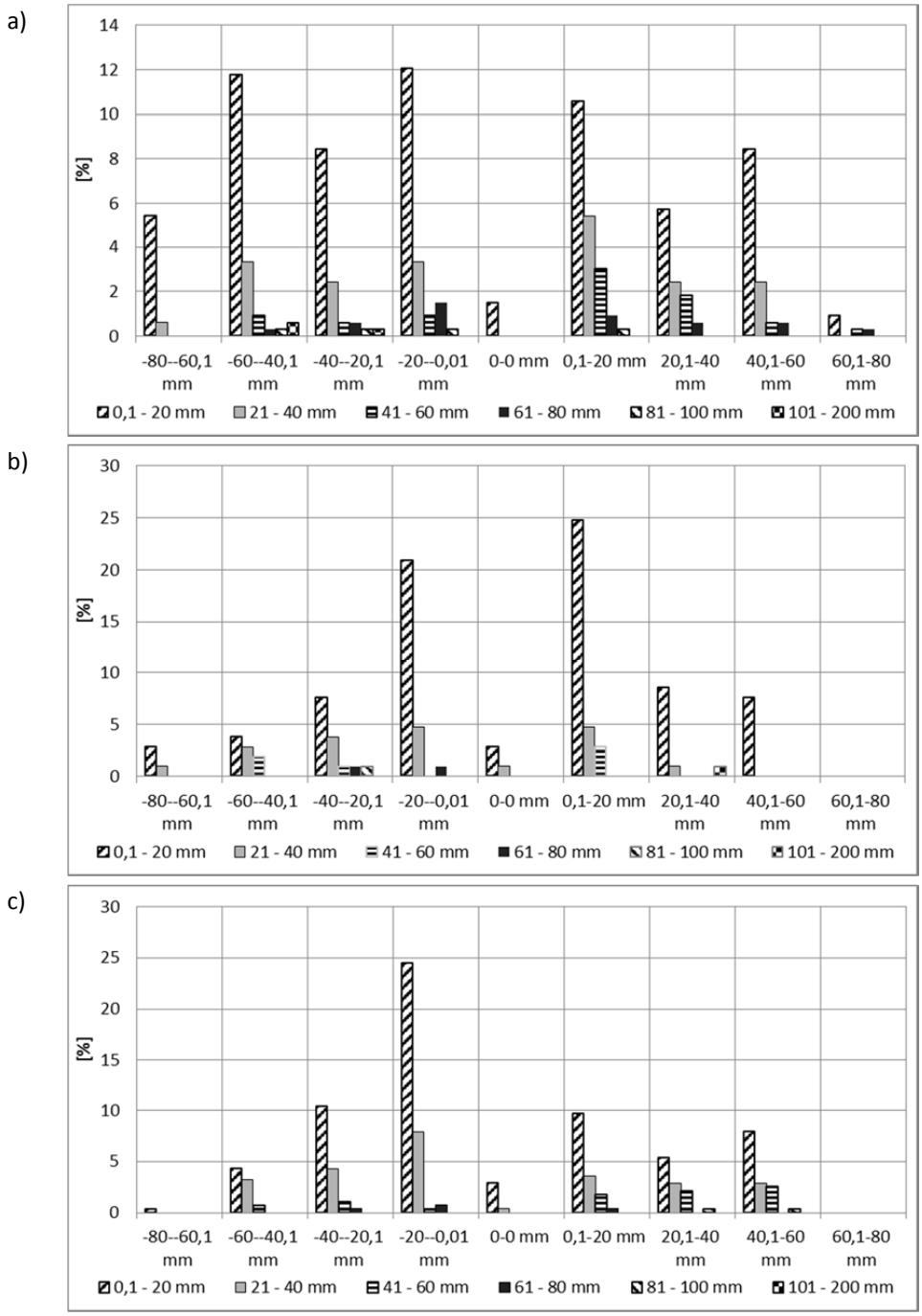

Figure J1.46: Distribution verticl depth from surface lines related to the point of origin in relation to the cutter groove for the core samples. Cracks with dip < 3 ° are not included. A) R_5437. B) R_5478. C) R_5458.

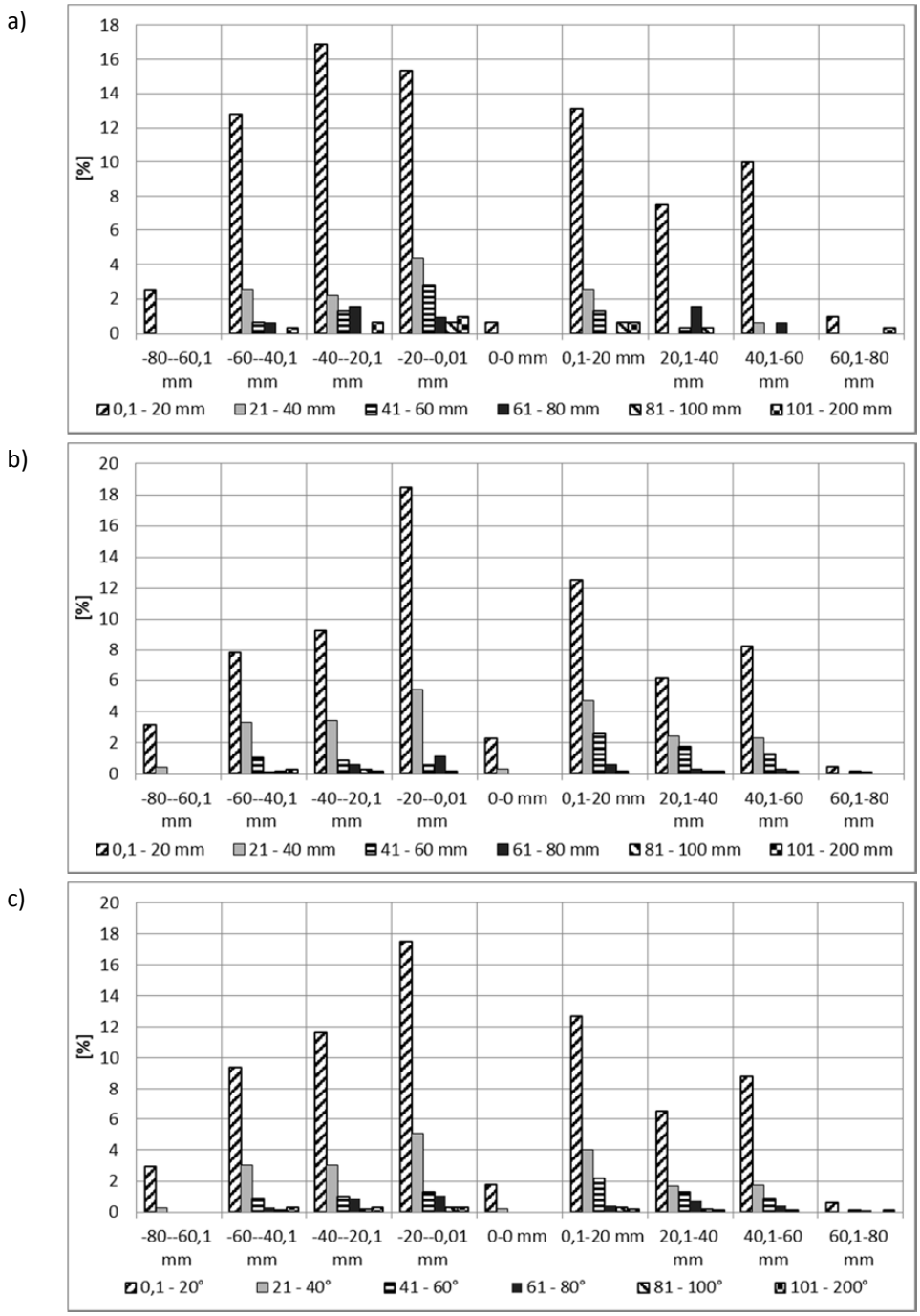

Figure J1.47: Distribution verticl depth from surface lines related to the point of origin in relation to the cutter groove for the core samples. Cracks with dip < 3 ° are not included. A) Geology 1. B) Geology 2. C) All cracks.

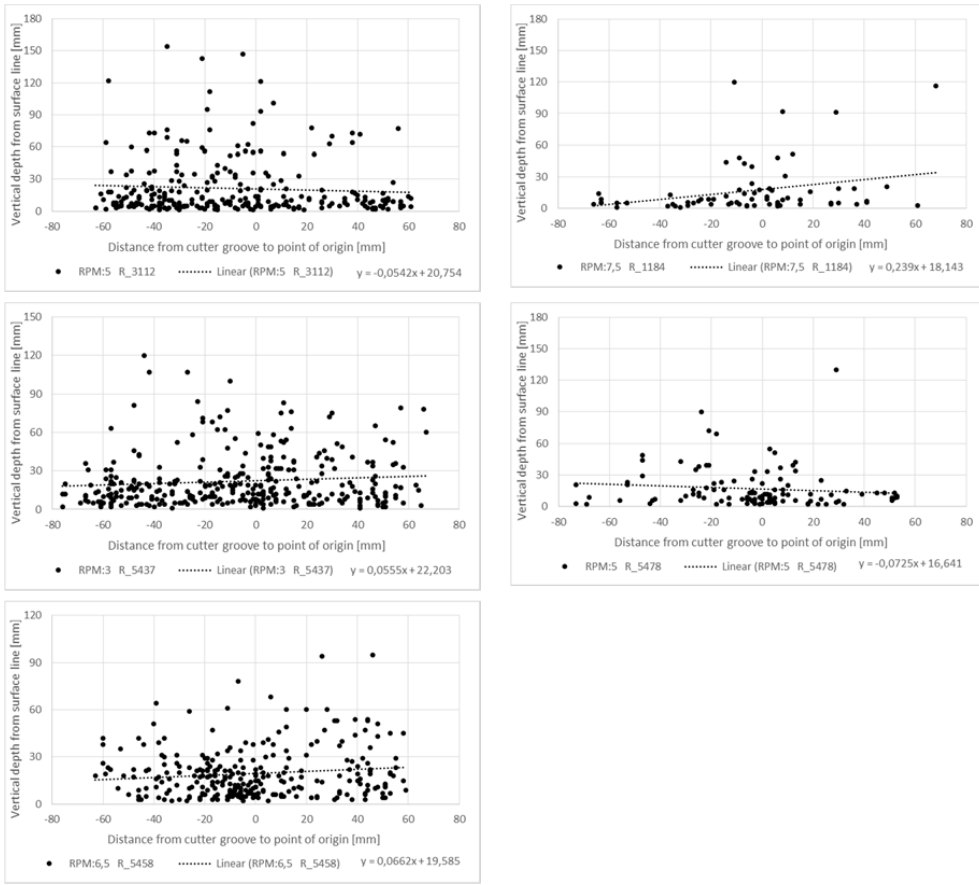

Figure J1.48: Vertical depth from surface line and exact point of origin in relation to the cutter groove for all cracks with dip >3° in the core samples.

J1.20 Horizontal distance from point of origin to cutter groove versus vertical distance from 0-line to end of crack

a)

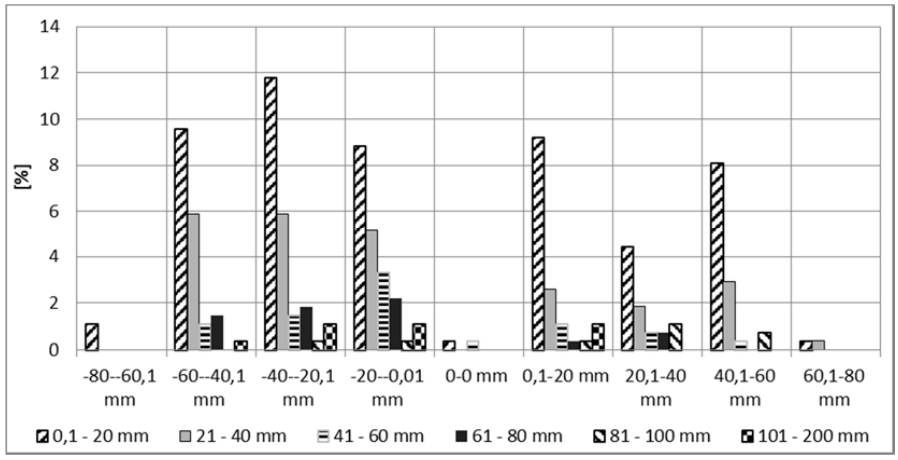

b)

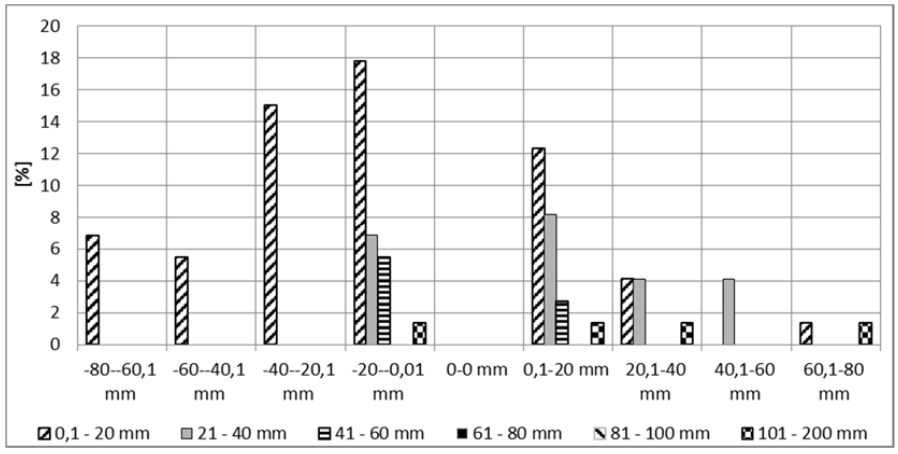

Figure J1.49: Distribution verticl depth from 0-lines related to the point of origin in relation to the cutter groove for the core samples. Cracks with dip < 3 ° are not included. A) R_3112. B) R_1184.

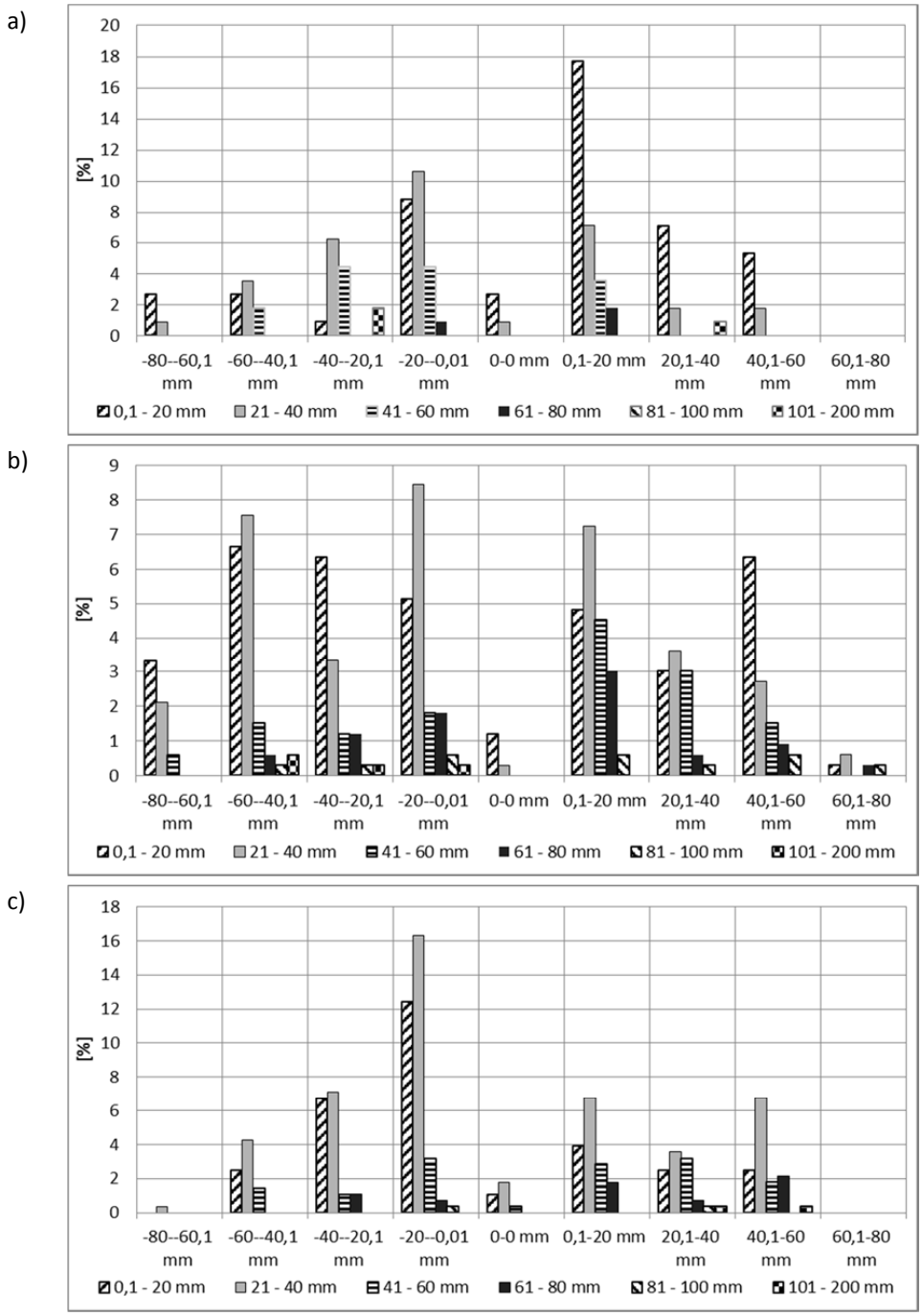

Figure J1.50: Distribution verticl depth from 0-lines related to the point of origin in relation to the cutter groove for the core samples. Cracks with dip < 3 ° are not included. A) R_5437. B) R_5478. C) R_5458.

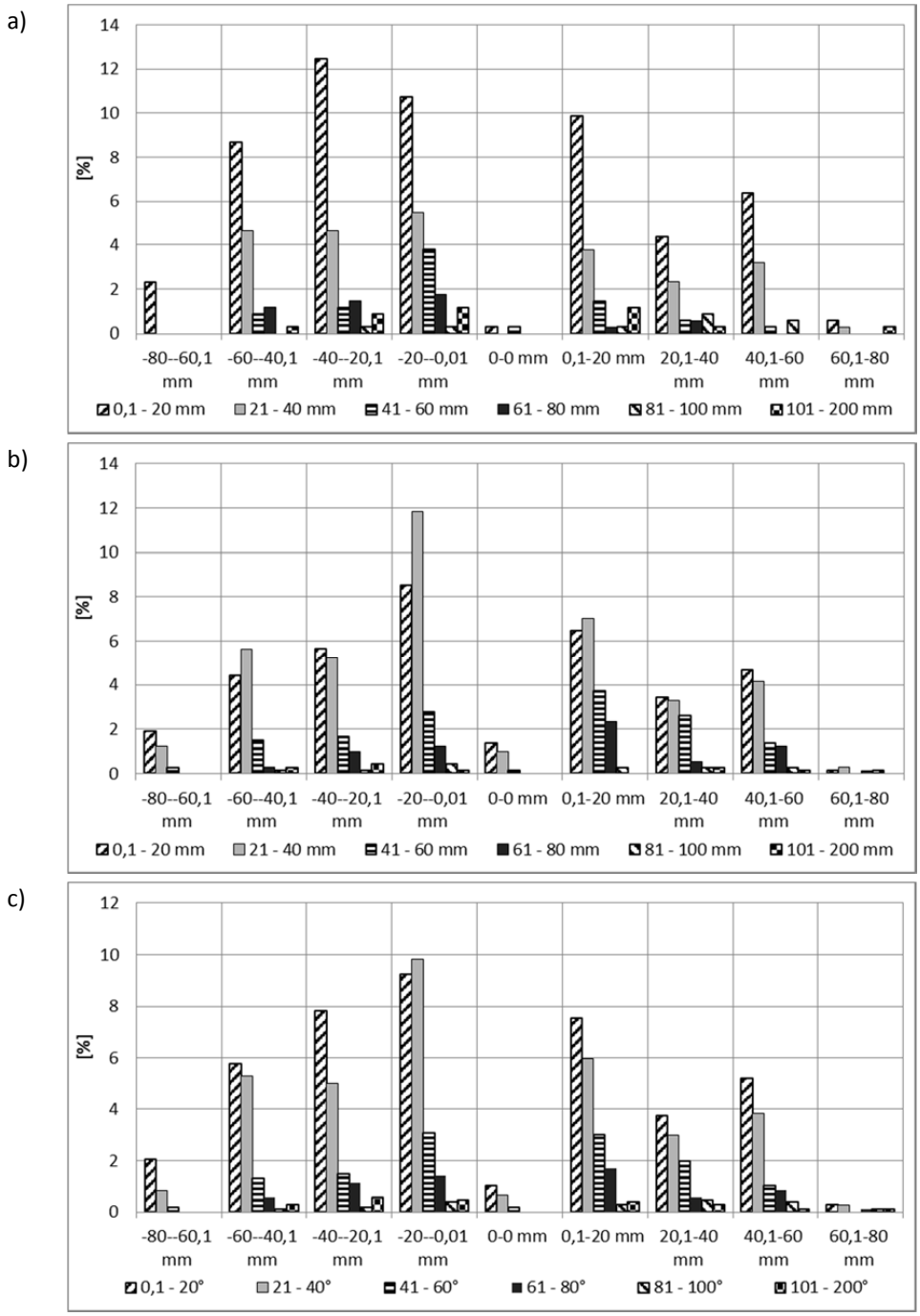

Figure J1.51: Distribution verticl depth from 0-lines related to the point of origin in relation to the cutter groove for the core samples. Cracks with dip < 3 ° are not included. A) Geology 1. B) Geology 2. C) All cracks.

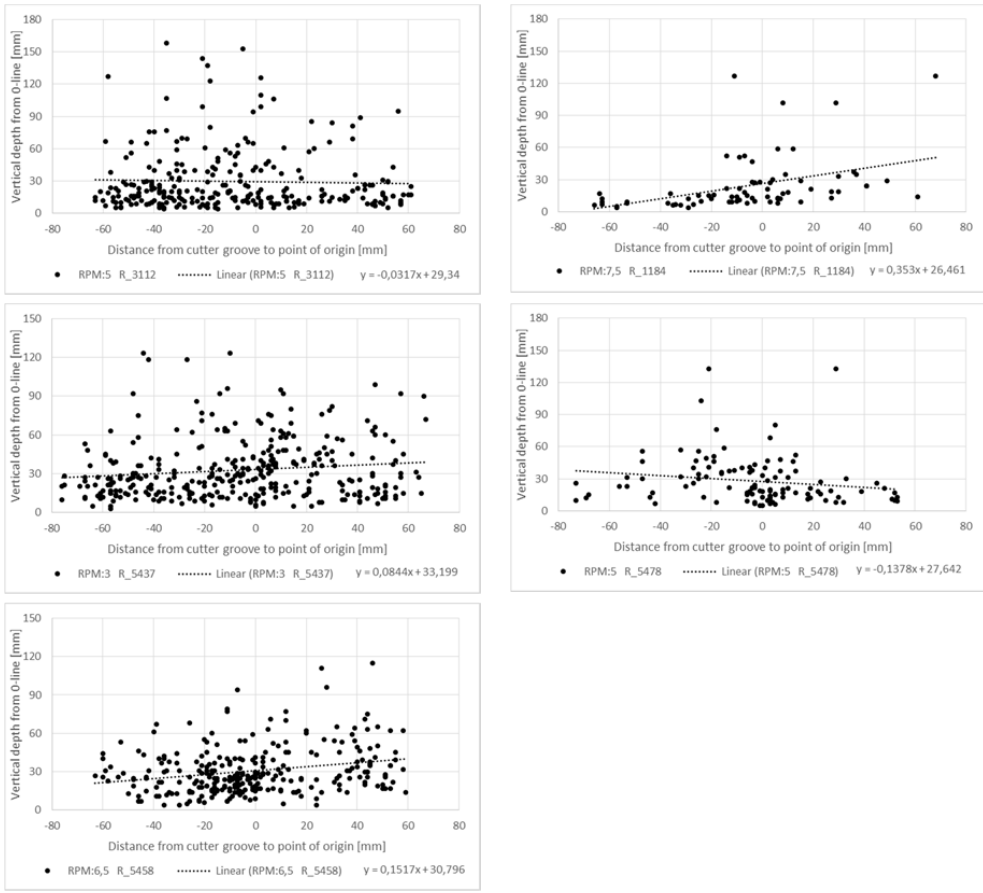

Figure J1.52: Vertical depth from 0-line and exact point of origin in relation to the cutter groove for all cracks with dip >3° in the core samples.

ISBN 978-82-326-3798-0 (printed version)
ISBN 978-82-326-3799-7 (electronic version)
ISSN 1503-8181

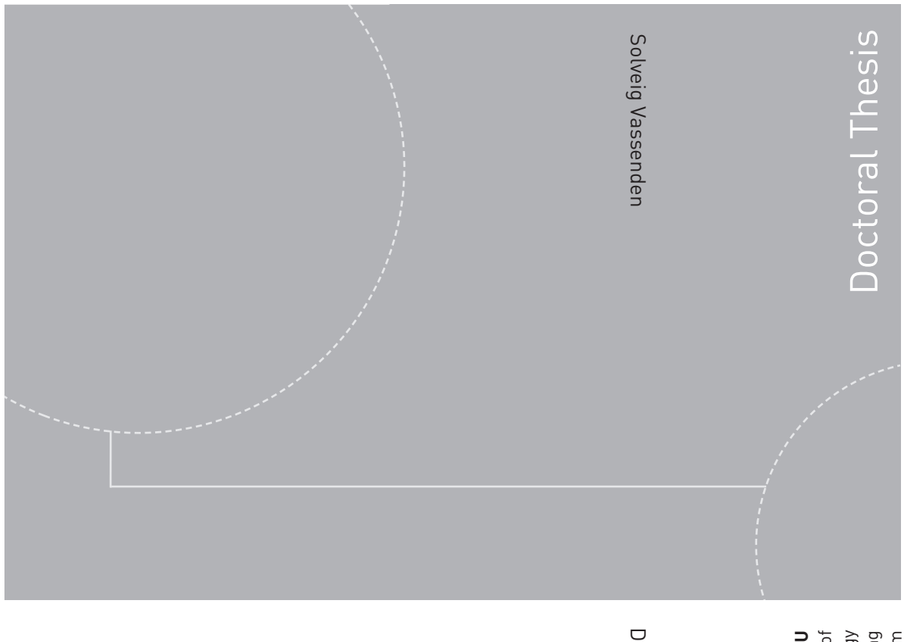

Doctoral theses at NTNU, 2019:100

Solveig Vassenden

Rock Breaking Under Rolling TBM Disc Cutters in Hard Rock Conditions

Visualization and documentation of craks

NTNU
Norwegian University of
Science and Technology

NTNU
Norwegian University of
Science and Technology
Faculty of Engineering
Department of Geoscienceand Petroleum

Doctoral theses at NTNU, 2019:100

NTNU
Norwegian University of
Science and Technology

NTNU
Norwegian University of
Science and Technology